

INTERNATIONAL COURT OF JUSTICE

**APPLICATION OF THE INTERNATIONAL CONVENTION FOR THE SUPPRESSION
OF THE FINANCING OF TERRORISM AND OF THE INTERNATIONAL
CONVENTION ON THE ELIMINATION OF ALL FORMS OF RACIAL
DISCRIMINATION**

(UKRAINE V. RUSSIAN FEDERATION)

REJOINDER

SUBMITTED BY THE RUSSIAN FEDERATION

VOLUME I

(ANNEXES 1 - 3)

10 MARCH 2023

TABLE OF CONTENTS

VOLUME I

Annexes 1-3

- Annex 1 Report of JSC Air and Space Defense Corporation "Almaz-Antey" on the results of studies related to the technical investigation into the crash of the Malaysian airlines Boeing 777-200 9M-MRD (flight MH17), 2023.
- Annex 2 Report of JSC Air and Space Defense Corporation "Almaz-Antey" on the conduct of a full-scale experiment, 2016.
- Annex 3 Report of JSC Air and Space Defense Corporation "Almaz-Antey" on a flight test of the air-route radar complex "Utes-T" located at the air-route radar position "Ust-Donetsk" at the Rostov Regional Centre of the Russian Federation Unified Air Traffic Management System, 2019.

Annex 1

Report of JSC Air and Space Defense Corporation "Almaz-Antey" on the results of studies related to the technical investigation into the crash of the Malaysian airlines Boeing 777-200 9M-MRD (flight MH17), 2023

(translation)



Air and Space Defense Corporation
"Almaz-Antey"

REPORT

on the results of studies related to the technical investigation into the crash
of the Malaysian airlines Boeing 777-200 9M-MRD (flight MH17)

PART 1

Moscow, 2023

TABLE OF CONTENTS:**PART 1**

page

1. Study Objects	5
2. Purpose and objectives of the research	6
3. Research conditions	7
4. Conclusion	8
5. Principal research materials	11
5.1. Identification of combat damage to a Boeing 777	12
5.1.1. Boeing 777 damage model	14
5.1.2. Fragmentation damage to the Boeing 777 aircraft	17
5.1.2.1. Fuselage outer skin damage boundaries	17
5.1.2.2. Number of hits in the outer skin of the forward part of the fuselage	30
5.1.2.3. Density of damage to the outer skin of the forward part of the fuselage	33
5.1.2.4. Damage to the primary structure	36
5.1.2.5. Damage to the cockpit floor and interior	42
5.1.2.6. Exit "inside-out" holes	45
5.1.2.7. Damage to the left engine and left wing plane	48
5.1.2.8. Direction of damage	53
5.1.2.9. Model of fragmentation damage to Boeing 777 aircraft	55
5.1.3. Bast damage to the Boeing 777	57
5.1.4. Criteria for comparing modelled and actual damage to Boeing 777.....	65
5.2. Identifying conditions under which damage was done to Boeing 777.....	66
5.2.1. Determining the detonation point	66
5.2.2. Warhead detonation model	68
5.2.3. Position of Boeing 777 in space	78
5.2.4. Methods for determining the orientation of the warhead relative to the aircraft structure (aircraft-missile encounter conditions).....	81
5.2.4.1. Consistency of fragmentation field boundaries	82

5.2.4.2. Consistency of fragmentation density distribution	87
5.2.4.3. Destruction of aircraft structure by a dense stream of projectiles ("scalpel")	95
5.2.4.4. Matching degree of blast effect of the 9H314M warhead	104
5.2.4.5. Verification of the results obtained on the basis of in-flight control data	108
5.2.4.6. Compliance with the radio trigger algorithm	109
5.2.5. Orientation of the warhead in relation to the aircraft structure	111
5.3. Determining the likely launch area	115
5.3.1. Missile flight model	116
5.3.1.1 The method of guiding a BUK missile	116
5.3.1.2 Model of BUK Missile of Almaz-Antey Corporation.....	117
5.3.2. Possible launch area	120
5.3.2.1 Calculation to identify the possible launch area	120
5.3.2.2 Comparative analysis of calculations to identify the possible launch area	121
5.4. Identification of weapon	126
6. Analysis of the results obtained	128

PART 2 Exhibits to the Report

1. Study Objects

1. The materials of the Dutch Safety Board (DSB) investigation report into the crash of the Malaysian airlines Boeing 777-200 9M-MRD (hereinafter referred to as Boeing 777), which crashed on 17 July 2014 during flight MH17 from Amsterdam to Kuala Lumpur, which were obtained with permission from the DSB.

2. The scheme prepared by DSB specialists, which shows how the aircraft fragments are linked to the structural design of Boeing 777,¹ as well as photo and video footage made by Almaz-Antey Corporation specialists and by Rosaviation and Central Research Institute of Air Force experts during inspections of the aircraft fragments at the Gilze-Rijen air base in February, May and August 2015.

3. Design and technical documentation for 9K37M1 SAMS.

4. Final report on the testing of the 9H314M warhead with preformed fragments, 1981.

5. Technical report on verification of the 9H314M warhead's zone of damage parameters, 1981.

6. Warhead 9H314M. Technical reports on control tests by explosion at ground stationary conditions, reports on results of control and periodic tests, 1981-1991.

7. Photo and video footage made during field experiments (31.07.2015 and 07.10.2015) as well as special research concerning the penetration capability of projectiles.

8. Elements of the target layout used in experiments and tests.

9. Samples of projectiles and missile (warhead) fragments collected from the sites of the experiments and recovered from the targets' structural components.

10. Design and technical documentation for the air-route radar complex (ARRC) "Utes-T".

11. Results of Utes-T ARRC tests.

12. Photo and video footage and in-flight recording control data obtained in the course of field experiments and studies to confirm the technical characteristics of the primary radar of Utes-T ARRC located at Ust-Donetsk position at the Rostov Regional Centre of the UATMS (Rostov Region, Russian Federation).

¹ The structural design of the Boeing 777 aircraft was obtained from DSB experts in February 2015 during the first phase of joint work at the place of preliminary layout of fragments.

2. Purpose and objectives of the research

The purpose of the studies was to determine the possible involvement of BUK 9M38 or 9M38M1 missiles in the attack on Boeing 777 and to assess the credibility of the findings of the Dutch experts.

In order to achieve this objective, the following tasks were carried out during the studies:

1. To assess the credibility of the findings of the Dutch experts as regards the weapon type and the conditions under which the Boeing 777 was hit in mid-air.
2. Comparing the damage to the Boeing 777 with the pattern of damage caused by the impact of the 9M38 or 9M38M1 missiles.
3. Identifying conditions under which the impact of 9M38 or 9M38M1 missiles on the Boeing 777 aircraft can cause the destruction of the aircraft in mid-air.
4. Identifying the possible launch area in light of the hypothesis of the Boeing 777 being hit by a 9M38 or 9M38M1 missile.

3. Research conditions

The source data for organising and conducting the research was the Preliminary Report, the Draft Report and the DSB Final Report to the extent related to the type of weapon and the conditions of its encounter with the Boeing 777 aircraft.

In the final version of the DSB Final Report "Crash of Malaysia Airlines Boeing 777-200, 9M-MRD, flight MH17" the Dutch experts concluded that the cause of the MH17 crash was the detonation of a 9H314M warhead delivered by a 9M38-series anti-aircraft missile from a BUK surface-to-air missile system, which was moving "in an opposite direction".

The conclusions about the type of weapon and the alleged location of the missile launch "from the east of Ukraine"² were made on the basis of "best matches" based on the results of the analysis of the location, size and boundaries of the damage area, assessment of the number and density of holes in the wreckage of Boeing 777,³ and identification of the mutual location (conditions of encounter) of the aircraft and the missile.

In the DSB Report, the "best match" refers to the aircraft-missile encounter conditions (angles in the horizontal and vertical planes, final missile speed)⁴ corresponding to the version that the aircraft was hit while flying in an "opposite direction" (Figure 3.1).

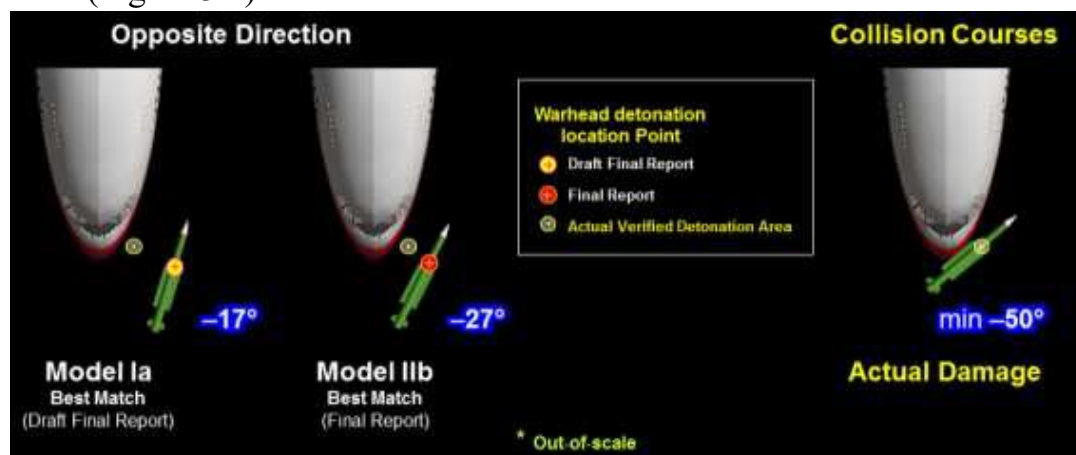


Figure 3.1 - Missile encounter conditions: left - "opposite course" (DSB); right - "collision course"

However, the area of detonation (destruct) of the 9H314M warhead, according to the Dutch experts, "was in a volume of space smaller than 1 m³, about 4 m above the tip of the nose of the aircraft to the left of the cockpit".⁵

² Final Report. 11. Missile flight parts, p.256

³ Final Report. 6. Fragmentation spray of pre-formed fragments, p.255.

⁴ Final Report. 3.8.3. Warhead simulations, p.140.

⁵ Final Report. 3.8.5. Volume of space containing the detonation position, p.142.

4. Conclusion

Based on the analysis of the operation of the BUK surface-to-air missile system and 9M38 and 9M38M1 guided missiles; damage to the outer skin, interior and the structure of the Boeing 777; and the results of experiments and special studies by specialists of Almaz-Antey Corporation, the following conclusions were drawn:

1. If the crash of the Boeing 777 was caused by a BUK missile, it could only have happened "on collision courses". The most probable angle of approach of the missile to the aircraft in the horizontal plane could be 72^{+2}_{-10} angle degrees. In such case, the launch area could be the area shown in the presentation⁶ at the Almaz-Antey Corporation press conference regarding the results of the full-scale experiment, which was held in October 2015 (Figure 4.1).



Figure 4.1 - Possible launch area: for 9M38M1 missiles (red area); for 9M38 missiles (blue area)

Table 4.1 shows the coordinate values for six points corresponding to the possible launch areas: points 1, 2, 3 and 4 correspond to the possible 9M38M1 launch area; points 3, 4, 5 and 6 correspond to the possible 9M38 launch area.

Table 4.1 - Coordinates of possible launch area

1	47.984290	38.482380	47° 59' 3.444" N	38° 28' 56.568" E
2	47.979410	38.535590	47° 58' 45.876" N	38° 32' 8.124" E
3	47.967230	38.467960	47° 58' 2.028" N	38° 28' 4.656" E
4	47.961720	38.536280	47° 57' 42.192" N	38° 32' 10.608" E
5	47.932970	38.465210	47° 55' 58.692" N	38° 27' 54.756" E
6	47.927220	38.530790	47° 55' 37.992" N	38° 31' 50.844" E

⁶ Results of the Field Experiment to Assess the Causes of the Crash of MH17, October 2015.

The study of the materials related to the missile fragments with unique serial numbers, specialists of the Almaz-Antey Corporation found, based on technical documents of the missile manufacturer, that both numbered fragments: the missile engine and the nozzle, were installed in the 9M38 missile (without the "M1" index, that is, an older modification) with the serial technical number "8868720. The missile was given the tail number "9M38 886847379" and on 31 December 1986 it was put into service.⁷

Accordingly, the most likely launch area for the 9M38 missile is limited by points 3, 4, 5 and 6 with their respective coordinates.

2. A missile from a BUK complex cannot approach an aircraft "on a collision course" from any of the three areas^{8,9,10} identified by experts of the Netherlands Aerospace Centre (NLR). This is confirmed by calculations made with the use of the software of the BUK missile control system previously provided to Dutch experts in response to their request for legal assistance.

3. The area of the missile launch from the side of Snezhnoye and Pervomayskiy towns (Donetsk Region, Ukraine), i.e. "in the opposite direction", is not confirmed by the in-flight control data recorded by the Utes-T radar complex located at the Ust-Donetsk radar position. In the primary data registration file "14-07-17.kt" of the Utes-T radar complex for the period from 13:02 to 13:32 UTC 17.07.2014, no markings from a weapon are registered, which indicates the absence of an object moving towards the Boeing 777 in "the opposite direction" in the observation space.

4. As a result of experiments, tests and special research carried out by Corporation, the credibility of the conclusion of the DSB report "Crash of Malaysia Airlines Boeing 777-200, 9M-MRD, flight MH17" about the aircraft being hit by a 9M38-series anti-aircraft missile with a 9H314M warhead "on the opposite course" is not confirmed.

5. The lack of complete objective data from metallurgical examinations and the mismatch between the weight and dimension characteristics of the fragments specified in the materials of the Dutch experts and the reference samples obtained during the tests do not allow for unequivocal identification of the type of projectiles or for reliably determining the type of warhead and weapon.

6. If other conditions of the missile aircraft encounter ("on an opposite course") are considered, the BUK missile could not have caused the crash of the Boeing 777.

The main points of this report are set out in official letter to the DSB No. 01-09/548k dated 29.07.2015.

Subsequently, the field experiments, tests and special studies confirmed the

⁷ PART 2. Exhibit E. Fragments of the 9M38 missile.

⁸ 250 km². Draft Final Report. 3.8 Launch area. Figure 47. Area of missile launch (Source NLR), p.132.

⁹ 320 km². Final Report. Visualisation of NLR fly out simulation result. Figure 62, p.144.

¹⁰ 75 km². More precise launch area identified by NLR specialists. Its image is available in open-source materials.

conclusions set forth in this letter and defined the most likely type of the missile more accurately.

5. Principal research materials

The report contains the results of studies carried out in accordance with the methodology developed by JSC Air and Space Defense Corporation "Almaz-Antey" to investigate the destruction of an airborne object by a BUK surface-to-air missile system.

The methodology draws on the Corporation's specialists' exceptional skills and their multi-year experience in developing, testing and operating air defence weapon systems, and is based on the established patterns of impact of anti-aircraft guided missiles on the structure of airborne objects. The methodology is based on the application of a set of engineering analysis methods and calculations and mathematical modelling, as well as on subsequent experimental confirmation of the results obtained.

The studies addressed a number of consistent and inter-related objectives:

- identifying combat damage done to the Boeing 777 aircraft caused by the main factors of remote action of a high-explosive missile warhead;

- determining conditions that cause combat damage (the conditions of missile aircraft encounter at the moment of detonation - position and mutual orientation of the aircraft and missile in space and their final velocities);

- identifying the possible launch area.

5.1. Identification of combat damage to Boeing 777

The effect of the warhead of a surface-to-air missile.

It follows from the basics of the surface-to-air missile (SAM) firing theory that generally the destruction of an airborne target can result from the fragmentation and blast effects of the missile's warhead.¹¹

The fragmentation effect of a SAM warhead is determined by the nature of the damage caused by the projectiles to the outer skin, the structure, and vulnerable components and assemblies of the target.

The fragmentation field can cause damage to a target in two ways:

1. By causing mechanical breakdown of the structure.
2. By hitting vulnerable sections (disabling engines, control systems, fuel ignition, detonation of explosives in bomb bay, etc.)

Depending on the vulnerability characteristics of the airborne object, the weight of the projectiles, their velocity and the conditions under which they encounter the obstacle, the following types of effect (in order of importance) are distinguished:

1. Penetration (mechanical action). The projectiles carry out mechanical destruction of the target's structure. If the fragments density is high enough, the structural elements (skin, power frame) of the target can be damaged to such an extent that the aerodynamic loads impacting the target in flight complete the destruction.
2. Initiating action (probability of initiation of a detonation wave in explosives and detonation of aircraft munitions, warheads, etc.).
3. Incendiary action (ignition of aviation fuel, etc.)
4. Eroding action (indentations, sinkholes or craters accompanied by the obstacle mass removal).
5. Aero- (hydro-) impact.

In general, the nature of destruction (damage to vulnerable sections) is most influenced by the density of fragments (amount of damage), kinetic energy (mass, velocity), shape of the fragments and the nature of the environment.

Under the influence of a dense stream of fragments and the resulting shock waves (ballistic waves of fragments in the air), the aircraft structure is penetrated and its compartments mechanically destroyed.

The region of intersection of the airborne target's (aircraft's) outer surface and the weapon's fragment dispersion sector (preformed and hull fragments) is the fragment cloud. The fragment cloud is characterized by respective boundaries on structural elements of the aircraft, the number of impact points and the distribution of damage density.

¹¹ Neupokoev F.K. Anti-Aircraft Missile Firing, p. 197-203.

At short distances (less than the blast radius taking into account the air density), the mechanical destruction from the dense flux of preformed fragments is supplemented by the blast impact.

The technical documentation for BUK missiles specifies that an airborne object (target) will be destroyed specifically by the blast effect if at least one of the points of the segment connecting the nose of the aircraft and the median of the wing is inside the sphere with a high-explosive radius R circumscribed around the geometric centre of the warhead. In the case under review (for the Boeing 777) this corresponds to the centreline of the aircraft, CLA.

A study was carried out in the period of development of the 9H314M warhead design and kill field parameters (in the 70-80s of the last century) specifically to determine how the blast impact high-explosive radius R depends on the detonation height H .

For conditions near the ground surface, the blast impact radius of a BUK warhead is about 5 meters, and for an altitude of $\sim 10,000$ meters (33,000 ft) it is about 3.5 meters (Figure 5.1.1).

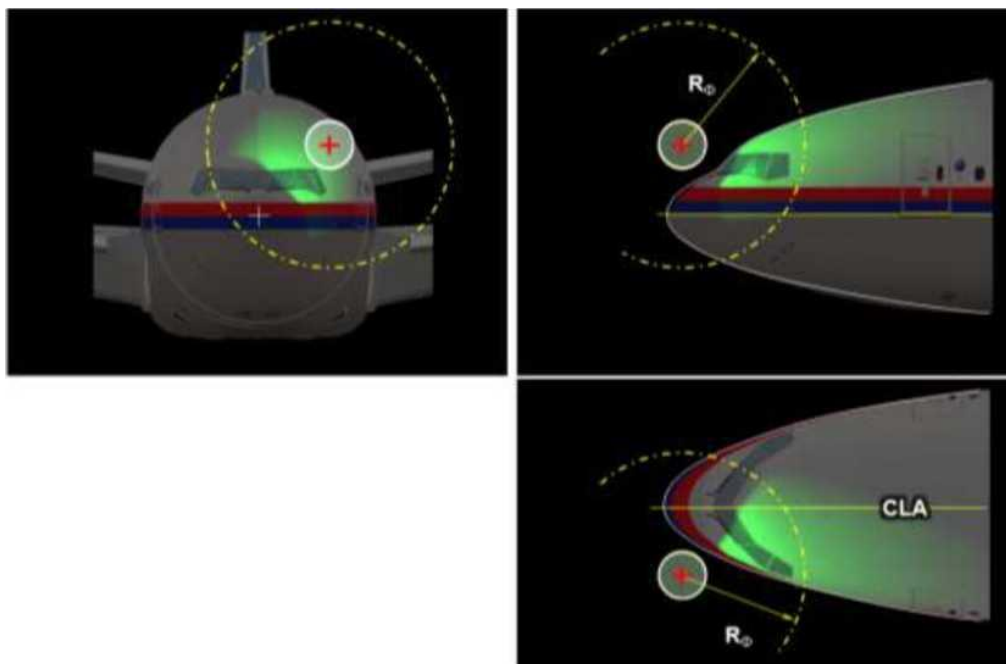


Figure 5.1.1 - Points located on the aircraft centreline (CLA) are inside the sphere with high-explosive radius R (~ 3.5 m) circumscribed around the geometric centre of the warhead when it is in a verified detonation area

Thus, in investigating the nature of damage from the remote impact of an anti-aircraft fragmentation warhead on the aircraft structure, it is necessary to:

investigate the traces of impact of nearby explosion factors;

determine the basic parameters of the fragment cloud, including boundaries, the amount of damage to the outer shell, the airframe, components and assemblies, and the aircraft's interior;

establish the distribution of fragmentation damage density in the aircraft structure fragments, including the airframe.

5.1.1. Boeing 777 Damage Model

The study of damage to the Boeing 777 (determining the fragment cloud boundaries, counting the number of and locating through-and-through holes) were carried out during the preliminary modelling phase of the research into Boeing 777 structural damage.

The study of photographs and visual inspection of fragments of the nose section of the aircraft revealed that many of the fragments show specific damage in the form of local holes and dents, which are characteristic of a high-speed impact by compact solid objects. Ten large fragments with relatively large amounts of such damage were identified in the nose section of the aircraft: fragments of the right side of the cockpit with part of the roof and preserved transparency on the right-hand pilot's side; elements of the cockpit transparency frame; the forward part of the fuselage with the first pressure bulkhead in front of the cockpit; fragments of the port side skin of the aircraft; and fragments of the roof behind the cockpit.

Seven of these fragments were used by DSB experts in the 3D reconstruction of the nose section of the MH17 fuselage.¹² Their referencing to the aircraft structure was made during the 3D reconstruction and does not need to be clarified.

Three important fragments: fragment of cockpit roof (Fig. 5.1.2), middle part of the port side (Fig. 5.1.3) and fragment of upper part of the port side and roof behind the cockpit (Fig. 5.1.4) were not included in the final layout.

The position of two of those fragment was accurately identified by DSB in relation to the aircraft's airframe structure based on the construction drawing of the Boeing 777 nose section (Section 41).¹³ However, after completion of the Draft Report, these fragments were not studied further or taken into consideration.

¹² Some of the fragments were not included in the preliminary layout shown during the joint work in February and May 2015.

¹³ Draft Final Report. Figure 52, p. 140.



Figure 5.1.2 - Fragment of the cockpit roof.
In the Preliminary Report materials it was one of the main pieces of evidence for the impact of high-energy objects (DSB submissions)



Figure 5.1.3 - Fragment of the middle port side (open-source photo)

The third fragment, a fragment of the upper port side,¹⁴ was not included in the final 3D reconstruction and was located in another room during the presentation of the DSB report.



Figure 5.1.4 - Fragment of the top of the port side (front) and the nose of the left engine air intake (rear) were located elsewhere in the final reconstruction (open-source photo)

There were no external reasons preventing the exact location of the fragment from being determined on the basis of easily identifiable structural features: joints, connections, marked elements of the airframe¹⁵ and there was no task to carry out its 3D-reconstruction.

The Boeing 777 fragments and the damage to it linked to the construction drawings using coordinates based on stringers and frames were added to the digital Damage Model. The coordinates of any point on the Boeing 777 fuselage are determined using the factory markings of the structural elements (stringers and frames), taking into account that the frame markings correspond to the distance in inches from the reference plane, which is perpendicular to the fuselage construction axis and is 92.5 inches from the end of the aircraft nose fairing.¹⁶

Directly in the Damage Model, an OXYZ coordinate system was adopted, which is linked to the aircraft such that the origin of the coordinates coincides with the end of the aircraft nose fairing, the OX axis coincides with the aircraft construction horizon along the centreline, the OY axis points to the right in the direction of flight and the OZ axis points upwards.

¹⁴ Was taken to Dutch territory at the request of JIT following a documentary aired on the RT television channel.

¹⁵ Factory markings on Boeing 777 airframe components.

¹⁶ Boeing 777-200/300 Aircraft Maintenance Manual, page 201.

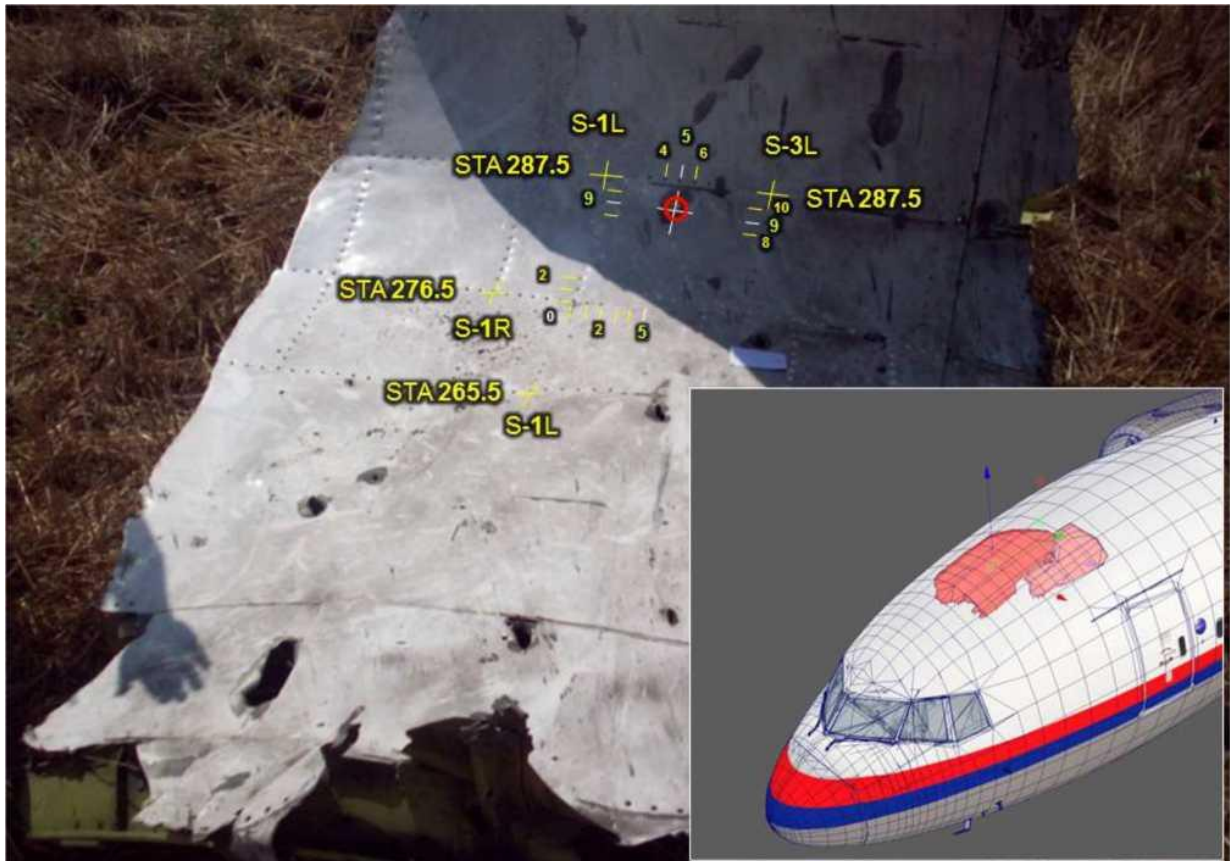


Figure 5.1.5 - Determining damage coordinates in fragments by referencing the marked elements of the airframe and visible structural components (sheet metal joints, numbered rivets)

As new data became available (photo and video footage of new fragments, results of inspections of fragments at pre-layout), the source data was refined.

5.1.2. Fragmentation damage to the Boeing 777 aircraft

5.1.2.1 Fuselage outer skin damage boundaries

An important parameter of the Damage Model is the outer skin fragments coverage zone boundaries (damage boundaries), which are one of the main indicators in determining the position of the weapon relative to the aircraft structure at the time of detonation (aircraft-missile encounter conditions).

Front boundary of damage area

Among the damaged parts that are important for determining a possible missile launch area, the forward pressure bulkhead shown in Figure 5.1.6 is of particular importance.

No through-and-through holes were found on its surface that could be identified as being caused by projectiles.

According to DSB experts, the forward pressure bulkhead (STA 132.5) is the objective forward boundary of the damage area where damage is caused by high-

speed elements.¹⁷



Figure 5.1.6 - Forward pressure bulkhead has no traces of fragmentation damage

The left side of the fuselage that is adjacent to the front airtight bulkhead (hermetic bulkhead, STA 132.5) has holes and dents. The right side of the fuselage attached to the front airtight bulkhead has no penetrating damage, as also noted by the Dutch specialists.¹⁸

At the front, in front of the cockpit windows, a fragment adjoins the pressure bulkhead, which is also the forward boundary of the fragment coverage area. The peculiarities of damage to this fragment are shown in several photographs (Figures 5.1.7-5.1.11).

¹⁷ Final Report. 3.5.3 Damage from external causes, p.121, 124.

¹⁸ Final Report. 2.12.2 General distribution and description of the wreckage, p.63-64.



Figure 5.1.7 - Fragment of the nose of Boeing 777 adjacent to the forward pressure bulkhead, from above (photo of February, 2015)



Figure 5.1.8 - Most of the fragment shows only clearly visible traces of close blast products: microcraters, thermal oxidation and soot (photo of February 2015)



Figure 5.1.9 - There are four through-and-through holes in the fragment. It is most likely that these through-and-through holes are the result of impact of secondary fragments rather than prefabricated projectiles, as evidenced by the shape, appearance and linear dimensions of the holes (photo of May 2015)



Figure 5.1.10 - Appearance of through-and-through holes. View from the inside of the fragment (photo of May 2015)



Figure 5.1.11 - Through-and-through holes identifiable as impact damage are located on the left side behind the bulkhead. Photo shows part of the port side adjacent to the bulkhead, with a clearly distinguishable forward boundary of the penetrating damage area.

These holes are the result of the impact of the rear front of the fragmentation field, which allows for their use as a marker for determining the orientation of the weapon in space (photo of February 2015)

Thus, the forward pressure bulkhead with fragments adjoining to it in front of the cockpit and port side windows is a clearly visible forward boundary of the fragment coverage field.

Lower boundary of damage area

Generally, the battle damage close to the lower boundary of the damage area (boundary of the coverage field) is elongated, clearly oriented rectilinear traces.

This damage is the result of contact with fragments (preformed and hull fragments) whose trajectories were oriented tangentially to the outer contour of the fuselage in this area.

The lower boundary of the fragmentation damage starts from the forward pressure bulkhead (STA 132.5) and can be traced almost to the front left door L1, up to the level of bulkhead STA 298.5.

Examples of damage constituting the lower boundary of the coverage field are shown in Figures 5.1.12 to 5.1.15.



Figure 5.1.12 - Non-penetrating damage at the lower boundary of the coverage field in the area of the forward pressure bulkhead (STA 132.5). Approximate position of the coverage field boundary corresponds to the bottom cut of the measuring ruler

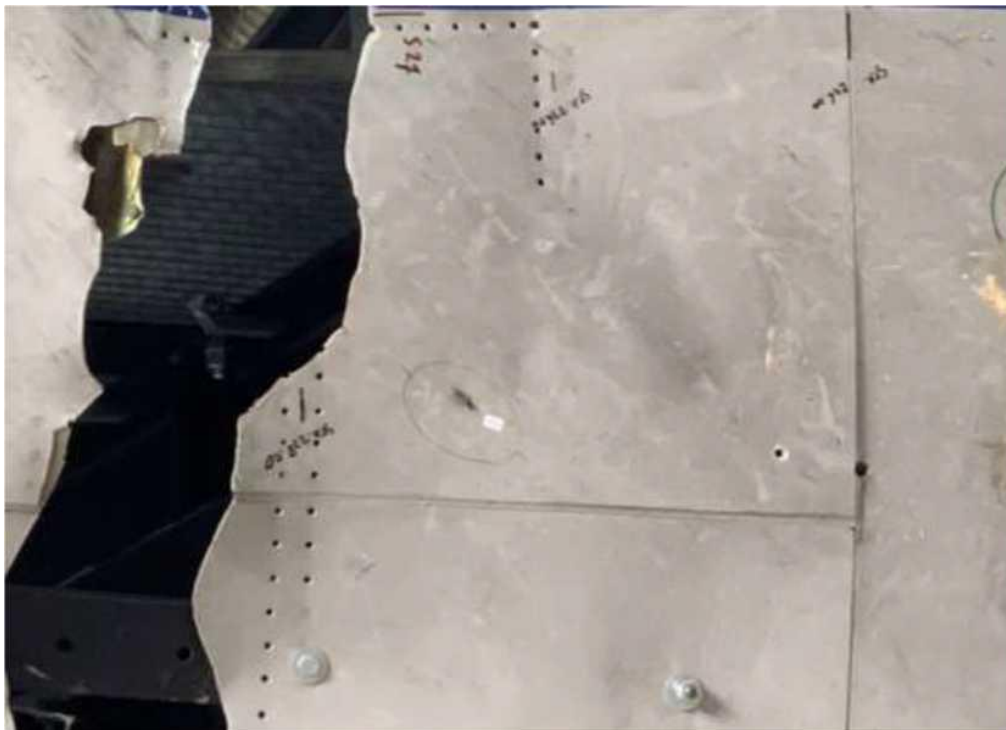


Figure 5.1.13 – Part-through non-penetrating damage at the lower boundary of the coverage field between bulkheads STA 228.5 and STA 236.5



Figure 5.1.14 – Though-and-through and part-through non-penetrating damage at the lower boundary of the coverage field near bulkhead STA 265.5



Figure 5.1.15 - Though-and-through and part-through non-penetrating damage at the lower boundary of the coverage field between bulkheads STA 276.5 (left), STA 287.5 (centre) and STA 298.5 (right)

Damage area boundary on the right-hand side of the cockpit

The right-hand boundary of the coverage field can be clearly seen on the fragment of the right-hand side of the cockpit with part of the roof and the preserved transparency on the right-hand side of the pilot (Figures 5.1.16-5.1.18).



Figure 5.1.16 - Fragment of the right-hand side of the cockpit with part of the roof and preserved transparency on the right-hand side



Figure 5.1.17 – Damage near the right boundary of the coverage field corresponds to the level of the upper right-hand corner of the right-hand pilot's front window



Figure 5.1.18 - Boundary damage to the right side of the cockpit

Upper rear boundary of damage area (along the roof)

The upper boundary of the coverage field on the right side of the nose of the Boeing 777 can be clearly seen on two roof fragments:

in the upper part of the fragment of the right side of the cockpit with part of the roof and the preserved transparency on the right-hand pilot's side (Fig. 5.1.19);

in the cockpit roof fragment (figure 5.1.20).



Figure 5.1.19 - Boundary damage in the upper part of the fragment of the right side of the cockpit



Figure 5.1.20 - A fragment of the cockpit roof objectively shows the boundary of the fragmentation field (photo - DSB resource)

The most important fragment that illustrates the location of the actual fragmentation damage area boundary is a fragment of the roof behind the cockpit. The furthest hole on the right-hand side is in the area of the STA 265.5 bulkhead.

The first bulkhead in this fragment where factory markings are clearly visible is the bulkhead STA 236.5. This is clearly visible in the figure used by the Dutch experts in the Preliminary Report (figure 5.1.21).



Figure 5.1.21 - Factory markings on the front bulkhead STA 236.5 and the bulkhead STA 246 which is behind it (rear cockpit wall) can be seen

The longitudinal centreline of the aircraft (CLA) runs through this fragment. That is, this roof fragment contains parts of both the left and the right side. This fragment contains damage both to the right (up to the level of STA 265.5) and to the left (up to STA 298.5) of the aircraft centreline. Multiple images of this fragment from different angles allow the rear boundary of the fragmentation damage area to

be determined.

Thus, the roof fragment behind the cockpit is an example of a clearly visible upper (rear) boundary of the fragment coverage field. This boundary is visible both on the right side of the roof (to the right of the longitudinal centreline of the aircraft CLA) and on the left side.

Upper left side of the rear boundary of the fragmentation damage area

The most important fragment illustrating the actual rear boundary of the fragmentation damage area is a fragment of the roof and the top of the port side behind the cockpit (Figure 5.1.22).



Figure 5.1.22 - Fragment of roof and top of port side behind cockpit. Through-and-through and part-through non-penetrating holes on the upper left side of the rear boundary of the coverage field are between the bulkheads STA 309.5 and STA 332.5

This fragment of the upper port side is closely adjacent to the roof fragment behind the cockpit (see Figure 5.1.20). The upper left part of the rear boundary of the coverage area in this fragment reliably matches the damage area boundary in the roof fragment behind the cockpit.

An important feature of the fragment is the presence of fragmentation damage beyond the STA 309.5 and STA 332.5 bulkheads (Figure 5.1.23).



Figure 5.1.23 - Example of damage to the outer skin at the boundary of the cover field beyond the level of the STA 332.5 bulkhead

Thus, in the roof fragment and the upper part of the port side that are immediately adjacent to the roof fragment behind the cockpit, the upper part of the left boundary of the fragmentation field is clearly visible, which is an important indicator in determining the orientation of the missile relative to the aircraft.

Rear boundary of the damage area (port side)

The most illustrative example of a rear boundary of fragmentation damage area is a fragment of the port central section which shows fragmentation damage to the outer skin and structural members around bulkheads STA 287.5, STA 298.5 and STA 309.5.

The fragment was not shown on the final layout, but its exact location was determined in the preparation phase and shown on the reconstruction diagram for the skin of the forward part of the Boeing 777 aircraft fuselage.¹⁹

This fragment is located at S-19L level and is adjacent to the fragment of the lower port side behind the cockpit (see Figure 5.1.15). An important feature of this fragment is that it is part of the flight crew rest compartment wall behind the cockpit on the port side (Figure 5.1.24).

¹⁹ Draft Final Report. Figure 52. Grid reconstruction of the outside skin of the forward fuselage, p. 140.



Figure 5.1.24 - Fragment of the central part of the port side behind the cockpit. Figure shows examples of through-and-through and part-through damage between the STA 287.5 and STA 309.5 bulkheads

Based on the layout of through-and-through (penetrating and non-penetrating) damage as well as part-through damage (ricochets) to all fragments examined, a general layout of the boundaries of the fragmentation field for the nose section of the Boeing 777 fuselage was prepared (Figure 5.1.25).²⁰

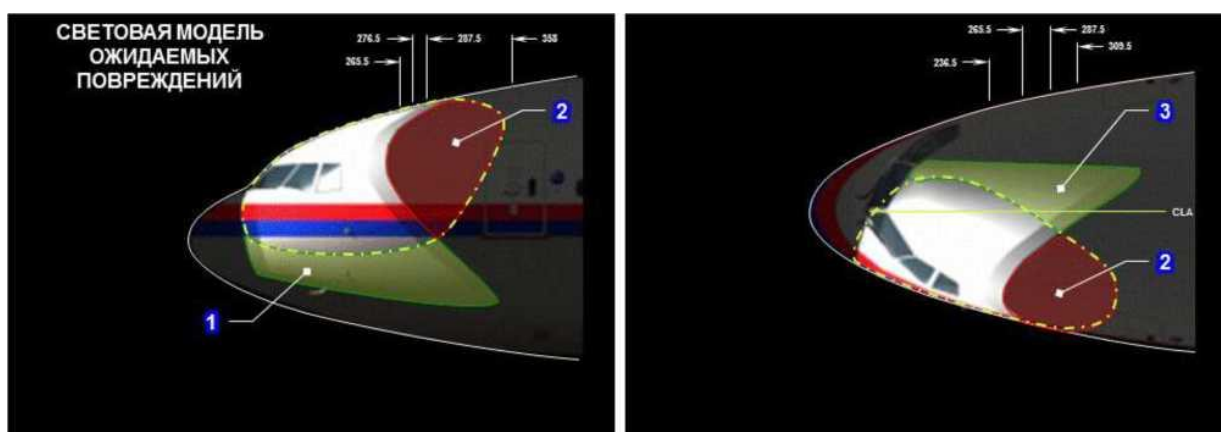


Figure 5.1.25 - Diagram of actual fragment coverage field boundaries as compared to DSB's "reference" model (light model of expected damage): left - left side view; right - top view

Figure 5.1.25*: the light model of expected damage

²⁰ For the sake of clarity, the fragmentation area boundary diagram used by Corporation specialists was superimposed on the light model of expected damage ("opposite course") presented in the DSB modelling material.

Comparison of the damage pattern (the fragmentation coverage boundary diagram) with the light model of expected damage ("reference model") shows that the actual fragmentation coverage area differs significantly from that which was modelled and accounted for by the DSB experts.²¹

Examples of inconsistencies between the actual fragmentation coverage area and the damage area boundaries of the 'reference damage model' are shown in Exhibit A.1.²²

Thus, examination of fragments of the fuselage forward part (taking into account the roof and port side fragments missing in the final 3D reconstruction) made it possible to obtain a clearly marked actual boundary of the fragment coverage field.

5.1.2.2. Number of hits in the outer skin of the forward part of the fuselage

As a result of visual inspection and examination of photographic evidence of fragments from the forward part of the Boeing 777, it was found that many of the fragments showed specific damage in the form of local holes and dents, which are characteristic of a high-speed impact by compact solid objects.

From the photographs and video footage obtained during the preliminary layout of the aircraft at Gilze-Rijen air base, the battle damage to the outer skin of the aircraft fragments in the cockpit area was visually identified and quantified.

The location of such holes in relation to each other and to easily identifiable structural components (marked elements of the airframe, joints, connections, rivets, etc.) was then evaluated from the photographs of the fragments taken from different angles (with a ruler in the field of view). Based on the assessment performed, damage coordinates were calculated in the adopted coordinate system. A total of 230 holes were counted and measured on the outer skin of the fragments presented in February 2015,²³ which were subsequently plotted on the three-dimensional Damage Model.

An example of a fragment with numbered holes under the transparency bezel of the cockpit commander is shown in Figure 5.1.26.

²¹ PART 2: Exhibit A.1. Description of figure A.1.17, pg. 15-18.

²² PART 2: Exhibit A.1.

²³ The Corporation's specialists used their measurements and data of experts from Rosaviatsia and the Central Research Institute of the Air Force obtained during inspections of the aircraft fragments at the Gilze-Rijen air base in February and May 2015.

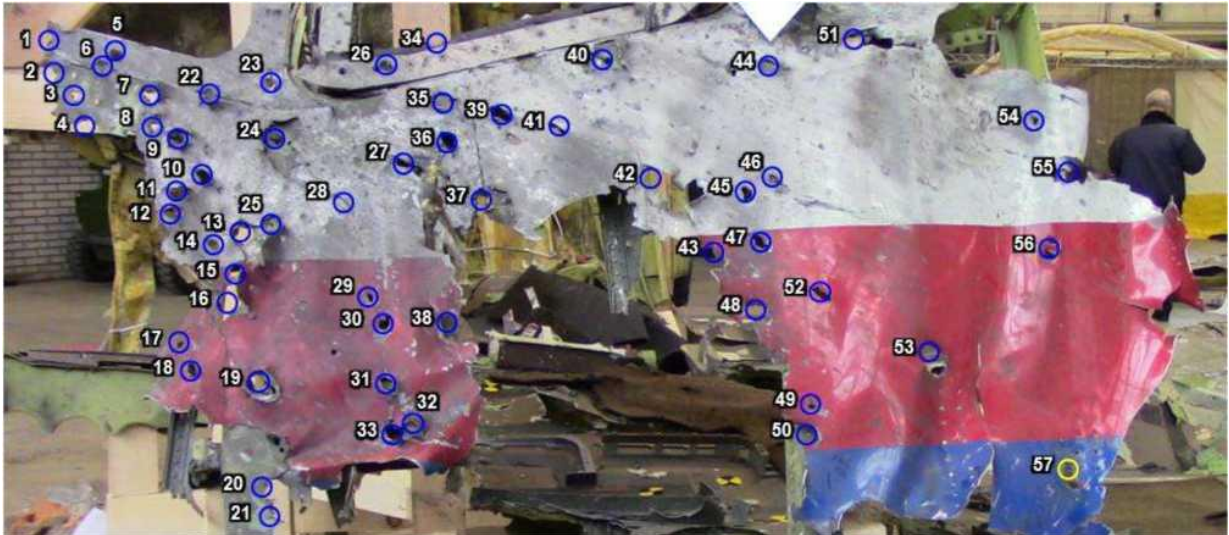


Figure 5.1.26 - Exterior view of a fragment of the aircraft's port side skin below the crew commander's transparency bezel with numbered holes resulting from battle damage

During the second inspection of the preliminary layout of aircraft fragments at Gilze-Rijen Air Base (May 2015), there were new fragments where battle damage to the outer skin was also visually identified and quantified. An example of a fragment from the top rear of the crew commander's window is shown in Figure 5.1.27.

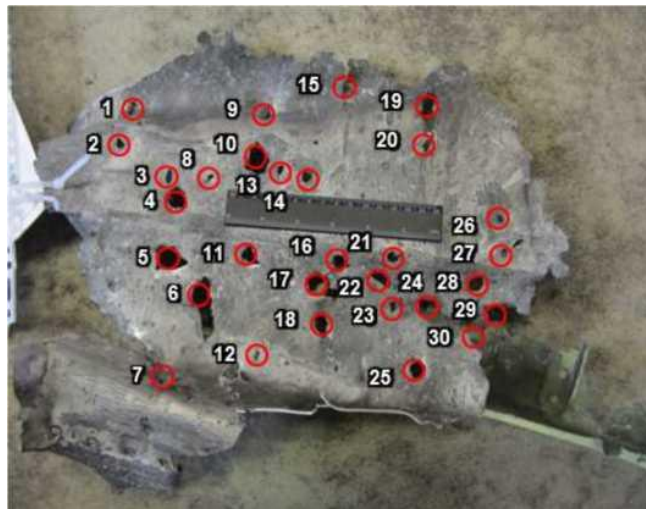


Figure 5.1.27 - Exterior view of the port side skin fragment from the top rear of the crew commander's vent with numbered holes resulting from battle damage

During the third inspection of the preliminary layout of the aircraft fragments at Gilze-Rijen air base (August 2015), many new fragments, not previously available for examination, appeared in the final display.

Using photographic and video material with new fragments obtained from open-source materials, similar work was carried out to identify the battle damage to the outer skin and quantify it.

All in all, taking into account data from Rosaviation and the Central Research Institute of Air Force (who worked as part of a joint team of experts), some 350 entry holes on the outer skin of the aircraft were accounted for.

In addition to the fragments that made it to the final layout, battle damage was studied on the three fragments shown in Figures 5.1.2-5.1.4.²⁴ As an example, a photograph of a portion of the upper port side skin fragment with numbered holes resulting from battle damage is shown (Figure 5.1.28).

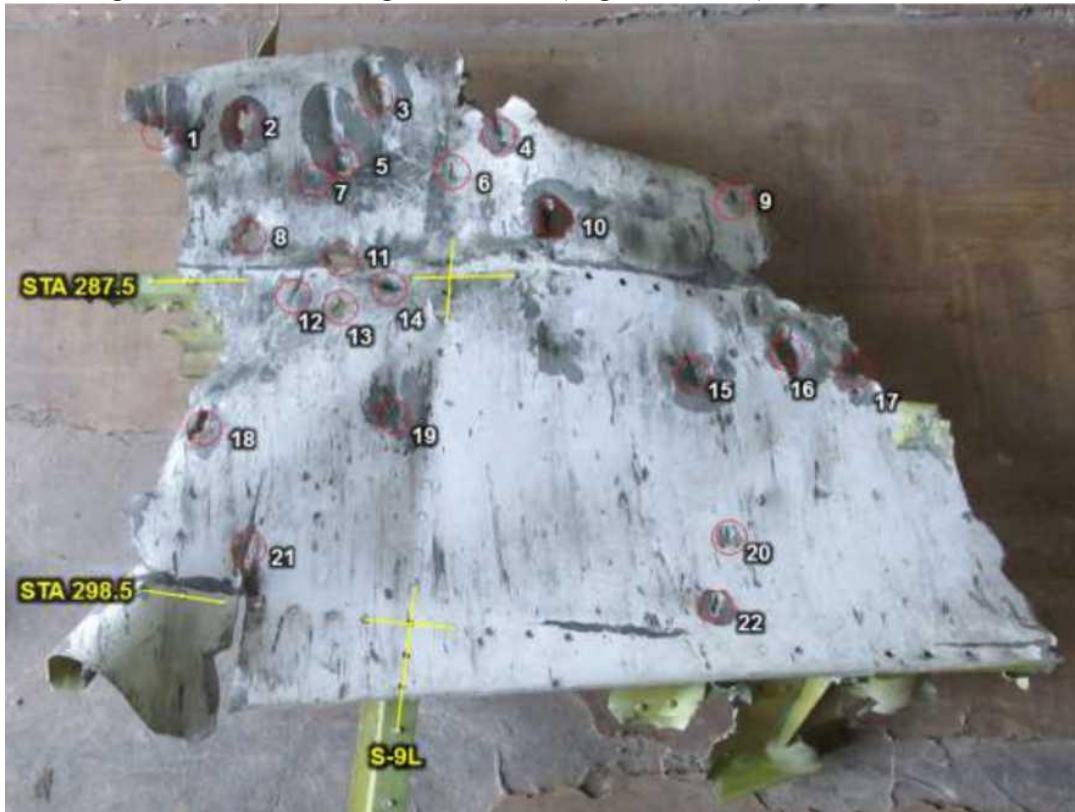


Figure 5.1.28 - Exterior view of the upper port hull fragment with numbered holes resulting from battle damage

Thus, around 350 entry holes were identified on the outer skin of the forward part of the aircraft, in the fragments presented in the final layout. Of these, 230 (more than 65 %) were actually measured during the inspections at Gilze-Rijen air base. In addition, about 70 more holes in fragments of the nose section of the Boeing 777 fuselage not represented in the final 3D display were taken into account.

²⁴ A total of about 70 through-and-through and part-through holes.

5.1.2.3. Density of damage to the outer skin of the forward part of the fuselage

In the materials of the Dutch experts, the transparency area on the left side of the cockpit is taken as fragments with the highest density of fragmentation damage, in particular, the second window of the cockpit commander (Fig. 5.1.29), where 102 holes were identified.²⁵

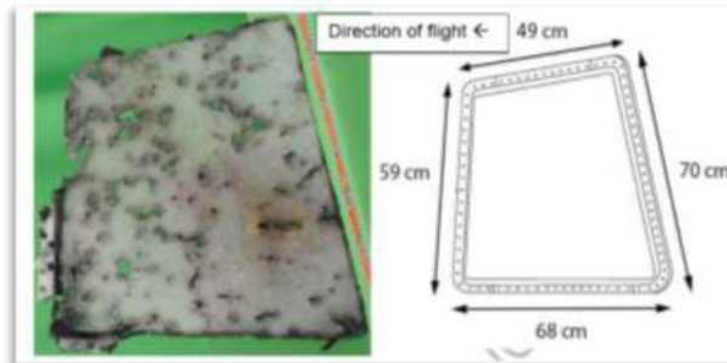


Figure 5.1.29 - Second crew captain window (left side)

The transparency area, which includes the second window, was a marker of sorts for the DSB specialists (the main reference point) corresponding to a maximum density of fragmentation damage of up to 250 per square metre.²⁶

In the course of studies of combat damage to the Boeing 777, specialists of Almaz-Antey Corporation identified several more fragments of the forward part of the aircraft with a high density of damage. Figures 5.1.30 to 5.1.34 show images of some of these fragments.



Figure 5.1.30 - Upper part of the frame of the left-hand cockpit window

²⁵ Final Report. 3.5.3 Damage from external causes, p.119-126.

²⁶ Final Report. Annex X (NLR report). 2.5 Number and density of hits, p.14.



Figure 5.1.31 - Lower part of the frame of the left-hand cockpit window



Figure 5.1.32 - Fragment of the port side below the cockpit window frame



Figure 5.1.33 - Fragment of the port side behind the cockpit windows



Figure 5.1.34 - Fragment of roof and upper port side (not included in final 3D reconstruction)

In addition to the fragments shown in Figures 5.1.30-5.1.34, the area of high fragmentation damage density includes fragments of the roof behind the cockpit (its left front part) and fragments of the port side, which are not shown in the final 3D reconstruction. Figure 5.1.35 shows the layout of the aircraft fragments with the highest density of damage.



Figure 5.1.35 - Layout of the outer skin and airframe fragments with the highest density of damage and signs of close blast effects

The highest density damage to fragments was entered into the Damage Model, where it was taken into consideration as part of an array storing the number of holes per site (polygonal object) in relation to the Boeing 777 aircraft model surface ("Damage Models").

The fragments of the outer skin of the forward part of the Boeing 777 fuselage with areas where the fragmentation damage has the highest density are spread from the left side of the cockpit transparency along the aircraft centreline or at a slight angle to it **along the port side and the left side of the roof** behind the cockpit.

5.1.2.4. Damage to the primary structure

Determining the extent and nature of damage to the primary structure is an important parameter of the Damage Model. This is due to the fact that the detonation of a BUK missile warhead with a mass of about 70 kg produces a dense stream of fragments, in which an area of maximum density of preformed fragments (the so-called "scalpel") stands out.²⁷

Under the influence of this dense stream of fragments and the resulting shock waves, the aircraft structure is penetrated and its compartments are mechanically destroyed, as was verified by conducting field experiments.^{28, 29}

Since the parameters for the formation of such area can be calculated and modelled fairly accurately, determining the concentration of damage to and destruction of the airframe will make it possible to determine the position of the missile's warhead relative to the aircraft at the time of detonation with sufficient accuracy.

An analysis of the Dutch material shows that in a technical study, all damage assessments are limited to the outer skin only – Only outer skin damage investigated.³⁰

However, the Corporation's investigation of damage to the aircraft's primary structure back in February and May 2015 revealed an important feature – the presence of a large number of fragmentation holes in the transverse structural elements (bulkheads) located along the roof of the cockpit and along the port side.

Such damage starts practically from the forward boundary of the fragmentation field (from STA 148 near the forward pressure bulkhead) and extends to the front passenger door L1, including the level below the cockpit floor.

²⁷ The "scalpel" accounts for more than 42% of the mass of all fragments and more than 50% of the kinetic energy of the fragment impact field.

²⁸ Report on the conduct of a full-scale experiment, pages 66-67; 75-88.

²⁹ PART 2. Exhibit B.3. Piercing the structure of an aircraft (target aircraft) through, pages 68-81.

³⁰ DSB submissions. Damage Investigation MH17. NLR Annex 13 - HEO_EN_3.



Figure 5.1.36 - Through-and-through holes in the bulkheads start from the forward boundary of the fragmentation field



Figure 5.1.37 - Examples of damage to bulkheads

At the same time, some of the damage to the aircraft structural elements along the port side and the left side of the roof extends beyond the visible damage limits on the outer skin and significantly beyond the damage pattern chosen by the Dutch experts as the "benchmark" damage. Examples of damage to the bulkheads are shown in Figure 5.1.37.

In total, there are about 60 holes in the transverse structural elements, the position of which can be ascertained with high accuracy.

The areas with the most damage to the transverse structural elements (bulkheads) coincide with the fragments that have the highest density of damage to the outer skin.

Several roof fragments behind the cockpit³¹ and the port side are shown as examples (Figures 5.1.38-5.1.41).



Figure 9: Part of the inside cockpit roof, indicating penetration with objects from outside. (Source: DCA)

Figure 5.1.38 - Left side of roof fragment behind cockpit (inside view). Multiple holes in STA 236.5, STA 246 and STA 254.5 led to deformation and failure of the structural elements
(Resource - Preliminary Report submissions)

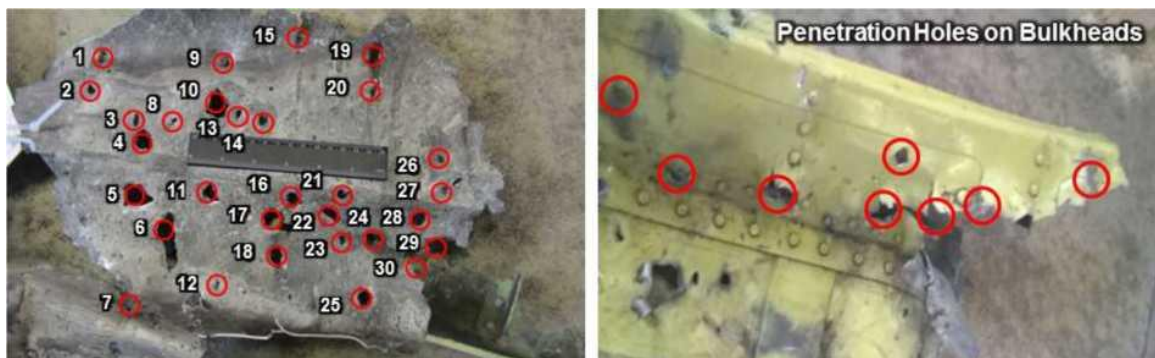


Figure 5.1.39 - Fragment of the port side skin from the top rear of the crew commander's window. Multiple holes in the bulkhead led to deformation and collapse of the structural element (photo on the right)

³¹ A fragment of the roof behind the cockpit with multiple damage to the structure was the main evidence of the impact of high-energy objects on the aircraft (Preliminary Report, figure 9).



Figure 5.1.40 – Fragment of roof and upper part of the port side: external (left) and internal (right) views. Multiple holes in bulkheads STA 287.5 and STA 298.5 led to deformation and collapse of the structural elements (red arrows indicate characteristic damage)



Figure 5.1.41 - Fragment of the centre port side behind the cockpit. Holes in the STA 287.5 and STA 298.5 bulkheads and traces of compression, deformation, tearing and breaking of structural elements are objectively observed

All of the examples of left side roof and port side fragments show penetrating and non-penetrating damage to the outer skin. Holes and traces of compression, deformation, tearing and destruction of the airframe elements are objectively observed in the airframe elements.

In addition to fragmentation damage, the outer skin and structural elements show traces of thermal burns and oxidation and traces of detonation products, unburned explosive particles, small particles of the warhead structure and projectiles.

All this, in conjunction with the maximum density of fragmentation damage to the outer skin and airframe, indicates that these fragments were in the area of impact by highest density (mass and kinetic energy) projectiles and factors associated with a close explosion.

Damage to the transverse structural elements (bulkheads) along the port side extends beyond the boundary of the fragmentation coverage field on the outer skin. As an example, Figure 5.1.42 shows damage to the bulkheads STA 212.5 and STA 228.5 on the port side fragment with the angle of attack sensor. The damage is below the floor level and the lower boundary of the outer skin coverage field.



Figure 5.1.42 - Holes in bulkheads STA 212.5 and STA 228.5 are beyond the lower boundary of the fragmentation field on the outer skin

This is also true for the top side of the roof. Figure 5.1.43 shows a section of the passenger compartment luggage shelf that is positioned further away from the STA 382 level.



Figure 5.1.43 - Fragment of passenger compartment luggage rack with (presumably) fragmentation damage

A further argument confirming the particular importance of investigating the damage to the airframe is the discovery in the luggage of a part of a bulkhead from the structure of the left side of the aircraft's fuselage. A metal fragment was also found in this part of the bulkhead, which was subsequently matched to a part of the missile.³²

The greatest damage to the structural elements of the aircraft is to the roof of the cockpit, the left side of the roof behind the cockpit, and to the port side.

Most of the destruction and damage to the airframe affected the transverse structural elements, i.e. the cockpit floor bulkheads and force beams.

Damage to the airframe of the Boeing 777 extends considerably further than damage to the outer skin and extends at a slight angle to the centreline of the aircraft along the left side of the roof behind the cockpit, along the port side (both to and below floor level).

³² Based on open-source materials.

5.1.2.5. Damage to the cockpit floor and interior

Cockpit floor damage studies are also important to determine the position of the missile's warhead relative to the aircraft on the basis of traces of structural damage to the aircraft from the dense flow of projectiles ("scalpel"), including the structure and the interior of the cockpit.

In total, there were more than 120 fragmentation holes in the cockpit floor, interior and transverse structural elements of the cockpit floor, which were available for examination by specialists of Almaz-Antey Corporation.

Damage to the cockpit floor and structure with examples of typical damage are shown in the diagram (figure 5.1.44).



Figure 5.1.44 – Diagram showing distribution of cockpit floor and structure damage with examples of characteristic damage

In the cockpit of the Boeing 777, the main damage to the cockpit floor and interior is concentrated near the left-hand seat (commander's seat) with a gradual decrease in the density of through-and-through holes along the left-hand side. On the right side of the cockpit floor, only single through-and-through holes are noted and then only at the rear of the cockpit.

Examples of typical damage to the cockpit floor and structure are shown in Figures 5.1.45 and 5.1.46.



Figure 5.1.45 - Damage to cockpit floor and structural elements along the port side



Figure 5.1.46 - Damage in the area of the commander's seat

Part of the cockpit floor along the port side (Figure 5.1.47) is almost completely destroyed. In addition, there are multiple through-and-through holes in the transverse elements of the cockpit floor structure, which led to the destruction of these structural elements and the bulkheads along the left side of the aircraft.



Figure 5.1.47 - Damage density in cockpit floor to the left of the aircraft commander's seat (along the port side)



Figure 5.1.48 - Fragmentation damage to cockpit floor to the left of the aircraft commander's seat (along the port side)

The density of holes in some elements of the cockpit floor located along the port side exceeds the average density of damage to the outer skin (Figure 5.1.48).

5.1.2.6. Exit "inside-out" holes

No exit "inside-out" damage was found in fragments of the starboard side of the Boeing 777 cockpit (Figure 5.1.49).



Figure 5.1.49 - Fragment of the right-hand side of the cockpit with part of the roof and retained transparency on the right-hand pilot's side

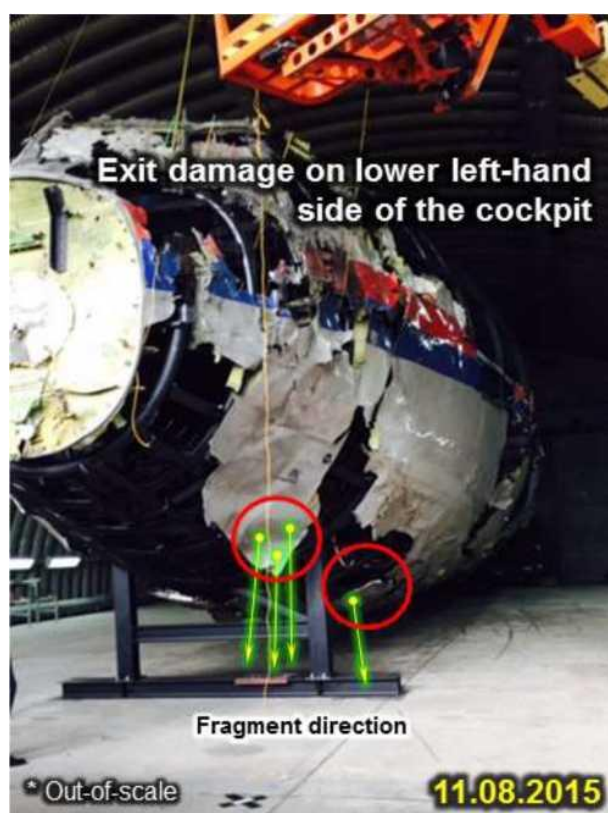


Figure 5.1.50 - Location of exit "inside-out" holes in the lower port side of the Boeing 777

At the same time, there is "inside-out" exit damage (holes and non-penetrating damage) in the cockpit fragments of the Boeing 777. It is, however, located not in the right, but in the left lower part of the fuselage. Figure 5.1.50 shows schematically the location of the main exit holes and the inside-out non-penetrating damage on the left side of the Boeing 777. The highest density exit damage is concentrated below the second left window and distributed further along the port side.

The available DSB's technical investigation materials (TNO and NLR materials) do not mention the presence of "inside-out" exit damage in the lower part **of the left side of** Boeing 777. Neither the Reports nor their annexes contain descriptions or photos of the exit ("inside-out") damage to the lower left side of Boeing 777. Examples of inside-out exit damage to the port side are shown in Figures 5.1.51 and 5.1.52.

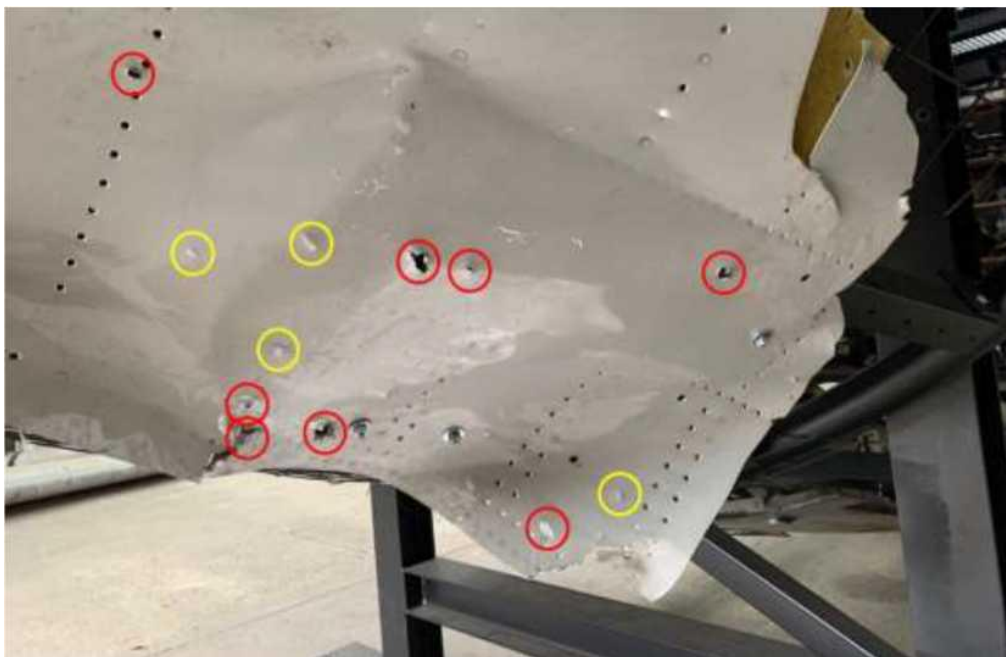


Figure 5.1.51 - "inside-out" exit damage in the lower port side of the Boeing 777 under the windows of the crew commander

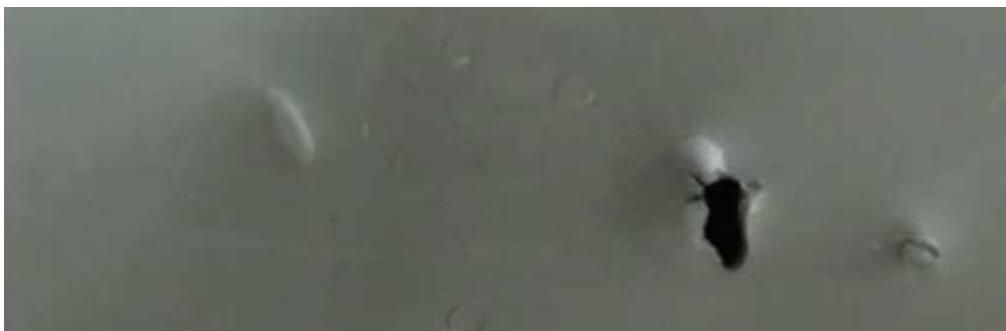


Figure 5.1.52 - Close-up of inside-out exit damage: non-penetrating damage (left) and through-and-through hole damage (right)

The location of "inside-out" exit holes and the direction of their distribution along the lower part of the port side is consistent with the location of areas with maximum density of fragmentation damage to the outer skin, structure and cockpit floor.

This indicates that the fragments with exit holes in the lower part of the port side were in the area of maximum density fragmentation flux.

5.1.2.7. Damage to the left engine and left wing plane

Preliminary layout inspections (February 2015 and May 2015) established that damage (mostly holes) that was identified as damage caused by "high-speed objects", was present in fragments of the left wing plane (Figure 5.1.53).



Figure 5.1.53 - Exterior view of fragment of Boeing 777 left wing tip with characteristic damage

Approximately similar damage, but slightly larger and less densely located, is found in the left engine air intake edge (Figure 5.1.54).



Figure 5.1.54 - Left engine air intake edge

Analysis of the nose of the left engine air intake showed that the left engine sustained combined damage: from the main fragmentation stream including ready (primary) damage, from fragments of the aeroplane structure collapsing in the air, and from falling to the ground.

Some of the damage is large in size (significantly larger than the linear dimensions of preformed fragments) and was probably caused by the aircraft structural failure. An example is the damage to the air intake, around which blue paint smears were clearly observed in the crash area.

The presence of blue-coloured smears indicates that this damage was most likely the result of a collision with a fragment of a destroyed aircraft structure (e.g. the outer skin of the port side of the aircraft is blue).



Figure 5.1.55 - Example of secondary damage to the left engine air intake edge

The left engine fragment, however, shows damage caused by the main fragmentation field, which was recognised by Dutch experts from TNO (Figure 5.1.55).

Damage to the left engine from the main fragmentation flux (preformed fragments) was even included in the six main conditions, the simultaneous matching of which was to show the greatest consistency with one or the other version in the work of the DSB experts.³³

In this connection, the most important of the fragmentation damage to the left engine are the exit through-and-through holes with linear dimensions of about 14 mm located in the structural elements behind the edge of the left engine air intake (Figure 5.1.56).

³³ TNO report. Damage reconstruction due to impact of high-energy particles on Malaysia Airlines flight MH17, Damage matching condition (6), p. 18/25.

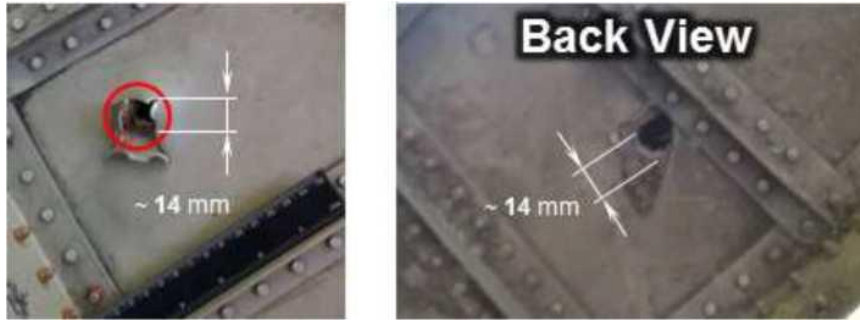


Figure 5.1.56 - Exit through-and-through "inside-out" holes in the left engine air intake edge (rear view).

The linear size of the holes is about 14 mm

It is also important that these exit holes correlate with the corresponding entry holes in the outer skin of the air intake. Figure 5.1.57 shows: the entry hole in the air intake edge (left) and the 'inside-out' exit hole in the structural element behind the air intake edge. To demonstrate their mutual relationship, the hole is illuminated by a flashlight from behind.



Figure 5.1.57 - Exit "inside-out" through-and-through hole in the structural element of the left engine air intake edge (right). The linear size of the exit hole is about 14 mm

As the test results have shown, only prefabricated projectiles can penetrate an aircraft structure (go through several successive combined barriers) and exit from the back side.³⁴

In such case, the entry hole shown in Figure 5.1.57 (left) is larger than the original dimensions of the preformed fragments. However, this is not a reason to attribute this damage to the impact of large missile body fragments, as was done in the DSB materials.

The attribution of this hole to battle damage caused by ready-made projectile is based on the results of experimental data from static and dynamic tests carried out by Corporation's specialists.

³⁴ PART 2. Exhibit B.3, pages 64-68.

For example, similar results were obtained by Russian specialists. Figure 5.1.58 shows a comparison of the appearance of "large" holes on the edge of the left engine air intake (in the middle) and holes in targets resulting from tests and experiments carried out in 2015 and 2016.³⁵



Figure 5.1.58 - "Large" holes caused by preformed fragments: left - from tests involving a 9H314M warhead; middle - on a Boeing 777 air intake; right - from special experimental studies assessing the penetrating effect of preformed fragments



Figure 5.1.59 - Fragment of composite body of left engine nacelle (presumably) with traces of fragmentation damage

³⁵ The large size of the hole is due to the dynamic nature of the event, variations in the velocity of the projectiles and the unknown level of deformation of the elastic parts of the outer skin (of the target).

Further confirmation that the left wing plane and the left engine of the aircraft were in the main fragmentation field can be seen in the photograph of a fragment of the composite body of the left engine nacelle shown in Figure 5.1.59.³⁶

The number, nature and shape of the holes taking into account their density and distance from the missile's detonation point suggest that the left wing plane and the left engine were in the main (primary) fragmentation field.

Accordingly, damage to the left wing plane and the left engine must be taken into consideration as one of the criteria using which the correlation between modelled and actual damage is determined.

³⁶ The fragment was not presented in the preliminary and final layout of the Boeing 777 aircraft.

5.1.2.8 Direction of damage

Using photographic images of the exterior skin and airframe fragments, construction drawings and digital models of the Boeing 777 aircraft, the trajectories of some of the projectiles were reconstructed.

Figure 5.1.60 presents a generalised diagram showing the main directions of damage reconstructed using studies of the damage to the outer skin and the airframe of the Boeing 777 airliner.³⁷

Similar directions are obtained from studies of damage to the cockpit floor and elements of the interior.

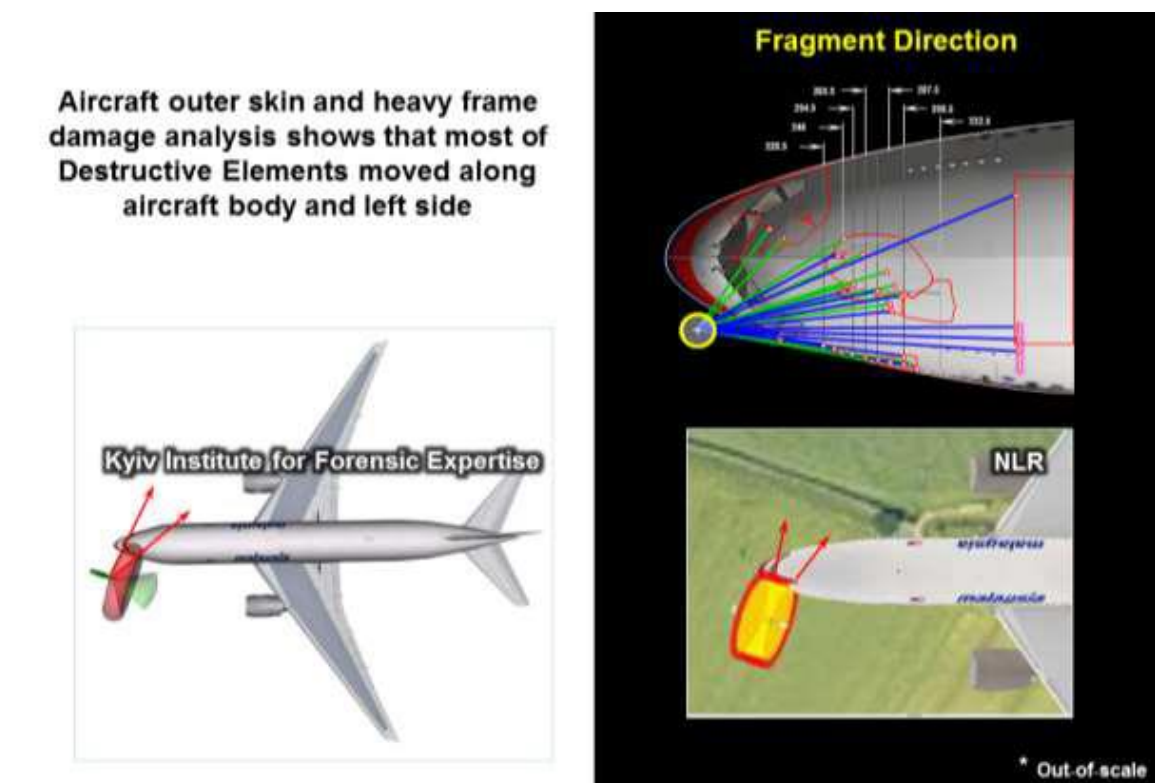


Figure 5.1.60 - Direction of fragment movement along the aircraft structure: the direction of damage to the outer skin is shown by green lines and the direction of the aircraft structural frame damage (through-and-through holes in the bulkheads) is shown by blue lines

As an example, Figure 5.1.61 shows the possible reconstructed trajectories of part of the projectiles for important fragments with a high density of fragmentation damage, which, however, are not present in the final 3D reconstruction.

³⁷ The red arrows at the bottom of the illustration show the direction of travel of the projectiles that corresponds to the results of the modelling by NLR (bottom right) and the Kyiv Institute for Forensic Expertise (bottom left).

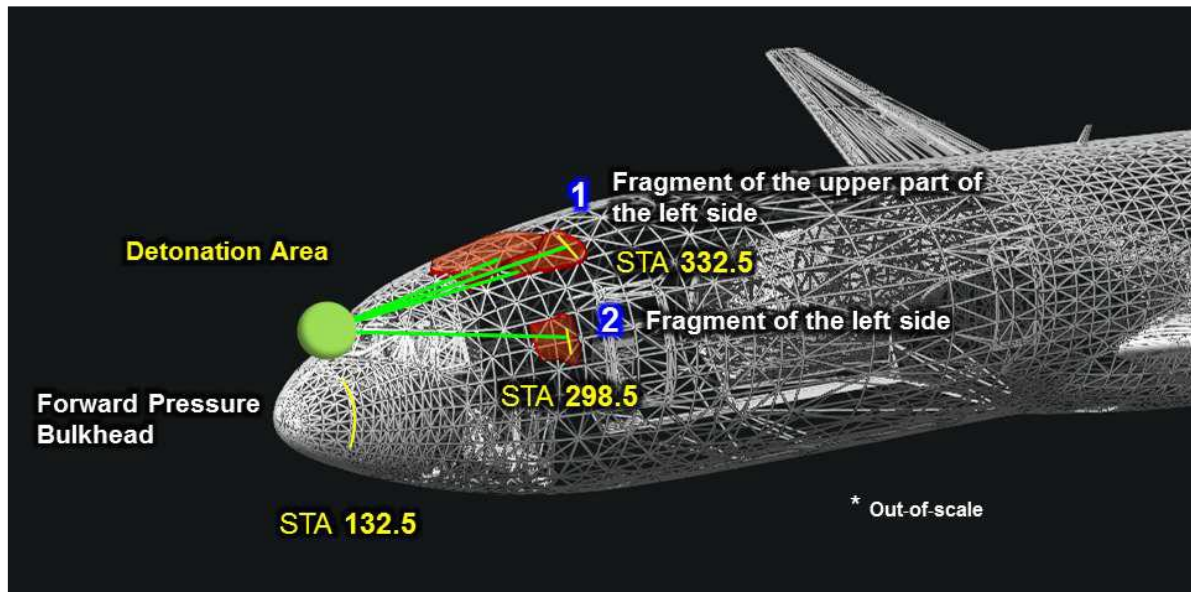


Figure 5.1.61 - Trajectories of projectiles along the aircraft structure as exemplified by two fragments at STA 298.5 and STA 332.5, where:
 1 is a fragment of upper port side (not included in 3D reconstruction);
 2 is a fragment of the port side (was not exported to the Netherlands)

During the technical investigation, the Dutch experts claimed that they did not see any damage beyond the STA 220.5 bulkhead just behind the cockpit windows.^{38, 39}

This approach ("opposite direction" version) implies that the main direction of the flow of projectiles across the aircraft structure was at angles of 40-45 degrees to the longitudinal axis of the aircraft as was demonstrated by Ukrainian and Dutch experts during the stages of joint work at Gilze-Rijen Air Base in February, May and August 2015.^{40, 41}

However, an analysis of the total damage to the outer skin and the airframe taking into account the fragments missing from the final reconstruction shows a different picture.

The main fragmentation flow spread along the port side and left side of the aircraft roof at a slight angle to the Boeing 777's structural axis.

³⁸ Final Report, p.121.

³⁹ TNO report, p.7.

⁴⁰ NLR materials. Presentatie Annex 13 - HEO_Amended. Fragment Spray Pattern Simulation, p. 60-61.

⁴¹ Results of examination of causes of MH17 crash over the territory of Ukraine 17.07.2014. 10-12.08.2015, Gilze.

5.1.2.9. Model of fragmentation damage to Boeing 777 aircraft

Based on a comprehensive analysis of the damage to the outer skin of the Boeing 777, the boundaries of the fragmentation field were determined.

Taking into account the boundaries of the fragmentation field affecting the forward part of the aircraft which were determined from fragments of the cockpit, port and starboard side, cockpit roof and behind the cockpit, and elements of the left wing plane and left engine, a model of damage to the outer skin of the Boeing 777 (fragmentation field) was constructed and is shown in Figure 5.1.62.

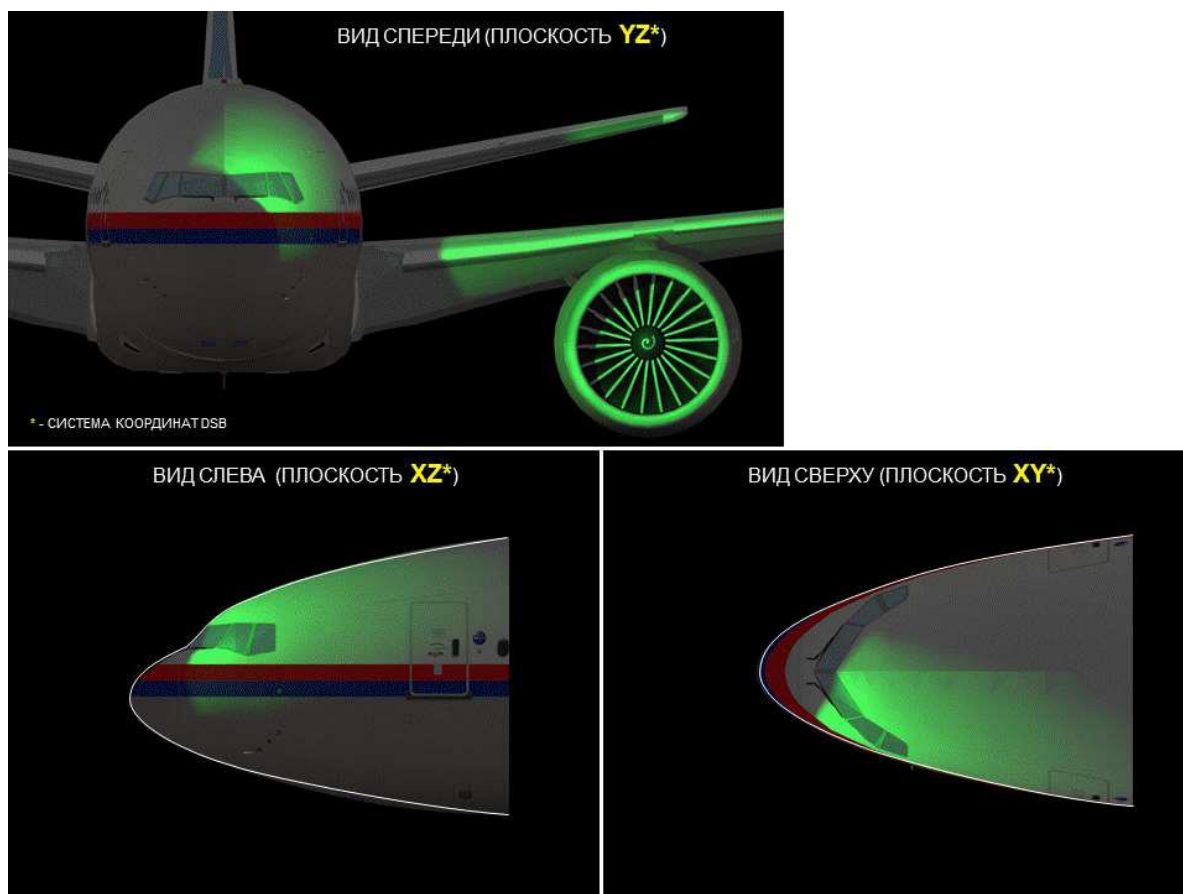


Figure 5.1.62 Fragmentation field model for the forward part of the fuselage, left wing plane and left engine of a Boeing 777 aircraft

As a result of a comprehensive examination of the combat damage to the forward part of the Boeing 777 fuselage:

A count of entry through-and-through holes and part-through holes (ricochets) in the available fragments was carried out. The fragmentation damage model accounted for about 350 entry holes in the fragments presented in the final layout.⁴² Of these, 230 (over 65%) were actually measured during inspections at Gilze-Rijen Air Base;

⁴² In addition, about 70 more holes were accounted for in fragments of the nose section of the Boeing 777 fuselage that are not represented in the final 3D rendering: fragments of the cockpit roof, the upper and middle portions of the port side.

the location of the outer hull fragments with areas of **maximum** fragmentation damage **density** was determined;

the location of **the area of the airframe destruction** was determined and about 60 through-and-through holes in the bulkheads were recorded, the position of which can be determined with a high degree of accuracy;

the "inside-out" exit holes were located and counted and the direction of their distribution **along the lower part of the port side** determined.

The result is a model of the fragmentation impact on the forward part of a Boeing 777 aircraft.

Figure 5.1.63 shows a visualisation of the fragmentation damage density distribution and areas of damage to the airframe elements as well as areas of "inside-out" exit holes caused by fragments.

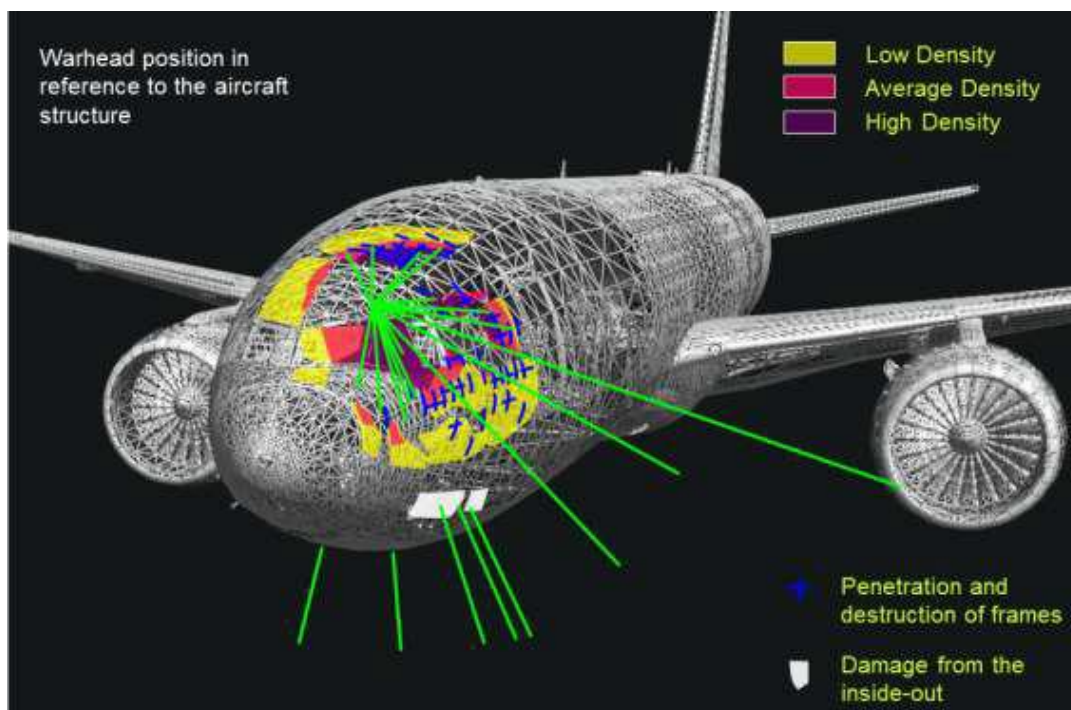


Figure 5.1.63 - Fragmentation damage density distribution coincides with the areas and directions of perforation and fracture of the Boeing 777 structural elements (along the port side and left side of the aircraft roof at a slight angle to the aircraft's structural axis)

Analysis of the location, distribution and direction of fragmentation damage shows that high density fragmentation impacted the front windows on the left side, along the top left side of the roof and further along the port side.

The main features of fragmentation damage (through-and-through holes and part-through holes) to the outer skin, airframe, floor and interior of the cockpit are:
 a clearly marked forward boundary of the coverage field - the damage starts from the forward pressure bulkhead STA 132.5;

on the starboard side of the pilot's roof the damage is recorded up to the level of bulkhead STA 265.5, while on the left side of the roof it is spread beyond the level of bulkhead STA 309.5, and in the upper part of the port side the damage to the outer skin is spread beyond the level of bulkhead STA 332.5;

damage to the airframe extends beyond visible damage to the outer skin;

the most damage is spread along the left side of the aircraft fuselage at a slight angle to the centreline (CLA).

5.1.3 Blast damage to the Boeing 777

It follows from the theory of anti-aircraft missile firing that an airborne target can be annihilated by destroying its structure with the high-explosive effects of the missile's warhead. The effective high-explosive radius of the warhead is relatively small and depends primarily on the mass⁴³ of the explosive and blast height.

The weight of the 9N314 and 9N314M warheads of BUK missiles is about 70 kg, including a mass of explosive material of $\sim 33.5^{+0.8} -0.4$ kg. The explosive substance (TG-24) is a mixture of TNT and hexogen.

Experiments have shown that, for conditions near the surface, the impact radius of a BUK warhead is about 5 metres, and for an altitude of 10,000 metres (33,000 ft) it is about 3.5 metres.

The DSB report only devotes about one page (on pages 124 and 125 of the Final Report) to the issue of blast impact.

However, in addition to the damage caused by projectiles, the structure of the Boeing 777 objectively shows damage from the effects of a nearby explosion.

Multiple traces of such effects are evident in the presence of microcrater areas, thermal effects (oxidation), compression of sheeting between the structural elements, deformation and tearing of outer sheeting, separation of sheeting from the structural elements, and deformation, tearing and destruction of the aircraft load-bearing structure elements.

On the surface of the outer skin of the Boeing 777-200 (MH17), a cratering effect is observed in the area of some relatively large breaches. A rash of microcraters is damage caused by high velocity "dust" (particles of unburned explosive material, small particles of warhead structure and projectiles) accompanying the blast wave at a short distance from the blast site.

Figures 5.1.64 and 5.1.65 show examples of fragments with the highest number of microcraters.

⁴³ Neupokoev F.K. Anti-Aircraft Missile Firing, pages 199-201.



Figure 5.1.64 - Microcrater areas: right side of cockpit roof (a), forward part with pressure bulkhead (b, c), transparency frame (d)



Figure 5.1.65 - Areas of microcrater formation on the port side

In the front left side of the cockpit, an area of thermal effects of the blast products in the form of thermal oxidation on the aircraft's skin and window frames can also be seen.

The features of the thermal impact and compression of the bulkheads observed in a fragment of the port side skin of the aircraft below the transparency bezel of the cockpit commander are shown in Figure 5.1.66.

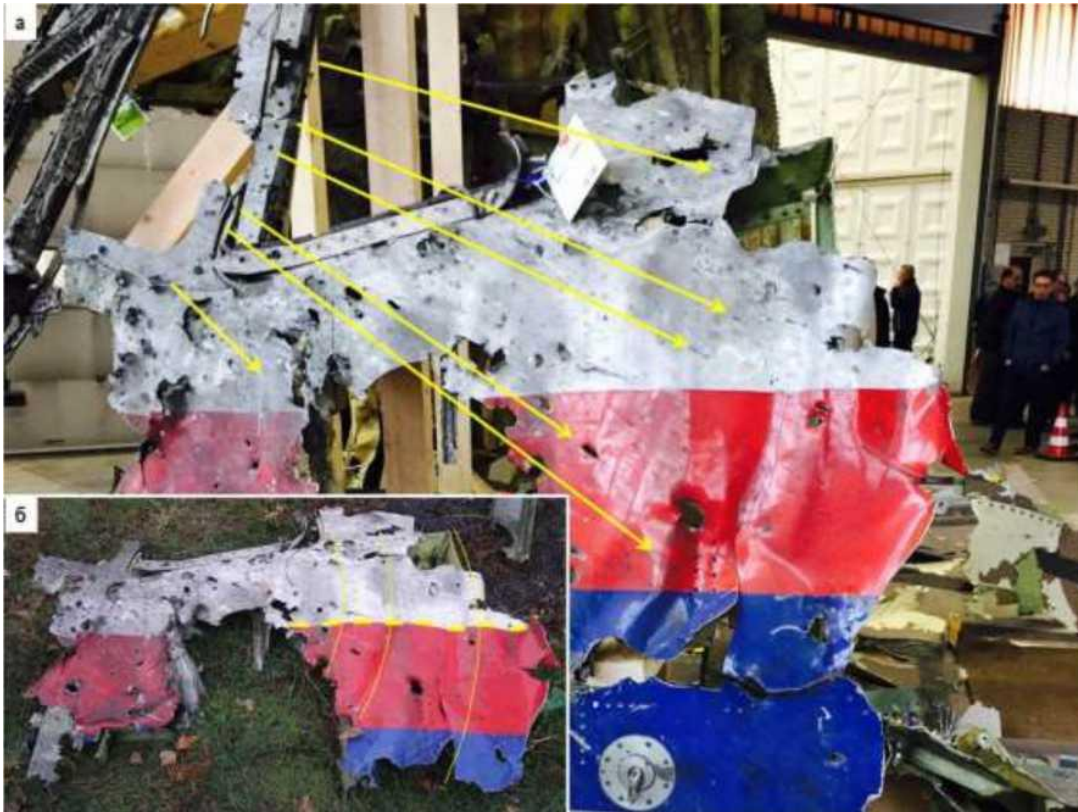


Figure 5.1.66 - Thermal stress and compression marks on bulkheads

In Figure 5.1.66(a), the yellow arrows indicate the direction of impact of the hot blast products, which resulted in oxidation of the paintwork and sooting of the skin on the port side of the aircraft. The significant divergence of the arrows over a relatively small area indicates that the fragment was no more than 2.0-2.5 m from the point of detonation.

The following types of short-range blast damage can also be observed on fragments of the nose section of the fuselage:

- compression of the sheathing sheets between the load-bearing members (bulkheads) without tearing the sheathing and without bending the frames and stiffeners;

- deformation of framing members (bulkheads and stringers);

- tearing of outer skin sheets from the load-bearing members (rivet tearing);

- breaking of skin sheets and destruction of load-bearing members.

An example of compression of the sheeting between the structural elements can be seen in figure 5.1.66(b). 5.1.66(b) which shows wavy compression of the skin around the STA 212.5-STA 228.5 bulkheads (yellow dashed line). At the same time, the deformation line of the outer skin on the port side of the aircraft is contrasted by traces of thermal oxidation, lying in waves (dark stripes) with maximums in the area of the bulkheads.

Another example of this damage to the aircraft structure is the part of the roof behind the cockpit shown in Figure 5.1.67.



Figure 5.1.67 - Impact of blast on roof fragment above cockpit

The wave deformation in the area of the five bulkheads of STA 236.5-STA 276.5 (shown in Fig. 5.1.67(b) with yellow dashed line) is also contrasted by traces of thermal oxidation of the outer skin, laying in waves with maximums in the area of the bulkheads.

You can also see in this picture numerous rivet holes caused by the outer skin tearing away from the airframe.

In addition to the damage listed above, the fuselage of the Boeing 777 contains other damage characteristic of a close explosion.

The main ones are: breaking and deformation of the outer skin sheets, tearing of the skin sheets from the load-bearing elements, destruction and deformation of the load-bearing elements of the airframe (Figure 5.1.68).



Figure 5.1.68 - Destruction and deformation of the aircraft nose structure

Examples of destruction and deformation of the outer skin sheets and structural members of the nose section of the aircraft are shown in Figures 5.1.68 and 5.1.70.

Thus, a fragment of the port sidewall skin with the angle-of-attack sensor, shown in Figure 5.1.69, shows all the main signs of damage typical of a close explosion (highlighted in red) - breaking and deformation of the skin sheets, destruction of the structural elements (bulkheads), and tearing of the skin sheets from the stringers and bulkheads.

Figure 5.1.70 shows examples of blast damage to the transparency frame (a), roof fragments (b) and (c) and the port side behind the cockpit transparency (d).



Figure 5.1.69 - Blast damage on a fragment with an angle of attack sensor on the outer (a) and inner (b) sides



Figure 5.1.70 - Deformation and destruction of structural elements

Figures 5.1.69 and 5.1.70 show in red the most typical damage, i.e. deformation of the load bearing elements and of the outer sheathing sheets. The airframe was destroyed by perforations (through-and-through holes from preformed fragments) in

the bulkheads.

Deformation and fragmentation of the Boeing 777 structure (outer skin and airframe) spread along the structure, predominantly on the left side (along the port side) – from the transparency towards the vertical stabiliser:

below floor level - up to STA 236.5;

above the floor level in the middle part of the port side - up to bunk STA 287.5;

in the upper part of the port side - up to bunk STA 309.5.

The internal equipment located in the Main Equipment Centre⁴⁴ shows signs of deformation on the port side up to the level of STA 409 (figure 5.1.71).

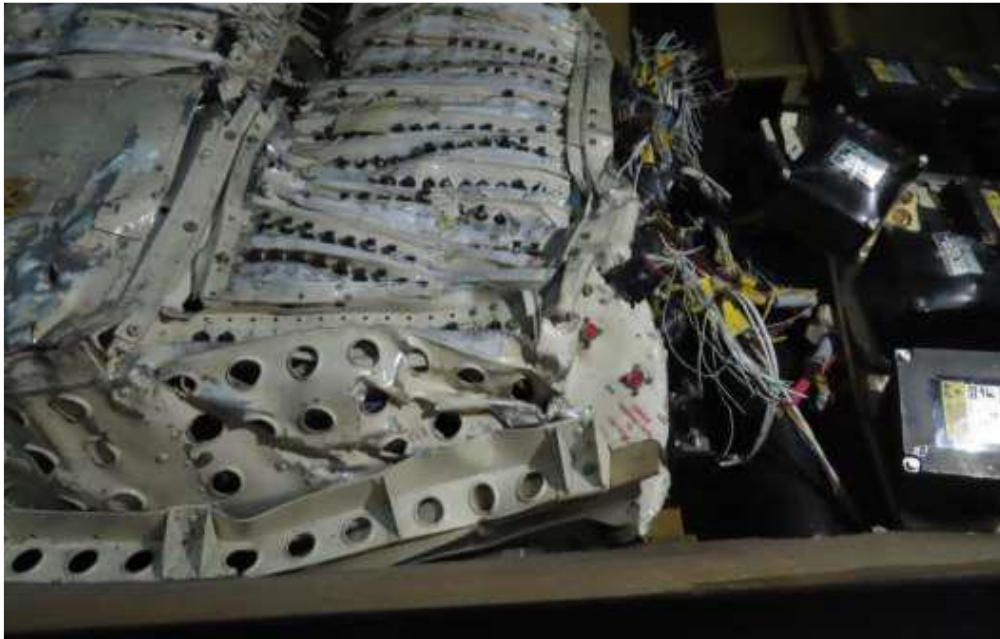


Figure 5.1.71 - Combined damage to avionics along the underside of the port side behind the cockpit (Main Equipment Centre)

Thus, the front left side of the Boeing 777 fuselage shows multiple traces of blast factors as manifested by microcraters, thermal effects, deformation and breaking of the outer skin sheets, separation of the skin from the structural elements, as well as deformation, tearing and destruction of the aircraft's load-bearing structure elements.

Figure 5.1.72 shows the area of damage caused by various blast factors: formation of microcraters, thermal effects and hot detonation product (HDP) tracks.

⁴⁴ Boeing 777-200/300 Aircraft Maintenance Manual, page 202.

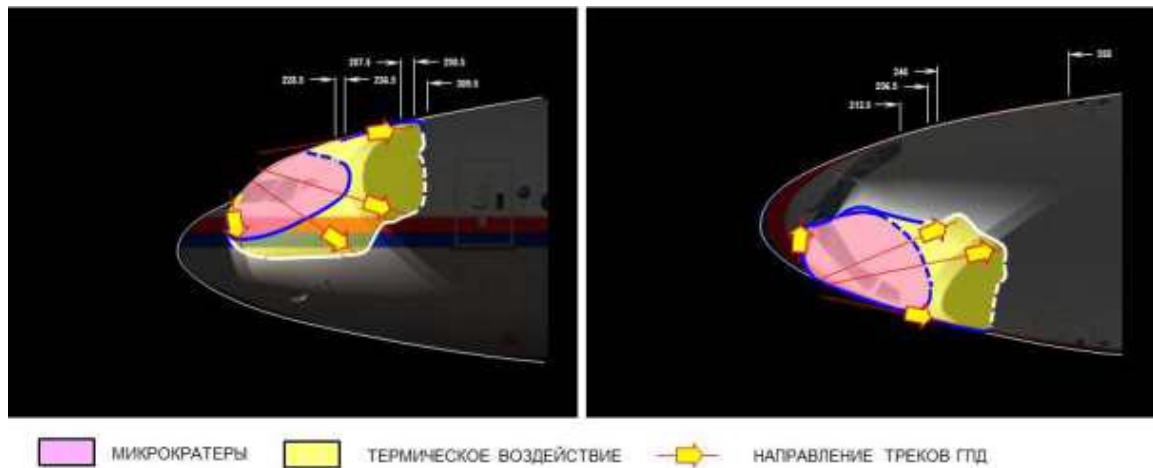


Figure 5.1.72 - Areas of the aircraft structure where traces of blast effects are observed

The amount, intensity and direction of spread of damage directly caused by blast factors suggest that the epicentre of the explosion was in the immediate vicinity of the transparency frames (between the windows of the crew commander) at a short distance (not more than 1.6-2.0 m) from the outer skin of the aircraft. A similar damage pattern in terms of intensity and location was obtained in the tests in the first experiment,⁴⁵ described in Exhibit A.4.3 of this report.⁴⁶

The impact of the high-explosive charge from the warhead caused significant deformation and fragmentation of the left side of the Boeing 777 structure.

The outer skin sheets were compressed and deformed and collapsed along the structure, predominantly on the left side (along the port side and left side of the roof) – from the transparency towards the vertical stabiliser.

The epicentre of the explosion was in close proximity to the transparency frames (between the windows of the aircraft commander) at a short distance from the outer skin of the Boeing 777.

⁴⁵ PART 2: Exhibit A.4.3 Comparative analysis of damage due to near blast factors, pages 44-51. 44-51.

⁴⁶ Was conducted under the conditions of an aircraft encountering a missile "on a collision course".

5.1.4 Criteria for comparing modelled and actual damage to Boeing 777

Based on an analysis of the combat damage features of the Boeing 777, the most significant were selected to act as criteria.

In order to obtain the best match when comparing modelled and actual damage, it is necessary to obtain the greatest match on a number of criteria.

These primarily include:

1. Conformity of the fragmentation coverage area boundaries.
2. No fragmentation damage to the forward pressure bulkhead.
3. Distribution of the impact density over the external surface of the aircraft (polygonal objects making up the digital model of the Boeing 777). It is imperative that the area of damage from preformed fragments is taken into account separately.
4. Consistency of the direction of impact of damage given the location of the detonation area (in particular the direction of ricochets).
5. Consistency in the nature of airframe damage from dense fragmentation flow.
6. Coincidence of areas of successive penetration of two or more structural barriers - external skin, load-bearing frame elements (floor etc.) and "inside-out" exit damage.
7. Consistency in the nature of the blast damage.
8. Damage to the left wing plane and left engine by the main fragmentation field - finished (primary) damage.

All or most of the listed conditions must be met at the same time for the greatest compliance.

The comparison should take into account objective markers (numerical indicators), the matching or maximum matching of which could be a certain criterion for compliance with an item in the list.

5.2 Identifying conditions under which damage was done to Boeing 777

To calculate the likely launch area, it is most important to determine the relative position in space of the aircraft and missile (angles between their axes), as well as the final velocity of the missile at the time of detonation.

The determination of the aircraft-missile encounter conditions is based on the best fit of the combination of three components: aircraft damage, the dynamic explosion model of the warhead (warhead characteristics) and the detonation point connecting them.

5.2.1 Determining the detonation point

The optimal solution for determining the detonation point area is based on a geometric analysis of the impact marks observed on the detected aircraft nose debris at the boundaries of the cover field.

Battle damage near the boundary of the cover field is an elongated, clearly oriented rectilinear track, formed by the contact between the outer skin sheets and the projectiles, whose trajectories were oriented tangentially to the outer contour of the fuselage at this point (Figure 5.2.1).



Figure 5.2.1 - Example of characteristic damage near the boundary of the overlapping field on the right side of the cockpit roof

These rectilinear tangential traces are, in fact, preserved and visible portions of the trajectories of the projectiles, allowing the position of these trajectories in three-dimensional space in a given coordinate system to be determined with sufficient accuracy.

Given the orientation of the tangential damage, the guide cosines of the trajectories were determined, from which, in combination with the measured damage coordinates, the position of the trajectories in space.⁴⁷

⁴⁷ In determining the position of the trajectories in space, the characteristics of the penetration capability of the GLE – the values of the range of angles at which the ricochet of the projectiles is possible (track formation) - were taken into account.

In turn, the coordinates of the intersection (crossing) points of the thus reconstructed trajectories of the projectiles in space allow the position of the detonation point to be estimated.⁴⁸

As a result of trajectory crossing calculations based on data from the Boeing 777 structure damage survey, it was determined that the point of detonation of the warhead was in the area bounded by the coordinates:⁴⁹

X (range), m	0.4... 1,0
Y (parameter), m	-1.9.-1.2
Z (height), m1,6. 1,9

The position of the detonation point in the Corporation's version has not changed significantly since May 2015. This can be easily seen, for example, in the Corporation's first press conference.⁵⁰

After calculations and modelling, the correspondence between the detonation point and the main marker points of the left side, the roof behind the cockpit and the right side of the cockpit roof were verified using a laser pointer on a Boeing 777 aircraft similar to MH17.

In addition, the validity of the resulting calculations was demonstrated directly at a 3D-reconstruction of the aircraft in August 2015 in a hangar at Gilze-Rijen Air Base.⁵¹



Figure 5.2.2 - Verification of the location of the detonation point area:
left - on the reference aircraft (Boeing 777-200);
right - on the 3D reconstruction in the hangar (Gilze-Rijen)

Table 5.2.1 shows the results of calculations of the detonation point position performed by specialists of Almaz-Antey Corporation, CNII Air Force, DSB⁵² and Kyiv Institute for Forensic Expertise.⁵³

⁴⁸ Given the linear dimensions of the warhead, which are comparable to the minimum detonation distance from the outer skin of a Boeing 777 aircraft.

⁴⁹ The coordinate system from the Draft DSB Final Report was used.

⁵⁰ The first Almaz-Antey press conference was held in June 2015.

⁵¹ Clearly demonstrating the inconsistency of the "Best Match" version used by the Dutch in the final DSB Report.

⁵² Final Report, Table 19, page 140; Table 20, page 142.

⁵³ Final Report, page 20, page 142.

Table 5.2.1 - Detonation point location coordinates

Organisation	X, m	Y, m	Z, m
"Almaz-Antey"	$0,4 < X < 1,0$	$-1,9 < Y < -1,2$	$1,6 < Z < 1,9$
CENTRAL RESEARCH INSTITUTE OF THE AIR FORCE	$0,8 < X < 1,3$	$-1,9 < Y < -1,5$	$1,6 < Z < 1,9$
DSB (Final Report)	$-0,7 < X < 0,5$	$-2,0 < Y < -3,5$	$3,4 < Z < 4,0$
Kyiv Institute for Forensic Expertise	0,0	-4,0	4,0
NLR (Draft Final Report) ⁵⁴	-0,5	-4,0	4,0
NLR (Final Report) ⁵⁵	-0,25	-3,0	3,7

The results of calculating the detonation point area, obtained using generally accepted methods involving trace studies based on objectively observed damage at the boundaries of the cover field, give similar results.

The volume containing the coordinates of all solution options for the detonation point area is less than 1 m³. It can be considered reliable due to the fact that it has been confirmed by various independent sources and methods, and verified. The distance to the nearest point on the cockpit was about 1.6 m.

5.2.2 Warhead detonation model

As input data for the static and dynamic detonation model of the 9H314M warhead, materials from the technical documentation for the 9H314M warheads and the results of their tests carried out between 1980 and 1991 were used.⁵⁶

The main technical characteristics of the warhead and their validation results are given in Exhibit B, and a description of the static and dynamic detonation models of the 9H314M warhead is given in Exhibit D.⁵⁷

⁵⁴ Draft Final Report. Table 15, p.130.

⁵⁵ Final Report, page 20, page 142.

⁵⁶ Warhead 9H314M. Technical specifications, 9H314M TU, 1980; Technical report No. 5-514 on verification tests by explosion at ground stationary conditions, 1980; Munitions 9H314M. Surveillance tests on verification of kill field parameters, 1981; Combat part 9H314M. Final report on testing of 9H314M ammunition with a shaped impactor, 1981; Reports on the results of control and periodic tests, 1990-1991.

⁵⁷ PART 2: Exhibit B, pages 52-88; Exhibit D, pages 94-105.

Fragmentation field of an anti-aircraft guided missile BUK

The fragmentation field produced by a missile assembly detonation has a number of features, the main ones being a significant increase in the number of fragments and an increase in their meridional angle of dispersion.^{58, 59}

Even if the warhead alone is detonated (without the missile bodies), in addition to the prefabricated projectiles, the field of effect is also formed by the detonation products. The 9H314M warhead weighs about 70 kilograms. If one subtracts the mass of prefabricated projectiles (~28.7 kg) and explosive charge (~33.5 kg) from the total mass of the warhead, then several kg would remain (cap, bottom, cap and other warhead shell elements) that create additional factors and have a noticeable impact on the engagement field. An even greater impact is caused by the missile's compartments close to the warhead.⁶⁰

As an example (Figure 5.2.3), an exterior view of a fragment of a target layout (witness sheet) containing three types of penetrations: prefabricated projectiles (PEAs), hull projectiles (fragments of compartment bodies which may not have the same dimensions as the PEAs) and detonation products (1-3 mm holes) are shown.



Figure 5.2.3 - General view of fragment 2.1 of target No. 2

⁵⁸ Report on the conduct of a full-scale experiment, pages 61, 74, 130.

⁵⁹ PART 2: Exhibit B.2.2, pages 57-60; Exhibit D, pages 94-105.

⁶⁰ Report on the conduct of a full-scale experiment, Exhibit A, pages 26-27; 112-113.

All types of through-hole are clearly visible in the close-up view of this fragment shown in Figure 5.2.4.

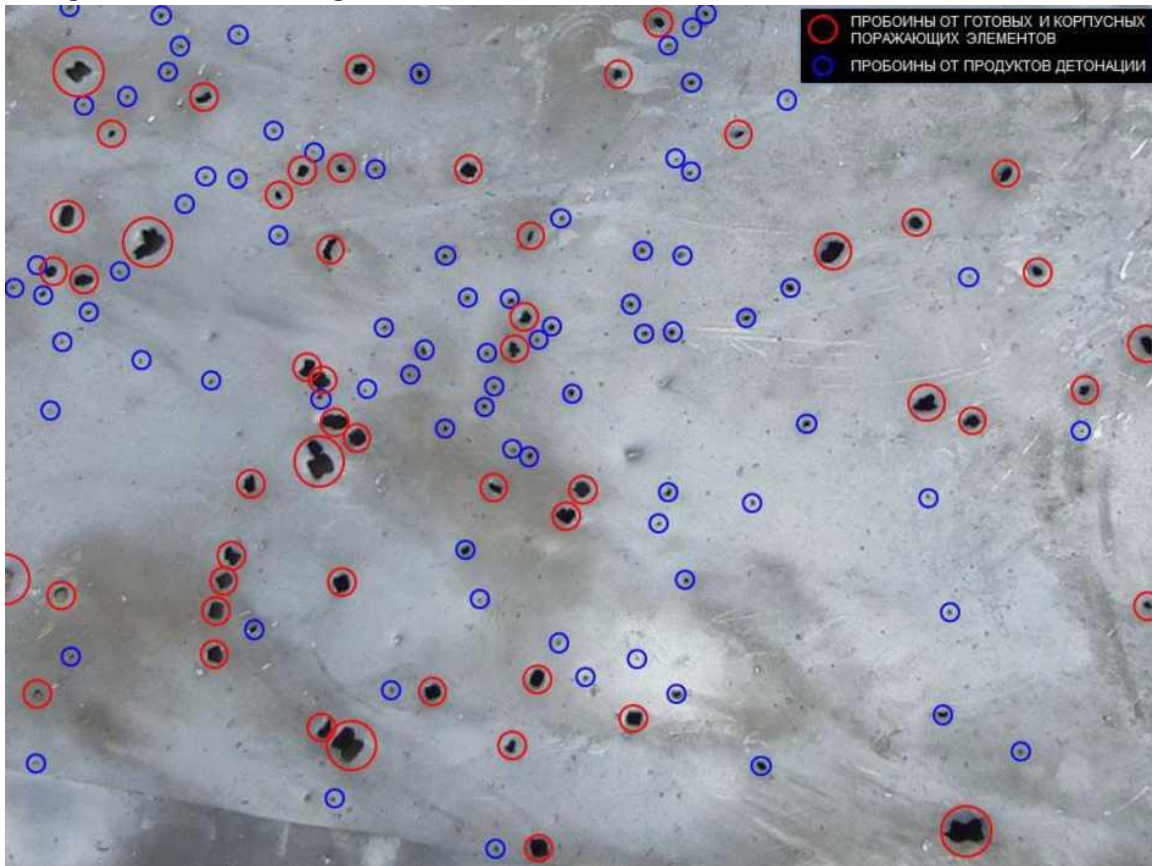


Figure 5.2.4 - Close-up of Fragment 2.1 of Target No. 2.

Entry holes vary in configuration from an elongated compact shape to a distinctive "butterfly" shaped hole for off-the-shelf projectiles and hull fragments, and small holes (1-3 mm) from detonation products

A similar pattern of damage was obtained in the second experiment with the IL-86 target aircraft, where a missile assembly was detonated. Figure 5.2.5 shows a photograph of a fragment of the target aircraft ("FR 2") with all three types of penetrations, including the distinctive butterfly-shaped penetration.

The damage characteristics of the 9H314M type 1-10 (I-beam, Bow-tie) are described in more detail in subsection 6.1 and paragraph 6.2.2 of Field Experiment Report (2016).⁶¹

⁶¹ Report on the conduct of a full-scale experiment, pages 131-141; 143-148.



Figure 5.2.5 - Close-up of fragment "FR 2" of target GB-86

Schematic representation of the fragmentation field in the meridional of the plane after the detonation of an assembled missile is depicted at figure 5.2.6.

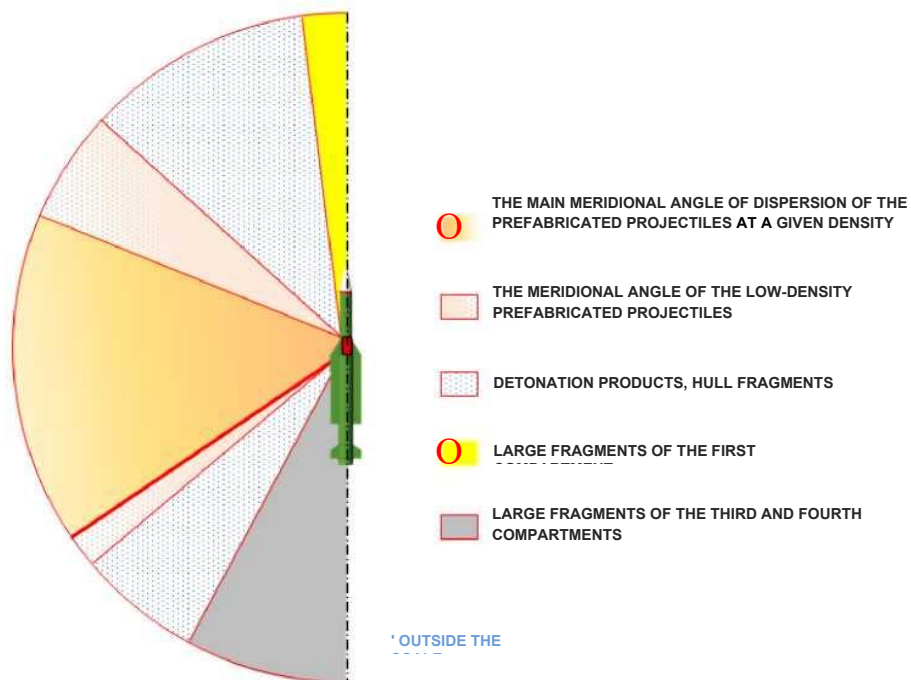


Figure 5.2.6 - Static fragmentation field in the meridional plane

That is, under static conditions, the fragments (prefabricated and hull-shaped projectiles) after detonation propagate in the meridional plane in virtually all directions, as confirmed by field experiments and tests conducted by the Corporation.

In doing so, a few of the most important parameters should be highlighted:

1. The position in space of the area of dense flow of the impacting elements (the area of maximum density of ready impacting elements, the so-called "scalpel") in which more than 42% of the mass of all fragments and more than 50% of the kinetic energy of the fragmentation field of destruction are concentrated. The presence of the "scalpel" and the results of its effects have been confirmed experimentally.⁶² The importance of determining the "scalpel" area is important because traces of its impact are one of the markers for determining the position of the missile relative to the aircraft at the time of detonation.

2. The positions in space of the trailing boundary of the debris field. The importance of defining it lies in the fact that the orientation of the trailing boundary of the debris field determines the forward boundary of the fragment cloud. Accordingly, the correct definition of the fragmentation trailing boundary affects the accuracy of determining the position of the missile relative to the aircraft at the moment of detonation.

"Scalpel"

Confirmation of the maximum density zone of preformed fragments is shown in Figure 5.2.7, where the two areas where the maximum density of preformed fragments is formed are highlighted. The area is highlighted in blue for the GGE light element fraction $\lambda_{L.PE}$ and in red for the heavy element fraction $\lambda_{H.PE}$.

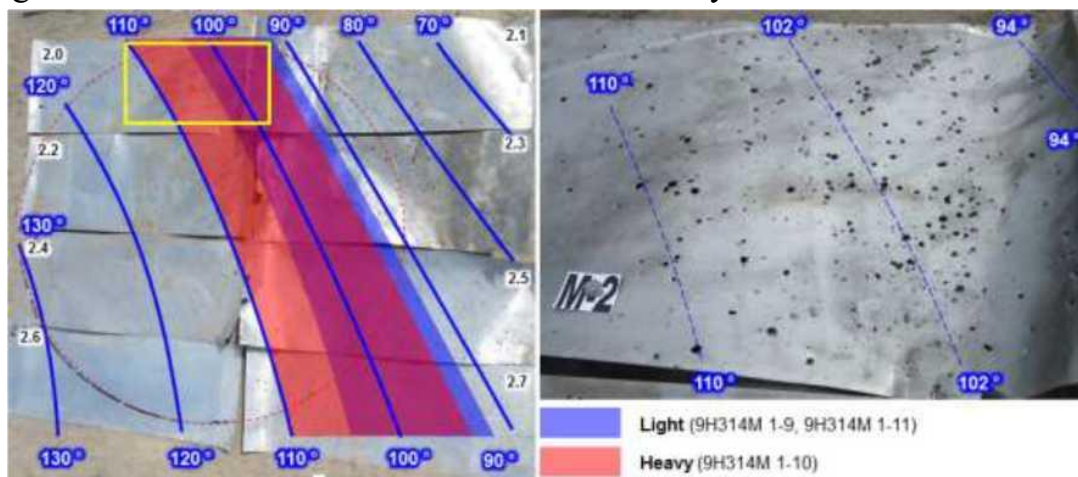


Figure 5.2.7 - Maximum density zones of preformed fragments: blue - Light fraction; red - Heavy fraction

The right-hand side of Figure 5.2.7 shows the maximum impact density zones obtained in full-scale tests using the example of a witness sheet (Shield 2.0 of target M-2).

⁶² PART 2: Exhibit B.3, pages 63-80; Exhibit D, pages 104-105.

In a static position, the maximum density zones of the Light and Heavy projectiles do not coincide completely and are offset in relation to each other. Under dynamic conditions there is a mutual overlap and the formation of a common zone of maximum density of preformed fragments.⁶³

Rear front of the shattering field

The main parameters that characterise the posterior front of the shattering field include:

The design sector for preformed fragments is 68-124 degrees; the low density area for preformed fragments is 48-68 degrees and 124-130 degrees;

Secondary fragment rear front – 150-160 deg.

This is confirmed by the results of full-scale tests - all the data on the parameters of the field of impact of the BUK warheads previously provided to the Netherlands by specialists of the Almaz-Antey Corporation has been confirmed experimentally.

The fragment dispersion model used by specialists of Almaz-Antey Corporation takes into account more than 12,900 fragments – preformed fragments separately heavy (Heavy) and light (Light) fractions as well as shell fragments.

The total number of fragments with sizes corresponding to the GGEs accounted for by the Diamond-Antey programme correlates with the results obtained in field tests.⁶⁴

In calculations and modelling, appropriate corrections are made to convert the static pattern of projectile dispersion (damage patterns, etc.) obtained from static in-situ experiments and laboratory studies into atmospheric specific dynamic models that take into account the position and speed of the missile and aircraft.

The magnitude and direction of the initial velocity of the preformed fragments (shrapnel) when the warhead is detonated under static conditions depends on the type of explosive, the ratio of explosives to fragment mass, the ratio of charge length to radius, and the position of the initiation point. The preformed fragments (and shrapnel) of warheads have a high muzzle velocity and travel a distance to a target (up to 10 metres) in a short time. Therefore, the effect of gravity on the flight of a preformed fragment (shrapnel) can be neglected and the trajectory (at up to 4-6 meters range) can be assumed to be rectilinear.

⁶³ PART 2: Exhibit D, pages 104-105.

⁶⁴ PART 2. Exhibit B.2.2, pages 56-60.

As a preformed fragment (shrapnel) flies in the atmosphere, its velocity decreases due to aerodynamic drag. A faster drop in fragment velocity occurs at low altitudes (near the ground).

The velocity of the projectiles, taking into account atmospheric conditions and reduced air density at 10,000 m (33,000 ft) at a distance corresponding to a verified detonation point (less than 2 m from the cockpit), increases by about 7-8% (for different types of fragments).

In order to hit (penetrate) a target, a fragment must have a certain kinetic energy at the moment of impact with the obstacle. Thus, for example, a fragment can penetrate an obstacle of thickness h if its kinetic energy at the moment of impact is greater than that required to displace the material of the obstacle, i.e. if the condition is met:

$$\frac{m_{se}V_{se}^2}{2} \geq Es sh,$$

where: m_{se} is the mass of one striking element;

V_{se} is the velocity of the striking element;

S is the area of the hole;

Es is the specific displacement energy per unit volume of the barrier material.

Thus, the ability to penetrate combined or successive obstacles is directly related to the velocity of the projectiles, their mass and shape.



Figure 5.2.8 - Comparative linear dimensions and mass of hull fragments (top) and preformed fragments (bottom)

Preformed fragments (Figure 5.2.8 below), which are compact in shape and heavy in weight, have a significantly higher penetration capacity. As confirmed by the results of experiments^{65, 66} sophisticated combined barriers can only be penetrated by preformed fragments.

⁶⁵ Almaz-Antey report on the full-scale experiment.

⁶⁶ PART 2. Exhibit B.3, pp. 64-81.

Dynamic conditions

When firing at an airborne target, the warhead is detonated while the missile is in flight. The velocity vector of the missile is always tangential to its trajectory.⁶⁷ The fragments of the warhead (preformed fragments + body) have a translational velocity equal to that of the missile V_M . When the warhead is detonated, the translational velocity is geometrically added to the intrinsic velocity V_{se} , which is obtained by the fragment from the energy of the warhead.

Since the velocity vector of the missile V_M does not coincide with the longitudinal axis of the missile ox_1 , the values of the flyaway angles are not the same for different cross sections of the dynamic region.

That is, under dynamic conditions, even when only the velocity of the missile is taken into account, the fragmentation field is not symmetric about the longitudinal axis of the missile. The asymmetry of the fragmentation field cross section is even more pronounced if the relative velocity of the projectiles, $V_{PE.OTH}$:

$$\overline{V_{PE.OTH}} = \overline{V_M} + \overline{V_{PE}} - \overline{V_A},$$

where:

$\overline{V_{PE}} - \overline{V_A}$ - the relative velocity vector of the missile

The nature of the fragment dispersion with respect to relative velocity (taking into account the velocities of the preformed fragments, missile and aircraft) is shown in Figure 5.2.9.

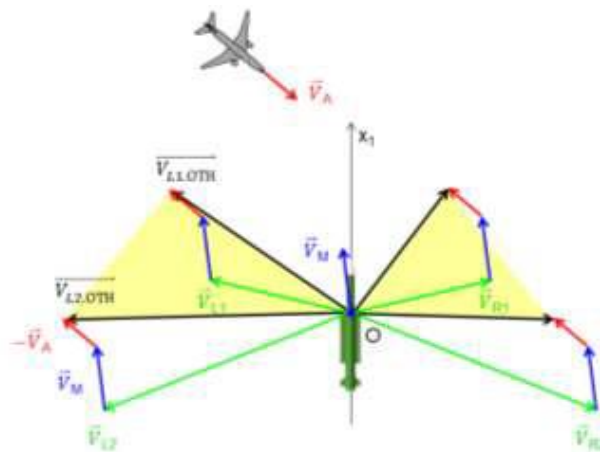


Figure 5.2.9 - Relative velocity of the impactor
(out of scale)

As shown above, the fragmentation field under dynamic conditions is not symmetric about the missile's axis, so a spherical diagram of fragment dispersion obtained by extrapolation by rotation around the missile's longitudinal axis will have significant errors.

⁶⁷ Neupokoev F.K. Anti-Aircraft Missile Firing.

The rear front of the shattering field is the most affected. Figure 5.2.10 shows the simulation results fragmentation field for conditions within the range of DSB conditions: missile velocity $V_M = 600$ m/s, angle between aircraft and missile axes $Az_{warhead} = -30^\circ$.

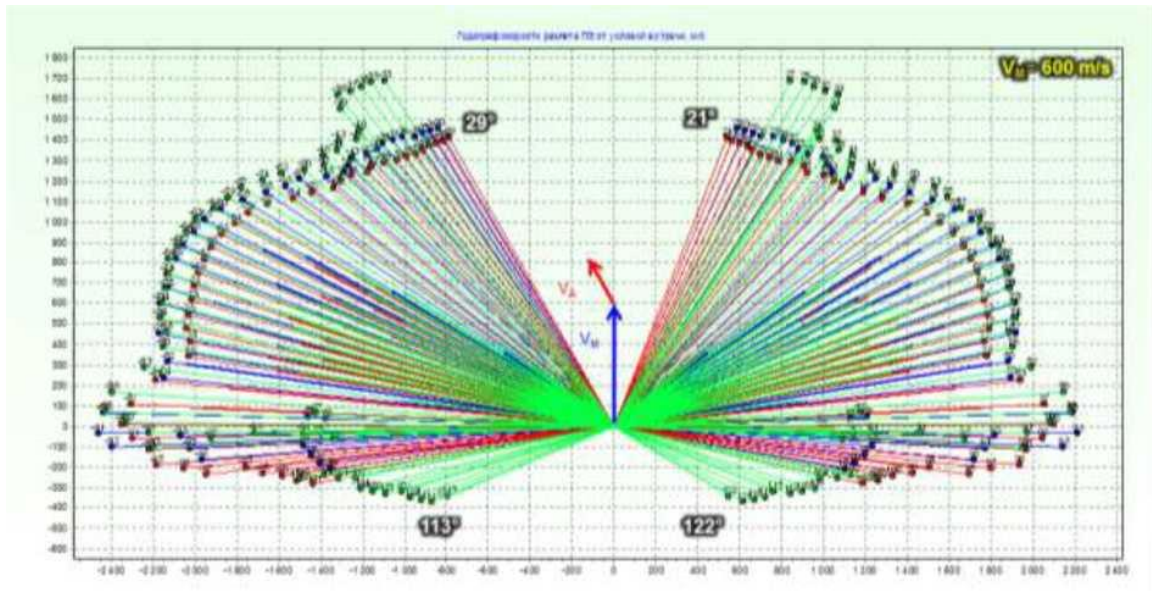


Figure 5.2.10 - Unbalanced cross-section of the fragmentation field in the meridional plane under dynamic conditions

The software used by the Corporation's specialists takes all these features into account and calculates the trajectories of each of the fragments, taking into account the influence of velocity projections in the three planes.

The results of the comparative modelling show that the asymmetry of the fragmentation field (left and right side relative to the longitudinal axis of the missile) depends primarily on the variation of angles between the missile and the aircraft and the final velocity of the missile:

As the angle between the longitudinal axes of the aircraft and the $Az_{warhead}$ missile increases at the moment of detonation, the value of the angle characterising the rear boundary of the fragmentation field increases (up to 3° in an angle range of -30° to -60°);

As the missile's final velocity V_M increases at the moment of detonation, the value of the angle characterizing the fragmentation field back-front also increases (up to 12° with an increase in the missile's final velocity from 600 m/s to 800 m/s).

The maximum differences occur when the angle between the longitudinal axes of the aircraft and rocket $Az_{warhead}$ and the terminal velocity of the rocket V_M are varied simultaneously.

In this case, errors can be as high as 15° or more (Figure 5.2.11), where: for the trailing boundary of the shattered field, the difference is $116^\circ - 101^\circ = 15^\circ$.

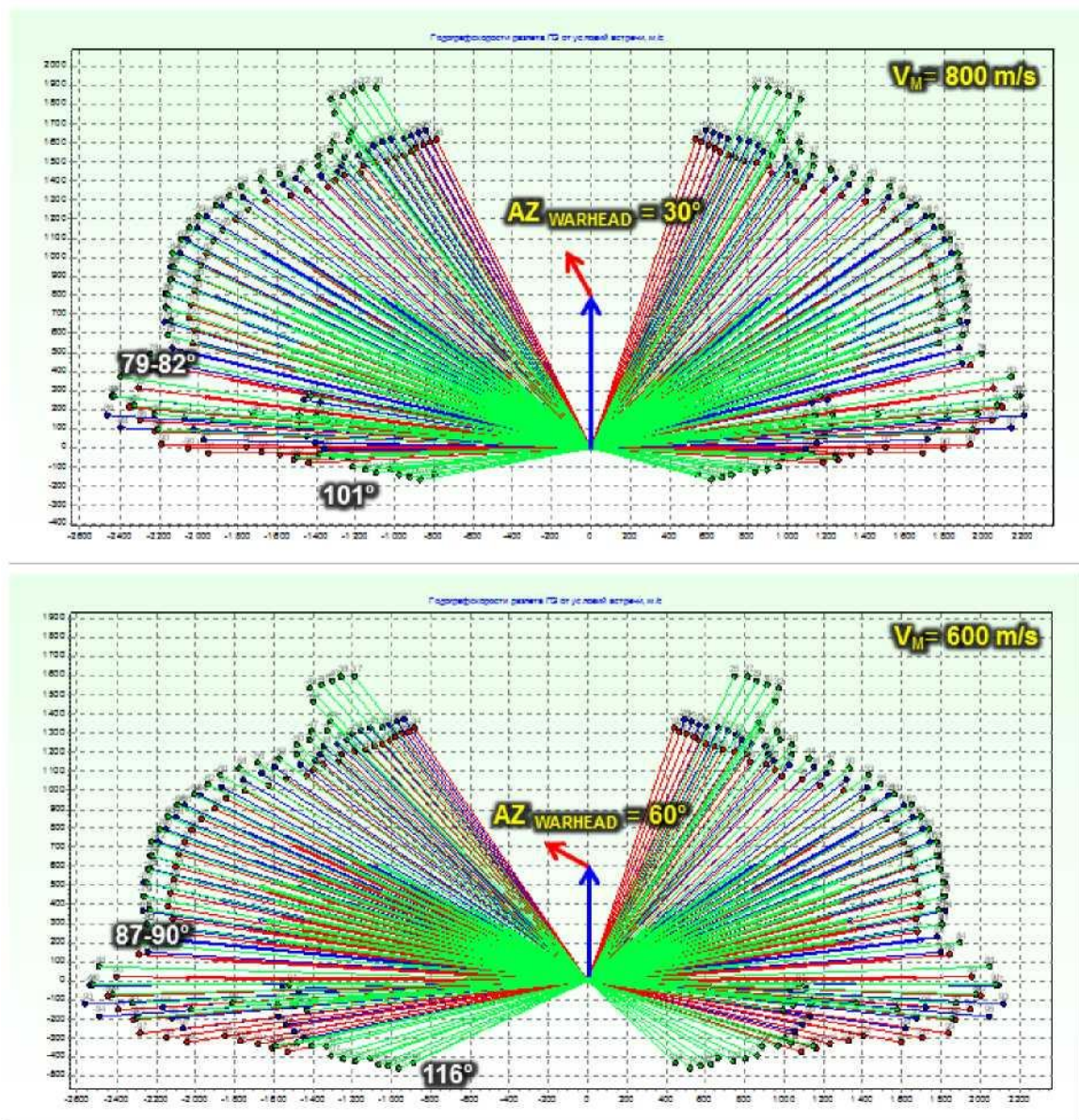


Figure 5.2.11 - Effect of simultaneous change in final missile velocity V_M and angle between longitudinal axes of aircraft and missile $AZ_{warhead}$:
top - $V_M = 800 \text{ m/s}$, $AZ_{warhead} = 30^\circ$; bottom - $V_M = 600 \text{ m/s}$, $AZ_{warhead} = 60^\circ$

The fragment dispersal model (preformed and hulled striking elements) used by specialists of Almaz-Antey Corporation calculates the velocity and coordinates of each of the fragments (more than 12,900 trajectories) at any time, as well as the fragment field density distribution at any selected distance and direction from the detonation point.

The fragments (separately Heavy and Light fractions, as well as Shell fragments) in the software package are modelled using material points and their motion is described by kinematic equations of motion, taking into account the initial (x_{0i}, y_{0i}, z_{0i}) and current coordinates (x_i, y_i, z_i) , and components of fragment velocities (v_{xi}, v_{yi}, v_{zi}) .

During computational experiments associated with the development of software modules responsible for simulating fragment dispersal under dynamic conditions, various variants of models were tested: fragment dispersal from a "point"; fragment dispersal from a "segment" corresponding to the linear dimensions of the warhead; fragment dispersal from an "elliptical cylinder" whose shape virtually coincides with the actual shape of the warhead. In the course of the experiments it was established that the shape of the warhead specified in the model had a considerable influence on the simulation results. This is due to the close proximity of the warhead to the surface of the aircraft (about 1.6-2.0 m), which is comparable to the linear dimensions of the warhead itself (over 0.5 m).

Therefore, the final version of the fragment dispersion model took into account the shape of the warhead.

5.2.3 Position of Boeing 777 in space

Consideration of the aircraft's actual position in space has a significant impact on the calculation of the likely launch area.

It should be noted, however, that during the DSB technical investigation all uncomfortable parameters were declared insignificant or "unimportant to the investigation" when determining the modelling inputs by the Dutch experts. For example, attack angles, wind drift angles and local magnetic declination associated with wind drift were considered to be insignificant.

**Relevant velocities have been obtained from the NLR and DSB (see Table 4 1)
A possible roll angle, angle of attack and drift angle of the airplane have been assumed to be negligible [7] The NLR has determined the probable terminal velocity of the guided weapon by means of a *fly out* simulation [7]**

Figure 5.2.12 - Recognition of "insignificant" corrections to determine the actual position of the aircraft's longitudinal axis in space

This can be seen in Figure 62 of the DSB Final Report,⁶⁸ which shows the 320 square kilometre "probable launch" area calculated by the NLR. The yellow line in the figure shows the projection of the path of the Boeing 777, corresponding to approximately 119 degrees.

In reality, the value of 119 degrees corresponds to the projection of the Boeing 777's course line on the map.

This is confirmed by materials of objective control (Fig. 5.2.13) – registration file of primary radar data of "Utes-T" radar complex in the part concerning the route of aircraft No. 0143.

⁶⁸ Final Report. Figure 62. Visualisation of NLR fly out simulation result, p.144.

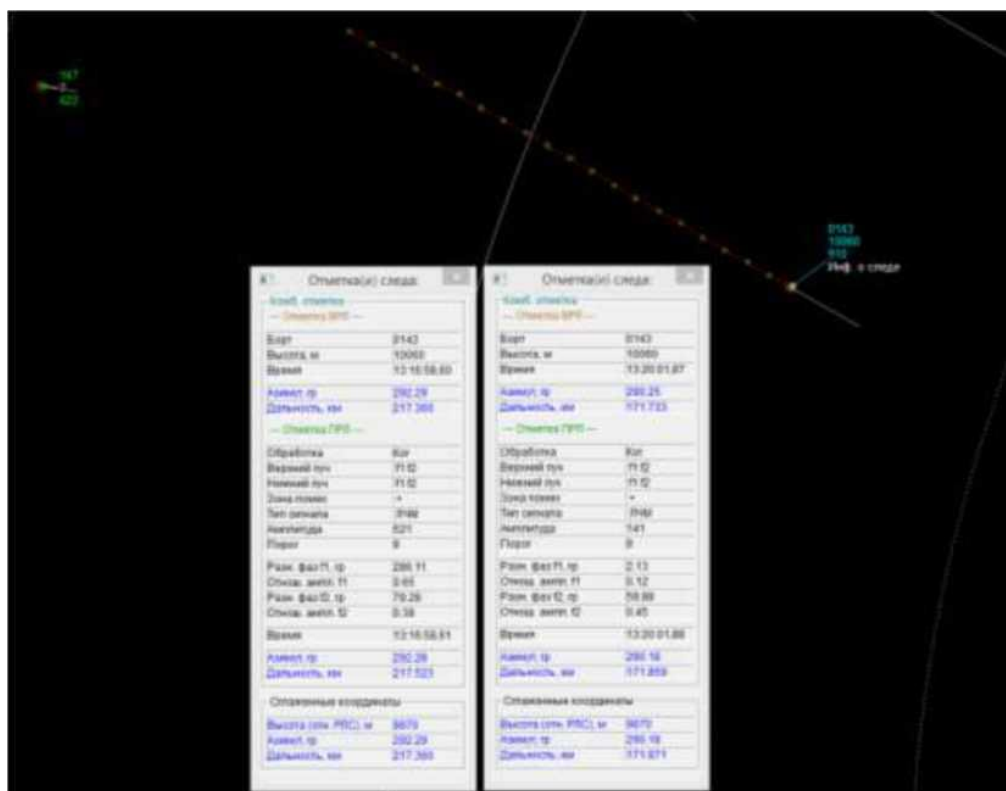


Figure 5.2.13 - Track of Aircraft No. 0143 (MH17) from 13:16:58.60 ETS to 13:20:01.88 ETS (objective control material)

The objective control data matches the Boeing 777 Flight Data Recorder (FDR) data when magnetic heading is converted to magnetic declination and drift angle is subtracted.^{69, 70}

Figure 5.2.13 shows the track of aircraft No. 0143 (MH17) immediately prior to the crash. The track of aircraft No. 0143 (MH17) corresponds to the projection of the Boeing 777 course line on the map at about 119 degrees.

The actual orientation of the aircraft's longitudinal axis (the position of the Boeing 777's axis relative to the north meridian), taking into account local magnetic declination and wind drift, was about 123 degrees.

Thus, a correction of about 4 degrees between the course line projection of the Boeing 777 on the map and the actual orientation of the aircraft's longitudinal axis must be considered when estimating the likely launch area.

⁶⁹ Preliminary Report, p.20.

⁷⁰ Final Report, p.111.

It is also important to bear in mind that the Boeing 777, which flew at 254 m/s at an altitude of over 10,000 m (FL 330), had a positive angle of attack (about 3°).

It follows from the basics of air navigation that the movement of an aircraft relative to the earth's surface is characterised by the vector of total speed W_n .

In general, an aircraft's total speed vector is directed towards the horizon at an angle called the vertical path angle θ .

This is shown in Figure 5.2.14, where:

SLA - spatial location of the aircraft - the point in space at which the centre of mass of the aircraft is located at a given time;

MC is the projection of the centre of mass of the aircraft onto the ground surface.

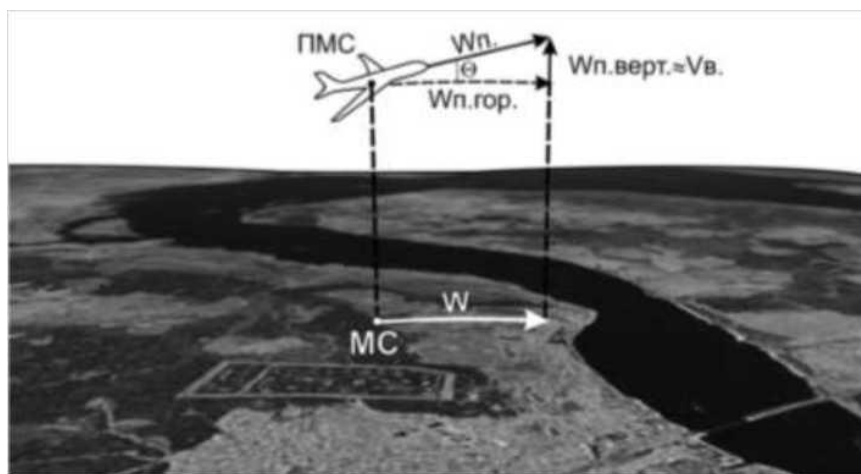


Figure 5.2.14 - Spatial position of the aircraft relative to the ground surface

Thus, it turns out that during flight the actual position of the aircraft's longitudinal axis is not parallel to the ground surface (Figure 5.2.15).

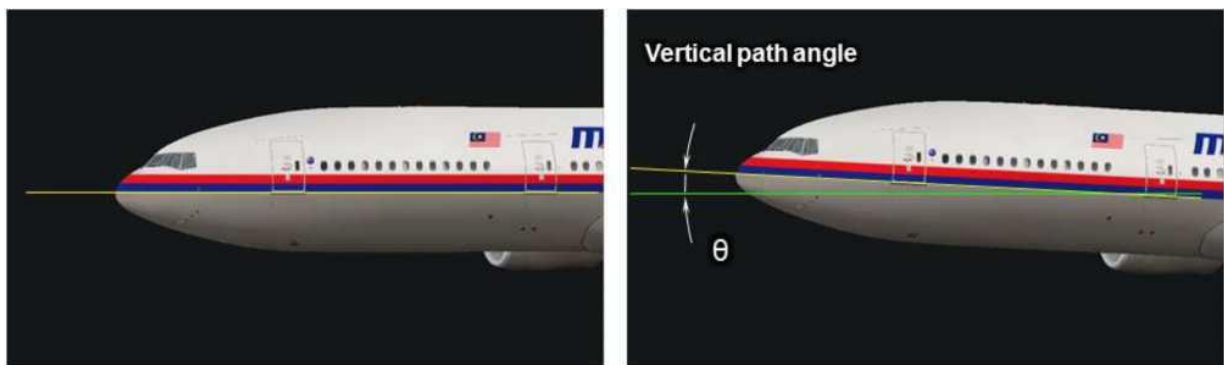


Figure 5.2.15 - Spatial position of the aircraft relative to the ground surface: left - without considering the angle of inclination of the trajectory; right - actual position of the longitudinal axis of the aircraft relative to the ground surface

This is important when calculating the position of the warhead [missile] relative to the aircraft in the vertical plane, especially considering the characteristics of the 9M38 missile.⁷¹

A key feature of the 9M38 missiles (compared to the 9M38M1) is that the missile always approaches high-altitude targets (e.g., at 10,000 m altitude) with a positive angle in the vertical plane, according to its hardwired algorithm. As an example, Figure 5.2.16 shows the effect of the aircraft's actual axis position on the missile's axis angle relative to the ground plane ($El^*_{warhead}$).

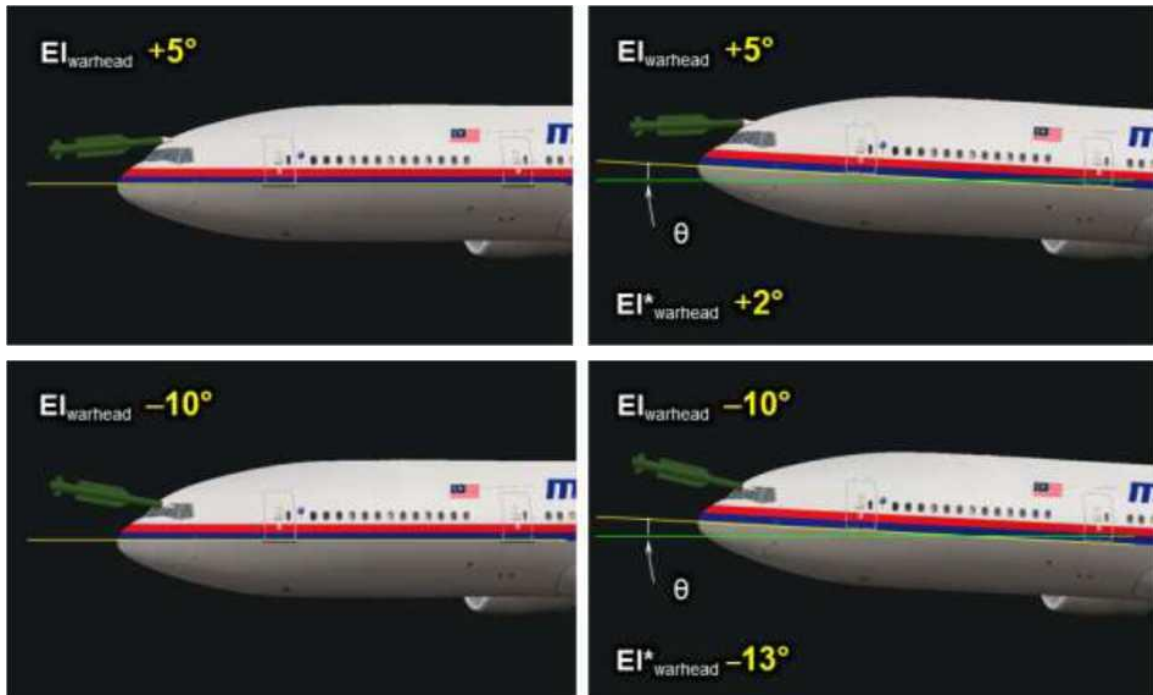


Figure 5.2.16 - Actual position of rocket axis $El^*_{warhead}$ relative to the earth's surface

Based on the characteristics of the 9M38 missile, variants that use zero or negative vertical angle $El_{warhead}$ should be excluded from the range of orientation of the missile relative to the aircraft.

5.2.4 Methods for determining the orientation of the warhead relative to the aircraft structure (aircraft-missile encounter conditions)

As noted above, the determination of the aircraft-missile encounter conditions is based on the best fit of a combination of three components: aircraft damage, the dynamic model of the warhead explosion (warhead characteristics) and the detonation point connecting them.

Almaz-Antey Corporation experts used several methods to determine the most

⁷¹ Based on the unique serial numbers of the engine and nozzle, the missile fragments demonstrated by JIT, the serial number of the product was established and the exact modification of the missile was determined - 9M38 - no "M1" index.

likely orientation of the warhead at the time of detonation, including:

by matching the field boundaries of the fragmentation cover;
on the distribution of the impact density of the projectiles on the aircraft fragments;

by traces of damage to the aircraft structure, including the power kit, from a dense stream of projectiles ("scalpel");

on matching the degree of blast effect of the 9H314M warhead, etc.

In general, the task of determining the orientation of the warhead relative to the aircraft structure can be divided into several specific tasks:

1. Creation of a damage model of the Boeing 777 aircraft, taking into account the main markers for the methods used to determine the conditions of the aircraft missile impact (field boundaries, density distribution, boundaries of the power kit failure zones, scale and nature of the blast damage).

2. Creation of a dynamic warhead detonation model with a spherical distribution of warheads (virtual warhead), taking into account the shape and linear dimensions of the warhead, mutual velocities, angles of position in space, including angles of attack, yaw and pitch.

3. Determine the area of space in which the munitions detonation has occurred (detonation point).

4. Determine the orientation of the virtual warhead for which the best match is achieved between the virtual warhead's impact pattern and the observed traces of impact and close detonation factors on the detected wreckage (taking into account the characteristics of the different methods).

The first three tasks were accomplished in examining the structural damage to the Boeing 777 (paragraph 5.1.2), creating a model of the detonation of the warhead (paragraph 5.2.2) and determining the location of the detonation point (paragraph 5.2.1).

The direct determination of the missile's (warhead's) orientation in space relative to the aircraft (determination of the conditions for meeting the aircraft with the missile) for each of the methods was carried out taking into account the markers.

5.2.4.1 Consistency of fragmentation field boundaries

The essence of the method for determining the orientation of a missile relative to an aircraft at the moment of a warhead explosion is to find the best match between the pattern of the overburden field generated during the flight of the virtual warhead and the observed overburden field boundaries on the studied debris. The result is the best overlap of the field boundaries between the three components: the damage model (1), the dynamic model of the warhead (2) and the detonation point that connects them (3).

A similar method was applied by NLR in the preparation of the DSB Final

Report. The difference was that the best solution was found using unverified data (warhead model and detonation point) with parameters specifically chosen for the assigned versions.⁷²

The damage "reference" used is a "light model" of damage created by NLR specifically for the "oncoming-only" version under predetermined encounter conditions (coordinates of the matching detonation point, orientation angles and final missile speed).⁷³

The main feature of this model was that the level corresponding to STA 220 was taken as the rear boundary of the cover field for comparison, which is almost 3 metres ($332.5-220.5=112$ inches ≈ 2.85 metres) closer than the actual boundaries of the cover field objectively observed on the upper port-side fragment.⁷⁴

The Technical Inquiry states that all independent experts (NLR and TNO) found no damage from of the projectile behind the windows of the crew commander, i.e. further down STA 220 frame.^{75, 76}

For this reason, when examining the combat damage fragments of the Boeing 777, special attention was paid to the boundaries of the fragmentation field. The following were investigated:

- fragments presented in the final 3-D reconstruction;

- fragments removed to the Netherlands, which are either not represented in the final reconstruction or were displayed in other rooms;

- fragments that, for unknown reasons, were not brought into Dutch territory, but their location in the aircraft structure has been reliably established (during the work of the DSB experts).

In comparing the modelled and actual damage, special attention was paid to the objectively observed forward boundary of the zone of damage from high-speed elements, which according to the DSB experts is the forward gullwing (STA 132.5)⁷⁷ and the rear boundary, which is a fragment of the port-side top with damage beyond STA 332.5 (see Figures 5.1.22, 5.1.23).

When comparing, for the best possible match of the damage, took into account the matching of the overlapping field boundaries (according to the polygonal objects that make up the digital damage model) and optimised the matching of the location and direction of the boundary damage ("ricochets").

The search was performed for a set of detonation point regions in a verified space of 1 m³ and took into account the final velocity range of the 9M38 missile

⁷² In the technical investigation, the "most appropriate for this investigation", contrary to data from the Almaz-Antey design and technical documentation, was found to be a warhead model with characteristics adapted to the main version - using less than 1/3 of the killing field factors.

⁷³ Final Report. 3.8.2. Fragmentation visualisation model, p.137-138.

⁷⁴ PART 2: Exhibit A.1, pp. 5-19.

⁷⁵ Final Report. Crash of Malaysia Airlines flight MH17. p.121.

⁷⁶ TNO report. Damage reconstruction due to impact high-energetic particles on Malaysia Airlines flight MH17, p.7.

⁷⁷ Final Report. Crash of Malaysia Airlines flight MH17. p.121.

from 600 to 730 m/s.

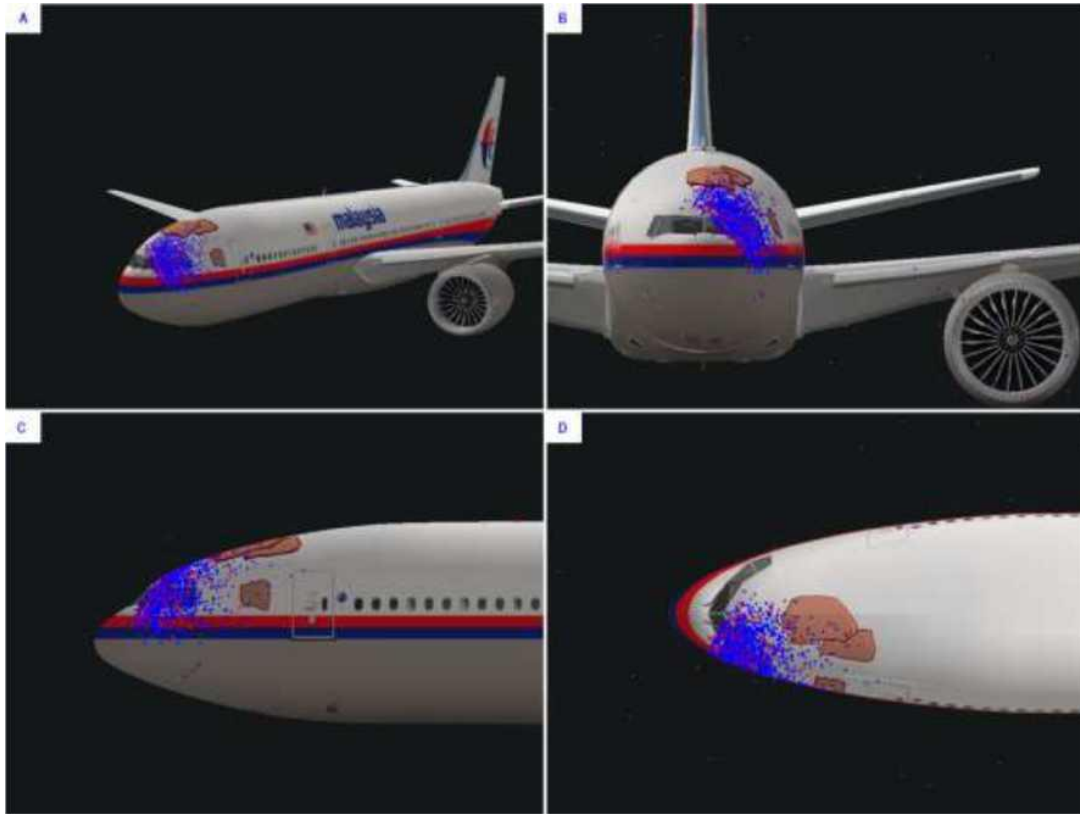


Figure 5.2.17 - Fragmentation cover field derived from modelling using a verified detonation area

The best results have been obtained for the horizontal angle of intersection of the missile with the aircraft's construction axis, ranging from -50° to -62° . The minimum missile velocity at impact (600 m/s) corresponds to the maximum intersection angle, while the velocity of 730 m/s corresponds to a minimum value of -50° .

The front and rear boundaries of the fragment cloud, as well as the boundary running along the right side of the cockpit roof and the roof behind the cockpit (hereinafter STA 236.5) were chosen as the main compliance markers.

Figure 5.2.18 shows the comparative modelling results for the three rocket end positions used by the different experts: -16 deg. (left), -37 deg. (centre) and -50 deg. (right).



Figure 5.2.18 - Comparison of left side damage modelling results of Boeing 777 for three values of crossing angle

Among the variants considered, only for the "Azimuth -50° " variant do the boundaries of the fragmentation overlap between modelled and actual damage most closely coincide on reference fragments No 1-No 5 with characteristic damage.

A description of the comparison results is provided in Exhibit E.⁷⁸

Using complete data on the actual field boundaries, verified fragment dispersion models and detonation point coordinates, only the aircraft impact conditions in a horizontal plane of at least -50° can be considered as minimum realistic input data, obtained using the methodology used by the Dutch experts in preparing the Final Report.

Accordingly, the impact of a BUK missile (9M38) as a cause of destruction of a Boeing 777 in mid-air can be considered only under the necessary condition that the missile crosses the plane course at an angle of at least -50° ... -60° in the horizontal plane (figure 5.2.19).

Otherwise, the boundaries of the fragmentation cover zone do not coincide: the front, running along the hermetic bulkhead and its adjacent fragments; the rear and the top, running through the roof and port side fragments described above, not included in the final reconstruction. In addition, only this condition explains the damage to the left wing plane and the left engine by prefabricated projectiles, the presence of damage from which was confirmed by TNO specialists.

⁷⁸ PART 2: Exhibit F, pages 114-126.



Figure 5.2.19 - Damage model visualisation for the "collision course" version, which explains all damage to the outer skin, airframe, left wing plane and left engine of the Boeing 777: left - damage boundary model; right - fragmentation coverage field

Figure 5.2.19 shows a visualisation of the fragmentation cover field for conditions ($AZ_{\text{Warhead}} = -55^\circ$; $EL_{\text{Warhead}} = 22^\circ$) showing the correspondence actual and modelled damage along the front fuselage overlap field boundaries, as well as including the left wing plane and left engine of the Boeing 777 aircraft.

It is at this orientation of the warhead (at least -50°) that comparison criteria No. 1 (conformity of cover field boundaries), No. 2 (no fragmentation damage to the forward gimbal), No. 4 (conformity of damage direction) and No. 8 (damage to the left wing plane and left engine preformed fragments), specified in paragraph 5.1.3, are met.

It should be particularly noted that the mandatory conditions under which the impact of a BUK missile can be considered as the cause of the Boeing 777 was verified and confirmed⁷⁹ in the course of a field experiment in a shielded target layout.

Thus, consideration of roof fragments and the top of the port side behind the cockpit significantly affects the reliability of determining the missile-aircraft rendezvous conditions.

Taking into account the boundaries of the fragmentation field objectively observed on the available fragments of the Boeing 777, the version of an aircraft hit by a BUK missile can **only** be considered "**on a collision course**", i.e. at an angle of at least $-50^\circ \dots -60^\circ$.

⁷⁹ This condition is that the missile crosses the course of the aircraft at an angle of at least "minus" 50-60 degrees in the horizontal plane.

5.2.4.2 Consistency of fragmentation density distribution

The essence of the method of determining the missile's orientation relative to the aircraft according to the density of fragmentation damage is to find the best correspondence between the picture of impact element distribution in the field of virtual warhead cover and the observed density of projectiles on the detected fragments (wreckage) of Boeing 777.

The result is the best fit of the dynamic fragment dispersion model to the damage density distribution model, taking into account the detonation point that connects them.

Most importantly, the Almaz-Antey specialists used the Damage Model as a benchmark for comparison, which takes into account the most important fragments of the roof and top of the port side beyond STA 220.5, characterising not only the actual rear boundary of the fragmentation field, but also being areas of high density of fragmentation damage.⁸⁰

The Almaz-Antey damage model takes into account the damage not only on the fragments presented in the 3D reconstruction, but also on the roof and upper port side fragments that did not make it to the final layout (see paragraph 5.1.2).

The fragmentation damage in the model is an array \mathbf{a} , which stores the number of penetrations for each of the \mathbf{M} sites that make up the nose of the Boeing 777.

For the Boeing 777 model used, the number of sites $\mathbf{M} = 5,365$. The array \mathbf{a} , storing the number of fragmentation impacts in each of the aeroplane's seats, was the reference.

The meaning of the algorithm for solving the problem of determining the conditions of meeting an aircraft with a missile (the orientation of the missile relative to the aircraft at the time of detonation) is as follows. At various points in the region of space (less than 1 m^3), which constitutes the verified detonation point region, the missile's payload is detonated, taking into account the mutual speed of approach to the aircraft with different angles of azimuth Az and angles of location El .

For each detonation, the trajectories of each fragment and the points of intersection of these trajectories with the planes that make up the surface of the aircraft are calculated. For each case, the points found are stored in a data array, each element of which represents the number of impacts falling on the area with the number corresponding to the element index. Such arrays are approximations (approximations).

For all the approximations found, error E is calculated, which quantifies the difference between the approximation array and the benchmark and is used as a criterion for selecting the approximation array that most closely matches the benchmark. The value of error E for it is the lowest among the values of other approximations.

⁸⁰ PART 2. Exhibit A.

As a result, the solution to the problem is reduced to a numerical solution to the optimisation problem:

$$E(\mathbf{p}^{\rightarrow*}) \rightarrow \min_{\mathbf{p}^{\rightarrow} \in P} E(\mathbf{p}^{\rightarrow}),$$

where, $\mathbf{p}^{\rightarrow} \equiv (x, y, z, Az, El)$ is a five-dimensional vector;

(x, y, z) are the Cartesian coordinates of the centre of the SAM system;

Az and El are the azimuth and the angle of engagement of the SAM system;

$\mathbf{p}^{\rightarrow*} \equiv (x^*, y^*, z^*, Az^*, El^*)$ is the desired solution that gives a minimum to the functional $E(\mathbf{p}^{\rightarrow})$.

For the numerical calculations, the following minimisation criterion was chosen:

$$E = \sum_{i=0}^{M-1} |e_i - a_i|$$

where M is the number of sites (polygonal objects) that make up the surface of the Boeing 777-200 ER aircraft model;

e - array storing the number of penetrations per site according to the simulation results (for each of the approximations);

a - an array storing the number of penetrations per site in the Benchmark - "Damage Models".

The number E in this criterion corresponds to the number of non-matched faults. The choice of this criterion is due to its obviousness and ease of implementation.

To solve such problems, it is necessary to enumerate many different positions of the warhead and compare them with the reference value. The position of the warhead in space is determined using five parameters: three Cartesian coordinates, elevation angle and azimuth (Figure 5.2.20).

The brute-force method is computationally intensive and time-consuming. For example, it takes about 2 seconds to calculate one explosion.⁸¹ A brute force attack (an ARM with a 2.4 GHz *Intel Xeon E5620* processor) would take about 4 years to compute and would be approximately 60 million variants.

The time required to complete a full search was reduced by performing calculations on the Orpheus-K supercomputer using parallel algorithm.⁸²

⁸¹ This figure is obtained by experimental measurements on the Orpheus-K supercomputer.

⁸² MPI - Message Passing Interface technology was used, which reduced the complete enumeration time for both the coarse and fine mesh to 12 days.

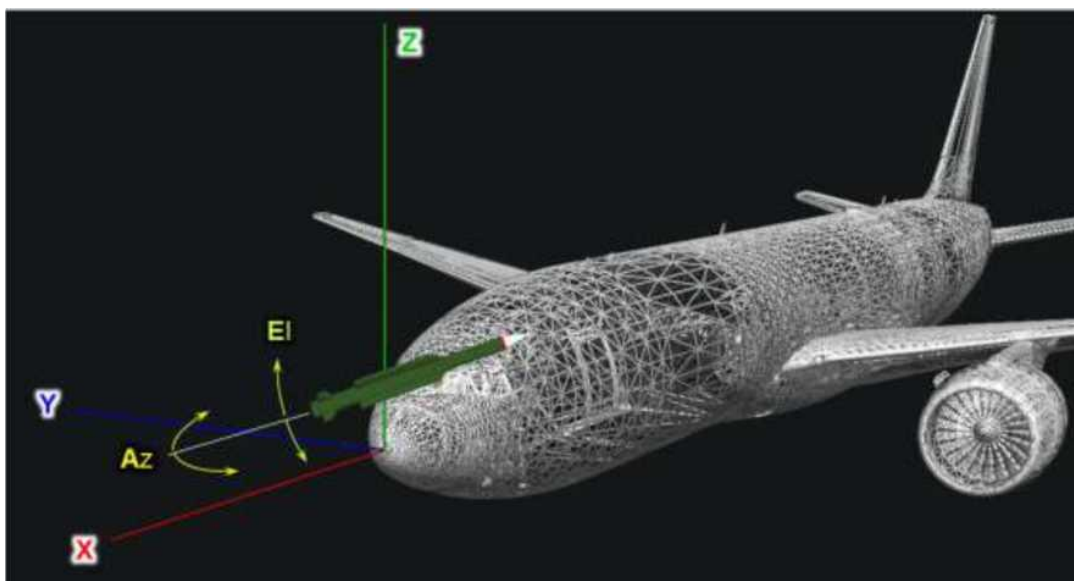


Figure 5.2.20 - Parameters for enumerating SAM position in space: X, Y, Z - position of the centre of the warhead relative to the origin of coordinates; Az, E1 - azimuth and location angle of the missile's longitudinal axis

The calculation was carried out. The range of best results for the spatial position of the missile's warhead relative to the aircraft at the time of detonation at a final missile velocity of 600 to 730 m/s was

Azimuth (Ag, horizontal plane), degrees-62... -68
 Angle of seating (E1, vertical plane), degrees20...24

One of the variants resulting from the calculations was used as a baseline for the first phase of the experiment. The calculated vector had values corresponding to the Corporation's version of the 'collision course':

Angles of the SAMS relative to the aircraft: azimuth angle -66° ; elevation angle 22° ; detonation point coordinates: $X = 0.5$ m, $Y = -1.5$ m, $Z = 1.7$ m; final rocket speed of 720 m/s.⁸³

If possible, the results of the calculations should be verified by other available methods.

One of the most acceptable markers, which can be easily checked, is the second window (vent) of the crew commander. Its exact dimensions are given in the DSB Report. There it is also shown that the second window was in the area of maximum fragmentation density and 102 fragmentation injuries were recorded on it.⁸⁴

This area, including the second window, was a kind of reference point for the Dutch experts, using which the experts searched for and verified the rendezvous conditions of the missile by plane.⁸⁵

In order to compare the actual and simulated damage in the second left window

⁸³ The results of the match with the benchmark were over 96%.

⁸⁴ Final Report. Cockpit window left hand side, Figure 34, p.79.

⁸⁵ Final Report. Annex X (NLR report). 2.5 Number and density of hits, p.14.

in terms of number and density of damage, simulations were performed for different values of the azimuth (horizontal angle) of the final missile position from the ranges obtained by different specialists:

- Missile end state (at time of warhead detonation): angle of location (E1, vertical angle), degrees(5)
- Detonation area coordinates, m (0.4; - 1.85, 1.85)
- missile speed, m/s 600

Only the value of the azimuth (the angle between the aircraft and rocket axes) was changed to the fixed values present in the various reports:

- azimuth (Az), degrees (-16; -37; -50; -62; -66; -68)

The options were compared using an interactive 'simulated damage' model and an 'actual damage' model of the second left window (102 fragmentation injuries according to the DSB Report).

As noted earlier, the dynamic fragment dispersion model takes into account the different types of fragments: ready-made two types of light fraction (Light) and heavy fraction (Heavy), as well as shell fragments (Shell).⁸⁶

When assessing fragmentation damage to windows, only prefabricated impactors should be considered. This assertion is based on experimental data obtained from in-situ experiments: cockpit transparency, 25mm laminated glass, can only be penetrated by prefabricated (primary) projectiles.⁸⁷

An example simulation for the Azimuth -16° variant is shown in Figure 5.2.21, where the set of areas (polygonal objects) corresponding to the second left window on the Boeing 777 is highlighted in orange on the interactive aircraft model.

A pop-up window indicates the number and types of fragments whose trajectories intersected the areas that make up the surface of the second left-hand cockpit window.

⁸⁶ Only hull fragments with linear dimensions corresponding to the size of the GGE are counted. Detonation products of 1-3 mm in size and large compartment fragments are not counted.

⁸⁷ PART 2. Exhibit B.3.

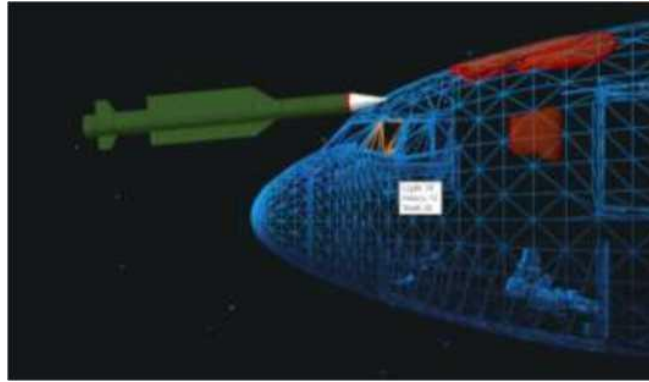


Figure 5.2.21 - Simulation of fragmentation damage to the nose of a Boeing 777 aircraft under Azimuth -16° conditions. The polygonal objects corresponding to the second left window are highlighted in orange on the interactive aircraft model

The simulation results in only 72 splinters in the second window:

Light	34	(light fraction projectiles of two types)
Heavy	12	(heavy fraction projectiles, "bowtie")
Shell	26	(hull splinters)

Accordingly, the simulation results show that only 46 prefabricated projectiles ($34+12= 46$) could damage the complex multi-layer barrier that is the cabin transparency (window).

The number of simulated damages (46 units) is 2.22 times less than the number actually recorded in the second window (102 units).

Similarly, a comparative analysis of modelled and actual damage for the other variants of the range of possible angles is performed. The results of two more important Azimuth -37° and Azimuth -50° variants characterising the range of missile impact conditions for the aircraft are shown in Figure 5.2.22.

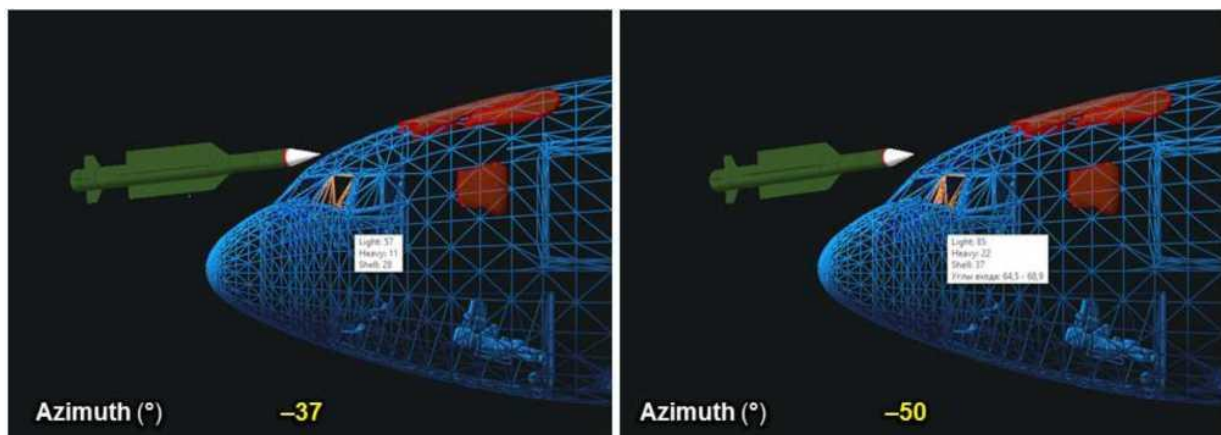


Figure 5.2.22 - Simulation of fragmentation damage to the nose of a Boeing 777 aircraft under Azimuth -37° (left) and Azimuth -50° (right) conditions

A. For "Azimuth -37° " conditions:

up to 96 fragments (Light- 57; Heavy- 11; Shell- 28) can reach the second window;

no more than 68 prefabricated projectiles (57+11= 68) could damage the complex multi-layer barrier that is the cab's transparency (window);

The number of simulated damages (68 units) is 1.5 times less than the number actually recorded in the second window (102 units);

The modelled damage density for Azimuth -37° conditions is 1.5 times lower than the actual damage density and is about 167 punctures per square metre.

B. For "Azimuth -50° " conditions:

The second window only receives up to 144 fragments (Light- 85; Heavy- 22; Shell- 37);

Up to 107 prefabricated projectiles (85+22= 107) could damage the complex multi-layer barrier that is the cab's transparency (window);

The number of modelled damage (107) is comparable to the number of actually recorded damage at the second window (102), and the modelled density is also comparable to the actual values recorded at the second window - about 250 punctures per square metre.

The modelling results for all variants are shown in Figure 5.2.23 as a histogram, from analysis of which the range of acceptable azimuth values is from -50° to -68° , with the best match for -66° .

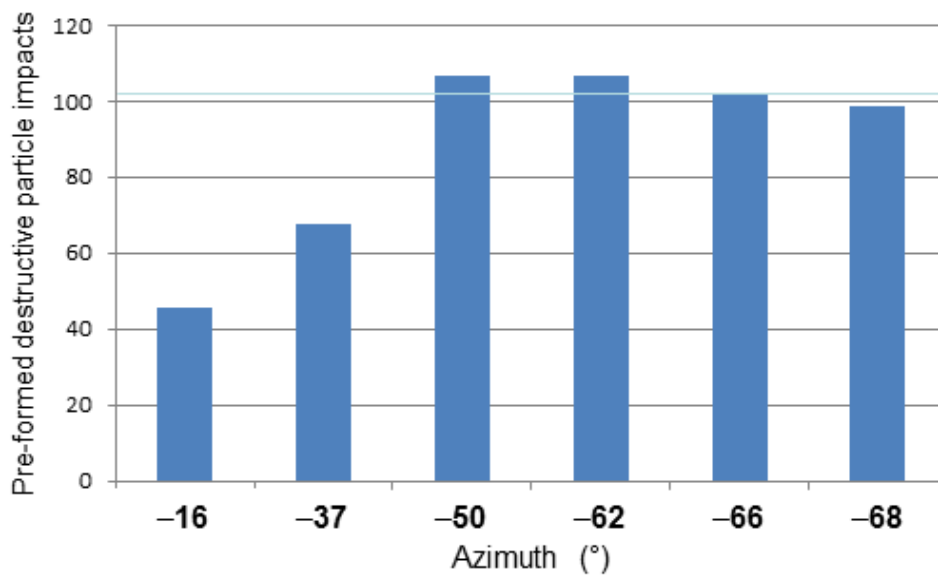


Figure 5.2.23 - Fragmentation damage to the second left window when the missile's warhead is oriented at horizontal angles ranging from -16° to -68°

Similar calculations were made for the other important roof and port top fragments not shown in the final layout.

For example, the upper port side fragment (Figure 5.2.24) shows a high density

of damage at the level of the STA 287.5 and STA 298.5 bulkheads.⁸⁸

The particular importance of this fragment lies in the fact that it is located twice as far from the boundary used in the NLR - STA 220.5 models and more than twice as far from the second left window (STA 164.75- STA 188.5). Taking into account that with distance from the detonation point - the fragmentation field density decreases inversely proportional to the square of the distance ("law of squares"), respectively, if the distance from the detonation point to the outer surface of the aircraft changes by half, the actual density of damage on this surface should change by a factor of four. Taking into account the additional fragments, the range of acceptable azimuth values is from -62° to -68° , and the best match remains for a value of -66° .

A damage model that does not include critical fragments such as the roof of the cockpit, the fragments with the highest density of projectiles is inaccurate.

Numerical experiments have found that areas of higher density have a greater influence on the target function, and accounting for missing roof and port side fragments provides a more accurate simulation.

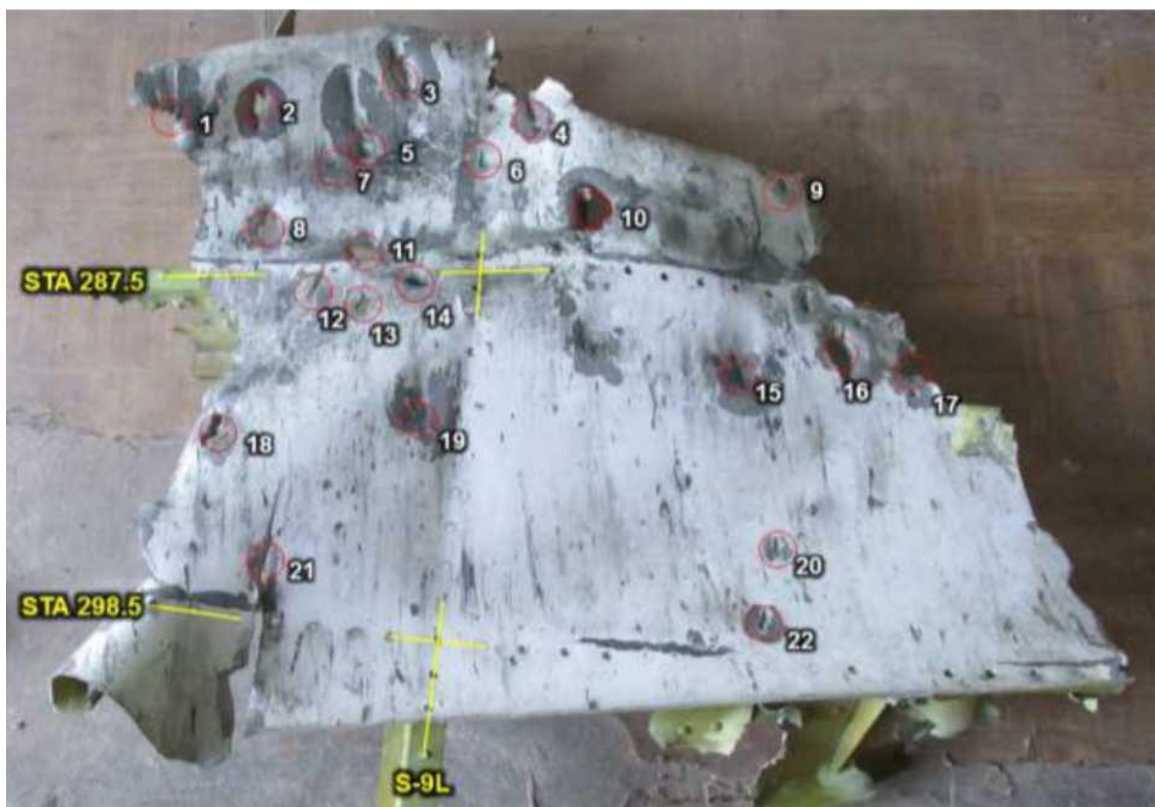


Figure 5.2.24 - Fragment with high density of fragmentation damage not included in final reconstruction and not included in NLR models

It should be noted that, as a result of a comparative analysis of the shielded target situation with damage to the outer hull fragments, elements of the structure of

⁸⁸ The fragment was not included in the final reconstruction, but was located in the Netherlands in another room.

the Boeing 777 (MH17) aircraft, it was the field of coverage of the main elements of the nose section of the aircraft and the distribution of the density of fragmentation damage were found to be consistent.

For the range of warhead orientation angles determined by this method (-62° to -68°), the comparison criterion No. 3 (impact density distribution) specified in paragraph 5.1.3 of the Corporation Report is best fulfilled.

Thus the consideration of fragments with a high density of fragmentation damage on the roof and upper port side behind the cockpit to the level of STA 287.5-STA 332.5 (not included in the 3D reconstruction and located almost 3 metres beyond the "reference" STA 220.5), significantly affects the credibility of the determination of the missile-aircraft encounter conditions.

The range of best results for the spatial position of the missile's warhead relative to the aircraft at the time of detonation for a final missile velocity of 600 to 730 m/s is -62° to -68° .

The destruction of a Boeing 777 aircraft by a BUK missile can only be considered on a "collision course", i.e. at an angle of at least -50° .

5.2.4.3 Destruction of aircraft structure by a dense stream of projectiles ("scalpel")

The piercing of an aircraft structure and the mechanical destruction of its compartments is caused by a dense stream of fragments and the resulting shock waves (ballistic waves of fragments in an airborne environment).

The ability to penetrate several successive or combined obstacles is directly related to the velocity of the projectiles, their mass and shape.

Experimental studies conducted show that:

1. Preformed fragments (Figure 5.2.25 below), having a compact shape and greater mass, have a significantly higher penetration.

2) The ballistic wave of fragments of the required intensity is generated only in areas of high density of preassembled projectiles (PDEs). The PGEs themselves must have a large mass and area in order to transmit the maximum impact force momentum to the barrier, which, for a BUK missile, corresponds to fragments of the heavy fraction 9H314M 1-10 ("double-barreled").



Figure 5.2.25 - Comparative linear dimensions and mass of hull fragments (top) and 9H314M heavy fraction preformed fragments 1-10 "doublet" (bottom)

This was confirmed by the results of experiments carried out by Almaz-Antey Corporation specialists.⁸⁹

Mechanical (penetration) capacity

Shell fragments, with their relatively low mass and large linear dimensions (Figure 5.2.25 above), decelerate faster in air and their impact on obstacles (penetration) under the same conditions is significantly lower than that of prefabricated projectiles. This is illustrated in more detail in Exhibit A of the Field Experiment Report (2016).⁹⁰

As one illustrative example, the differences in the penetration (mechanical)

⁸⁹ Almaz-Antey report on the full-scale experiment (2016).

⁹⁰ Exhibit A to the Field Experiment Report, section 3.1, pages 17-27.

capacity of off-the-shelf and body-mounted projectiles when secured in a particularly strong "trap" barrier are shown.⁹¹

Prefabricated projectiles of all fractions, taking into account the outer skin of the trap and three layers of stopping foam, penetrated the complex combined obstacle to a depth of 400.0-450.0 mm (Figure 5.2.26).



Figure 5.2.26 - Removing a ready-made impactor from the "L. 1" trap: left - depth of penetration of a ready-made impactor into the trap; right - ready-made impactor 9H314M 1-9 stuck in the trap

Figure 5.2.27 shows the hull impactor (compartment hull fragment) extracted from the third layer of stopping foam of the heavy-duty booby trap "L.1".

This fragment penetrated the outer barrier of the trap (2.0 mm aluminium alloy sheet AMg6M), two of the three sheets of stopping foam PS-1-150 and was stopped at the boundary of the third layer.

⁹¹ The trap is designed to trap debris and consists of several consecutive layers: an outer trap barrier (2.0mm aluminium alloy sheet AMg6M); three layers of stopping foam PS-1-150 with a total thickness of 260mm and a layer of boards with a total thickness of 750mm.



Figure 5.2.27 - Hull impactor (compartment hull fragment) lodged in the third layer of stopping foam PS-1-150 of trap "L.1" of the shielded target layout (31.07.2015)

The analysis of the results of the field tests confirms two important claims made by Almaz-Antey Corporation specialists:

1. At angles close to normal (shielded target conditions), aluminium barriers (similar to the outer skin of a Boeing 777) are capable of penetrating not only prefabricated projectiles but also hull fragments.

2. Ready-made projectiles provide a much more destructive effect after piercing the fuselage of any aircraft and will cause a great deal of damage to the interior of the aircraft.

Combat damage studies of the Boeing 777 show that penetrating and non-penetrating damage on the aircraft structure fragments was caused not only by prefabricated projectiles, but also by other parts of the weapon. This is especially true for the rear front of the fragmentation field (when impacted at angles close to normal).

As an example, Figure 5.2.28 shows photographs of through-and-through holes at the forward boundary of the fragmentation field on the fragment in front of the front windows of the Boeing 777 cockpit.

These photos were taken at Gilze-Rijen airbase in May 2015 and show examples of through-hull penetrations caused by hull-mounted projectiles.

That these injuries were not caused by prefabricated projectiles is confirmed by the shape, appearance and linear dimensions of the holes (Figure 5.2.28).

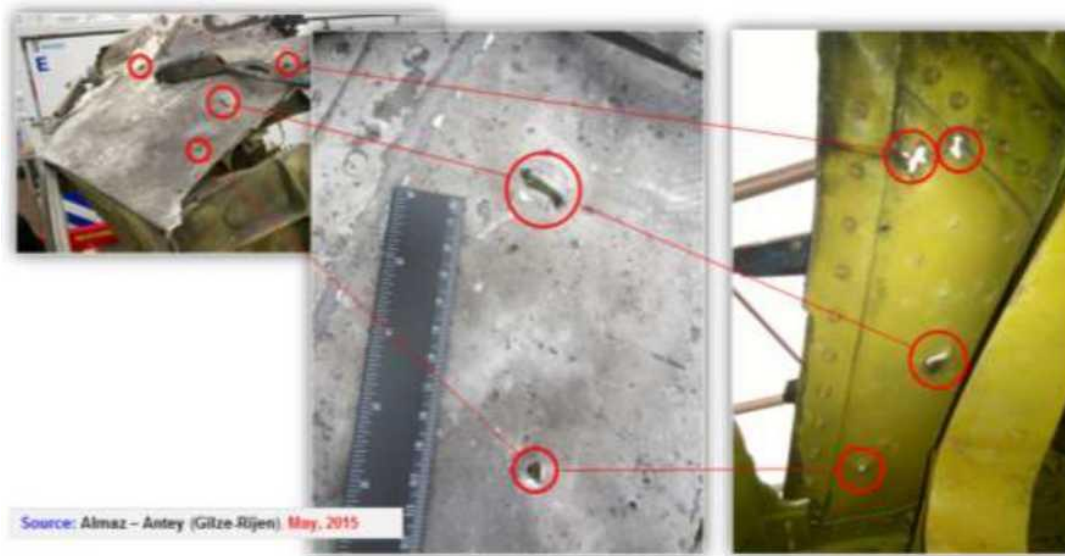


Figure 5.2.28 - Hull damage to the nose section of a Boeing 777 (external and internal view)

In this case, at small angles between the velocity vector and the plane of the obstacle, the housing fragments, unlike preformed fragments,⁹² do not preferentially penetrate beyond the obstacle and the element ricochets without penetrating the obstacle as shown in Figure 5.2.29.



Figure 5.2.29 - At small angles between the velocity vector and the plane of the obstacle, hull fragments do not penetrate beyond the obstacle and ricochet occurs

Areas of high density of ready-to-use destruction elements

The presence of the maximum fragmentation field density region of the 9H314M warhead ("scalpel") and its parameters have been confirmed experimentally.

⁹² PART 2. Exhibit B.4. Specific experimental studies to assess piercing action of ready-made projectiles.

The results of the conducted static tests confirm the formation of a dense fragment flow - the coincidence in space of the area of maximum concentration of the number of fragments with the area of their maximum velocity.⁹³ That is, the combination in space of the three most important components: the number of fragments, their total mass and velocity - the area of maximum kinetic energy of the killing field, which is called the "scalpel".

The results obtained during the second experiment allow us to conclude that when the warhead 9H314M of a BUK missile is detonated under the conditions of the DSB Report, a dense stream of projectiles penetrates the cockpit structure through. This is confirmed by the video and photographic material presented in the Corporation Report (2016)⁹⁴ and Exhibit B.3.

It is the "scalpel" that pierces through the structure of the aircraft and causes the most damage to the aircraft's interior.

An example of inside-out punctures on the starboard side of an IL-86 target aircraft is shown in Figure 5.2.30.



Figure 5.2.30 - Examples of through-hole exit punctures ("inside-out") on the starboard side of the IL-86 target aircraft

A dense stream of projectiles penetrating the aircraft hull successively overcome at least three to five combined dispersed obstacles in varying combinations (elements of the outer skin of the aircraft on the port side and/or roof; thermal insulation and decorative panels of the port side and/or roof; panels or cabinets of equipment on the port side or roof; cockpit floor, including longitudinal

⁹³ PART 2: Exhibit B.2.2.

⁹⁴ Report on the conduct of a full-scale experiment, pages75-88; 149-157. 1

or transverse force components; panels or cabinets with equipment on the starboard side or under the cockpit floor; thermal insulation and decorative panels on the starboard side or underside; elements of the external skin of the aircraft on the starboard side or underside of the aircraft).⁹⁵

Also, the results of the experiment confirmed the coincidence of the calculated model of the impact of the dense flux of the preformed fragments with the actual experimental result.⁹⁶

Accordingly, the use of a methodology to determine the orientation of the missile relative to the aircraft structure is justified, as the methodology has experimental validation and acceptable accuracy.

As noted in paragraph 5.1.2.9 of this report, the damage study of the Boeing 777 found that the distribution of fragmentation damage density coincides with the areas and directions of perforation and destruction of the Boeing 777 airframe, cockpit floor and the areas of "inside-out" exit fragmentation damage (Figure 5.2.31).

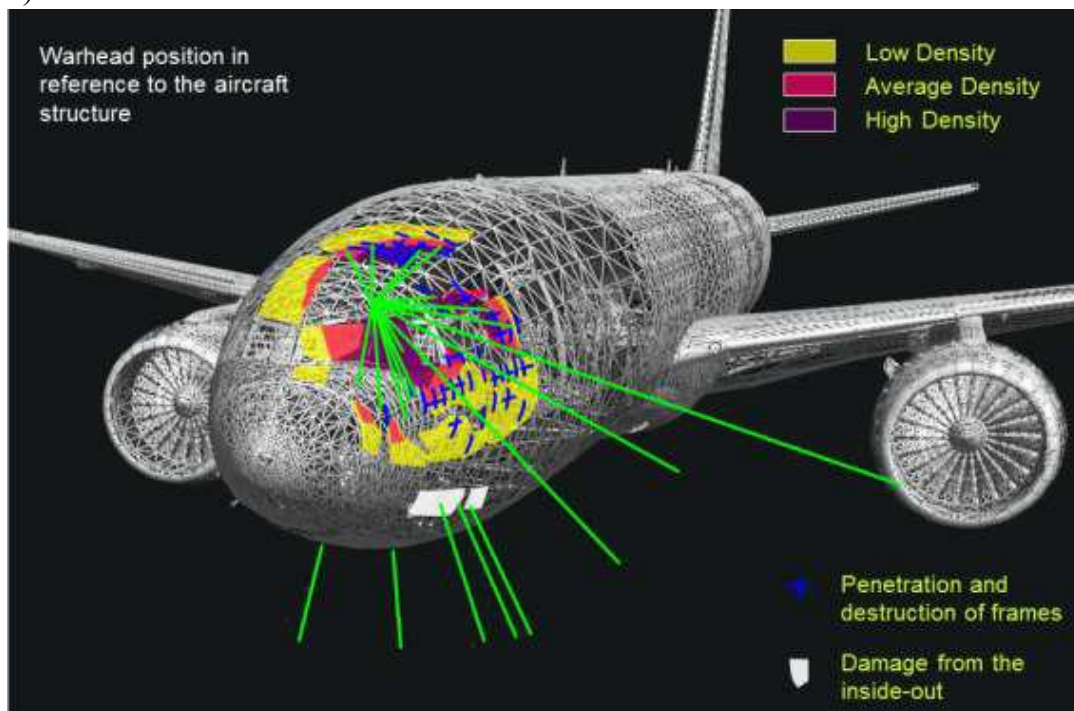


Figure 5.2.31 - Fragmentation damage density distribution coincides with the areas and directions of perforation and fracture of the Boeing 777 airframe elements

The essence of the method for determining the orientation of a missile relative to an aircraft at the moment of a warhead explosion is to find the best match between the spatial position of the dense fragmentation flow under dynamic conditions and the observed pattern of perforation and destruction of the outer hull, structure, cockpit floor and exit holes on the studied debris.

⁹⁵ Report on the conduct of a full-scale experiment, pages90-107; 157.

⁹⁶ PART 2: Exhibit B.3, section "Piercing the Structure of the Aircraft (Target Aircraft) Through".

The result of the search is the best possible alignment of the 'scalpel' area with the damage model, taking into account the detonation point linking them.

Studies carried out by the Corporation's specialists on fragments of the roof, port side, transparency frame, cockpit floor and structure of the aircraft,⁹⁷ which were available for study, revealed evidence of compartment damage caused by the dense flow of debris and the resulting shock waves (aero-impact) on the Boeing 777 structure.

Exhibits A.3 and A.4 present several examples of damage corresponding to exposure to a dense fragmentation flow region where the fragmentation density was so high that the mechanical effects of the preformed fragments (number, mass, speed), together with the aerodynamic loads acting on the aircraft in flight, caused its structure to break or puncture through.

Such damage can be traced from the outside skin of the port side through the cockpit, including the floor - outwards (at the bottom of the port side).

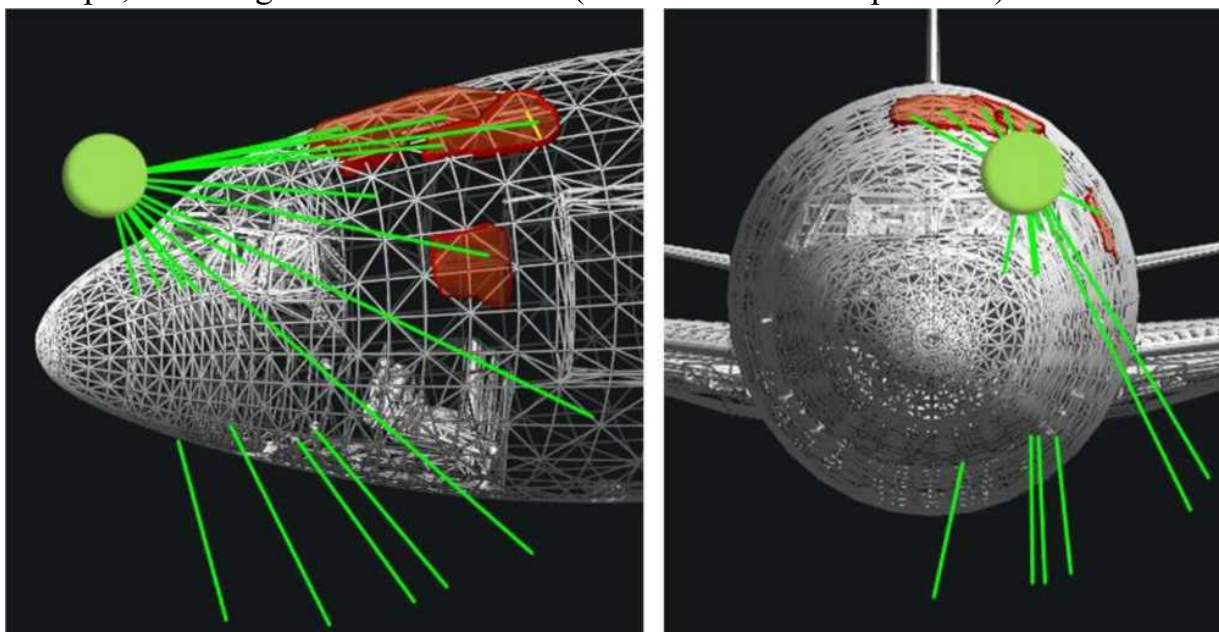


Figure 5.2.32. Visualization of approximate trajectories of ready-made projectiles in a dense fragmentation stream as it passes through or along the structure of the Boeing 777. The green ball indicates the verified detonation area, the green spokes show the directions of trajectories of preformed fragments in a dense fragmentation flow ("scalpel")

Using construction drawings and a digital model of the Boeing 777 aircraft, reference trajectories were constructed (Figure 5.2.32), which correspond to the directions of the most significant structural damage to the Boeing 777:

through-hole with exit punctures "inside-out";

penetration of two or three or more obstacles resulting in the destruction of fragments of the cockpit floor (including the transverse structural elements) along

⁹⁷ At the preliminary layout site in the large hangar at Gilze-Rijen airbase in February and May 2015.

the port side;

penetration of two or more barriers resulting in failure (by perforation) of the force mainframe along the left side of the roof and the port side;

Coincidence of dense fragmentation flow traces along the outer skin (ricochets) with areas of continuous failure of the bulkheads behind them.

The best results for matching the spatial position of the dense fragmentation flux with the reference trajectories were obtained for values of the horizontal angle of intersection of the missile with the aircraft's construction axis ranging from -66° to -74° .

Further confirmation of the range of angles of orientation of the missile relative to the aircraft (in terms of the position of the dense fragmentation stream and its effect on the aircraft structure) was obtained in the first full-scale experiment conducted under Corporation conditions - the "collision course" version.



Figure 5.2.33 - Distribution of target coverage density combined with Boeing 777 contour across the STA 220.5 level cross section

By aligning the target layout with the aircraft structure cross sections, taking into account the detonation point corrections adopted for safety conditions, confirmation was obtained that the direction of the dense fragmentation flow along the left side of the roof and the port side.

The highest fragmentation flux density is on the left side of the cockpit roof, the top and centre of the port side, the left side of the cockpit floor, as well as the area of "inside-out" exit holes at the bottom of the port side below the cockpit commander's transparency (Figure 5.2.33).

For the range of warhead orientation angles determined by this method (-66 degrees to -74 degrees), mapping criterion #5 (matching the nature of the damage from to the structure by dense fragmentation flow) and #8 (damage to the left wing plane and the left engine of the PTE) as specified in subsection 5.1.4 are best met.

In view of the destruction of the aircraft structure by the dense stream of projectiles ("scalpel") objectively observed on the available Boeing 777 fragments, the version that the aircraft was hit by a BUK missile can only be considered on a "collision course".

The best results for matching the missile's orientation to the aircraft at the moment of warhead detonation with the spatial position of the dense fragmentation stream are obtained for values of the horizontal angle of intersection of the missile with the aircraft's structural axis in the range of -66° to -74° .

5.2.4.4. Matching degree of blast effect of the 9H314M warhead

Data recorded by the Boeing 777's parametric recorder at the time of its termination at 13:20:03:

height: 32,998 ft;

instrument speed: 293 knots;

magnetic heading: 115°;

drift angle: minus 4°.

Weather: wind direction: 219°;

wind speed: 36 knots;

ambient temperature: minus 44°C.

For these conditions, the effective high-explosive range of the 9H314M warhead of a BUK missile is about 3.5m.

It is known from the theory of anti-aircraft missile firing that the effectiveness of the shock wave on an airborne target depends not only on the altitude, but also on the geometric shape of the warhead, the direction of flight of the target relative to the missile and their final mutual velocity. At high missile velocities, the initial blast pressure could be two times higher than for the same explosive charge (HE) under static conditions.⁹⁸ The combined effect of the PM geometry and final velocity can result in a difference of more than 2.5 times in the pressure maximum of the blast wave front (depending on the direction).

Similar conclusions were reached by the Dutch experts from TNO. Annex Z of the DSB Final Report⁹⁹ shows the simulation calculations for a warhead detonation at an altitude of 10,000 m at a final velocity of 600 m/s.

TNO calculations show that 0.91 ms after the explosion, when the blast front reached a range of 3.0-3.3 metres, the difference in maximum pressure depending on direction is more than 2.3-2.6 times.

For example, the pressure peak in the direction perpendicular to the missile's axis (radial) is about 1,400 kPa and in the 45° downwind direction (45°) 600 kPa, which significantly affects the distribution of blast damage.

Structural damage to the Boeing 777 from near blast factors is presented in paragraph 5.1.3, which shows that deformation and fragmentation of the Boeing 777 structure (external skin and structure) has spread along the left side of the aircraft structure and reaches the level of bulkheads STA 287.5-STA 309.5. Damage along the port side has spread to more than 4 meters from the front border of damage - front hermetic bulkhead STA 132.5.

To assess the orientation of a warhead by the nature of the close blast damage, it is most important to examine the fragments closest to the point of blast and having surfaces oriented frontally to the direction of blast wave propagation.

⁹⁸ Neupokoev F.K. Anti-Aircraft Missile Firing. Pages 200-201.

⁹⁹ TNO Report 2015M10626. Numerical simulation of blast loading on Malaysia Airlines flight MH17 due to a warhead detonation.

Such a fragment that satisfies these requirements is the nose section of the Boeing 777, adjacent to the front bulkhead at the top (Figure 5.2.34).



Figure 5.2.34 - Fragment of the nose of a Boeing 777, adjacent to the front bulkhead from above (photo February, 2015)

There are several important facts that come to mind when assessing the blast effect:

Minor tearing of the bulkhead wall as well as the sheathing failure with deformation of the bulkhead flange to the left and below the fragment in question;

the anterior boundary of the shattered cover field runs along the rear of the fragment (shatter action is observed on transparency remnants), with no residual macro deformation of the glass and its destruction is due to shattering perforation;

No noticeable permanent deformation of the left-hand windscreen wiper close to the point of detonation;

the remaining surface of the fragment before transparency shows only clearly distinguishable traces of close blast products: microcratering, thermal oxidation and soot (Figure 5.2.35).



Figure 5.2.35 - Most of the fragment shows only clearly visible traces of close blast products: microcratification, thermal oxidation and soot (photograph February 2015)

Thus, despite the close blast (not more than 2.0 m from the fragment), the high-explosive effect on this fragment was very low and did not exceed the critical (destructive) value with respect to the fuselage front structure in the cockpit area.

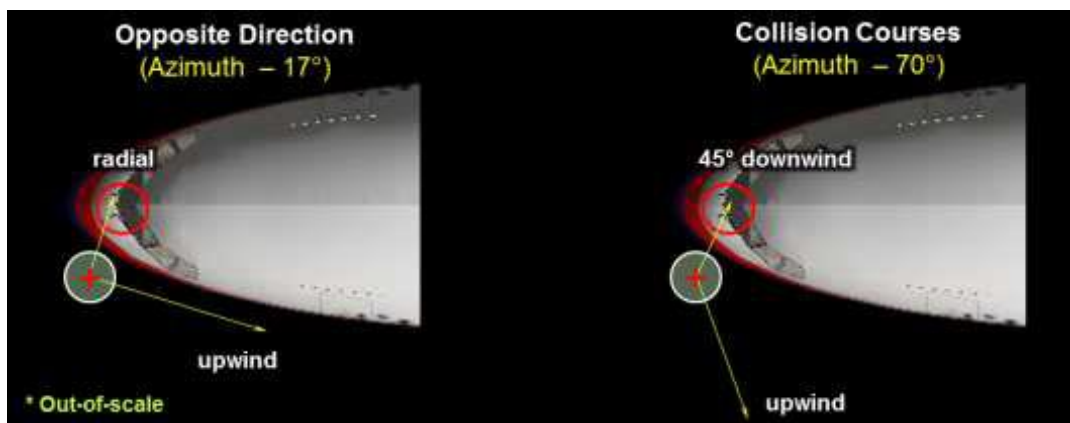


Figure 5.2.36 - Comparison of impact conditions on a fragment of Boeing 777 nose section adjacent to the front bulkhead from above: left - "on an oncoming course"; right - "on a collision course"

Figure 5.2.36 shows a diagram derived from the calculations, showing the blast wave impact directions from the verified detonation region for the two versions of the 9M38 missile impact considered.

As can be seen from the diagram, the preservation of a fragment located at a short (no more than 2.0 m) distance from the detonation point of the 9M38 warhead can only be explained for the "collision course" version.¹⁰⁰

Calculations have shown that if the explosion occurred within 1.6-2.0 m, the most likely conditions are that the missile crosses the course of the aircraft between -68° and -72° (Criterion #7).

The non-compliance of the landmine impact of the basic DSB version ("opposite course") was also demonstrated in the Air Force Central Research Institute contribution to the joint work of the international expert group.¹⁰¹

The in-situ tests resulted in experimental confirmation of the non-compliance of the blast effect of the 9H314M warhead with the basic DSB ("opposite course") version. A comparative analysis of the damage to the IL-86 and Boeing 777 (MH17) target aircraft from close blast factors is given in Exhibit A.4.3.

The main conclusion of the studies is that the orientation of the warhead, under the conditions of the IL-86 target aircraft experiment (according to the DSB version an opposite course", i.e. about -17°), is not consistent with the spread and nature of damage to MH17 from close blast factors.

Thus, as a result of calculations confirmed by field tests, it is established that the nature of damage from close blast factors on the Boeing 777 structure is not consistent with the "opposite course" version (test results significantly exceed the level of damage observed on the MH17 fragments).

The angle of intersection of the longitudinal axes of the aircraft and missile in the horizontal plane at which it is possible to consider a version of aircraft damage as a result of a near missile explosion was more than -50° , and the most probable conditions were that the missile crossed the aircraft course between -68° and -72° .

¹⁰⁰ PART 2: Exhibit A.4.3 Dynamic conditions, pages 50-52.

¹⁰¹ Calculation Results of Warhead Location at the Moment of Detonation.

5.2.4.5. Verification of the results obtained on the basis of in-flight control data

An analysis of the objective control materials recorded by the Utes-T air-route radar complex located at the Ust-Donetsk radar position showed that in the primary data registration file "14-07-17.kt" for the period from 13:02 to 13:32 UTC 17.07.2014, no markings from the weapon were registered. This indicates the absence of an object moving towards the Boeing 777 "on an oncoming course" (according to the DSB) in the observation space.

In order to confirm the technical characteristics of Utes-T, a full-scale experiment (flight test of the Utes-T ARRC) was conducted, approximating as closely as possible to the conditions at the time of the crash.¹⁰² Main results:

1. The radar detection capability of Utes-T has been confirmed to match the radar signature of the 9M38 missile. A missile flying at altitudes above the radio horizon can be detected by the primary radar at ranges greater than 200 km.

2. Utes-T 's ability to detect and track supersonic objects without interference has been confirmed (Figure 5.2.37).



Figure 5.2.37 - Supersonic Air Object Escort

3. The conditions under which the absence of primary marks from the missile in the logging file is possible have been theoretically determined and practically confirmed during a series of overflights.

The main conclusion: the unregistered radar-guided BUK missile **could only approach the Boeing 777 from a southerly direction - "on a collision course"**, which rules out collision course angles in the horizontal plane of less than -60° .

¹⁰² Report "On conducting a flight check of the Utes-T track radar complex located at the Ust-Donetsk track radar position of the Rostov zonal centre of the Unified Air Traffic Management System of the Russian Federation", 2019.

5.2.4.6. Compliance with the radio trigger algorithm

The inconsistency between the "opposite direction" version and the logic of the non-contact fuse was first brought to the attention of the Dutch experts in a letter sent to the DSB in July 2015.¹⁰³

Additionally, the inconsistency of the missile's detonation point area for the NLR/DSB version ("opposite direction") was also highlighted in a presentation given during the August 2015 expert panel (Gilze-Rijen, Netherlands).¹⁰⁴

If the missile were to approach on a head-on course (according to the Dutch experts), the point of detonation of the BUK missiles would have to shift at least 3.0-5.0 meters from the nose of the aircraft towards the keel (vertical stabilizer). The damage to the Boeing 777 would have been of a fundamentally different nature.

This non-contact fuzing feature is not unique to the 9M38 or 9M38M1 BUK missiles.

A similar principle underpins the algorithms of most surface-to-air missiles.



Figure 5.2.38 - Features of the algorithms incorporated in the non-contact fuse of BUK missiles (9M38 or 9M38M1) are not unique. A similar principle underpins the algorithms of most surface-to-air missiles

¹⁰³ Letter No. 01-09/548k dated 29.07.2015. Annex A, pages 9-10.

¹⁰⁴ Findings of Expert Assessments on MH17 Accident.

As an example, Figure 5.2.38 shows still images from tests of the Patriot and MEADS anti-aircraft guided missiles in service with NATO countries. As can be seen from the pictures in the "opposite course" picture, the missile is detonated near the centerline (MEADS) or behind it (Patriot), that is, at least 5 meters from the tip of the nose of the target aircraft.

In the verified detonation region, the initiation of a 9M38 BUK missile could only take place if the projection of the angle between the velocity vectors of the missile and the aircraft on the horizontal plane was at least -50° .

The nature of the damage objectively observed on the Boeing 777 fragments, as well as the location of the verified detonation point area when considering the "opposite course" version, contradict the operating algorithm of the non-contact fuse of the BUK missiles.

5.2.5 Orientation of the warhead relative to the aircraft structure

To determine the optimum orientation of the warhead relative to the aircraft structure at the moment of detonation, methodologies were used that took into account the appropriateness of all the main factors of lethal (fragmentation and blast) effects of the anti-aircraft guided missile warhead.

In the techniques, the orientation of the warhead was optimised to match the main factors of the field of attack, which include:

the field boundary of the fragmentation cover;

the distribution of the density of the impact of the projectiles;

Destruction of the aircraft's power kit by a dense stream of projectile elements ("scalpel");

the degree of the blast effect of the warhead, etc.

The results obtained by the different methods are summarised in Table 5.2.1.

Table 5.2.1 - Orientation of the warhead to the aircraft structure

The method	Value range, deg.	Best match, deg.
Conformity of the boundaries of the field of cover	-50 to -62	-55
Matching impact density distribution	-62 to -68	-66
Exposure to a dense stream of projectiles ("scalpel")	-66 to -74	
Blast effect of the warhead	-68 to -72	

In addition, the missile's orientation relative to the aircraft was checked for consistency with the objective control material and the fuzzer algorithm. The result of this correspondence check ensures that the missile does not cross the course of the Boeing 777 in a horizontal plane less than $-50^{\circ} \dots -60^{\circ}$.

As a result of determining the optimum orientation of the warhead relative to the aircraft structure at the moment of detonation, based on a comprehensive application of techniques that take into account the correspondence of the main factors of the warhead's impact, as well as the results of experiments and special studies conducted by specialists of Almaz-Antey Corporation, the following conclusions were drawn. It is most likely that the missile and the aircraft met on collision courses:

in the horizontal plane - 72^{+2}_{-10} deg;

in the vertical plane - 22^{+4}_{-3} deg.

For the specified range of orientation angles of the warhead, all the comparison criteria specified in paragraph 5.1.4 are best fulfilled.

Taking into account the actual boundaries of the fragmentation cover, the distribution of fragmentation damage to the roof and the area of destruction of the structure, objectively observed on the available fragments of the Boeing 777, the version of an aircraft hit by a BUK missile can be considered only on a "collision course", i.e. at an angle of at least -50°..-60°.

Comparing results

The results obtained by Almaz-Antey were compared with those of the Dutch specialists.

Various reports by Dutch experts during the DSB-led technical investigation in 2015 applied methodologies related to only one factor in the remote operation of combat units - matching the boundaries of the fragmentation field:

- NLR (light damage model);
- TNO (ready-to-use destruction model).

The results are summarised in Table 5.2.2.

Table 5.2.2 - Overview of previously submitted calculations of warhead orientation in relation to aircraft design

Source	The method	Azimuth (Az) , deg.	
		Value range	Best match
Draft Final Report NLR	Conformity of the boundaries of the field of cover		-17
Final Report NLR ¹⁰⁵ ; TNO	Conformity of the boundaries of the field of cover	-17 to -35	-20; -27

The results obtained by the NLR and TNO in the DSB technical investigation using the field-of-cover matching methodology cannot be used for comparison.

This is because these results were obtained using all three components of Best Match (damage model (#1), warhead model (#2)¹⁰⁶ and the detonation point linking them (#3)¹⁰⁷), whose parameters were pre-agreed and adapted to fully match the pre-defined version - "counter course".^{108, 109}

The non-compliance of all three components included in the "Best Match" DSB Report has been confirmed by subsequent studies, field experiments and tests.

¹⁰⁵ NLR report (Annex X). 6.17 Matching modelled and observed fragmentation damage, p.56.

¹⁰⁶ TNO report. 4.3. Warhead, p.13.

¹⁰⁷ TNO report. 5.1. Variation of warhead position and orientation, p.17.

¹⁰⁸ TNO report. 4.3.2. Warhead implementation (designs), p.14-15.

¹⁰⁹ TNO report. 4.2. Closing velocities, p.13.

Damage model (no. 1)

The damage model used as a 'benchmark' takes into account less than half of the damage to the port side skin of the Boeing 777. A strip width of about 2.24 m is taken into account, while the actual damage to the upper port side is more than 5 m away from the forward boundary of the field of cover. Damage to the airframe, interior, left wing plane and left engine are not accounted for, nor is damage caused by a landmine.¹¹⁰

Model DSB warhead (No. 2)

In the warhead model used as a "benchmark" instead of the data transmitted by the designer and reflected in the design and technical documentation, confirmed by state and inspection test certificates, the Dutch experts selected a set of parameters that are suitable precisely to support the investigation version.¹¹¹

Without explaining the final reasons for the rejection of the data transmitted by the manufacturer, the Dutch experts chose "Model II / Design II" as the "reference" of the warhead in the Final Report materials. In this model, **only the correct name "9H314M" and a picture of this very warhead were used** out of the whole set of technical specifications based on the real technical documentation and test results transmitted and demonstrated by the Russian side.

The "reference" model warhead accounted for about 1/3 of the fragmentation kill field and less than 60% of the fragmentation angles, as confirmed by field tests.¹¹²

All other parameters of the "benchmark" warhead were selected for Best Match in order to justify the main "9M38-series missile on an oncoming course" theory that formed the basis of the Final Report conclusions.¹¹³

Detonation point (no. 3)

The technical investigation material shows that the Dutch specialists selected many coordinate values for the detonation points - different for each of the simulations. Only one parameter remained unchanged: the 'oncoming course'.

As a result, for different variants of the warhead models (Model Ia, Model IIb), which at different stages of the technical investigation were taken as "Best Match", completely different coordinates of the detonation area were obtained, where the distance from the outer skin of the aircraft hull varied in wide ranges. For example, on the Y co-ordinate from 4.0 metres in February to 2.0 metres in October 2015, which is contrary to the objectively observed damage and which in fact cannot be.¹¹⁴

The distance from the Boeing 777 aircraft structure of the volume containing

¹¹⁰ PART 2: Exhibit G, Exhibit G.1.

¹¹¹ TNO report. Damage reconstruction due to impact of high-energy particles on Malaysia Airlines flight MH17.

¹¹² PART 2: Exhibit B.2.

¹¹³ PART 2: Exhibit G, Exhibit G.2.

¹¹⁴ PART 2: Exhibit G, Exhibit G.3.

the coordinates of all the solution options for the detonation point area, obtained using conventional methods (including trace studies) based on objectively observed damage at the boundaries of the fragment cloud, differs from the results from the DSB Report by a factor of two or more.

Exhibit G.3 shows that using verified data on BUK missiles and their warheads, aircraft structural fragments affecting the result,¹¹⁵ and the combined use of techniques to calculate the final position of the missile relative to the aircraft at the time of detonation, the results come close to those of the Almaz-Antey Corporation.

¹¹⁵ PART 2: Exhibit G, Exhibit G.2.

5.3 Determining the likely launch area

The methodology for calculating the likely launch area is based on a feature of the 9M38 surface-to-air guided missile guidance system used in the BUK surface-to-air missile system (SAM).

This feature consists in the fact that once the radar homing head has locked onto the target, the BUK missile is guided to the target using the proportional navigation method.

The essence of the method is that the flight of the missile to the rendezvous point with the target in the homing section follows a trajectory at each point of which the angular velocity of the missile's velocity vector remains proportional to the angular velocity of the missile-target line.¹¹⁶

Accordingly, with proportional navigation, if the aerial target moves uniformly and straightly at the same altitude, the missile's trajectory in the horizontal plane is almost straight.

target. Proportional-navigation guidance systems use the target tracking information obtained from the seeker, to steer the missile directly towards the collision point with the target. If the target does not change its direction or velocity, the missile will follow a more or less straight path towards this collision point.

Figure 5.3.1 - Features of Proportional Convergence Approach Missiles (Final Report, p. 134)

These features were taken into account by Dutch experts in the initial stages of the DSB technical investigation.^{117, 118, 119}

Similar principles also underpin the calculations of Ukrainian specialists¹²⁰ and those of the Almaz-Antey Corporation.

This methodology is fully acceptable because the Boeing 777 flew on a straight trajectory with constant bearing, constant speed and constant altitude, as confirmed by the Flight Data Recorders (FDR) of MH17.¹²¹

Therefore, for the calculation of the launch area, the most important is to determine the relative position in space of the missile relative to the aircraft (encounter conditions) at the time of detonation of the warhead, which indicate the direction to the intended launch area, as well as the final velocity of the missile, which determine the distance of the launch area from the point of detonation of the warhead.

¹¹⁶ Neupokoev F.K. Anti-Aircraft Missile Firing, p. 108. 108.

¹¹⁷ Draft Final Report. 3.4.9 BUK surface to air weapon system, p.114; 5.4.4 BUK missile, (NLR Appendix), p.319.

¹¹⁸ NLR report (Appendix X). 6.6 BUK missile, p.46-47.

¹¹⁹ Final Report. BUK operating characteristics, p.134.

¹²⁰ Results of examination of causes of MH17 crash over the territory of Ukraine 17.07.2014. 10-12.08.2015, Gilze.

¹²¹ Submitted by the DSB - Preliminary Report and Final Report.

5.3.1. Missile flight model

5.3.1.1. The method of guiding a BUK missile

The 9M38 and 9M38M1 missiles use a combined guidance method: inertial guidance¹²² in the initial guidance section and semi-active homing in the final trajectory section.

Targeting begins with the azimuthal turn of the launcher rails in the direction of the target (the pre-emptive rendezvous point of the missile with the target).

The rocket autopilot in pre-launch mode accelerates the gyro motors of the sensing elements to stabilise the missile on the launch pad in relation to the launch line.¹²³

After the missile leaves the launcher, it begins its movement along the firing line (in the direction of the preemptive point). The missile is controlled and the angular and Doppler guidance of the radar homing head (RGH) before the target is acquired by the onboard computer, with or without the use of a radio correction line (RLC).¹²⁴

For missiles launched from a self-propelled firing system (TELAR), the RGS captures the signal reflected from the target after the missile leaves the launcher during its flight.

For a large airborne object with high radar visibility (Boeing 777), this means that almost after launch, the missile's RGS will carry out a target acquisition.

In the absence of interference, the homing of the missile to the target is done by the signal reflected from the target. The illumination of the target, necessary for semi-active homing of the missile, is performed by a ground-based microwave transmitter (illumination station) located on the self-propelled firing system (TELAR).

After the RGS captures the target, the BUK missile is guided to the target using the proportional navigation method.

¹²² With radio correction capability for effective targeting of manoeuvring missiles.

¹²³ In march mode, after receiving commands from the rocket control unit, the autopilot controls the missile according to the commands generated by the rocket control unit and stabilises the missile in its roll.

¹²⁴ Radio-correction mode is not used when firing the third rocket of the salvo and when firing from the launcher. the loader.

5.3.1.2. A model of the Almaz-Antey Corporation's BUK missile

When modelling the trajectories of the 9M38 and 9M38M1 missiles, Almaz-Antey Corporation specialists used a software package based on the combat algorithms described in the design and technical documentation for these missiles.

The Manned Missile Guidance Model (MPGM) is part of this system. The SAM model consists of an on-board hardware operation unit, including a remote fuse, radar homing head, autopilot, steering drives, and the SAM flight dynamics unit, which is most important in terms of calculating the possible launch area.

The missile flight dynamics block calculates the full state vector (coordinates of the centre of mass, pitch, roll and yaw angles, velocities and accelerations of the three axes in the coupled and velocity coordinate systems) at each instant of time.

The calculation takes into account all relevant factors, including the aerodynamic characteristics of SAMs, variations in air rudder effectiveness under different conditions, time delays in the development of control commands, and others.

The validity of the SAM model calculations is confirmed by the convergence of the modelling results with the out-of-track measurements and telemetry information obtained from the actual launches of the 9M38 and 9M38M1 missiles.

An analysis of the available material shows that the results obtained from the respective rocket flight models used by independent specialists to calculate the possible launch area are broadly consistent with the Corporation's calculations: using the agreed input data, the calculated areas and the final velocities of the rocket are the same.

Trajectories and speeds

To illustrate the fit of the Almaz-Antey models, Figure 5.3.2 shows the projected trajectories of the 9M38 and 9M38M1 missiles when simulating guidance on a uniformly and straightly moving target at an altitude of 10 km. The coordinates within the range of input data used in the technical investigation (horizontal range 27 km; horizontal angle between -35° and -37°) are taken as the launch point.

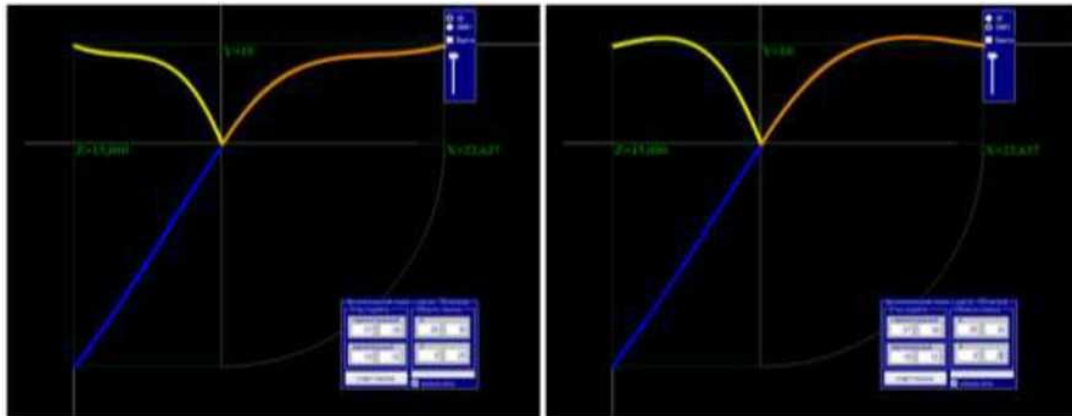


Figure 5.3.2 - Projected trajectories of 9M38 (left) and 9M38M1 (right) missiles

In this case, the guidance process is calculated with the Boeing 777 course line in mind, and the difference between the aircraft's velocity vector and its longitudinal axis, due to the drift angle and local magnetic declination, is added only to the final state of the missile.

The end state of the 9M38 and 9M38M1 missiles (at the time of detonation of the warhead) have some differences:

1. The 9M38 missile:
 - azimuth (horizontal angle), deg -36,2
 - angle of location (vertical angle), deg 11,7
 - horizontal range, km 27,2
 - rocket velocity, m/s 595.8
2. The 9M38M1 missile:
 - azimuth (horizontal angle), deg -36,3
 - angle of location (vertical angle), deg -9,6
 - horizontal range, km 27,2
 - rocket velocity, m/s 603.7

In this case, in the horizontal plane, the projections of the missile trajectories (blue lines) are almost straight lines, which is a clear confirmation that for calculating the launch area, the most important thing is to determine the relative position in space of the missile relative to the aircraft at the moment of detonation of the warhead, which indicates the direction to the intended launch area.

Thus, in the horizontal plane, the trajectory of a BUK missile aiming at a non-maneuvering target is practically a straight line. Accordingly, the final state of the missile in the horizontal plane at the time of detonation of the warhead is the most important input parameter for calculating a possible launch area.

The terminal velocity of the missiles at a horizontal range of about 27 km is also approximately the same and is ~ 596 m/s and ~604 m/s for the 9M38 and 9M38M1 missiles respectively. These data are consistent with the results obtained by the Dutch experts in the initial phase of the technical investigation.¹²⁵

The largest difference in trajectories is in the vertical plane (at an altitude of 10 km): the angle of departure for the 9M38 is positive, in this case about 12 degrees, while for the 9M38M1 in this case the pitch is negative, about "minus" 10 degrees.

Figure 5.3.2 shows the projected trajectories of the 9M38 and 9M398M1 missiles in the vertical plane with the yellow and orange lines.

The results of the comparative modelling show that using the same "missile end state" input data (aircraft-missile encounter conditions), the resulting parameters of the BUK missile trajectories, their velocities and possible launch areas are the same.

Based on the similarity between the results obtained with the Almaz-Antey SAM and the independent missile flight model for the same missile end states, the model can be considered validated.

¹²⁵ Final Report (Annex Y). TNO report. 4.2. Closing velocities, Table 4.1, p.13/25.

5.3.2. Possible launch area

5.3.2.1 Calculation to identify the possible launch area

The inputs for calculating the possible launch area are the conditions of the aircraft-missile encounter - their relative position in space¹²⁶ and the final velocity of the missile at the time of detonation.

The position in space of the missile relative to the aircraft:

- in the horizontal plane – 72^{+2}_{-10} deg;
- in the vertical plane – 22^{+4}_{-3} deg.

The missile's final velocity range, corresponding to the "cross-course" rendezvous conditions, is 620 to 730 m/s.

The launch area, which was calculated in October 2015, even before the identification of the missile model, was shown in a presentation at the Almaz-Antey Corporation press conference.¹²⁷ This launch area, calculated for two types of missiles, is shown in Figure 5.3.3.

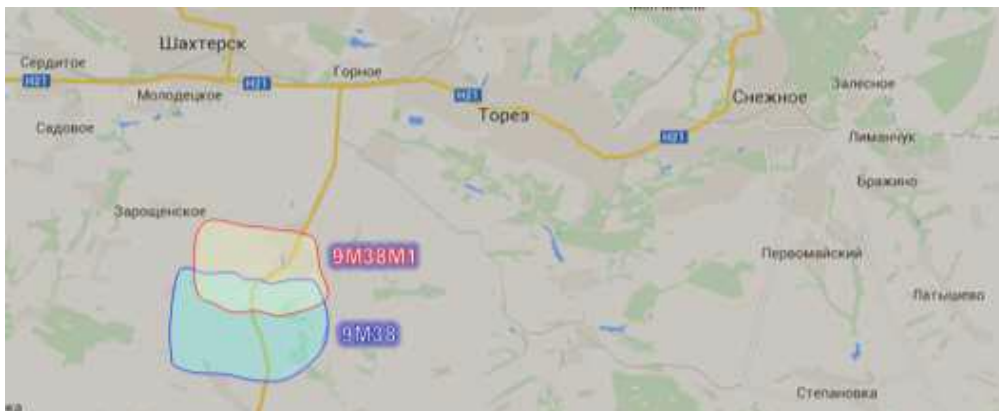


Figure 5.3.3 - Possible launch area: for 9M38M1 missiles (red area); for 9M38 missiles (blue area)

The coordinates corresponding to a possible missile launch area are given in Table 5.3.1.

Table 5.3.1 - Coordinates of possible launch area

1	47.984290	38.482380	47° 59' 3.444" N	38° 28' 56.568" E
2	47.979410	38.535590	47° 58' 45.876" N	38° 32' 8.124" E
3	47.967230	38.467960	47° 58' 2.028" N	38° 28' 4.656" E
4	47.961720	38.536280	47° 57' 42.192" N	38° 32' 10.608" E
5	47.932970	38.465210	47° 55' 58.692" N	38° 27' 54.756" E
6	47.927220	38.530790	47° 55' 37.992" N	38° 31' 50.844" E

¹²⁶ Taking into account drift angles, attack angles and associated magnetic declination.

¹²⁷ "Results of a field experiment to assess the causes of the crash of MH17", October 2015.

By examining the materials relating to the rocket fragments recovered, which have unique serial numbers, the serial number of the item in which the fragments were found was established.

This product is an older modification of the missile, the 9M38, produced in late 1986.¹²⁸ Without the "M1" index, which can definitely be confirmed by relevant technical documentation.

Accordingly, the most likely launch area for the 9M38 missile is limited to points 3, 4, 5 and 6 with their respective coordinates.

5.3.2.2. Comparative analysis of calculations to identify the possible launch area

A comparison will be made for variants of the launch area calculation carried out by Dutch experts.

Missile flight model and estimated launch area NLR

During the DSB technical investigation, calculations of the possible launch area were carried out by experts from the Netherlands National Laboratory for Aeronautics and Space Research (NLR).^{129, 130}

There is no detailed description of the flight models of the NLR missile in the DSB report materials, but it is stated that the Dutch specialists took into account the peculiarities of the guidance method of the BUK missiles. Therefore, the validity of the model can only be assessed from the results obtained.

The initial modelling carried out by NLR was announced during a joint team effort in Gilze-Rijen (Kingdom of the Netherlands) in February 2015.

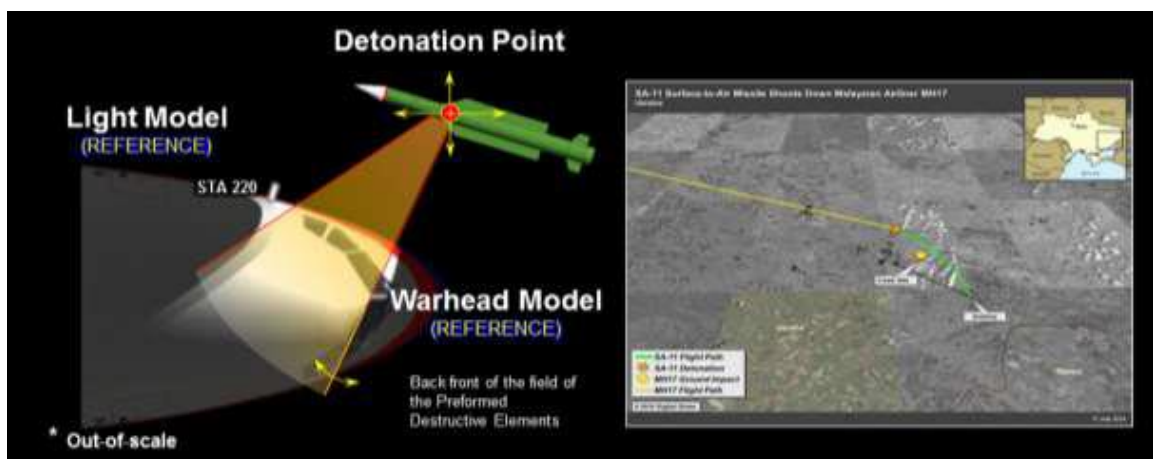


Figure 5.3.4 - Model Ia - First "Best Match" option (NLR, February 2015)

In NLR's first version (Model Ia), all three "Best Match" components were matched so well that an exact "almost pixel-for-pixel" match was obtained for the

¹²⁸ PART 2: Exhibit E: Fragments of the 9M38 missile.

¹²⁹ As follows from the caption to Figure 47 of the Draft DSB Final Report (Figure 47, p.132).

¹³⁰ As follows from the caption to figure 62 of the DSB report (Final Report. Figure 62, p.144).

figure published on the Ukrainian embassy website (Figure 5.3.4).¹³¹

As a result of the resulting matching of the selected parameters with the original "Best Match" version, the NLR experts calculated the first₂ version of the possible missile launch area. This 250 km area in the Draft Final Report was shown in Figure 47, page 132.

After abandoning the original "benchmark" warhead and detonation point, a second possible missile launch area was calculated by NLR experts on the basis of the new "Best Match" version, which formed the basis of the findings of the DSB Report on the possible missile launch area "from eastern Ukraine".¹³²

This 320 km² area was represented in the DSB (Final Report) by Figure 62 (page 144)¹³³, and the conclusions drawn from it are presented on page 256.

The new location of the possible launch area has some differences from the one given in the Draft Report. For comparison, both variants of the possible missile launch area calculations are shown in Figure 5.3.5.

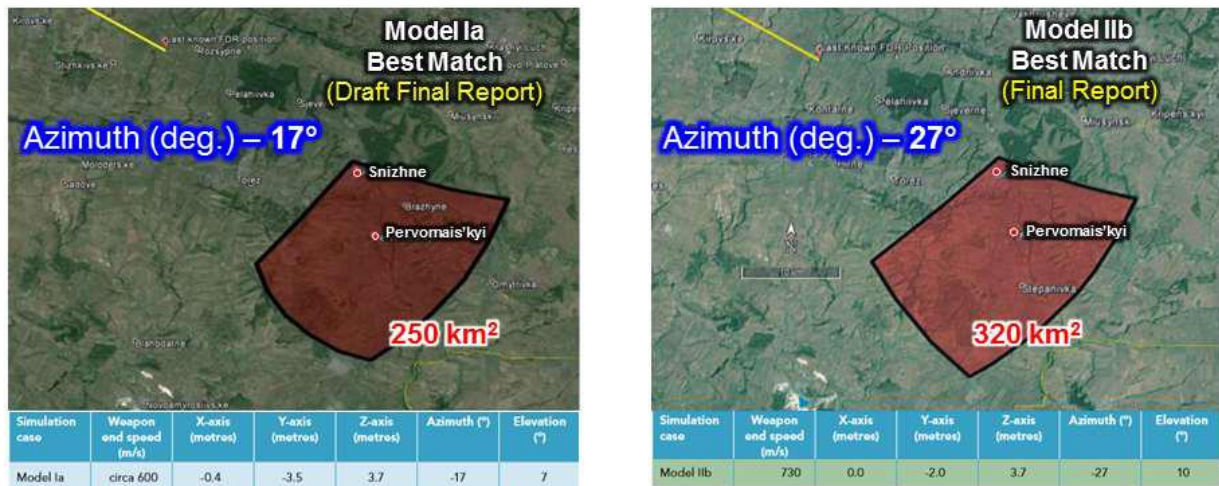


Figure 5.3.5 - Calculated missile launch areas by NLR experts for two different "Best Match" variants at 250 and 320 km

The comparison results show that the main difference between the two calculations is the significant increase, of more than 25%, in the area of this range from 250 to 320 km², which contradicts the technical characteristics of the BUK missiles. Moreover, compared to the initial calculations (February 2015), the NLR specialists had an opportunity to refine their "Missile Flight Model" using data provided in May-August 2015 by Ukrainian specialists and specialists of the Almaz-Antey Corporation.

¹³¹ The inconsistency of all three "Best Match" components underlying the findings of the DSB Report is given in Exhibit G.1. (PART 2. Exhibit G.1)

¹³² Final Report. 11. Missile flight parts, p.256.

¹³³ Visualisation of NLR fly out simulation results.

For example, the model demonstrated by Ukrainian specialists in August 2015 determined the launch area (less than 10 square kilometres) and the amount of allowable error in the missile approach angles in the horizontal plane within $\pm 2.5^\circ$.¹³⁴

According to the data provided by the specialists of Almaz-Antey Corporation, errors in approach angles when aiming the missile at a non-maneuvering aerodynamic target in the horizontal plane under specified conditions and normal autopilot operation amount to $\pm 4-6^\circ$.

The second important feature of the second version of NLR's calculations is that by changing the position of the missile axis relative to the aircraft in the horizontal plane in the second version of Best Match by 10 degrees (from -17° to -27°), the right upper bound of the calculated area has not changed. It again includes Snizhne, even though the probability of launching from this point is close to zero, given the parameters presented by the NLR in the new Best Match.

The retention of Snezhnoye as part of the "possible launch area" when the conditions of the missile's encounter with an aircraft change significantly (more than 18°)^{135,136} contradicts the claims made in the NLR material about the way this area is determined by the final conditions of the missile's orientation at the moment of detonation (due to the use of the proportional navigation method).^{137, 138, 139}

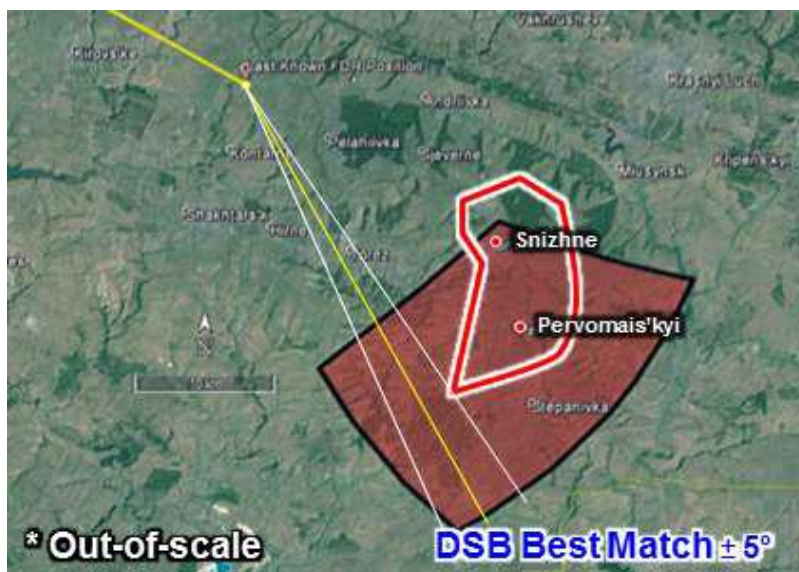


Figure 5.3.6 - "Refined Possible Launch Area" presented in the new NLR report has shifted north. "Best Match" value from Final Report

¹³⁴ Results of examination of causes of MH17 crash over the territory of Ukraine 17.07.2014. 10-12.08.2015, Gilze.

¹³⁵ In the second Best Match variant, the angle of intersection of the aircraft and missile axes in the horizontal plane increased by 10 degrees: from -17 to -27 .

¹³⁶ Taking into account the actual relative position in space of the aircraft and missile due to local magnetic declination (minimum 4 degrees) and the overestimated final velocity of the missile (an additional minimum 4 degrees).

¹³⁷ Draft Final Report. 3.4.9 BUK surface to air weapon system, p.114; 5.4.4 BUK missile, (NLR Appendix), p.319.

¹³⁸ NLR report (Appendix X). 6.6 BUK missile, p.46-47.

¹³⁹ Final Report. BUK operating characteristics, p.134.

[-27° with a tolerance of ±5° does not fall within the new "refined launch area"](#)

As a result of the calculation of the "refined probable launch area" in the new NLR report, a new 75 km² area is shown, the main feature of which is that the boundaries of the calculated launch area have shifted significantly northwards (Figure 5.3.6), compared to the Final Report.¹⁴⁰

Accordingly, the results obtained are radically different from those of the final DSB Report: the range of angles of direction to the "Last recorded FDR position" from the new "clarified area" is about 34° (-5° ±17°),¹⁴¹ that is in the range from "plus" 12° to "minus" 22° (instead of the range from "minus" 35° to "minus" 17° Final Report). This directly contradicts the results previously obtained by the Dutch experts during the technical investigation and reflected in the Final Report,¹⁴² including the results obtained directly by the NLR experts.¹⁴³

The new calculated area not only does not match the conclusions of the DSB "best fit" report obtained for -27° conditions,¹⁴⁴ but even taking into account errors of ±5 degree excludes these conditions (see Figure 5.3.6), i.e. **directly contradicts the results obtained** in the DSB-led technical investigation.

Thus, during the technical investigation, NLR specialists carried out calculations of the "likely launch area" three times using different models. The main feature of these calculations was that, despite changing the parameters of the warhead model, damage model, detonation point areas, and missile flight models, the calculated area always "included the town of Snizhne. In all cases, the "matching" was done by fitting the parameters of the warhead, damage model, and detonation region, as well as by fitting the parameters in the missile flight model.

[Alternate calculated launch area](#)

As shown in Exhibits E and G.3,¹⁴⁵ the most reliable from the range of initial conditions of the technical investigation documents is a horizontal angle of the missile crossing the longitudinal axis of the aircraft of at least -50°. The results show that when using "missile end state" input data (aircraft-missile encounter conditions), no contradicting the actual damage, the version of a launch from the area of Snezhnoye and Pervomayskoye settlements **is not confirmed**.

¹⁴⁰ An image of the new area is freely available (in open-source materials)

¹⁴¹ These values are obtained for the angles of intersection of the aircraft course line projection on the map taking into account the real position of the aircraft longitudinal axis in space, i.e. taking into account the local magnetic declination and the drift angle

¹⁴² Final Report. 3.8.3 Warhead simulation, p.140.

¹⁴³ NLR report (Appendix X). 6.17 Matching modelled and observed fragmentation damage, p.56.

¹⁴⁴ Final Report, p.140.

¹⁴⁵ PART 2: Exhibit F, Exhibit G.3.

Using the baseline not contradicting the actual damage to the Boeing 777 from fragmentation and high-explosive effects, and using the characteristics of the BUK missiles from the technical documentation, **the version of a BUK missile launched from the area of Snezhnoye and Pervomaisky settlements is not confirmed.**

5.4 Identification of weapon

As a result of the investigation of the combat damage on the Boeing 777 fragments, it was established that the aircraft was hit by a remote-controlled high-explosive warhead loaded with ready-to-use high-explosive fragments. The warhead exploded no more than 1.6-2.0 metres from the window of the cockpit on the left side.

The number of damage of all types from prefabricated and hulled destructioners is:

on fragments of the outer skin of the nose section of a Boeing 777 installed in a 3D reconstruction of about 350;¹⁴⁶

there are about 60 holes in the airframe elements, the position of which can be established with a high degree of accuracy;

more than 120 fragmentation injuries on the cockpit floor, interior and transverse structural elements of the cockpit floor;

The "inside-out" portside exit holes (punctures and non-pitch damage) are concentrated below the second portside window and distributed further along the portside;¹⁴⁷

The left wing and left engine have combined fragmentation damage, which includes through holes from prefabricated projectiles up to 14 mm in size.

Most of the high-energy objects that struck the aircraft moved predominantly along the longitudinal axis of the aircraft or at slight angles to it. The highest density of damage to the outer skin and the structure was recorded in the area of the windshield and the vent on the left side of the cockpit, and further along the port side and the upper left part of the aircraft roof. This is confirmed by the mutual location of fragments of the outer skin, the structure and the cockpit floor with maximum damage densities on the 3 D-reconstruction. Damage to the cockpit floor is concentrated along the port side, while damage to the power structure (bends) - on the left side of the roof and on the port side - is spread further than the outer skin damage.

In accordance with the missile manufacturer's technical documents (DNPP), it was established that both numbered fragments: the engine part marked "9D1318869032" and the nozzle part marked "9D131.05.000 No. 8.30.113" were installed in the 9M38 missile (without the "M1" index, i.e. an older modification) with the factory technical number "8868720".

¹⁴⁶ There are no "inside-out" exit punctures on the starboard side of the Boeing 777.

¹⁴⁷ About 70 more holes have been accounted for by Almaz-Antey specialists in the fragments that were not represented in the final 3D rendering.

The analysis showed that **the 9M38 missile** of the BUK system **could only be the cause of the** destruction of the aircraft in mid-air if it **encountered the aircraft "on a collision course"**.

This is confirmed by the actual boundaries of the fragmentation area, the direction of damage, the shape, number and density distribution of the holes to the outer skin, structure, floor and internal equipment of the cockpit, as well as the characteristics of the 9H314M warhead impact field confirmed experimentally.

When considering the conditions of the aircraft missile encounter "on an opposite course", the 9M38 missile could not be the cause of the crash of the Boeing 777. In this case, the nature of the damage to the starboard side and the structure does not correspond to the most important characteristics of the impact field - the density of the fragmentation field and the penetration effect of the flow of preformed projectiles produced by the detonation of the BUK warhead, and the location of the detonation point area contradicts the non-contact fuse algorithm.

In the "opposite direction" version, the aircraft was hit by another unidentified weapon with a high-explosive fragmentation warhead loaded with preformed fragments of one or two fractions.

6. Analysis of the results obtained

As a result of the research including calculations and modelling confirmed by a series of full-scale experiments and tests, specialists of Almaz-Antey Corporation have confirmed their conclusions, which were first announced in May 2015 during a meeting at Gilze-Rijen Air Base.

The essence of these conclusions is as follows:

1. If the crash of the Boeing 777 was caused by a BUK missile, it could only have happened "on a collision course" and it could only have been an older version of the missile, the 9M38.

2. Based on the results of the analysis of the full-scale experiment carried out under the conditions in the findings of the Dutch experts, the results of special studies of the penetration capability of projectiles, assessment of the damage to the outer skin, internal equipment and the structure of the Boeing 777, and the full-scale experiments involving the Utes-T ARRC, it was established that the DSB findings that the aircraft was hit by a 9M38M1 missile flying "in an opposite direction" were not confirmed.

3. If the Boeing 777 had been hit by a BUK missile with a 9H314M warhead "on an opposite direction", the damage pattern would have been radically different – the number and density of holes in the outer skin would have been 2-3 times greater than what is actually observed. The structure of the aircraft would have been penetrated through from the starboard side, and the outer skin of the cockpit would have many holes with a "butterfly" shape which is characteristic of "bowtie shaped" projectiles.¹⁴⁸

4. Calculations and experiments¹⁴⁹ proved that taking into account the detonation point area corresponding to the actual damage to the Boeing 777 and considering all the basic characteristics of the 9H314M warhead damage area, the version about the impact of BUK missiles can only be considered under the missile aircraft encounter conditions where the missile crosses the aircraft course in the horizontal plane with angles 72^{+2}_{-10} degrees.

5. The methodologies used by the Almaz-Antey Corporation specialists to calculate the missile launch areas are largely the same as those used by independent specialists. When the same source data are used, the calculation results for the main parameters are the same.

By making necessary adjustments to the source data for the aircraft damage model (fragments with a high density of damage) taking into account the fragmentation field boundary and the actual position of the aircraft in space (taking into account local magnetic declination), the possible launch area calculated according to the methodology of independent specialists will shift to the west, which

¹⁴⁸ Experiment in a combined target layout conducted on 07.10.2015.

¹⁴⁹ Shielded target experiment conducted on 31.07.2015.

is closer to the results of Almaz-Antey specialists' calculations.

Thus, the studies using adjusted source data in the models do not support the version of a missile launch from the area of Snezhnoye and Pervomaysky settlements.

6. BUK missiles launched from any of the three areas^{150, 151, 152} determined by calculations of specialists from the "Netherlands Air and Space Centre" (NLR) cannot approach an aircraft under actual encounter conditions that can explain the damage to the outer skin and airframe which is objectively observed in the airliner's fragments. This is confirmed by calculations made by the 9M38 and 9M38M1 missile (including the non-contact fuse) control system software and in-flight control data recorded by Utes-T ARRC.

7. The lack of complete objective data from metallurgical examinations and the mismatch between the weight and dimension characteristics of the fragments specified in the materials of the Dutch experts and the reference samples obtained during the tests do not allow for unequivocal identification of the type of warhead and weapon. This does not exclude the possibility that the aircraft was also hit by another, unspecified, weapon.

¹⁵⁰ **250** km². Draft Final Report. 3.8 Launch area. Figure 47. Area of missile launch (Source NLR), p.132.

¹⁵¹ **320** km². Final Report. Visualisation of NLR fly out simulation result. Figure 62, p.144.

¹⁵² **75** km². A new area, images of which have been published in the public domain.



Air and Space Defense Corporation
"Almaz-Antey"

Exhibits to the Report

PART 2

Moscow, 2023

TABLE OF CONTENTS:**PART 2**

	Page
Exhibit A. Analysis of combat damage to the Boeing 777	5
Exhibit A.1. Boundaries of the fragmentation field covering outer skin of the Boeing 777 aircraft	5
Exhibit A.2. Characteristics of fragmentation damage to the cockpit.....	20
Exhibit A.3. Damage to the elements of the load-carrying structure	25
Exhibit A.4. Comparative analysis of damage to the IL-86 target aircraft and fragments of the Boeing 777	33
Exhibit A.4.1: Comparative analysis of damage to the outer skin	33
Exhibit A.4.2 Comparative analysis of damage to the framework	41
Exhibit A.4.3 Comparative analysis of damage due to near blast factors ..	44
Exhibit B. 9H314M warhead	53
Exhibit B.1. Specifications of the 9H314M warhead	53
Exhibit B.2. Confirmation of fragment dispersion sector in static position ...	55
Exhibit B.2.1 Results of control tests of 9H314M warheads (1980-1981)	55
Exhibit B.2.2 Testing of the warhead as part of the compartment hull	57
Exhibit B.2.3 Missile warhead tests	61
Exhibit B.3. Confirmation of the mechanical effect (penetration) of prefabricated projectiles	64
Exhibit B.4. Special experimental studies to assess the penetration of projectiles	82
Exhibit C. Rationale for the selection of the target aircraft	90
Exhibit D. Warhead Detonation Model	95
Exhibit E. Fragments of the 9M38 missile	107
Exhibit F. Comparative modelling for different final positions of the missile	114

Exhibit G. Main inconsistencies of DSB version	128
Exhibit G.1. Best Match	129
Exhibit G.1.1. Model of damage to Boeing 777 aircraft.....	132
Exhibit G.1.2. Warhead model	140
Exhibit G.1.3. Warhead detonation point	148
Exhibit G.2. Comparison of actual damage with "reference" models	157
Exhibit G.3 Calculation of possible launch area as per "Best Match" options	162
Exhibit G.4: Identification of projectiles and warhead	166
Exhibit G.4.1: "Distinctly shaped" projectiles	166
Exhibit G.4.2 Characteristic damage in fragments of the Boeing 777 structure	173
Exhibit G.4.3: Summary analysis of data on projectiles.....	176
Exhibit G.5: Missile fragments recovered from aircraft structure.....	179

Exhibit A: Analysis of combat damage to the Boeing 777

The combat damage included in the Boeing 777 Damage Model comprises damage to the outer skin of the aircraft, the aircraft's structure (longitudinal structural members - stringers and transverse structural members - bulkheads) and major elements of the cockpit's interior.

Exhibit A.1. Boundaries of the fragmentation field covering outer skin of the Boeing 777 aircraft

The study of damage to the Boeing 777 and identification of the boundaries of the fragment coverage area were carried out in the preliminary modelling phase of the Boeing 777 structural damage studies. As new data became available (photographs and video footage of new fragments, results of examining fragments in the preliminary layout), the source data was updated.

The structural damage to the Boeing 777-200 (MH17) was assessed using photographs and video footage of the aircraft's structure fragments obtained:

with the permission of the DSB in the course of an inspection by a team of Russian experts during visits to the military airbase near Gilze-Rijen (Kingdom of the Netherlands) in February, May and August 2015;

materials of the DSB Preliminary Report;

materials of the DSB Draft Final Report;

materials of the DSB Final Report;

working documents handed over by DSB to Russian experts during meetings of authorised representatives;AA

open-source materials.

An examination of photographic material and visual inspection of fragments of the aircraft's nose section established that many of the fragments have specific damage in the form of local holes and dents, which are characteristic of a high-speed impact by compact solid objects. A total of ten¹ large fragments with relatively large amount of such damage were identified in the first stage:

fragment "F.1" - fragment of the right-hand side of the cockpit with part of the roof and preserved glazing on the right-hand side of the pilot (figure A.1.1);

fragment "F.2"- elements of the cockpit glazing frames (Figure A.1.2);

¹ Photographic and video evidence allowing for the assessment of the nature of fragmentation damage was available for these ten fragments only.

fragment "F.3" – forward section of the fuselage with the first pressure bulkhead in front of the cockpit (figure A.1.3);

fragment "F.4" - part of the aircraft's port side skin below the commander's window glazing bezel (figure A.1.4);

fragment "F.5" - fragment of the aircraft's port side skin - the lower part of the port side from the STA 228.5 bulkhead to passenger door L1 (figure A.1.5);

fragment "F.6" - fragment of the roof behind the cockpit (figure A.1.6);

fragment "F.7" - of the top of the port side and the roof behind the cockpit (figure A.1.7);

fragment "F.8" - fragment of the port side in front of passenger door L1 (figure A.1.8);

fragment "F.9" - fragment of the port side outer skin with the angle of attack sensor (figure A.1.9);

fragment "F.10" - fragment of the port side outer skin in the area of the forward pressure bulkhead (figure A.1.10).



Figure A.1.1 - Exterior view of fragment "F.1



Figure A.1.2 - Exterior view of fragment "F.2" (a) and areas of the fragment with characteristic damage (b, c, d) highlighted in red



Figure A.1.3 - Exterior view of fragment "F.3" (a) and areas of the fragment with characteristic damage on the port side (b) and in front of the glazing (c)



Figure A.1.4 - Exterior view of fragment "F.4



Figure A.1.5 - Exterior view of "F.5" (bottom of port side from bulkhead STA 228.5 to door L1)



Figure A.1.6 - Exterior view of F.6 (roof behind the cockpit)



Figure A.1.7 - Exterior view of fragment "F.7" (a) and areas of fragment with characteristic damage from outside (b, d) and inside (c) the port side and roof behind the cockpit



Figure A.1.8 - Exterior view of fragment "F.8" (port side fragment)

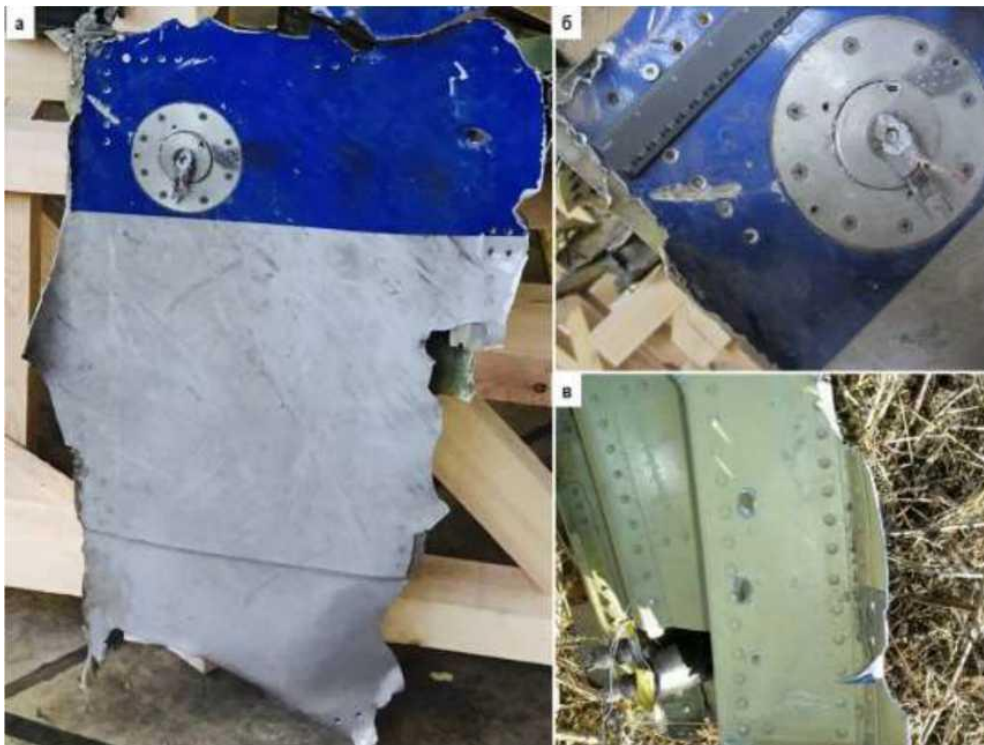


Figure A.1.9 - Exterior view of fragment "F.9" (a) and areas of the fragment with characteristic external (b) and lateral damage (c)

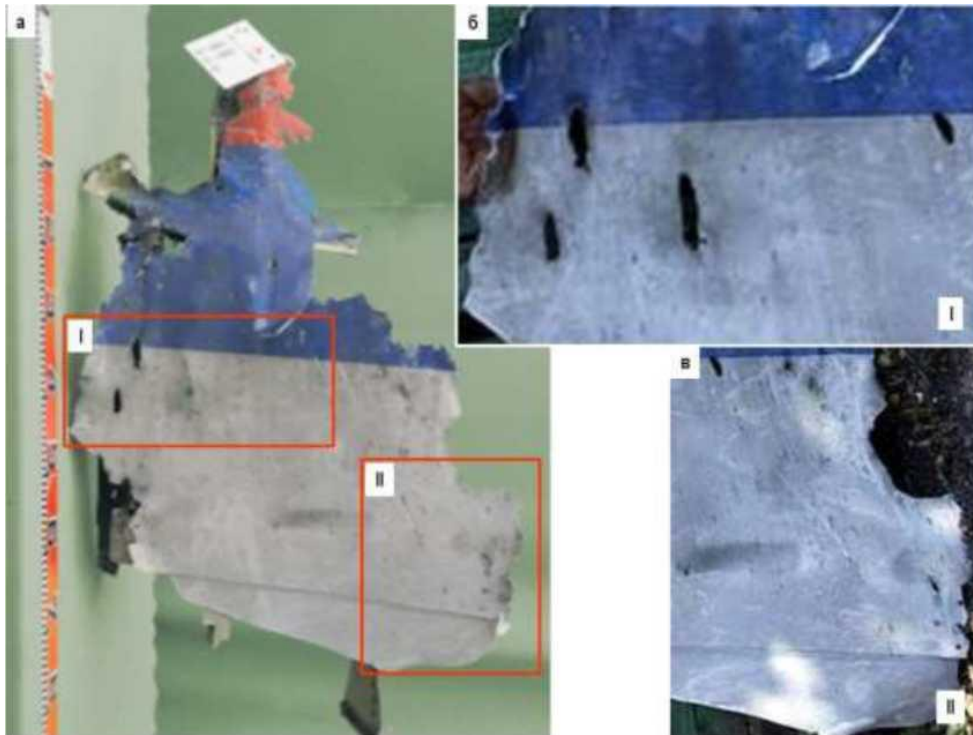


Figure A.1.10 - Exterior view of fragment "F.10" with characteristic damage (b, c)

Most of the above fragments were used by the DSB specialists in the 3D reconstruction of the nose section of the MH17 fuselage.² The referencing of fragments F.1 to F.5, F.9 and F.10 to the aircraft structure was done during the 3D reconstruction and no update is required.

In order to make an objective assessment of the boundaries of the fragmentation damage to the aircraft structure, it was necessary to clarify the locations of fragments F.6, F.7 and F.8, which are not present in the exhibit.

One of the most important and informative fragments that did not make it into the 3D reconstruction is the fragment "F.6", the fragment of roof behind the cockpit. It was one of the images of this fragment³ that was the main argument that allowed the DSB experts to conclude in the Preliminary Report (September 2014) that the aircraft had been destroyed by high-speed, high-energy objects acting from outside.

² Fragment F.10 was not presented in the preliminary layout shown during the joint work in February and May 2015.

³ Preliminary Report. Figure 9, p. 24/34.



Figure A.1.11 - Locating fragment "F.6" based on DSB materials

The location of this fragment in the MH17 structure was identified as early as September 2014 and is shown in the Preliminary Report (Figure A.1.11(a), A.1.11(c)).

In the working papers used during the joint work of the authorised representatives and the expert team in February 2015, the linking of the fragment to the airframe structure (Figure A.1.11(b)) was shown by the DSB specialists. However, later in both the working papers (Figure A.1.11(d)) and in the final Report, the exact location of the fragment was not shown.⁴

An analysis of multiple images of this fragment of the roof above the cockpit allowed to link it to the structure of the airframe. The location of fragment "F.6" is shown in Figure A.1.12.

Figure A.1.12 shows in red the places where the fragment F.6 is coincident with the characteristic structural elements of the nose section of the aircraft:

- "1" place where the outer skin sheets are connected with the bulkhead STA 246;
- "2" place of STA 246's intersection with the centre line of the aircraft;
- "3" place of STA 265.5 's intersection with the stringer S-1R.

Similarly, fragments F.7 and F.8 were located with reference to easily identifiable elements of the aircraft structure (skin sheet joints, skin-bulkhead and skin-stringer junctures, location of rivets and other features).

⁴ In the Draft Final Report, the location of fragment "F.6" was shown in Figure 52.

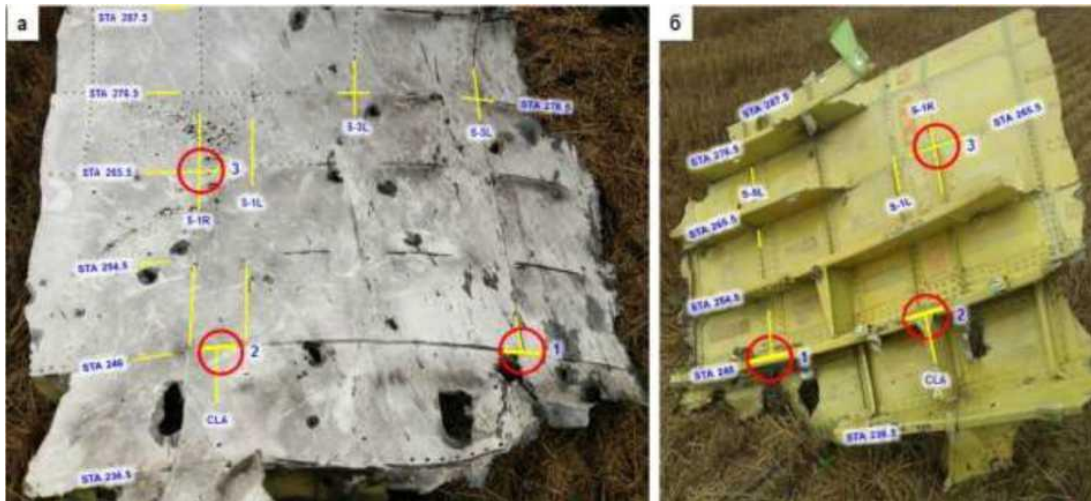


Figure A.1.12 - Exterior view of fragment "F.6" from outside (a), from inside (b) with points of reference to the primary structure

The fragment "F.7" (fragment of the upper part of the port side and the roof behind the cockpit) is also important for determining the nature and extent of the damage. Figure A.1.13 shows the exterior view of this fragment in one of the hangars at the layout site in the Netherlands. The fragment was handed over to the DSB specialists but was not included in the final 3D reconstruction of the fuselage, the analysis of its damage features was either not performed or not reflected in the Report.



Figure A.1.13 - Exterior view of upper port side and roof fragment behind the cockpit (fragment "F.7")

Result of locating fragments "F.6", "F.7" and "F.8" in the 3D model is shown in Figure A.1.14.



Figure A.1.14 – Distribution of fragments in the structure of MH17

An analysis of the relative location of fragmentation damage on the surface of fragments of Boeing 777-200 (MH17) aircraft showed that, despite the absence of a large portion of the outer contour of the cockpit among the fragments, obvious boundaries of the coverage area can be identified.

In locating the boundaries of the fragment coverage area through-and-through (penetrating and non-penetrating) holes and part-through holes (ricochets) were taken into account.

In fragments "F.1", "F.3"- "F.7" "F.9" and "F.10", the damage near the boundary of the fragment coverage area comprises elongated, well-aligned rectilinear sections ("tracks") caused by a contact with projectiles whose trajectories were tangential to the outer contour of the fuselage (Figure A.1.15).

The location of these holes in relation to each other and to easily identifiable structural components of the aircraft was assessed using photographs of the fragments taken from different angles: the joints of the outer skin sheets, the junctures of the outer skin sheeting and bulkheads and stringers.



Figure A.1.15 - Examples of boundary damage in fragment "F.1" (left) and fragment "F.9" (right)

Based on this assessment, fragmentation damage patterns were plotted in the airframe coordinate system and the actual boundaries of the overlapping field were determined.

An example of an analysis of the fragment coverage area observed in the fragments is shown in Figure A.1.16.

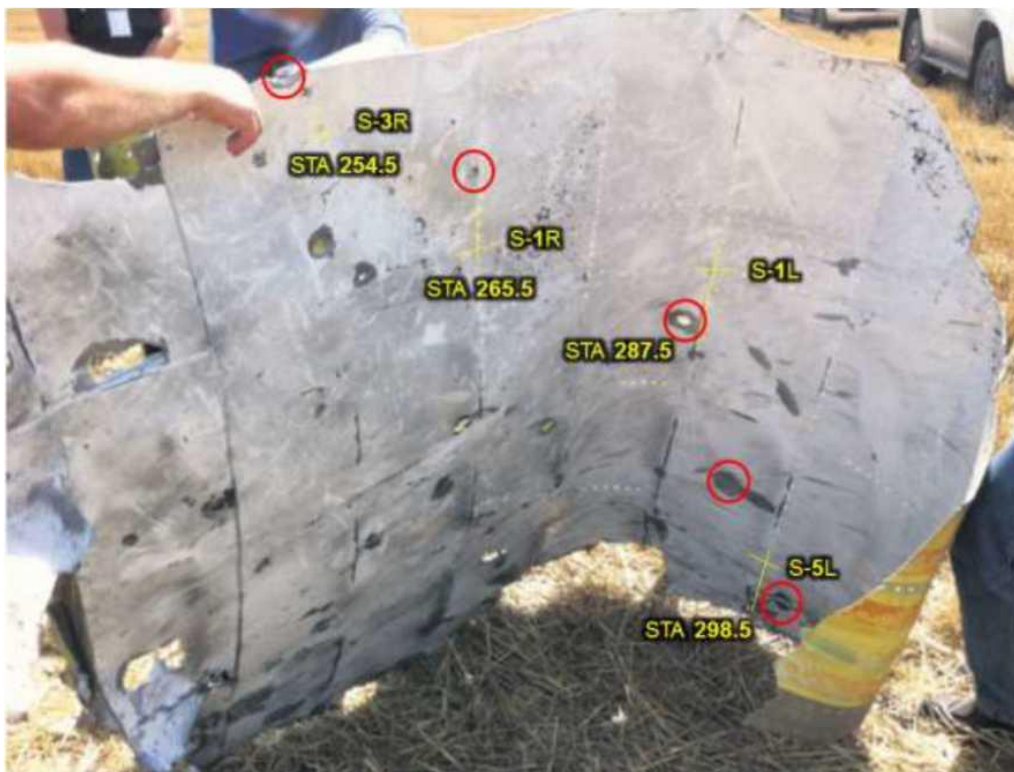


Figure A.1.16 – Fragment coverage area boundary on the fragment of roof behind the cockpit - fragment F.6 (photo by DSB)

The schematics of through-and-through (penetrating and non-penetrating) damage as well as part-through damage (ricochets) for all fragments were used to build a general diagram of the boundaries of the fragment area covering the nose section of the Boeing 777 fuselage, which is shown in Figure A.1.17.

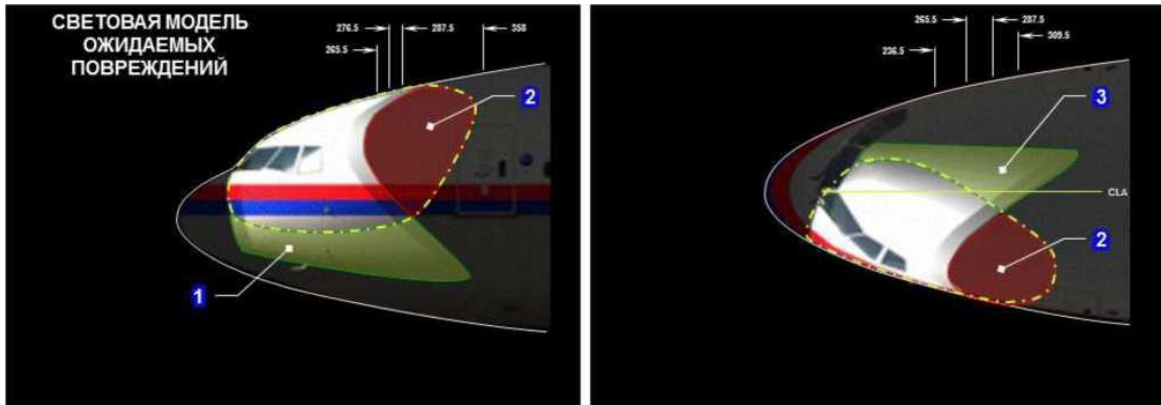


Figure A.1.17 - Schematic of actual fragment coverage area boundaries: left - port side view; right - top view

For the sake of clarity, the diagram of actual boundaries of the fragment coverage area used by Corporation specialists was superimposed on the light model of expected damage ("on-course") presented in the DSB (NLR Light Model) modelling material.

Figure A.1.17 shows two projections of the light model of expected damage (left and top views).

Comparison of the damage pattern (fragmentation zone boundary pattern) with the light model of expected damage shows that the actual fragmentation zone differs significantly from that modelled and accounted for by the DSB. The greatest differences are observed in the three zones shown in Figure A.1.17:

Zone "1" is the lower boundary of the damage on the port side. In this zone, unlike the DSB light model, there is no fragmentation damage to the MH17 fuselage.

Zone "2" is the top of the port side up to the front left passenger door and the left side of the cockpit roof. In this area, unlike the DSB light model, fragmentation damage to the MH17 fuselage can be observed on fragments "F.6", "F.7" and "F.8" (which are missing from the final 3D rendering). Moreover, the "F.7" fragment was located in the Netherlands, but was located in a different room.

The F.7 fragment shows fragmentation damage near the bulkheads STA 287.5 and STA 298.5 (Figure A.1.18)⁵ and STA 309.5 and STA 332.5 (Figure A.1.19), which is almost 3 metres beyond the damage accounted for in the DSB model.

⁵ For unknown reasons, the fragment was split into three pieces before being transported to the territory of the Netherlands.

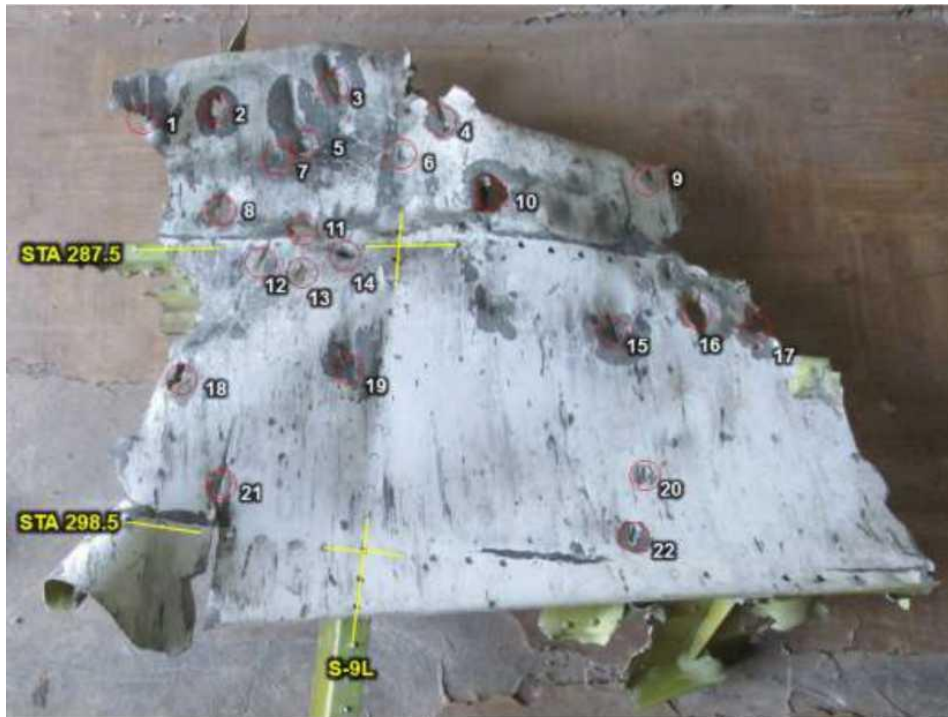


Figure A.1.18 - Forward part of fragment "F.7".
Fragmentation damage is located between bulkheads STA 287.5 and STA 298.5,
which is 2 metres further than the DSB 'reference'



Figure A.1.19 - Fragment of the roof and top of the port side behind the cockpit. The
fragmentation damage is located between bulkheads STA 309.5 and STA 332.5,
which is almost 3 metres further than the DSB 'reference'

During the technical investigation, the Dutch experts claimed that they did not see any damage beyond the STA 220.5 bulkhead just behind the cockpit windows.^{6, 7}

a small part of the fuselage immediately aft of that. At the rearward edge of the panel, positioned on the left hand side of the aeroplane between approximately STA220 and STA410 close to the forward passenger door and on panels further away from the cockpit, no high-energy object damage was noted. The cockpit panel at STA132.5 appeared to be the leading edge of the high-energy object damage.

Figure A.1.20 - No damage beyond the STA 220 bulkhead (Final Report)

A narrow strip on the cockpit between bulkheads STA 132.5 to STA 220.5, i.e. only of about 2.24 m (220.5-132.5= 88 inches), was chosen as the damage "reference". Whereas the objectively observed damage in the upper part of the port side is spread considerably further, beyond the STA 332.5 bulkhead (Figure A.1.21), i.e. about 5.1 m (332.5-132.5= 200 inches) from the front bulkhead STA 132.5, taken as the front boundary of damage area.



Figure A.1.21 - Example of damage to the outer skin at the edge of the coverage area beyond the level of the STA 332.5 bulkhead

⁶ Final Report. Crash of Malaysia Airlines flight MH17. p.121.

⁷ TNO report. Damage reconstruction due to impact of high-energy particles on Malaysia Airlines flight MH17, p.7.

Zone "3" is on the roof behind the cockpit. In this zone, unlike the DSB light model, there is no fragmentation damage on the MH17 fuselage.

As an example, Figure A.1.22 shows a diagram comparing the objectively observed boundaries of the fragmentation area on the roof fragment behind the cockpit with the "simulated damage location and boundaries on the Boeing 777 fuselage" NLR,⁸ adopted in the DSB report as the damage "reference".

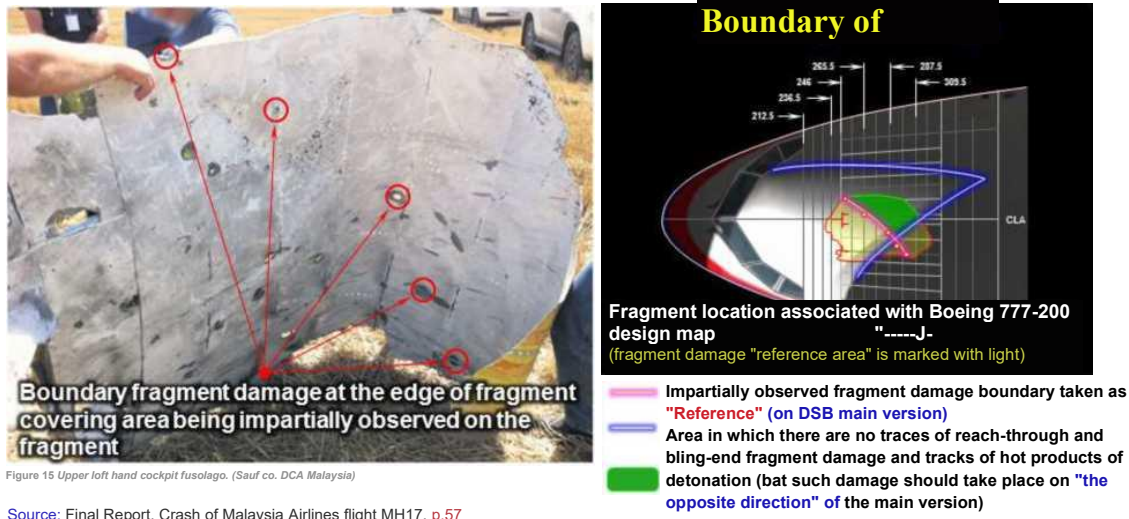


Figure A.1.22 - Objectively observed boundary of the fragmentation area on the roof section behind the cockpit as compared to the "reference" boundaries of the virtual model of NLR, which are shown by the illuminated area

Analysis of the relative location of fragmentation damage on the surface of the Boeing 777 fragments showed that, despite the absence of a large part of the outer contour of the cockpit among the fragments, the obvious boundaries of the fragmentation field can be identified.

The fragmentation field boundaries objectively observed on the outer hull fragments of Boeing 777-200 (MH17) differ significantly from the damage model expected for "opposite direction" conditions.

⁸ Final Report. 3.8.2 Fragment visualisation model, Figure 58, p.138.

Exhibit A.2. Characteristics of fragmentation damage to the cockpit

Fragmentation damage to fragments the Boeing 777-200 (MH17) cockpit has a number of peculiarities. At short distances from each other on different fragments, fragmentation damage has a different exterior view and density, depending on the location (orientation) of the fragments in the aircraft structure. In a number of cases, even in different parts of the same fragment at relatively short distances, a significant change in the nature, density and direction of the damage can be observed. Thus, in one part of a fragment, penetrations may be present not only through the outer skin sheets, but also through the structural elements of the structure, while at a short distance from them only non-penetrating damage (ricochets) is present.

An example of the changing nature of the damage is the "F.4" fragment - part of the port side under the windows of the crew commander, shown in Figure A.2.1.

Figure A.2.1(b) shows a through hole in the front of the fragment (area "I"; the hole is highlighted in blue). In areas of skin reinforced from the inside by the force assembly, the edges of the breach are deformed in the opposite direction to the impact direction of the hitting element. This deformation is characteristic of the shock wave reflected from the force plate. In addition, a rash of microcraters and traces of thermal oxidation is observed on the surface of the skin, confirming that this breach is located at a short distance from the point of detonation (the site of the explosion).

Figure A.2.1(c) shows the non-penetrating damage (area "II"; the hole is highlighted in yellow), which was also located a short distance from the point of detonation. This is also confirmed by the presence of micro-craters and traces of thermal exposure adjacent to this lesion. At the same time, the external exterior view of the damage, taking into account the results of special tests of the penetration capability of preformed fragments⁹ shows that the angle of attack of the striking element during interaction with the outer skin sheet of fragment "F.4" did not exceed 5-10 degrees, i.e. the trajectory of the striking element was almost parallel to the aircraft structure.

⁹ Determining conditions for the formation of non-penetrating damage (ricochets).

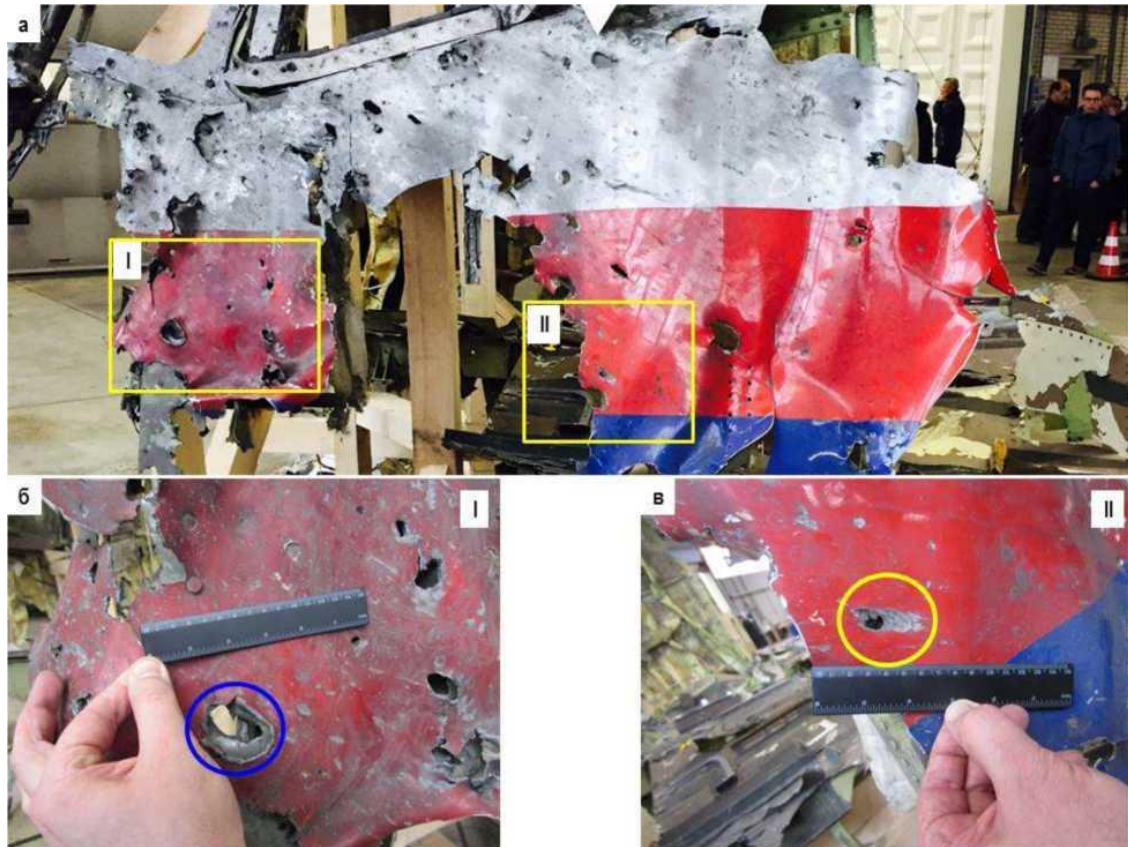


Figure A. 2.1 - Change of damage pattern on the outer skin of F.4



Figure A.2.2 - Exterior view of non-penetrating damage to the port side of the Voinp-777: the damage is under the cockpit glazing

This type of damage indicates that the projectiles did not travel across the board ("opposite direction"), but tangentially along the board, which is consistent with the "collision course" version.

Similar damage was sustained under controlled conditions (on a special stand using a ballistic setup) only at low angles to the firing line (Figure A.2.3). The velocity range corresponded to the dynamic conditions under consideration.

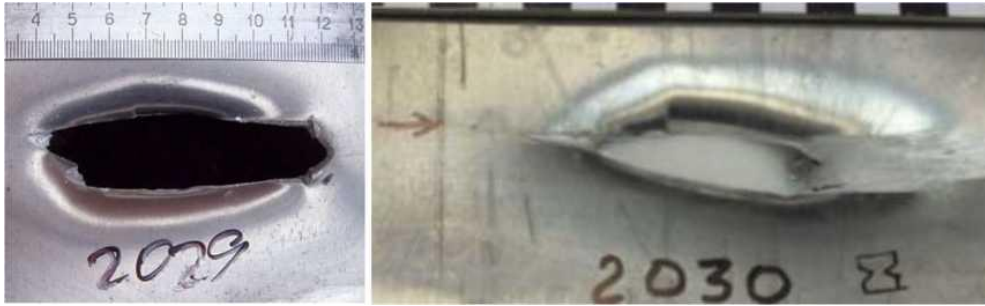


Figure A.2.3 - Exterior view of damage at low angles to the firing line (tangential) under controlled conditions on the bench: left - angle 15°, speed 1683 m/s; right - angle 5°, speed 1640 m/s

The cockpit glazing frame (F.2) is located in close proximity to F.4.

The glazing frame elements shown in Figure A.2.4 show multiple through holes from projectiles (highlighted in yellow) in a substantially more robust structure incorporating additional metal reinforcements and frame corners in addition to the outer sheathing sheets.

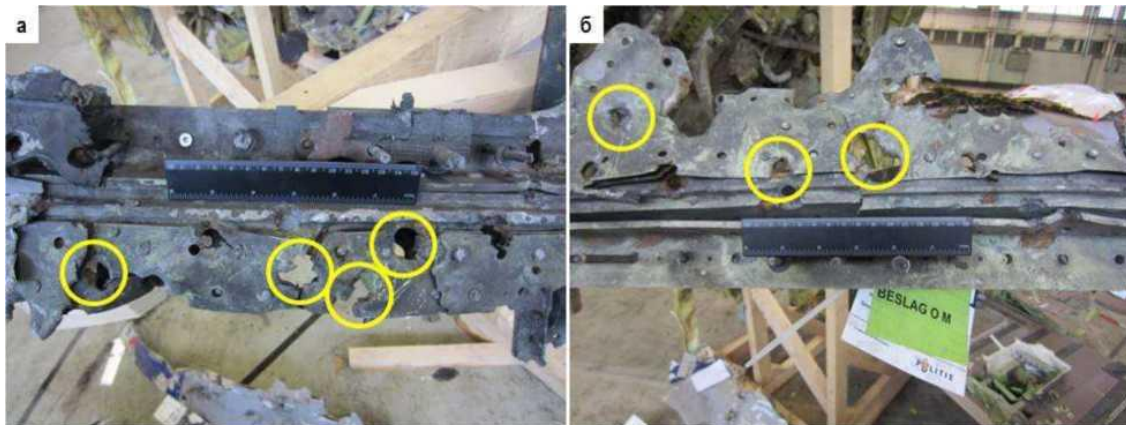


Figure A.2.4 - Penetrating damage to the cockpit glazing frame

There are no obvious ricochet marks on parts of the frame, although non-penetrating damage is also present. An example of such damage is the part of the F.2 fragment shown in Figure A.2.5.



Figure A.2.5 - Example of non-penetrating damage to a glazing frame

Non-penetrating damage (highlighted in red) is an example of the erosive action of a warhead.¹⁰

Similar damage was observed in the full-scale Almaz-Antey tests when the projectiles interacted with particularly hard target structure elements (Figure A.2.6).



Figure A. 2.6 - Characteristic non-penetrating damage: left - MH17; right - target acquisition (experiment)

Another feature of cockpit fragmentation damage is the significant change in the density of fragmentation damage. Figure A.2.7 shows the distribution of combat damage density on fragment "F.4" (part of the port side below the windows of the cockpit commander).

¹⁰ Indentations, sinkholes or craters accompanied by the obstacle mass removal.

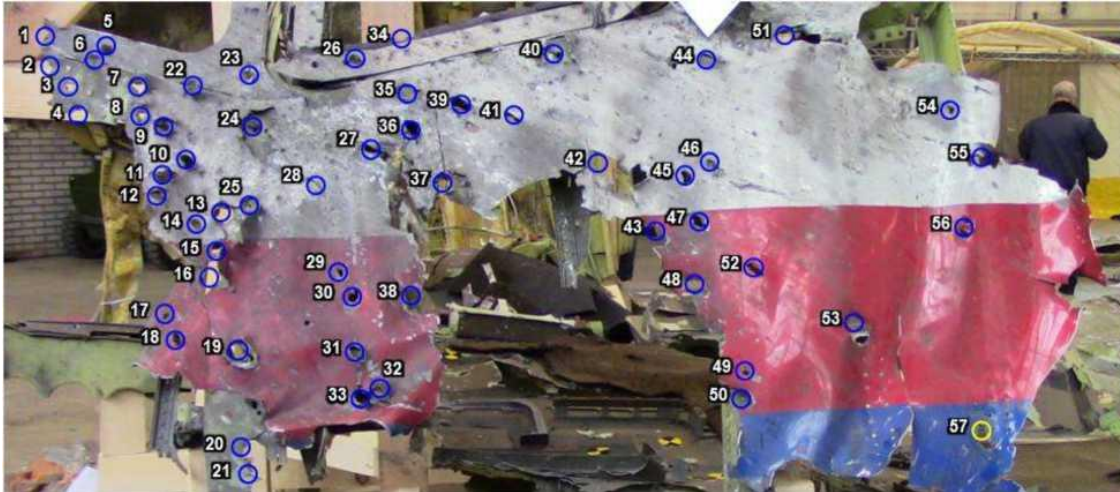


Figure A.2.7 - Exterior view of fragment "F.4" with numbered battle damage

Combat damage from the projectiles in a relatively small area is extremely unevenly distributed. The density of damage decreases significantly from left to right (from the nose towards the tail section) and from top to bottom.¹¹

Considering the change in the exterior view and density of the damage, it can be stated with sufficient certainty that this change in the nature of damage located on fragments close to the point of explosion can only be explained by a significant change in the angles of approach of the projectiles to the outer skin of the fragments. In the middle and lower part of the port side, already in the area of the cockpit glazing, the trajectories of the PEs were practically parallel to the aircraft structure.

Behind the cockpit glazing, the projectiles predominantly moved along the port side of the aircraft.

¹¹ This is the damage pattern with the change in maximum density from left to right and from top to bottom was obtained on shield 1.1 of target No. 1 and shield 2.3 of target No. 2 in the first stage of the experiment (according to the Concern's version).

Exhibit A.3. Damage to the elements of the load-carrying structure

Damage analysis of the Boeing 777's load-bearing structure shows that the transverse load-bearing elements, the load-bearing members, suffered the most damage among the structural elements of the aeroplane's load-bearing structure.

Through-and-through-and-through damage in the port side bulkheads starts almost from the front edge of the fragmentation area (from STA 148 next to the front pressure bulkhead) and extends to the front passenger door L1.

Figures A.3.1-A.3.7 show examples of through holes in the bulkheads located in the nose of the fuselage and along the port side.



Figure A.3.1 - Through-and-through-and-through damage to the forward fuselage bulkheads

Figure A.3.1 shows through-holes in a bulkhead up to the cockpit glazing frame.

Figure A.3.2 shows through-holes in the skewers below the glazing on the left side of the cockpit.

Figure A.3.3 shows the through-holes in the bulkhead and outer skin of the fragment at the top at the rear of the third crewmember's window.

Figure A.3.4 shows the through-holes in the bulkheads located on the fragment of the centre port side behind the cockpit.

Figure A.3.5 shows the damage to the deck members located on the fragment of the top of the port side behind the cockpit.

Figures A.3.6 and A.3.7 show the damage to the port side bulkheads which resulted in their rupture and subsequent structural failure of the mid and upper port side.



Figure A.3.2 - Punctures in bulkheads STA 196.5 - STA 212.5 under the glazing of the left side of the cockpit



Figure A.3.3 - Fragment of the port side skin from the top behind the third window of the crew commander. Multiple holes in the bulkhead led to deformation and failure of the force element (photo right), indicating that this fragment was exposed to maximum density (mass and kinetic energy) of the projectiles and factors accompanying a close explosion



Figure A.3.4 - Fragment of the centre port side behind the cockpit. Objectively observed holes in the STA 287.5 and STA 298.5 bulkheads, traces of compression, deformation, rupture and destruction of structural members



Figure A.3.5 - Fragment of the upper port side behind the cockpit: external (left) and internal (right) views. Multiple holes in the STA 287.5 and STA 298.5 bulkheads resulted in deformation and failure of the structural elements (red arrows indicate characteristic damage)



Figure A.3.6 - Destruction of port side bulkheads by perforation



Figure A.3.7 - Perforation, thermal oxidation and deformation of the transverse strength members (bulkheads) resulted in their rupture and subsequent structural failure of the upper port side

Analysis of the damage (through holes) to the bulkheads shows that damage to the aircraft's primary structure is much more widespread than to the outer skin, including non-penetrating damage (ricochets). As an example, damage to the primary structure of F.9 (part of the port side, Figure A.3.8) and F.6 (the roof behind the cockpit, Figure A.3.10) can be seen.

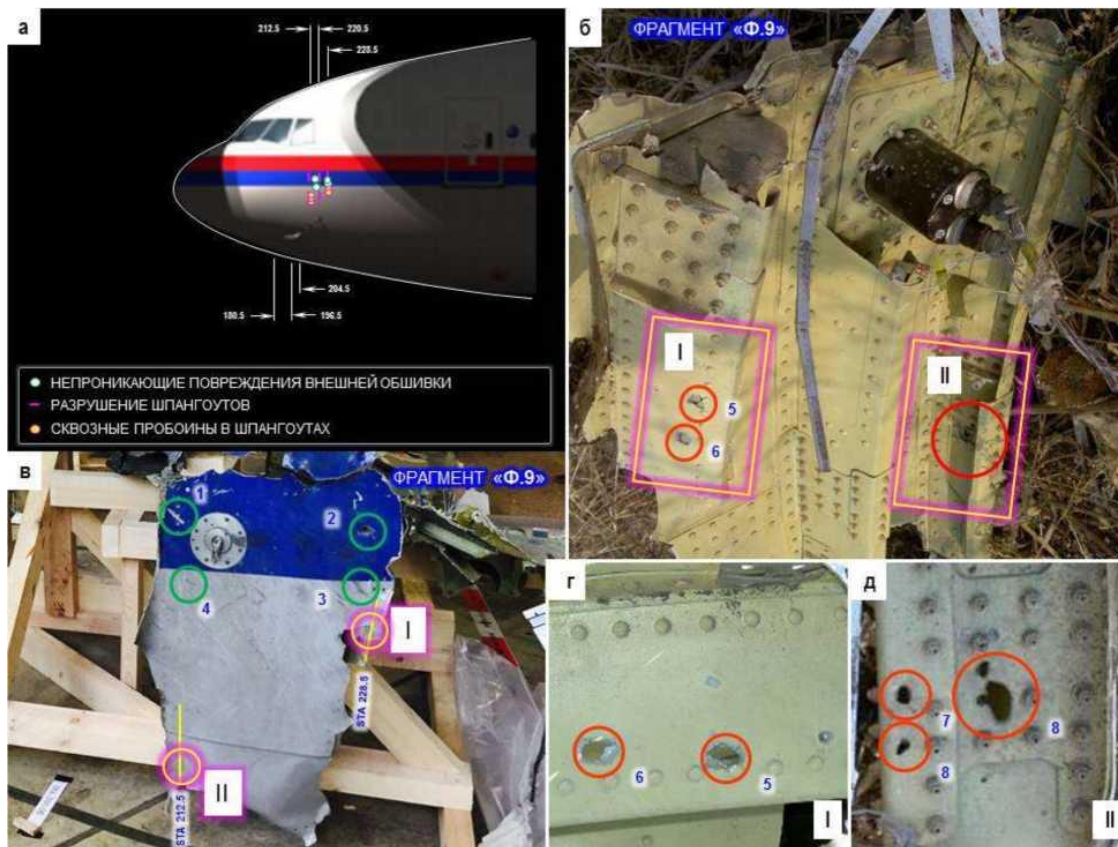


Figure A.3.8 - Damage diagram of the port side fragment with ROV (a), inside (b), outside (c) and through-holes in the bulkheads (d, e)

Figure A.3.8 shows a fragment of the port side outer skin with the F.9 angle-of-attack sensor located below the windows of the crew commander. On the outer skin of the fragment (Figure A.3.8(c)), there are four non-penetrating holes marked "1" through "4" in the upper part of the fragment. All of these damages, with the exception of track "2", are non-penetrating - there is partial damage to the duralumin plate of the outer skin ("1") or only the paint coating ("3", "4").

On the inside of this fragment there are five through-holes in the bulkheads marked with numbers from "5" to "9" (Figures A.3.8(b), A.3.8(d) and A.3.8(e)). A comparison of the exterior view of the damage located on the F.9 fragment with the results of special GSE penetration tests shows that the angle of attack of the projectiles when interacting with outer skin sheet was no more than 5 degrees, i.e. almost parallel to the aircraft structure (Figure A.3.9).



Figure A.3.9 - Exterior view of non-penetrating ricochet damage: on F.9 fragment of the left side of a Boeing 777 (left) and on the barrier after interaction with preformed fragments at an angle of 5° to the firing line (right)

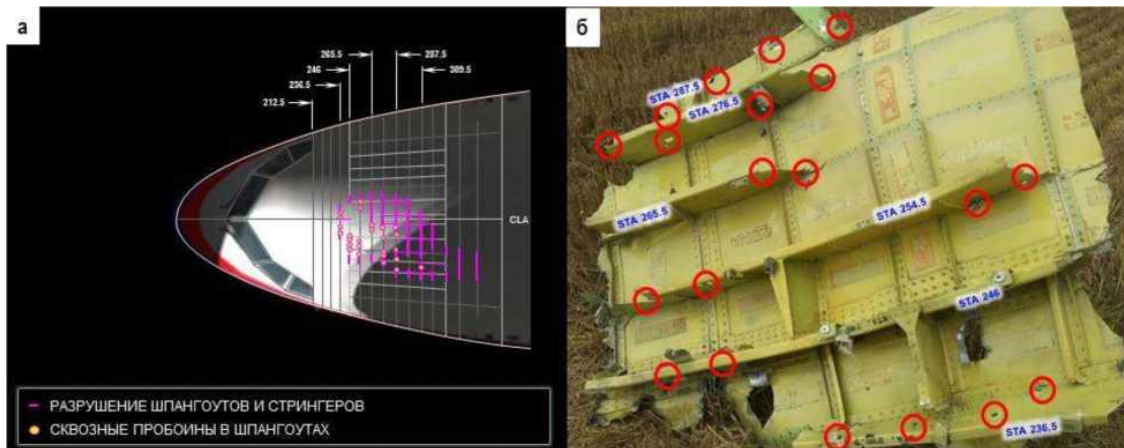


Figure A.3.10 - Schematic of damage to the roof structure behind the cockpit in the F.6 area (a) and through holes in the bulkheads (b)

Analysis of the force structure failure pattern (Figure A.3.10) shows that the area of through holes and destruction and deformation of the structural elements (bulkheads and stringers) exceeds the fragment coverage area. Through penetrations in the bulkheads are located well beyond the penetrating damage to the outer skin.

The main conclusion is that in the port side and roof area behind the cockpit, **the projectiles moved predominantly along the aircraft structure** - from the nose to the tail or at a slight angle to the centreline of the aircraft. At the same time, a large proportion of the fragments moved inside the aircraft structure, which explains why the damage to the force structure inside the aircraft is much further than the damage to the outer skin of the fuselage.

Examples of damage to the bulkheads are shown in figure A.3.11.



Figure A.3.11 - Examples of damage to bulkheads

Figure A.3.12 shows a section of the passenger compartment luggage rack, which is located further away from the STA 382 level.



Figure A.3.12 - Fragment of passenger compartment luggage rack with (suspected) fragmentation damage

In total, more than 100 holes were recorded in the transverse structural elements (taking into account photographic images from public sources), of which 60 holes can be established with a high degree of accuracy in the aircraft structure.

The greatest damage among the structural members of the Boeing 777 structure was sustained by the transverse structural members, the bulkheads. The main area of localisation of through holes in the bulkheads is along the port side from the front edge of the fragmentation field to the front passenger door L1, along the left side of the roof to STA 332.5 and further to the passenger cabin on the port side to STA 382+, and to the forward cargo compartment (Forward Cargo) corresponding to STA 409.

Multiple holes in the upper port side and left side roof members led to the deformation and destruction of the force mainframe.

The projectiles in the dense fragmentation stream moved predominantly along the aircraft structure (or at a slight angle to the centreline) along the port side and the left side of the roof.

Exhibit A.4. Comparative analysis of damage to the IL-86 target aircraft and fragments of the Boeing 777

A comparative analysis of damage to the IL-86 and Boeing 777 target aircraft was carried out in relation to the outer skin of the aircraft, the aircraft's structure (longitudinal load-bearing elements - stringers and transverse load-bearing elements - bulkheads) and the main elements of the internal equipment of the cockpit.

The missile detonation experiment was carried out according to the conditions (detonation point coordinates, encounter angles) calculated by the DSB.¹²

Exhibit A.4.1: Comparative analysis of damage to the outer skin

The main peculiarities of the damage to the outer skin of the IL-86 target aircraft resulting from the experiment:

1. The area of damage to the outer skin of the IL-86 target aircraft is significantly larger than that to the Boeing 777.
2. On the left side of the cockpit, in the area of the crew commander's windows, there are no ricochet marks left by preformed fragments, unlike in the case of MH17.
3. On the right side of the cockpit, in the area of the second pilot's windows, along the starboard side and the right side of the roof and underbody there are, unlike in the case of MH17, multiple exit holes from projectiles that penetrated through the fuselage of the aircraft.
4. One of the main distinguishing features of the nature of damage to the outer skin of the IL-86 target aircraft from the Boeing 777 is the presence of multiple through-holes on the port side and roof, having a characteristic "butterfly" exterior view.

Ricochets

Figure A.4.1 shows fragments of the port side under the windows of the Boeing 777 crew commander (left) and the IL-86 target aircraft (right). Analysis of the photographs shown in the figure shows that on the port side fragments of Boeing 777 (left)¹³ many tangential non-penetrating holes (ricochets) from preformed fragments are observed, while on similar fragments of the left side of IL-86 target aircraft (right) there is no such damage.

¹² Report on the conduct of a full-scale experiment, pages 6-9.

¹³ The figure shows in purple the fragments of the port side of MH17 that were missing from the site of the temporary lay-up during the joint work of the authorised representatives (February and May 2015). Until August 2015, neither the fragments themselves nor their images were available to Russian experts for examination.



Figure A.4.1 - Fragments of the left side of a Boeing 777 (left) and an IL-86 target aircraft (right)

As an example, Figure A.4.2 shows a comparison of port side fragments located in approximately the same location - behind the cockpit glazing of the Boeing 777 and the IL-86 target aircraft.

The main difference between the fragments of the port side of MH17 and the IL-86 target aircraft compared is the nature of the damage caused by preformed fragments. On the port side of MH17 there are many non-penetrating, non-piercing holes (both with partial metal damage, or only damage to the paint coating on the outer skin sheets). The IL-86 target aircraft shows clear penetrating penetrations, both from prefabricated projectiles and hull projectiles.



Figure A.4.2 - Fragment A3 of the port side of the Boeing 777 (left) and B3 of the port side of the IL-86 target aircraft (right)

Such a significant difference in the nature of damage to the port side skin can only be explained by different angles of approach of the projectiles to the obstacle (the surface of the outer skin of the aircraft's fuselage). Accordingly, different conditions of the aircraft's encounter with the missile (coordinates of the detonation point and angles between longitudinal axes).

Exit through-holes "from the inside out"

During the experiment, the structure of the target aircraft was holed, as evidenced by multiple through holes and non-skid exit damage "from the inside out" on the starboard side and the right lower part of the bottom of the IL-86 target aircraft (IL-86)¹⁴ (Figure A.4.3).



Figure A.4.3 - Examples of through-hole exit holes on the starboard side of the IL-86 target aircraft (left) and no exit holes on the starboard side of the Boeing 777 (right)

At the same time, on the cockpit fragments of the Boeing 777, the inside-outside exit damage (holes and non-piercing damage) is located on the lower left side of the fuselage, rather than on the right side of the fuselage.

The highest density of exit damage is concentrated under the second left-hand window of the crew commander and spread further along the port side.

The available technical investigation materials (TNO, NLR and DSB materials) **do not mention** the presence of "inside-outside" exit damage on the lower port side of the Boeing 777.

There are no descriptions or photos of the exit ("inside-outside") damage to the lower left side of the Boeing 777 in the Reports and their appendices.

Examples of inside-outside exiting damage of non-clearance damage and through holes in the underside of the port side are shown in Figures A.4.4 and A.4.5.

¹⁴ Report on the conduct of a full-scale experiment, pages 75-88; 149-157.

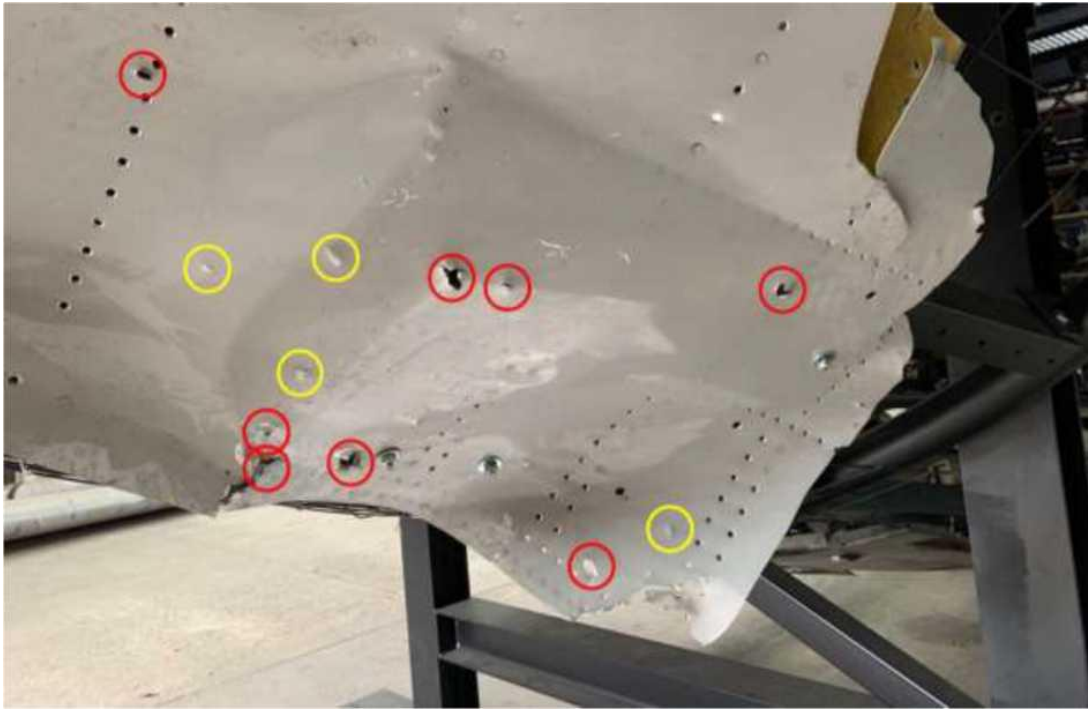


Figure A.4.4 - Exit damage "inside-out" on the lower port side of the Boeing 777 under the windows of the crew commander



Figure A.4.5 - Close-up of inside-outside exit damage: non-clearance damage (left) and through-hole damage (right)

When a BUK missile is detonated, the projectiles of the 9H314M warhead pierce through the structure of the aircraft (given the orientation of the dense fragmentation flow - "scalpel"), which is confirmed by the presence of dozens of through exit holes in the right side, the right side of the roof and the right side of the bottom of the IL-86 target aircraft.

The absence of distinctive starboard exit wounds on the fragments of the Boeing 777 disproves the Dutch experts' conclusions that MH17 was hit "in an "opposite direction" by a missile equipped with a 9H314M warhead.

The characteristic exterior view of the "butterfly" holes

None of the fragments of the Boeing 777's exterior skin, load-bearing structure and internal equipment examined directly by the Corporation's specialists, as well as photographic and/or video material, **showed any** through holes with the characteristic "butterfly" exterior view. It should be noted that no such holes were subsequently found in the fragments or **their images are missing from all the official documents of the DSB technical investigation.**

Analysis of the test results from the full-scale experiments showed that the characteristic butterfly-shaped holes on the outer skin sheets are not isolated or random.

Dozens of such through-holes with a pronounced "butterfly" exterior view, left by the 9H314M 1-10 "bowtie" projectiles, have been observed on fragments of the outer hull of the IL-86 target aircraft (IL-86).

Examples of some holes with the characteristic "butterfly" exterior view are shown in Figures A.4.6-A.4.9.

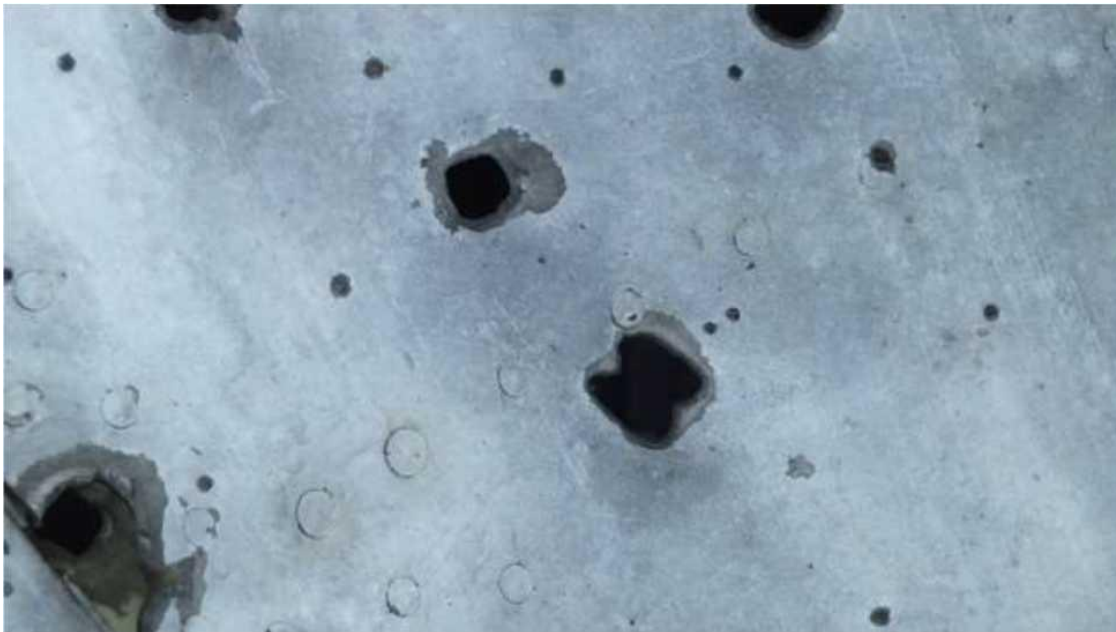


Figure A.4.6 - The skin of the port side of the IL-86 target aircraft (close-up)



Figure A.4.7 - The skin of the port side of the IL-86 target aircraft (close-up)



Figure A.4.8 - Fragment of the outer skin above the glazing of the aircraft commander (IL-86 target aircraft)



Figure A.4.9 - Cladding of the upper port side of the target aircraft "IL-86

In order to assess the shape of the holes formed by the interaction of the 9H314M preformed fragments with the spaced obstacles, an additional experiment was conducted in a shield target layout simulating other warhead detonation conditions (approach angles and distances from the detonation point).¹⁵

Examination of the damage (through-holes) to the fragments of the shielded targeting environment showed that all targets made of a duralumin alloy similar to the outer skin of the Boeing 777 aircraft had a large number of "butterfly" shaped holes, which leave the 9H314M 1-10 heavy fraction "hollowed-out" projectiles (Figure A.4.10).

Test results show that the finished 9H314M 1-10 warheads leave a distinctive "butterfly" punch not only on the first obstacle of a shielded target, but also on all subsequent obstacles.

¹⁵ Report on the conduct of a full-scale experiment, pages 142-148.



Figure A.4.10 - Characteristic "butterfly" shaped holes in shielded target sheets

Analysis of the results of two experiments carried out under different conditions of interaction between the projectiles and the obstacles (angles of approach to targets, distance from the detonation point) as a result of a 9H314M type warhead, leads to the conclusion that the characteristic "butterfly" shape holes in the outer skin are not isolated or accidental.

Dozens of photos of these characteristic butterfly-shaped holes were presented in the "Field Experiment Report" sent to the Dutch¹⁶ in 2016.

A comparative analysis of the shape of the projectile penetrations from the experiments and the data in the Final Report indicates that fragmentation damage to the port side skin of the Boeing 777 could not have been caused by 9H314M projectiles under the conditions described in the DSB report.

Thus, in the course of tests carried out under different conditions, it was found that the shape of the holes on the first obstacle is not related to the mutual orientation of the missile and the aircraft at the moment of detonation, and has no correlation with the dynamics of missile movement and the point of detonation of the warhead. As a consequence, the shape of the holes on the first obstacle is one of the main attributes for identification of the type of warhead and its orientation at the time of detonation relative to the target (target).

¹⁶ Report on the conduct of a full-scale experiment, pages 131-141; 143-148. Annex to the Report, pages 89-94.

This is also true for dynamic situations.

As an example, the result of tests in dynamic situations using an airborne target simulator is shown (Figure A.4.11).

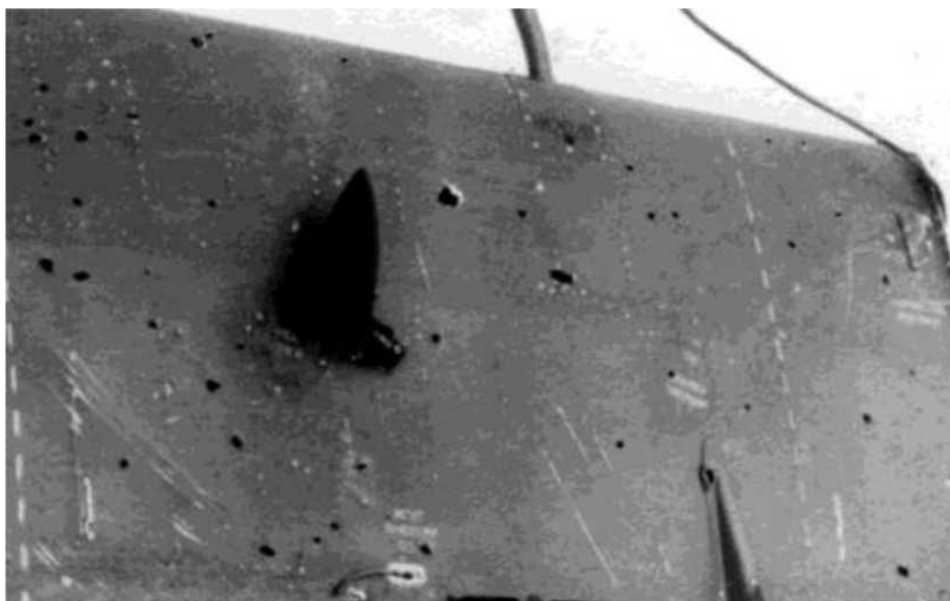


Figure A.4.11 - Exterior view of damage to an airborne target in a dynamic situation: "opposite direction"; mutual speed of target and missile is comparable to the conditions in question

The absence of distinctive "butterfly" holes in the fragments of the Boeing 777 disproves the conclusions of the Dutch experts that it was hit "in an "opposite direction" by a missile equipped with the 9H314M warhead.

Exhibit A.4.2: Comparative analysis of damage to the framework

The analysis of damage to the Ilyushin-86 target aircraft's load-bearing structure shows that the longitudinal load-bearing elements - stringers - have sustained the most damage among the elements of the aircraft's load-bearing structure.¹⁷ At the same time, on the Boeing 777, the greatest damage is observed on the transverse structural elements - stringers.

The rocket detonation experiment was conducted under the conditions (detonation point coordinates, encounter angles) calculated by the DSB specialists. The simulation results show that with this orientation of the warhead relative to the aircraft, the trajectories of all preformed fragments are directed at large angles to the longitudinal axis of the aircraft structure.

The results of the modelling were confirmed during the tests - Figures A.4.12 and A.4.13 show two fragments of the left side of the cockpit of the IL-86 target aircraft, in which the angles of entry

¹⁷ Report on the conduct of a full-scale experiment, pages 107-113. 107-113.

of the projectiles into the aircraft structure (by successive penetrated obstacles and tracks) can be observed. The directions of projectiles movement are shown by arrows in the figures.



Figure A.4.12 - Through-holes in the outer skin of the port side (1) and in the reinforced stringer of the port side (2)



Figure A.4.13 - Direction of projectiles movement through the fragment of the upper port side (above the crew commander's window)

Another example showing the direction of the trajectory of the projectiles through an aircraft structure would be Fragment 5.¹⁸ Figure A.4.14 shows photographs of the fragment from different angles. View from inside the cockpit.



Figure A.4.14 - Direction of motion of the projectiles through the outer skin fragment and the port side bulkhead

The transverse structural elements (bulkheads) of the IL-86 target aircraft have damage of a nature that is radically different from the through holes in the bulkheads observed on the MH17.

The difference in the nature of damage to the transverse structural elements can only be explained by a significant difference in the conditions of impact of projectiles on the aircraft structure. First of all, this can be explained by the angles of approach of the projectiles to the outer skin of the aircraft, and, consequently, by the missile-airplane encounter conditions, which are radically different from the DSB's main "opposite direction" version.

¹⁸ Left side fuselage element of the IL-86 target aircraft, located behind the commander's seat (Report on the conduct of a full-scale experiment, pages 114-115).

Exhibit A.4.3 Comparative analysis of damage due to near blast factors

Unlike the MH17, in the IL-86 target aircraft, compression and deformation of the outer skin sheets occurred predominantly along stringers, the longitudinal load-bearing elements of the aircraft's structure.

One example of such deformation of the outer skin sheets can be seen in the fragments of the port side in the area of the aircraft commander's windows,¹⁹ shown in Figures A.4.15 and A.4.16.



Figure A.4.15 - Fragment of the left side of the IL-86 target aircraft below the windows of the aircraft commander



Figure A.4.16 - Deformation of the outer skin of the IL-86 target aircraft

¹⁹ Figure A.4.15 shows the rows of multiple rivet holes which formed as a result of the outer skin being torn away from the primary structure. The main characteristic of this damage is that the tearing of the outer skin was predominantly along the bulkheads.

The impact of the explosion on the structure of the IL-86 target aircraft caused part of the left side of the roof and the left side to be pressed inwards into the aircraft structure (towards the right side). Figure A.4.17 shows traces of the impact on the cockpit of the IL-86 target aircraft obtained during the experiment.



Figure A.4.17 - Destruction of the target aircraft's load-bearing structure of the IL-86

The area of greatest damage is marked in yellow. In the centre there is an area of severe damage to the aircraft's primary structure (red dotted oval).

Significant differences between MH17 and the Ilyushin-86 target aircraft can also be observed in the areas of micro-craters and traces of thermal influence of explosion products (thermal oxidation) on the cockpit skin (Figures A.4.18 and A.4.19).



Figure A.4.18 - Thermal influence marks on the left side of the IL-86 target aircraft



Figure A.4.19 - Aircraft commander's windscreen and small window

From the analysis of the drawings, it appears that the greatest intensity of traces of Thermal influence is observed behind the third window of the crew commander. In contrast to MH17, there are virtually no thermal oxidation traces in the area of the windscreen and the left-hand side window.

As shown in subparagraph 5.1.2.4 of the Corporation's report,²⁰ the fragments of Boeing 777 (MH17) show the destruction of the aircraft's primary structure **along the port side**.

This collapse was accompanied by fragmentation of the roof and port side structural components at the points of collapse of the framework, primarily the bulkheads. The area of greatest damage to the Boeing 777 is between the bulkhead and the glazing frame.

At the same time the damage to the outer skin and force structure of the Boeing 777 from near blast factors is spread along the left side of the aircraft structure and reaches the level of STA 287.5-STA 309.5. Respectively the damage along the port side is spread over 4 m from the damage front boundary - STA 132.5 forward pressure bulkhead.

This difference in blast impact results can be explained by a significant difference in the angles of approach of the missile in the horizontal plane, as well as a firing point which is different from that specified in the DSB Report (the "opposite direction" version).

²⁰ PART 1. 5.1.2.4 Damage to the primary structure.

Fragmentation of the left side structure of the Boeing 777 was made possible as a result of multiple through-and-through holes (perforations) in bulkheads of the port side and the left side of the roof (see Exhibites A.3 and A.4.2) and the impact of the blast directed along the left side of the aircraft structure.

This is only possible if the missile crosses significantly (at least -50° ... -60°) the course of the aircraft. Figure A.4.20 shows the combined impact of the 9H314M warhead on the target during the first stage of the full-scale experiment²¹ (in the Corporation's "collision course" version).



Figure A.4.20 - Destruction of the target environment (Stage 1 of the experiment)

The first phase of the experiment (31.07.2015) was conducted under missile-aircraft encounter conditions according to the Corporation's version. The first photo (left) shows how, before the shockwave impact started, all projectiles overcome five obstacles making part of the shield target layout (up to a total of 12-14 mm in dural equivalent). The other photographs (in the middle and on the right) show the impact of the shockwave.

This caused destruction of the shield target layout along the structure, predominantly on the left side. The impact of the explosive charge of the warhead caused significant deformation and fragmentation of the shield target.

Figure A.4.21 shows fragments of target No. 1 (M.1) and No. 2 (M.2).

²¹ A photo report is presented in Annex A of the Report on the conduct of a full-scale experiment (2016).



Figure A.4.21 - Fragments of targets No. 1 and No. 2 (Stage 1)

An analysis of fragments of targets No. 1 (top) and No. 2 (bottom) shows that it is when the missile warhead is oriented across the aircraft structure (according to the Corporation's version) that the main blast impact occurs along the left side of the structure. Photographs of the left side of the targets²² show evidence of much greater deformation and local ruptures and fractures (highlighted in red in Figure A.4.21).



Figure A.4.22 - Fragment of target 1.1 (full-scale experiment in a shield target layout conducted on 31.07.2015)

²² The side of the shield target simulating the port side of the Boeing 777-200 airliner (MH17).

Figure A.4.22 shows a photograph (close-up of a fragment of a target - witness sheet 1.1) after exposure to the 9H314M's killing field factors.

It is important to point out that during the experiment in a shield target layout the fragment of target 1.1 was placed almost twice as far away from the detonation point as the actual one, which was due to adjustments for safety requirements.

Figure A.4.23 shows a schematic of a shield target layout simulating the contours of a Boeing 777 aircraft during tests at ground static conditions (according to Almaz-Antey Corporation's version).²³

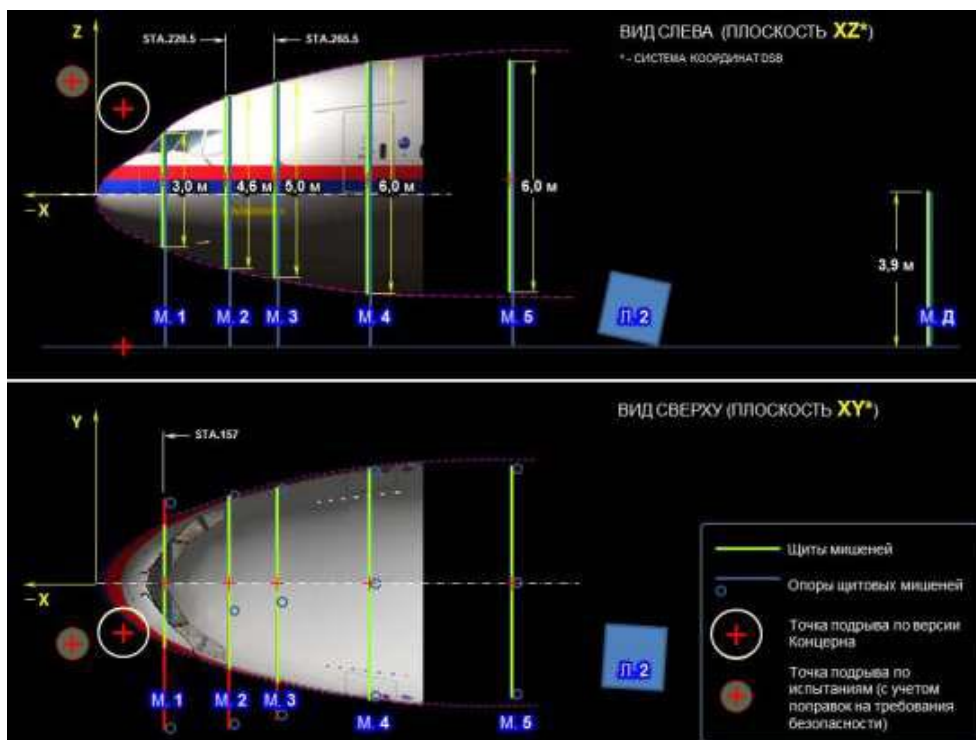


Figure A.4.23 – Plan of shield target layout (31.07.2015). The detonation point for safety reasons was located twice as far away as the detonation point calculated by Corporation's specialists. The position of target No. 1 is marked with the symbol "M.1" in the figure.

In order to avoid total destruction of the witness sheets in the target layout, the detonation point of the test was proportionally placed further away from the detonation point area in question (a red cross in a white circle in the figure).

In reality, if the 9H341M warhead had been detonated near target No. 1 at a distance corresponding to the distance of the detonation point from the nose of the Boeing 777 aircraft (not more than 1.6-2.0 m), the number of fragmentation

²³ Report on the conduct of a full-scale experiment, pages 142-143. 142-143

hits in the fragment of target 1.1 would have been three to four times larger than that in the photo (Figure A.4.22).²⁴

Given the blast effect, this would have resulted in the complete destruction of witness sheet 1.1 of target M.1.

Thus, the comprehensive full-scale experiment of Almaz-Antey Corporation proved that in the event of the missile being detonated when flying in an "opposite direction" (according to the DSB's version), the blast damage to the MH 17 aircraft's structure would have been of a fundamentally different nature.

In addition, the difference in static and dynamic conditions must be taken into account when assessing the blast effect.

Dynamic conditions

It is known from the theory of anti-aircraft missile firing that the effectiveness of the shock wave on an airborne target depends not only on the altitude (thin air), but also on the geometric shape of the warhead, the direction of the target flight relative to the missile, and their final relative velocity. At high missile's velocity, the initial blast pressure could be up to two times higher than in case of detonation of the same explosive charge under static conditions.²⁵ The joint effect of the particularities of the geometric shape of the warhead and the final velocity leads, at short distances, to more than 2.5 times difference in the maximum pressure of the blast wave front (depending on the direction).

Similar conclusions were reached by the Dutch experts from TNO. Annex Z to the DSB Final Report²⁶ shows the simulation calculations for a warhead detonation at an altitude of 10,000 m, at a final velocity of 600 m/s.

The TNO's calculations show that 0.91 ms after the explosion, when the blast front reached a range of 3.0-3.3 meters, the difference in maximum pressure is more than 2.3-2.6 times depending on the direction (Figure A.4.24).

²⁴ With distance from the detonation point, the fragmentation field density decreases in inverse proportion to the square of the distance increase ("law of squares"). Accordingly, if the distance from the detonation point to the barrier changes by a factor of two, the actual damage density on that surface must change by a factor of four.

²⁵ Neupokoev F.K. Anti-aircraft missile firing, pages 200-201.

²⁶ TNO Report 2015M10626. Numerical simulation of blast loading on Malaysia Airlines flight MH17 due to a warhead detonation, p. 9/17.

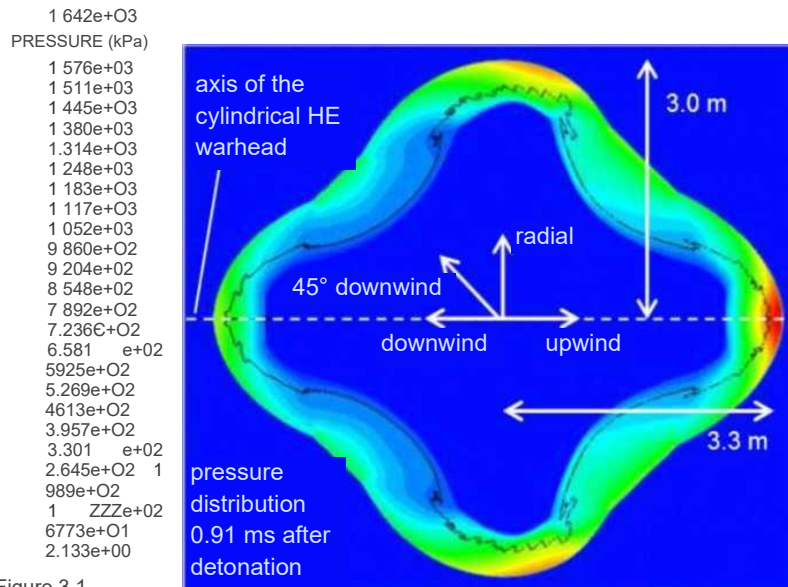


Figure 3.1

Pressure distribution of the blast wave from the warhead 0.91 ms after detonation. At this time the blast front reaches a distance of 3.0 m in radial direction and 3.3 m in longitudinal direction. The blast is not spherical due to the cylindrical shape and the velocity of the warhead. The initial velocity of the warhead points to the right, causing the peak pressure to be highest in upwind direction (approximately 1600 kPa).

Figure A.4.24 - Pressure distribution in a short distance blast wave is not symmetrical (TNO report materials)

According to calculations carried out by TNO specialists the pressure peak in the direction of missile movement (upwind) is 1600 kPa (15.79 atm), in the direction perpendicular to the missile's axis (radial) is about 1400 kPa (13.82 atm), and in the direction 45° from the missile's axis (45° downwind) is 600 kPa (5.92 atm). Accordingly, at a distance of about 3 metres from the detonation point the difference in maximum pressure depending on the direction is more than 2.3 times (1600:600 = 2.66 and 1400-600 = 2.33).

Damage to the structure of Boeing 777 from near blast factors is presented in paragraph 5.1.3 of the Almaz-Antey Corporation Report. Where it is shown that deformation and fragmentation of Boeing 777 structure (external skin and power frame) spread along the left side of the aircraft structure and reached the level of STA 287.5-STA 309.5, i.e. damage along the left side spread over 4 m from the leading edge of damage - STA 132.5 forward pressure bulkhead.

Summary

The nature of the damage caused by the factors of the close explosion of the target aircraft and the Boeing 777 differ significantly in all respects: the direction of deformation of the aircraft structure, the areas of micro-crater formation, and the traces of thermal effects of the explosion products (thermal oxidation) on the outer skin.

The main difference is the direction of deformation of the structure:

"IL-86 - compression and deformation of the outer skin sheets was predominantly along stringers - the longitudinal load-bearing elements of the aircraft load-bearing structure, which resulted in indentation of the left side of the roof and the port side into the aircraft structure (in the direction from the port side to the starboard side).

Boeing 777 - compression and deformation between the transverse strength members (members) of the skin sheets along the port side, which combined with tearing and perforation (of the members and outer skin) resulted in fragmentation of the left side of the aircraft structure.

However, the nature of the blast damage sustained in the first phase of the experiment (according to the Corporation's version) is broadly consistent with that observed on MH17.

The nature of the damage caused by close blast factors on the IL-86 target aircraft differs significantly from the structural damage to the Boeing 777-200 (MH17).

It is experimentally confirmed that the detonation point and orientation of the warhead under the IL-86 target aircraft experiment conditions (DSB version) does not correspond to the area of distribution and nature of damage to the Boeing 777 resulting from close blast factors.

Exhibit B. 9H314M warhead

The Exhibit presents the technical characteristics of the 9H314M warhead and its test results.

Exhibit B.1. Specifications of the 9H314M warhead

This material has been prepared on the basis of extracts from the design and technical documentation for the 9M38 and 9M38M1 anti-aircraft guided missiles that were handed over to the DSB in July 2015²⁷.

The weight of the 9H314 and 9H314M warheads is about 70 kg, including a mass of explosive material of $\sim 33.5^{+0.8}_{-0.4}$ kg. The explosive substance (TG-24) is a mixture of TNT and hexogen.

Fragments mass ~ 28.7 kg. The material of the fragmentation is steel.

The exterior view and placement of the 9H314M warhead in the No. 2 compartment are shown in Figures B.1.1 and B.1.2.



Figure B.1.1 - 9H314M warhead

²⁷ Specifications for 9H314 and 9H314M warheads transmitted to the DSB on 29.07.2015 as Annex to letter No. 01-09/548k.

Exhibit B.2. Confirmation of fragment dispersion sector in static position

Exhibit B.2.1: Results of control tests of 9H314M warheads (1980-1981)

1. Basic information on the warheads used in the tests:

Body weight, kg	33.57- 33.97
Weight of explosives, kg	33.51 - 33.63
Weight of the assembled warhead, kg	67.15- 67.65

2. Basic information on the projectiles:

There are three types of projectiles:

light fraction 9H314M 1-9 "	"parallelepiped"
average dimensions, mm	8x8x5
average weight, g.....	2.35
quantity, pcs.	4,042
light fraction 9H314M 1-11 "	"parallelepiped"
average dimensions, mm	6x6x8,2
average weight, g.....	2.1
quantity, pcs.	1823
heavy fraction 9H314M 1-10 "	"bowtie"
dimensions, mm	13x13x8,2
weight, g	8.1
quantity, pcs.	1,823

3. Test conditions

Detonation of the warheads (in the compartment hulls) was carried out in a target layout consisting of two shields of 4.5x18 m and 10x18 m set in arcs of circles of 10 and 20 metres respectively.

The thickness of each of steel plates on the shields was 5 mm.²⁸

4. Test results

The weight of the projectiles selected from the trap and collected on the ground:

Average weight of projectiles collected in the field:

"parallelepiped" 8x8x5, g	2.23
"parallelepiped" 6x6x8, g	1.92
"bowtie" 13x13x8, g.....	7.62

Average weight of projectiles selected from the trap:

"parallelepiped" 8x8x5, g	2.12
"parallelepiped" 6x6x8, g	1.80
"bowtie" 13x13x8, g.....	7.34

²⁸ The use of steel shields allows for identifying preformed fragments only.

According to the results of ground stationary explosive tests in the rocket compartment, the number of survivable projectiles of the heavy 13x13x8.2 mm fraction (9H314M 1-10 "bowtie") is 96 %, the mass loss of an individual element is 6-7 %.

Distribution of the number and initial velocities of ready-to-use targets elements by 2° zones in angle of dispersion: A) Light fractions 8x8x5 and 6x6x8.2:

Fragment dispersion sector, deg. 48-130
 Including outside the projected fragment distribution travel time curve: 48-66
 deg, % 0.....51
 126-130 degrees, % 0.....08
 In the design sector of 68-124 degrees, % 99.41

B) Heavy fraction 13x13x8.2

Fragment dispersion sector, deg. 50-126
 Including outside the projected fragment distribution travel time curve:
 50-68 deg, % 028
 124-126 degrees, % 0.....03
 In the design sector of 68-124 degrees, % 99.69

B) The initial velocities of the projectile fragments are within the design parameters and are 68-124 deg:

Light fractions 8x8x5 and 6x6x8.2, m/s 1340 - 2,340

Heavy fraction 13x13x8.2, m/s 1380 - 2,380

D) The maximum initial projectile velocities as determined by the tests are

Light fractions, m/s2440 - 2 580

Heavy fraction, m/s2460 - 2 570

The mechanical (piercing) effect of the bowtie-shaped 9H314M 1-10 projectiles, as determined by experiment, is in dural equivalent:

The angle between the velocity vector and the plane of the obstacle:
 90 deg. 23.0-26.3 mm
 30 deg. 10.0-12.2 mm

The elements were oriented in different positions, the magnitude of the obstacle pierced being the average for all positions and velocities (in the range of 1,000 m/s to 2,500 m/s).

Exhibit B.2.2 Testing of the warhead as part of the compartment hull

Tests were carried out on 31.07.2015 specifically to confirm the specifications of the warhead given to the DSB specialists.

During the test, the number and distribution of through-holes in the target witness sheets were counted. The punch count in the target witness sheets was carried out separately for the whole witness sheet and separately for the simulated contour section of the Boeing 777 ("in circumference").

As an example, Table B.2.1 shows the result of the punch count in target sheets 2 and 3.²⁹

Table B.2.1 - Number of holes in target sheets No. 2 and No. 3

Shield no.	sheet no.	Number of holes		Shield no.	sheet no.	Number of holes	
		total	within the circle			total	within the circle
2	2.0	619	560	3	3.0	594	533
	2.1	695	225		3.1	640	340
	2.2	293	290		3.2	246	245
	2.3	865	580		3.3	660	500
	2.4	94	94		3.4	141	141
	2.5	690	380		3.5	365	265
	2.6	14	13		3.6	43	43
	2.7	350	80		3.7	198	111
	Σ	3620	2222		3.8	2	0
			3.9	74	0		
			Σ	2963	2178		

Three types of penetrations are present on the shielded target fragments: from preformed fragments, from hull fragments (fragments of the compartment hull) and from detonation products³⁰ (holes of 1-3 mm in size).

As an example, Figure B.2.1 shows the exterior view of fragment (witness sheet) 2.1 of target No. 2.

All types of through-holes are clearly visible in the close-up view of this fragment shown in Figure B.2.2.

²⁹ Exterior view of all the target layout sheets is shown in Annex A of the Report on the conduct of a full-scale experiment (2016).

³⁰ Particles of unburned explosive material, small particles of ammunition components and fragments of destroyed projectiles.



Figure B. 2.1 - General view of fragment 2.1 of target No. 2

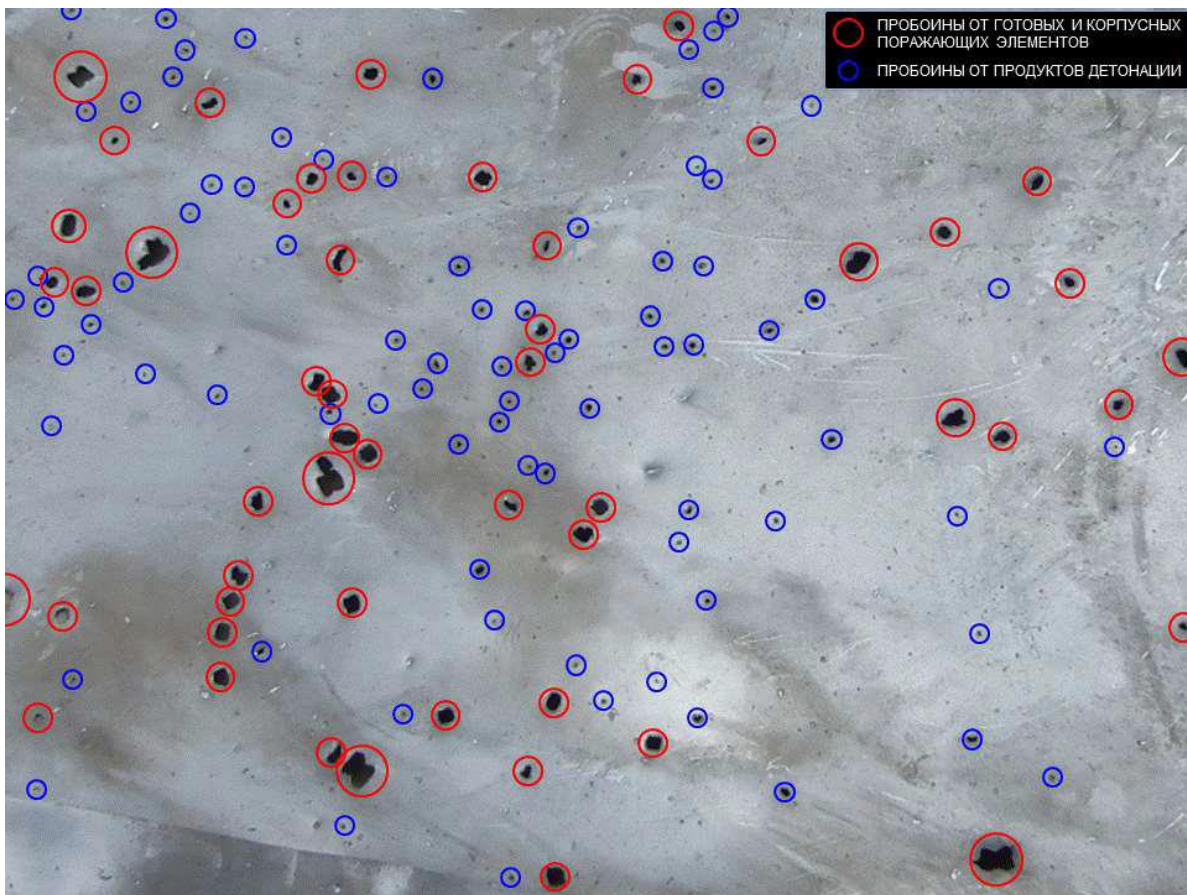


Figure B. 2.2 – Close-up of fragment 2.1 of target No. 2. Number of holes. During the tests, it was proven experimentally that the kill field of the 9H314M warhead when detonated as part of a missile compartment is up to three times larger than in virtual models that consider only preformed fragments.

The number of through-holes in 2 or 4 mm thick target shields is on average 2.4 to 2.6 times greater than when modelling prefabricated projectiles alone. When considering penetrations with linear dimensions corresponding to those of finished projectiles (6 to 13 mm), the number of penetrations is, on average, 1.8 to 2.0 times greater than when modelling finished projectiles only.

The modelling software used by the specialists of Almaz-Antey Corporation takes these features into account and calculates the trajectories of the fragments, taking into account the hull fragments (detonation products are not taken into account).

The fragment dispersal calculation software module takes into account more than 12,900 fragments. The simulation separates prefabricated projectile fragments (PFAs) and hull fragments:

- heavy fraction 9H314M 1-10 "bowtie" weighing ~ 8.1g (Heavy);
- light fractions 9H314M 1-9 and 9H314M 1-11 "parallelepiped" masses ~ 2.1-2.35 g (Light);
- hull fragments with linear dimensions of 6-13 mm (Shell).

Figure B.2.3 compares the simulation results with the actual fragment cloud covering target No. 2 obtained during field tests.³¹

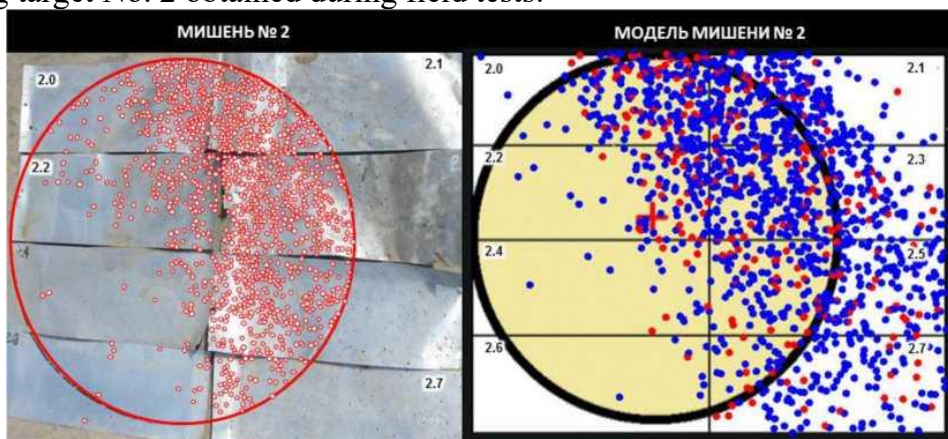


Figure B. 2.3 - Comparison of simulation results with the area covering target no. 2 based on tests

The left side of Figure B.2.3 shows the condition of Shield Target No. 2.³² The dots indicate the penetrations of the projectiles that have penetrated into

³¹ Modelling was carried out using the initial conditions for the first stage of the experiment (centre coordinates of the 9H314M warhead relative to the target environment and angles of orientation of the warhead in space corresponded to the Concern's "collision course" version)

³² Shield target No. 2 is chosen as the reference as it accommodates the meridional angle of the finished projectiles, ranging from 60° to 130°.

the circle.³³ The right-hand side of Figure B.2.3 shows the result of one implementation of the fragment coverage model of shield plate target No. 2.

The comparative analysis showed a high correlation between the results of the computer simulation of the static detonation of the 9H314M warhead (in the compartment housing) and the results of the conducted field test.

The discrepancy in the relative number of holes from the M_S simulation results with the relative number of holes on the No. 2 shield target sheets M_{EXP} , obtained during the tests, does not exceed 2.0% for each of the shields.

The estimated RMS deviation of the in-situ test results from the simulation results was about 1.1 %.

The use of a shield target made it possible to assess the distribution of penetrations from all types of projectiles over the two-degree zones of the PE meridional angle, as well as to determine the limits of the posterior front of the meridional angle of projectile fragments in a static detonation of a 9H314M warhead in a compartment shell.

Analysis of the distribution of the projectiles over the two-degree zones of the meridional angle of separation shows that in the static position the rear boundary of the fragmentation field of the 9H314M warhead is at least 124°-126°.

Thus, the results obtained in the field experiment, confirmed the consistency of the initial modelling data based on statistical data from government, control and series tests of the 9H314M.³⁴

The results of the analysis of the test results under static conditions are consistent:

1. A mathematical model of the static detonation of the 9H314M warhead, which includes not only projectiles, but also body fragmentation, and which is used by Corporation specialists to carry out the calculations.

2. The meridional angle of the 9H314M warhead's prefabricated projectiles, which is in accordance with the technical documentation, is 68°-124° according to the 1980s test data.

³³ In Figure B.21, the dots indicate only penetrations from prefabricated and hulled projectiles within the circumference - cross-section of the Boeing 777-200 fuselage.)

³⁴ Source data on the meridional angle of projectiles from the reference and series tests (during 9H314M development and production) were provided to the DSB experts in May and July 2015.

Exhibit B.2.3 Missile warhead tests

The tests were conducted on 07.10.2015 to verify the findings of the Dutch Safety Board (DSB) Report on the type of weapon that impacted the Malaysian Boeing 777-200 9M-MRD passenger aircraft that crashed on 17.07.2014 over Ukrainian territory during flight MH17 from Amsterdam to Kuala Lumpur.

As a result of the tests on the IL-86 target aircraft, the radio-transparent nose fairing and the weather radar equipment were perforated. More detailed photos of the damage to the nose fairing and weather radar can be found in the Field Experiment Report.³⁵

Using the damage to the radio-transparent nose fairing and the Ilyushin-86 target aircraft's weather radar equipment, the meridional angle of the posterior front of the fragmentation field can be calculated. Figure B.2.4 shows the raw data for estimating the rear edge meridional angle of the fragmentation field of the 9H314M warhead.

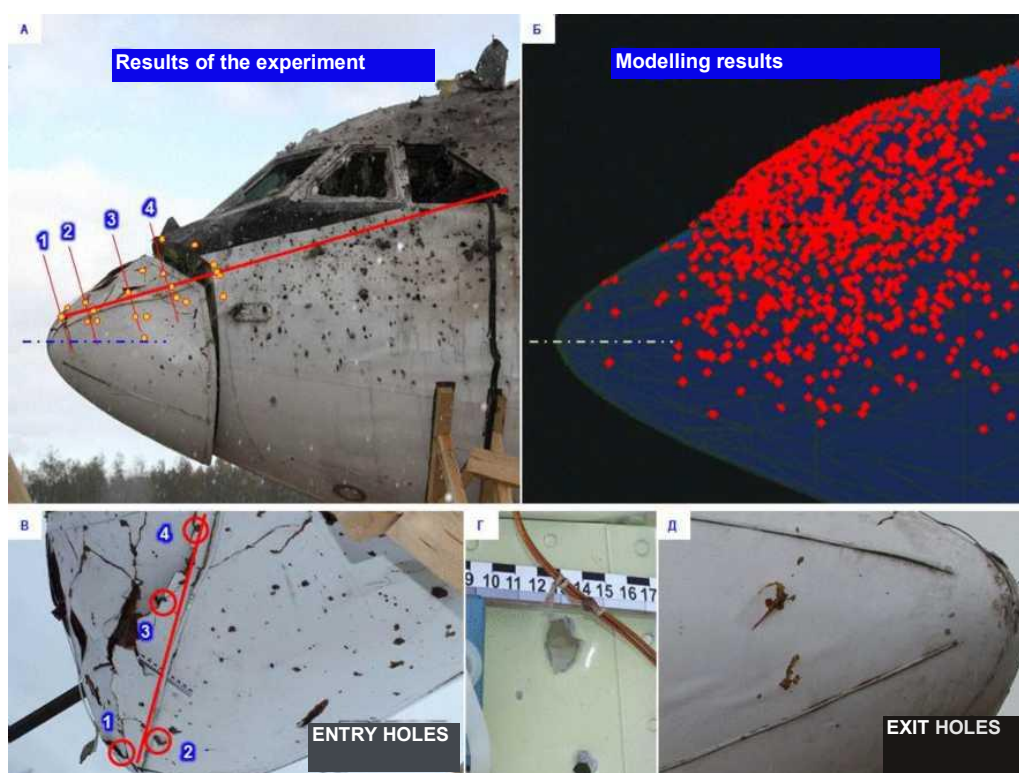


Figure B. 2.4 - Source data for estimating the rear edge of the 9H314M warhead's fragmentation field

The upper left corner (Figure B.2.4) shows the radio-transparent nose fairing of the IL-86 target aircraft. On it, numbers from "1" to "4" denote through-holes in the fairing, where "1" is the furthest single hole, and point "4" corresponds to the section where these hole marks are already present in high density.

³⁵ Report on the conduct of a full-scale experiment, pages 37-40.

For calculations of the posterior front of the meridional angle of fragment dispersion, a plane containing the formant (red line) offset from point "1" and located at an angle of 16.5 degrees, i.e. parallel to the centerline of the missile during the tests³⁶ is chosen.

On the top right (Fig. B.2.4) is the result of modelling the damage to the nose section of the IL-86 model under static experimental conditions. At the bottom of the figure are photographs illustrating entry and exit holes in the radio-transparent fairing, as well as damage to the weather radar equipment mounting bracket (corresponding to the section near point "3").

Calculations show that the through-holes located on the fairing and on the elements of the weather radar³⁷ correspond to a meridional angle of 120°-122°. The boundary of the furthest damage (cross-sections at points "2" and "1") corresponds to a value of over 124°-126°.

The missile's warhead tests under static conditions resulted in conformity:

1. The mathematical model of the static detonation of the 9H314M warhead used by the Corporation's specialists to carry out the calculations.
2. The values of the trailing edge of the meridional angle of the finished 9H314M warheads, which correspond to the technical documentation, to test data from the 1980s and are 124°-126°.

In addition, in the course of comprehensive tests, it was proven experimentally that the kill field of the 9H314M warhead is up to three times larger when the warhead is detonated as part of the missile compartment than in the virtual models, which consider only the preformed fragments.

The number of through-holes in the shield target and in the outer skin of the target aircraft is, on average, three times greater than when simulating only preformed fragments.³⁸

Low-density areas of PGE and hull exposures in the rear hemisphere were represented by witness targets (first stage of the full-scale experiment). These targets recorded areas of low DLE and hull impactor density in the rear hemisphere at angles greater than 150°-160°, i.e., under static conditions, fragments (prefabricated and hull impactors) propagate in a meridional plane in almost all directions after detonation.

³⁶ Including compensatory correction in the vertical plane for static +9.5° of the field experiment, Figure 3.2 and caption on page 8)

³⁷ Report on the conduct of a full-scale experiment, Figures 5.14 and 5.15, p.40.

³⁸ Report on the conduct of a full-scale experiment, pages 46, 61, 74.

Additionally, consistency between the experimental data and the data provided by the manufacturer of the Almaz-Antey equipment has been demonstrated in a number of independent in-situ tests.

A schematic representation of the fragmentation field generated by an exploding missile assembly in the meridional plane is shown in Figure B.2.5.

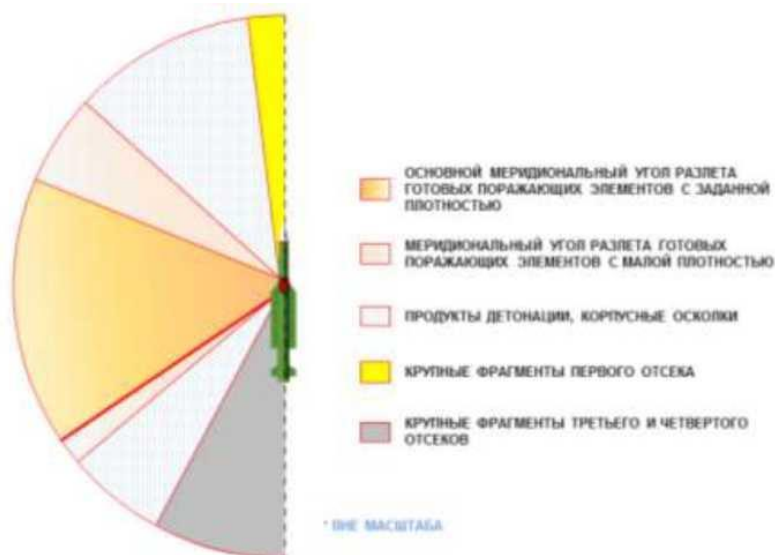


Figure B.2.5 - Static fragmentation field in the meridional plane

Thus, as a result of several in-situ experiments (including independent ones), confirmation of the value of the meridional angle of the finished 9H314M warheads' dispersion was obtained, which corresponds to the technical documentation and data from the control and periodic tests of the 1980s and amounts to 68°-126°.

Experimentally confirmed the presence of a low density region of projectiles and hull fragments in the posterior hemisphere (up to 150° or more).

Exhibit B.3. Confirmation of mechanical effect (penetration) of prefabricated projectiles

When modelling the impact of an anti-aircraft warhead on a target, the main characteristics of the killing field that must be identified are the mechanical (penetration) characteristics. Because it is indicators such as penetration depth (together with the configuration of the breach) and kinetic energy that determine the degree of impact of the warhead: the effectiveness of the impact on a range of target elements - cables, control circuits, hydraulic systems, etc., deformation and destruction of target structural elements.

The basic parameters characterizing the mechanical (piercing) effect of the hit elements of BUK missile warheads were communicated to the Dutch experts in a letter sent to the DSB at the end of July 2015. At the beginning of August 2015, during a meeting with DSB experts, the technical characteristics were visually confirmed by an illustration of the materials of full-scale tests carried out specifically for this purpose (Figures B.3.1 and B.3.2).

The need to assess the mechanical (piercing) effect of the projectile was again stressed during discussions.³⁹

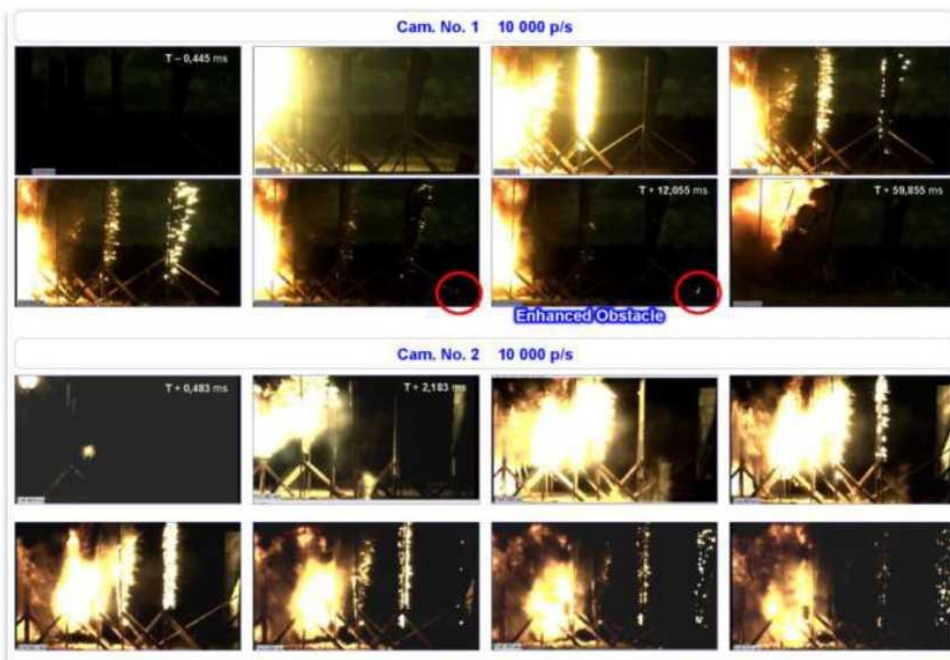


Figure B.3.1 - Demonstration of the mechanical (penetration) capability of the 9H314M projectile. The projectiles successively penetrate up to 5-6 combined obstacles

³⁹ Presentation of Almaz-Antey. JSC Concern Almaz-Antey. Findings of Expert Assessments on MH17 Accident. August, 2015, Gilze.



Figure B.3.2 - Fragments of material characterizing the mechanical (penetration) capacity of 9H314M warheads provided to DSB experts during the joint work phase in August 2015 (Gilze-Rijen, Netherlands)

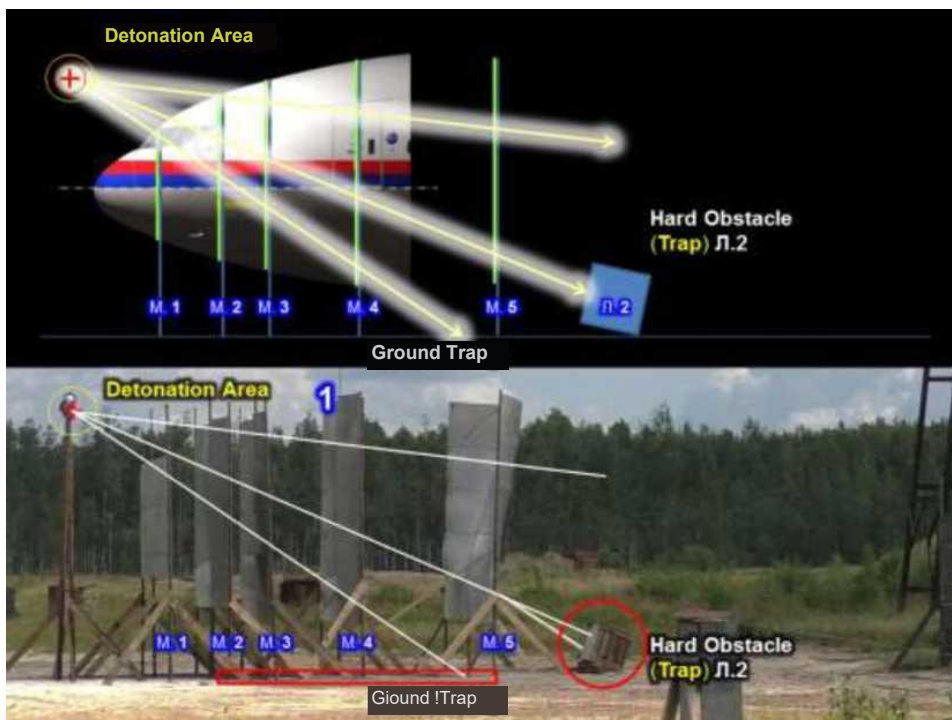


Figure B.3.3 - Approximate trajectories of the projectiles: top - layout of the target environment; bottom - photo before the test

During the first tests, the projectiles of all three fractions penetrated up to 5-6 obstacles made of aluminium alloy AMg6M with thickness from 2.0 to 4.0 mm. The leading projectiles retained a high velocity of up to 1670-1990 m/s after penetrating even 3 obstacles.⁴⁰

The diagram (Figure B.3.3) shows the approximate trajectories of some of the finished projectiles - penetrating successive obstacles, Ground Trap and Special Trap "L.2" (Hard Obstacle/Trap).

Figures B.3.4-B.3.7 (still images) show the moments of detonation, of the projectiles crossing certain obstacles and entering the Ground Trap and Hard Obstacle/Trap No. 2, which is marked "L.2" in the diagram.



Figure B.3.4 - Momentum T+0.383 ms after detonation (top left corner)

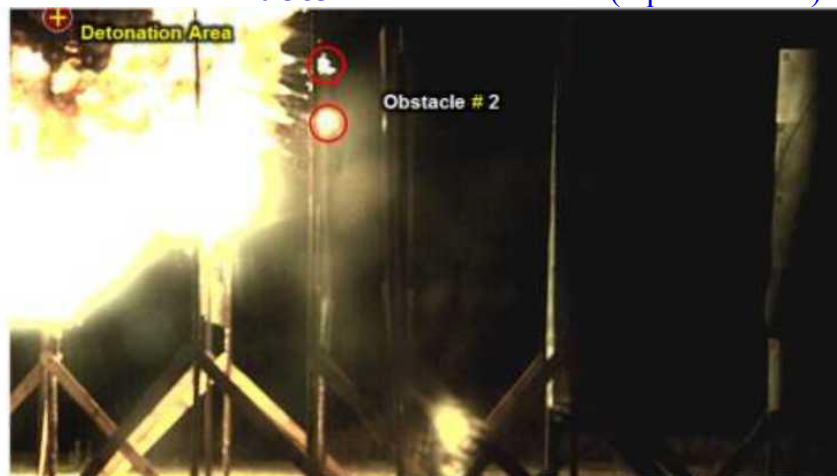


Figure B.3.5 - Overcoming obstacle No. 2 (highlighted in red)

⁴⁰ Report on the conduct of a full-scale experiment, pages 157, 158.

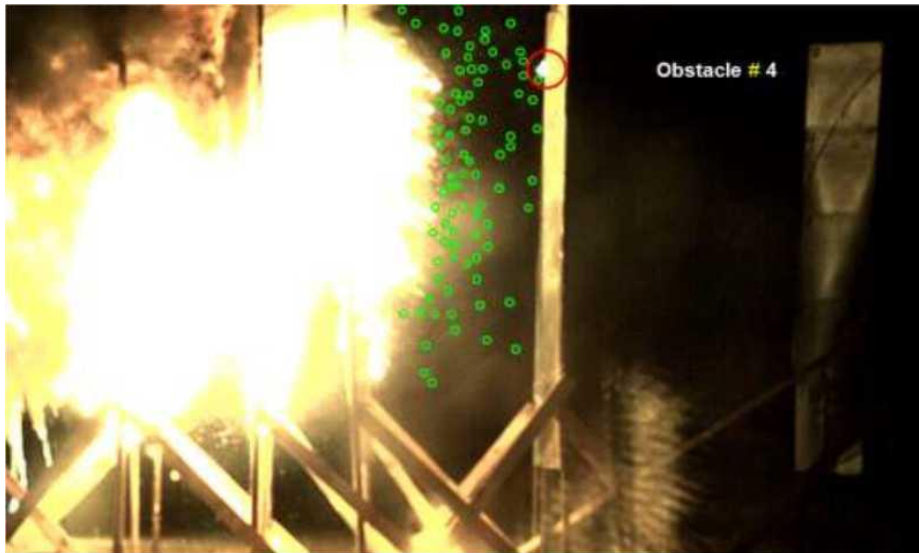


Figure B.3.6 - Overcoming Obstacle #4 by the first GGE (highlighted in red). In green are the leading hitters



Figure B.3.6 - Overcoming obstacle No. 5 (highlighted in red above right) and hitting the Ground Trap (below)



Figure B.3.7 - Causing a group of casualties to enter the special "L.2" trap (highlighted in red in the lower left corner)

A penetration test revealed that the 9H314M type 1-10 ("bowtie") projectile penetrated a complex combined trap barrier to a depth of 400.0-450.0 mm, taking into account the outer skin of the trap (2.0 mm aluminium alloy AMg6M) and the stopping foam PS-150 (three layers of 260.0 mm total thickness).⁴¹

Piercing the structure of the aircraft (target aircraft) through

When considering the "opposite direction" version (the basic DSB version), the preformed projectiles from the 9H314M warhead can penetrate an aircraft structure (several successive combined obstacles) and exit out the back side.

In order to assess the penetration of the Boeing 777's structure, the IL-86 target plane experiment was carried out in preparation for and during the experiment:

1. Modelling of PE trajectories (different fractions and hulls), the conditions of PE interaction with obstacles (outer skin) and their distribution over different parts of the nose of the aircraft were determined. For this purpose, various variants of the Boeing 777 aircraft model were used, including a 'transparent' (Wireframe) and an Interactive model.

Part of the modelling results are shown in Figure B.3.8 (based on the preparation of the second phase of the in-situ experiment).

⁴¹ Report on the conduct of a full-scale experiment, p.162.

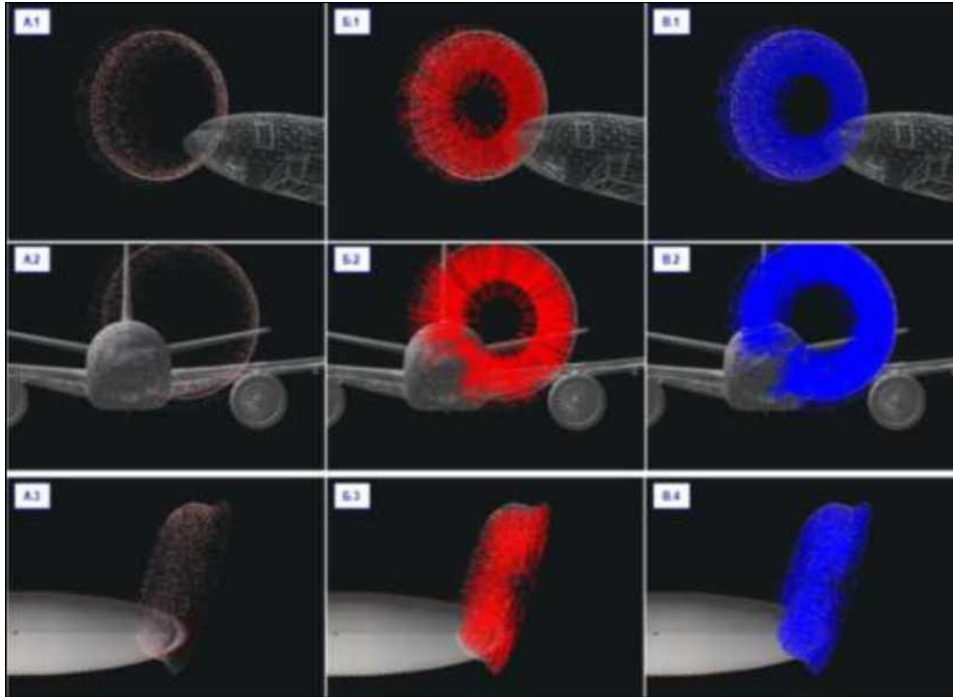


Figure B.3.8 - Preliminary modelling of GGE trajectories: left - leading preformed fragments front; centre - heavy preformed fragments trajectories; right - light preformed fragments trajectories

2. Appropriate recalculations were made for the IL-86 target aircraft and static ground conditions (Figure B.3.9).

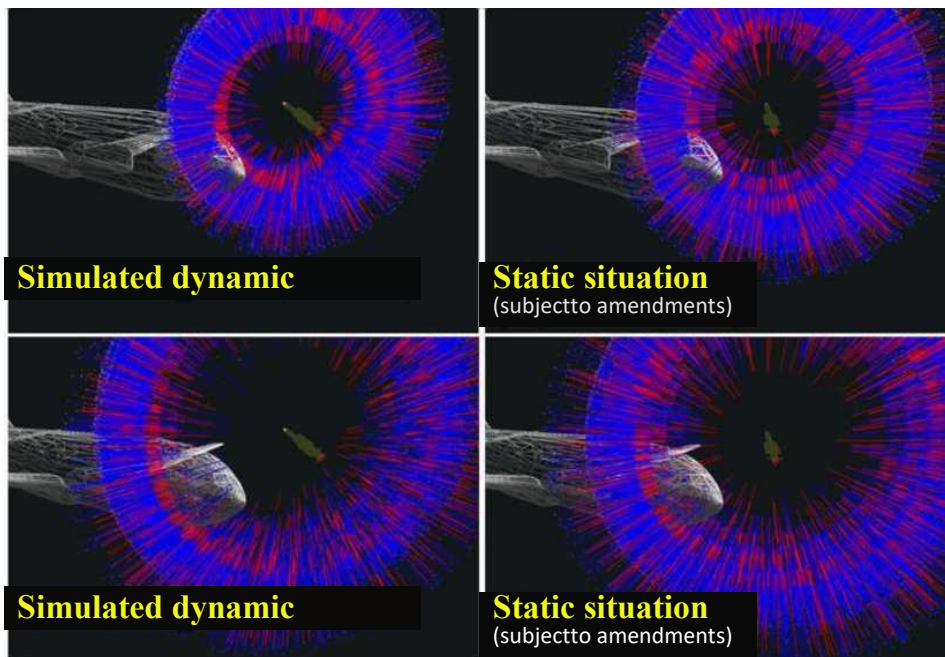


Figure B.3.9 - Simulation of dynamic (left) and static (right) corrected situations for target aircraft IL-86

Based on the simulation, a target environment was generated (Figure B.3.10), primarily for fixing starboard through-punching (area and box traps, speed sensors, fixing video cameras, etc.).

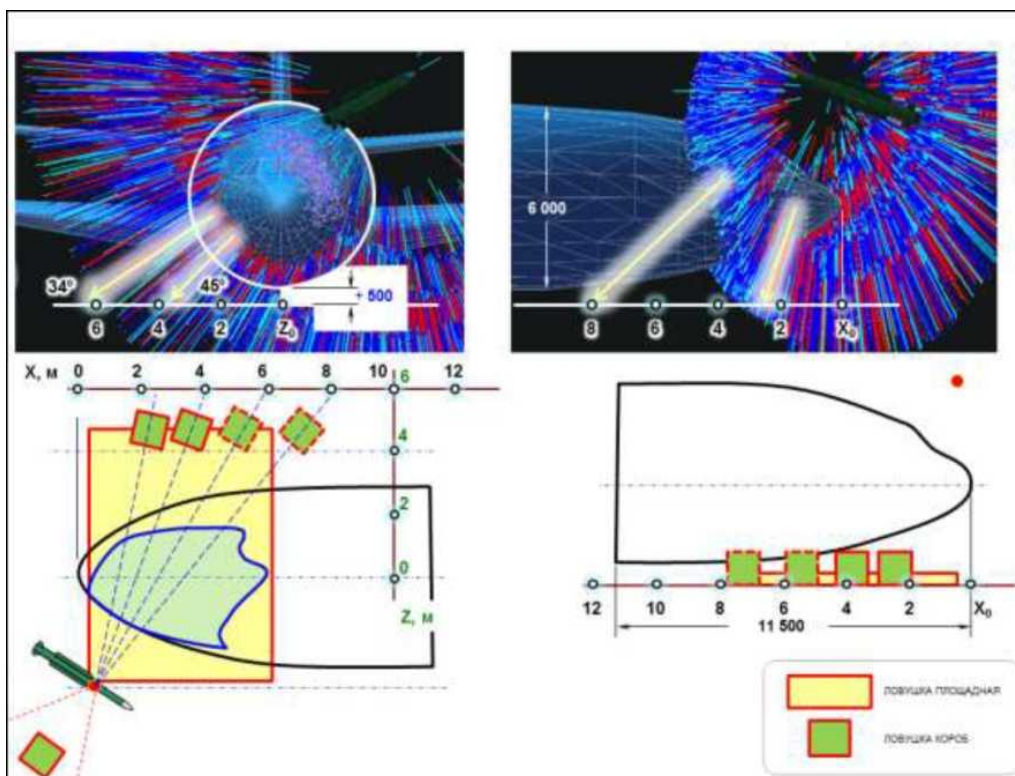


Figure B.3.10 - Target Correction Using the Interactive Model of the IL-86 Target Aircraft

3. The starboard piercing was recorded using video equipment and speed sensors.

Some of the consecutive video footage is shown in Figures B.3.11-B.3.16.

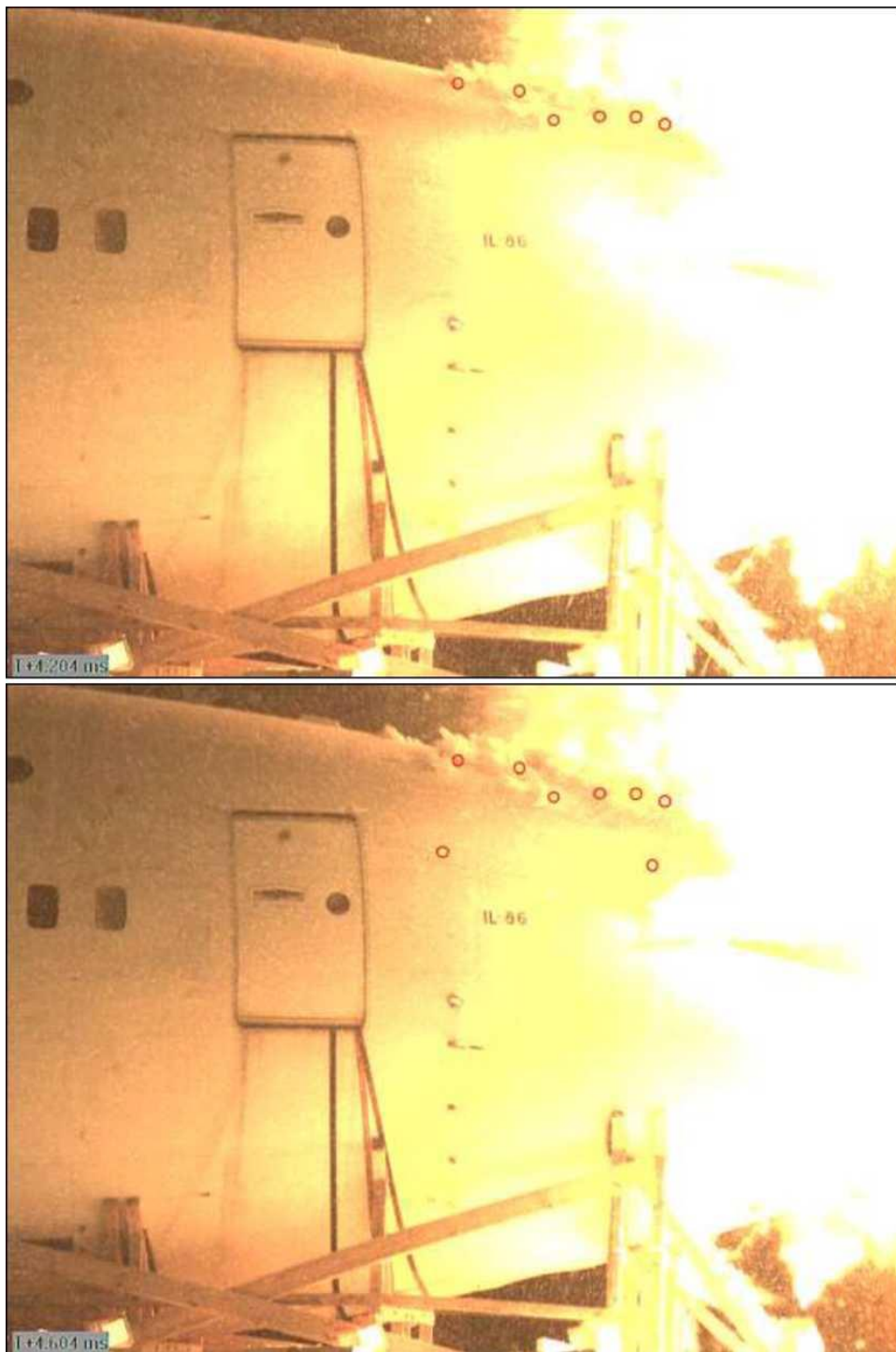


Figure B.3.11 - Puncturing the starboard side of target aircraft b-86 (top - T+ 4.204 ms; bottom - T+ 4.604 ms)



Figure B.3.12 - Puncturing the starboard side of the target aircraft IL-86 (top - T+ 5.204 ms; bottom - T+ 5.404 ms)

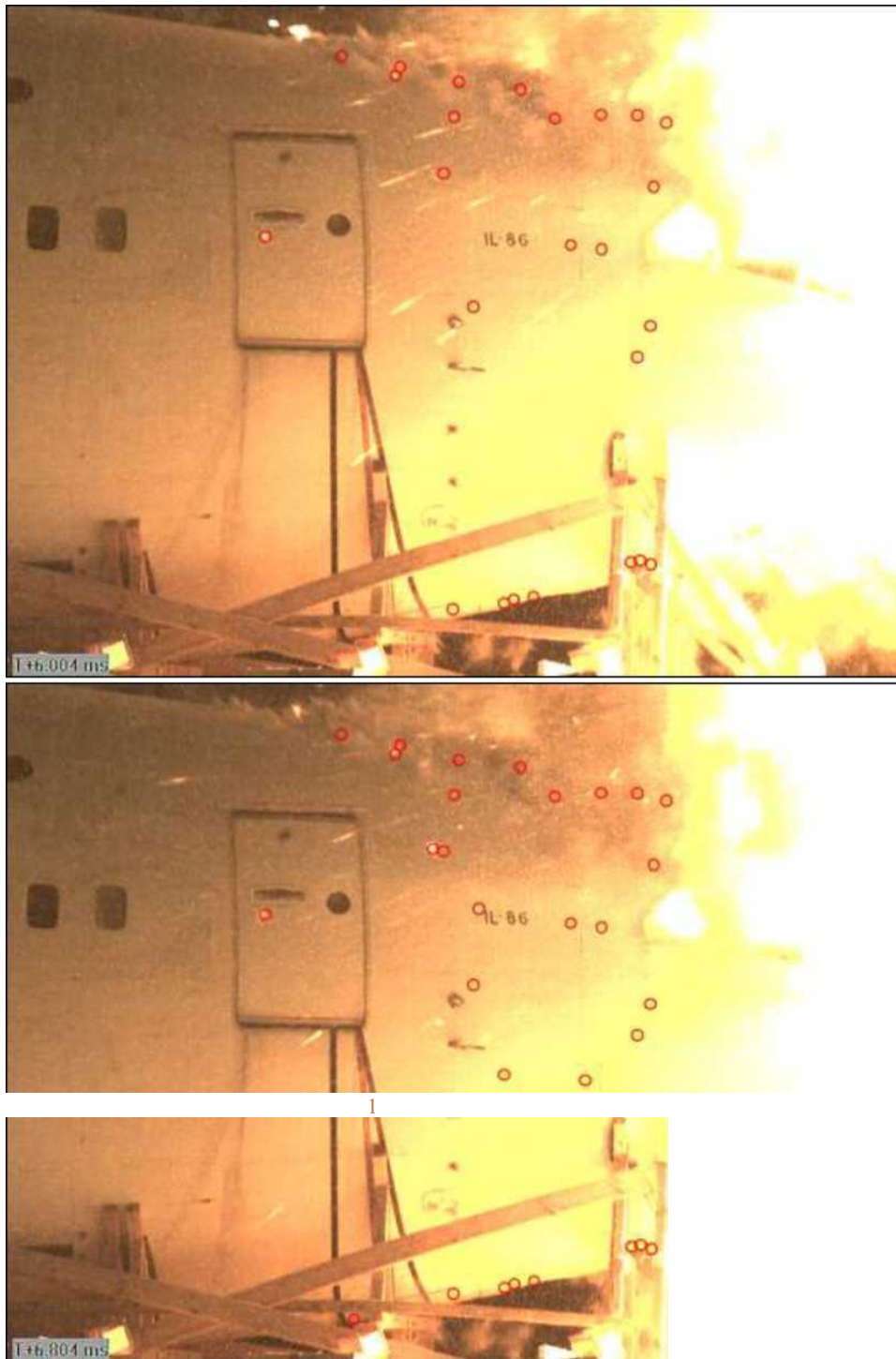


Figure B.3.13 - Puncturing the starboard side of the target aircraft IL-86 (top - T+ 6.004 ms; bottom - T+ 6.804 ms)

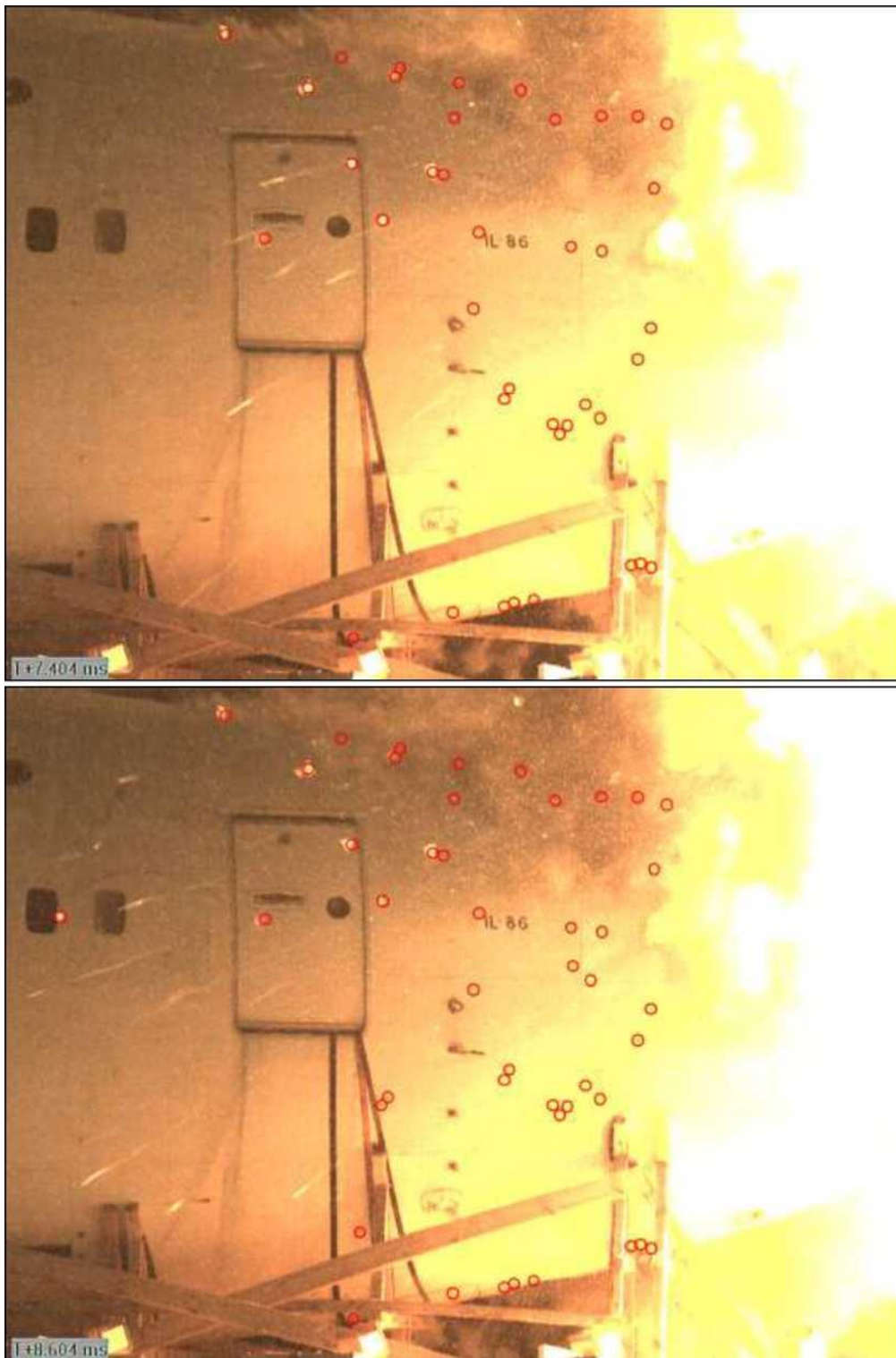


Figure B.3.14 - Puncturing the starboard side of the target aircraft IL-86 (top - T+ 7.404 ms; bottom - T+ 8.604 ms)



Figure B.3.15 - Puncturing the starboard side of the target aircraft IL-86 (top - T+ 9.004 ms; bottom - T+ 10.604 ms)



Figure B.3.16 - Puncturing the starboard side of target aircraft IL-86 (top - T+ 11.004 ms; bottom - T+ 12.204 ms)

4. Photo-fixation of damage (exit holes) on the starboard side, as well as the floor and internal equipment of the target aircraft cockpit was carried out. Materials are presented in the Field Test Report.

In the second experiment, the 9H314M warhead of the 9M38M1 missile was found to penetrate the cockpit structure when detonated according to the DSB report, as confirmed by the video and photographic evidence presented in the Corporation's report.⁴²

The projectiles that pierced the hull of the aircraft successively overcame at least three to five combined dispersed obstacles in varying combinations:

- elements of the outer skin of the aircraft on the port side and/or roof;
- thermal insulation and decorative panels of the port side and/or roof;
- panels or cabinets with equipment on the port side or roof;
- cockpit floor, including longitudinal or transverse power elements;
- panels or cabinets with equipment on the starboard side or under the cockpit floor;
- thermal insulation and decorative panels on the starboard side or underbody;
- elements of the outer skin of the aircraft on the starboard side or underbody aircraft.⁴³



Figure B.3.17 - Example of through holes in the cockpit floor and framework of the B-86 target aircraft cockpit floor

On the port side, penetrating fragmentation damage from preformed fragments was recorded from the nose fairing and weather radar to the front left passenger door L1 inclusive. Non-penetrating damage (ricochets) in the cockpit glazing area, unlike that of the Boeing 777, was not recorded (Figures B.3.18 and B.3.19).

⁴² Report on the conduct of a full-scale experiment, pages 75-88; 149-157.

⁴³ Report on the conduct of a full-scale experiment, pages 90-107; 157.



Figure B.3.18 - No non-penetrating damage (ricochets) from preformed fragments on the port side of target aircraft b-86

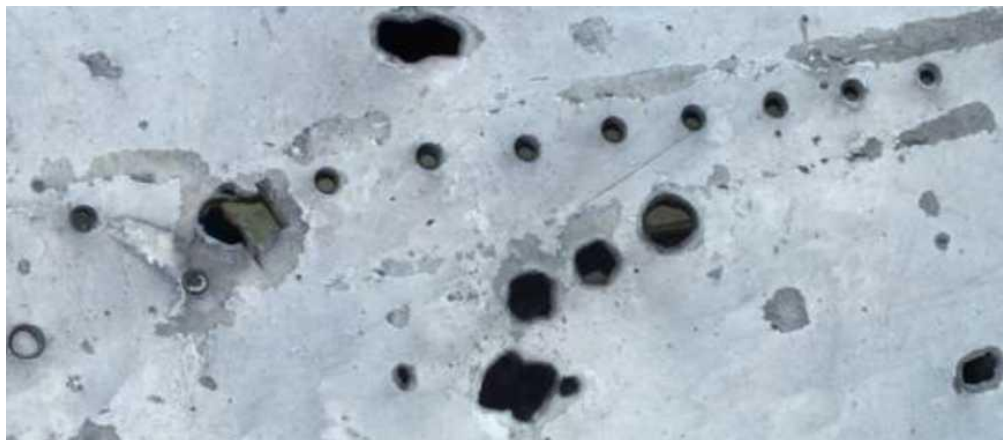


Figure B.3.19 - Fragment of the left side skin of the target behind the windows of the aircraft commander (close-up). No non-penetrating damage from any of the projectiles was observed. The fragment shows the characteristic "bowtie" holes from 9H314M 1-10 projectiles.



Figure B.3.20 - Characteristic view of the damage to the dovetails on the left side of the cockpit of the B-86 target aircraft (L-shaped reinforcements of the dovetails have been holed). The direction of motion of the projectiles is transverse to the structure of the aircraft. No piercing holes in the bulkheads

5. A comparative analysis was made of the results obtained from the preliminary modelling and from the experiment. Based on archival data, as well as tests conducted under dynamic conditions on missile stands and with airborne targets (Figures B.3.21-B.3.23), conclusions were drawn about the penetration of the aircraft structure through.

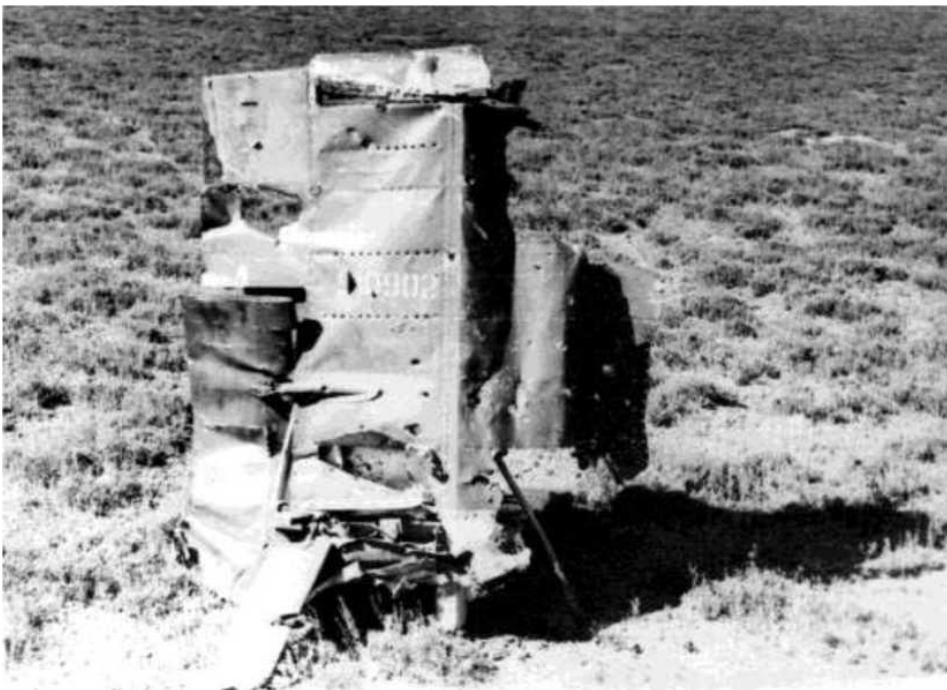


Figure B.3.21 - Target structure pierced through, outer skin and power frame perforated, deformed and destroyed (Resource: Almaz-Antey Archive)

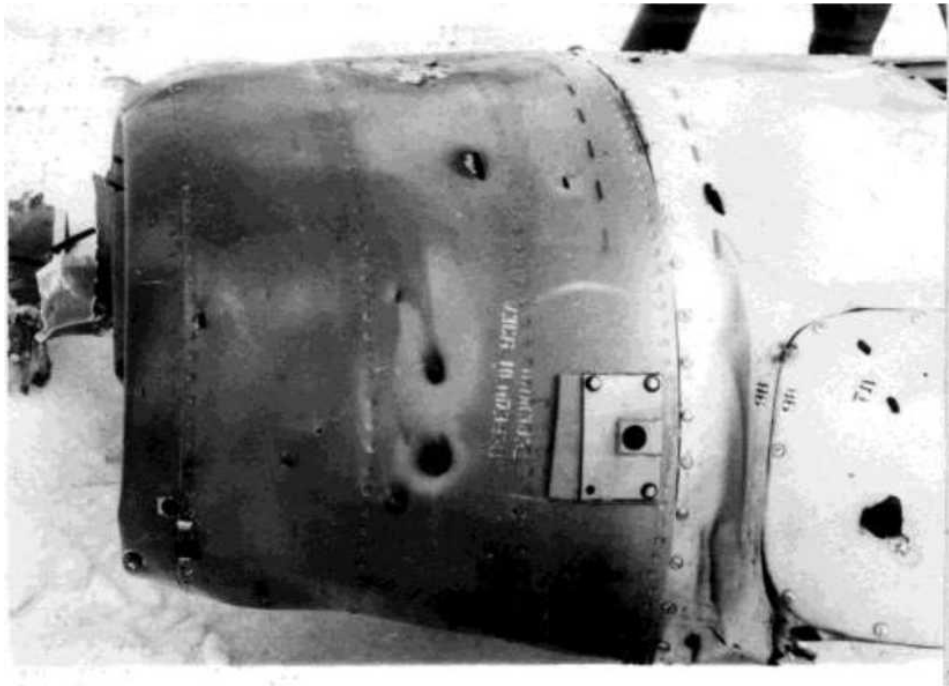


Figure B.3.22 - Target jet engine structure perforated, outer skin and power frame perforated and deformed (Resource: Almaz-Antey archive)

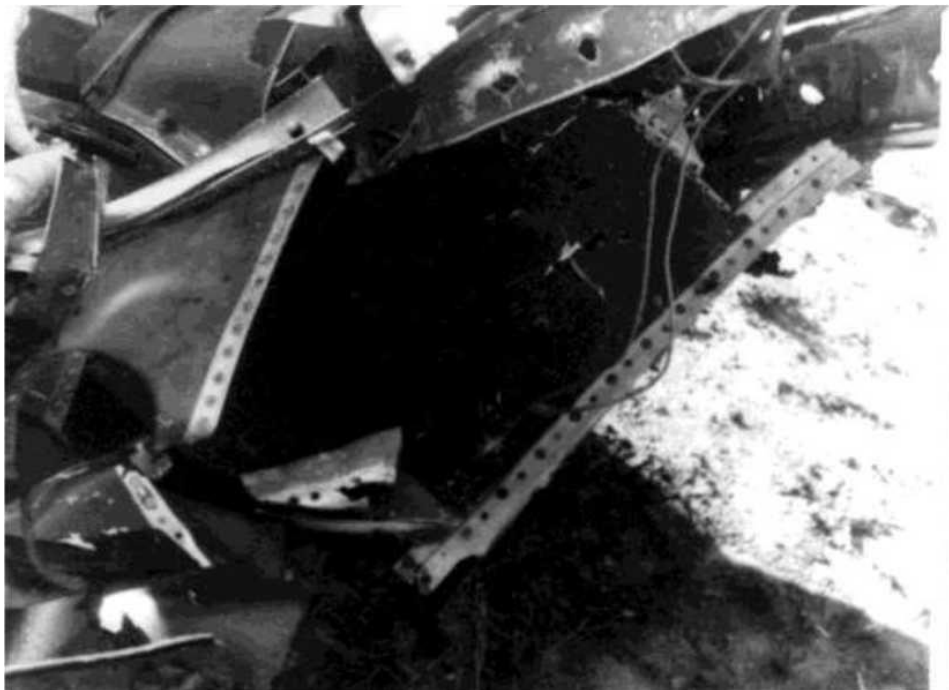


Figure B.3.23 - Target pierced through, outer skin and power frame perforated, deformed and destroyed (Resource: Almaz-Antey Archive)

The results of two experiments and additional special tests of the mechanical (piercing) action of preformed fragments revealed a discrepancy between the piercing action of the flow of finished projectiles produced by the 9H314M warhead and the piercing action of the projectile that hit the Boeing 777 according to DSB, which also excludes the "opposite direction" version for the BUK missiles.⁴⁴

Analysis of the mechanical (piercing) action of the prefabricated projectiles showed that the characteristics declared in the technical documentation are confirmed - the prefabricated projectiles are capable of piercing combined and/or consecutive obstacles (up to 26 mm in dural equivalent), depending on the entry angles.

When considering the version of the missile being detonated on a "head-on" course, **the 9H314M's warheads penetrate the structure of the aircraft**, as evidenced by the presence of dozens of "**inside-out**" exit holes in the right side, the right side of the roof and on the bottom of the IL-86 target aircraft.

⁴⁴ Report on the conduct of a full-scale experiment, pages 149 - 164, 190.

Exhibit B.4. Special experimental studies to assess the penetration of projectiles

In order to verify the simulation results, the damage observed on the Boeing 777-200 (MH17) airframe fragments corresponded to the mechanical (piercing) capacity of the 9H314M projectiles, special experimental studies were carried out to assess the piercing effect of the projectiles.

The test objects were 9H314 1-10 heavy fraction projectiles ("bowties") and two 9H314 1-11 and 9H314 1-9 light fraction projectiles ("parallelepipeds") of the 9H314M product. Exterior view of elements and pallets for them is shown in Figures B.4.1- B.4.3.

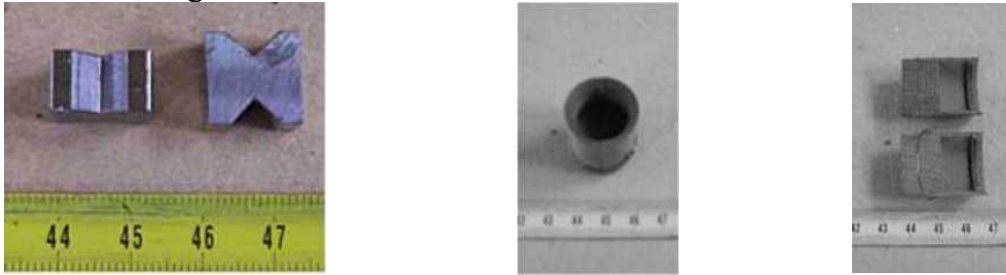


Figure B.4.1 - Exterior view of projectile No. 1 and its pallet

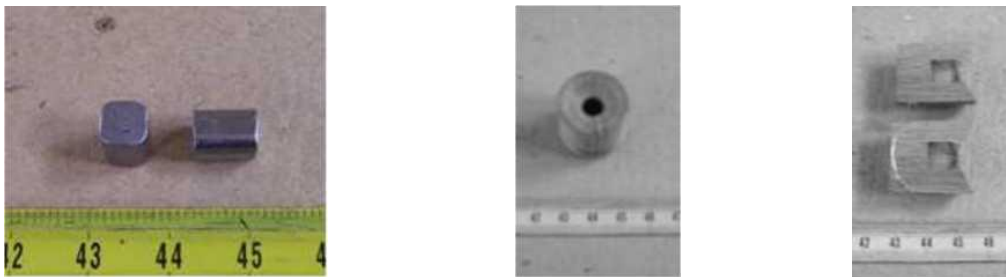


Figure B.4.2 - Exterior view of projectile no. 2 and its pallet

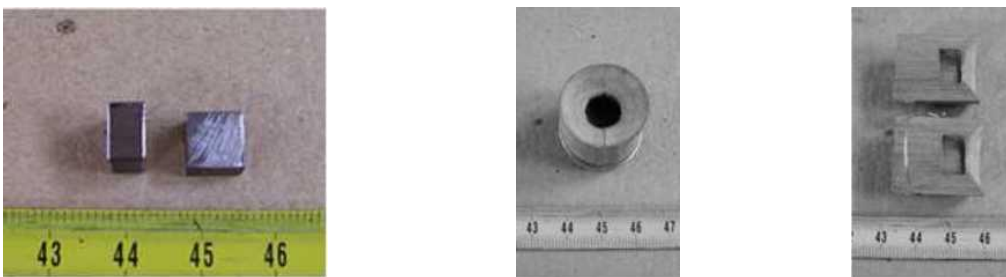


Figure B.4.3 - Exterior view of projectile no. 3 and its pallet

The weight and size characteristics of the projectiles used in the 9H314M product (in accordance with the requirements of the technical documentation) are given in Table B.4.1.

Table B.4.1 - Weight and size characteristics of ready-made 9H314M projectiles

Projectiles	Dimensions, mm			Weight, g	Weight distribution, g
	Base length	Base width	Height		
9H314M 1-10	13.0 ^{+0,6} - 0,4	13,0- 0,7	8,2 ⁺ 0,2	8,1	± 0,6 - 0,1
9H314M 1-11	6,0- 0,08	6,0- 0,08	8,2± 0,2	2,1	± 0,01 - 0,17
9H314M 1-9	8,0- 0,09	8,0- 0,09	^{+ 0,1} 5,0 - 0,2	2,35	± 0,15

The weight and size characteristics of the projectiles involved in special piercing studies are given in Table B.4.2.

Table B.4.2 - Weight and size characteristics of the projectiles

Projectiles	Dimensions, mm			Weight, g
	Base length	Base width	Height	
Item No. 1 9H314M 1-10	12,8-13,1	12,8-13,1	8,1-8,2	8,1-8,2
Item No. 2 9H314M 1-11	6,0	6,0	8,1-8,2	2,03-2,07
Item No. 3 9H314M 1-9	7,95-8,0	7,95-8,0	4,9-5,1	2,36-2,48

Tests were carried out to assess the penetration of projectiles in an aluminium barrier. The characteristics to be determined are the ricochet angles of the projectiles when penetrating a 2.0 mm thick duralumin barrier.

The tests were conducted by firing projectiles at AMg6M aluminium alloy sheets from the PPN-23 ballistic unit using textolite pallets and polyethylene thrusters.

The barrier sheets were set at angles of 5, 10 and 15 degrees to the firing line (horizon), with all three types of projectiles being thrown into the sheet at each set angle.

The projectiles were thrown into the obstacle at a velocity range of 1640 to 1770 m/s. These conditions correspond to the minimum velocities for the dynamic detonation conditions of the warhead.⁴⁵

The values for the test parameters are given in Table B.4.3.

⁴⁵ The velocity of the projectile (element) approaching the obstacle, V_0 was determined from the measuring base span times measured by the frequency meters.

Table B.4.3 - Test parameters

Description	Value
Angle of inclination of obstacle, deg.	5, 10, 15
Velocity of the element meeting the obstacle, m/s: - 9H314M 1-10 - 9H314M 1-11 - 9H314M 1-9	1640 - 1770 1655 - 1729 1648 - 1663

The interaction of the projectiles with the target was recorded by an electro-optical camera. In order to cut off the influence of the tray on the barrier, a cut-off device was installed between the unit and the barrier.

The projectiles to be thrown were fixed rigidly in the pallet with the base perpendicular to the line of sight.⁴⁶

The trays with the projectiles were installed in PPN-23 and additionally sealed with a pusher.

A diagram of the experiments for testing the mechanical (penetration) capacity of the projectiles is shown in figure B.4.4.

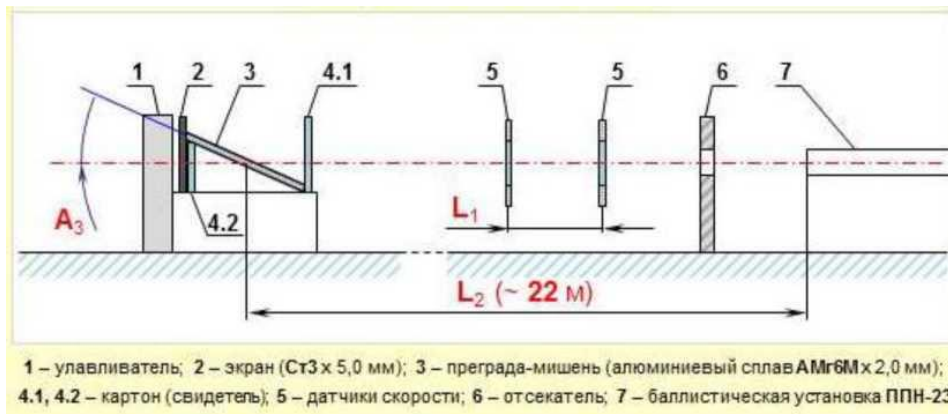


Figure B.4.4 - Test scheme

Figures B.4.5-B.4.7 show still images from a high-speed camera capturing the order in which the projectiles interact with the obstacles of the target environment.

⁴⁶ The base of element no. 2 ("parallelepiped" 9H314M 1-11) is a square face.

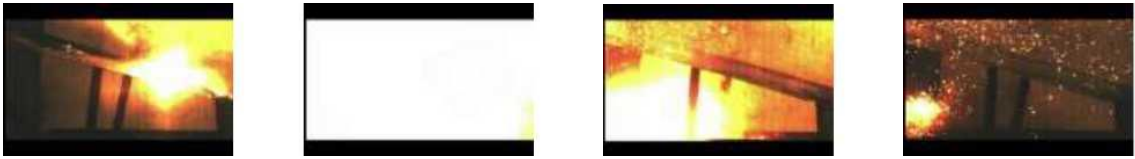


Figure B.4.5 - Barrier set at an angle of 15 degrees



Figure B.4.6 - Barrier set at an angle of 10 degrees



Figure B.4.7 - Barrier set at an angle of 5 degrees

The orientation of the element on the approach to and behind the barrier was determined using cardboard witnesses.

Examples of the exterior view of barriers and witnesses after interaction with the projectiles are shown in the photographs (Figures B.4.8-B.4.15).



Figure B.4.8 - Exterior view of barriers after interaction with the projectiles



Figure B.4.9 - Witness appearance after interaction with the element

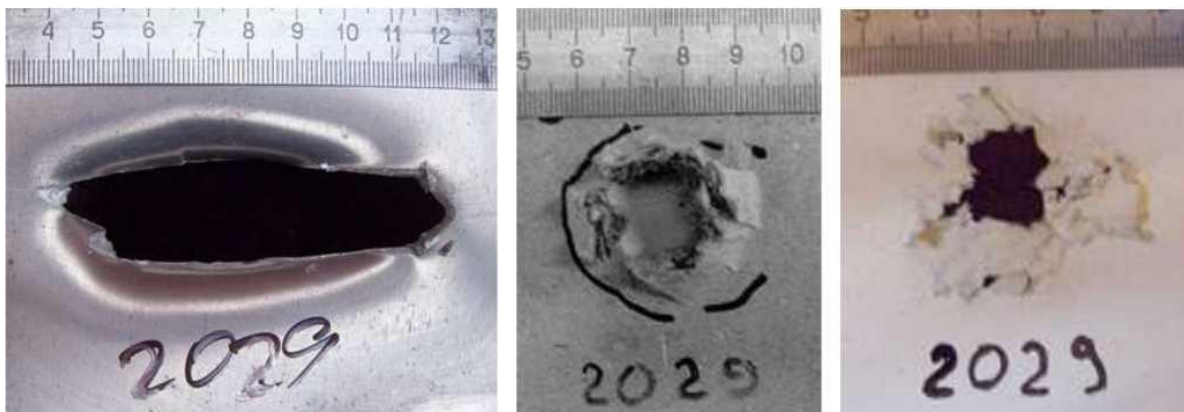


Figure B.4.10 - Experiment 2029. Exterior view of the barrier (left) and witnesses before (centre) and after the barrier (right) as a result of interaction with element no. 1 at an angle of 15° to the firing line at 1683 m/s



Figure B.4.11 - Exterior view of obstacle after interaction with projectiles Nos. 1-3 at an angle of 10° to the firing line



Figure B. 4.12 - Experiment 2040. Exterior view of obstacle after interaction with element no. 1 at an angle of 10° to the firing line at 1688 m/s



Figure B.4.13 - Experiment 2030. Exterior view of obstacle (Exterior view) after interaction with element no. 1 (9H314M 1-10) at an angle of 5° to the firing line at 1640 m/s



Figure B.4.14 - Experiment 2030. Exterior view of obstacle (inside view) after interaction with element No. 1 (9H314M 1-10) at an angle of 5° to the firing line at 1640 m/s

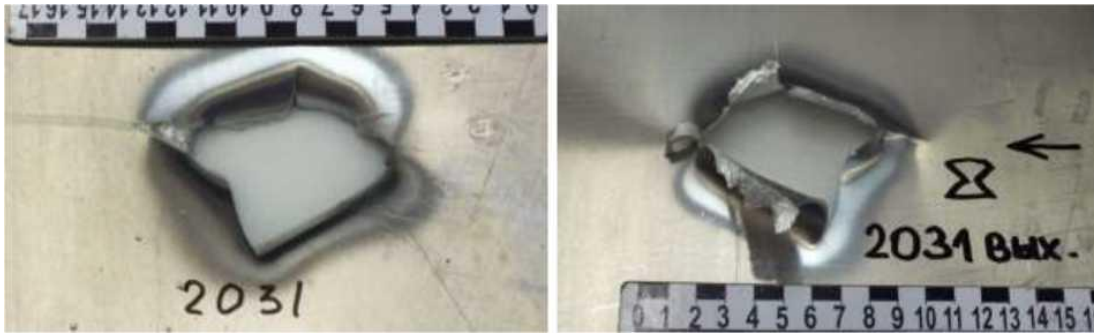


Figure B.4.15 - Experiment 2031. External (left) and internal (right) exterior view of the barrier after interaction with element no. 1 (9H314M 1-10) at an angle of 5° to the firing line at a velocity of 1770 m/s

Main test results:

1. In all cases, a 15° angle barrier and a flush approach by the element to the barrier resulted in the element penetrating the barrier and penetrating behind the barrier.
2. In most cases of a 10° and 5° barrier, a penetration through the barrier with a ricochet of the element (without penetration beyond the barrier) occurred.
3. In a number of cases, a penetration of the barrier at angles of 10° and 5° resulted in a penetration of the barrier with the element penetrating behind the barrier.
4. In one case (experiment 2012) the element ricocheted into the barrier without penetrating the barrier (Figure B.4.16).

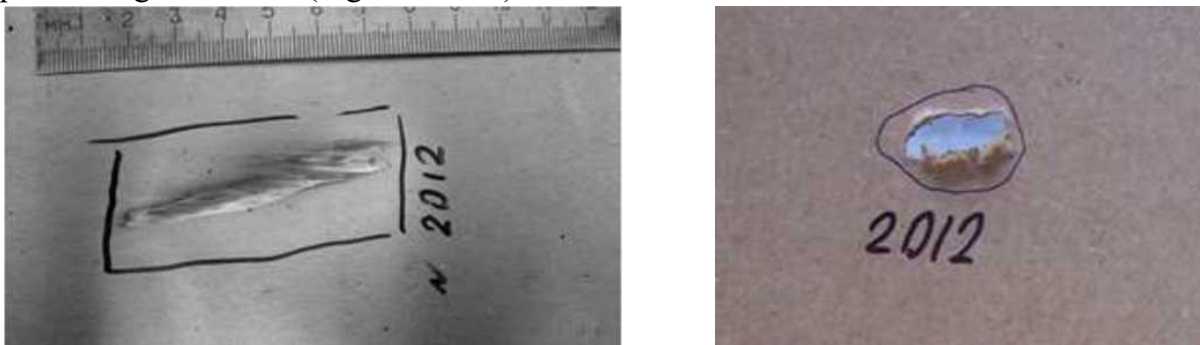


Figure B.4.16 - Experiment 2012. Exterior view of the barrier and witness after interaction with the element (no through penetration of the barrier)

5. Projectiles penetrating behind the barrier and approaching the barrier flat maintained their orientation and ensured subsequent penetration of the 5.0 mm thick steel St3 shield (Figure B.4.17).



Figure B.4.17 - Exterior view of steel shield (St3 x 5.00 mm) after interaction with projectiles penetrating beyond the barrier (left side is a breach from element 9H314M 1-10 "bowtie")

In this way, the tests confirmed the penetration capability of the projectiles - the projectiles are guaranteed to pierce and penetrate behind duralumin barriers at angles to the firing line of 15 degrees or more.

When prefabricated projectiles meet duralumin barriers at angles of 15 degrees or more to the direction of impact of the fragmentation field, a guaranteed through penetration of the barrier and penetration of the projectiles beyond the barrier is assured.

Conditions for ricochets from duralumin barriers occur in the encounter angle range of 5°... 10° or less.

Exhibit C: Rationale for the selection of the target aircraft

The choice of the target aircraft for the second test was based on three main parameters:

Firstly, the diameter of the target plane's fuselage had to match that of the Boeing 777 as closely as possible.

When selecting a target aeroplane, Almaz-Antey specialists used aircraft construction drawings which show that the difference between the fuselage diameter of the Boeing 777-200 and that of the IL-86 is (6.08:6.20 0.9806), that is less than 2%:

The fuselage diameter of the Boeing 777-200 is 6.20 metres;

The fuselage diameter of the IL-86 is 6.08 metres.

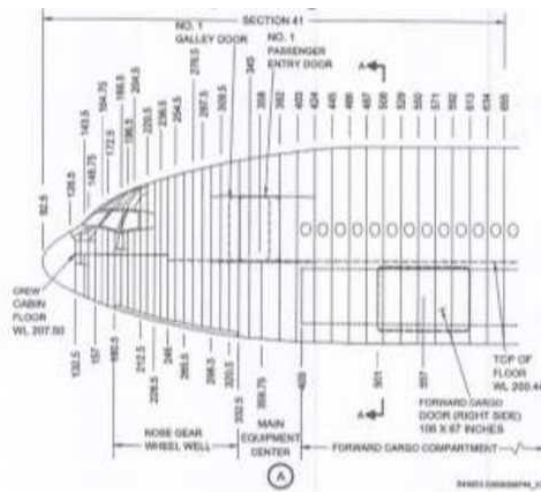


Figure C.1 - Fragment of the construction drawing of the Boeing 777 nose section



Figure C.2 - Fragment of the IL-86 nose section drawing used to select and prepare the target for the experiment

Secondly, it was necessary to achieve the best possible match between the roof contour of the target aircraft and the Boeing 777.

An analysis of the drawings and 3D models shows that the nose section of the IL-86 and Boeing 777 target cockpit has a high degree of overlap in level and roof outline in the glazing area.

When aligned with the cockpit roofline, the discrepancy in the cockpit glazing area and up to the level of the left-hand front passenger door is no more than 4-5 %.

The maximum divergence (up to 8%) is from the tip of the nose (radio transparent cowl) and up to the level of the forward pressure bulkhead. On the Boeing 777 (MH17), the front boundary of the fragmentation zone is the forward pressure bulkhead (level STA. 132.5), therefore the area of the radio transparent cowl is not critical for the experiment - it is located before the actual front damage boundary.

In addition, to compensate for inaccuracies in the mounting of the target aircraft on the test stand, a tray was used, the alignment of which allowed the roof contours in the cockpit area - the main object of study for the experiment - to be aligned as closely as possible.

In the 2016 Almaz-Antey Corporation Field Experiment Report, paragraph 3.1.2 on page 11. 11 of 190 states that the target pile No. 1 (the IL-86 target aircraft) was designed and built in agreement with specialists from JSC "Ilyushin".



Figure C.3 - Stand to align cockpit roof contours. (Figure from Almaz-Antey Experiment Report, page 12 of 190)

In addition, the Report indicates that compensatory corrections were used to compensate for static conditions and target differences (page 8 of 190 Field Experiment Report).

Considering that the missile was located to the left and above the level of the cockpit floor, the projection area of the nose of the IL-86 target aircraft (from the forward gimbal, excluding the radio transparent cover, to the left front door of the passenger cabin) from the detonation point was not less than 94 % of that of the Boeing 777. Including compensatory corrections, up to 95-98 %.

The target environment for the experiment with the target aircraft was chosen to be as close as possible to the distance of the detonation point (about 4 metres), as in the Final Report materials.

Thirdly - and most importantly - the strength of the cockpit hull in the port and starboard area of the target aircraft must be greater than that of the Boeing 777.

The third parameter, which formed the basis for target selection, certainly needs to be explained. In order that the results of the evaluation of the mechanical (piercing) effect of the projectiles obtained during the tests can be used to assess the nature of objectively observed damage on the Boeing 777, the strength characteristics of the cockpit of the target aircraft are very important. It was because the IL-86 ("IL-86") was designed much earlier than the Boeing 777 that it was chosen.

The design features of the IL-86 that distinguish it from the Boeing 777 are

1. Additional metal cabinets with on-board electronic equipment and a steel safe on the port side⁴⁷ (Fig. C.4).



Figure C.4 - Metal cabinet and steel safe on the port side, located behind the crew commander's seat: left - before the experiment; right - after the experiment

⁴⁷ Report on the conduct of a full-scale experiment, pages 90-94.

2. The presence of a flight engineer's workstation. This seat is located behind the starboard pilot and equipped with a metal cabinet with instrumentation and control panel located all along the starboard side and the right side of the cockpit roof (Figure C.5).⁴⁸



Figure B.5 - Control panel of the flight engineer of the IL-86 target aircraft (starboard, after the experiment)

3. The analogue version of the GB-86 ("IL-86") aircraft's avionics with its many material-intensive electronic and electromechanical components from the 1970s-80s (Figure C.6).⁴⁹

⁴⁸ Report on the conduct of a full-scale experiment, pages 94-96.

⁴⁹ Report on the conduct of a full-scale experiment, pages 104-105.



Figure C.6 - Material-intensive components of on-board avionics equipment of the IL-86 target aircraft (starboard and starboard side of the roof)

On Boeing aircraft, behind the right-hand pilot (co-pilot) there are shelves for technical documentation and landing places for instructors.

Thus, the IL-86 target aircraft, chosen as the Boeing 777 counterpart with compensation corrections and a stockpile, matches its geometric dimensions as closely as possible.

The cockpit projection area from the detonation point according to the experiment is not less than 95% of MH17, and the strength of the Ilyushin's left and right side cabinets, taking into account the right, left and top cabinets with analogue instrumentation of the 70s, is not inferior to the Boeing 777.

Exhibit D: Warhead Detonation Model

A static fragmentation region is created if the warhead (missile) is detonated in a stationary state. For example, in range conditions. For a BUK missile, the static fragmentation region is symmetrical about the longitudinal axis of the missile ox_1 .

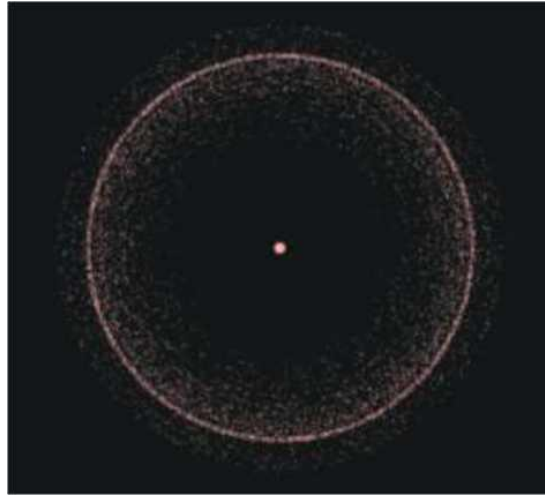


Figure D.1 - Static fragmentation field in the equatorial plane

The static fragmentation region is characterized by the static fragmentation angle α_{ct} and the inclination φ_{ct} of the bisector of this angle to the longitudinal axis of the missile. For a given missile type the static fragmentation angle remains unchanged.

When an explosive charge is initiated from the side of the warhead, as implemented in the 9M38 missile (9M38M1), under static conditions the fragmentation area is deflected backwards ($\varphi_{ct} > 90^\circ$).

As input data for the static and dynamic detonation model of the 9H314M warhead, materials from the technical documentation for the 9H314M warheads and the results of their 1980-1991 tests, as well as field experiments conducted during the technical investigation of the MH17 crash were used.

The characteristics of the meridional angle of projectiles under static conditions (travel time curve) are shown in Exhibit B.

Static conditions

In order to fulfil the tasks of modelling the engagement field of a BUK missile, a modelling software package was created, of which the fragment dispersal calculation software module is an integral part.

The distribution density of lethal projectiles λ is one of the most important characteristics of a high-explosive fragmentation warhead.

The simulation of projectile dispersion in a static detonation of a warhead is carried out using statistical data on

Two-degree zones of meridional angle of dispersion of projectiles accumulated by the manufacturer during numerous field tests.⁵⁰

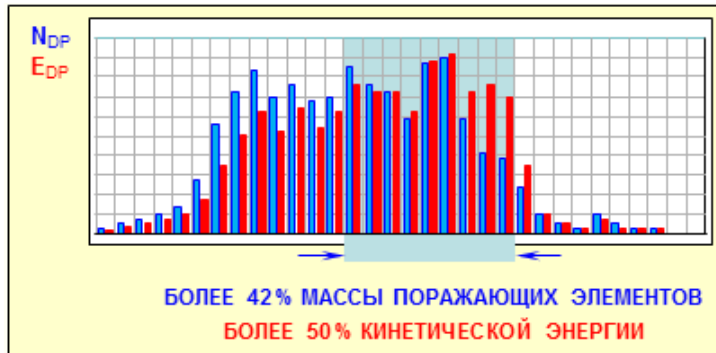


Figure D.2 - Source data for the density and kinetic energy distribution of the 9H314M warhead

The source data on the distribution of projectiles are the weights of the number and initial velocities of the projectiles with a course angle deviation step of two degrees. The distribution of the hit item parameters within the specified intervals follows a continuous uniform law.

Dynamic conditions

When firing at an airborne target, the warhead is detonated while the missile is in flight. The velocity vector of the missile is always tangential to its trajectory. The fragments of the warhead (projectiles + hull) have a progressive velocity equal to that of the missile V_M . When the warhead is detonated, the progressive velocity is geometrically combined with the fragment's own velocity V_{PE} , obtained by the energy of the warhead charge. In a dynamic situation, the fragments will disperse with an initial velocity ($V_{PE,D}$):

$$V_{PE,D} = \vec{V}_M + V_{PE}$$

The dynamic region of fragment dispersion is characterised by the dynamic angle of dispersion φ_D and the bisector angle in a given plane passing through the longitudinal axis of the missile.

The nature of the fragment dispersion (out of scale) is shown in Figure D.3.

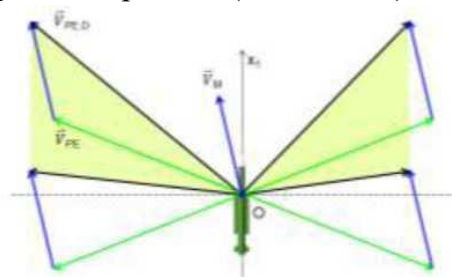


Figure D.3 - Fragmentation pattern during flight of an anti-aircraft missile (without regard to target velocity)

⁵⁰ The software module is designed to work with any modification of the SAM, as it reads the travel time curve data from the configuration file, stores them in a special database and uses them for calculations in the model.

Since the velocity vector of the missile V_M does not coincide with the longitudinal axis of the missile x_1 , the values of the fragmentation angles are not the same for different cross sections of the dynamic region, i.e., under dynamic conditions even when only the missile velocity is considered, the impact field is not symmetric about the missile's longitudinal axis. Therefore, a spherical diagram of the fragment dispersion obtained by extrapolation by rotation around the longitudinal axis of the missile will have significant errors.

The asymmetry of the fragmentation cross section is even more pronounced when the relative velocity of the projectiles is considered, $U_{PE,OTH}$:

$$V_{PE,OTH} = V_M + V_{PE} - V_A$$

where: $V_{PE} - V_A$ is the vector of the relative velocity of the missile.

The fragment dispersion pattern with respect to relative velocity (taking into account the velocities of projectiles, missile and aircraft) is shown in Figure D.4.

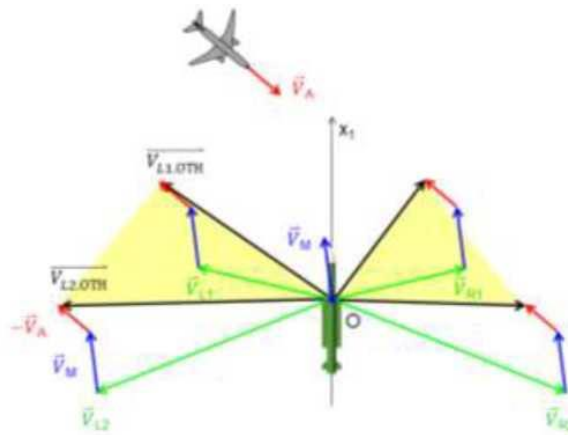


Figure D.4 - Relative velocity of the impactor

The irregularity of the fragmentation cross-section has the greatest effect on the parameters of the trailing edge, which is used to calculate the position of the warhead relative to the aircraft structure.

Figure D.5 shows the results of a fragmentation field simulation for dynamic conditions similar to those of the spherical projection simulation range of the projectile dispersion model used in the DSB technical investigation:

final velocity of the rocket $V_M = 600$ m/s;

the angle between the axes of the aircraft and the missile $Az_{warhead} = 30^\circ$.

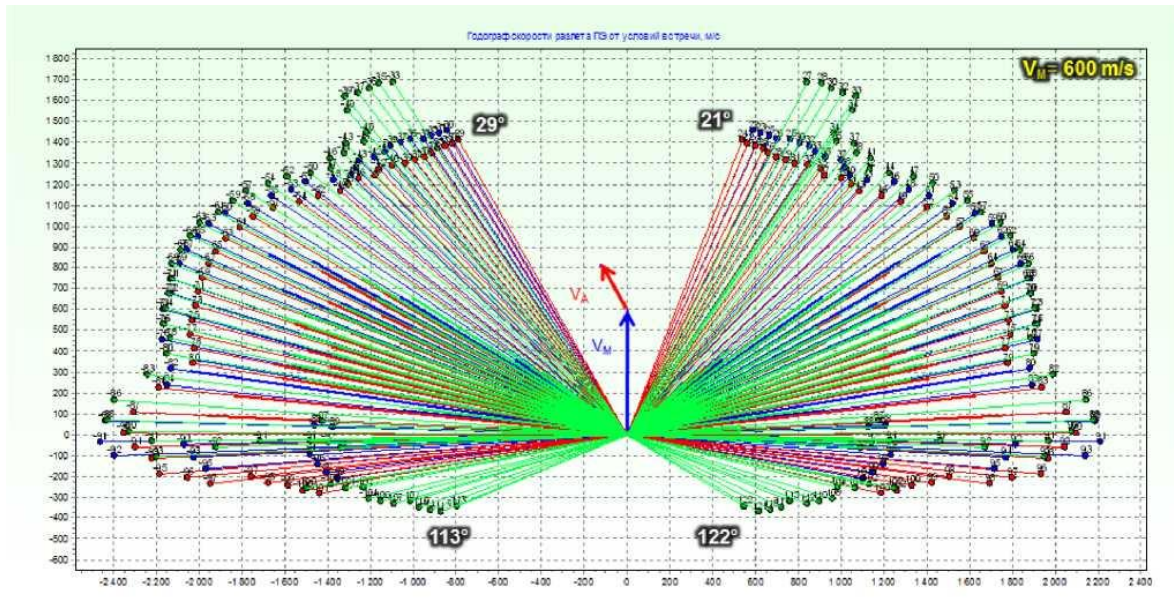


Figure D.5 - Unbalanced cross-section of the fragmentation field in the meridional plane

Analysis of Figure D.5 shows that the cross section of the fragmentation field in the meridional plane is asymmetrical. This is particularly evident in the value of the meridional angle of the trailing edge of the fragmentation field: towards the target (left) the trailing edge of the dynamic angle of departure is 113° and in the opposite direction (right) it is 122° .

Figures D.6, D.7 and D.8 show the results of a comparative simulation when the missile-missile encounter parameters change: the final missile velocity V_M (at constant airspeed) and the angle between the missile and aeroplane axes $Az_{warhead}$ at the time of detonation.

The results of the comparative modelling show that the asymmetry of the fragmentation field (left and right side relative to the longitudinal axis of the missile) depends significantly on the variation of angles between the missile and the aircraft and the final velocity of the missile.

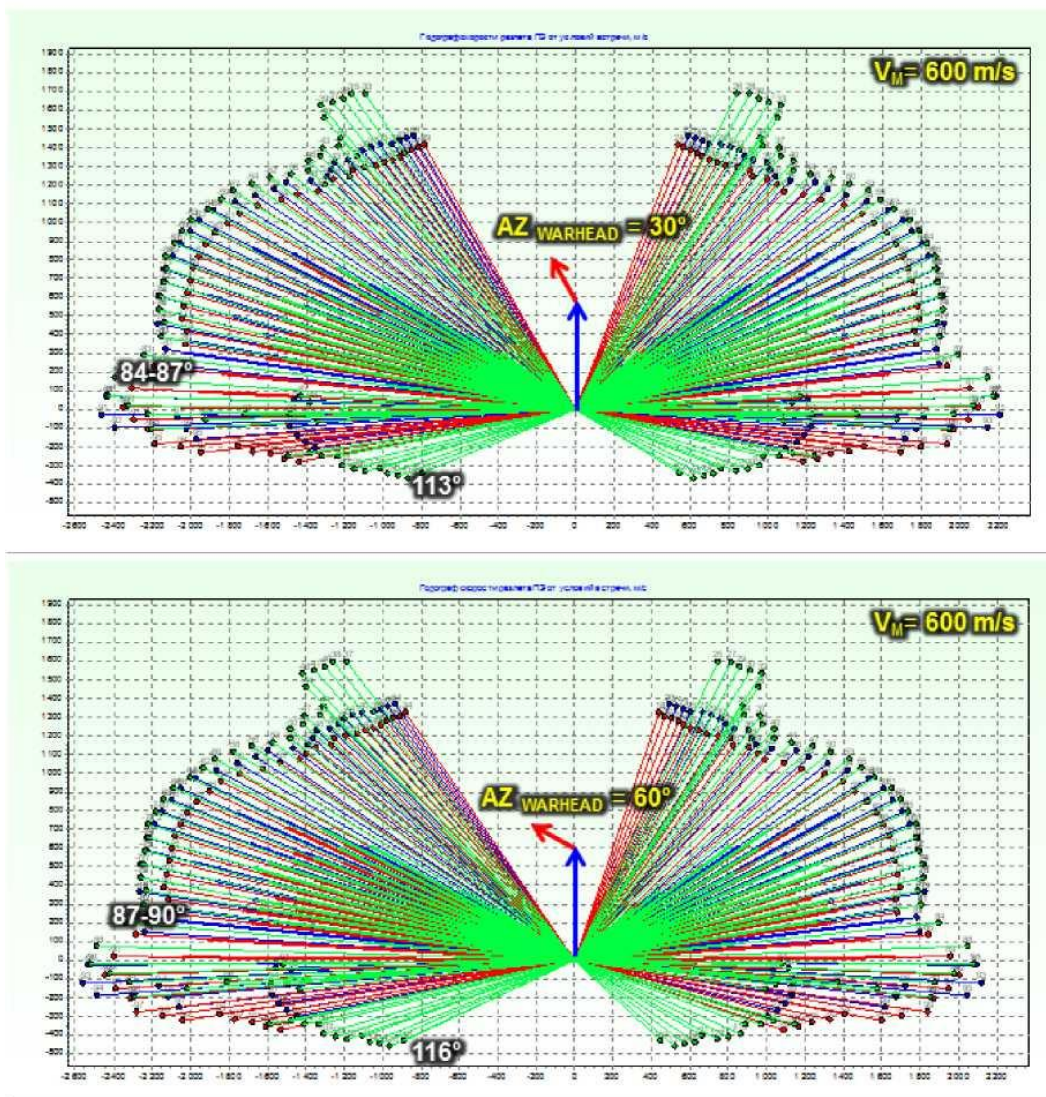


Figure D.6 - Effect of angle between aircraft and missile longitudinal axes $Az_{warhead}$ at the moment of detonation at the same rocket velocity $V_M = 600$ m/s: top - $Az_{warhead} = 30^\circ$; bottom - $Az_{warhead} = 60^\circ$

As the angle between the longitudinal axes of the aircraft and the missile increases ($Az_{warhead}$) at the moment of detonation, the value of the angle characterizing the posterior front of the fragmentation field increases.

In this case in the left hemisphere, towards the target from 113° to 116° .

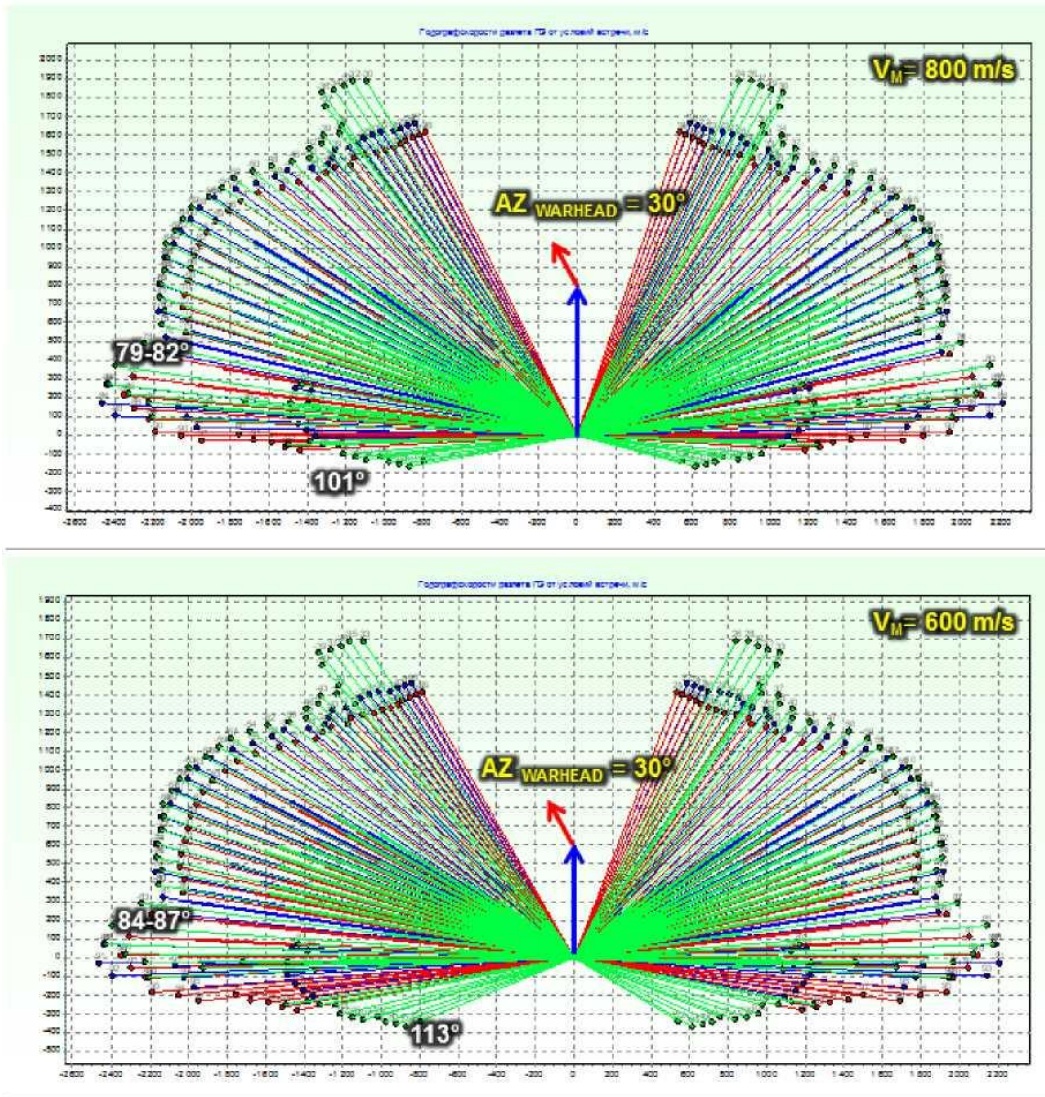


Figure D.7 - Effect of final missile velocity V_M at the moment of detonation at constant angle between the longitudinal axes of the aircraft and the $Az_{warhead}$ missile: top - $V_M = 800$ m/s; bottom - $V_M = 600$ m/s

As the final velocity of the missile increases, V_M at the moment of detonation, the value of the angle characterizing the trailing edge of the fragmentation field decreases. In this case, from 113° at 600 m/s to 101° at 800 m/s (in the left hemisphere).

In an analysis of the calculation results, the effect of a change in final missile velocity on the result of determining the relative position of the missile relative to the aircraft structure is determined. If a "density peak" (aka "scalpel") is used as a marker, the estimate of the effect of a change in velocity is about 5°.

This is confirmed by the calculations made by the specialists of the Almaz-Antey Corporation (see Figure D.7).

The position of the rear "scalpel" marker does change by about 5° : ($87^\circ-82^\circ=5^\circ$). At the same time, the effect of changing the terminal velocity of the missile gives an angle change of up to 12° , which characterizes the trailing edge of the fragmentation field, to the "opposite direction" version specifically ($113^\circ-101^\circ=12^\circ$).

The maximum difference appears when the angle $Az_{warhead}$ between the longitudinal axes of the missile and aircraft changes simultaneously with the missile's terminal velocity V_M . In this case, errors in favour of the "opposite direction" version could be as much as 15° deg or more (see Figure D.8), where: for a trailing edge of fragmentation $116^\circ-101^\circ=15^\circ$.

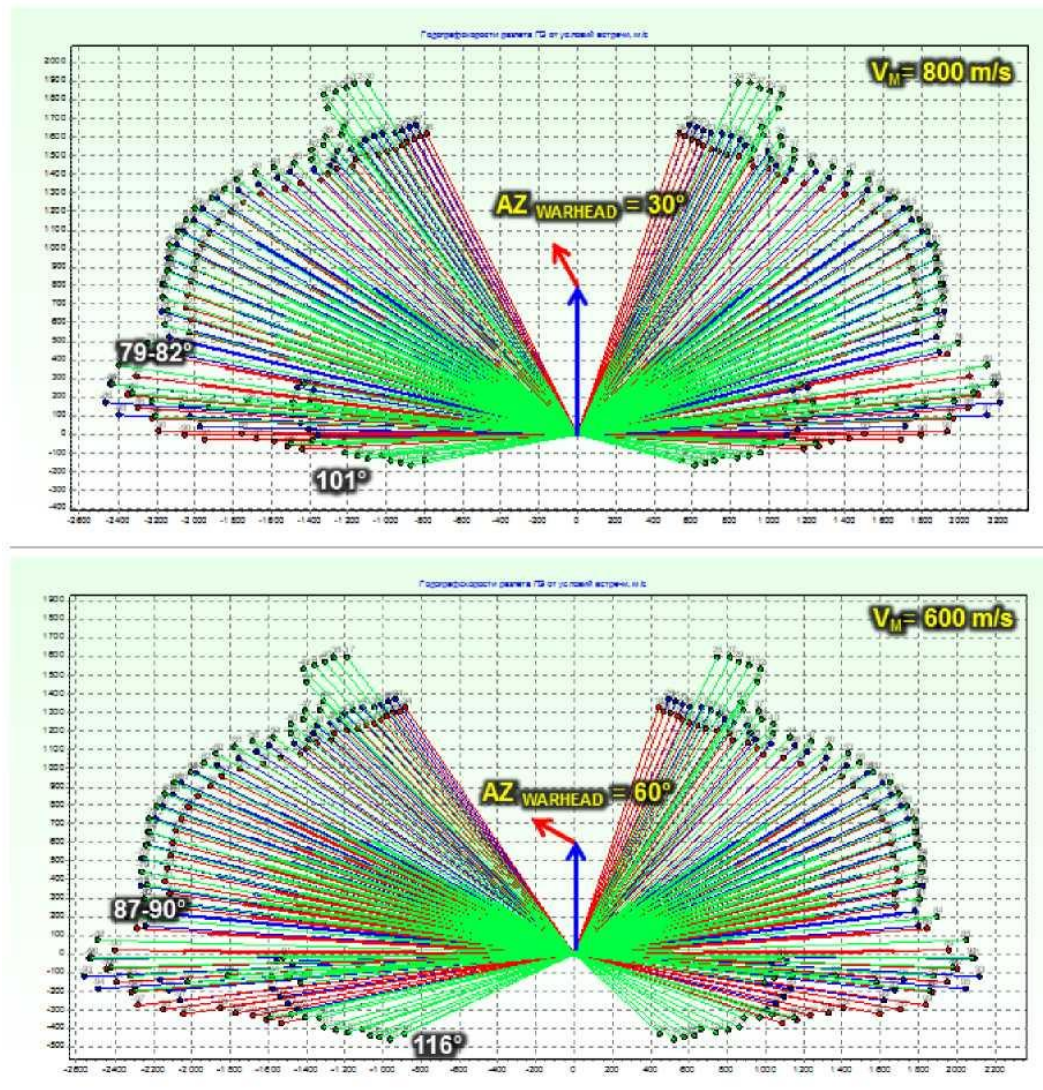


Figure D.8 - Effect of simultaneous variations in final missile speed V_M and the angle $Az_{warhead}$ between the longitudinal axes of the aircraft and the missile.
top - $V_M = 800 \text{ m/s}$, $Az_{warhead} = 30^\circ$; bottom - $V_M = 600 \text{ m/s}$, $Az_{warhead} = 60^\circ$

The speeds of 600m/s and 800m/s have been chosen for modelling because a final missile speed of about 600m/s is considered to be the most realistic for the "opposite direction" version. This is consistent with the results of calculations by Almaz-Antey and the NLR during the drafting phase of the Report.

The missile's terminal velocity of 800 m/s is the velocity value that falls within the speed range used by experts in calculating missile-landing conditions (orientation of the warhead relative to the aircraft).

The initial value of the angle between the longitudinal axes of the missile and the aircraft of 30° ($Az_{warhead} = 30^\circ$) is within the range used by the DSB experts.

The modelling software used by specialists from Almaz-Antey Corporation takes these features into account and calculates the trajectories of each of the fragments, taking into account the influence of velocity projections in the three planes.

The fragment dispersal calculation software module takes into account more than 12,900 fragments. The simulation separates prefabricated projectile fragments (PFAs) and hull fragments:

Heavy fraction 9H314M 1-10 "bowtie" weighing $\sim 8.1\text{g}$ (Heavy);

light fractions 9H314M 1-9 and 9H314M 1-11 "parallelepiped" masses $\sim 2.1\text{-}2.35\text{g}$ (Light);

hull fragments with linear dimensions of 6-13 mm (Shell).

A fragment dispersal model calculates the velocity and coordinates of each fragment at any instant in time, as well as the distribution of the fragment field flux density at any selected distance and direction from the detonation point.

The fragments (separately Heavy and Light fractions, as well as Shell fragments) in the software package are modelled using material points, their motion is described by kinematic equations of motion, taking into account the initial (X_{0i} , Y_{0i} , Z_{0i}) and current coordinates (X_i , Y_i , Z_i), and components of fragment velocities (V_{xi} , V_{yi} , V_{zi}).

During computational experiments associated with the development of software modules responsible for modelling fragment dispersal, various model variants were tested: fragment dispersal from a "point"; fragment dispersal from a "segment" corresponding to the linear dimensions of the warhead; fragment dispersal from an "elliptical cylinder" whose shape virtually coincides with the actual shape of the warhead (Figure D.9).

Numerical experiments have shown that the shape of the warhead specified in the model has a significant influence on the simulation results.

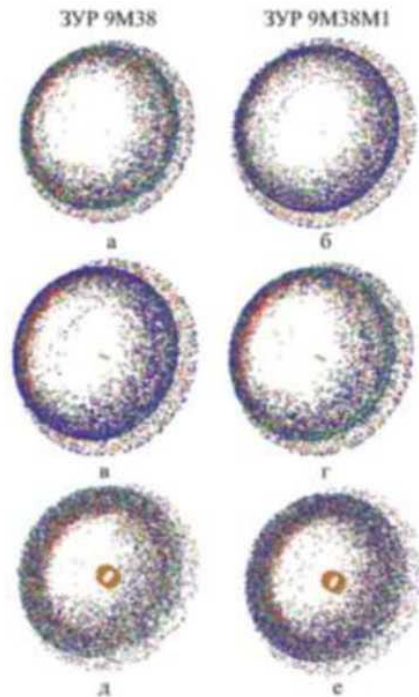


Figure D.9 - Fragment dispersion patterns of 9H314 and 9H314M: a), b) - dispersion from a "point"; c), d) - dispersion from a "segment"; e), f) - flying off the "elliptical cylinder"

This is due to the close proximity of the warhead detonation point area to the surface of the aircraft (about 1.6-2.0 m to the nearest cockpit surfaces), which is comparable to the linear dimensions of the warhead itself (over 500 mm).

In this regard, the final version of the static fragmentation model takes into account the shape of the warhead, unlike other models which use "point" models and do not take into account the linear dimensions of the warhead.

As noted in Exhibit B.2.2, in the course of the experiment in the shield target layout the conformity of the mathematical model of static detonation of the 9H314M warhead used by the Corporation's specialists for the calculations was confirmed. The discrepancy in the relative number of holes between the results of the simulation and the in-situ experiment did not exceed 2.0% for each of the shields, and the standard deviation of the in-situ test results from the results of the simulation was about 1.1%.

"Scalpel"

The diagram in Figure D.10 shows an overlay on the image of target No. 2 (M-2) of the meridional angle of the finished projectiles ranging from 70° to 130°.

The diagram on the left side of Figure D.10 shows two areas where the maximum density of finished projectiles should be formed. For preformed fragments of the light element fractions $\lambda_{L,PE}$ the area is highlighted in blue, and for the heavy element fraction $\lambda_{H,PE}$ the area is highlighted in red.

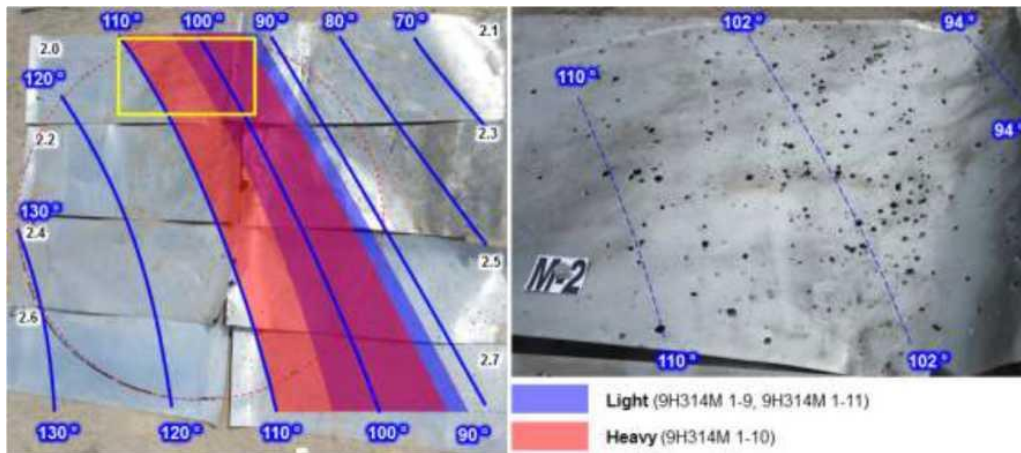


Figure D. 10 - Maximum density zones of finished projectiles: blue - Light fraction; red - Heavy fraction

The right side of Figure D.10 shows the maximum impact density zones obtained in full-scale tests using the example of a witness sheet (Shield 2.0 of target M-2).

The left side of Figure D.11 shows the relative density of projectiles in areas of maximum density divided into 2-degree zones. It is these 2-degree zones of meridional angle of fragment dispersion (bright red and bright blue) that have the maximum relative density and form the so-called "scalpel".

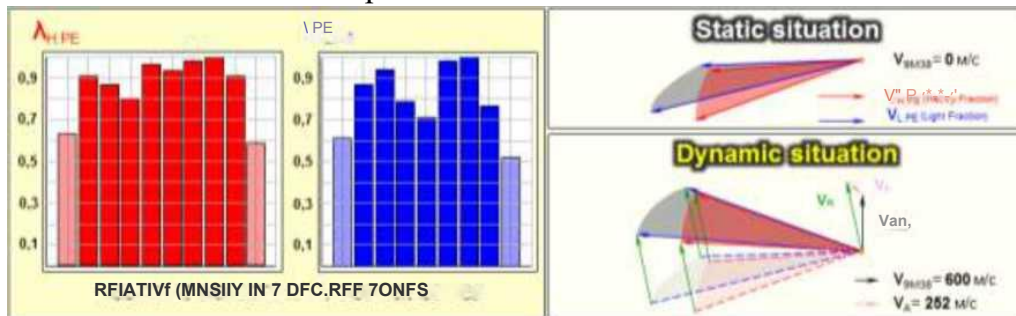


Figure D.11 - Formation of the Maximum Shrapnel Density Area under Dynamic Conditions

In the other two-degree zones, the relative density is slightly lower (highlighted in pale red and pale blue).

In a static position, the maximum density zones of the Light and Heavy ready projectiles do not coincide completely and are offset in relation to each other (Figure D.11, top right).

When recalculating dynamic conditions, corrections and adjustments are made to the relative velocity V_R , the relative position of the longitudinal axes of the missile and the target, and the flight altitude.

Under dynamic conditions, due to the fact that heavy fraction projectiles in this angle range have a slightly lower average initial velocity ($V_{H.PE}$) than the average initial velocity of light fraction projectiles ($V_{L.PE}$), a mutual overlapping and formation of a common zone of maximum density of preformed fragments (Figure D.11, bottom right).

This area (the so-called "scalpel") concentrates more than 42% of the mass of all fragments and more than 50% of the kinetic energy of the fragment impact field.

That is, the coincidence in space (under dynamic conditions) of the three most important components is confirmed: the maximum number of fragments (primarily projectiles of the heavy fraction), their total mass and velocity - the area of maximum kinetic energy of the field of impact, which is called "scalpel".

The presence of an area of high fragmentation field density is confirmed by tests, including those carried out by independent specialists.

Thus, in the fragmentation field of a BUK missile, under dynamic conditions, **a region of maximum fragment density is formed**. The position of this region is determined by the velocities and the relative position of the missile relative to the aircraft structure at the time of detonation.

Consistency between static and dynamic test results

Almaz-Antey Corporation has a methodology that has been repeatedly tested in calculations, modelling and field experiments (tests) to convert the values obtained in static conditions into any dynamic conditions and to estimate the expected impact (damage) pattern.

This technique has been validated both in static tests on the ground in different target environments (test benches, etc.) and in dynamic tests - on the ground using missile test benches (Figure D.13) and in the air using different target systems (Figure D.14).



Figure D.13 - Ground tests in a shield target layout under dynamic conditions at the rocket booth. Velocity of the experimental setup at the moment of detonation - 1,010 m/s

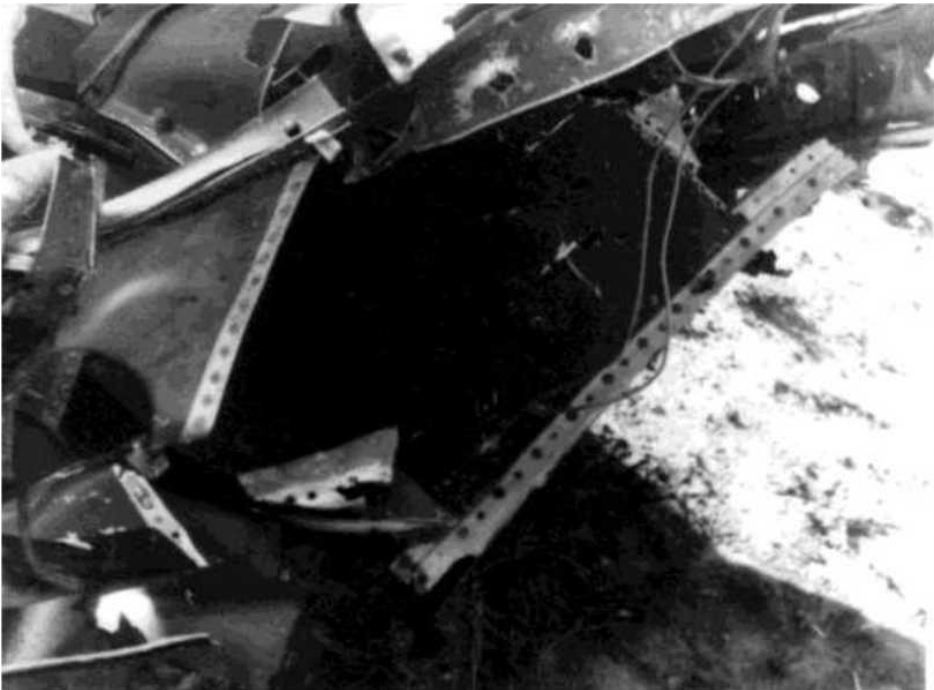


Figure D.14 - Fragment of an air target destroyed in an airborne dynamic test. Target perforated, outer skin and primary structure perforated, deformed and collapsed

Supercomputer technology tools are used to verify and adjust the compensation corrections. The used methods and tools, taking into account accumulated statistical data on different types of tests in static and dynamic conditions, give a reliability of simulation results up to $\eta = 94... 99 \%$.

Exhibit E: Fragments of the 9M38 missile

At a JIT (international investigation team) press conference, fragments of a missile that JIT claims were found in the vicinity of the Malaysian Boeing 777 (MH17) crash were shown.

In particular, the green-painted rear engine (part of compartment 3) of the 9M38 missile with the engine serial number and the date of assembly were presented (Figure E.1).

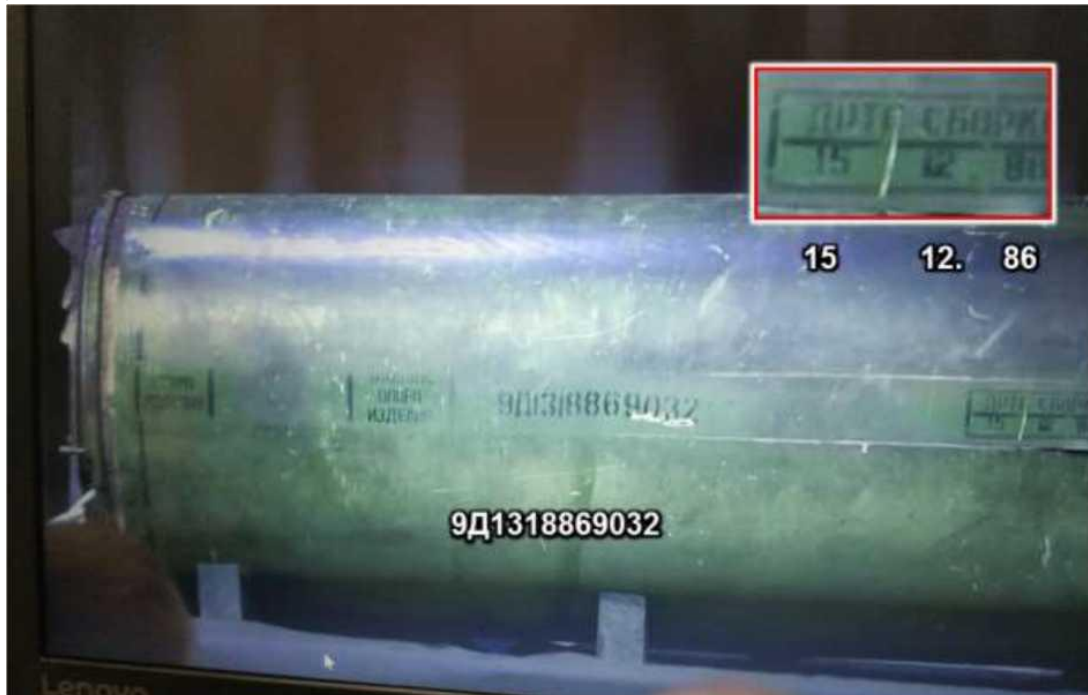


Figure E.1 - Missile fragment: rear of the 9D131 engine of the 9M38 missile (resource - JIT press conference)

This piece is stamped with serial number 9D1318869032, where:

9D131 - engine brand;⁵¹

8 - Manufacturer's index (PAO Dolgoprudnoye Research and Development production enterprise", abbreviated as "DNPP");⁵²

86 - year of manufacture (1986);

9032 - serial number (90 - series, 32 - engine number in the series).

A "Nozzle" bearing the factory name Block "C" was also demonstrated, a fragment of which with the factory number is shown in Figure E.2.

⁵¹ 9D131 engine was used in the 9M38 and 9M38M1 missiles.

⁵² From 1975 to 1991, the company was called Dolgoprudnenskoye Machine-Building Association (DMPO)



Figure E.2 - Rocket fragment: part of the nozzle, block "C" (resource - JIT press conference)

This fragment has serial number 9D131.05.000 No. 8.30.113.

A check in the archive of data sheets for the products manufactured by the DMPO (DNPP) in 1986 revealed that the 90xx series engines were installed in two series of 9M38 missiles manufactured in Q4 1986 - series "86" and "87".

The engine with serial number "9032" was installed in the 9M38 missile with serial engineering number "8868720".

According to the rocket data sheet and the engine form, the final assembly of the engine was carried out on 24 December 1986.⁵³

The nozzle (C Block) with serial number "9D131.05.000 No. 8.30.113" was also reactivated and on 24 December 1986 installed in the rocket with serial number "8868720", as evidenced by the entries in the "C Block Passport" and "9D131 Product Form" with serial number "8869032".

Record of filling (filling) with gunpowder of pyrotechnic products, included in the rocket: product 9B155M1, Serial No. KT 10613341 is filled with gunpowder mixture 9X94M1 and 9X265 on 23.12.86, and its installation is performed on 24 December 1986.

According to the technical data sheet, final acceptance of the missile with serial number "8868720" took place on 27 December 1986.⁵⁴

⁵³ Section 3 of the "Certificate of 9D131 Assembly" form indicates that the assembly of the unit with serial number 8869032 was carried out at the Enterprise p/y A-7144 (now known as Voskresensk Aggregate Plant) on 24.12.86. Section 4 "Information on final assembly of unit 9D131" indicates that final assembly of the engine as part of unit 9M38 No. 8868720 with installation of unit "C" was carried out on 24.12.86.

⁵⁴ The date of handover/acceptance is indicated in folders No. 1 and No. 2 of the missile's data sheet, serial No. 8868720

Thus, in accordance with the technical certificate, both numbered fragments: rocket motor No. 9D1318869032; nozzle (block "C") No. 9D131.05.000 No. 8.30.113 were installed in the 9M38 rocket with the factory technical number "8868720".

The date of final assembly of the engine as part of product 9M38 No. 8868720 with installation of block "C" was 24.12.86, the date of transfer/acceptance of the missile was 27 December 1986.

The 9M38 missile (serial number 8868720) was assigned an airborne number "9M38 886847379" in accordance with the 1986 regulations in force.

According to the entries in the "9M38 Shipment Logbook", the missile, serial number "8868720", was received by the customer with the serial number "9M38 886847379". 31 December 1986.

In some open sources one can find allegations about alleged discrepancies between the technical documentation and the found fragments. For example, the date of assembly of the rocket engine indicated in the technical documents (24 December 1986) does not correspond to the date of the stamp on the engine casing found during the investigation (15 December 1986).

The conclusions that the technical certificate for the 9M38 anti-aircraft guided missile with the factory technical number "8868720", debris from which is presented by DSB and JIT as having been involved in the crash, provided by Russia, are untenable.

In order to dispel any doubts about the coincidence or "non-coincidence" of the dates in the technical documentation and on the fragments in the possession of the investigation, it is sufficient to make an enquiry to the manufacturer, DNPP.

In order to understand how and when the marking is applied, it is necessary to familiarise yourself with the workflow for the final assembly of the missile.

The stamp with the inscriptions "DATE OF ASSEMBLY" and "15.12.86" is a technology stamp.

The experts could easily ascertain this from the materials provided to the investigation by Ukraine⁵⁵ and publicly available as annexes to the DSB report.

Thus, in Figure E.3 below, the 9M38 missile (white in colour) given by Ukraine to the investigation clearly shows the stamp "DATE OF CONVENTION" and "06.09.85". In addition, the photograph shows that the paint in the area of the stamp differs from the rest of the engine paint.

⁵⁵ For example, the presentation Results of examination of causes of MH17 crash over the territory of Ukraine 17.07.2014. (10-12.08.2015, Gilze), shown during an expert meeting in August 2015.



Figure E.3 - Stamp "ASSEMBLY DATE" on the 9M38 missile delivered by Ukraine to the investigation. The expert shows with his hand the attachment point of the wing on the shell of the third compartment. In order to see the stamp "Assembly date", the wing must be dismantled (resource - materials of KNIISE)

This stamp ("COMBINED DATE") is placed on the engine after it has been self-assembled, before the wings are fitted, when it looks as shown in figure E.4.



Figure E.4 - 9M38M1 missile engine provided by Ukraine to the investigation (resource - materials of KRISE)

The 9M38M1 engine (green) is pictured assembled, but the fourth and second compartments, the nozzle block, and the wings have been removed.

After the "ASSEMBLY DATE" stamp has been applied to the engine, both the engine itself and the rocket as a whole, a number of other manipulations are carried out in accordance with the "Technological Process", some of which include:

1. The assembly of the fourth compartment, including the filling (filling) with gunpowder of the pyrotechnic articles included in the missile. For the rocket with serial number "8868720", this operation was carried out on 23.12.86, as evidenced by the corresponding record in the technical documentation.⁵⁶ Due to safety requirements, the filling (filling) with powders of pyrotechnic products of the fourth compartment is carried out at another enterprise, not in Dolgoprudny, which requires transportation of the missile to the place of carrying out the filling and final assembly.

2. Assembly (docking) of rocket compartments with sealing of joints with U30MES-5H type sealant (figure E.5). In accordance with the "Technological Process", the complete joint readiness occurs not earlier than 24 hours after the application of the last layer of sealant.



Figure E.5 - Docking of the third and fourth compartments. At the front of the fourth compartment there is also a wing attachment point: before the fourth compartment is docked to the engine, the wing cannot be installed on the rocket (resource - preparation materials for the second field experiment)

3. Installing the "C" unit (nozzle). Final installation of block "C" (nozzle) on the engine is possible only after the fourth compartment is fully assembled and docked with the third compartment. In Section 4 ("Information on Final Assembly of the Product 9D131") of the data sheet for the missile with serial number "8868720" there is a record that "final assembly of the engine as part of the 9M38 No. 8868720 with installation of block "C" was carried out on 24.12.86.

⁵⁶ Certificate of acceptance for product 9B155M1, Serial No. KT 10613341.

4. Twenty-four hours after the sealing of the rocket compartments with serial number "8868720" was completed, the sealant was coated with dark green enamel EP-140 (Notice 9M38.7373 to Technical Requirements 9M38.0000.000D3). The drying time of the enamel EP-140 in the conditions of the assembly shop was set within 8-9 hours.

5. After completion of the drying of the EP-140 enamel, the installation of the missile's connecting (transit) harnesses and wings is carried out. In accordance with the technical documentation for the missile 9M38 with the factory technical number "8868720", the wings installed on the missile were manufactured on 17.12.1986.⁵⁷ That is, two days after the engine was stamped with the inscriptions "ASSEMBLY DATE" and "15.12.86".



Figure E.4 - 9M38M1 missile delivered by Ukraine to the investigation (SBN materials). After installation of the wings, the process stamp "Assembling Date" is not visible - it is covered by the relevant wing

6. Then, in accordance with the "Technological Process", the final (final) painting of the missile with enamel EP-140 dark green (GOST 24709-81) is carried out. The drying time of the enamel EP-140 in the conditions of the assembly shop is set at 8-9 hours.

7. The missile is then painted with black enamel on the flight number.

8. Full resistance of the paint coating to the specified effects is achieved after 24 hours. Therefore, in accordance with the "Technological Process", the transfer of the missile to the test bench for

⁵⁷ The docking list for item number 8868720 shows the date of issue of Kr I wings, Kr II, Kr III and Kr IV installed in the rocket - 17.12.1986.

acceptance testing takes place no earlier than 24 hours after the marking has been applied.

9. After the tests, the missile is packaged, the documentation is completed and it is handed over to the customer. According to the datasheet, final acceptance of the missile with serial number "8868720", which included the 9D131 engine with serial number "8869032", was carried out on 27.12.86.

10. The missile was assigned the tail number "9M38 886847379" and on 31 December 1986 it was put into service.

Conclusions:

1. The numbered missile fragments demonstrated during the JIT press conference (engine part with serial number "9032" and nozzle with serial number "8.30.113") were installed in an older version of the BUK missile, **the 9M38 missile** with serial technical number "8868720".

2. In a fully assembled missile, the technological inscriptions on the engine "DATE OF ASSEMBLY" cannot be seen - as they are located under the wing, which is mounted after the final assembly of the rocket and engine compartments, respectively.

3. According to the manufacturing process, after the assembly of the engine (without the C Block), it takes several days for the final assembly of the rocket to achieve full resistance to the specified effects of the sealing and paint means.

4. The Act of Acceptance/Transfer of the 9M38 missile number 8868720, containing numbered fragments, was signed on 27 December 1986.

Exhibit F. Comparative modelling for different final positions of the missile

The DSB Report shows that the range of missile end states (angles of intersection of aircraft and missile longitudinal axes) in the horizontal plane is from -35° to -17°.

Although -17° was discarded by the Dutch experts already at the Draft Report stage, source data values that include the full range of final values used in the technical investigation will be used for the comparative modelling:

- The end state of the missile (at the time of detonation of the warhead):
- azimuth, deg (-37, -16)
- angle of location (vertical angle), deg(5)
- Detonation area coordinates, m (.....0.4; - 1.85, 1.85)
- missile speed, m/s 600

Coordinates within the verified range as well as the agreed realistic velocity for the 'opposite direction' version in question are used as the detonation point.

As an additional value for comparison, a value of -50° was used, corresponding to the minimum angle of intersection of the missile and aircraft longitudinal axes according to the Almaz-Antey Corporation version, at which all damage to the Boeing 777 is logically explained.

Five fragments with characteristic lesions were used as marker points for comparison, which can be verified in the final 3D layout in Gilze-Rijen.

The first four fragments No 1, No 2, No 3 and No 4 were included in the final 3D reconstruction, while fragment No 5 is not installed in the 3D reconstruction, but is located in the Netherlands:

No 1 is the forward pressure bulkhead (STA 132.5), which according to DSB experts is the objective front boundary of the high-speed damage zone.⁵⁸ It is described in detail in subparagraph 2.1.2.1 of the Almaz-Antey Corporation Report.⁵⁹

No 2 - the second window (window No 2) of the crew commander, on which DSB experts recorded 102 fragmentation holes and this window was in the area with the highest density of fragmentation damage – about 250 fragmentation holes per square metre.⁶⁰

⁵⁸ Final Report. 3.5.3 Damage from external causes, p.121.

⁵⁹ Investigation report related to the technical investigation into the crash of Malaysian passenger aircraft Boeing 777-200 9M-MRD (flight MH17). Frontal damage boundary, pages 17-21.

⁶⁰ Final Report. 3.5.3 Damage from external causes, p.121, 126.

Figure F.1 shows the condition of one of the restored layers of window No 2 and its position in the aircraft structure, based on NLR material.⁶¹

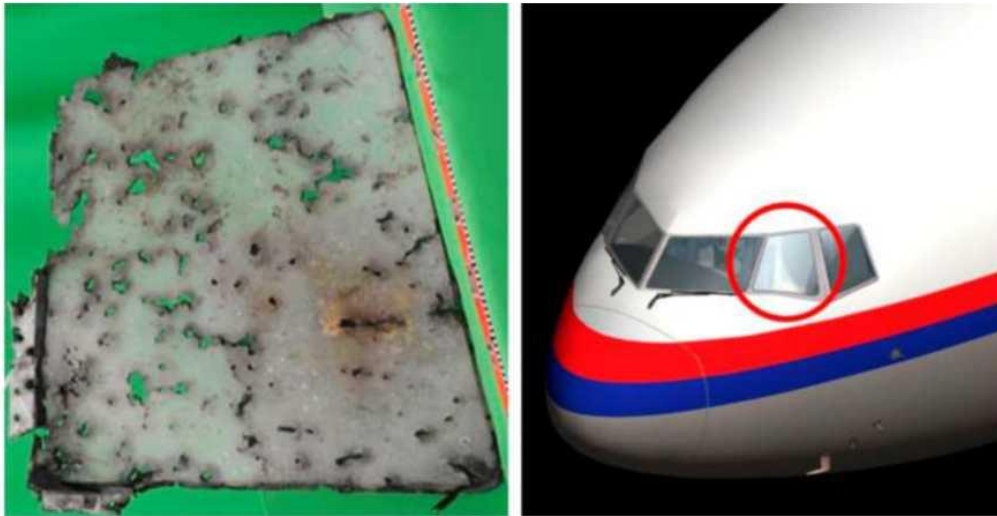


Figure F.1 - According to the NLR report (Annex X of the DSB report), the second window on the left side of the cockpit has a maximum impact density of approximately 250 damage per square metre (Resource - NLR)

No. 3 - fragment of the upper port side (behind the crew commander's windows), which was in the area of maximum density (mass and kinetic energy) of projectiles and factors accompanying a close explosion.

The location of this fragment has been accurately identified by indigenous experts.⁶²



Figure F.2 - Fragment of the port side planking from the top at the rear of the third window of the Crew Commander with evidence of multiple holes in the outer planking (left) and in the bulkhead (right)

⁶¹ NLR report (Annex X). 2.5 Number and density of hits, p.14

⁶² This is evidenced by a fragment form that was present at the pre-launch site in May 2015.

No 4 - fragment of lower port side from frame STA 228.5 to passenger door L1 with pronounced non-penetrating damage (ricochets) to the port side skin at the edge of the covering field.



Figure F.3 - Fragment of the underside of the port side with fragmentation damage at the edge of the covering field

No 5 is a fragment of the upper port side, which, despite being present in the Netherlands since 2015, is not installed in the 3D reconstruction and is not part of the "reference" damage model.⁶³

In doing so, the fragment has two crucial markers:

its forward section shows a high density of fragmentation damage, as well as multiple holes in the STA 287.5 and STA 298.5 bulkheads, which led to deformation and structural failure of the Boeing 777 (Figure F.4);

the rear part of the fragment has damage located between bulkheads STA 309.5 and STA 332.5 (figure F.5).

⁶³ Exhibit A.1.



Figure F.4 - Fragment of upper port side: external (left) and internal (right) views. Multiple penetrations in bulkheads STA 287.5 and STA 298.5 caused deformation and failure of the structural members (red arrows indicate characteristic damage)



Figure F.5 - At the rear of the fragment, fragmentation damage is located between bulkheads STA 309.5 and STA 332.5, which is almost 3 metres beyond the accepted "reference" damage

For ease of reference, all of the specified fragments, which will act as marker points, are plotted on the 3D-reconstruction image shown in Figure F.6.

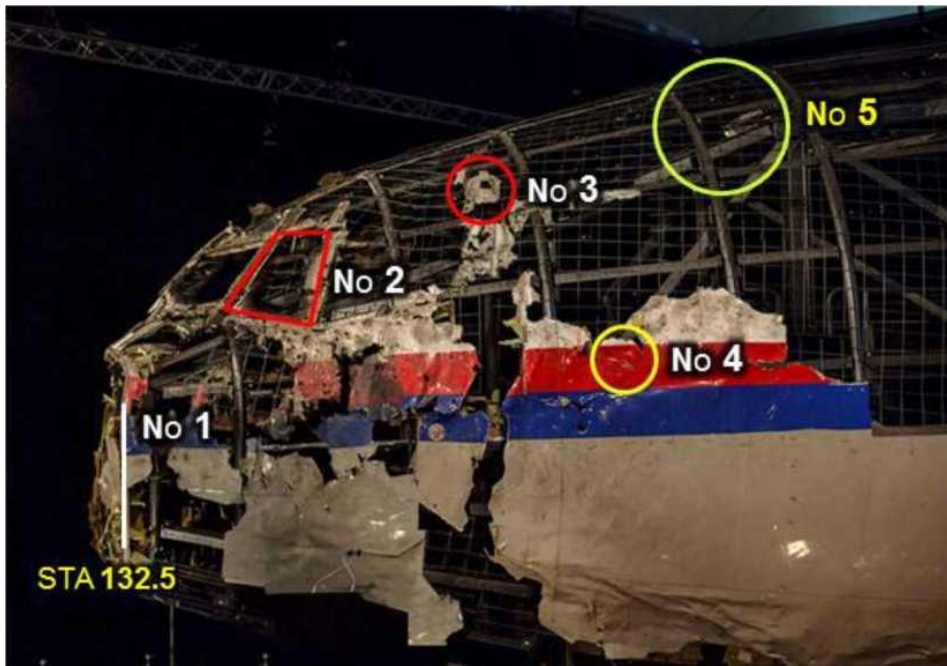


Figure F.6 - Fragments No 1, No 2, No 3 and No 4 are included in the final 3E reconstruction, while fragment No 5 is missing

Consider the comparison of objective damage on control fragments No 1-No 5 with simulation results as a function of angle change in the horizontal plane:

Azimuth -16° variant

Figure E.7 shows the results of the fragmentation field modelling of the Boeing 777 outer hull model (left) compared to the 3D reconstruction (right).

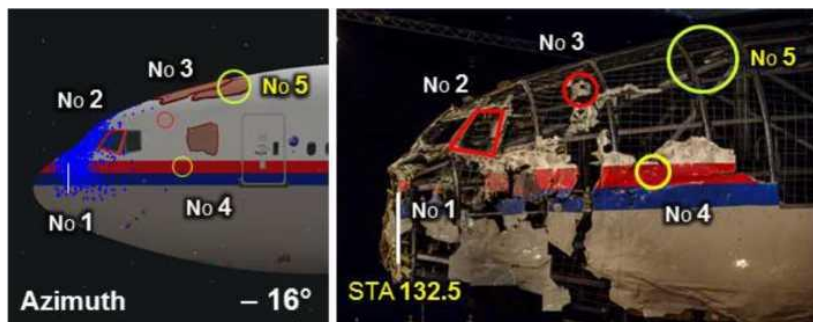


Figure F.7 - Simulation of Boeing 777 nose section damage under Azimuth -16° conditions

1. The anterior boundary of the fragmentation cover from prefabricated projectiles is much closer to the nose than the real one, starting behind the level of the forward pressure bulkhead (Fragment No 1). In reality this would have resulted in multiple through-holes in the forward pressure bulkhead and weather radar of the Boeing 777. For example, as happened during the second

A full-scale experiment using an IL-86 target aircraft in a rocket detonation with similar "Azimuth -17°" conditions (Figure F.8).



Figure F.8 - Example of through-holes in the weather radar equipment of target aircraft IL-86 (Proceedings of the Experimental Report)

At the same time, as noted in the Final Report, there were no hit holes in the forward herringbone and weather radar of the Boeing 777.⁶⁴

In addition, the fragment in front of the cockpit windshields should show multiple GVE damage from modelling and in-situ testing (Figure F.9).

In fact, there is no multiple damage from preformed fragments on this fragment.⁶⁵



Figure F.9 - Inconsistency of damage in front of cockpit windshields: according to modelling results, the fragment should show multiple GPE damage (left); the fragment in front of windshields does not have a high density of damage (right)

⁶⁴ Final Report. 3.5.3 Damage from external causes, p.123

⁶⁵ Investigation report related to the technical investigation into the crash of Malaysian passenger aircraft Boeing 777-200 9M-MRD (flight MH17). Frontal damage boundary, pages 17-21.

Figure F.10 shows the exterior view of a fragment of witness sheet 1.1 of target M.1 after the full-scale experiment on 31.07.2015. This witness sheet was twice as far from the detonation point as the fragment in front of the cockpit windows adjacent to the forward pressure bulkhead.



Figure F.10 - Fragment of Witness Sheet 1.1 of Target M. 1 (field experiment in a shield target layout conducted on 31.07.2015)

In reality, if the 9H341M detonated near target No. 1 (M.1) at a distance corresponding to the distance of the detonation point from the nose of the Boeing 777 (not more than 1.6-2.0 m), the number of fragmentation holes on Witness 1.1 would be three to four times greater than in the photograph (figure F.10).⁶⁶

Accordingly, given the blast effect, the fragment in front of the cockpit windows of the Boeing 777 would have been completely destroyed.

The nature of the simulated damage to the forward pressure bulkhead (as confirmed by the experimental results) is radically different from the actual damage to the Boeing 777.

2. The second left window (fragment no. 2), which has the maximum damage density according to the Final Report, is not included in the maximum damage area according to the simulation results.

In order to compare the actual and simulated damage on the second left window in terms of damage number and density, simulations were carried out for different values of the rocket's final position azimuth (horizontal angle) from the ranges used in the technical investigation and the final rocket speed of 600 m/s.⁶⁷

⁶⁶ With distance from the detonation point, the shrapnel field density decreases in inverse proportion to the square of the distance ("law of squares"); accordingly, if the distance from the detonation point to the barrier changes by a factor of two, the actual damage density on that surface must change by a factor of four.

⁶⁷ Final Report (Annex Y). TNO report.

The options were compared using an interactive 'simulated damage' model and an 'actual damage' model of the second left window (102 fragmentation holes according to the DSB Report).^{68,69}

Almaz-Antey's dynamic fragmentation model takes into account the different types of fragments: two types of Light and Heavy ready-made fragments, as well as Shell fragments.⁷⁰

When assessing fragmentation damage to windows, only prefabricated impactors should be considered. This assertion is based on experimental data obtained from in-situ experiments: cockpit glazing, 25mm laminated glass, can only be penetrated by prefabricated (primary) projectiles.

An example simulation for the Azimuth -16° variant is shown in Figure F.11, where the set of areas (polygonal objects) corresponding to the second left window on the Boeing 777 is highlighted in orange on the interactive aircraft model.

A pop-up window indicates the number and types of fragments whose trajectories intersected the areas that make up the surface of the second left-hand cockpit window.

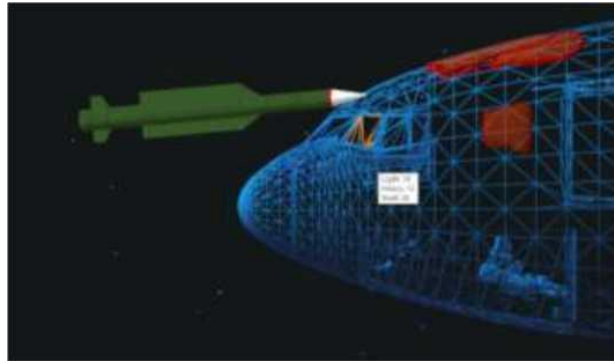


Figure F.11 - Simulation of fragmentation damage to the nose of a Boeing 777 aircraft under Azimuth -16° conditions. The polygonal objects corresponding to the second left window are highlighted in orange on the interactive aircraft model

The simulation results in only 72 splinters in the second window:

Light	34	(GGE light fraction of two types)
Heavy	12	(GPE heavy fraction, "bowtie")
Shell	26	(hull splinters)

⁶⁸ Final Report. 3.5.3 Damage from external causes, p.121, 126.

⁶⁹ 9 NLR report (Annex X). 2.5 Number and density of hits, p.14.

⁷⁰ Only hull fragments with linear dimensions corresponding to those of preformed fragments are taken into account. Detonation products of 1-3 mm in size and large compartment fragments are not taken into account.

Accordingly, the simulation results show that only 46 prefabricated projectiles (34+12= 46) could damage the complex multi-layer barrier that is the cabin glazing (window).

The number of simulated damages (46 units) is 2.22 times less than the number actually recorded in the second window (102 units).

The nature of modelled damage to the second left window, recognized by the DSB experts as the area of maximum density, is fundamentally different from the actual damage to the Boeing 777: the number of damage (46 units) is 2.22 times less than the actual damage to the second window (102 units), while the density of damage is less than the actual damage and is about 110 holes per square meter.

3. The area of the outer skin behind the second and third windows is not included in the tight fragment cloud at all, according to the modelling results (Figure F.12).



Figure F.12 - Inconsistency of damage in the area of the second and third windows on the left side of the cockpit

In fact, in the area behind the third window, there is multiple damage to both the outer skin and the load-bearing structure (the bulkheads).

The port side fragments (No 3, No 4 and No 5), which objectively have damage caused by projectiles, are, according to modelling results, outside the area of fragment coverage.

The nature of modelled damage for fragments No 3, No 4 and No 5 is fundamentally different from the actual damage to the Boeing 777. According to the simulation results these fragments are outside the fragment coverage area.

4. In contrast to the actual damage to the Boeing 777, according to the simulation and field experiment with the IL-86 target aircraft, there should be multiple through-hole exit holes on the starboard side.

Thus, the nature of the modelled damage for Azimuth -16° conditions for all marker fragments from No 1 to No 5 is radically different from the actual damage to the Boeing 777.

The differences in modelled damage have been confirmed by field experiments and tests.

Azimuth -37° option

Figure F.13 shows the results of the fragmentation field modelling of the Boeing 777 outer hull model (left) compared to the 3D reconstruction (right).

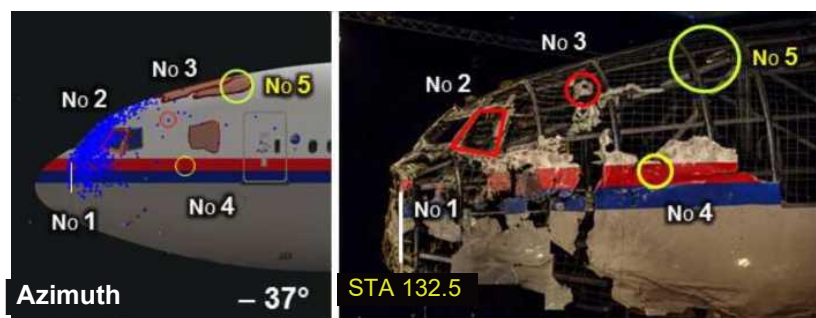


Figure F.13 - Simulation of Boeing 777 nose section damage under Azimuth -37° conditions

1. The forward boundary of the fragment cloud formed by prefabricated projectiles is closer (to STA 132.5 level) than the real one, starting behind the level of the forward pressure bulkhead (Fragment No. 1).



Figure F.14 - Actual through holes, identified as impact damage, located to the right of the bulkhead no closer than 5-10 cm from the level of STA 132.5

2. The second left window (Fragment No. 2), where the maximum density of damage was recorded according to the Final Report, is included in the damage area, but the calculated density of damage is not fully consistent with the recorded objective data.

The simulation result for the Azimuth -37° variant is shown in Figure F.15, where the set of areas (polygonal objects) corresponding to the second left window on the Boeing 777 model are highlighted in orange on the interactive aircraft model.

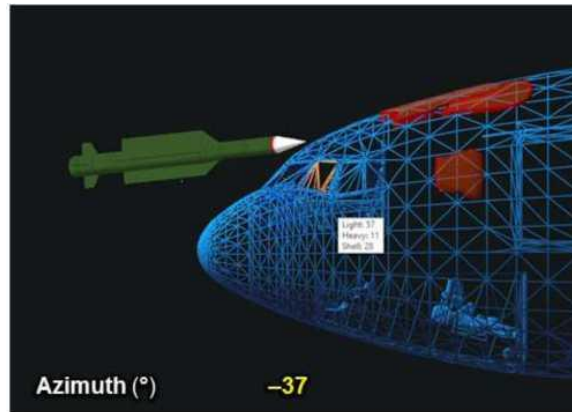


Figure F.15 - Simulation of fragmentation damage to the nose of a Boeing 777 under Azimuth -37° conditions

Simulation results for "Azimuth -37° " conditions:

up to 96 fragments (Light- 57; Heavy- 11; Shell- 28) can reach the second window;
no more than 68 prefabricated projectiles ($57+11= 68$) could damage the complex multi-layer barrier that is the cab's glazing (window);

The number of simulated damages (68 units) is 1.5 times less than the number actually recorded in the second window (102 units);

The modelled damage density for Azimuth -37° conditions is 1.5 times lower than the actual damage density and is about 167 holes per square metre.

The nature of modelled damage to the second left window, recognised by the DSB experts as the area of maximum density, is different from the actual damage to the Boeing 777: the number of damage (68 units) is 1.5 times less than the actual number of holes in the second window (102 units), while the density of damage is less than the actual number of holes per square metre and is about 167.

3. The port side fragment no. 3 does not fall within the calculated zone of maximum density (mass and kinetic energy) of the projectiles and factors associated with a close explosion.

Accordingly, the modelled density damage to the fragment differs from the actual damage (Figure F.16).



Figure F.16 - Fragment of port side no 3 actually has multiple damage to the outer skin and force element, indicating that the fragment was in a dense fragmentation stream

On the fragment the following was objectively fixed: high density of damages (30 holes of various sizes in area about 0,1 sq. m); strongly expressed traces of microcraterization, thermal oxidation, compression and rupture of sheets of outer hull; multiple through-holes in a bulkhead, accompanied by deformation and destruction of a force element on perforation.

3. The port side fragments no 4 and no 5, which objectively show GHE damage, do not fall within the modelled fragmentation cover for the Azimuth -37° variant.

The Azimuth -37° variant, out of the range of input data used in the technical investigation, is the most consistent with the actual damage observed on the fragments present in the 3D reconstructions. The main inconsistencies of this variant come from the fragments that are not accounted for by the 'damage reference models':

fragment No 3, which is located further back than the STA 220.5 'reference' level;
 fragments missing from the final display (for various reasons not removed from the crash site or placed elsewhere), e.g. fragment No 5.

Azimuth -50° variant

Figure F.17 shows the results of the fragmentation field modelling of the Boeing 777 outer hull model (left) compared to the 3D reconstruction (right).

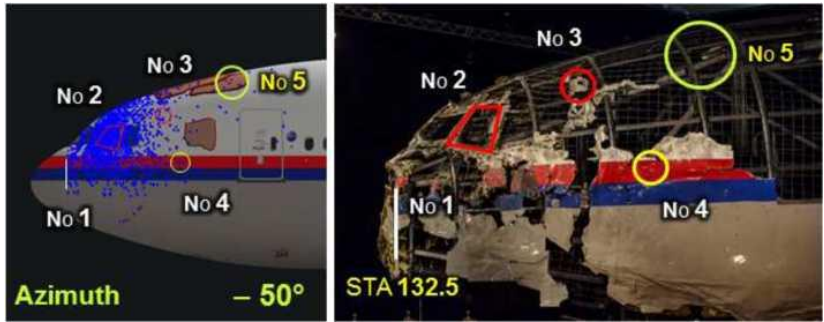


Figure F.17 - Simulation of Boeing 777 nose section damage under Azimuth -50° conditions

1. The front boundary of the fragmentation area from prefabricated projectiles is at the level of STA 132.5, which generally coincides with the actual front boundary of the fragmentation field.

2. The second left window (fragment No 2), where the Final Report recorded the highest density of damage, enters the damage area, with a modelled damage density comparable to the actual values recorded in the area of the second window - about 250 gaps per square metre.

The simulation result for the Azimuth -50° variant is shown in Figure F.18, where the set of areas (polygonal objects) corresponding to the second left window on the Boeing 777 is highlighted in orange on the interactive aircraft model.

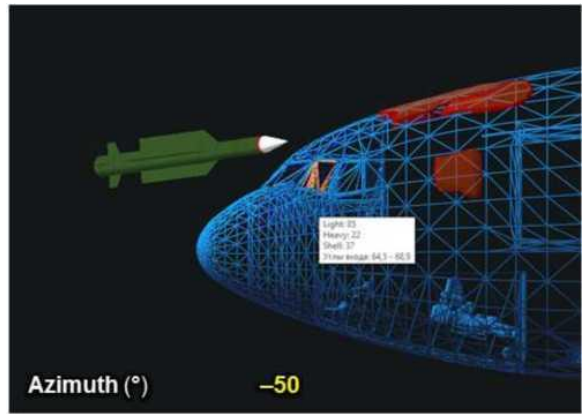


Figure F.18 - Simulation of fragmentation damage to the nose of a Boeing 777 under Azimuth -50° conditions

Simulation results for "Azimuth -50°" conditions:

The second window only receives up to 144 fragments (Light- 85; Heavy- 22; Shell- 37);

Up to 107 prefabricated projectiles (85+22= 107) could damage the complex multi-layer barrier that is the cab's glazing (window);

The number of modelled damage (107) is comparable to the number of actually recorded damage at the second window (102), and the modelled density is also comparable to the actual values recorded at the second window - about 250 holes per square metre.

3. The port side fragments No 3, No 4 and No 5, which objectively have GBE damage, fall within the modelled fragmentation cover for the Azimuth -50° variant.

4. The Azimuth -50° option is the minimum value pertaining to "missile end state" in the horizontal plane which provides a logical explanation to the actual boundary of the fragment coverage area taking into account the characteristics of a BUK missile (Figure F.19).

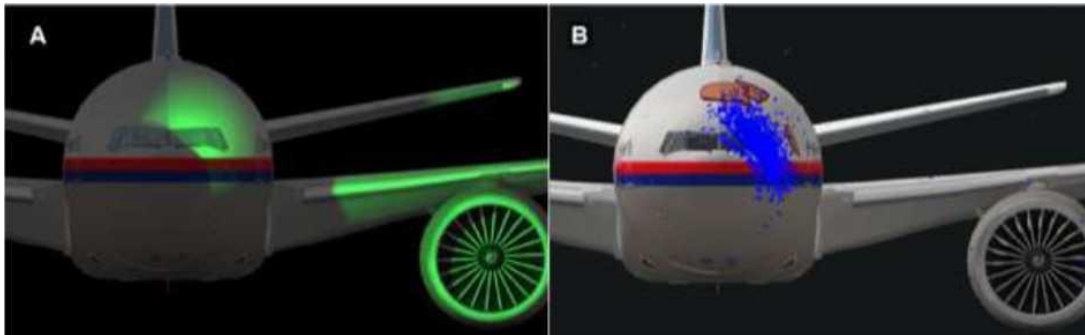


Figure Frfr .19 - Boundaries of the fragment coverage area for a "collision course", which explains all damage to the outer skin, power structure, left wing plane and left engine of the Boeing 777: left - area of expected damage; right - results of the simulated fragment coverage area for the "Azimuth -50°" option

Among the options considered, only for the "Azimuth -50°" option do the boundaries of the fragmentation overlap between modelled and actual damage most closely coincide on reference fragments No 1-No 5 with characteristic damage.

Thus, as minimally realistic baseline data to explain all damage to the outer skin, power frame, left wing plane and left engine of the Boeing 777 aircraft, and which does not contradict the characteristics of the BUK missiles, only the missile impact conditions in the -50° horizontal plane can be considered.

Exhibit G. Main inconsistencies of the DSB version

In the final version of the DSB Final Report "Crash of Malaysia Airlines Boeing 777-200, 9M-MRD, flight MH17" the Dutch experts concluded that the cause of the MH17 crash was the detonation of a 9H314M warhead delivered by a 9M38-series BUK surface-to-air missile "on the opposite course".

Conclusions on the type of weapon and the intended location of the missile "from eastern Ukraine"⁷¹ are made on the basis of "best matches" based on the results of analysis of the location, size and boundaries of the damage area, assessment of the number and density of holes in the wreckage of the Boeing 777,⁷² and determination of the relative location (meeting conditions) of the aircraft with the missile (Figure J.1).

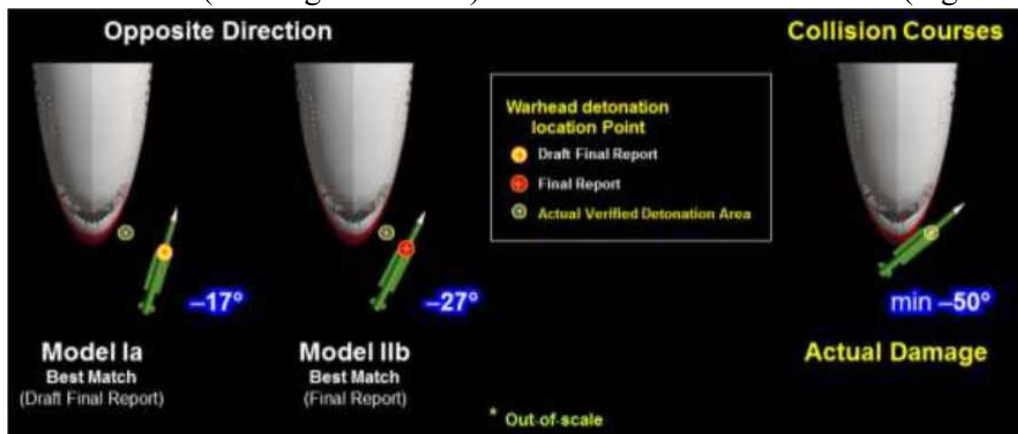


Figure G.1 - Missile encounter conditions: left - "opposite direction" DSB version; right - "collision course"

The "Best Match" in the DSB Report lists the missile encounter conditions (angles in the horizontal and vertical plane, final missile speed)⁷³ as appropriate for the "opposite direction" version of the aircraft.

As "Best Match" at various stages of the technical investigation, two versions of the aircraft missile encounter conditions were recognised:

1. **Model Ia** - with horizontal angle $Az = -17^\circ$ in the draft DSB report.⁷⁴
2. **Model IIb** - with horizontal angle $Az = -27^\circ$ in DSB Report.⁷⁵

⁷¹ Final Report. 11. Missile flight parts, p.256.

⁷² Final Report. 6. Fragmentation spray of pre-formed fragments, p.255

⁷³ Final Report. 3.8.3. Warhead simulations, p.140.

⁷⁴ Draft Final Report, Final Report. 3.8.3. Warhead simulations, Table 19, p.140.

⁷⁵ Final Report. 3.8.3. Warhead simulations, Table 19, p.140.

Exhibit G.1. Best Match

The main feature of the surface-to-air guided missiles of the BUK complex is that the missile is guided toward a target using the method of proportional navigation.

The DSB report confirms that the features of the BUK's guidance method were taken into account by Dutch technicians during the DSB's technical investigation.^{76,77,78}

The main feature of the guidance method using proportional navigation is that if the airborne target moves uniformly and in a straight line at the same altitude, the trajectory of the missile in the horizontal plane is almost straight.

target. Proportional-navigation guidance systems use the target tracking information obtained from the seeker, to steer the missile directly towards the collision point with the target. If the target does not change its direction or velocity, the missile will follow a more or less straight path towards this collision point.

Figure G.1.1 -Features of Proportional Convergence Approach Missiles (Final Report, p. 134)

Similar principles also underlie calculations of Ukrainian specialists,⁷⁹ specialists of Almaz-Antey Corporation and other independent experts. This methodology is fully acceptable because the Boeing 777 flew on a straight trajectory with a constant bearing, and at constant speed and constant altitude.

An analysis of the Annexes to the DSB Report and of in-flight recording control data confirms that the Boeing 777 flew on a straight trajectory with a constant bearing, constant speed and constant altitude, which is confirmed by the Flight Data Records (FDR) of flight MH17.⁸⁰

Therefore, for calculations identifying the launch area, the most important thing is to determine the relative position of the missile in space with reference to the aircraft (encounter conditions) at the moment of the warhead detonation, which indicates the direction to the intended launch area, as well as the final speed of the missile, which determines the distance between the launch area and the point of the warhead detonation.

⁷⁶ Draft Final Report. 3.4.9 BUK surface to air weapon system, p.114; 5.4.4 BUK missile, (NLR Annex), p.319.

⁷⁷ NLR report (Annex X). 6.6 BUK missile, p.46-47.

⁷⁸ Final Report. BUK operating characteristics, p.134.

⁷⁹ Results of examination of causes of MH17 crash over the territory of Ukraine 17.07.2014. 10-12.08.2015, Gilze.

⁸⁰ Submitted by the DSB - Preliminary Report and Final Report.

As noted in the Corporation's Report,⁸¹ determining the conditions of missile-aircraft encounter is based on the best match of three components: damage to the aircraft, the dynamic model of the warhead explosion (warhead properties) and the detonation point linking them.

Thus, each of the Best Matches represents three interrelated 'references':

1st "Reference" is a damage model.

2d "Reference" is a warhead model (model of fragment dispersion under dynamic conditions).

3d "Reference" is the position of the detonation point where simulated detonations of a "reference warhead" are carried out under different conditions regarding relative position of the aircraft and the missile.

Based on the results of each of the variants, a comparison is made between the damage caused by a simulated detonation of the "reference warhead" and the "reference" damage.

The result is the best match between the dynamic fragment dispersion model and the damage model taking into account the detonation point linking them:

the values of the angles between the longitudinal axes of the missile and the aircraft in the horizontal plane $Az_{Warhead}$ and in the vertical plane $El_{Warhead}$;

final velocity of the missile V_M at the moment of the warhead detonation.

As an example, the original version of the model developed by NLR was articulated during the work of a joint team effort in Gilze-Rijen (Kingdom of the Netherlands) in February 2015.

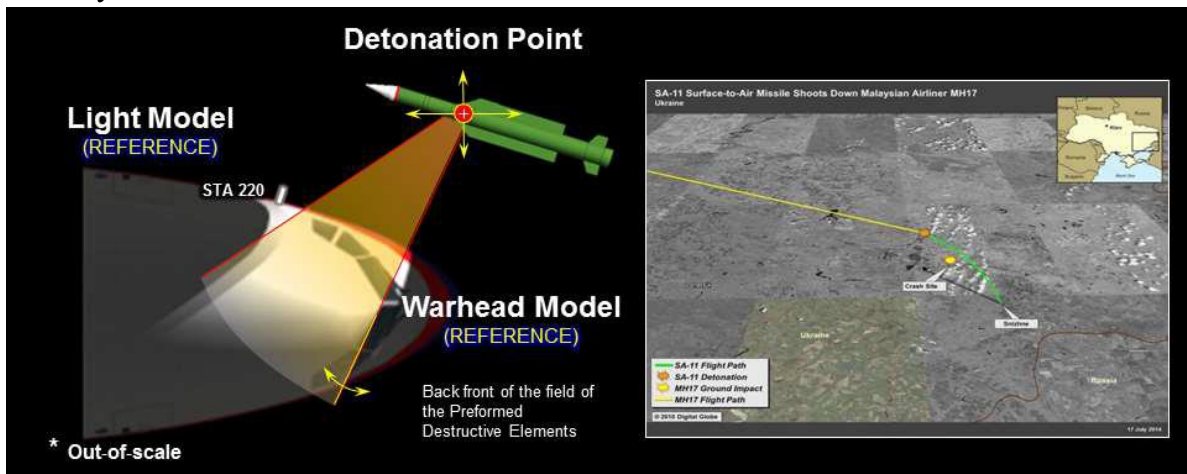


Figure G.1.2 - Model Ia - First "Best Match" option (NLR, February 2015)

⁸¹ PART 1. Sub-section 5.2. Determination of damage conditions of the Boeing 777 aircraft.

In NLR's first version (Model Ia), all three components of the "Best Match" were chosen so well that an exact, almost "pixel-for-pixel" match was obtained for the figure published on the website of the US Embassy in Ukraine.

A reverse trajectory simulation of a BUK missile targeting a non-maneuvering aircraft, using the missile encounter conditions considered by the DSB ("Best Match" - Model Ia) would indeed result in an area considered as a "firing position" in the "Pervomaisky" area.

"The "References" for this Best Match were:

the Light Model of expected damage (NLR);

dynamic warhead detonation model (Warhead Model/Design I);

detonation point which is more than 4 metres away from the outer skin of the aircraft, coordinates X= -0.5 m; Y= -4.0 m; Z= 4.0 m.⁸²

The above "references" will be discussed in Exhibites G.1.1- G.1.3, and the calculations identifying the possible launch area using this data are given in Exhibit G.2.

⁸² Draft Final Report. Table 15, p.130.

Exhibit G.1.1. Model of damage to Boeing 777 aircraft

In investigating the nature of the damage caused by the remote impact of the high-explosive fragmentation warhead of an anti-aircraft missile on the structure of an aircraft it is necessary to:

- study the traces of impact by the factors of a nearby explosion;
- determine the basic parameters of the fragment coverage area, including boundaries, the amount of damage to the outer shell, the airframe, components and assemblies, and the aircraft's internal equipment;
- establish the distribution of fragmentation damage density in aircraft structural fragments, including the airframe.

High-explosive effect (effect of close blast factors)

The DSB's damage model ("reference") does not take into account the blast effect of the warhead.

Fragment coverage area boundaries

In order to justify the main DSB's version that the "aircraft was hit by a 9M38-series BUK missile travelling in an "opposite direction", the Dutch experts used only selected fragments of the aircraft that could fit the pre-determined version (Figure G.1.3).

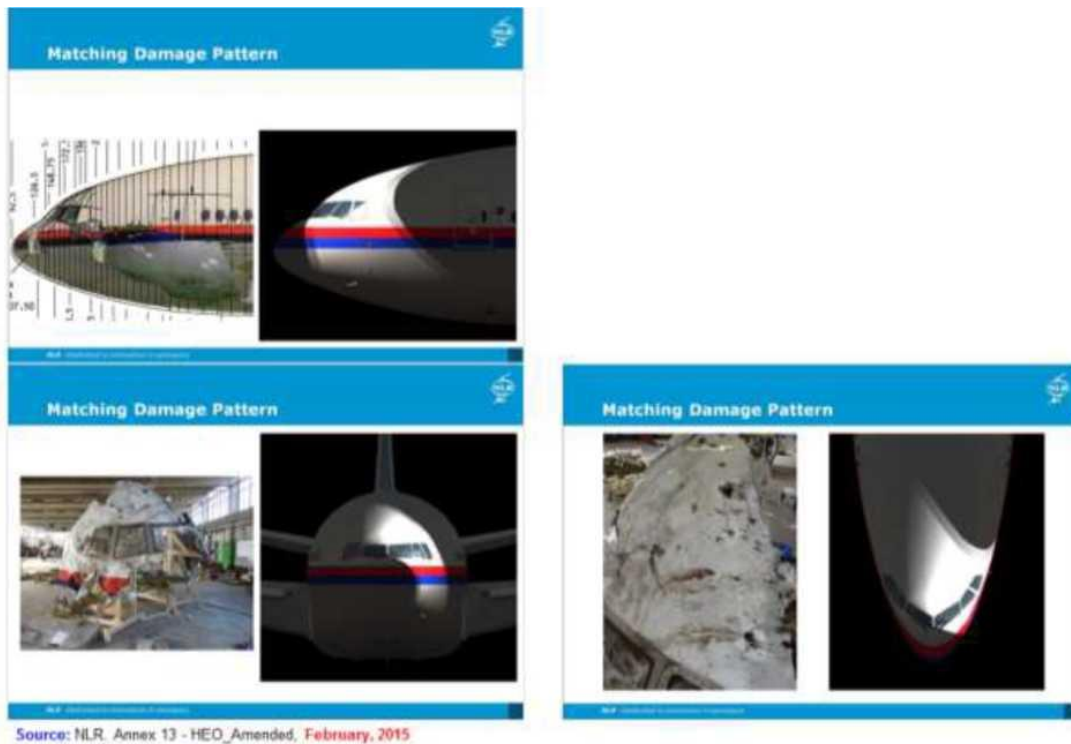


Figure G.1.3 - Replacing the damage survey with a computer model

Only a few sample fragments were included in the 'reference'⁸³ damage model (Light Model, NLR):

- of the cockpit glazing frames;

- Fragment of the right-hand side of the cockpit with part of the roof and the remaining glazing on the right-hand pilot's side;

- part of the port side trim below the crew commander's glazing bezel (level STA 220.5);

- Fragment of the port side plating with angle of attack sensor; forward pressure bulkhead (level STA 132.5).

In this case, the front pressure bulkhead with fragments adjacent to it was located in another room. The other fragments were either ignored or not displayed at all in the public areas of the hangar.

Figure G.1.4 shows the state of lay-out of the aircraft fragments at the time of replacement of the actual damage survey by computer modelling.



Figure G.1.4 - The "reference" damage model is based on only a few sample fragments: left - front view; right - port side view

It was these fragments that formed the basis of the "reference". Despite the emergence of important new fragments, the 'reference' has not changed, as the final DSB report shows. During the technical investigation,

⁸³ Final Report, p.137-138.

the Dutch experts claimed that they did not see any damage beyond the STA 220.5 bulkhead, located just behind the cockpit windows.^{84, 85}

a small part of the fuselage immediately aft of that. At the rearward edge of the panel, positioned on the left hand side of the aeroplane between approximately STA220 and STA410 close to the forward passenger door and on panels further away from the cockpit, no high-energy object damage was noted. The cockpit panel at STA132.5 appeared to be the leading edge of the high-energy object damage.

Figure G.1.5 - No damage beyond the STA 220 bulkhead (Final Report)

The factory markings for the Boeing 777's structural members (bulkheads and stringers) correspond to the distance in inches from the reference plane perpendicular to the fuselage's structural axis and 92.5 inches away from the end of the aircraft's nose fairing.⁸⁶

As a "reference" of the damage, the Dutch specialists took the narrow strip between the bulkheads from STA 132.5 to STA 220.5, i.e. the one of **only about 2.24 m** (220.5-132.5= 88 inches), on the port side of the cockpit.



Figure G.1.6 - Fragment of roof and upper part of the port side behind the cockpit. The fragmentation damage is located between bulkheads STA 309.5 and STA 332.5, which is almost 3 metres further than the DSB 'reference'

⁸⁴ Final Report. Crash of Malaysia Airlines flight MH17. p.121.

⁸⁵ TNO report. Damage reconstruction due to impact of high-energy particles on Malaysia Airlines flight MH17, p.7.

⁸⁶ Boeing 777-200/300 Aircraft Maintenance Manual, page 201.

Objectively observable damage in the upper port side spread considerably beyond STA 332.5, i.e. about 5.1 metres ($332.5-132.5=200$ inches) from the forward STA 132.5 bulkhead, taken as the leading edge of the damage.⁸⁷

Accordingly, the "reference" accounts for less than 1/2 of the actual damage to the top of the port side. Figure G.1.6 shows a fragment of the roof and top of the port side behind the cockpit which was not accounted for in the final reconstruction.

Unlike the original plans, the final reconstruction was carried out in a small hangar, where only the nose section of the aircraft is represented. All other fragments were located in other rooms. At the same time, some of the fragments were arranged in such a way that the damage that does not fit in the main version was not visible. For example, the vertical stabiliser (keel) was turned towards the blind wall of the hangar with its left side showing signs of the effects of the explosion of the killing agent (Figure G.1.7).



Figure G.1.7 - Vertical stabiliser in final reconstruction

Also shown separately from the main display were a fragment of the roof and top of the port side behind the cockpit and the nose of the left engine air intake, shown in figure G.1.8.

⁸⁷ Final Report. 3.5.3 Damage from external causes, p.121.



Figure G.1.8 - Fragment of the roof and top of the port side (front) and toe of the left engine air intake (rear) were located elsewhere in the final reconstruction



Figure G.1.9 - Source data for the model that has become the "reference": on the left are the fragments included the "reference"; on the right, the final layout

Figure G.1.9 compares the condition of the aircraft fragments layout at the time when the actual damage study was replaced with computer modelling.

The left-hand side of Figure G.1.9 shows what the left-hand side fragments, which were used by the NLR as a 'reference' to support their version, would have looked like in the final 3D reconstruction.

The right side of Figure G.1.9 shows the final layout of the nose section of the aircraft. A large number of additional fragments of the aircraft structure presented in the reconstruction were not used during the ongoing investigations and were not available in the preliminary layout during the entire technical investigation.

The yellow polygon in the right top corner shows where the fragment of the roof and upper part of the left-hand side should have been located, which in the final lay-out was located in a different room.

The model used by the DSB experts in the technical investigation as damage "reference" takes into account less than 1/2 of the actual damage to the upper part of the port side and does not correspond to the actual fragmentation field boundaries objectively observed in the 3D reconstruction of the Boeing 777.

Number of hits and distribution of damage density

During the technical investigation, the Dutch specialists made little use of the most important parameters for studying combat damage to the airliner's structure, such as the amount of damage and the distribution of the density of damage.

However, during the course of the technical investigation, these critical indicators were modified based on the "main story" options.

So in the version of the NLR that formed the basis of the Draft Final Report, the Dutch experts found only about 300 damage to all types.⁸⁸

The total number of hits, of all types of impact damage, on the available wreckage of the cockpit equals around 300. An extrapolation of the number of hits on the fuselage, accounting for the structure that was not available, suggests that the total number of hits of high-energy objects was well over 600. The highest density of hits was on the upper window frame of the captain's left hand side front window. The density of hits in this area is calculated to be around 80 hits per square metre.

Figure G.1.10 - Description of the number and maximum density of damage for the "Best Match" version from the Draft Final Report

Taking into account the spread of damage to missing fragments, the total number of lesions was estimated at more than 600, and a maximum density of damage was stated at 80 holes per square metre.

These damage parameters fit the NLR version with the detonation point to the left of the aircraft's longitudinal axis at 4.0 metres.⁸⁹ Subsequently, the Draft Final Report identified this version (Model Ia) as "Best Match".

In the new 'Best Match' in Final Report, the main indicators - damage count and maximum density - have been changed. At the same time

⁸⁸ Draft Final Report. 3.7.4. Physical measurements, p.119-124; Investigation of the impact damage due to high-energy objects on the wreckage of flight MH17. 5.5 Number of hits and density, p.289.

⁸⁹ Damage Investigation MH17. NLR Annex 13 - HEO_EN_3.

the maximum measured density on the same fragments more than tripled, from 80 to 250 holes per square metre.⁹⁰

The total number of hits (over 350), of all types of impact damage, on the available wreckage of the cockpit suggests that the total number of hits of high-energy objects was well over 800. The highest density of hits on the left hand side of the cockpit was calculated to be over 250 hits per square metre. The highest density of hits was on the left front windows.

Figure G.1.11 - Description of number and maximum damage density for the "Best Match" version from the Final Report

It should be noted, however, that the actual number and density of fragment damage cannot depend on the type of computer models used and the conditions and/or coordinates selected - the actual number and distribution of the holes on the Boeing 777 fragments could not have changed in reality after the crash.

Thus, the damage model used by the NLR specialists during the technical investigation as a "reference" did not take into account the most important parameters of combat damage studies: the actual number and distribution of damage density. These objectively unchangeable parameters were modified, if necessary, to fit variants of the "Best Match" versions.

Damage to the airframe of the aircraft

The Dutch experts did not consider the damage to elements of the aeroplane's force structure, the floor and internal equipment of the Boeing 777's cockpit, which need to be assessed for an objective and comprehensive investigation.

When assessing damage during a technical investigation, all investigations are limited to the outer skin only (figure G.1.12).

Only outer skin damage investigated

Figure G.1.12 - Damage Investigation MH17

The refusal to substantively study almost half of all the actual damage to the forward part of the aircraft⁹¹ is justified by references to "the complexity and unpredictability of such studies due to the deviation of the projectiles from their original direction after overcoming the obstacle (Figure G.1.13).

⁹⁰ Final Report. 3.5.3 Damage from external causes, p.119-126.

⁹¹ The amount of damage to the bulkheads, floor and internal cockpit equipment is comparable to the amount of damage to the outer skin.

The Dutch Safety Board has made a reconstruction of the forward part of the aeroplane. It is a well known fact in the study of terminal ballistics of fragments that a fragment hitting a plate at an oblique angle (not perpendicular to the plate) changes its direction of travel after penetration. The initial angle is typically reduced after penetration. This change in angle is dependent on several factors and can be as small as several degrees or as large as the original oblique angle. As a result, it is usually not possible to obtain accurate data on the direction of travel of fragments outside the structure by studying parts inside the structure.

Figure G.1.13 - Failure Cause of Aircraft Strength Framing Study (Final Report)

However, no research has been done on how, to what extent and under what conditions different types of projectiles of a particular warhead may deflect when passing a variety of obstacles. Only some theoretical materials were used that do not give any numerical values. In contrast, specialists at Almaz-Antey paid particular attention to studies of mechanical (penetration) capability - in addition to two experiments, special Studies.⁹²

At the same time, the NLR (DSB) experts, without explanation, rejected the use of materials on the penetration capability of BUK missile projectiles provided by Almaz-Antey Corporation,⁹³ as well as the results of the first full-scale experiment demonstrated in August 2015 during the final phase of the joint work.⁹⁴

The damage "reference" does not take into account damage to the power frame, floor and internal cockpit equipment, meaning that almost half of all damage is ignored under the pretext of "research complexity".

As it appears from the NLR material, the light model of expected damage, taken as a "reference" of damage, was originally created for pre-assigned conditions on the main version. Only for a specific BUK missile warhead (9H314M warhead),⁹⁵ coming precisely "on the opposite direction to the **direction of flight of the aeroplane...**" from the eastern direction, as explicitly shown in the technical study materials.⁹⁶

⁹² Report on the conduct of a full-scale experiment, pp. 149-164.

⁹³ Letter No. 01-09/548k dated 29.07.2015 with extracts from technical documentation and field visits tests

⁹⁴ Final Report. Presentation (August, 2015). Findings of Expert Assessments on MH17 Accident. Simulation Results Validation, p.41-50.

⁹⁵ Final Report. 3.8.2. Fragmentation visualisation model, p.137.

⁹⁶ Final Report. 3.8.2. Fragmentation visualisation model, p.138.

In other words, the virtual NLR model, taken as a "reference" of damage, **did not allow** any other versions than the "main story" of the investigation to be considered.

Thus, the model (Light Model, NLR) used during the DSB technical investigation as a damage "reference", of all the main parameters characterizing the distance effect of a high-explosive SAMG warhead, took into account only the outer hull fragmentation damage boundaries. At the same time, a narrow band of selected fragments 2.24 m wide, which is less than¹ L of the port side damage area, was taken into account from the outer hull.

Objectively unchanged parameters (number and distribution of damage density) were modified as necessary to suit variants of the "Best Match" versions.

"**The damage reference** was created by NLR specialists specifically to justify a version of hitting a Boeing 777 with a specific type of 9H314M warhead and only for predetermined parameters of "**opposite direction**" encounter conditions.

Exhibit G.1.2: Warhead Model

An important part of the technical investigation is the warhead model. The Dutch experts assigned the type of warhead even in the initial research phase before the first joint experts' meeting in Gilze-Rijen in February 2015.⁹⁷

It is the specific warhead that contains the preformed "bowtie" ("bowtie") type of projectile.

In doing so, the NLR experts used unverified information as input data to justify their version, which made it possible to obtain, during modelling, the results necessary to confirm the "main version". For example, data from analogues of warheads used in NATO countries with a different, "mirrored" detonator location was used to justify the "convenient" direction of the projectile's dispersion (Figure G.1.14).⁹⁸

⁹⁷ Damage Investigations MH17. NLR_Presentatie Annex 13 - HEO_Amended. February, 2015.

⁹⁸ Fragment Spray Zone of a static detonation of a cylindrical warhead. Source: The Fundamentals of Aircraft Combat Survivability Analysis and Design, Robert E. Ball.

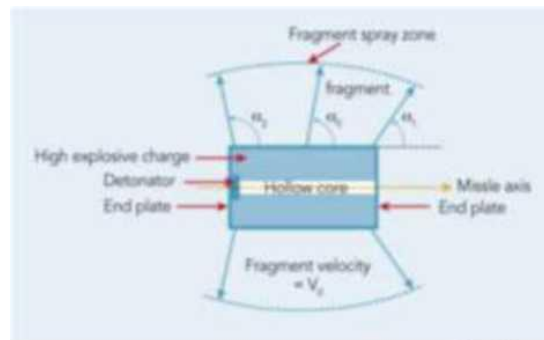


Figure G.1.14 - Source data from DSB Report documents for the modelling of the warhead, later called "Design I", which became the basis of the first "Best Match" - Model Ia

After analyzing the materials received in February 2015 from DSB experts, Almaz-Antey Corporation specialists identified serious inaccuracies in the source data on the characteristics of the warheads used by the NLR experts. In order to eliminate these inaccuracies, a process was initiated to lift the "classified" and "top secret" design documentation and reports on state and periodic tests of the combat parts used in the 9M38 and 9M38M1 BUK missiles.

As a result, in May 2015, the Corporation's specialists presented data on the main characteristics of the 9H314M warhead of the 9M38M1 missile during the second meeting at Gilze-Rijen Air Base (Netherlands) to DSB representatives in the presence of a group of international experts.⁹⁹

However, analysis of the Draft Final Report¹⁰⁰ shows that the DSB experts ignored the developer's data and continued to use warhead models using fundamentally different parameters as inputs.

On 29.07.2015, the Corporation sent to the DSB extracts of technical documentation for 9H314M warheads and test results of these warheads conducted between 1980 and 1991. The letter also invited DSB experts to review the originals of these materials (technical descriptions, manuals, test procedures and test results) in the Russian Federation.¹⁰¹

On 31 July 2015, two days after the letter was sent, validation tests were carried out specifically to confirm the characteristics of the warheads conveyed in the letter. During these tests, all the main parameters of the warhead's field of attack were taken in a ground targeting environment.

⁹⁹ Presentation (May, 2015). Findings of Expert Assessments on MH17 Accident, p.5-8.

¹⁰⁰ Draft Final Report. Crash of Malaysia Airlines Boeing 777-200, 9M-MRD. Figure 28, p.111.

¹⁰¹ Letter No. 01-09/548k dated 29.07.2015 with extracts from technical documentation and field test reports.

The express analysis carried out on the basis of the results of the tests showed that all the main characteristics were fully consistent with the data previously sent in letter No. 01-09/548k dated 29.07.2015.

This test was necessitated by the fact that a review of the technical investigation materials showed that the materials previously provided **had not been used**.



Figure G.1.15 - Fragment of materials submitted to the DSB experts

In early August 2015, during the final meeting with the Dutch experts, the main test results were communicated to the Commissioners in the form of a visual illustration of the technical specifications transmitted (Figure J.1.15).¹⁰²

In addition to the demonstration of the main results of the full-scale test, the Dutch experts were shown the original technical documentation, the materials of previous tests and even the raw data of the full-scale experiment: the description of the experimental procedure, photo and video images, target sheets, control samples of the projectile, etc.

Ignoring the Corporation's suggestion, the Dutch experts for the new 'Best Match' variant in the Final Report used a new electronic model of the warhead, the 'Model II' ('Design II').

In this latest "reference", instead of the data transmitted by the developer and reflected in the design and technical documentation and confirmed by state and inspection test certificates,

¹⁰² Presentation (August, 2015). Findings of Expert Assessments on MH17 Accident. Simulation Results Validation. Experimental Objective, p.41-50.

the Dutch experts have chosen a set of parameters that are suitable precisely to justify the investigation version.

TNO rates design II as being the most realistic for the purpose of this investigation because of the physical basis of the design.

Figure G.1.16 - Virtual model with convenient characteristics found to be the most suitable for this investigation, contrary to data from the design and technical documentation

Explanation of the final reasons for the rejection of the data transmitted by the manufacturer, other than a reference to some "physical basis of calculation" in no technical investigation file is available.¹⁰³

However, as the subsequent analysis of the annexes to the Final Report shows, for the "most realistic model" the Dutch experts used input data that differed significantly from the original.

For example, the explosive charge of the warhead used for the simulation was some kind of "composition "B" consisting of 60 per cent hexogen and 40 per cent TNT.^{104, 105} In the 9H314M warhead, the TNT/hexogen mixture ratio is significantly different, with the TG-24 composition using 24 per cent TNT.

The model used a different shape and geometric dimensions for the body and side plates of the warhead, as well as the location of the detonator, which does not correspond to the warhead drawings.

In creating the "reference" model of the warhead, unreliable input data was used, directly contradicting the manufacturer's technical documentation and the results of field tests.

However, according to the Kyiv Institute for Forensic Expertise, which was shown during the expert meeting in August 2015,¹⁰⁶ the Dutch experts had all the necessary comparative material at their disposal (Figures J.1.17 and J.1.18).

¹⁰³TNO report. Damage reconstruction due to impact of high-energy particles on Malaysia Airlines flight MH17

¹⁰⁴Numerical simulation of blast loading on Malaysia Airlines flight MH17 due to a warhead detonation (Annex Z, TNO report - 2015 M10626), p.7.

¹⁰⁵Draft Final Report, p.360.

¹⁰⁶Results of examination of causes of MH17 crash over the territory of Ukraine 17.07.2014. (10-12.08.2015, Gilze).

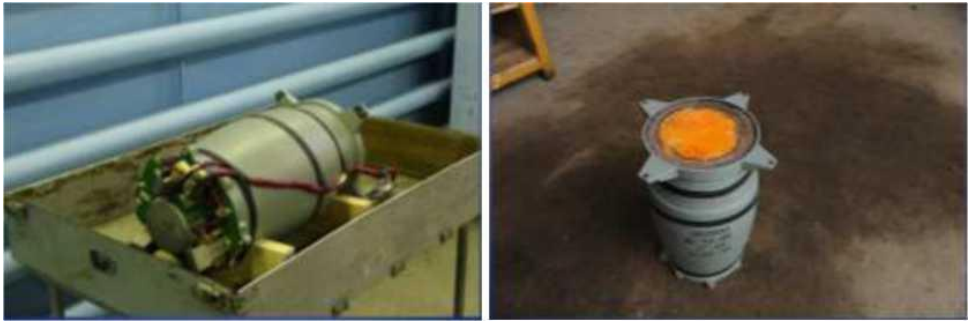


Figure J.1.17 - Detonator placement on the warhead (left) and correct name of the 9H314M warhead indicating the type of explosive charge TG-24 (right). Proceedings of Ukraine



Figure J.1.18 - Test samples of a bursting charge (left) and three fractions of projectiles (right). Materials of Ukraine

Warhead Model

Initial data from DSB Draft Final Report to model the warhead referred to as "Design I" and "Design II" later.

Source: Draft Final Report, Figure 26

Source: Draft Final Report, Figure 32

As a matter of fact, from all the data concerning 9H314M warhead characteristics, delivered in May – August, 2015 DSB Final Report used only the **Right Name of the Warhead**, which contained figured destructive elements (Bow-tie or Butterfly), and here is the **Picture of this Warhead appearance** (low to the right)

Figure G.1.19 - Dutch use of source data for warhead characteristics

As a result, the Final Report chose the Model II / Design II as the 'reference' warhead.

In this "reference" model only **the correct name "9H314M"** and **a photograph** of this very warhead were used from the whole array of technical specifications based on real technical documentation and test results, which were handed over and demonstrated by the Russian side (Figure J.1.19).

All other parameters of the "reference" model were picked up for another "Best Match" to justify the main version "destruction by a 9M38-series missile travelling in an opposite direction" which formed the basis of the Final Report conclusions.

According to DSB experts, the Design II differed from the data provided by Almaz-Antey only in "a smaller meridional angle of the elements".¹⁰⁷

However, this statement is not true.

Firstly - the Design II model takes into account only the finished projectiles,¹⁰⁸ which is less than half of the fragmentation impact field.¹⁰⁹

the smaller angular range for the fragment ejection. Note that the warhead model only contains preformed fragments. Other fragments that occur with the break-up of the SAM are not included in the model.

Figure G.1.20 - The model of a warhead used by the Dutch experts considered only prefabricated warheads. Hull warheads were not included in the model

Second, -the difference in the meridional sector of fragment dispersion is **significant**. The virtual "Design II" model adopted as a "reference" takes into account less than ½ of the meridional sector of fragment dispersion under static conditions (Table G.1.1).

Table G.1.1 - Comparison of meridional fragment dispersion sector under static conditions

Parameter	9H314M	"Design II"	Included in the "reference" model
Meridional sector of fragment dispersion:			
- separately from the warhead	68°-124°	76°-112°	64,28 %
- as part of compartment hull	48°-130°		43,9 %
- as part of missile	40°-150°		32,72 %

¹⁰⁷ TNO report. 4.3.2. Warhead implementations (designs), p.15.

¹⁰⁸ TNO report. Damage reconstruction due to impact of high-energy particles on Malaysia Airlines flight MH17, p. 15.

¹⁰⁹ It has been proven experimentally (including through independent tests) that when a missile is detonated in an assembly, the number of fragments capable of penetrating the outer hull of an aircraft is two to three times greater than the projectiles considered in the Design II "reference" model.

The field performance of BUK missiles has been confirmed by numerous tests,¹¹⁰ including field experiments: the impact field of the 9H314M warhead when detonated as part of a missile is two to three times larger than in the virtual Design II model.¹¹¹

Thirdly, the parameters of the Design II are chosen in such a way that the greatest distortions (programmed errors) refer to the rear front of the fragmentation field. Of particular importance is the fact that, according to the methodology adopted by the Dutch specialists, it is the alignment of the rear edge of the fragmentation field with the front edge of the covering field that determines the conditions of the aircraft's encounter with the missile.

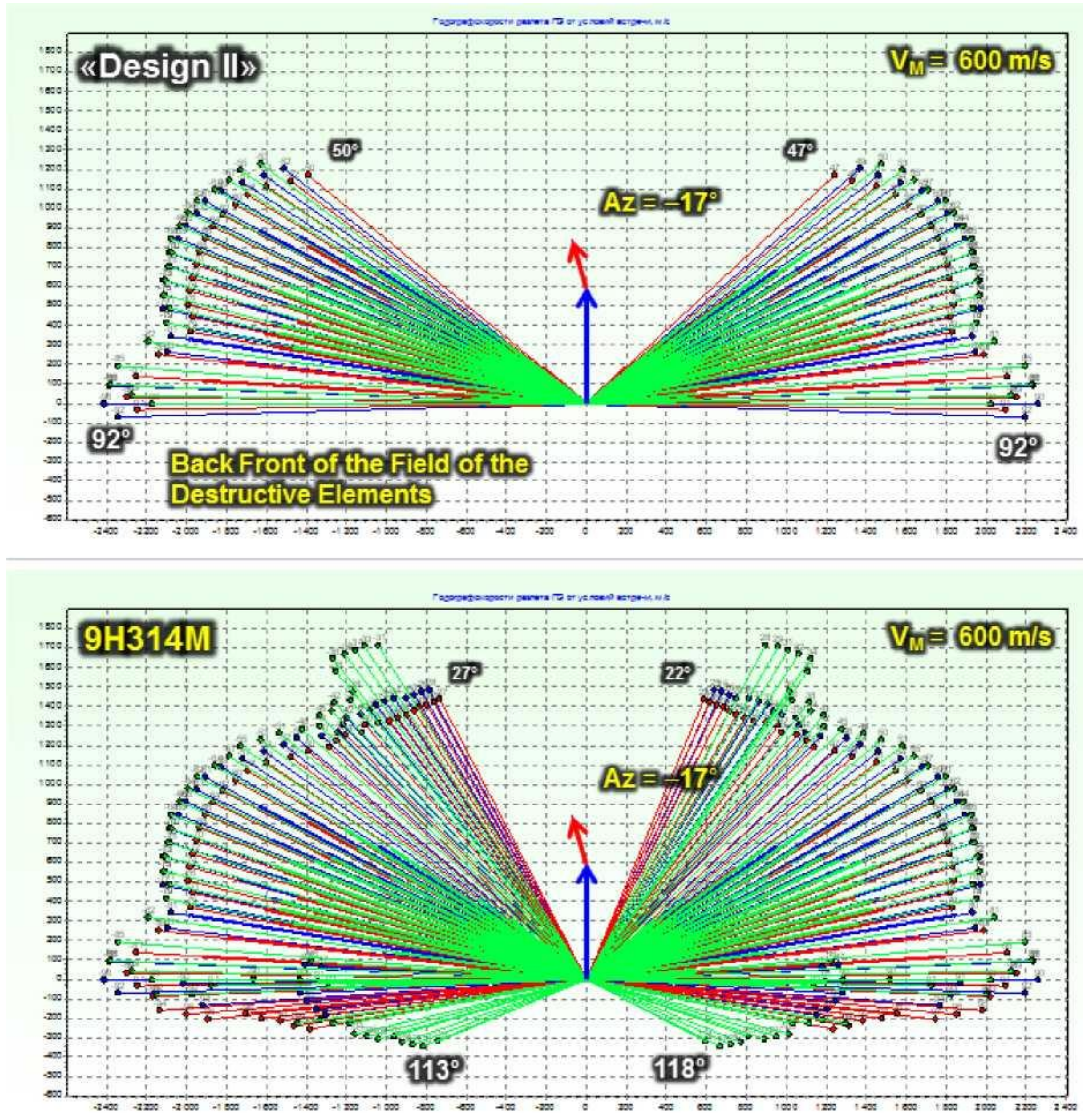


Figure G.1.21 - Comparison of the Design II 'reference' model (top) with the verified performance of the 9H314M (bottom)

¹¹⁰ Exhibit B.2.

¹¹¹ Report on the conduct of a full-scale experiment, pages 46, 61, 74..

Figure G.1.21 shows the results of a comparative dynamic fragmentation field simulation for "Best Match" DSB conditions corresponding to the basic version at most: missile velocity $v_M = 600$ m/s;

the angle between the axes of the aircraft and the rocket $Az_{warhead} = -17^\circ$.

For the conditions considered, the error in determining the missile encounter conditions reaches -21° , where: for the trailing edge of the fragmentation field the difference is $113^\circ - 92^\circ = 21^\circ$.

Accordingly, when determining the final position of the missile relative to the aircraft using the methodology adopted by the Dutch experts during the DSB, even without taking into account other factors, the "Best Match" (Model Ia) value in the Draft Report would be -38° , not -17° .

For the second "Best Match" value (Model IIb from the DSB Report), the conditions for the aircraft to meet the missile in the $Az_{warhead}$ horizontal plane were not -27° , but a minimum of -48° .

In both cases, based on the technical characteristics of the BUK missiles, the probability of launch from the Snezhnoye ("Pervomayskiy") area given the conditions of the refined "Best Match" (-38° and -48°) is close to zero.

The parameters of the "reference" warhead for each of the variants (Model I, Model II) were agreed upon in advance¹¹² and, contrary to the manufacturer (Corporation Almaz-Antey), adapted to fully match the "opposite direction" version best suited to the predetermined version;¹¹³

Analysis of the DSB Report material shows that in all versions of the "reference" warhead models, the main adaptation of the projectile dispersion parameters was focused on the distortion of the back-front of the fragmentation field.

In other words – the virtual missile was forcibly turned towards Snezhnoye/Pervomaysky during the simulation.

The Model II warhead model, considered the most appropriate for the purposes of this investigation ("reference model"), is based on raw data contradicting the manufacturer's technical documentation and the results of field tests.

The "**reference**" warhead model was created by NLR and TNO specifically to justify the Boeing 777 being hit only for the predetermined parameters of "**opposite direction**" encounter conditions.

¹¹² TNO report. 4.3. Warhead, p.13.

¹¹³ TNO report. 4.3.2. Warhead implementation (designs), p.14-15.

Exhibit G.1.3. Warhead detonation point

The primary objective of aircraft damage research is to find the area of the warhead detonation point.

It should be noted that the event (detonation of a high-explosive fragmentation warhead) resulting in the destruction of the Boeing 777 can have only one region of space in which the detonation occurred. And the location of this region of space does not depend on the variants of the electronic models used - the "standards". The actual location of the detonation point area can only be determined from the actual damage objectively observed on the aircraft fragments.

All the research to find the original location of the detonation point by the NLR was completed as early as February 2015, based on just a few fragments.

The NLR experts used only two fragments, the same fragments used to determine the port-side rear damage boundary and to create a damage "reference" (Light Model), as shown in Figure G.1.22.

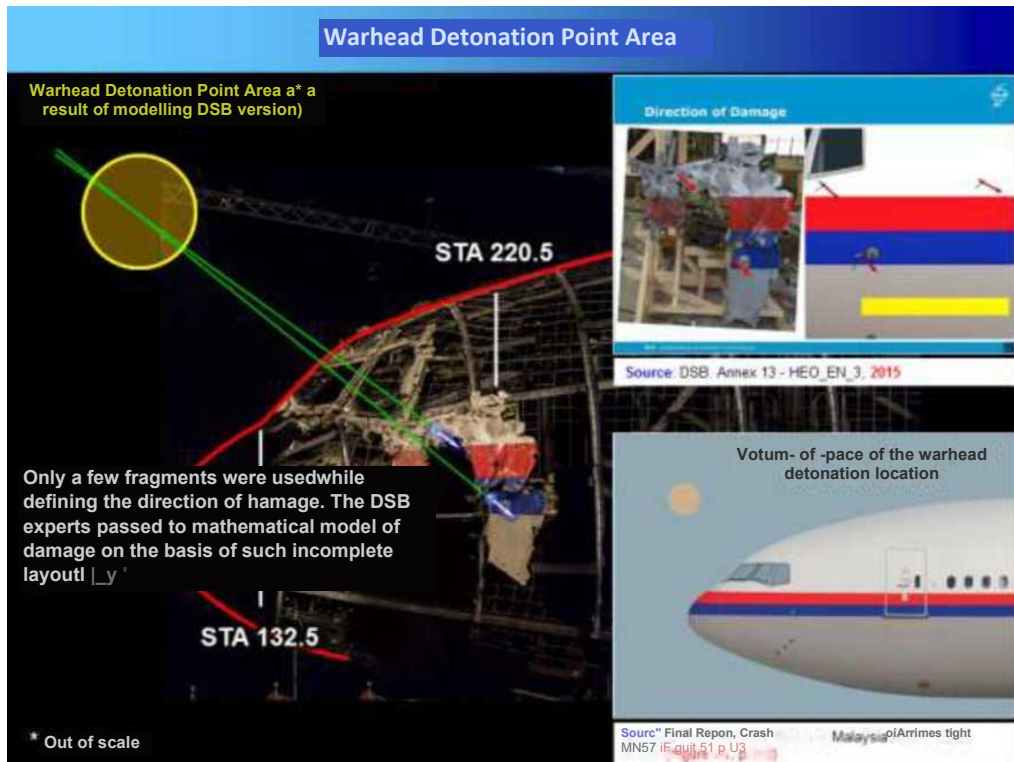


Figure G.1.22 - Determining the detonation point location by coincidence of damage directions on the two port-side fragments

The figure schematically shows how certain damage directions indicate the area of space where, in the opinion of the NLR experts

NLR, the detonation of the warhead occurred. Other DSB experts (from TNO) did not independently search for the detonation point - the coordinates of the detonation point, the angles of orientation of the warhead for each "Best Match" variant were assigned by NLR experts.¹¹⁴

At the bottom right of Figure G.1.22 is an image from the Final Report¹¹⁵ showing the area in which the main version "opposite direction" (launch from the Pervomayskiy area) indicated that a particular warhead, 9H314M, detonated.

In the course of justifying the position of the detonation point, the NLR experts had to adjust the facts to a pre-assigned version.

For example, the forward pressure bulkhead in the crash area was a single piece with the right side of the cockpit. Subsequently, without apparent necessity, this single piece was not only separated, but its component parts - the front pressure bulkhead itself and the right side of the cockpit at Gilze-Rijen airbase were placed in different hangar rooms (Figure G.1.23).



Figure G.1.23 - Separation of the forward pressure bulkhead with a fragment of the starboard cockpit and their subsequent location in different rooms led to a serious error in determining the detonation area

¹¹⁴ TNO report. 5.1. Variation of warhead position and orientation, p.17.

¹¹⁵ Final Report. Figure 61. Simplified representation of the volume of space the warhead detonation location according to three independent simulations, p.143.

As can be seen from Figure G.1.24, it was the absence of a germoprop in the reconstruction during the damage direction survey that led to the serious error of fitting the location of the warhead detonation point to a predetermined version.

An example projection of the trajectory of an impactor that has left a track on the boundary of the debris field on the forward containment shell, contrary to the NLR version, is shown in Figure G.1.24 as shown by the blue line.

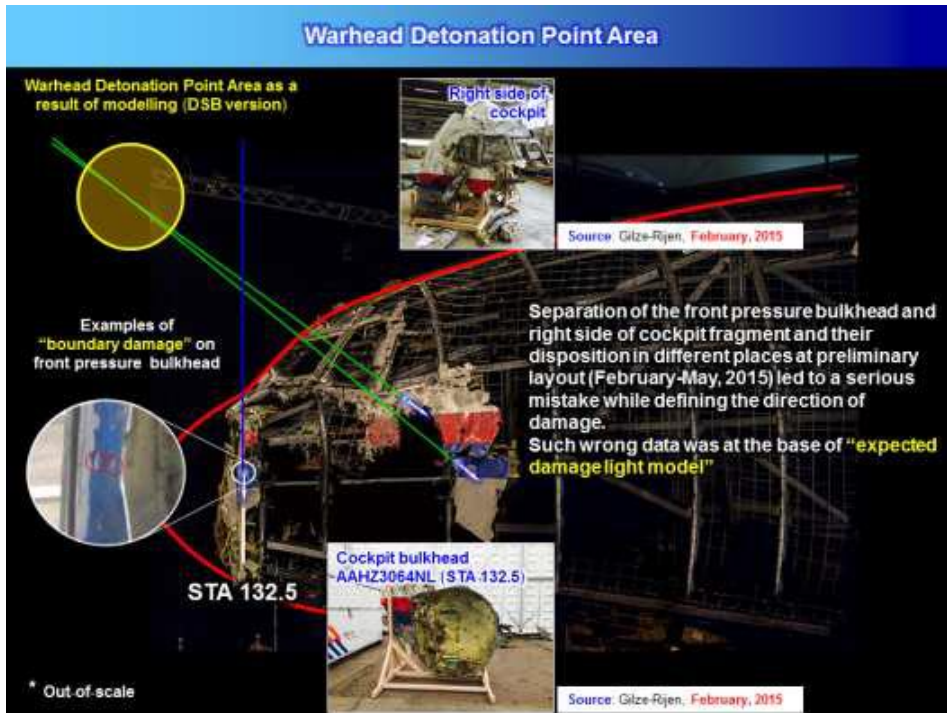


Figure G.1.24 - Damage to the forward furling bulkhead contradicts the detonation point area assigned by the fitting method

A significant portion of the port side fragments were not present at the pre-deployment site and were not available for examination by the Russian experts during the joint work in February and May 2015. Accordingly, the damage on these fragments was also not taken into account by the DSB (NLR) experts in determining the direction of the damage and justifying the location of the detonation point area.

The blue lines in the diagram (Figure G.1.25) show the projections of the trajectories of the projectiles that left rectilinear tangential traces on the boundaries of the debris field on the port side fragments, which only appeared in the final plotted after comments to the draft DSB report were discussed in August 2015.

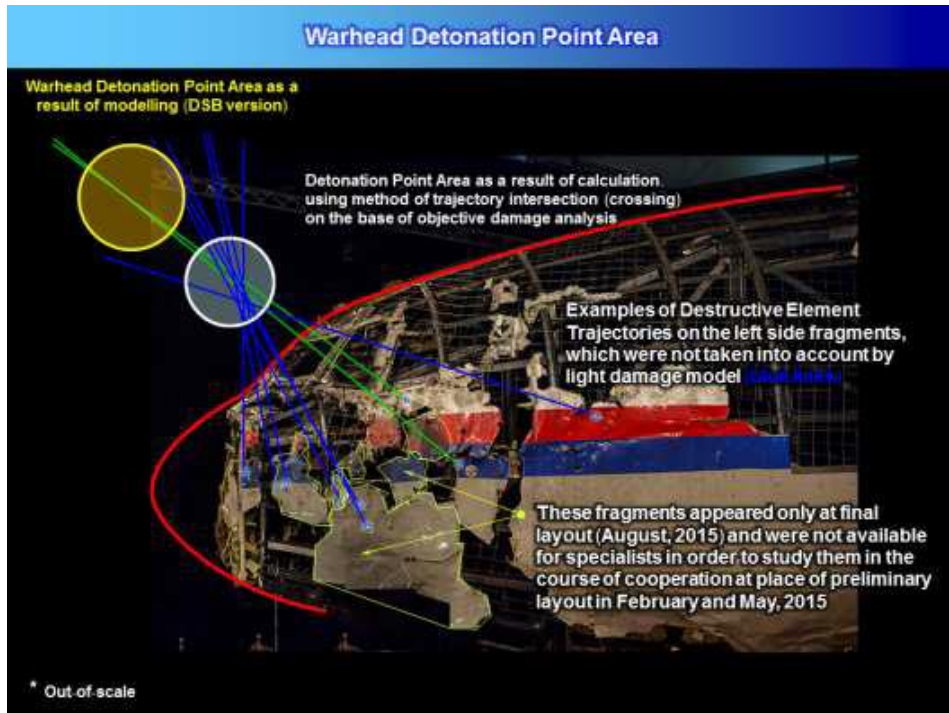


Figure G.1.25 - Damage on fragments unavailable for examination in February and May 2015 contradicts the detonation point area determined by the fitting method for a given result

All damage directions (tracks) converge to approximately one limited area of space. But this area, determined by crossing the tangents to the actual boundary damage, is quite different from the detonation area that the NLR specialists determined by the fitting method specifically for the first version of the "opposite direction".

The difference between the location of the detonation point area obtained and verified by the actual damage study and the detonation point area obtained by the fitting method is shown in Figure G.1.26.



Figure G.1.26 - Detonation point areas

And it was the manipulation of the location of the detonation point area that allowed the NLR specialists to select a combination of a damage "reference" and a warhead "reference"^{116, 117} and thereby create the "Best Match" option required to confirm the main version - "attack on an opposite course" (Figure G.1.27).

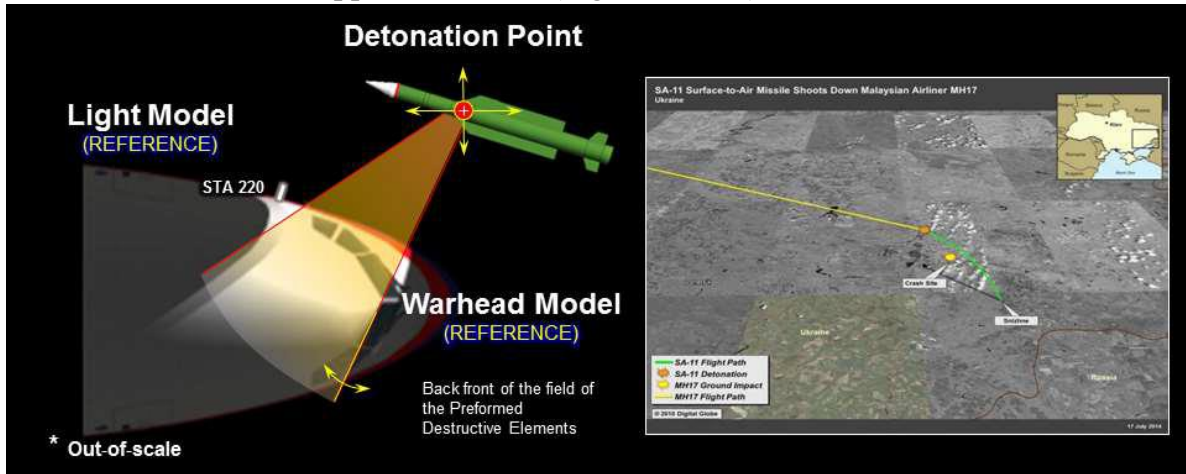


Figure G.1.27 - Combining the combination of the "reference" warhead model with the detonation point damage "reference" obtained by the fitting method resulted in an encounter condition value ("Best Match") ostensibly fully consistent with the "opposite direction" version

The figure shows how by fitting the rear edge of the fragmentation field in the "reference" warhead model (Model I) and selecting the detonation point coordinates to match the assigned light boundaries of the damage "reference" (Light Model) a "Best Match" (Model Ia) was obtained. This combination formed the basis of the Draft Final Report and was ideally suited to justify the "main version", providing the "Best Match" image shown in Figure G.1.27 at right.

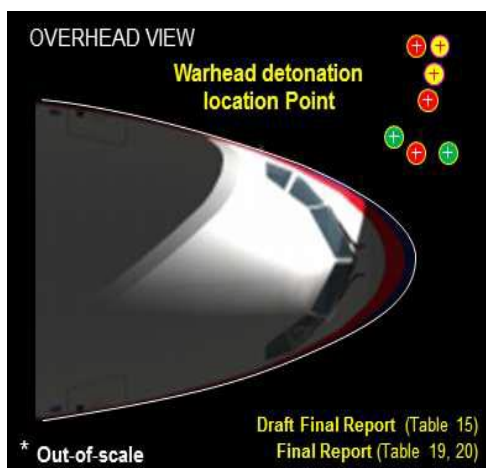
Analysis of the technical investigation material shows that the Dutch experts selected many different detonation point area coordinates – different for each of the modelling options. The coordinates of the detonation point locations are shown in Table J.1.2, and a visualisation of the scatterplots of the detonation point locations in space (top view) is shown in Figure J.1.28.

¹¹⁶ Final Report, pages 137-138; 139-140.

¹¹⁷ TNO report. Damage reconstruction due to impact of high-energy particles on Malaysia Airlines flight MH17, p.12-13.

Table G.1.2 - Detonation point location coordinates from DSB technical investigation,
118119

Organisation	X, m	Y, m	Z, m
DSB (Final Report)	$-0,7 < X < 0,5$	$-2,0 < Y < -3,5$	$3,4 < Z < 4,0$
NLR (Draft Final Report)	-0,5	-4,0	4,0
NLR (Final Report)	-0,25	-3,0	3,7
DSB "Best Match"	0,0	-2,0	3,7



During search of warhead detonation area using damage "light model" by trial-and-error method practically all the parameters changed: detonation point coordinates, missile final velocity; warhead characteristics (destructive element velocity and meridional spray angles).
"The opposite direction" was the only invariable parameter.

Figure G.1.28 - Variety of Detonation Point Locations Present in DSB Technical Investigation Material

As a result, for the various model variants (Model Ia, Model Iib), which at different stages of the technical investigation were taken as the "Best Match", the parameters of the "reference" warhead were changed and completely different coordinates of the detonation area were selected.

Only one parameter remained unchanged: the "opposite direction".

This contradicts the basic principle: the real position of the detonation point area does not depend on changes in the parameters of virtual "references" and is determined only by the actual damage objectively observed on the aircraft fragments.

During the selection of conditions, in addition to changing the parameters of the "reference" models of warheads, almost all parameters were changed. For example, the distance of the detonation point from the aircraft hull varied widely - for some coordinates by a factor of two (Y coordinate from 4.0 metres in February to 2.0 metres in October 2015).

Although the parameters of Best Match varied so widely that they often conflicted with technical specifications, each new variant chosen by NLR was recognised as the "best".

¹¹⁸ Draft Final Report. Table 15, p.130.

¹¹⁹ Final Report, page Table 20, page 142.

Both of these "Best Match" were declared at various stages of the investigation to be a "reference", fully consistent with the actual pattern of the lesions "in terms of boundaries, location, nature, number, density and angle of attack."^{120, 121, 122}

As an example to illustrate the contradictions of the "Best Match" search method of parameter matching, the diagram (Figure G.1.29) shows an example of "matching" damage directions on three aircraft nose section fragments for the two Model Ia and Model IIb variants which are the basis of the "Best Match" findings in Draft Final Report and Final Report.

The diagram in Figure J.1.29 shows that the damage directions from different areas of the detonation point differ significantly (**up to tens of degrees**) from each other and from the objectively observed damage on the Boeing 777 fragments.

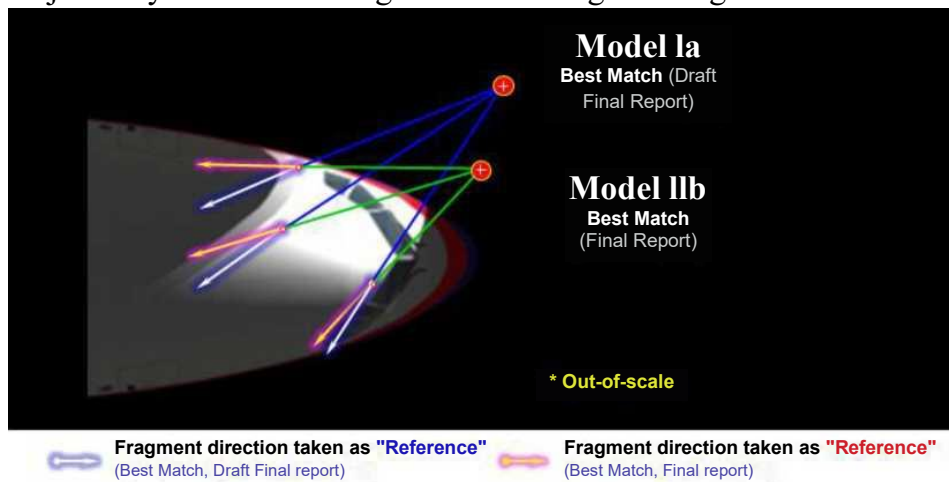


Figure G.1.29 - Non-matching of damage directions in two "reference best match" variants

In addition to inconsistent damage directions, using different detonation point coordinates (differing by up to a factor of two) **makes it impossible to obtain** "the closest match of modelled and actual damage", primarily in terms of the impact density distribution over the outer surface of the aircraft.

In reality, this cannot be the case because if the distance from the detonation point to the outer surface of the aircraft changes by a factor of two, the actual damage density on this surface must change by a factor of four (Figure G.1.30).¹²³

¹²⁰ Draft Final Report. 3.7.3 NLR projection, p.125.

¹²¹ NLR Report, p.63.

¹²² Final Report. 3.8.2 Fragmentation visualisation model, p.138.

¹²³ The fragmentation field density decreases in inverse proportion to the square of the increase in distance ("law of squares"), accordingly if the distance from the detonation point to the outer surface of the aircraft changes by half, the actual density of damage on that surface must change by a factor of four.

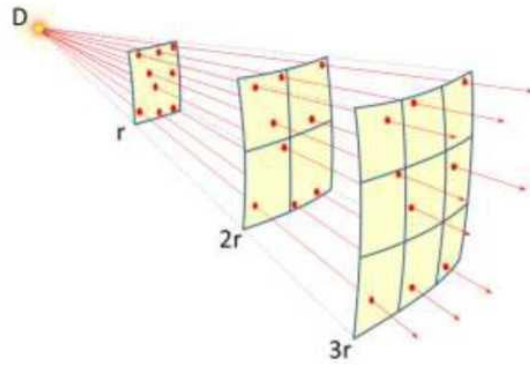


Figure G.1.30 - Variation of fragmentation density as a function of distance from the detonation point (P). At $2g$, the damage density decreases by a factor of four compared to distance d , and at $3g$, it decreases by a factor of nine

These theoretical data are confirmed by both calculations and field tests carried out by the Corporation's specialists under controlled conditions as part of the technical investigation (Fig. G.1.31).

Figure G.1.31 shows photographs of three elements of targets No. M-1.1, No. M-2.1 and No. M-3.1 arranged in sequence at increasing distances from the detonation point of the warhead.^{124, 125}

The images shown in the figure illustrate the change in fragmentation density as the distance from the warhead to the obstacle (target) increases.



Figure G.1.31. Variation of the fragmentation field density as a function of the distance of the target elements from the detonation point. In the shield target layout created for the full-scale experiment, target No. M-3.1 (right) was placed approximately twice as far from the detonation point as target No. M-1.1 (left)

As can be seen from the images in the photographs, the density of damage on target No. M-1.1 and No. M-3.1 at different detonation point distances, which differ by a factor of two, **is not the same**.

¹²⁴ Report on the conduct of a full-scale experiment, p.142.

¹²⁵ Report of the field experiment. Annex A. Figure A.5, page 3.

The actual impact density distribution of the impact of the same warhead on the outer surface of an aircraft **cannot simultaneously correspond to** different detonation points separated by distances differing by a factor of two.

In reality, neither the density nor the direction of the damage (holes, tracks) on the Boeing 777 fragments could have changed when combining the "reference" DSB models, changing their parameters and the coordinates of the detonation point.

However, during the DSB technical investigation, as the "reference" models, and consequently the coordinates of the detonation point, changed, so did the results of the punch count and damage density.

For example, the maximum density of damage depending on the coordinates of the detonation point varied from 80 holes per square metre^{126, 127} to 250 holes per square metre.^{128, 129} Which is an indication of the fitting of the parameters.

This situation was only possible as a result of the fact that the actual damage study back in February 2015 was replaced by a virtual model taken as a damage "reference". However, the damage "reference" does not take into account the direction of the damage, the number of damage, the distribution of the density of holes or the damage to the aeroplane's airframe.

In addition, as is now evident, the Dutch experts at the NLR laboratory changed the coordinates of the detonation point by a matching method, so that the simulation results corresponded to a predetermined version - "hitting the aircraft with a BUK missile in an "opposite direction".

Therefore, the apparent discrepancy between the "reference" damage models (Light Model, NLR), the detonation point coordinates (assigned by NLR)¹³⁰ and the actual damage by the Dutch experts in forming the Final Report conclusions went unnoticed.

The detonation point coordinates from Best Match do not correspond to the actual damage on the Boeing 777 fragments and contradict the specifications of the 9H314M warhead.

The "**reference**" coordinates of the detonation point of the warhead were determined by NLR's experts using a matching method specifically to justify the Boeing 777 hit for the predetermined parameters of "**opposite direction**" encounter conditions.

¹²⁶ Draft Final Report. 3.7.4 Physical measurements, p.119-124.

¹²⁷ Draft Final Report. Annex-NLR Report NLR-CR-2015-155. 5.26. Density, p.310.

¹²⁸ Final Report. 3.5.3 Damage from external causes, p.119-126.

¹²⁹ Final Report. Annex X. NLR report. NLR Report NLR-CR-2015-155-PT-1. 2.5 Number and density of hits, p.14.

¹³⁰ TNO report. 5.1. Variation of warhead position and orientation, p.17.

Exhibit G.2. Comparison of actual damage with "reference" models

There are no criteria in the papers of the Dutch technical investigators to determine the best or, conversely, the worst match for the actual damage and "reference models"¹³¹.

Beforehand, no criterion was defined for the quality of the match. The results from this investigation are considered a subject matter of expert judgment.

Figure G.2.1 - Lack of criteria for determining "Best Match

Conclusions about greater or lesser compliance with a version or model are simply stated without explaining the resulting discrepancies or coincidences between modelled and actually observed damage on the Boeing 777 fragments (location, size and boundaries of fragment damage zones, number and density of holes, etc.).

The final result of the comparison is simply announced: the most suitable, in the experts' opinion, type of kill vehicle and the conditions of its encounter with the aircraft (speed, coordinates and angular position of the kill vehicle axis in relation to the aircraft) are named.

What the lack of best match criteria and quantitative indicators leads to can be illustrated by the decision to "better match" damage from a 70kg warhead.¹³²

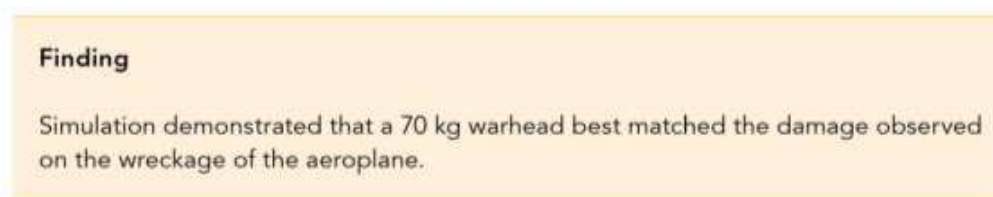


Figure G.2.2 - Final Report Materials

A few important points will be highlighted:

1. A comparison of a 70 kg warhead and a 40 kg warhead is made for different coordinates of the detonation area (Figure G.2.3).

In terms of detonation point coordinates for the two variants compared, the difference ranges from 40-80 centimetres to 1.7 metres, which completely **rules out identical baseline conditions for comparison**.

¹³¹ TNO report. Damage reconstruction due to impact of high-energy particles on Malaysia Airlines flight MH17, p.4.

¹³² Final Report. 3.8.3. Warhead simulation, p.141.

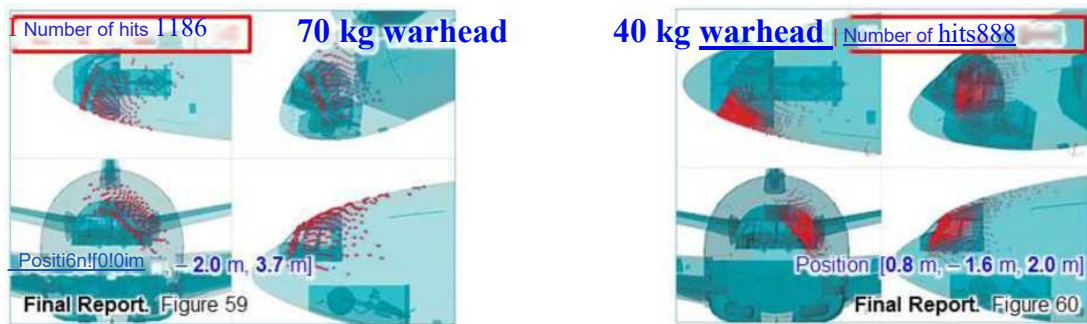


Figure G.2.3 - Features

comparison of the two

Figures (Figure 59, Figure 60) are provided in the Final Report for visual confirmation of the "best match", but the conditions (coordinate values) under which the modelling of the versions for this comparison was carried out can only be found in the various annexes to the TNO Report.¹³³¹³⁴

2. Lack of consideration of the number of fragmentation holes leads to paradoxical results.

Thus, when examining the actual damage to the outer skin, the DSB experts counted only about 350 hits of all types. Taking into account the distribution of the average observed density to the missing sections of the outer hull, the number of hits determined by the DSB experts is "more than 800".¹³⁵

According to the results of a simulation of a 70kg warhead detonation conducted by TNO specialists, 1,186 ready-to-use warheads alone should hit the outer hull. In the 40 kg warhead simulation, 888.

This said, while the number of actual damage ranges from 800 to 900 hits, the "best match" is Model IIb, where the number of hits alone (number of hits 1,186) must be 1.5 times the number of documented damage of all types.

3. Lack of comparative analysis with test results.

The number of fragmentation damage of all types detected on the Boeing 777 fragments and documented, even taking into account the spread of the average density of damage to all missing fragments, is at least half that of the 9H314M warhead detonation under the "opposite direction" version.

¹³³ TNO report. Annex A, Figure A.4, p.5/9.

¹³⁴ TNO report. Annex B, Figure B.3, p.5/7.

¹³⁵ Final Report. 3.5.3 Damage from external causes, p.121

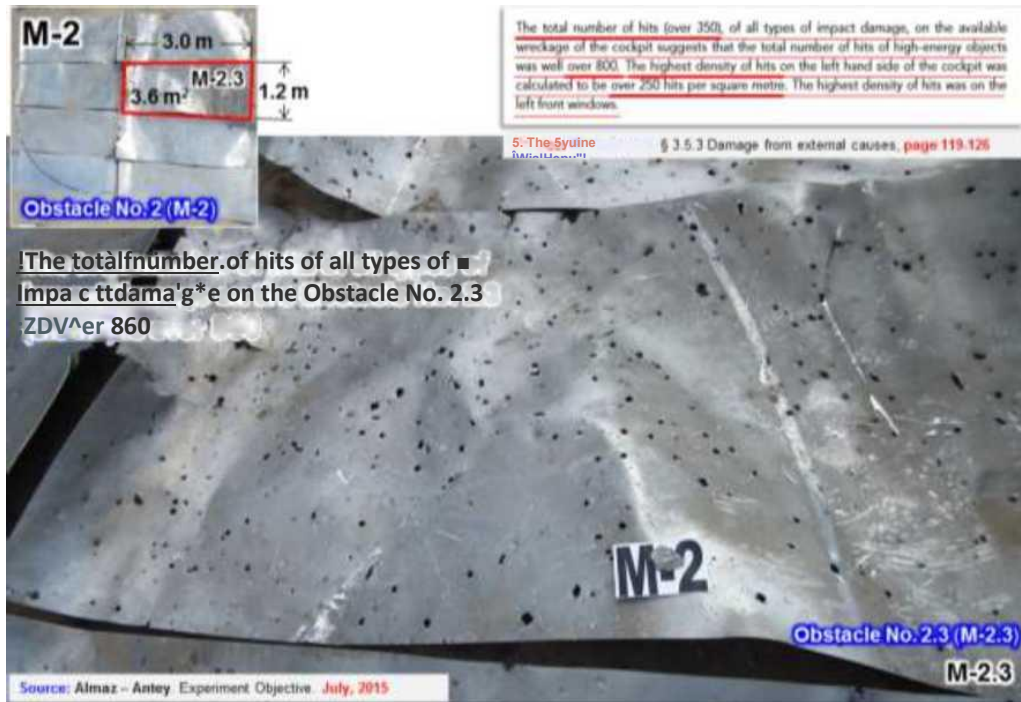


Figure G.2.4 - Over 860 through-holes of all types were recorded on Feature No. 2.3 of 3.6 m of Target No. M-2

When the 9H314M warhead was detonated at a distance corresponding to the distance of the detonation point according to the NLR, only one element of the 3.6 square metre shielded targeting area had more holes of all types (865) than were objectively recorded on all fragments of the Boeing 777 nose section.¹³⁶

A total of 3,620 holes of all types were recorded on the target and more than 2,200 within the circumference (cross section) (Figures G.2.4 and G.2.5).



Figure G.2.5 - Comparison of target area No. 2 and its element No. 2.3 with the Boeing 777 aircraft model and final lay-out (scale observed)

The results of simulations of fragmentation damage to the aircraft under the initial conditions of the "opposite direction" version, carried out using an interactive model, show that the nose of the aircraft should have been hit by

¹³⁶ Final Report, p.121.

approximately 2,800 fragments, of which 1,800 are ready-made light and heavy fracture fragments.

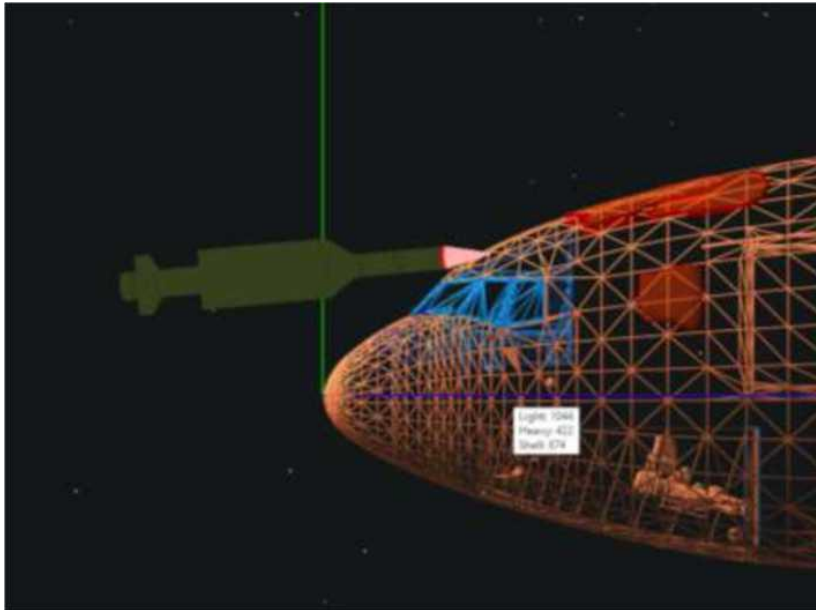


Figure G.2.6 - Simulation of fragmentation damage to the nose of a Boeing 777 aircraft. The nose section, excluding cockpit glazing, is selected (highlighted in orange) for evaluation: total of 2,340 fragments (Light - 1,044; Heavy - 422; Shell - 874)

The value of 2,800 fragmentation damage resulting from the modelling is more than **3.5** times higher than the number of penetrations on the entire aircraft hull indicated by the DSB experts (800 penetrations). If only prefabricated projectiles are taken into account, the excess is **2.28** times (1,822:800 2,277).

In fact, it turns out that the "Best Match", carried out without regard to criteria and numerical indicators, was determined on the basis of a subjective visual comparison of figures showing the results of two mathematical models, all parameters of which are agreed exactly for the basic version¹³⁷.

A brief analysis of the conditions for which the Dutch experts believed a simultaneous match should have shown the greatest the consistency of the "main version"¹³⁸ shows that the hypothesis of the Boeing 777 being hit by a BUK missile in an "opposite direction" not only does not meet all the specified conditions for comparing damage simultaneously, but is completely or partially contradicted by most of the specified conditions.

¹³⁷ TNO report. Damage reconstruction due to impact high-energetic particles on Malaysia Airlines flight MH17, p.13, 17.

¹³⁸ TNO report. Damage reconstruction due to impact high-energetic particles on Malaysia Airlines flight MH17, p.18.

For example, the conditions required for a simultaneous match specify that there is damage to the left engine from preformed fragments directly from the warhead.¹³⁹ For all possible variants of the counter-combat version of the simulation, there is no damage to the left engine by the main fragmentation stream (prefabricated projectiles). This was confirmed in two full-scale experiments conducted by the Corporation in July and October 2015.¹⁴⁰

As a result of not using criteria¹⁴¹ and numerical indicators to compare¹⁴², using models with unreliable parameters and detonation point co-ordinates as 'references', the Dutch experts chose 'Best Match' conditions, selected to justify a predetermined version.

¹³⁹ TNO report. Damage matching condition (6), p.18.

¹⁴⁰ Report on the conduct of a full-scale experiment. Item 5.1.5 Damage to the left engine simulator, page 89. Main results of the first stage of the full-scale experiment, pages 35-37. 35-37.

¹⁴¹ TNO report. (Final Report, Annex Y), p.4.

¹⁴² TNO report. (Final Report. Annex Y), p.18.

Exhibit G.3: Calculation of possible launch area as per "Best Match" options

As noted in the Corporation Report, a feature of missiles using proportional navigation is that when aimed at a uniformly and linearly (at the same altitude) moving airborne target, the trajectory of the missile in the horizontal plane is almost linear.¹⁴³

This methodology is acceptable because the Boeing 777 flew on a straight trajectory with a constant bearing, constant speed and constant altitude, as confirmed by the Flight Data Recorders (FDR) of MH17.¹⁴⁴

These principles form the basis of the calculations of Ukrainian specialists,¹⁴⁵ specialists of Almaz-Antey Corporation and other independent experts, and according to the DSB Report, the Dutch specialists also took these features into account during the ^{146, 147, 148} technical investigation.

It should be noted that, at the request of the NLR experts, specialists from Almaz-Antey Corporation also carried out calculations based on raw data from the Netherlands¹⁴⁹ Experts,¹⁵⁰ used to determine the original "Best Match" option (from the Draft Report).



Figure G.3.1 - Using images provided by Almaz-Antey specialists in the Final Report to show a "match" of the launch area calculations

Some of the material provided by Almaz-Antey Corporation in August 2015¹⁵¹ was subsequently used in the Final Report as some kind of "proof of match". Some of the material provided by Almaz-Antey in August 2015 was subsequently used in the Final Report as some kind of

¹⁴³ Final Report. BUK operating characteristics, p.134.

¹⁴⁴ Submitted by the DSB - Preliminary Report and Final Report.

¹⁴⁵ Results of examination of causes of MH17 crash over the territory of Ukraine 17.07.2014. 10-12.08.2015, Gilze.

¹⁴⁶ Draft Final Report. 3.4.9 BUK surface to air weapon system, p.114; 5.4.4 BUK missile, (NLR Annex), p.319.

¹⁴⁷ NLR report (Appendix X). 6.6 BUK missile, p.46-47.

¹⁴⁸ Final Report. BUK operating characteristics, p.134.

¹⁴⁹ Final Report. Table 20, p.142

¹⁵⁰ Final Report. Figure 64, p.146.

¹⁵¹ Presentation (August, 2015). Findings of Expert Assessments on MH17 Accident. Missile Launch Area Simula3.tion. INT'L Investigation Team's Version, p.20.

"proof" that the calculations matched, without the disclaimer that the Corporation's experts did not agree with the version itself or with the source data used for this "Best Match", including the real position of the aircraft in space¹⁵² (Figure G.3.1).

The coincidence of the results of the calculation of possible launch areas was intended by the Dutch experts to be a technical confirmation of the intended launch area "south of the village of Snezhnoye", coinciding with the area shown in the drawing published on the website of the US Embassy in Ukraine in the first days after the disaster.

Several objective adjustments need to be made to calculate the possible launch area according to the "Best Match" options from the DSB Report:

1. Actual position of the aircraft in space. As shown in the Corporation Report, taking into account the objective control data and data from the Boeing 777 recorder (FDR), the actual orientation of the aircraft's longitudinal axis (axis position relative to the north meridian) taking into account local magnetic declination and wind drift was approximately 123°. ¹⁵³

Accordingly, a correction of about 4 degrees between the course line projection of the Boeing 777 on the map and the actual longitudinal axis orientation of the aircraft must be taken into account when calculating the likely launch area.

2. Exclusion of deliberately unreliable variants. TNO acknowledged in their Report that the original version of their Model I warhead model was inaccurate because it used incorrect initiation point data – a different location for the detonator. ¹⁵⁴ It is known that using a different initiation point leads to a drastic change in performance as it affects one of the basic characteristics of the static fragmentation region - the slope φ_{ct} of the bisector of the static angle of dispersion α_{ct} to the longitudinal axis of the missile (a "mirrored" dispersion sector is obtained, where the bisector slope is not greater than 90°, but vice versa $\varphi_{ct} < 90^\circ$). ¹⁵⁵

Accordingly, only the final "Best Match" version corresponding to Model IIb - with horizontal angle $Az = -27^\circ$ from the DSB Report¹⁵⁶ – is taken into account in calculating the likely launch area.

3. Clarification of an anti-aircraft guided missile modification.

Until August 2015, Almaz-Antey experts allowed for two missile modifications: 9M38 and 9M38M1. Two areas were presented in the submissions to the DSB: for the 9M38M1 missile

¹⁵² Final Report. Figure 65, p.146.

¹⁵³ PART 1. Item 5.2.3. Position of Boeing 777 in space, pages 78-79.

¹⁵⁴ TNO report. 4.3.2. Warhead implementation (designs), Figure 4.4, p.14.

¹⁵⁵ Neupokoev F.K. Anti-aircraft missile firing, p. 187. 187.

¹⁵⁶ Final Report. 3.8.3. Warhead simulations, Table 19, p.140.

("red" small area) and separately for the 9M38 missile ("blue" large area).¹⁵⁷

Accordingly, given the subsequently identified missile modification (9M38), the area corresponding to the 9M38M1 missile is excluded.

The results are shown as diagrams in Figures G.3.2 and G.3.3, using the image of the calculated launch areas from the DSB report as a substrate.



Figure G.3.2 - Launch area calculated for "Best Match" DSB Report taking into account actual aircraft longitudinal axis orientation

When using the DSB Final Report source data for the launch area calculation with encounter conditions recognized as "Best Match" ($Az = -27^\circ$) and considering the real position of the aircraft longitudinal axis in space "firing position at coordinates 47.974605, 38.760549" is not included in the calculation results (Figure G.3.2).



Figure G.3.3 - Launch area calculated using missile-aircraft encounter methodology, taking into account actual aircraft longitudinal axis orientation and verified warhead data

¹⁵⁷ Presentation (August 2015). Findings of Expert Assessments on MH17 Accident. Missile Launch Area Simula3.tion. INT'L Investigation Team's Version, p.20, 21, 24.

It was shown in Exhibit G.1.2 that the use of inaccurate data on the impact field of a BUK missile (especially on the trailing edge of the fragmentation field) leads to serious errors.

Using the NLR's methodology for determining the missile encounter conditions used in the DSB technical investigation, with these errors compensated for, the "Best Match" value (aircraft encounter conditions in the *Azwarhead* horizontal plane) would have been at least -48° , not -27° .

Accordingly, using verified data on the engagement field characteristics of the BUK warhead confirmed experimentally, **the calculation result will not have a single point of intersection** with the 320 square km area "in eastern Ukraine" specified in the DSB Report as the likely launch area (Figure G.3.3).

It should also be added that it was based on the initial "Best Match" data that Almaz-Antey Corporation specialists conducted a full-scale experiment in a combined target environment using an IL-86 target aircraft¹⁵⁸ on 07.10.2015.

The results of the experiment did not confirm the "opposite direction" version.

Thus, the results of the experiment together with the verified characteristics of the warhead, the coordinates of the detonation point, the actual damage to the Boeing 777 and the actual location in space of the aircraft's longitudinal axis exclude the version of a BUK missile being launched from the area of Snezhnoye and Pervomaisky townships.

¹⁵⁸ Report on the conduct of a full-scale experiment, pages 6-8, 190.

Exhibit G.4. Identification of projectiles and warhead

The available technical investigation material identified 20 fragments that were found to be from the 9H314M warhead.

This conclusion was reached by the experts of the NFI Institute (briefing at the NFI during the second phase of the joint work in May 2015), later confirmed during the presentation in August 2015¹⁵⁹ and in the DSB Final Report.

Exhibit G.4.1: "Distinctly shaped" projectiles

As the main argument underlying the assumption of the type of warhead, the technical investigation materials use the claim that "in the wreckage of the aircraft structure and the bodies of the three crew members in the cockpit", "Bow-tie" and "Cubes" projectiles were found. These "are present only in the 9H314M warhead used in the 9M38M1 missile of the BUK complex"¹⁶⁰.

A total of four "distinctly shaped" fragments are mentioned and photographed in the technical investigation, among which the Final Report identifies two "bowties" and two "cubes"¹⁶¹.



Figure 37: Four distinctly shaped fragments. Top left: cockpit. Top right: Captain's body. Bottom left: Purser's body. Bottom right: First Officer's body. (Source: NFI). Scale is in millimetres.

Figure G.4.1 - Four distinctly shaped fragments (Final Report)

¹⁵⁹ Investigation MH17. High Energy Objects (Annex 13 meeting. Gilze-Rijen). 11 August, 2015.

¹⁶⁰ Final Report. 3.6.5. Surface-to-air weapon system common in the region. p.132.

¹⁶¹ Final Report. Figure 37 (p.89), Table 11 (p.92).

Certain inconsistencies were detected in determining the locations of these "distinctly shaped" fragments positioned as 9H314M warheads, as well as in their classification (in terms of exterior view), residual mass and dimensions. First of all, this concerns the most important fragments that relate specifically to the 9H314M warhead: the heavy fraction projectiles (9H314M 1-10), called "bowtie".

1st "distinctly shaped" fragment (fragment # 1)

The location of the first "bowtie-like" impactor (Figure G.4.2) is not known with certainty. Unlike the other light fragments, no form (passport) was provided for this fragment during the NFI briefing (May, 2015), and during the Commission's work, fragments of starboard noise insulation, technical documentation and other locations were also cited as locations for discovery and retrieval.



Figure G.4.2 - Fragment similar to an "bowtie" with variable mass:
5.5 g (February, 2015); 6.1 g (October, 2015)

As a result, in the Final Report, the residual mass for this fragment was increased from 5.5 grams to 6.1 grams, and its original location statements were replaced by the streamlined wording "in the cockpit".¹⁶²

2d "distinctly shaped" fragment (fragment # 2)

During the Gilze-Rijen collaboration phase (11 August 2015), the fragment shown in Figure G.4.3 was positioned as a 'Bow-tie' weighing 1.2 g and measuring 12 by 12 by 1 mm in the DSB presentation on high-energy object research.¹⁶³ As can be deduced from

¹⁶² Final Report. Figure 37 (p.89), Table 11 (p.92).

¹⁶³ Investigation MH17. High Energy Objects. Fragments from human remains, p.11.

the drawing, the body of the Captain, who was in the cockpit on the left-hand pilot's seat, was identified as the extraction site.

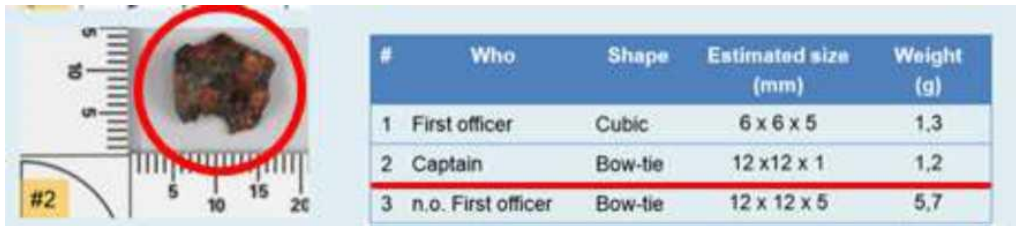


Figure G.4.3 - Variable shape fragment: "Bow-tie" (August, 2015); "Cubic" (October, 2015)

In the Final Report this fragment has not only changed shape from a "Bow-tie" to a "Cubic" (without specifying "Square" or "Filler"), but it has also changed "location of discovery". According to the caption under "Figure 37" in the Final DSB Report, this fragment was found in the Purser's body.¹⁶⁴

3d fragment of a "distinctly shaped" (fragment # 3)

The fragment shown in Figure G.4.4 first appeared in the Draft Final Report. With reference to the NFI resource, this fragment, which resembles a 'bowtie', was positioned as having been found in the body of a flight crew member, without specifying which one in particular.¹⁶⁵

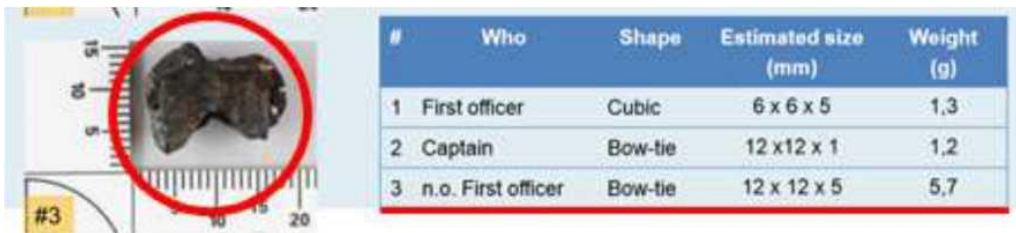


Figure G.4.4 - Fragment similar to a "bowtie"

In the presentation of the DSB (11.08.2015) on the study of high-energy objects, this fragment was positioned as a "Bow-tie" weighing 5.7 g and measuring 12 by 12 by 5 mm. The place of extraction indicated the body of the co-pilot of "Team B" (n.o.First officer), who was not controlling the aircraft at the time of the crash (was not in the right cockpit seat).¹⁶⁶ According to paragraph 2.5.1 of the Final Report, it is common practice for the Team B co-pilot to rest on bunks located behind the cockpit, on business class seats or on observer seats in the cockpit.

¹⁶⁴ Final Report. 2.16.1 Forensic examination, p.88-89.

¹⁶⁵ Draft Final Report. 2.16.1 Forensic examination. Figure 21, p.75.

¹⁶⁶ Final Report. 2.5.1 Flight crew, p.29.

The Final Report presents this fragment as having been found in the body of the crew commander, Captain of the A-team (Captain's body),¹⁶⁷ who was in the left pilot's seat at the time of the crash.

4th "distinctly shaped" fragment (fragment #4)

The fourth "distinctly shaped" fragment, positioned as a "Cubic", belongs to a different group of steel from the two NFI "combat related" groups. According to the technical investigation, it was found in the body of the First Officer's body,¹⁶⁸ who was in the right-hand pilot's seat at the time of the crash.

In accordance with the materials of the DSB Report, NFI experts conducted examinations (detailed autopsies and toxicological examinations) with the bodies of four crew members (flight and cabin crew): "Team A" co-pilot (First Officer); Purser; "Team B" captain (Captain non-operation flight crew); "Cabin crew member".¹⁶⁹ The examination data given in the Final Report differ from the materials previously displayed in the Draft Final Report¹⁷⁰ and the DSB presentation¹⁷¹ where there is no mention of cabin crew members, there are discrepancies among the flight crew members with whom the examination was carried out, and passengers were indicated.

In this regard, according to the available technical investigation materials (with reference to NFI, NLR and DSB resources) the locations of "certain shape" fragments in the aircraft wreckage and crew members' bodies have no unambiguous explanation (see Table G.4.1):

Fragment # 1 (similar to "Bow-tie") - exact location and circumstances of discovery and recovery are unknown, but the fragment has changed its mass from 5.5g (February, 2015) to 6.1g (October, 2015);

Fragment # 2 (shape change from "Bow-tie" to "Cubic") - was found in the body of the Captain, who was in the cockpit on the left pilot seat (August, 2015) or the Purser, whose exact location at the time of the crash is unknown, but is stated to have been in the cockpit (October, 2015);

fragment #3 (similar to "Bow-tie") - was found in the body of the Team B co-pilot (n.o. First officer), who was not flying the aircraft at the time of the crash, or in the body of the Team A captain, who was in the left-hand pilot's seat. At the same time, the bodies

¹⁶⁷ Final Report. 2.16.1 Forensic examination. Figure 37, p.89.

¹⁶⁸ Final Report. 2.16.1 Forensic examination. Figure 37, p.89.

¹⁶⁹ Final Report. 2.13.2 Crew autopsy, p.84, 85.





¹⁷⁰ "Bodies of the flight crew members and one passenger." Draft Final Report. 2.16.1 Forensic examination, p.76.

¹⁷¹ Investigation MH17. High Energy Objects. Objects in/on human remains (2); Flight crew; Non-operating flight crew; Others, p.6-8.

of the Team B co-pilot and the Team A captain according to DSB Final Report no detailed studies have been carried out;¹⁷²

Fragment #4 ("Cubic") – was found in the body of the co-pilot of "Team A" (First Officer), but it belongs to a different steel group from the two groups according to the NFI "combat correlation" findings.

Table G.4.1 - The four "distinctly shaped" fragments

"Distinctly shaped" fragments		Key features	NLR: Damage Investigation MH17	Draft Final Report	DSB: High Energy Objects	Final Report
#1		Shape Size, mm Weight, g Place of discovery	"Bow-tie." 5,5 1)	"Bow-tie." Wreckage	"Bow-tie." 14x14x4.5 6,1 Cockpit wreckage	"Bow-tie." 14x14x4.5 6,1 Cockpit
#2		Shape Size, mm Weight, g Place of discovery	-	-	"Bow-tie." 12x12x1 1,2 Captain (Team A)	"Cubic" 12x12x1 1,2 ²⁾ Purser
#3		Shape Size, mm Weight, g Place of discovery	-	"Bow-tie." Body of a flight crew member	"Bow-tie." 12x12x5 5,7 Non-operating First Officer	"Bow-tie." 12x12x5 5,7 Captain (Team A)
#4		Shape Size, mm Weight, g Place of discovery	-	-	"Cubic" 6x6x5 1,3 First officer (Team A)	"Cubic" 6x6x5 1,3 ³⁾ First officer (Team A)

1) Initially (February, 2015) the location was cited as elements of the starboard side noise insulation, technical documentation and other locations.

2) The fragment belongs to 'Group 2' (by impurity), distinct from the other fragments classified by NFI experts as 'potential bowties'.

3) The fragment belongs to the (impurity) "Other" group, distinct from the other two ("Group 1" and "Group 2"), which the NFI has concluded are "related to the warhead".

¹⁷² Final Report. 2.13.2 Crew autopsy, p.84, 85.

There are also discrepancies in the technical investigation regarding who was actually in the cockpit at the time of the crash.

According to paragraph 2.11.2 "Cockpit Voice Recorder" of the DSB Report, at the moment of the crash, there was one member of the cockpit crew besides the flight crew ("Team A") in the cockpit.¹⁷³ Probably it was the chief flight attendant, as stated in paragraph 2.13.2 "Crew autopsy"¹⁷⁴ of the DSB Report.

At the same time, in the materials given in the DSB presentation (August, 2015) as the third crew member who was (most probably, presumably) in the cockpit the co-pilot of "Team B" (Non-operating First Officer) from whom 81 fragments, including fragment #3 (similar to a "bowtie") were allegedly extracted for examination.¹⁷⁵ According to the Final Report the body of the Team B co-pilot was not subjected to a detailed examination (detailed autopsy and toxicological examination).

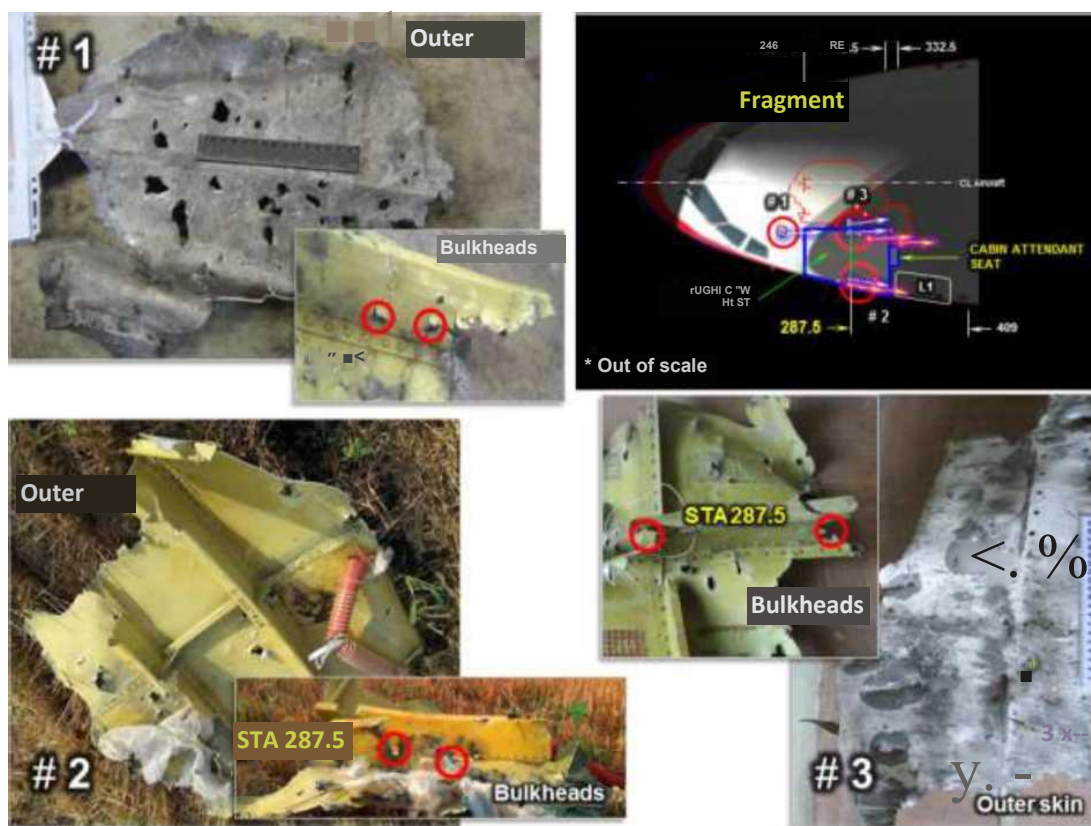


Figure G.4.5 - Possible locations of flight and cabin crew in the diagram are highlighted in blue: rest area behind the cockpit (Flight Crew Rest and Cabin Attendant Seat)

¹⁷³ Final Report. 2.11.2 Cockpit Voice Recorder, p.45.

¹⁷⁴ Final Report. 2.13.2 Crew autopsy, p.85.

¹⁷⁵ Investigation MH17. High Energy Objects. Objects in/on human remains (2); Non-operating flight crew, p.7.

According to the DSB Report, there was only one person in the cockpit in addition to the flight crew ("Team A") (according to different sources it was either the co-pilot of "Team B" or the chief flight attendant).

As can be seen from Figure G.4.5, the possible locations of "Team B" flight crew members¹⁷⁶ and cabin crew (rest area behind the cockpit and flight attendant's work station) were in the zone of maximum density (mass and kinetic energy) of the projectiles and factors accompanying a close explosion.

This is evidenced by the condition of the external plating and force-frame of the port-side sections numbered #1, #2 and #3 in the figure.

Two facts unite these fragments:

1. All of the fragments show distinct traces of microcratering, thermal burns, oxidation, compression and tearing of the outer skin sheets, deformation and destruction of the structural elements, as well as through holes in the bulkheads, indicating that they were exposed to the maximum density (mass and kinetic energy) of the projectiles and factors accompanying a close explosion.

2. The possible locations of the "Team B" and cabin crew (from which "distinctly shaped" fragments were recovered) **are outside** the fragmentation cover of the "reference" used by the NLR specialists (the "expected" damage zone is shown by the light) for the "**opposite direction**" version.

Thus, three of the four "distinctly shaped" fragments, including the two "double-edged" fragments from which it is concluded that they belong to a 9H314M type warhead, are not reliably documented by the location and circumstances of their discovery and extraction. For the fourth "distinctly shaped" fragment belonging to the same warhead is not obvious due to the difference in the chemical composition of the impurities in the two groups "correlated with the warhead".

¹⁷⁶ Final Report. 2.5.1 Flight crew, p.29.

Exhibit G.4.2 Characteristic damage in fragments of the Boeing 777 structure

No characteristic "butterfly" shape damage was found on the structural fragments of the Boeing 777 examined by the Corporation's specialists at the layout site, as well as on photographs from open sources.

In this case, through holes are observed from 13-14 mm large projectiles, which may belong to the "heavy fraction".

Figure G.4.6 shows an image of one of the inlet openings in the power section of the Boeing 777 cockpit glazing frame in comparison with a ruler to estimate the actual dimensions of the inlet opening.



Figure G.4.6 - Entry hole in the structural member has a linear dimension of about 14 mm

All of the 8-11 mm and 13-14 mm holes (presumably from light and heavy projectiles) observed on Boeing 777 structure elements have a characteristic rectangular shape. The red crosses in Figure G.4.7 show the likely orientation of the impactor (PI) when penetrating the barrier.

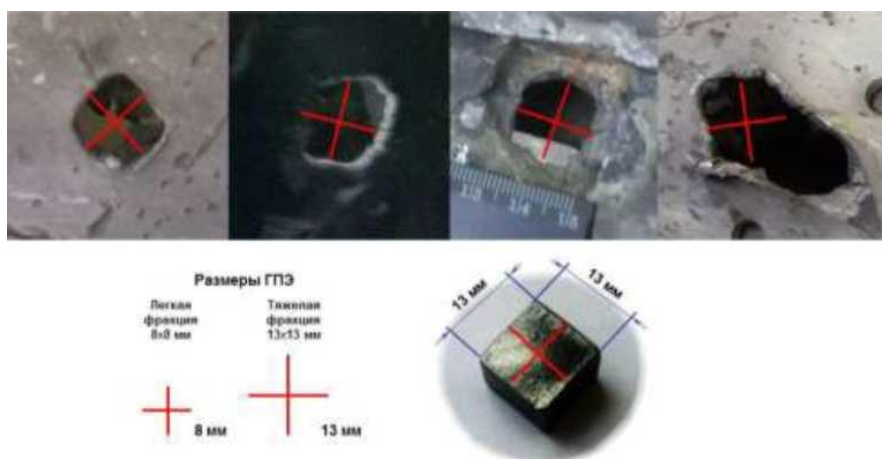


Figure G.4.7 - Characteristic through-holes on Boeing 777

If one considers the hypothesis of a BUK missile being used, such a shape could be left by the lightweight 8x8x6mm and the heavyweight 13x13x8mm fractions that have the "parallelepipedic" shape of the 9H314 warhead (without the bowties), which the obsolete 9M38 missile models were equipped with.

At the same time, photographs of "butterflies made by bowties" holes allegedly found on structural elements of the Boeing 777 appeared on the Internet. Some examples of such "butterfly holes" are shown in Figure G.4.8.

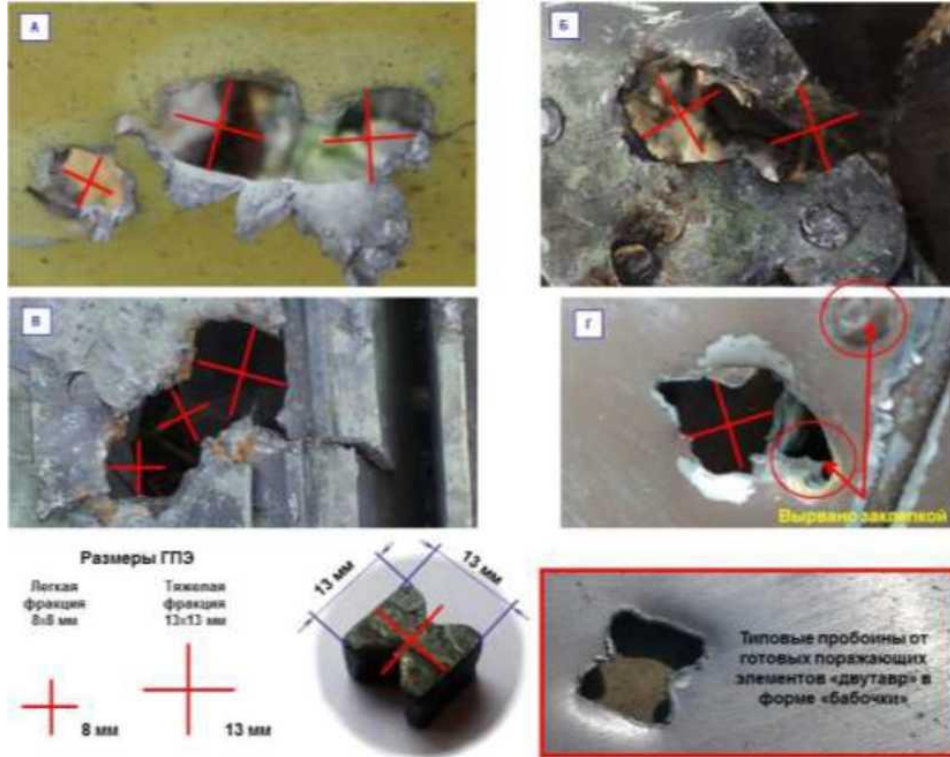


Figure G.4.8 - Through-holes on Boeing 777 (MH17) misrepresented as "butterflies"

Figure G.4.8 shows the orientation of the PE when penetrating the barrier with red crosses. An analysis of the dimensions of the penetrations which try to pass off as bowtie "butterfly" marks shows that the aspect ratio (height - width) is significantly greater than 1:2 - 1:3.

This can only be explained by the impact of two or three projectiles. Figure G.4.8 (d) shows a hole that resulted from the penetration of a structural element and the failure of a riveted joint of two elements (ripped out by a rivet).

However, not a single fragment of the outer hull of the aircraft has a distinctive "butterfly" hole from the bowtie-shaped projectiles (9H314M 1-10).

The results of both the first and second phases of the experiment clearly showed that the characteristic bowtie holes, which have a clear "butterfly" shape, on the

of the outer skin are not isolated or random.¹⁷⁷ An example of such an opening is shown in figure G.4.9.



Figure G.4.9 - Characteristic hole in the outer skin of the IL-86 target aircraft (experiment 07.10.2015)

Thus, a comparative analysis of the cross-sectional linear dimensions and shape features of penetrations from the projectiles obtained in the course of experiments and the data given in the technical investigation materials indicates significant differences. This, together with the lack of complete objective data from metallurgical examinations, does not permit unequivocal identification of the type of the projectile and reliable determination of the type of the weapon's warhead.

The absence of characteristic "butterfly-shaped" holes in the fragments of the Boeing 777 disproves the conclusions of the Dutch experts that it was hit by a missile travelling "on an opposite course", which was equipped with the 9H314M warhead.

¹⁷⁷ Report on the conduct of a full-scale experiment, pages 131-141; 143-148. Annex A to the Report on the conduct of a full-scale experiment, pages 89-94.

Exhibit G.4.3: Summary analysis of data on projectiles

The Dutch experts' conclusions about the type of weapon¹⁷⁸ are based on the consistency of the exterior view of the holes on the Boeing 777 fragments, the exterior view of the projectile elements, their number and the distribution of their types.

As a result of research carried out by Almaz-Antey Corporation specialists, it has been established that

1. No penetrations were found on the outer skin of the Boeing 777 with the characteristic "butterfly" exterior view of the "bowtie" warheads. At the same time, it was established by experiment that the shape of the penetrations on the first obstacle is one of the main attributes for identifying the type of warhead.

2. The distribution of the available cross-sectional dimensions of the entry holes in the outer skin of the Boeing 777 is correlated to a warhead loaded with one or two fractions of projectiles. However, the results of an experiment conducted with the 9H314M warhead in a combined target environment (IL-86 target aircraft) show the impact of three different fractions of prefabricated projectiles.¹⁷⁹

3. The "distinctly shaped" fragments, including the two "bowtie" looking fragments from which it is concluded that they belong to the 9H314M type warhead, have no unequivocal explanation of their location and circumstances (see Table G.4.1 and explanations thereto).

4. For all fragments with an "bowtie-like" shape, the weight and size characteristics (degree of deformation, shape, dimensions and residual mass) differ dramatically from the archival data from the state tests and the results obtained in the 2015 tests and field experiments.¹⁸⁰

5. Of the 16 fragments that the NFI has suggested are potential remnants of 'double-barrels', at least two have images indicating their presumed shape as "parallelepiped".¹⁸¹ In this case, at least one of the "potential bowties" belongs to a different group of steel (in terms of impurities), different from other "bowtie-like" fragments. But its residual mass of 3.2 grams unambiguously excludes it from the number of fragments of light fractions, whose initial mass does not exceed 2.35-2.5 grams (figure Zh.4.10).

¹⁷⁸ The DSB report identifies the 9M38-series missile equipped with the 9H314M warhead as the medium of attack.

¹⁷⁹ Subsection 5.3. Report on the conduct of a full-scale experiment, pages 128-130.

¹⁸⁰ Section 8. Report on the conduct of a full-scale experiment, pages 165-177.

¹⁸¹ Paragraph 8.4.2. of the Report on the conduct of a full-scale experiment, pages 181-182.

7	Wreckage	Irregular, -	3.2	2
---	----------	--------------	-----	---

Figure G.4.10 - Fragment #7 weighing 3.2 g has an "Irregular" shape and belongs to the second impurity group (from Table 11 of the DSB Report)

The 3.2g projectile in the technical investigation was identified as #7 (Final Report, Table 11, page 92) and was in the second impurity group, different from the other "bowties", which **does not meet the State Standard requirements for the same type of projectiles from a single warhead.**

6. According to the assumptions of NFI,¹⁸² the projectiles include a fragment weighing 16 grams, which is almost twice the weight of the heaviest hitter of any type of BUK missile. of the heaviest high-explosive warhead of any type of BUK missile.

Number	Location	Shape and dimensions (millimetres)	Mass (grams)	Group (see below)
18	Human remains	Irregular, -	16	2

Source: Final Report (Table 11, page 12)

size
13X13X8,2 mm

weight
8,1 grams

shape
«BOWTIE»

quantity
1 870 pieces.

?

Bow-tie (Butterfly) or Cubic (Square)

- These 20 fragments are assessed to be high energy objects originating from outside the plane.
- As such, these fragments are assessed to originate from a warhead.

Source: MH17 Annex 13 – Progress Meeting_HED, August, 2015



Source: Almaz – Antey (Gize-Rijen) May, 2015

Figure G.4.11 - Fragment # 18 weighing 16 g from Table 11 of the DSB Report cannot be a 9H314M warhead

In accordance with the technical documentation for the 9H314M warhead, the heavy fraction warheads have a mass limit of no more than 8.7 grams, subject to tolerances. According to the drawing, the mass of the 9H314M 1-10 is $8.1^{+0.6}_{-0.1}$ g¹⁸³

7. As a mandatory third fraction of the warhead ("Filler"), the documents list only one element that appeared later than,¹⁸⁴ and yet does not correspond chemically (impurities) to the other two groups – **Other**.

¹⁸² Investigation MH17. High Energy Objects, p.16.

¹⁸³ Paragraph 8.1.1. of the Report on the conduct of a full-scale experiment, p. 166.

¹⁸⁴ There are no "Filler" fragments in the DSB Draft Report. In the investigation materials, the only item of the light fraction identified as "Cubic" appeared only after a letter was sent to the DSB in July 2015.

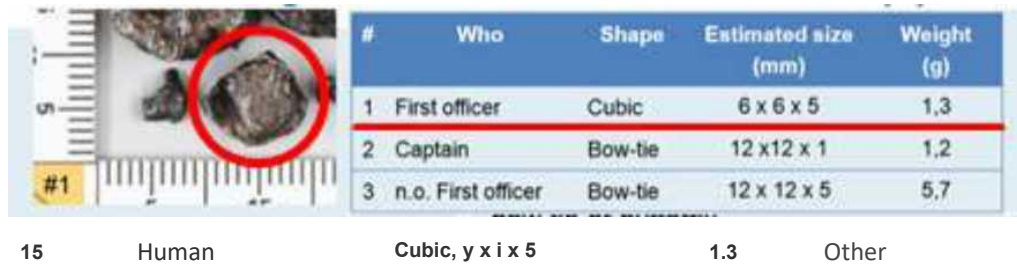


Figure G.4.12 - Fragment # 15 with a mass of 1.3 g is in the "Cubic" shape and does not belong to the two impurity groups "correlated with the warhead" (Table 11 from the DSB Report)

The fragment therefore does not clearly belong to a single warhead.

8. There is a lack of complete objective data from metallurgical examinations. At the same time, some of the data (e.g. different steel groups for the same type of warheads) clearly contradict the technical characteristics of the warhead. The statement that it is inexpedient to carry out detailed examinations because, quote: "Most likely, such an analysis will not yield anything, because the projectiles are made of low-quality steel, which may be of the most varied origin..."^{185, 186} does not correspond to reality. High-tech military products, such as anti-aircraft guided missiles, **use certified construction materials**.

The projectiles are manufactured in strict accordance with the requirements of the technical documentation: dimensions and weight in accordance with the drawing; the material used complies with the national standard.

In sum, there is no objective fact linking the detected warheads to a particular missile class, other than the fact that two of the fragments presented "look like an bowtie".

The Corporation's specialists are of the opinion that without establishing the steel grade of the warheads and without conducting a full examination of the warheads, it is impossible to definitively identify the type of warhead, much less to state that the 9M38 or 9M38M1 missile was the cause of the crash.

The lack of complete objective metal examination data makes it impossible to unequivocally identify the type of warhead and reliably determine the type of warhead and means of destruction.

¹⁸⁵ Final Report. Annex V.

¹⁸⁶ NLR. "Annex 13 - HEO_EN_3". Chemical composition found fragments.

Exhibit G.5. Missile fragments recovered from aircraft structure

According to the Final Report (p. 93) one of the missile fragments ("metal fragment") was found stuck in the left window frame. Figure G.5.1 shows both the fragment and where it was found.



Figure G.5.1 – Place of discovery of a "metal fragment" (DSB contribution)

What makes this fragment particularly important is that it is the only one of all the fragments, including prefabricated warheads, presented by Dutch experts trapped in a part of the aircraft's structure and photographed at the discovery site to document the missile strike of the aircraft.

The following picture is a still image from a JIT press conference held in 2016, showing a completely different location for this 'metal fragment' discovery.



Figure G.5.2 - The new location of the "metal fragment" and its presumed location in the missile airframe (JIT materials)



Figure G.5.3 - Two different 'metal fragment' detection locations under the hold-down bar of the second window of the aircraft commander (DSB, 2015); in the third windowframe break (JIT, 2016)

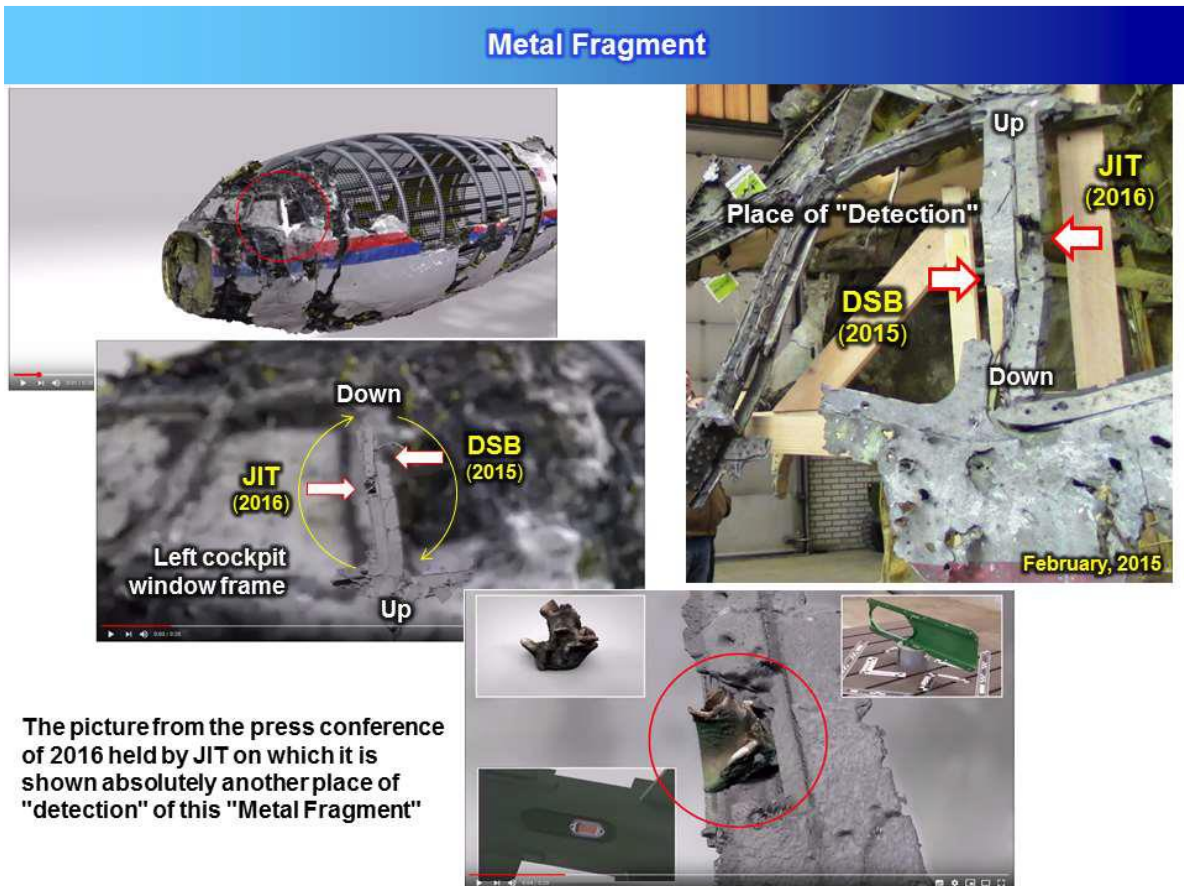


Figure G.5.4 - To show the new location of the 'metal fragment' detection, the JIT experts changed the real location of the frame fragment in the virtual 3D reconstruction

At the JIT press conference, this fragment is presented as important evidence of the detonation of a BUK-type SAM near the cockpit of a Boeing 777 (Figure G.5.5).

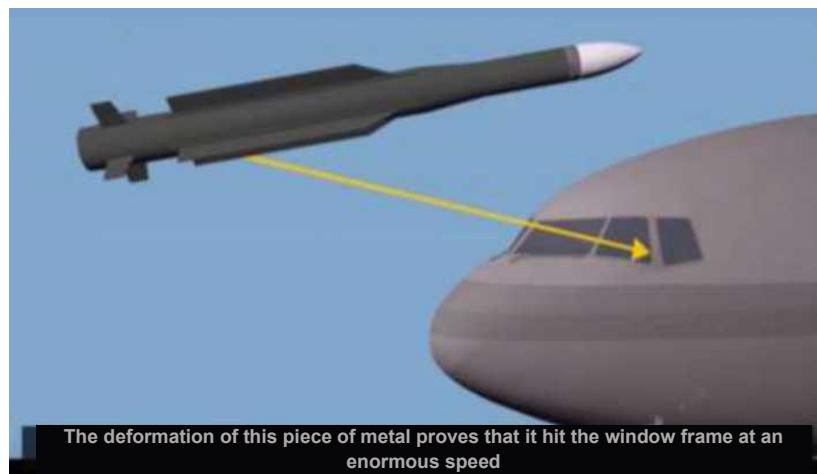


Figure G.5.5 - Representation of possible fragment trajectory (JIT materials)

However, this "metal fragment" cannot be unequivocally identified as a BUK missile fragment according to the materials available to the Corporation's specialists.

In addition to the variation in the location of the "metal fragment", there are several other points that have no explanation.

First, - the position of this fragment in the rocket airframe in flight shown in the footage (Fig. G.5.5) contradicts the design features of BUK missiles. The 9M38 missiles are stabilized on roll. Therefore, the breakaway connector is at the bottom of the hull all the time in flight and cannot "turn" 90 degrees towards the right side of the missile.

Secondly - the diagram in the JIT shot (yellow arrow in Fig. G.5.5), not only does not answer the question of how in the main version this "metal fragment" could get under the hold-down bar of the window frame, but also calls into question the "opposite direction" version itself (Fig. G.5.6).

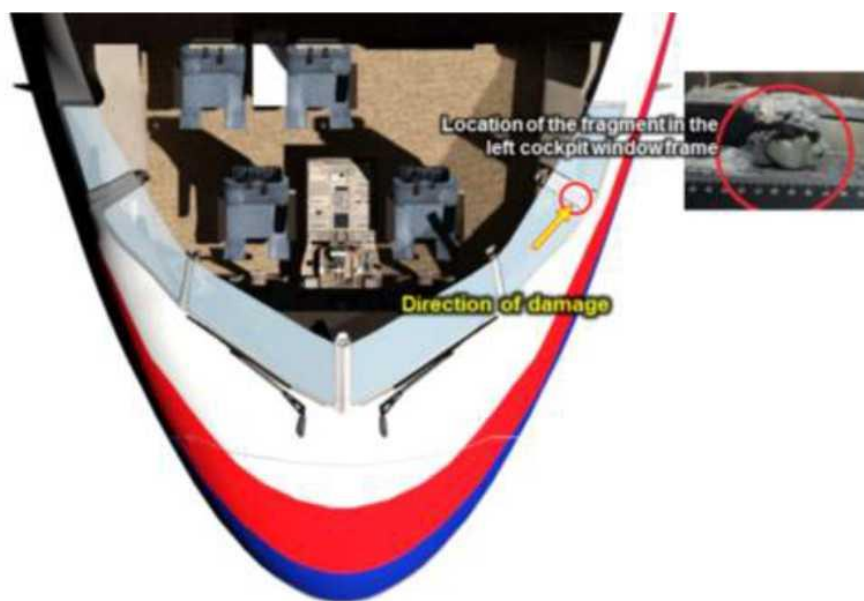


Figure G.5.6 - Possible trajectory of the "metal fragment" detected under the window frame clamping strip - along the glass consistent with Corporation's "collision course" version

The only fragment that was shown in the DSB technical investigation materials as "photographed at the point of discovery in the aircraft structure" in order to support the version that the aircraft was hit by a BUK missile has no ambiguous place or circumstances of the "fragment" discovery of the in the aircraft structure, according to the available materials.

Annex 2

Report of JSC Air and Space Defense Corporation "Almaz-Antey" on the conduct of a full-scale experiment, 2016

(translation)

JSC Air and Space Defense Corporation "Almaz-Antey"

REPORT

on the conduct of a full-scale experiment

Moscow, 2016

Contents

INTRODUCTION	4
1. Study Object	4
2. Purpose and Objectives of the Experiment	5
3. Conditions for the Experiment	5
3.1. Preparing the experiment.....	9
3.1.1. Preliminary preparation of 9M38M1	9
3.1.2. Preparing the target layout	11
3.1.3. Final preparation of item 9M38M1	12
3.2. Recording the results of the experiment.....	13
4. Conducting the experiment	16
5. Evaluation of the fragmentation and blast effects of the 9H314M warhead	32
5.1. Damage to the outer skin of the aircraft's fuselage	32
5.1.1. Damage to the cockpit.....	32
5.1.2. Port	46
5.1.3. Cockpit roof.....	61
5.1.4. Cockpit starboard	75
5.1.5. Damage to the left-hand engine simulator	89
5.2. Damage to the interior and structure of the cockpit.....	89
5.2.1. Damage to the interior of the cockpit.....	89
5.2.2. Damage to the cockpit structure.....	107
5.2.3. Damage to typical fragments of the outer skin and structure of the target aircraft's cockpit	114
5.3. Cross-sectional dimensions of holes on the outer skin of the target aircraft caused by preformed fragments	129
5.4. Conclusions based on the analysis of the exterior of the target after detonation of the 9H314M warhead	131
6. Characteristic holes caused by 9H314M 1-10 preformed fragments.....	132
6.1. Peculiarities of fragmentation damage to the outer skin of the target	132
6.2. Supplementary experiment in a shield target layout	142
6.2.1. Conditions for the supplementary experiment	143
6.2.2. Results of the supplementary experiment in the shield target layout	145

6.3. Conclusions on the peculiarities of fragmentation damage to the outer skin	151
7. Analysis of the mechanical (penetration) capability of 9H314M warhead's preformed fragments	151
8. Analysis of weight and size characteristics of preformed fragments of 9H314M warhead before and after the experiment.....	168
8.1. Weight and size characteristics of preformed fragments before the experiment.	168
8.1.1. Heavyweight 9H314M 1-10 (bowtie shaped) projectiles	169
8.1.2. Lightweight 9N314M 1-9 and 9N314M 1-11 ("parallelepiped"-shaped) projectiles	169
8.2. Weight and size characteristics of the ready-made projectiles after the experiment	170
8.3. Results of a supplementary experiment in the shield target layout.....	174
8.3.1. Heavyweight 9H314M 1-10 projectiles	176
8.3.2. Lightweight 9H314M 1-9 and 9H314M 1-11 projectiles	179
8.4. Comparative analysis of the projectiles	181
8.4.1. Comparative analysis of the projectiles with archival data.....	181
8.4.2. Comparative analysis of projectiles recovered following the experiment and those specified in the DSB Report	182
9. Analysis of the pattern of destruction of missile's structural elements	188
MAIN CONCLUSIONS FROM THE RESULTS OF THE EXPERIMENT	196

Exhibit A. Photo report in relation to the full-scale experiment in a shield target layout.

INTRODUCTION

In order to verify the conclusions in the Report of the Dutch Safety Board (DSB) regarding the type of weapon that impacted the Malaysian airliner Boeing 777-200 9M-MRD, which crashed on 17 July 2014 over the territory of Ukraine during flight MH17 from Amsterdam to Kuala Lumpur, Air and Space Defense Corporation "Almaz-Antey" (Almaz-Antey) has prepared and conducted a full-scale experiment.

The test was performed on 9H314M warhead, which consists of a shell with preformed fragments (projectiles) and a destructive charge sealed at the ends with covers. The warhead was tested both as part of the second section body and as part of the item (9M38M1 missile). The blasting of the warhead charge was initiated from the face of a special assembly with an ED-8M electric detonator mounted in it.

The overall straddle pattern and the times of fragment arrival at the target were recorded using Phantom V7.3 high-speed video cameras and certified panoramic video cameras mounted on the sides of the target layout.

The tests determined the parameters of the target impact areas, the hole density distribution and the size and weight of the fragments which were captured after punching holes in the obstacles.

1. Study Object

1. The materials of the DSB's investigation report on the crash of the Malaysian airliner Boeing 777-200¹ 9M-MRD, which crashed on 17 July 2014 during flight MH17 from Amsterdam to Kuala Lumpur, which were obtained with permission from the Dutch Safety Board (DSB).

2. Photographic and video evidence obtained during the field experiment and as a result of special research concerning the penetration capability of the projectiles.

3. Elements of the target layout.

¹ Which is referred to hereinafter as Boeing 777.

4. Samples of projectiles and missile (warhead) fragments collected on the ground and recovered from structural components of the targets.

2. Purpose and Objectives of the Experiment

The purpose of the experiment was to experimentally assess the reliability of the findings contained in the DSB Report to the extent they relate to the type of munitions that hit Boeing 777.

In order to achieve this purpose, the following tasks were to be solved during the experiment:

1. Evaluating the characteristics of the fragment cloud covering the targets after detonation of 9H314M warhead.
2. Evaluating the nature and appearance of fragmentation damage to the targets and the characteristics of the projectiles after they punched holes in the barriers.
3. Evaluating the mechanical (penetration) capability of 9H314M warhead's preformed fragments.
4. Evaluating the blast characteristics after explosion of 9H314M warhead.
5. Evaluating the pattern of destruction and damage caused by the explosion of 9H314M warhead to the structural parts of 9M38M1 missile airframe.
6. Comparative analysis of the pattern of damage to the targets and fragments of Boeing 777 aircraft.

3. Conditions for the Experiment

The source data for the experiment was taken from the DSB Report "Crash of Malaysia Airlines Boeing 777-200, 9M-MRD, flight MH17" as it relates to the type of weapon and the conditions under which it encountered Boeing 777:

The following is said on page 253 of the DSB Report, the main conclusions:²

“At 13.20:03 (15.20:03 CET), a warhead detonated outside, on the left above the cockpit of flight MH17. This was a 9H314M warhead carried by a 9M38-series missile,³ which are mounted on Buk surface-to-air missile systems.”

² Para. b of Section 10.1 (1) "Main conclusion". ³

³ Name of the weapon in the DSB Report.

The following is said on p. 143 of the DSB Report, under “result” in section 3.8.5, “Volume of space containing detonation position”:

“The simulations performed showed that the detonation position of the 9H314M warhead was in a volume of space of less than 1m³, about 4 meters above the tip of the nose of the aircraft, to the left of the cockpit.”

There are quantitative characteristics of the missile-aircraft encounter conditions on pages 139-143, in section 3.8.5 “Volume of space containing the detonation position” of the DSB Report, and on p. 363 of the Draft DSB Report. It was these conditions that, according to the DSB experts, existed at the moment of detonation of the 9H314M warhead of the 9M38-series missile on the left side of Boeing 777.

These conditions are illustrated in figure 3.1, which is a photograph of p. 363 of the Draft Final Report of the Dutch Safety Board (DSB).

The main quantitative characteristics of the missile-aircraft encounter conditions are as follows:

A. Aircraft and missile velocities at the position of the warhead detonation:⁴

Boeing 777, m/s	252-254
“9M38-series” missile with 9H314M warhead, m/s	~ 600

B. Angular position of the longitudinal axis of 9H314M warhead (9M38-series missile) relative to the aircraft fuselage at the detonation position:⁵

in the horizontal plane (AZ _{DSB}), deg.	- 17
in vertical plane (El _{DSB}), deg.	7

C. Position of the centre of the 9H314M warhead⁶ of "9M38-series" missile relative to the aircraft fuselage (from the geometric centre of the aircraft nose)⁷ :

⁴ Paragraph 5.61.2 (p. 363) of the Draft Final Report of DSB; Table 19 (p. 140) in section 3.8.3 'Warhead simulation' of the DSB Report.

⁵ Figure O.5 (page 363) of the DSB's Draft Final Report; Table 19 (page 140) in section 3.8.3 "Warhead simulation" of the DSB Report.

⁶ The coordinate system used in the DSB's materials is different from that accepted for Buk surface-to-air missile system. Y (height) and Z (parameter) coordinates are swapped. For their internal calculations the experts of Almaz-Antey used Buk SAM coordinate system. The numerical values of the coordinates correspond to the parameters specified in the DSB Report.

⁷ Table 20 (page 142); Figure 61 (page 143) in section 3.8.5 "Volume of space containing the detonation position" of the DSB Report; Table 15 (page 130), figures O.4 and O.5 (page 363) in the Draft Final DSB Report.

X_{DSB} (range), m - 0.4 ... 0.0
 Y_{DSB} (parameter), m - 3.5 ... - 3.0
 Z_{DSB} (height), m 3.7 ... 4.0

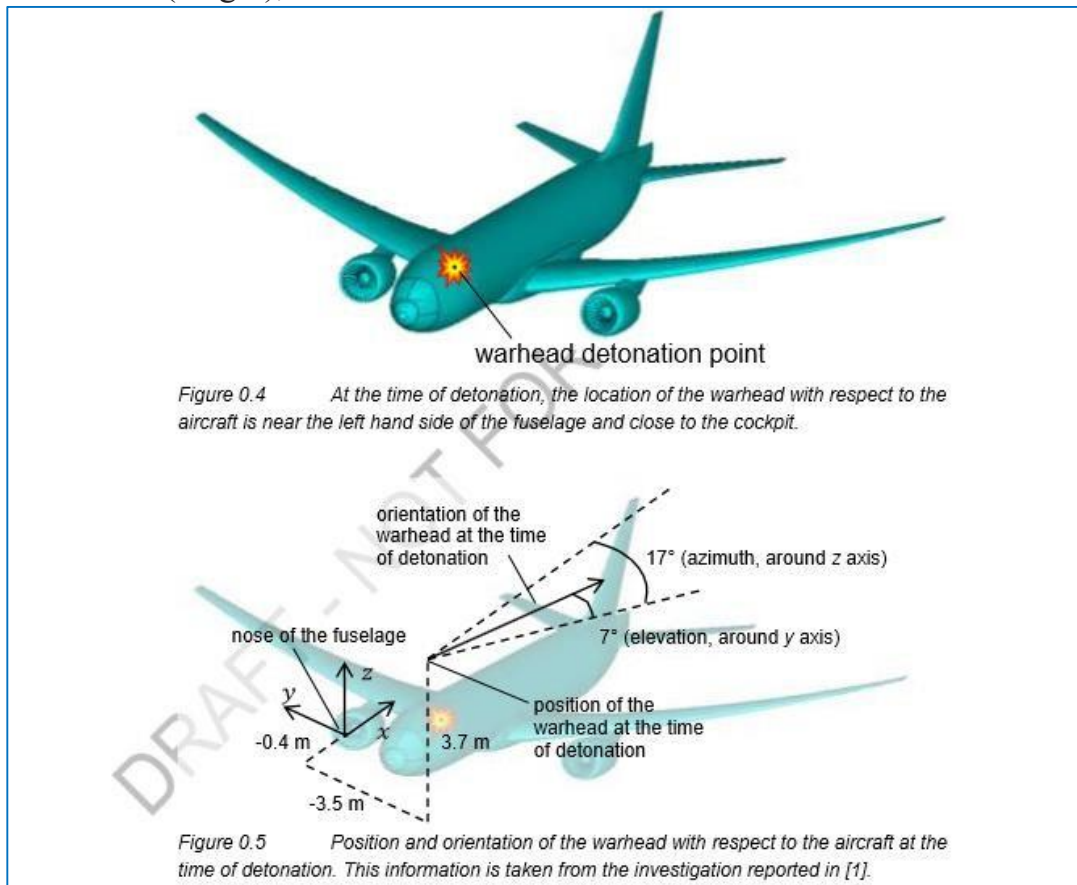


Figure 3.1 - Source data (missile-aircraft encounter conditions) according to DSB experts

Thus, the source data on the conditions of the missile-aircraft encounter used in preparing and conducting the experiment were the DSB Report materials.

To conduct the experiment at ground static conditions (at aircraft and missile velocities of 0 m/s), compensatory corrections for the missile and aircraft dynamics (missile velocity, V_{9M38-s} - 600 m/s, aircraft velocity V_{B777} - 252 m/s) at the encounter position were calculated.

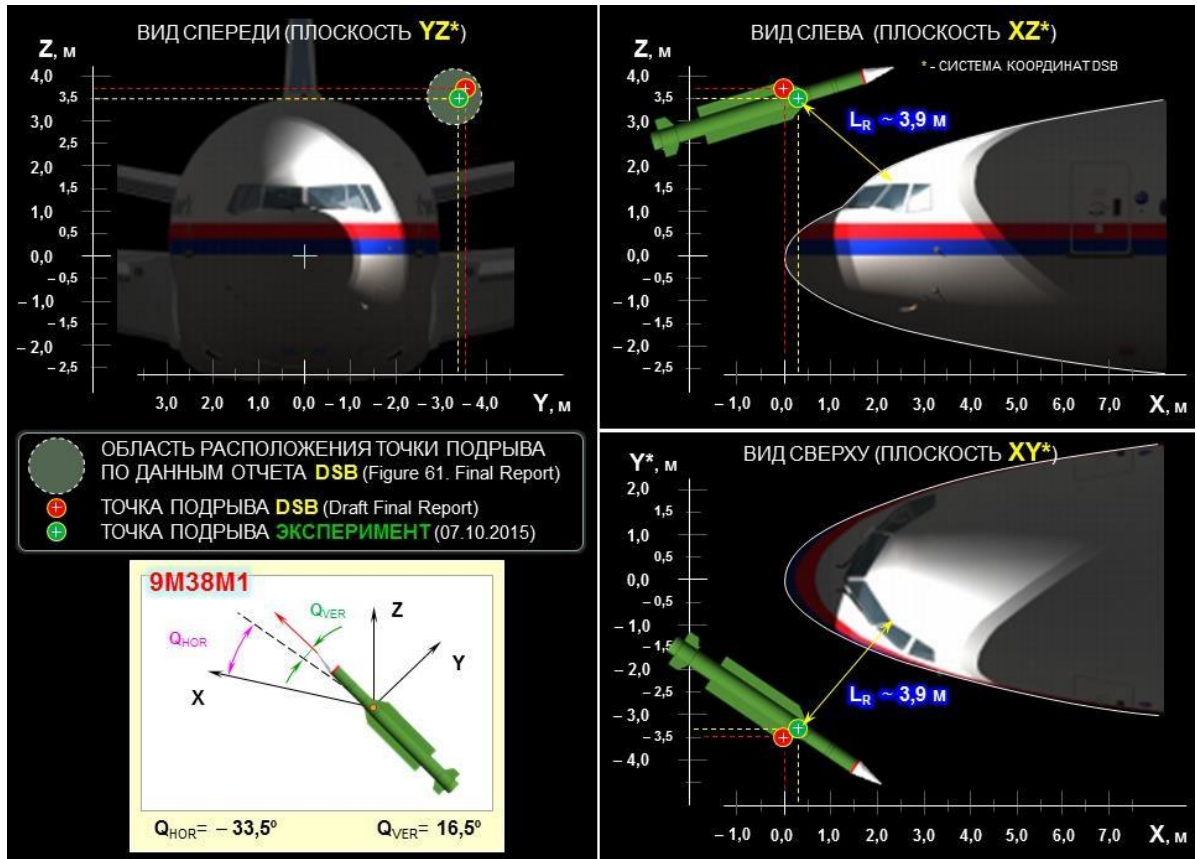
The resulting compensatory corrections were as follows:

in the horizontal plane, Q_{HOR} (Az), deg. - 16.5

in the vertical plane, Q_{VER} (El), deg. + 9.5 at the detonation position:

$$\Delta X, \text{ (range) m} \dots\dots\dots + 0.25 \Delta Y, \text{ (parameter) m} \dots\dots\dots + 0.15 \Delta Z, \text{ (height) m} \dots\dots\dots - 0,20$$

These corrections were used to create the target layout. The target layout is shown schematically in figure 3.2.



FRONT VIEW (YZ* PLANE)

LEFT VIEW (XZ* PLANE)

AREA WHERE THE DETONATION POSITION IS ACCORDING TO DATA IN THE DSB REPORT

TOP VIEW (XY* PLANE)

DETONATION POSITION

DETONATION POSITION EXPERIMENT

Figure 3.2 - Schematic target layout. The missile's orientation angles correspond to the data in the DSB Report taking into account the compensatory corrections.

To assess the characteristics of the fragmentation field at the time of 9H314M warhead detonation under conditions other than those in the selected target layout (figure 3.2), an

additional experiment was conducted.⁸ A shield target layout was used in this experiment. Shields made of aluminium alloy AMg6M mounted at different distances and angles from the detonation position of the 9H314M warhead were used as targets.

3.1. Preparing the experiment

In order to conduct the full-scale experiment at ground static conditions, the requirements for the preparation of the item (9M38M1 missile), the test stand (the tower and the item support) and the target layout were defined.

Following the elaboration of a procedure and timelines for fulfilling the main technical requirements, a "Programme and Methodology for Testing 9M38M1 Item through an Explosion in the Target Layout" was developed.

3.1.1. Preliminary preparation of 9M38M1

Using the source data (from the DSB Report materials), representatives of Almaz-Antey and institutions and organisations which cooperate with Almaz-Antey carried out preliminary preparation of the 9M38M1 item and the test stand (support) for the testing:

A. The item 9M38M1 was prepared for the experiment. The state of the item 9M38M1 corresponds to 33^d-40th second of the missile flight cyclogram.⁹

Specific configuration of the item prepared:

- A burnt-out motor is installed on the item 9M38M1 (solid charge is made blank), the state of all pyrotechnic components of the article (pyrogen igniters, gas generators) corresponds to 33^d-40th second of the flight cyclogram;

- the safety and arming unit have been removed from the item 9M38M1 and a connector- plug on the safety and arming unit cable is fitted;

- the second compartment of the item has a temporary hole (Ø 20.0 mm) for power take-off of the special assembly in the safety and arming unit area.

The stages of 9M38M1 preliminary preparation process are shown in figure 3.3.

⁸ The conditions for the additional experiment in the shielded target layout are provided in section 6.2.1. of Almaz-Antey's Report.

⁹ As per the conditions set forth in the DSB Report, according to the version of the missile encountering the aircraft "on an opposite course", with the missile velocity of $V_{\text{"9M38-series"}} \sim 600$ m/s.



Item 9M38M1

Logbook 9M38M1.0000.000 FO
for the item 9M38M1

9N314M warhead

9M38M1 MISSILE HAS BEEN PREPARED AND CORESPONDS TO 40TH OF FLIGHT

Figure 3.3 – Preliminary preparation of the item 9M38M1 for the experiment

B. The item orientation unit (support) has been manufactured which meets the respective requirements:

- it is provided that the distance from the front support (in compartment 3 area) to compartment 2 is at least 30-35 cm (to avoid distortion of 9H314M warhead damage area characteristics);

- it is provided that the item 9M38M1 is oriented at the elevation angle of 16-17 degrees (in the vertical plane);

- it is provided that the item 9M38M1 is oriented along the azimuth of 33-34 deg. (in the horizontal plane) by rotating the support on the test bench (tower);

- the support has a wooden structure (to avoid ricochet of projectiles and fragments), except for the rear bearing of the item;

- the design of the support ensures that the item 9M38M1 can be mounted as part of the assembly on the test bench using the standard lifting fixtures.

After completion of the preliminary preparations, the item, tooling and lifting fixtures were delivered to the area of the experiment.

3.1.2. Preparing the target layout

The target layout consists of two targets:

Target No. 1 - Ilyushin-86 (IL-86) target aircraft (nose section of the aircraft "IL-86" on a special support);

Target No. 2 is a simulation of the aircraft's left engine - a shield target made of 3.0 mm steel plates (St3).

IL-86 target aircraft was prepared with the assistance of specialists from cooperating enterprises and organisations using drawings and assignments agreed with Almaz-Antey's specialists.

In consultation with OJSC "IL" specialists, the support for Target No. 1 (IL-86 target aircraft) was designed and built.

The appearance of the support is shown in figure 3.4.



Figure 3.4 – Support for IL-86 Target Aircraft

Upon completion of IL-86 target aircraft transportation to the experimental site, the target layout was assembled in accordance with the target layout plan (figure 3.5).

Mounting of Target No. 1 (nose section) Mounting of the test bench



Target No. 2 (left engine)

Figure 3.5 - Mounting of the target layout

3.1.3. Final preparation of item 9M38M1

In the final stage of preparing item 9M38M1 for testing, facilities for remote detonation were mounted. Final preparation of the item 9M38M1 was carried out on the technology site in the experimental area. The preparation (mounting of a special remote detonator assembly) was carried out by explosive experts.

The process of the item final preparation is shown in figure 3.6.



Figure 3.6 - Final preparation of the item 9M38M1

Once the preparation of the item was complete, it was mounted on the test bench (figure 3.7).



Figure 3.7 - Mounting the item 9M38M1 on the test bench

After checking the relative orientation of the item¹⁰ and the target layout, first of all IL-86 target aircraft, the preparation of the experiment was completed.

3.2. Recording the results of the experiment

The 9H314M warhead detonation process, the overall straddle pattern and the times of fragment arrival at the target layout were recorded using:

- certified panoramic video cameras mounted on the sides of the target layout (figures 3.8 through 3.11);
- GoPRO cameras mounted inside the cockpit (figure 3.12);
- Phantom V7.3 high-speed video cameras (5,000 fps) mounted on the sides of the target layout (figure 3.13);
- The GGE speed sensors installed on the windscreen and in the cockpit seats (figure 3.14).

¹⁰ The closest distance from the centre of the 9H314M warhead to the outer skin of the IL-86 target aircraft was ~3.9m.



Figure 3.8 - Camera No. 1P



Figure 3.9 - Camera No. 2P



Figure 3.10 - Camera No. 3P



Figure 3.11 - Camera No. 4P



Figure 3.12 - Camera No. 1B



Figure 3.13 - Camera No. 2C



Figure 3.14 – Control velocity sensor GPE on the windscreen of the cockpit

The test was followed by photographing and videotaping of the target layout, the removal of projectiles and the counting of holes in the target fragments.

4. Conducting the experiment

The explosive charge of the warhead was initiated from the front end from the centre of the special assembly MSNI.773979.011-01 with electric detonator ED-8M mounted inside it.

High detonation of the warhead occurred.

Figure 4.1 shows a still image from panoramic video camera 4P showing the moment the 9M38M1 missile is detonated.



Figure 4.1 - Camera No. 4P. Detonation of the 9H314M warhead as part of the item 9M38M1

The process of detonation of 9H314M warhead (as part of the 9M38M1) is shown in figures 4.2 through 4.31.

One can see in these figures (figures 4.2 through 4.31) still images from the high-speed video camera No. 2C ("Phantom V7.3", shooting mode: 5,000 frames per second).

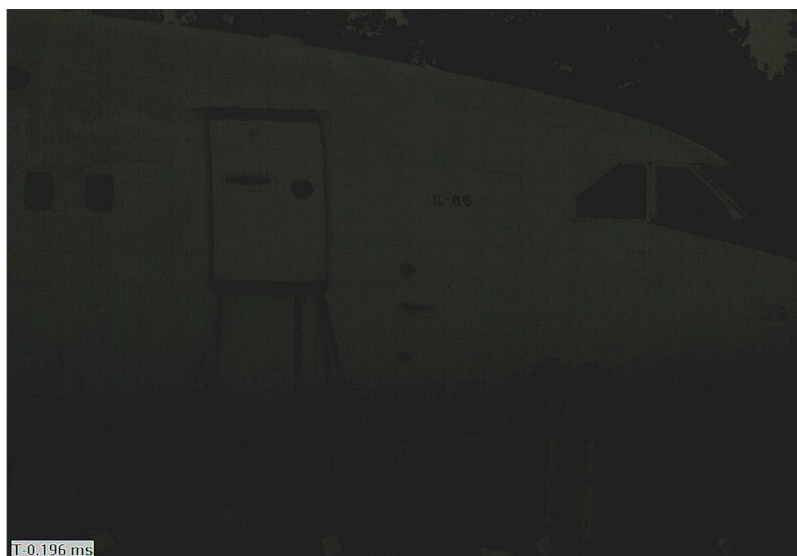


Figure 4.2 - Target layout prior to detonation of the 9H314M warhead (as part of the item 9M38M1)



Figure 4.3 - Detonation of the 9H314M warhead

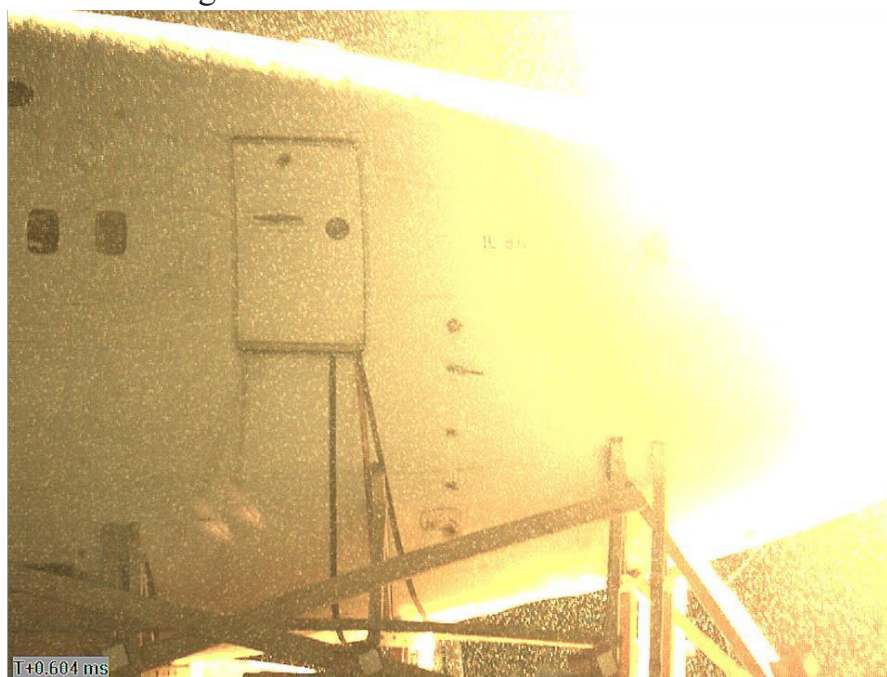


Figure 4.4 - Detonation of the 9H314M warhead

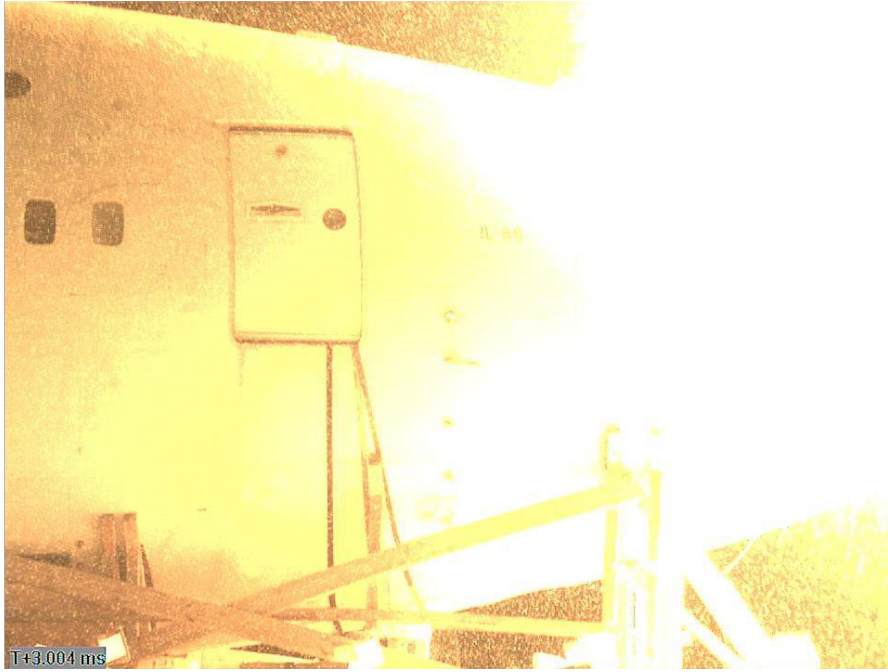


Figure 4.5 - Detonation of the 9H314M warhead



Figure 4.6 - Detonation of the 9H314M warhead



Figure 4.7 - Detonation of the 9H314M warhead



Figure 4.8 - Detonation of the 9H314M warhead



Figure 4.9 - Detonation of the 9H314M warhead



Figure 4.10 - Detonation of the 9H314M warhead



Figure 4.11 - Detonation of the 9H314M warhead



Figure 4.12 - Detonation of the 9H314M warhead



Figure 4.13 - Detonation of the 9H314M warhead



Figure 4.14 - Detonation of the 9H314M warhead



Figure 4.15 - Detonation of the 9H314M warhead



Figure 4.16 - Detonation of the 9H314M warhead

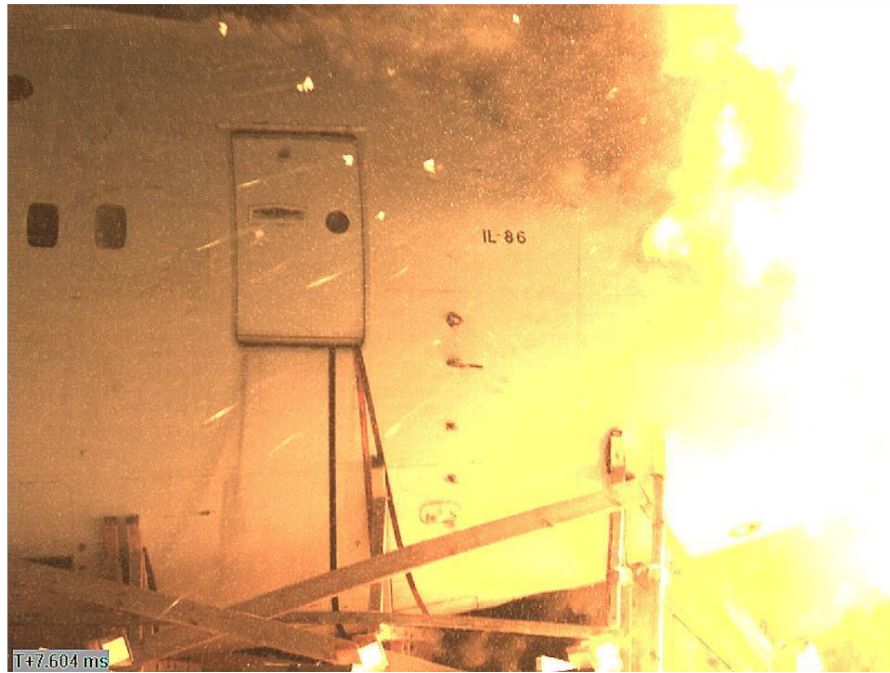


Figure 4.17 - Detonation of the 9H314M warhead



Figure 4.18 - Detonation of the 9H314M warhead



Figure 4.19 - Detonation of the 9H314M warhead



Figure 4.20 - Detonation of the 9H314M warhead



Figure 4.21 - Detonation of the 9H314M warhead



Figure 4.22 - Detonation of the 9H314M warhead



Figure 4.23 - Detonation of the 9H314M warhead



Figure 4.24 - Detonation of the 9H314M warhead

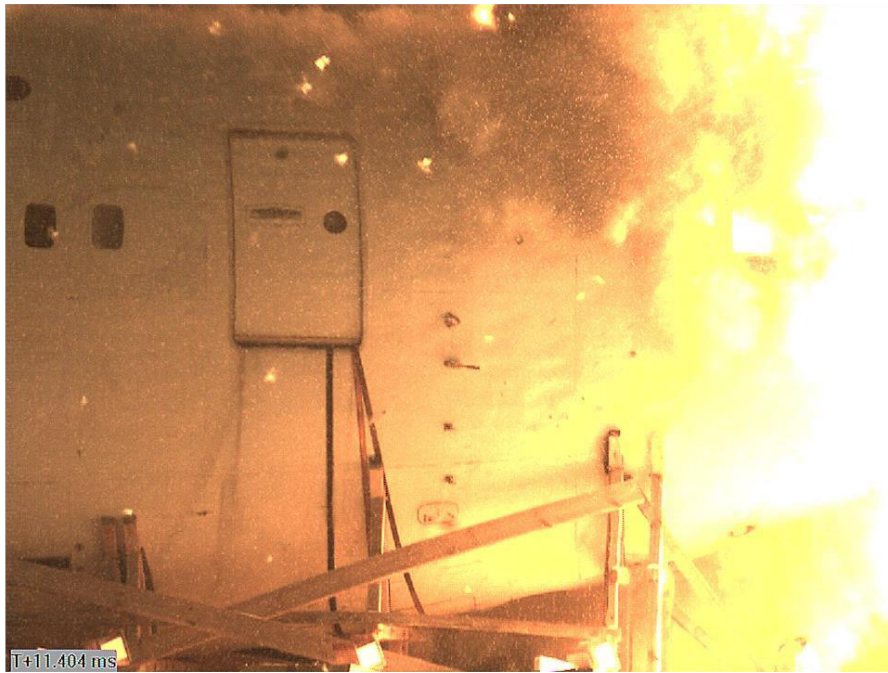


Figure 4.25 - Detonation of the 9H314M warhead

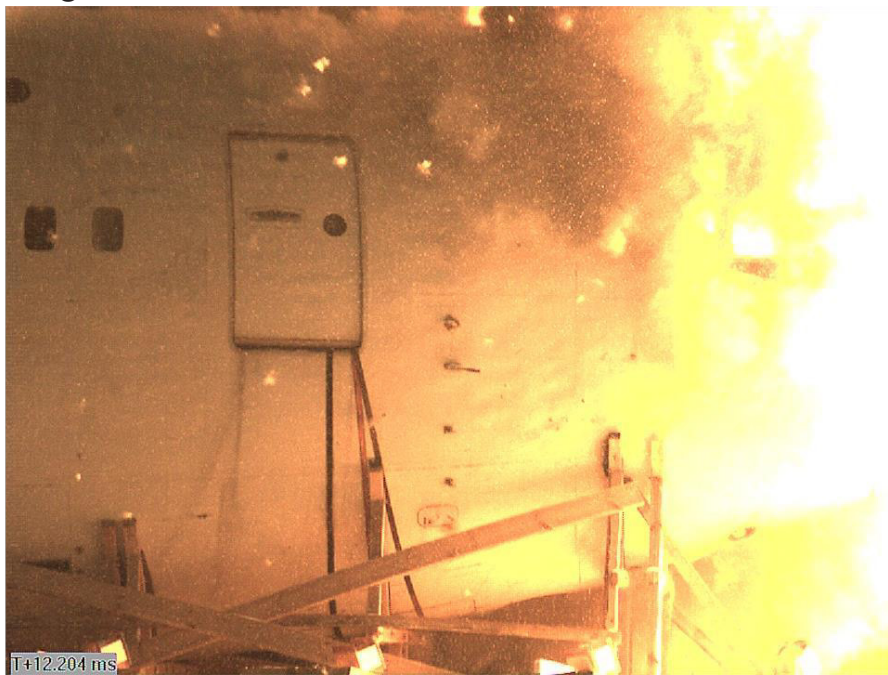


Figure 4.26 - Detonation of the 9H314M warhead

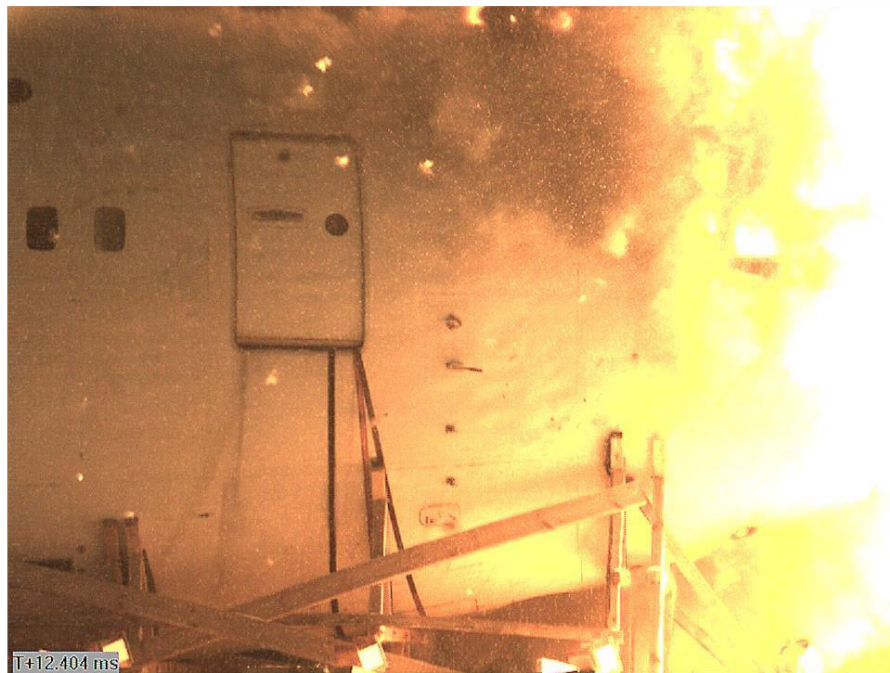


Figure 4.27 - Detonation of the 9H314M warhead



Figure 4.28 - Detonation of the 9H314M warhead

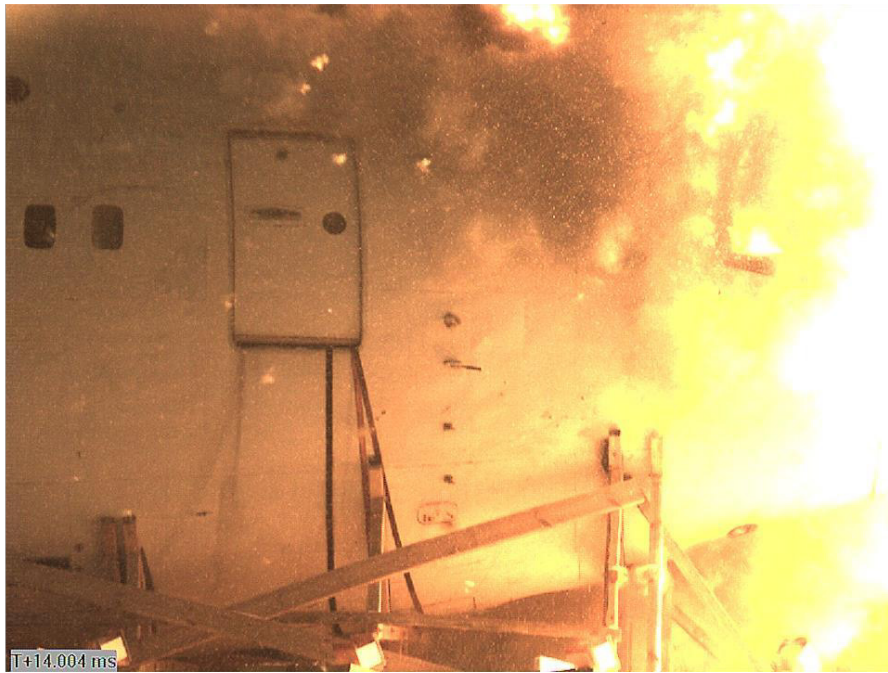


Figure 4.29 - Detonation of the 9H314M warhead



Figure 4.30 - Detonation of the 9H314M warhead



Figure 4.31 - Detonation of the 9H314M warhead

5. Evaluation of the fragmentation and blast effects of the 9H314M warhead

Following the experimental detonation of the 9H314M warhead as part of the item 9M38M1, an inspection and video and photo registration of the fragmentation field and of the effects of the blast on the targets were carried out.

The registration of damage to the structure of the target aircraft was done on a stage-by-stage basis. At the first stage, before sorting out the debris inside the cockpit, video and photo registration of the damage to the outer skin of the aircraft was carried out. Subsequently, after the destroyed elements of the cockpit structure were sorted out, video and photo registration of damage to the aircraft load-bearing structure (longitudinal structural elements - stringers and transverse structural elements - frames), elements of internal cockpit equipment, galley unit, lavatory, first passenger cabin, and technological spaces under the cockpit was performed.

5.1. Damage to the outer skin of the aircraft's fuselage

5.1.1. Damage to the cockpit

Cockpit damage is shown in figures 5.1 through 5.25.



Figure 5.1 - Left side of the cockpit



Figure 5.2 - Cockpit. Rear left view



Figure 5.3 - Cockpit. Rear view



Figure 5.4 - Cockpit. Wide shot. Top left view



Figure 5.5 - Cockpit. Wide shot. Front left view



Figure 5.6 - Left side of the cockpit



Figure 5.7 - Cockpit (front view)



Figure 5.8 - Cockpit (front view)



Figure 5.9 - Cockpit (front view)



Figure 5.10 - Cockpit (front view)



Figure 5.11 - Entry holes in the radiotransparent radome

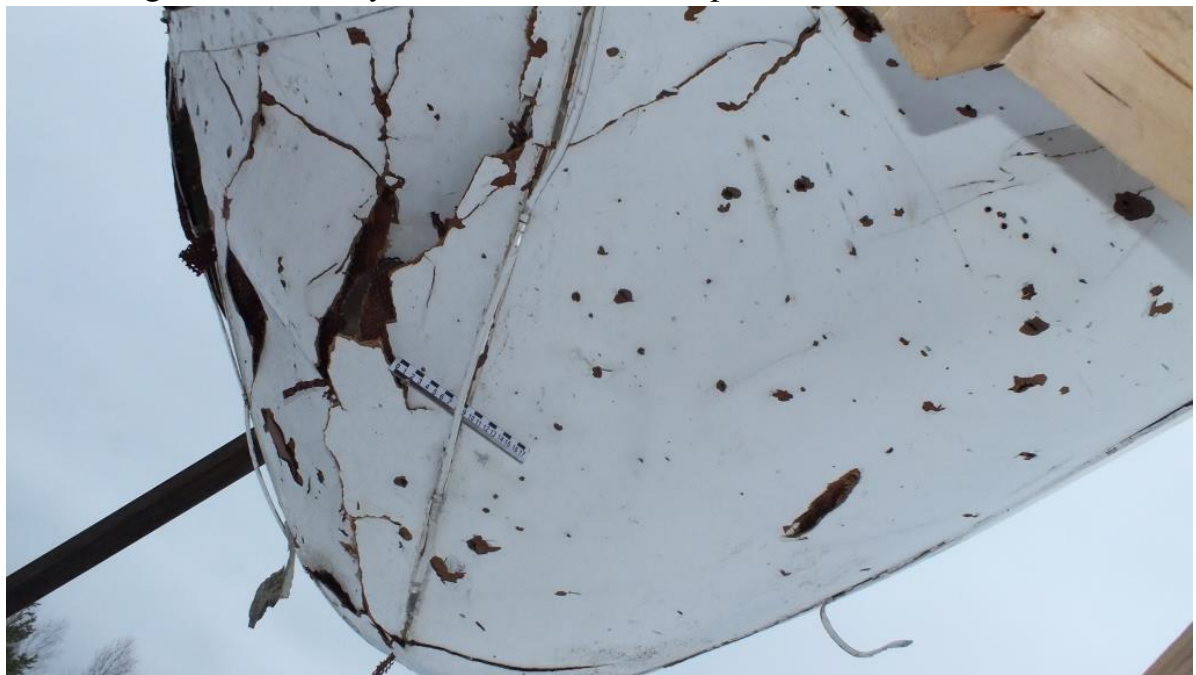


Figure 5.12 - Entry holes in the radiotransparent radome



Figure 5.13 - Output holes in the radiotransparent radome

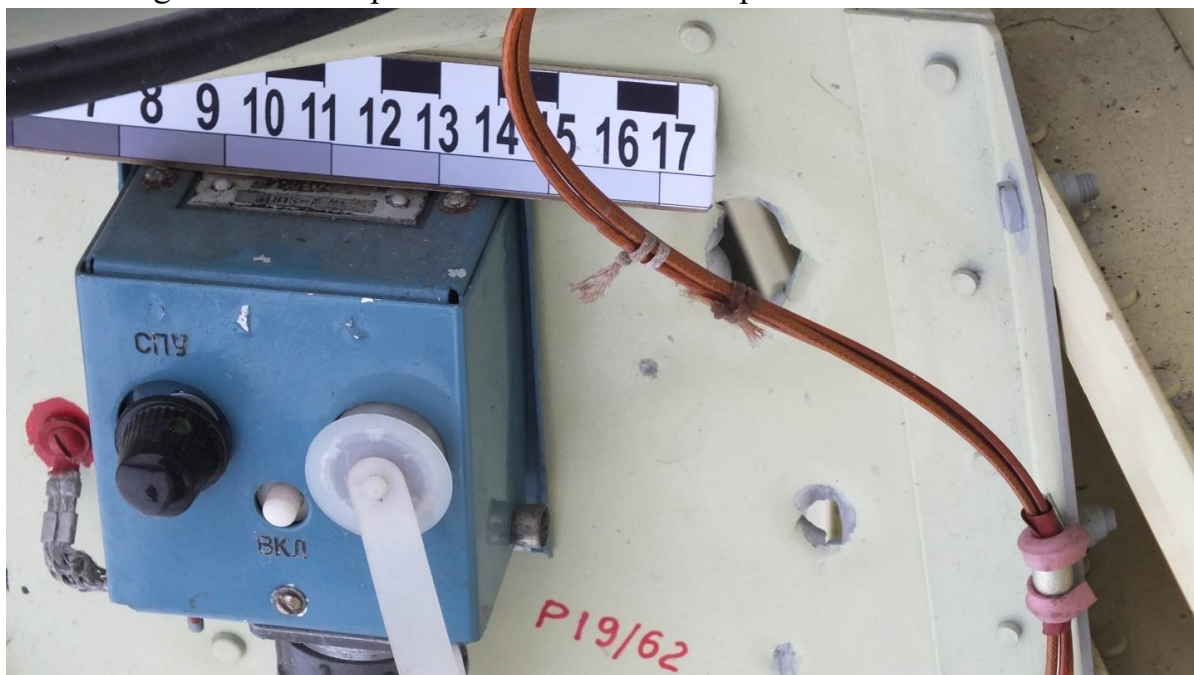


Figure 5.14 - Through-and-through holes in weather radar equipment



Figure 5.15 - Through-and-through holes in weather radar equipment



Figure 5.16 - Aircraft commander's windscreen (front view)



Figure 5.17 - Second and third windows of the aircraft commander



Figure 5.18 - Cockpit glazing. Left view



Figure 5.19 - Aircraft commander's windscreen frame



Figure 5.20 - Aircraft commander's second and third windows
(top left view)



Figure 5.21 - Third window of the aircraft commander



Figure 5.22 - Aircraft commander's window frames



Figure 5.23 - Aircraft commander's windscreen and direct-vision window



Figure 5.24 - Aircraft commander's windscreen and direct-vision window
(left front view)



Figure 5.25 - Upper part of the aircraft commander's direct-vision window
(left view)

An analysis of the exterior of the cockpit showed destruction of the entire left side of the cockpit glazing (windscreen of the aircraft commander, left direct-vision window and left rear window). There is significant deformation of the structural frame of the glazing, especially the rear left window. There is a significant density of fragmentation holes. At the same time, the shape of the entry holes varies from elongated compact shape to a distinctive butterfly-shaped hole. The entry holes in the area of the glazing have clear outlines, no traces of non-penetrating damage (ricochets) caused by preformed fragments have been recorded under the glazing.

There is damage to the framework and the outer skin of the cockpit.

There is a significant deformation of the outer skin of the fuselage in the cockpit area in the direction from outside to inside, exposing the contours of the framework. The entire outer surface of the cockpit on the left side shows traces of debris impact¹¹ in the form of a rash of microcraters and thermal oxidation (burns).

The size of the fragmentation field on the target is 2-2.5 times larger than the size of the fragmentation field on the Boeing 777 fragments. In particular, this is objectively observed in the area of the upper right and lower left side of the cockpit. In addition, unlike

¹¹ Particles of unburned explosive material, small particles of ammunition components and fragments of destroyed projectiles.

the Boeing 777, multiple traces of fragmentation damage are observed on the nose cone and the weather radar equipment.

The nature of the destruction and damage to the cockpit caused by the blast factors is far superior to that on the Boeing 777 fragments.

Thus, the characteristics of the fragmentation field and the nature of the destruction and damage to the cockpit of the aircraft target caused by the blast factors differ significantly from the characteristics of the fragmentation field and the nature of the damage observed on the Boeing 777 fragments.

5.1.2. Port

The appearance (from different angles) of the damage caused during the tests to the outer skin of the target aircraft's port is shown in figures 5.26 through 5.53.



Figure 5.26 - Port under the aircraft commander's windscreen



Figure 5.27 - Port under the windows of the aircraft commander



Figure 5.28 - Port under the windows of the aircraft commander



Figure 5.29 - Port outside the windows of the aircraft commander with signs of deformation of the outer skin, elements of the framework and thermal burn



Figure 5.30 - Port outside the windows of the aircraft commander



Figure 5.31 - Port side in L1 door area. Characteristic holes caused by hull fragments are seen the dimensions of which are significantly greater than those of holes caused by ready-made projectiles



Figure 5.32 - Port side and front left-hand passenger door L1



Figure 5.33 - Port side in L1 door area (overall view)



Figure 5.34 - Top of port side
(close-up over the windows of the aircraft commander)



Figure 5.35 - Top of port side (overall view above the aircraft commander's windows). The fragment shows deformation and tearing of the outer skin



Figure 5.36 - Port side skin (overall view). The fragment shows detachment of the outer skin from the framework resulting from the detachment of rivet heads



Figure 5.37 - Fragment of the outer skin of the port side (overall view). The fragment shows deformation of the outer skin in the direction from outside to inside, exposing the contours of the framework and detachment of outer skin elements



Figure 5.38 - Port side skin (overall view, bottom view)



Figure 5.39 - Port side skin showing signs of significant deformation of outer skin in the direction from outside to inside



Figure 5.40 - Port side skin (close-up). No traces of non-penetrating damage (ricochets) caused by preformed fragments on the port side of the target aircraft

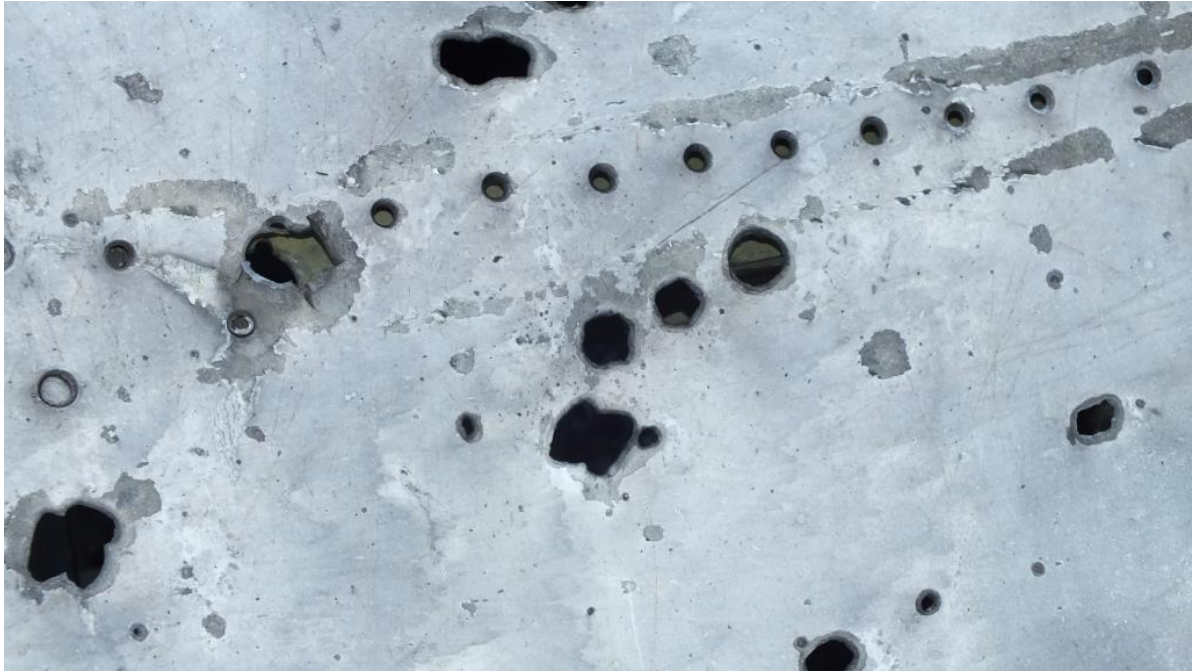


Figure 5.41 - Fragment of the port side skin (close-up).
The fragment shows the characteristic butterfly-shaped holes from the 9H314M 1-10
projectiles

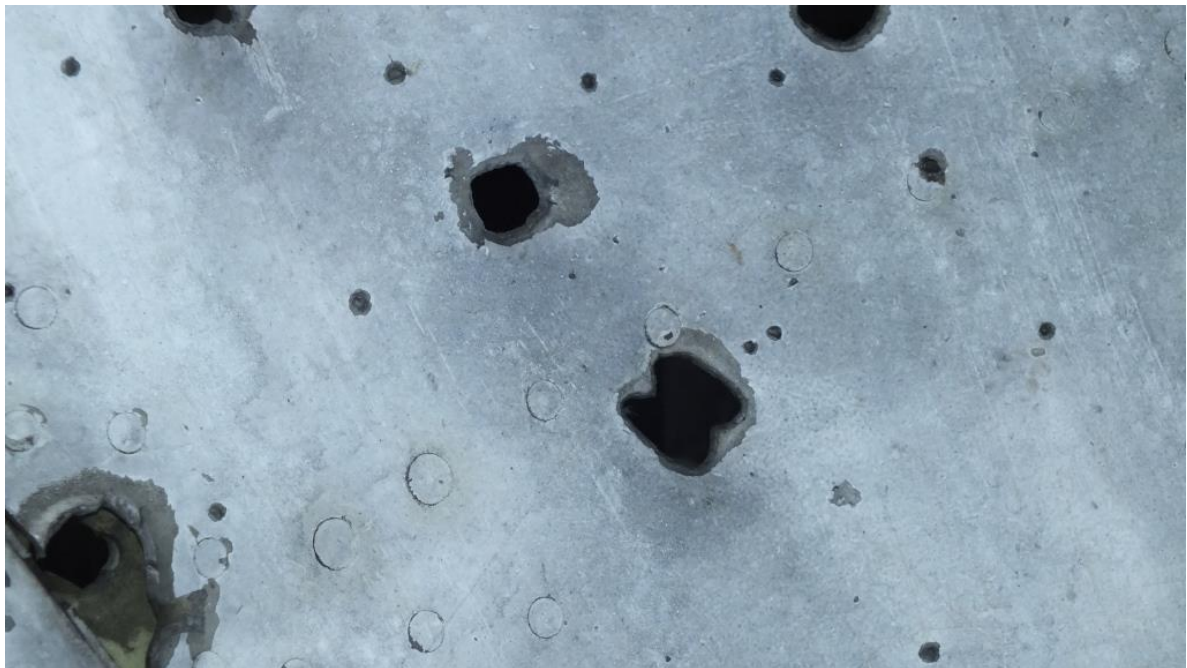


Figure 5.42 - Port side skin with a characteristic butterfly-shaped hole caused by a
projectile of 9H314M 1-10 (close-up)

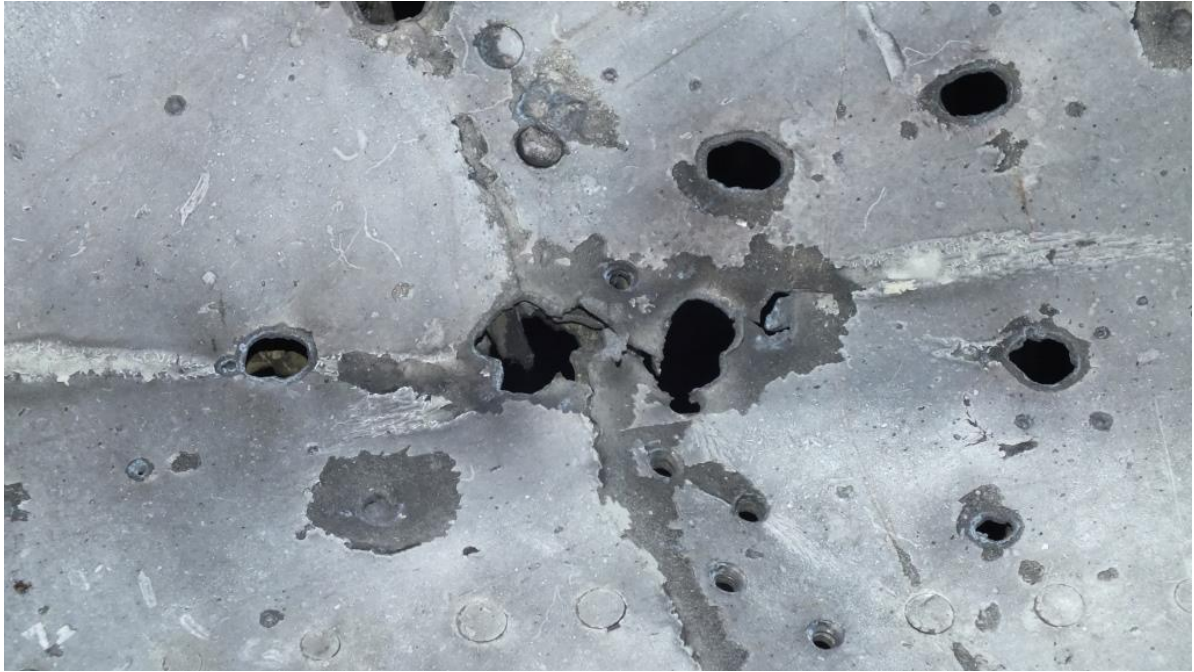


Figure 5.43 - Fragment of the port side skin with holes caused by all types of preformed fragments of 9H314M warhead (close-up)



Figure 5.44 - Port side skin with micro-crater marks and characteristic butterfly-shaped holes caused by 9H314M 1-10 projectiles (close-up)



Figure 5.45 - Port side skin with characteristic butterfly-shaped holes caused by 9H314M 1-10 projectiles (close-up)



Figure 5.46 - Overall view of the port and left side of the roof



Figure 5.47 - Fragment of the upper part of the port with through-and-through holes caused by ready-made projectiles and missile hull fragments (inside view)



Figure 5.48 - Fragment of upper part of the port with characteristic butterfly-shaped holes caused by 9H314M 1-10 ready-made projectiles (inside view)



Figure 5.49 - Fragment of upper part of the port (inside view). The fragment shows deformation of the framework elements and detachment of the outer skin from the framework resulting from the detachment of rivet heads



Figure 5.50 - Fragment of the port side behind the aircraft commander's seat (close-up, inside view)



5.51 - Fragment of the port side behind the aircraft commander's seat
(overall view, inside view)



Figure 5.52 - Upper part of the port behind the aircraft commander's seat
(inside view)



Figure 5.53 - Fragment of the port side in the area of the aircraft commander's direct-vision window

An analysis of the damage to the port side showed that the number of entry holes and the total dimensions of the fragmentation field on the port side are also significantly greater than those on the fragments¹² of the Boeing 777. Penetrating fragment damage caused by ready-made projectiles was observed in the section from the nose cone and the weather radar to the front left passenger door L1 inclusive.

The shape of the entry holes varies from an elongated compact shape to distinctive butterfly-shaped holes caused by ready-made projectiles and large (30 to 250 mm) shapeless holes caused by the second compartment (warhead compartment) fragments and small (1-3 mm) holes caused by detonation products.

There is significant deformation of the outer skin of the port in the direction from outside to inside, exposing the contours of the framework. Also, there are ruptures in the outer skin and its detachment from the framework as a result of the rivet heads detachment.

¹² Para 3.2.2, "Observed fragment damage", in Appendix Y (Appendix-Y-TNO-Report) to the final DSB Report states that the fragments of Boeing 777's port show no damage caused by preformed fragments in the section from the frame STA.220 (just behind the cockpit glazing) to the frame STA.410.

The entire external surface of the port side up to the front left passenger door L1 (at a distance of up to 5.8-6.2 m from the aircraft nose) shows traces of explosion products in the form of deformation, rash of microcraters and thermal oxidation (burns).

The density of holes on the port side and the size of the fragmentation field are 2-3 times greater than the density of holes and the size of the fragmentation field on similar Boeing 777 fragments.

Thus, the characteristics of the fragmentation field and the nature of the destruction and damage to the port of the target caused by the blast factors differ significantly from the characteristics of the fragmentation field and the nature of the damage on the Boeing 777 fragments.

5.1.3. Cockpit roof

The appearance (from different angles) of the damage done during the tests to the roof of the target aircraft's cockpit is shown in figures 5.54 through 5.78. The photographs show the fragments that were cut out for subsequent analysis (for more details see section 5.2.3.).



Figure 5.54 - Cockpit roof after removal of fragments
(front view)

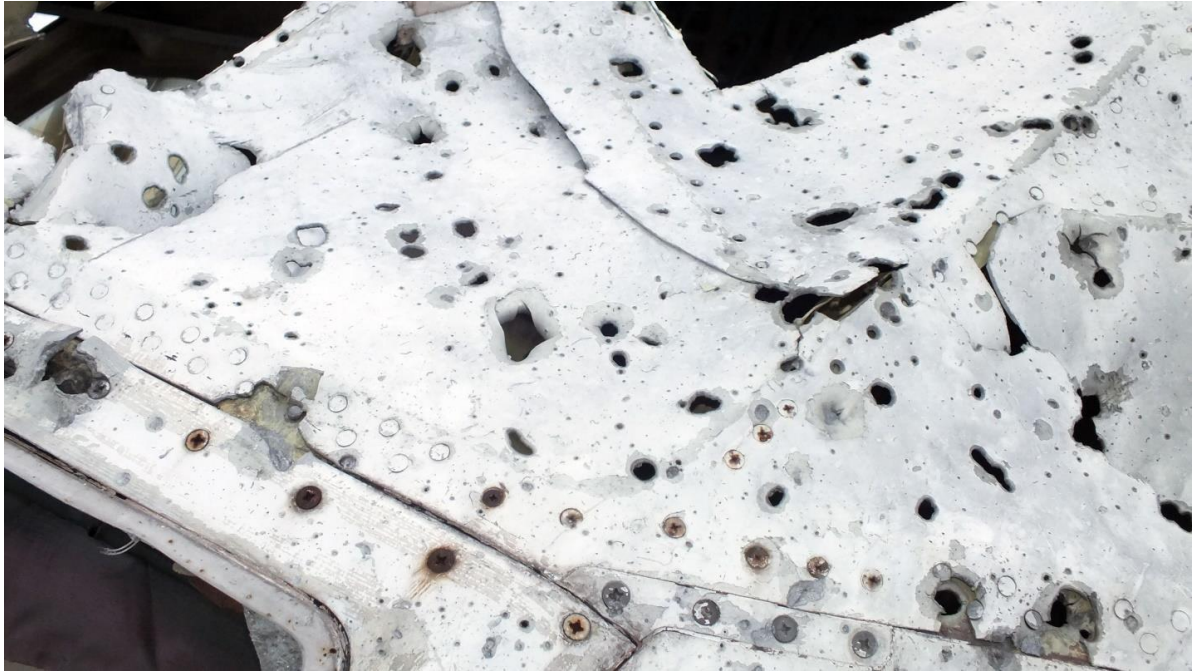


Figure 5.55 - Cockpit roof (left view)



Figure 5.56 - Fragment of cockpit roof over the aircraft commander's windscreen

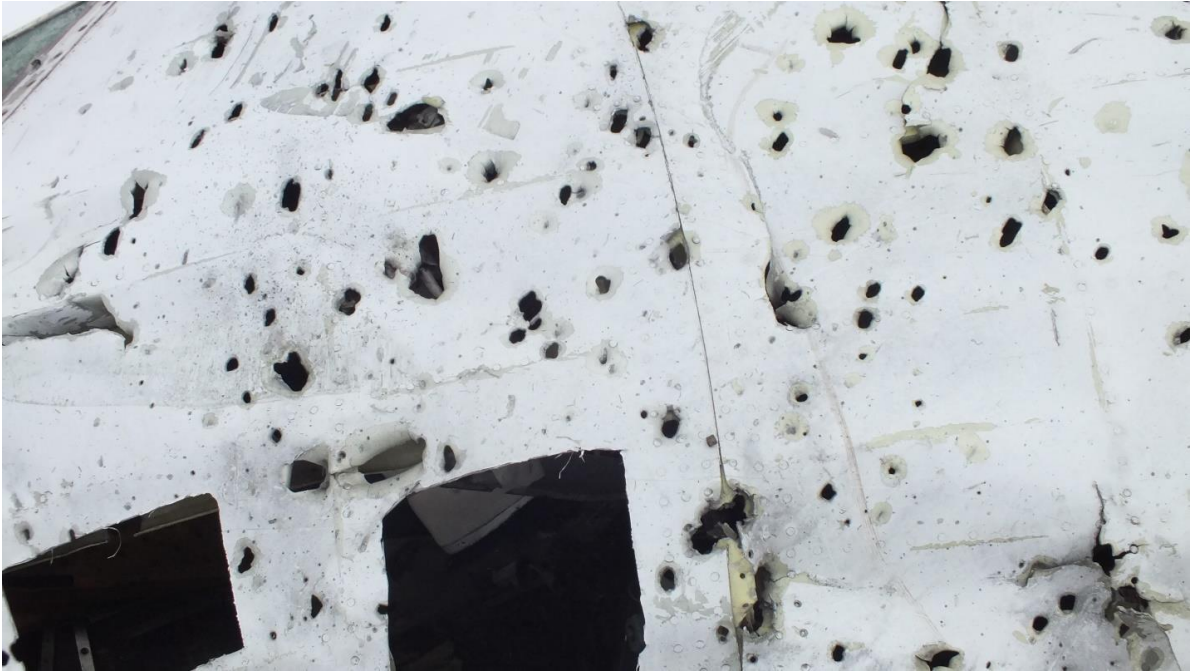


Figure 5.57 - Cockpit roof (top view)

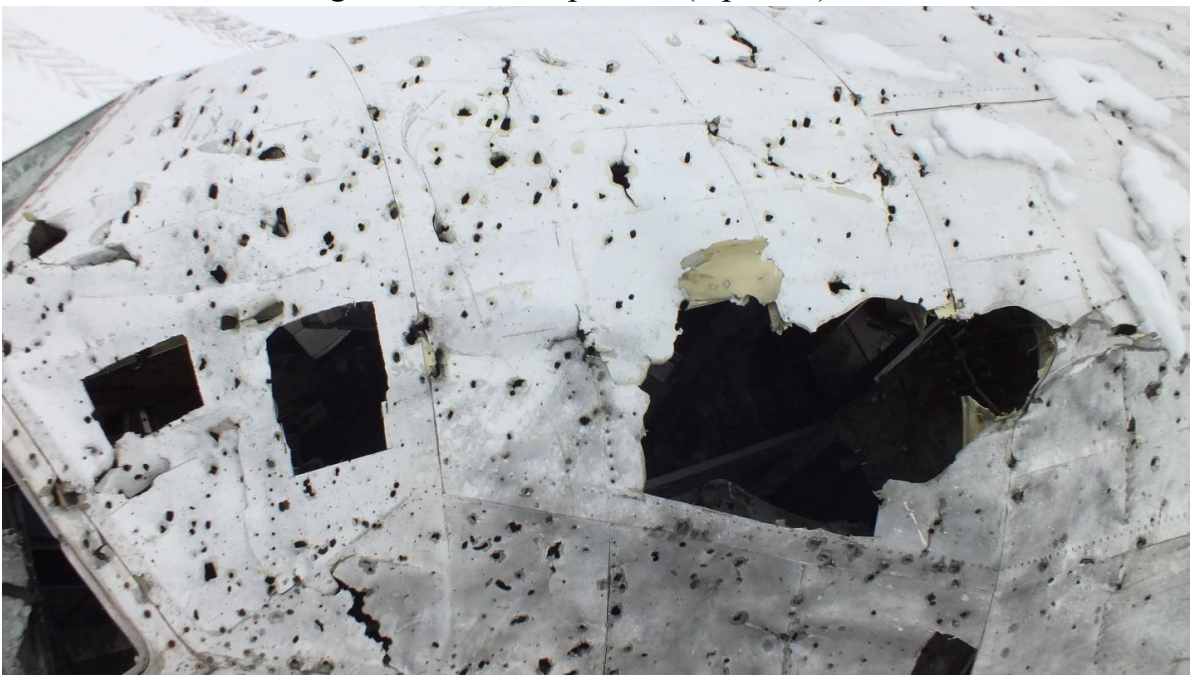


Figure 5.58 - Cockpit roof (top view)



Figure 5.59 - Cockpit roof at the level of the front left passenger door L1 (top view). The roof fragment shows that through-and-through holes caused by ready-made projectiles are present on both left and right side on the roof



Figure 5.60 - Cockpit roof after removal of fragments (top front view)



Figure 5.61 - Right side of cockpit roof (top view)



Figure 5.62 - Left side of cockpit roof before removal of fragments (top left view)



Figure 5.63 - Fragment of cockpit roof (close-up).

The direction of deformation of the roof structure elements from inside to outside indicates that an aero-strike resulted from the impact of 9H314M warhead explosion factors



Figure 5.64 - Cockpit roof with aero-strike marks (overall view)



Figure 5.65 - Cockpit roof near the centre (axial) line of the aircraft. The fragment shows traces of damage caused by ready-made projectiles to both the left and right sides of the roof



Figure 5.66 - Cockpit roof above the aircraft commander's seat (inside view)



Figure 5.67 - Cockpit roof above the aircraft commander's seat with signs of destruction of transverse structural elements (stringers)



Figure 5.68 - Characteristic butterfly-shaped through-and-through holes in a fragment of the cockpit roof



Figure 5.69 - Cockpit roof on the port side



Figure 5.70 - Through-and-through holes on the right side of the cockpit roof (inside view)



Figure 5.71 - Through-and-through holes in the cockpit roof (inside view)



Figure 5.73 - Through-and-through holes in the cockpit roof (inside view)



Figure 5.74 - Through-and-through holes in the outer skin and thermal and noise insulation panels on the right side of the cockpit roof (inside view)

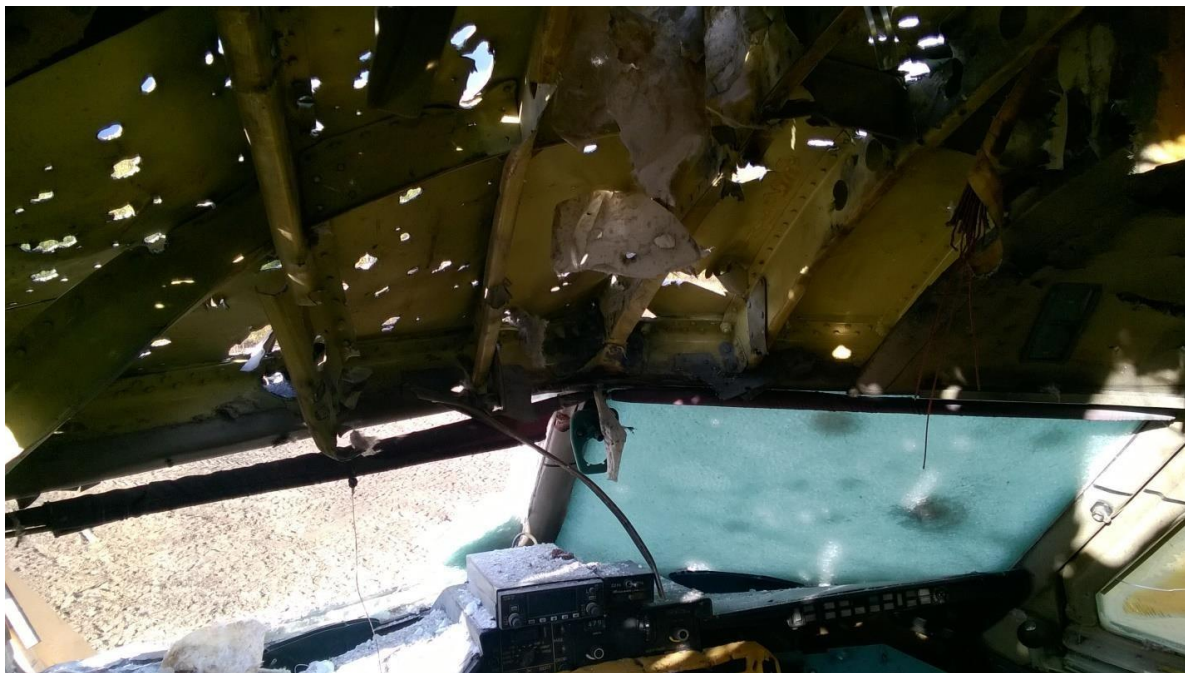


Figure 5.75 - Through-and-through holes in the central and right sections of the cockpit roof (inside view)



Figure 5.76 - Through-and-through holes in the central and right sections of the cockpit roof (inside view)



Figure 5-77 - Characteristic butterfly-shaped holes (inside view)



Figure 5.78 - Missile compartment hull fragments (left) and holes caused by them (right)

An analysis of the damage to the target roof showed that the number of entry holes and the total size of the fragmentation field on the target's roof¹³ are significantly greater than those on the Boeing 777 fragments.

The shape of the entry holes varies from an elongated compact shape to distinctive butterfly-shaped holes caused by ready-made projectiles and large (30 to 150 mm) shapeless holes caused by the second compartment (warhead compartment) fragments.

In the left section of the cockpit roof, there is destruction of the structure and the outer skin. The direction of deformation of the aircraft's structural elements from inside to outside indicates that an aero-strike resulted from the impact of the explosion (figures 5.63, 5.64). Fragments of Boeing 777 show no traces of aero-impact.

There is significant deformation of the outer skin of the roof in the direction from outside to inside, exposing the contours of the structure. Also, there is detachment of the outer skin from the structure resulting from the detachment of rivet heads.

A large part of the outer surface of the roof (up to 5.2 m from the tip of the aircraft nose) shows signs of exposure to detonation products, manifested as small (1-3 mm) through-and-through holes, rashes of micro-craters and thermal oxidation (burns).

The density of holes on the roof and the size of the fragmentation field are two to four times greater than the density of holes and the size of the fragmentation field on similar Boeing 777 fragments.

Thus, the characteristics of the fragmentation field and the nature of the destruction and damage to the target's cockpit roof caused by explosion factors differ significantly from the characteristics of the fragmentation field and the nature of damage on the Boeing 777's fragments.

¹³ Through-and-through holes on the target aircraft's roof caused by preformed fragments are located on both the left and right sides of the roof, at a distance of up to ~ 7.2 m from the aircraft's nose tip.

5.1.4. Cockpit starboard

The appearance (from different angles) of damage done during the tests to the starboard side of the target aircraft's cockpit is shown in figures 5.79 through 5.82.



Figure 5.79 - Cockpit starboard side



Figure 5.80 - Cockpit starboard side near door R1 (bottom view)



Figure 5.81 - Cockpit starboard side near door R1. Thermal burn marks can be seen in the upper right corner of the photograph



Figure 5.82 - Cockpit starboard side

Examples of through-and-through holes and non-penetrating damage to the starboard side and cockpit floor (from different angles) are shown in figures 5.83 through 5.105.



Figure 5.83 - Exit holes and non-penetrating damage



Figure 5.84 - Exit holes and non-penetrating damage



Figure 5.85 - Exit holes and non-penetrating damage



Figure 5.86 - Exit hole



Figure 5.87 - Exit holes and non-penetrating damage



Figure 5.88 - Exit hole (left) and non-penetrating damage (right) close-up



Figure 5.89 - Exit holes and non-penetrating damage



Figure 5.90 - Exit holes



Figure 5.91 - Exit holes



Figure 5.92 - Exit holes



Figure 5.93 - Exit hole



Figure 5.94 - Exit holes and non-penetrating damage

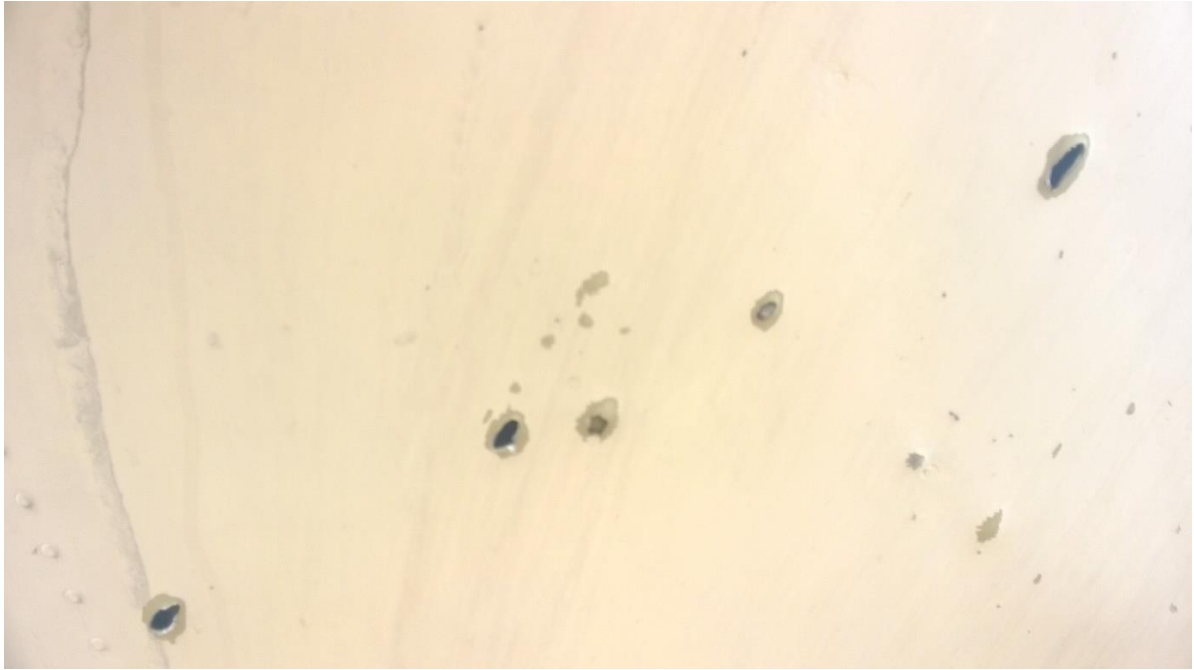


Figure 5.95 - Exit holes and non-penetrating damage



Figure 5.96 - Exit holes



Figure 5.97 - Exit holes and non-penetrating damage



Figure 5.98 - Exit holes and non-penetrating damage



Figure 5.99 - Exit holes and non-penetrating damage



Figure 5.100 - Exit holes and non-penetrating damage



Figure 5.101 - Exit holes and non-penetrating damage



Figure 5.102 - Exit holes and non-penetrating damage



Figure 5.103 - Exit holes and non-penetrating damage



Figure 5.104 - Exit holes in R1 door area



Figure 5.105 - Through-and-through hole in door R1 (inside view)

An analysis of the damage to the starboard side showed the following:

no damage to the outer skin or structure of the starboard has been identified;

the rear window is destroyed and there is fragmentation damage to the right direct-vision window in the direction from inside to outside;

more than 30 exit holes caused by preformed fragments of 9H314M warhead are observed on the starboard surface, the lower part of the roof and the bottom in the cockpit area (including the front right passenger door R1).

Part of the external surface of the starboard (near the roof) shows signs of exposure to explosion products in the form of thermal oxidation (burns), which differs significantly from the condition of the fragments of Boeing 777's starboard side.

Thus, the presence of fragmentation damage (exit holes) and marks of explosion products on the starboard side of the target creates a significant difference from the characteristics of damage to Boeing 777 fragments.

5.1.5. Damage to the left-hand engine simulator

Figure 5.106 includes photos showing the condition of Target No. 2 (left engine simulator) after the tests: the left photo is the front view, the right photo is the rear view.

front view

rear view



Figure 5.106 - Target No. 2 (left engine) after testing

The left engine simulator suffered no damage by preformed fragments.

Thus, when 9H314M warhead, which has been oriented under the conditions specified in the DSB Report materials, is detonated no damage is done to the left engine by preformed fragments.

5.2. Damage to the interior and structure of the cockpit

5.2.1. Damage to the interior of the cockpit

The damage done to the cockpit's interior during the tests is shown in figures 5.107 through 5.141.



Figure 5.107 - Appearance of the cockpit's interior on the port side of the target aircraft: before the tests (left) and after detonation of the 9H314M warhead (right)



Figure 5.108 - Cockpit after the tests (inside view)



Figure 5.109 - Cockpit after the tests (inside view)



Figure 5.110 - Through-and-through holes in the aircraft commander's safe
(on the port side of the cockpit)



Figure 5.111 - Cockpit after the tests (inside view)



Figure 5.112 - Decorative panel of the cockpit roof



Figure 5.113 – Exit holes in the instrumentation cabinet on the port side (view from inside the cockpit)



Figure 5.114 - Exit holes in the instrumentation cabinet on the port side (view from the cockpit)



Figure 5.115 - Damage to the flight engineer's control panel (starboard side of the cockpit)



Figure 5.116 - Through-and-through holes in the control panel (cockpit roof)



Figure 5.117 – Flight engineer's control panel
(ride side of the cockpit)



Figure 5.118 - Flight engineer's control panel (starboard)



Figure 5.119 - Cockpit floor, port side(near the aircraft commander's seat)

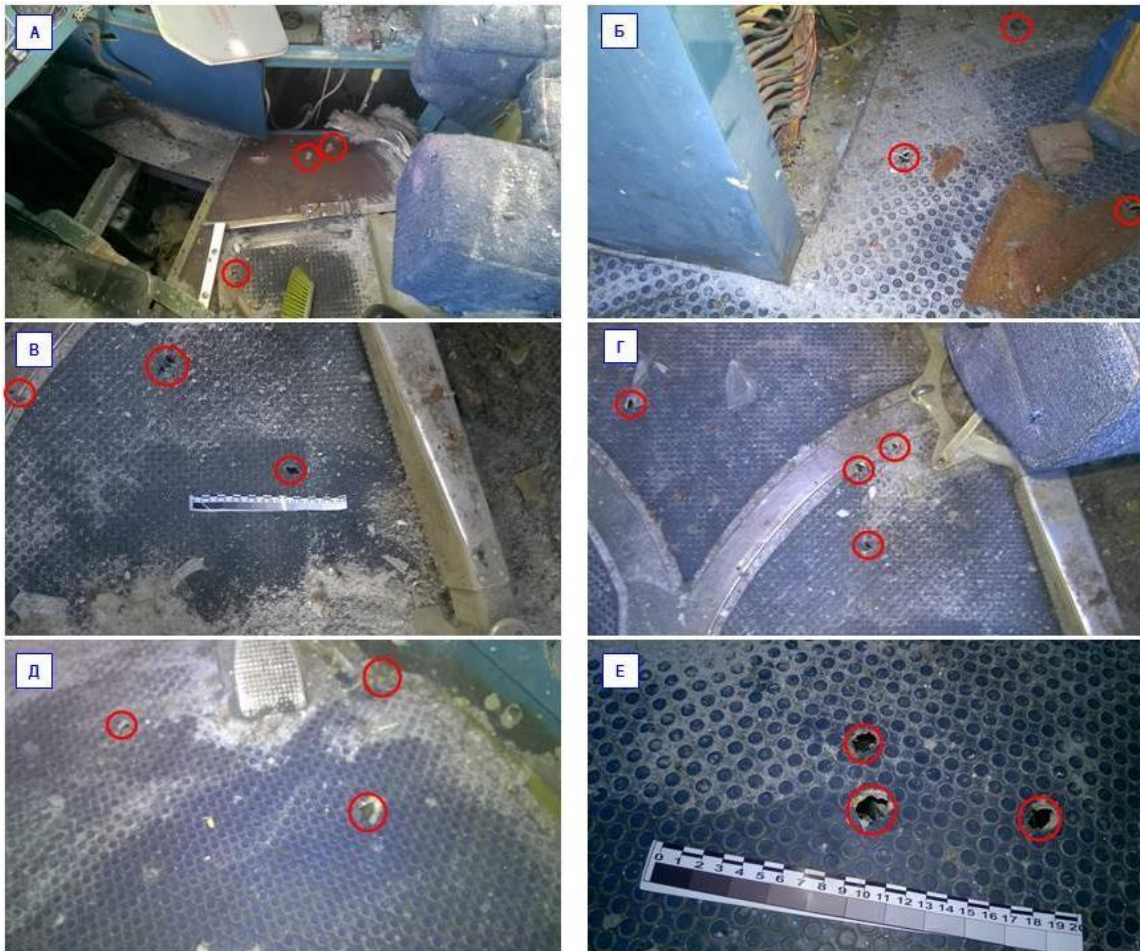


Figure 5.120 - Cockpit floor (central and right sections)

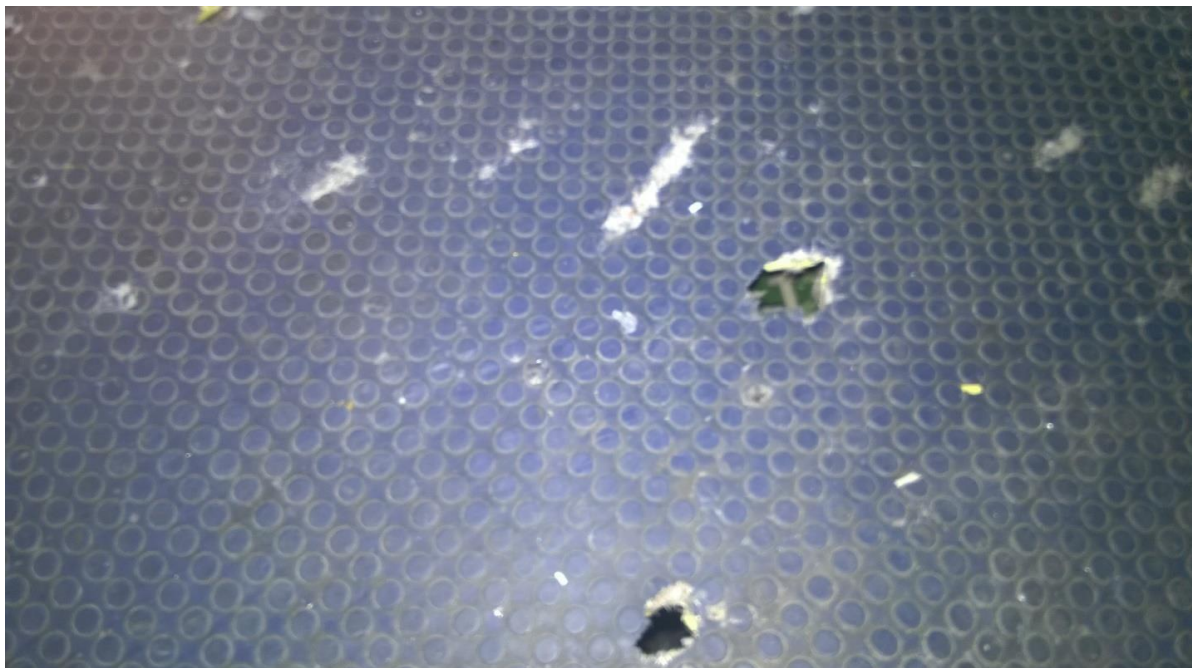


Figure 5.121 - Through-and-through holes in the cockpit floor



Figure 5.122 - Through-and-through holes in the cockpit floor (starboard)



Figure 5.123 - Through-and-through holes in the cockpit floor (starboard)



Figure 5.124 - Through-and-through holes in the cockpit floor (starboard)



Figure 5.125 - Through-and-through holes in the cockpit floor (central part of the cockpit)



Figure 5.126 - Through-and-through holes in the cockpit floor



Figure 5.127 - Cockpit floor in the aircraft commander's seat area



Figure 5.128 - Cockpit floor in the aircraft commander 's seat area



Figure 5.129 - Through-and-through holes in the cockpit floor in the aircraft commander 's seat area



Figure 5.130 - Through-and-through holes in the cockpit floor (bottom view)



Figure 5.131 - Through-and-through holes in the cockpit floor (bottom view)



Figure 5.132 - Through-and-through holes in the cockpit floor (bottom view)

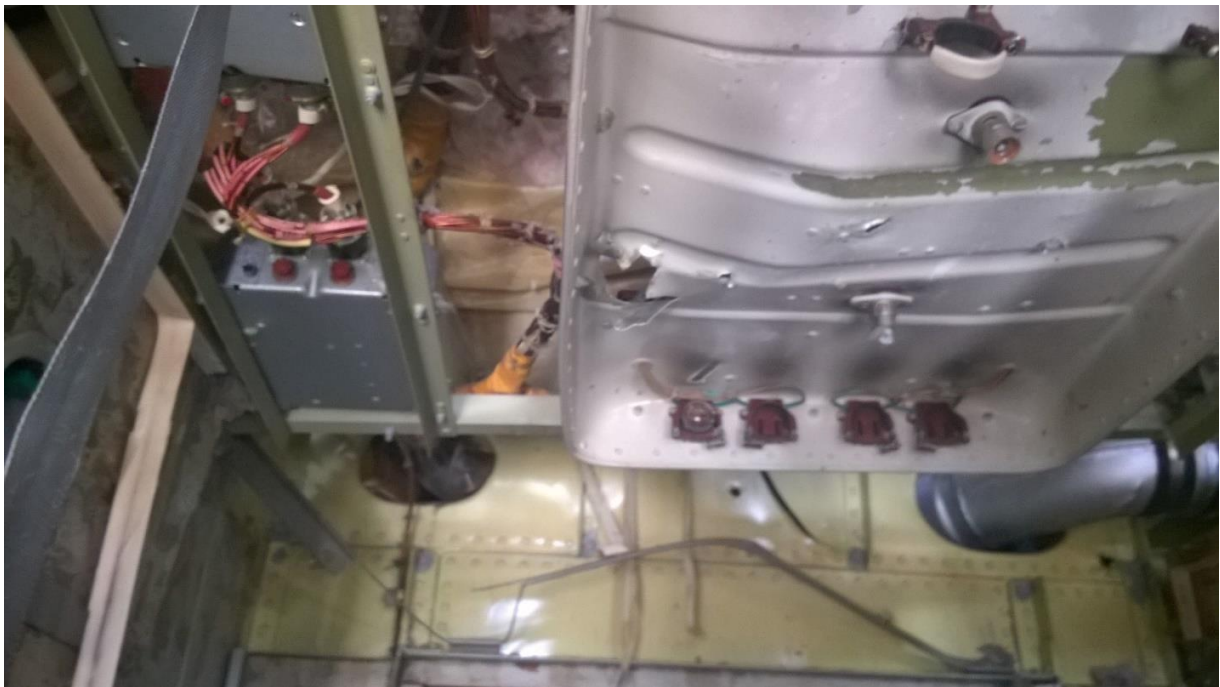


Figure 5.133 - Through-and-through holes in the floodlamp lighting (corridor behind the cockpit)

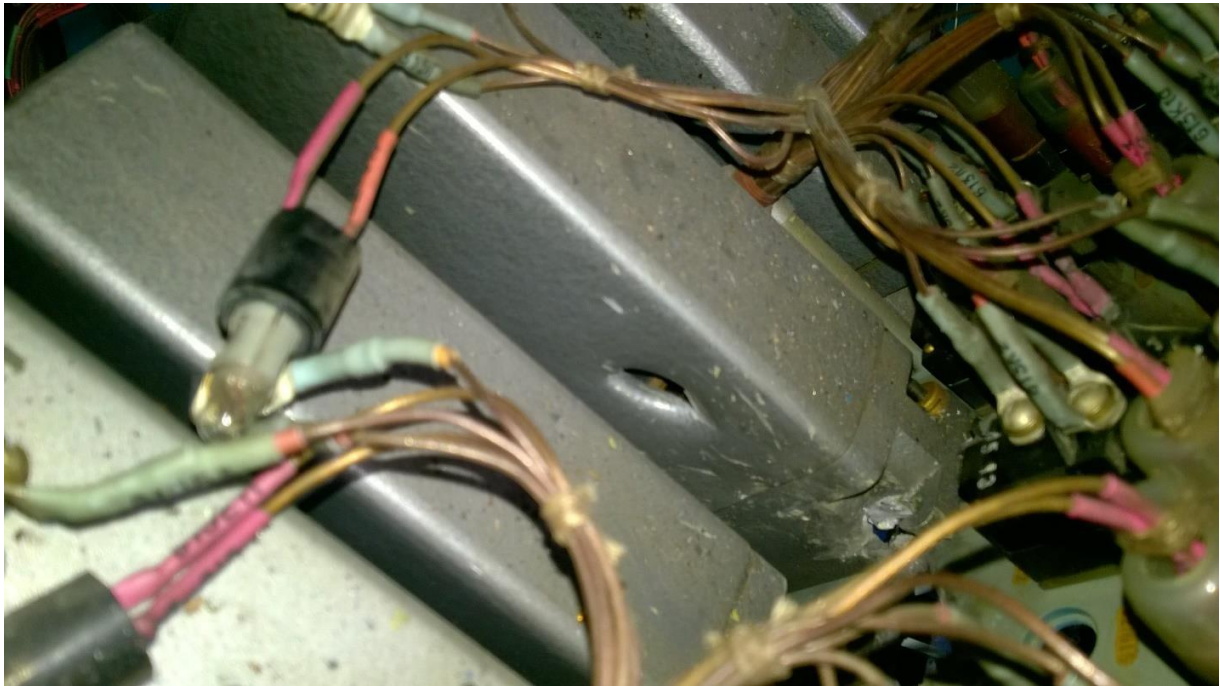


Figure 5.134 - Material-intensive components of avionics equipment in the cockpit



Figure 5.135 - Material-intensive components of avionics equipment in the cockpit



Figure 5.136 - Material-intensive components of the avionics equipment



Figure 5.137 - Material-intensive components of the avionics equipment. Instrumentation panel in the top section of the starboard (in the top right corner, there is an exit hole in the right section of the cockpit roof)



Figure 5.138 – Exit holes in the lower right section of the first passenger compartment (rear view)



Figure 5.139 - Through-and-through holes in toilet cladding panels (starboard)



Figure 5.140 - Characteristic butterfly-shaped holes in the fragments of the cockpit's interior

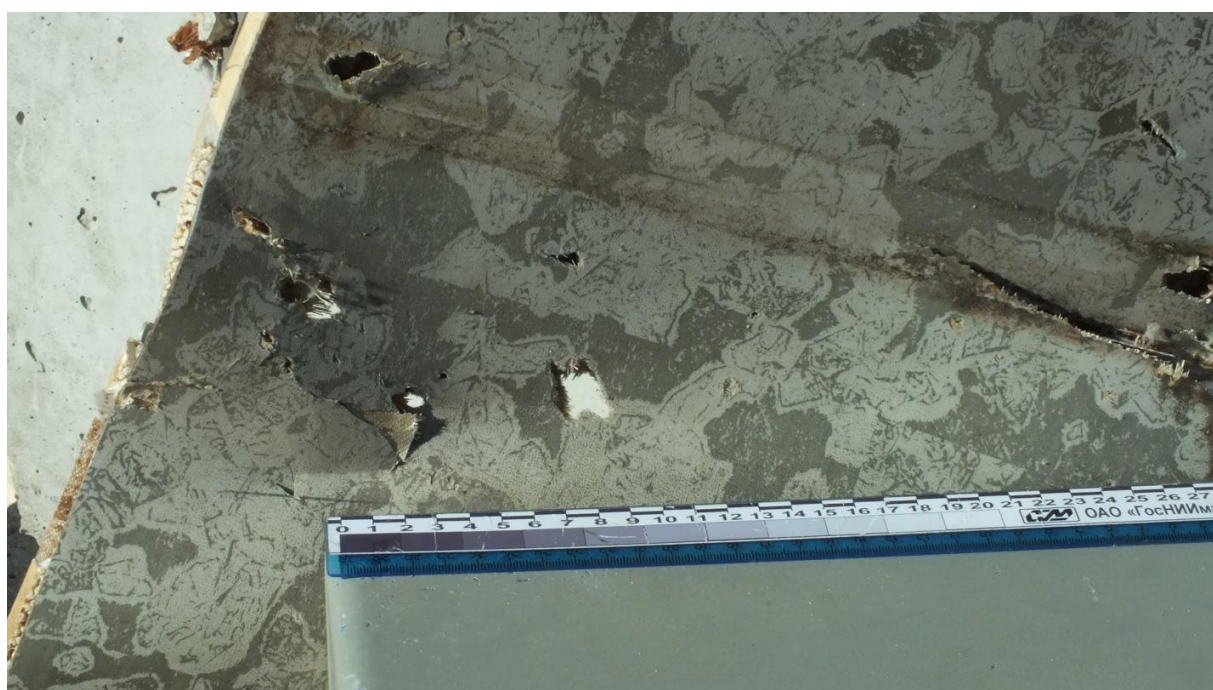


Figure 5.141 - Through-and-through holes in the galley wall

5.2.2. Damage to the cockpit structure

Examples of damage to the structural elements of the cockpit are shown in figures 5.142 through 5.152.

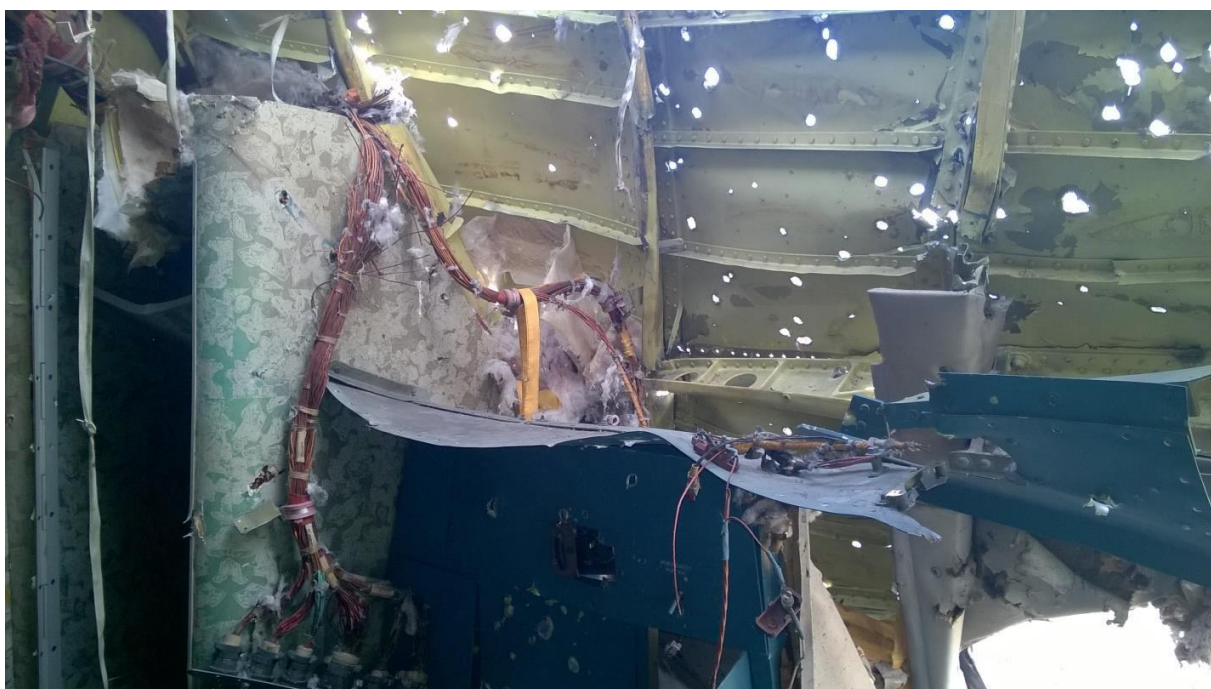


Figure 5.142 - Fragment of the port side with a broken frame



Figure 5.143 - Cockpit roof with through-and-through holes in stringers and signs of damage



Figure 5.144 - Through-and-through holes in a power kit element



Figure 5.145 - Through-and-through holes in a structural element of the airframe (stringer)



Figure 5.146 - Through-and-through holes in the roof and cockpit stringer (right side)



Figure 5.147 - Damage to stringers in the structure of the target aircraft's cockpit roof



Figure 5.148 - Through-and-through hole in L-shaped frame reinforcement on the left side of the cockpit



Figure 5.149 - Through-and-through hole in L-shaped frame reinforcement (port side of the cockpit)



Figure 5.150 – Destruction of a frame (top of the port side)



Figure 5.151 - Characteristic view of damage to frames on the left side of the cockpit (punctured L-shaped frame reinforcements). The direction of the motion of the projectiles is transverse to the aircraft structure. There are no through-and-through holes in the frames.



Figure 5.152 - Appearance of the port side frames

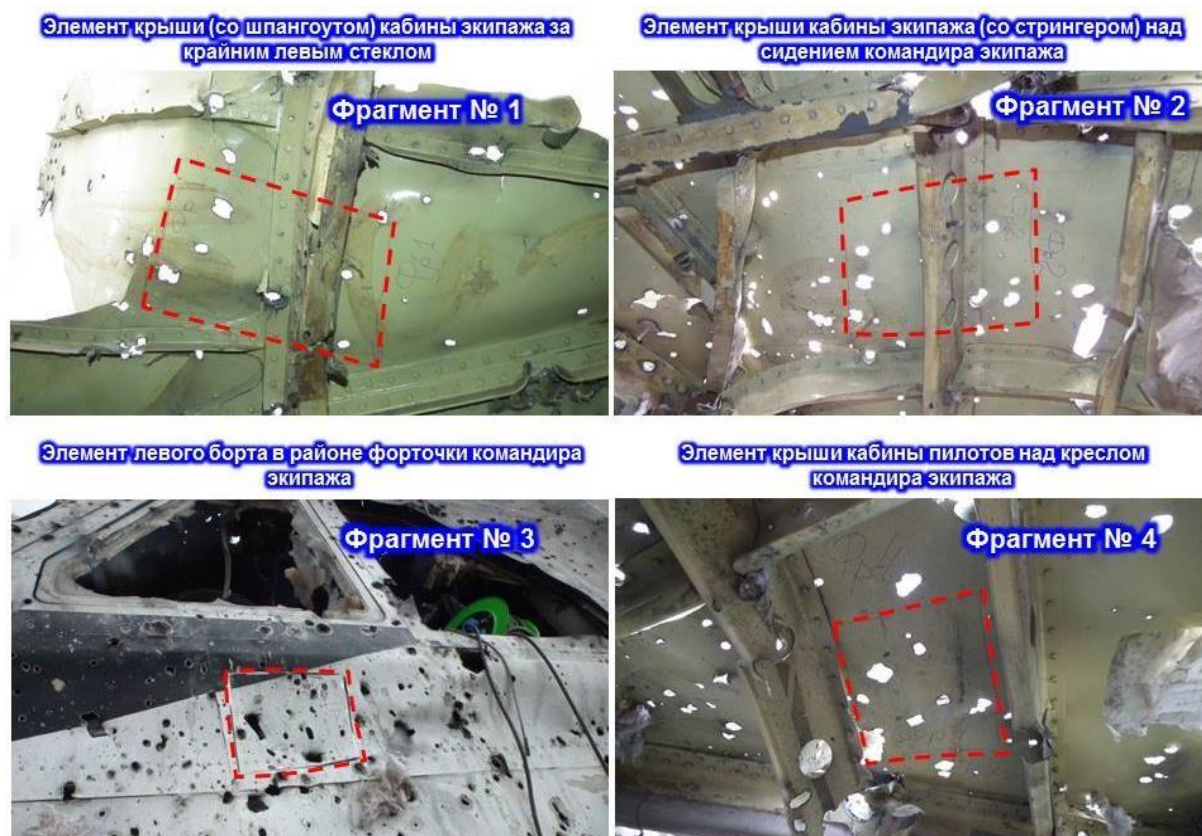
5.2.3. Damage to typical fragments of the outer skin and structure of the target aircraft's cockpit

Fragments of the outer skin of the target aircraft were recovered for examination.

A total of five fragments were recovered:

1. Fragment No. 1: element (with a frame) of the outer skin of the cockpit roof behind the outermost left window.
2. Fragment No. 2: element (with a stringer) of the outer skin of the cockpit roof above the aircraft commander's seat.
3. Fragment No. 3: element of the outer skin of the port side in the area of the aircraft commander's direct-vision window.
4. Fragment No. 4: element of the outer skin of the cockpit roof panel above the aircraft commander's seat.
5. Fragment No. 5: element of the outer skin of the port behind the aircraft commander's seat.

Figure 5.153 shows the location of fragments Nos. 1 through 4 before they were removed from the outer skin of the target aircraft.



Element of the cockpit roof (with a frame) behind the outermost left window

Fragment No. 1

Element of the cockpit roof (with a stringer) above the aircraft commander's seat

Fragment No. 2

Element of the port side in the area of the aircraft commander's direct-vision window

Fragment No. 3

Element of the cockpit roof above the aircraft commander's seat

Fragment No. 4

Figure 5.153 – Locations of fragments recovered, fragments Nos. 1-4

Fragment No. 5, a port side element behind the commander's seat, was also recovered. The fragment includes part of the port side skin panel and part of a transverse structural element (frame). A photograph of the fragment recovery location and its appearance are shown in figure 5.154.



Figure 5.154 - Fragment No. 5

In fragments No.1, No. 2, No. 4 and No. 5, characteristic butterfly-shaped through-and-through holes are clearly seen. They are left on the outer skin of the aircraft by bowtie-shaped ready-made projectiles of 9H314M 1-10.

Fragments No. 1 and No. 5 show the peculiarities of the damage to the transverse structural elements of the airframe, the frames. Fragment No. 2 demonstrates the peculiarities of the damage to longitudinal structural elements of the airframe (stringers). Fragments No. 3 and No. 4 show the peculiarities of the damage to the outer skin of the aircraft in the area of the glazing of the left side of the cockpit – there are no ricochets caused by ready-made projectiles.

Figures 5.155 through 5.158 contain photographs of a fragment of the outer skin of the cockpit roof (Fragment No. 1).



Figure 5.155 - Fragment No. 1 before extraction (inside view)



Figure 5.156 - Fragment No. 1 (close-up, inside view). Characteristic holes caused by preformed fragments of 9H314M 1-10 are seen on the inner surface of the skin.



Figure 5.157 - Fragment No. 1 extraction place (internal view)



Figure 5.158 - Fragment No. 1 after extraction
(close-up, inside view)

Figures 5.159 and 5.160 contain photographs of a detail of the outer skin of the cockpit with a stringer (Fragment No. 2).

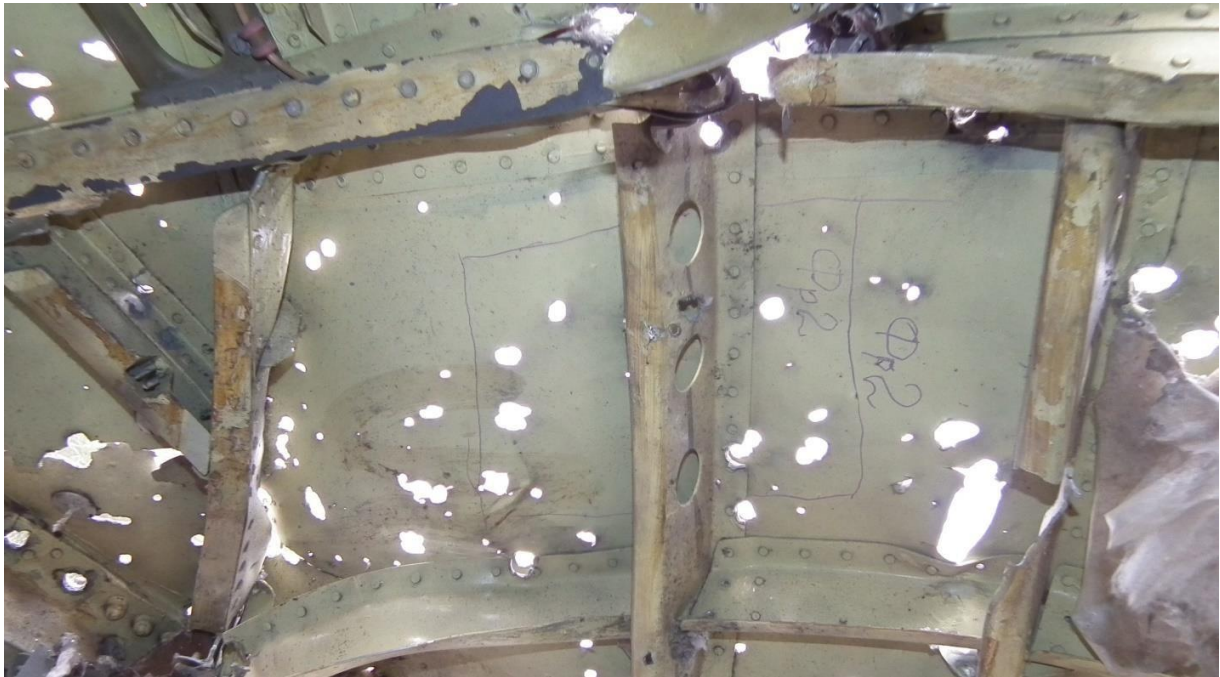


Figure 5.159 - Fragment No. 2 before extraction (inside view)



Figure 5.160 - Fragment No. 2 after extraction (inside view)

Figures 5.161 through 5.165 contain photos of a fragment of the outer skin of the left side of the cockpit (Fragment No. 3).



Figure 5.161 - Fragment No. 3 before extraction (external view)



Figure 5.162 - Extracting fragment No. 3



Figure 5.163 - Fragment No. 3 extraction place (external view)



Figure 5.164 - Fragment No. 3 after extraction (external view)



Figure 5.165 - Fragment No. 3 after extraction (internal view)

Figure 5.166 contains a photograph of a fragment of the outer skin of the cockpit roof (fragment No. 4) before extraction.



Figure 5.166 - Fragment No. 4 before extraction (internal view)



Figure 5.167 - Place of extraction of fragments No. 2 and No. 4 (internal view)

Figures 5.168 through 5.176 contain photographs of a fragment of the outer skin of the port side of the cockpit (Fragment No. 5).



Figure 5.168 - Fragment No. 5 before extraction (internal view)



Figure 5.169 - Fragment No. 5 before extraction (internal view). The blue bar shows the trajectory of entry of a projectile of 9H413M 1-10, which, after piercing the outer skin, penetrated the L-shaped reinforcement of a frame



Figure 5.170 - Fragment No. 5 after extraction (external view)



Figure 5.171 - Fragment No. 5 after extraction (internal view)

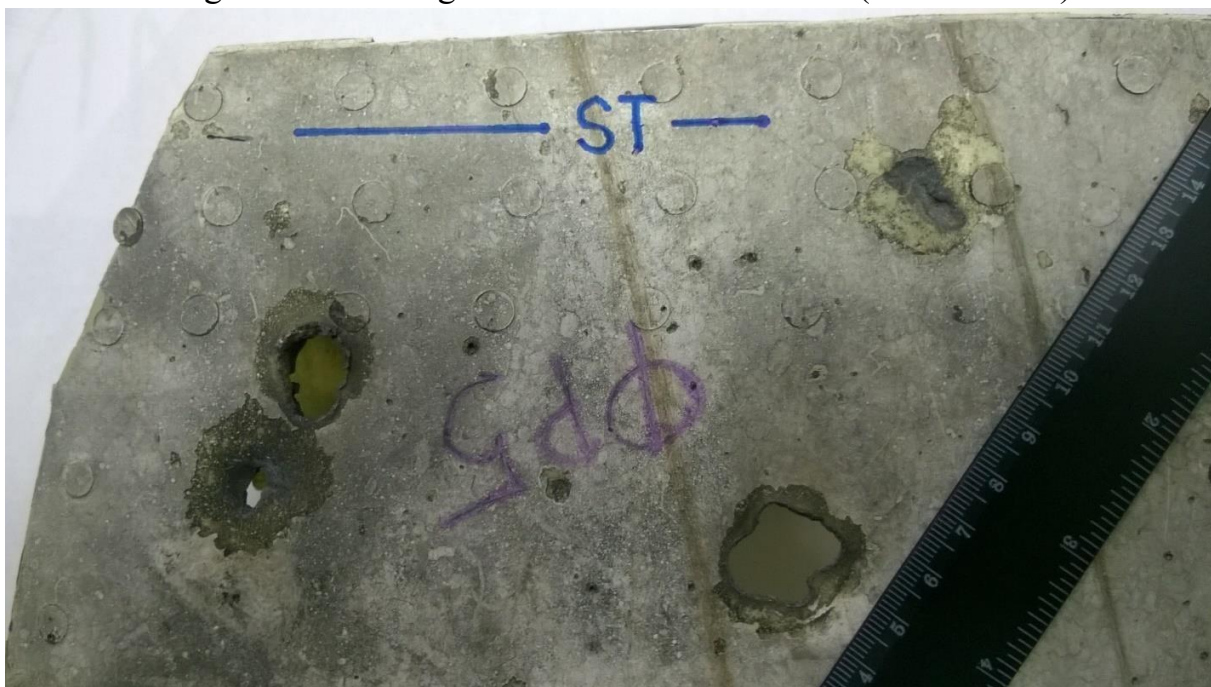


Figure 5.172 - Condition of the outer skin of the port with traces of blast effects (micro-craters, thermal influence) and penetrating and non-penetrating damage caused by ready-made projectiles and missile hull fragments

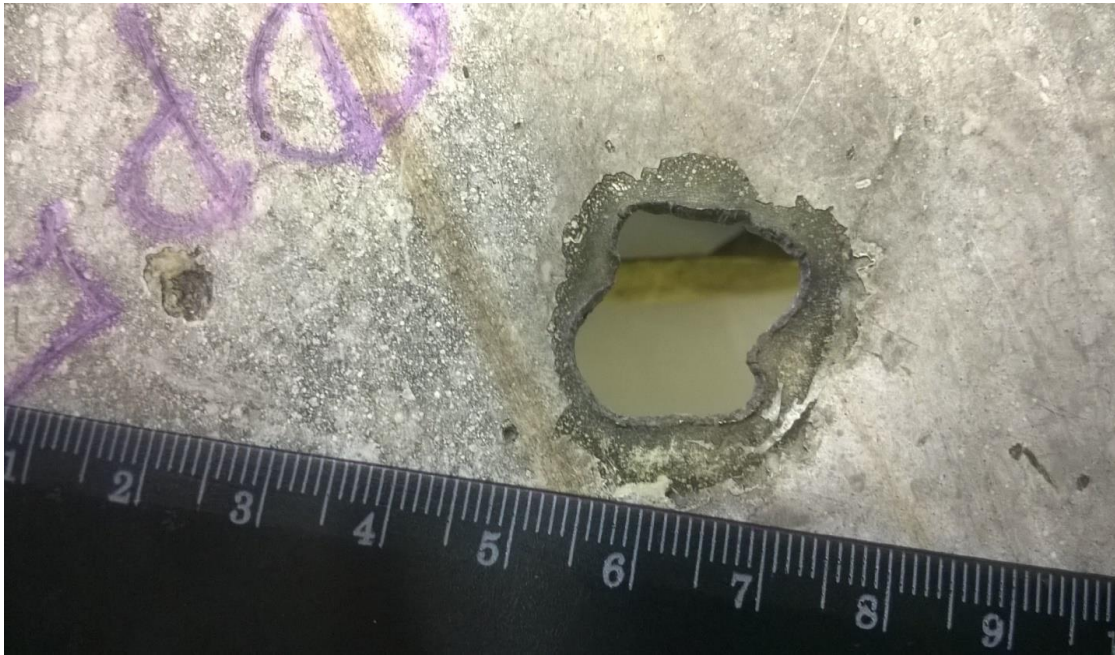


Figure 5.173 - Characteristic butterfly-shaped hole in the outer skin of the port caused by a bowtie shaped preformed fragment of 9H314M 1-10 (Fragment No. 5, outside view)



Figure 5.174 - Characteristic butterfly-shaped hole in the outer skin of the port caused by a bowtie shaped preformed fragment of 9H314M 1-10 (inside view)

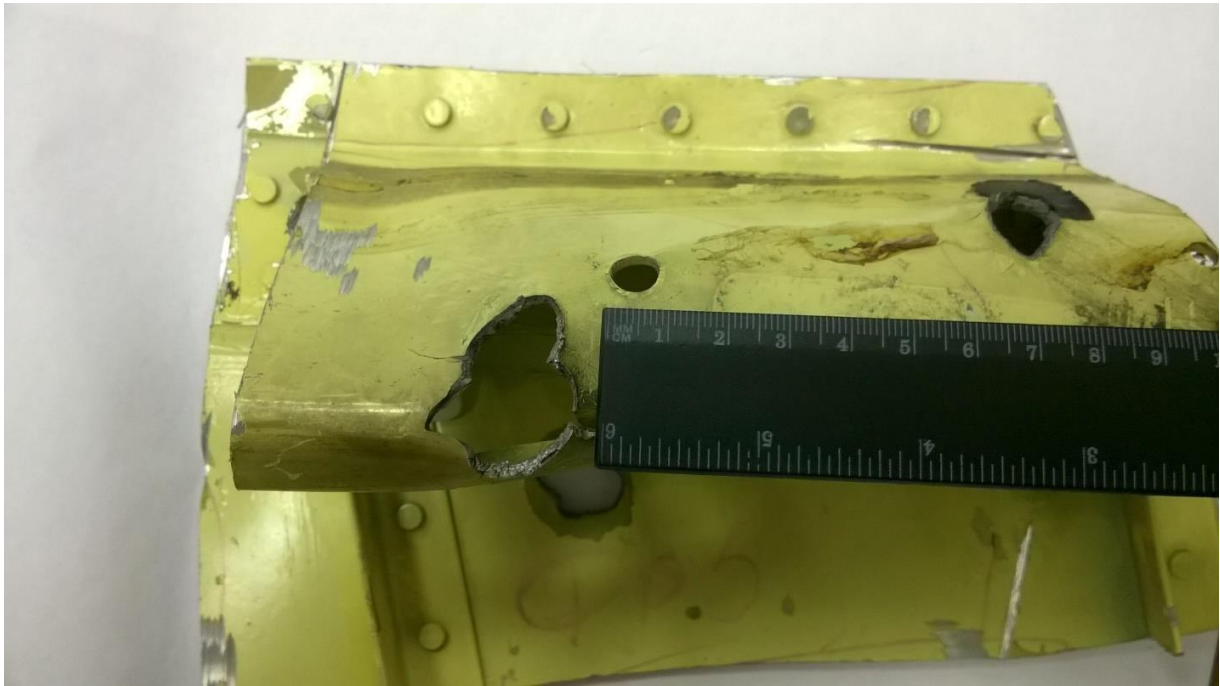


Figure 5.175 - Through-and-through holes in the frame in fragment No. 5

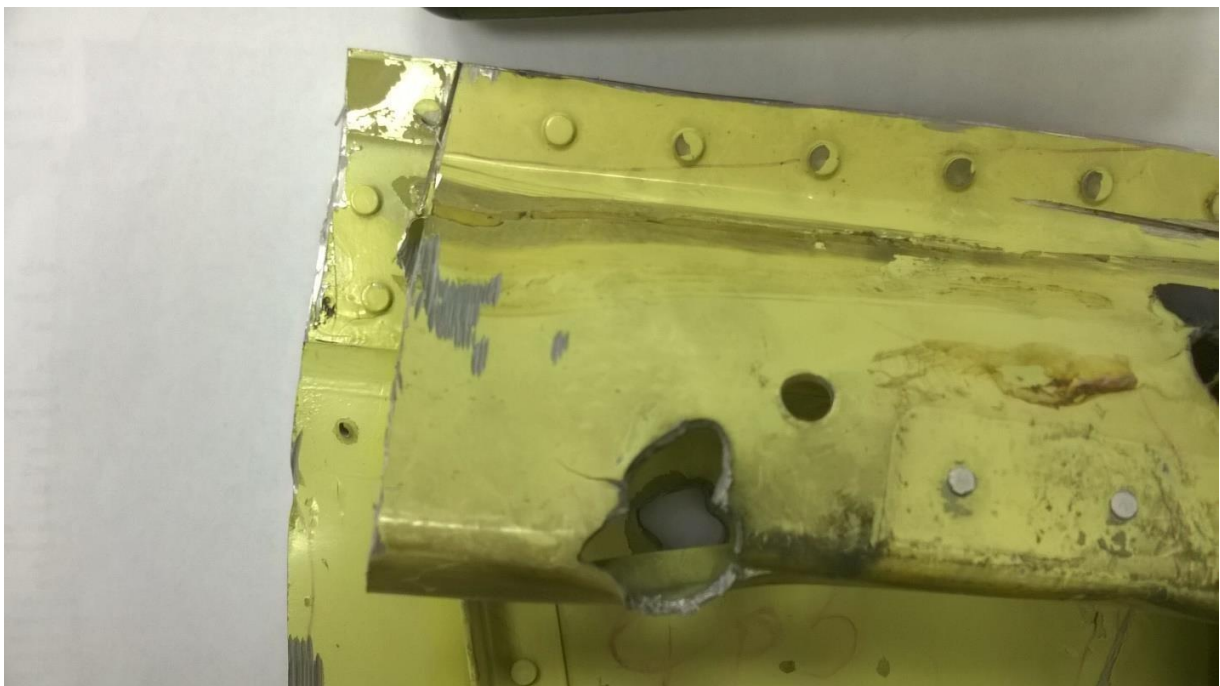


Figure 5.176 - Alignment of through-and-through holes in the frame and outer skin of fragment No. 5

Figures 5.177 and 5.178 contain photographs of the fragment extraction locations. Figure 5.177 shows the inside view and Figure 5.178 shows the outside view.



Figure 5.177 - Locations of extracted fragments No. 1, No. 2, No. 4 and No. 5 (inside view)



Figure 5.178 - Locations of extracted fragments (external view)

An analysis of damage to the interior and structural elements showed that elements of the interior of the cockpit, kitchen, lavatory and forward part of the first passenger cabin had multiple fragmentation damage, including characteristic "butterfly"-shaped holes.

The internal components of the cockpit and the forward part of the fuselage are destroyed and deformed by the effects of the explosion.

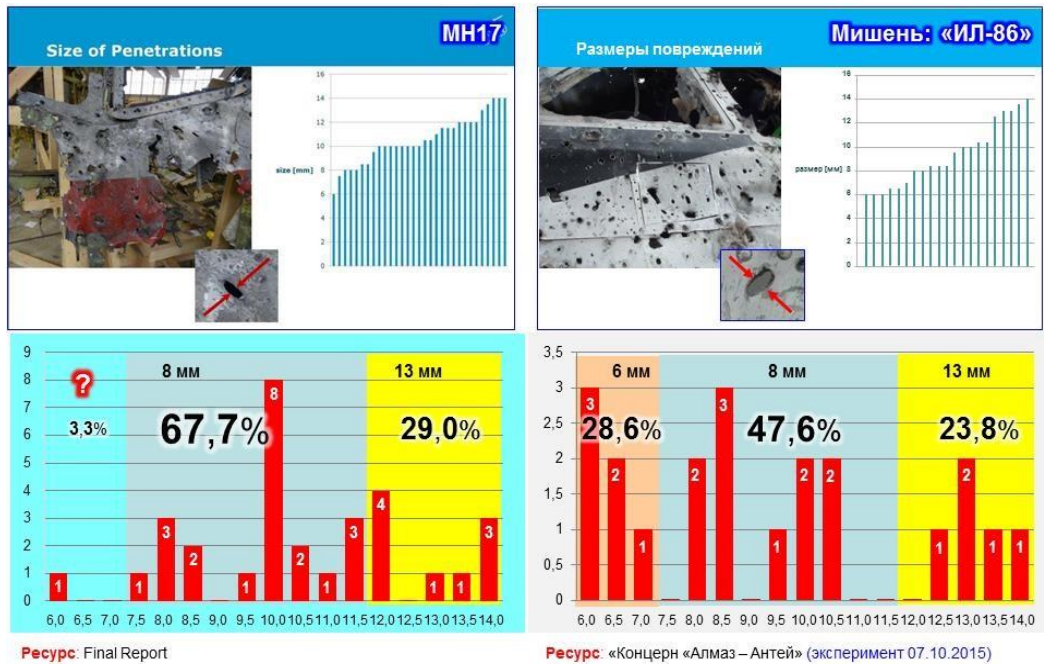
The fragmentation damage to the structural elements is mainly concentrated in the longitudinal elements, the stringers. With regard to the frames, the holes are mostly found only on the L-shaped reinforcements of the frames.

The pattern of the fragmentation damage distribution and the shape of the holes in elements of the interior and structural elements of the cockpit differ significantly from the characteristics of damage to the corresponding structural elements of the Boeing 777.

5.3. Cross-sectional dimensions of holes on the outer skin of the target aircraft caused by preformed fragments

The DSB Report (figure 14, Appendix X) contains statistical data on the cross-sectional dimensions of holes left by projectiles in a fragment of the outer skin of the aircraft Boeing 777.

The Dutch experts performed measurements in relation to one of the port side fragments and measured 31 holes. Similar measurements were carried out on a fragment of the outer skin of the target aircraft (in the area of fragment No. 3), which has similar distribution in the aircraft structure. The cross-sectional dimensions of the entry holes and the results of their analysis are shown in figure 5.179.



MH17

Target: IL-86

Figure 5.179 - Cross-sectional dimensions of entry holes on the outside skin of the port side

The statistical data from the DSB Report on the cross-sectional dimensions of the holes (figure 5.179 top left) were put in an analyzable form and presented as a histogram (figure 5.179 bottom left).

The results of the analysis showed that the cross-sectional size of the overwhelming number of holes on the outer surface of the fragment (21 out of 31, which makes up 67.7 %) is within the range of 7.5 to 11.5 mm.

The size of the nine holes (29.0 %) is within the range of 12.0 to 14.0 mm. And only one hole (3.3 %) has a cross-sectional size of about 6 mm.

Figure 5.179 (to the right) shows the results of measurements of the cross-sectional dimensions of the holes taken during the experiment (histogram in the lower right part of figure 5.179). The cross-sectional size of most of the holes (10 out of 21, which makes up 47.6 %) is within the range of 7.5 to 11.5 mm, which corresponds to the lightweight 9H314M 1-9 of the 9H314M warhead. Six holes (28.6 %) have a cross-sectional size of 6 to 7 mm and five holes (23.8 %) have dimensions between

12 and 14 mm, corresponding to the heavyweight projectiles 9H314M 1-10 of the 9H314M warhead.

A comparative analysis of the distribution of the cross-sectional dimensions of the preformed fragments (according to DSB data and data obtained during the experiment) allows a conclusion that the cross-sectional dimensions of the entry holes in the outer skin of the Boeing 777 do not correspond to the ratio between preformed fragments in the 9H314M warhead, which contains three different fractions of preformed fragments. This is evidenced by the number of holes (~ 68 %) the dimensions of which are within the range of 7.5 to 11.5 mm and by almost complete absence of holes with cross-sectional dimensions of ~ 6 mm.¹⁴

Thus, a comparative analysis of the cross-sectional dimensions of the holes caused by preformed fragments indicates that the fragmentation damage to the Boeing 777 structure could not have been caused by preformed fragments of the 9H314M warhead.

5.4. Conclusions based on the analysis of the exterior of the target after detonation of the 9H314M warhead

Thus, the analysis of the exterior of the target after the detonation of the 9H314M warhead and the examination of the nature of destruction and damage to the target established that the penetration damage to the target is significantly different from the penetration damage to the Boeing 777 aircraft fragments.

The main differences are related to: the size and density of the fragmentation field; the number and shape of penetration holes; the percentage ratio between cross-sectional dimensions of the holes; and the size and nature of the destruction and damage caused by blast factors.

¹⁴ The DSB materials (Appendix X) refer to one hole with dimensions of about 6 mm. Such a hole could be created when a projectile approached the aircraft with its lateral edge facing the obstacle (the thickness of the lateral edge being ~ 5-6 mm).

6. Characteristic holes caused by 9H314M 1-10 preformed fragments

6.1. Peculiarities of fragmentation damage to the outer skin of the target

One of the main peculiarities of the damage to the outer skin of the target aircraft distinguishing it from damage to the Boeing 777 is the presence of multiple through-and-through holes on the port side and the cockpit roof, which have a characteristic butterfly-shape.

Examples of such penetrations are shown in figures 6.1 through 6.20.



Figure 6.1 - Port side and left side of the cockpit roof of IL-86 target aircraft

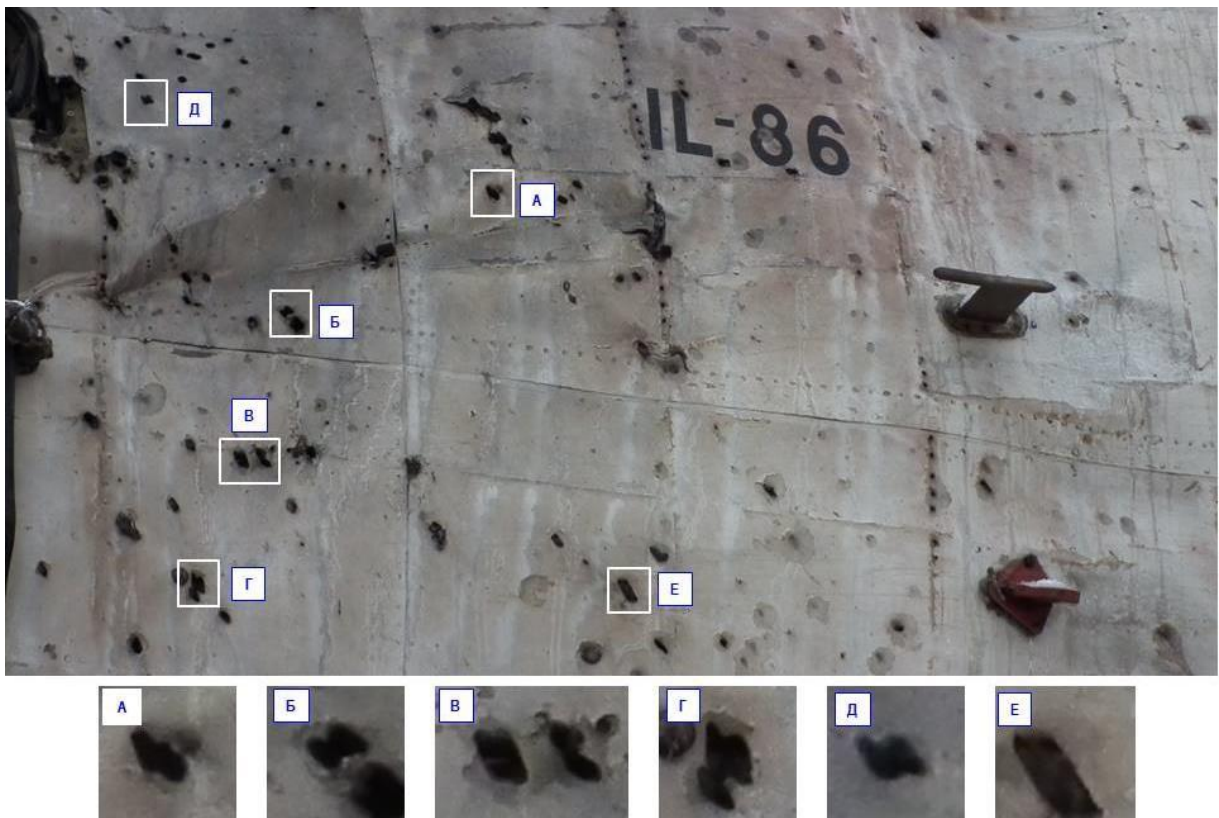


Figure 6.2 - Port side of the cockpit



Figure 6.3 - Port side of the cockpit (inside view)



Figure 6.4 - Left-hand side of cockpit roof



Figure 6.5 - Cockpit roof



Figure 6.6 - Fragment of the upper section of the port behind the aircraft commander's seat



Figure 6.7 - Appearance of a characteristic butterfly-shaped hole in a fragment of the cockpit roof (external view)



Figure 6.8 - Fragment of the left-hand side of the cockpit roof (inside view)



Figure 6.9 - Appearance of characteristic butterfly-shaped holes in a fragment of the cockpit roof (external view)



Figure 6.10 - Fragment of the port side



Figure 6.11 - Fragments of the port side and the cockpit roof

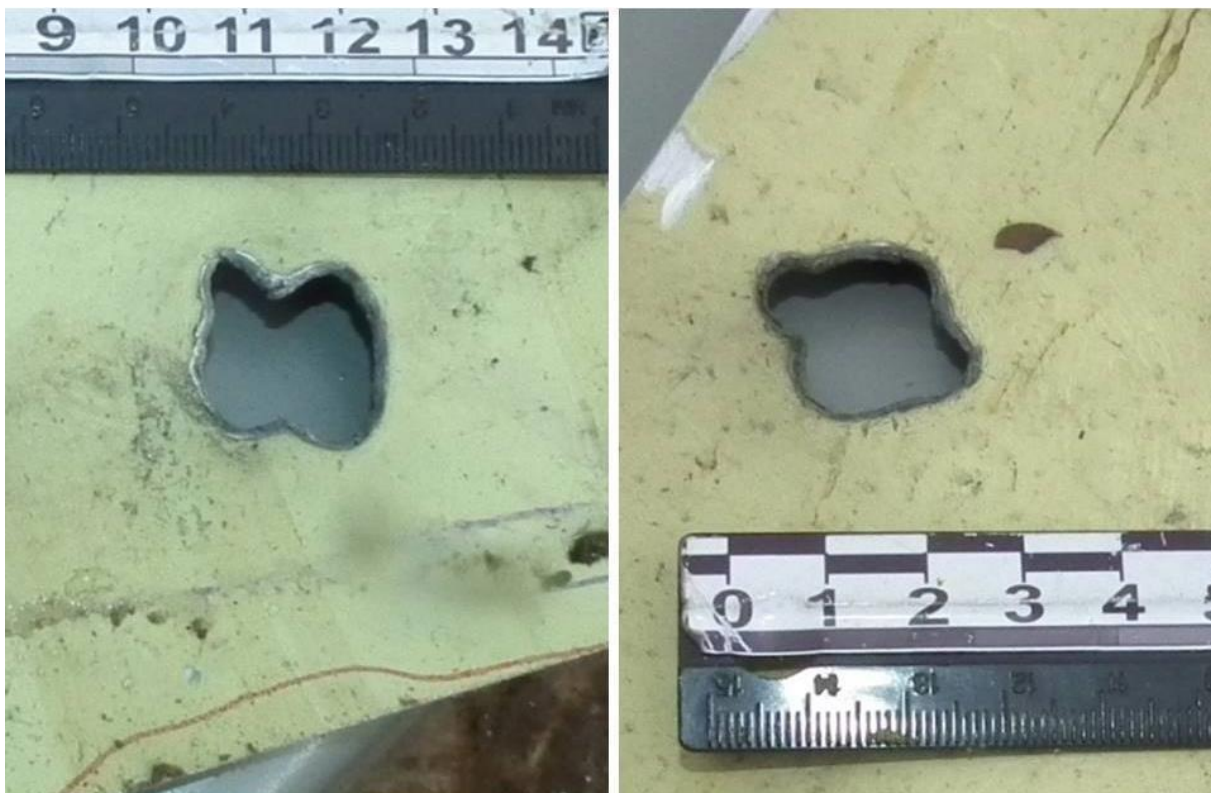


Figure 6.12 - Appearance of characteristic butterfly-shaped holes in the outer skin of the target aircraft (inside view)



Figure 6.13 - Appearance of a characteristic butterfly-shaped hole in the outer skin of the target aircraft (external view)

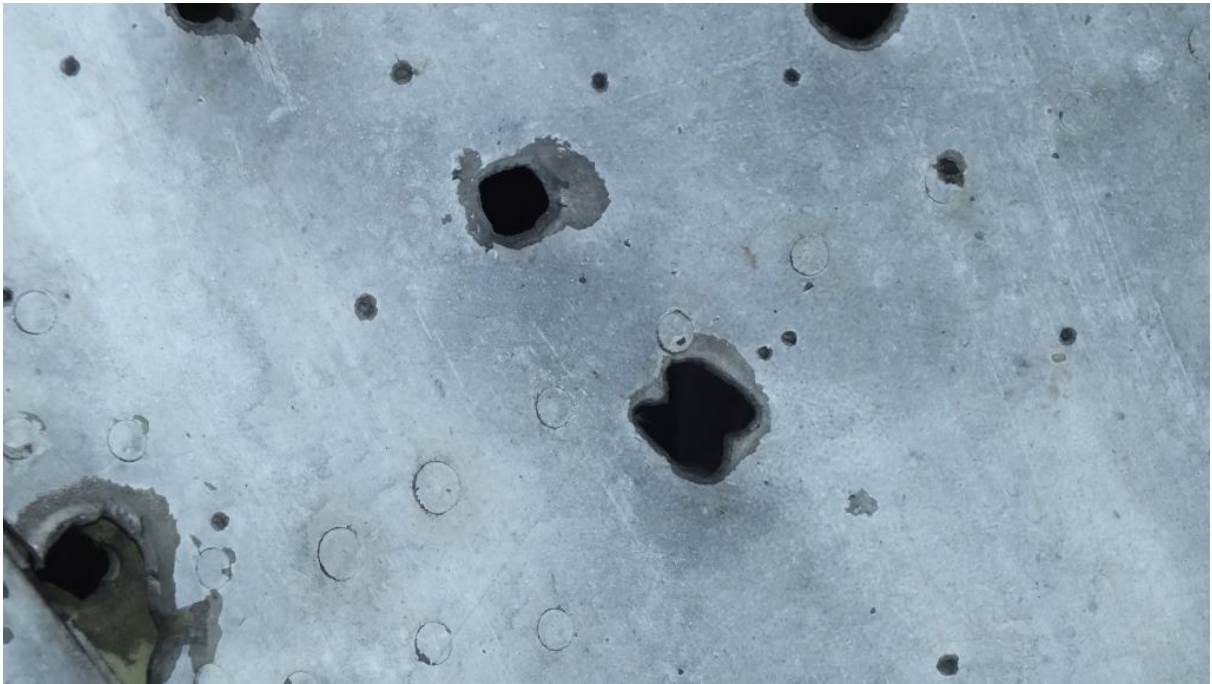


Figure 6.14 - Skin of the port side (close-up)



Figure 6.15 - Skin of the port side (close-up)



Figure 6.16 - Fragment of the outer skin above the aircraft commander's window



Figure 6.17 - Characteristic butterfly-shaped hole in the outer skin of the port hull caused by a preformed fragment 9H314M 1-10 (inside view)



Figure 6.18 - Fragment of the left-hand side of the cockpit roof



Figure 6.19 - Skin of the upper section of the port side (close-up)



Figure 6.20 - Characteristic butterfly-shaped penetration

The through-and-through holes which have a characteristic "butterfly" appearance were created by projectiles of 9H314M 1-10 fractions which initially had "bowtie" shape.

There are dozens of such through-and-through holes with a distinct 'butterfly' appearance on fragments of the outer skin of the IL-86 target aircraft. No characteristic butterfly-shaped penetrations were found on the fragments of the structure of the Boeing 777 examined by the Almaz-Antey's specialists at the deposition site or in photographs from open sources.

6.2. Supplementary experiment in a shield target layout

In order to evaluate the shape of the holes created by the interaction of preformed fragments of the 9H314M warhead with mutually spaced obstacles, an additional experiment was conducted in a shield target layout simulating other warhead detonation conditions (approach angles and distances from the point of detonation).

A photo report of the field experiment in the shield target layout is described in Appendix A.

6.2.1. Conditions for the supplementary experiment

In order to conduct testing at ground static conditions, a shield target layout was developed to simulate the contours of a Boeing 777 aircraft. The the target layout is schematically shown in figures 6.21 and 6.22.

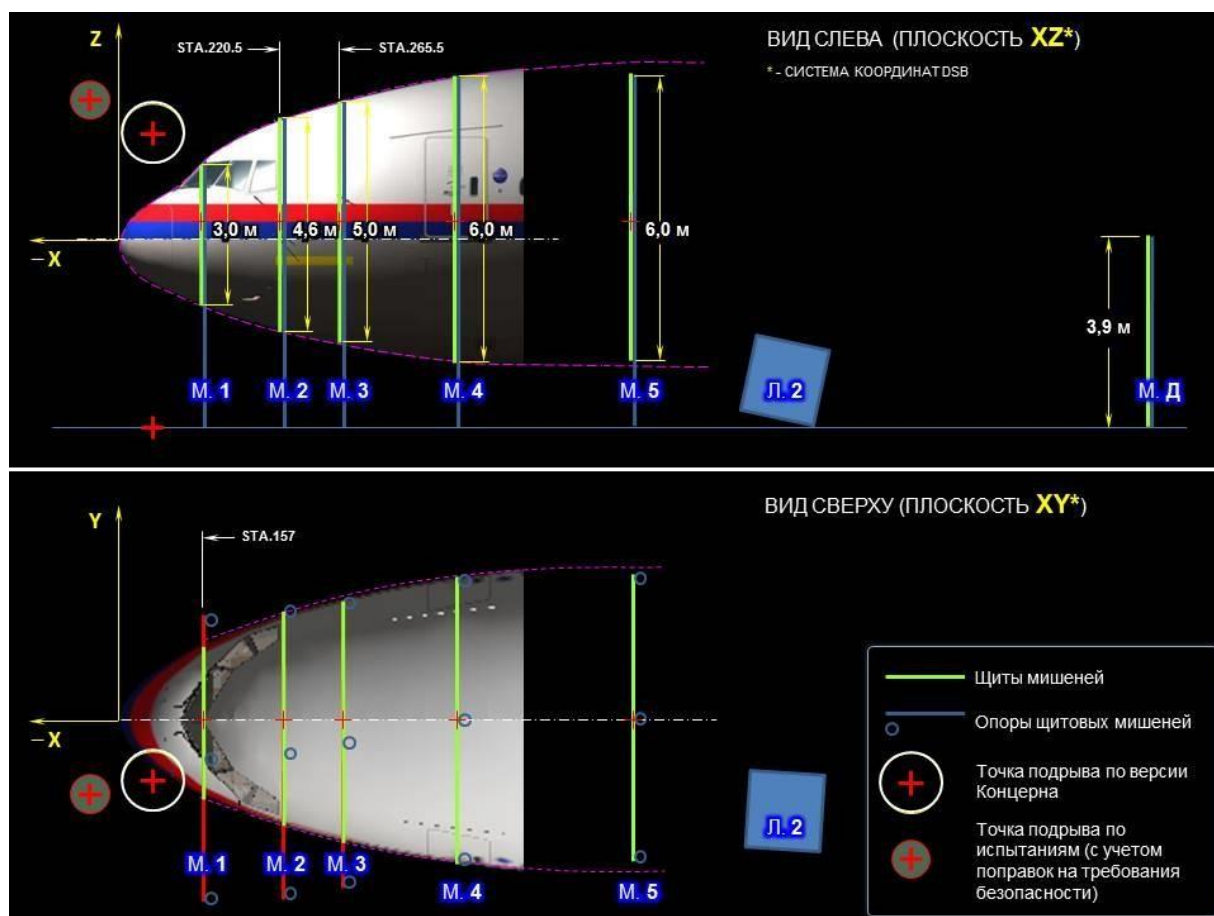


Figure 6.21 - Schematic diagram of shield target layout

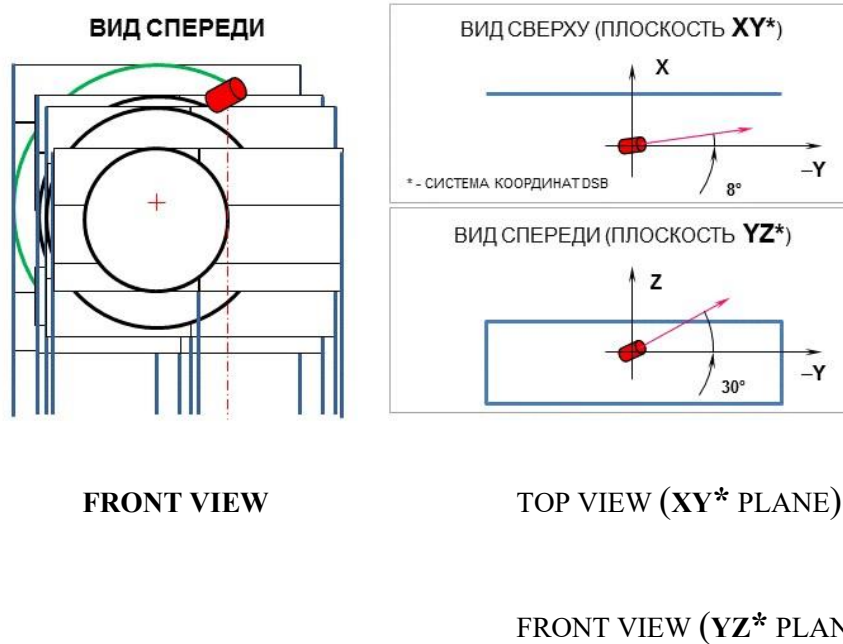


Figure 6.22 - Layout of the 9H314M warhead in the shield target layout

The 9H314M warhead (in the compartment hull) was mounted on a horizontal wooden table stand with a height of~ 6.83 m oriented in the horizontal plane at an angle of 8 degrees to the shield target layout. The orientation of the warhead in the vertical plane was provided by the support mounted at an angle of 30 degrees from the ground.¹⁵ The shield target layout prepared for testing¹⁶ is shown in figure 6.23.

¹⁵ Subject to compensatory corrections for testing at ground static conditions - corrections for the dynamics of the missile and aircraft at the rendezvous point.

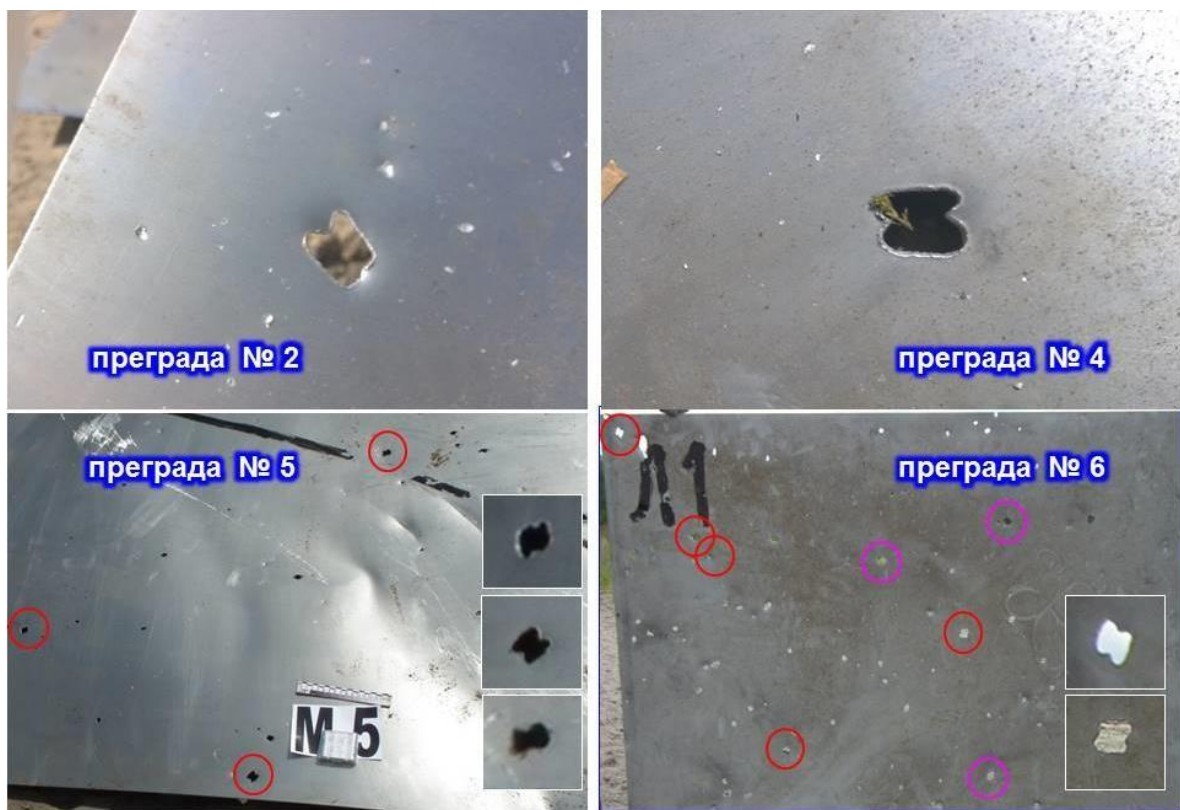
¹⁶ Refer to section 1 of Appendix A for procedures used for mounting the target layout..



Figure 6.23 - Target layout in the compartment hull prior to 9H314M warhead testing

6.2.2. Results of the supplementary experiment in the shield target layout

The test results show that the preformed fragments of 9H314M 1-10 warhead leave distinctive butterfly-shaped holes not only on the first obstacle in the shield target layout, but also on all subsequent obstacles. Figure 6.24 shows examples of butterfly-shaped holes left on mutually spaced obstacles in the shield target layout: obstacles Nos. 2, 4 and 5 (shields simulating the contour of the aircraft) and obstacle No. 6 - the outer layer of trap No. 1.



obstacle No. 2

obstacle No. 2

obstacle No. 5

obstacle No. 6

Figure 6.24 - Characteristic butterfly-shaped penetrations on different mutually spaced obstacles in the shield target layout

These characteristic penetrations are not random and are present on various sheets of shield targets. Examples of the peculiarities of the appearance of fragmentation damage on sheets of shield targets are shown in figures 6.25 through 6.33.

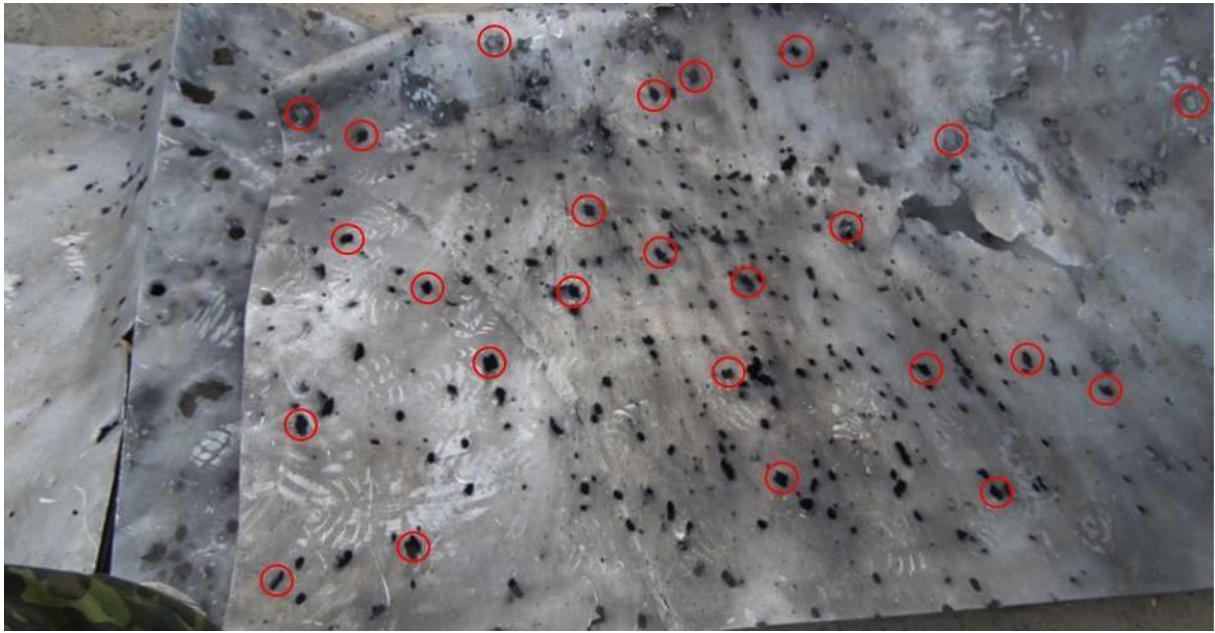


Figure 6.25 - Overall view of target No. 1.1

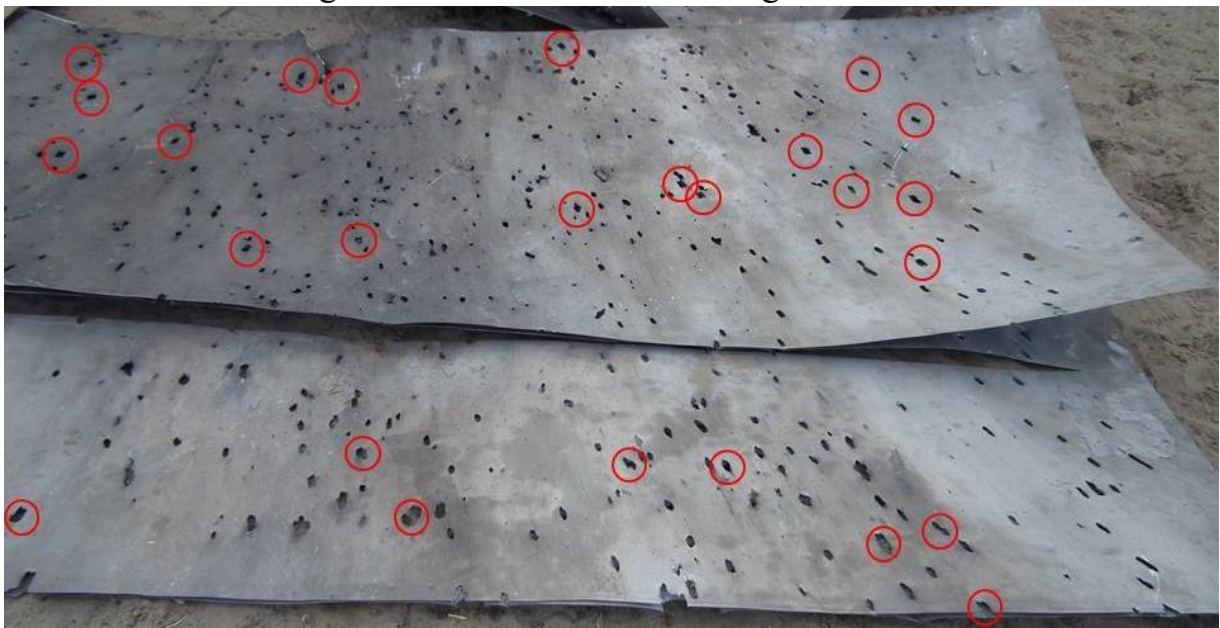


Figure 6.26 - Overall view of target No. 1.3 (top view) and target No. 1.5 (bottom view)



Figure 6.27 - Fragments of target No. 1.1



Figure 6.28 - Fragments of target No. 1.3



Figure 6.29 - Fragments of target No. 1.3

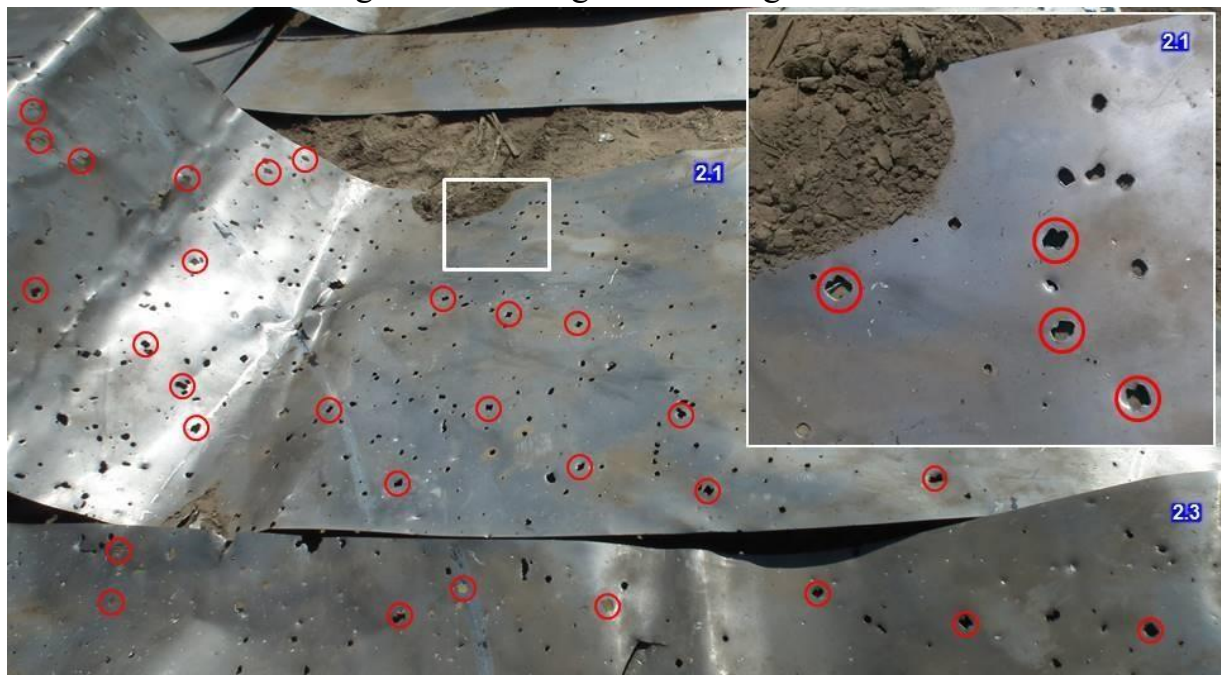


Figure 6.30 - Target No. 2



Figure 6.31 - Fragment of target No. 2.3



Figure 6.32 - Fragment of target No. 2.5



Figure 6.33 - Examples of holes on targets No. 3 and No. 4

6.3. Conclusions on the peculiarities of fragmentation damage to the outer skin

An analysis of the results of two experiments conducted under different conditions of interaction between the preformed fragments and the obstacles (angles of approach to targets, distance from the detonation point) as a result of a 9H314M type warhead detonation allow an unequivocal conclusion that the characteristic butterfly-shaped holes in the outer skin sheets are not isolated or accidental.

Thus, the absence of distinctive butterfly-shaped holes in the fragments of the Boeing 777 does not support the conclusions of the DSB Report that it was hit by a missile equipped with the 9H314M warhead.

7. Analysis of the mechanical (penetration) capability of 9H314M warhead's preformed fragments

As a result of the experiment, an analysis of the mechanical (penetration) capability of preformed fragments of 9M38M1 missile warhead 9H314M was carried out.

Special sensors located on the windscreen and in the aircraft commander's seat were used to determine the maximum velocities of the preformed fragments impacting the left side of the target's cockpit. The appearance of the sensors before the experiment is shown in figure 7.1.



Figure 7.1 - Location of velocity sensors

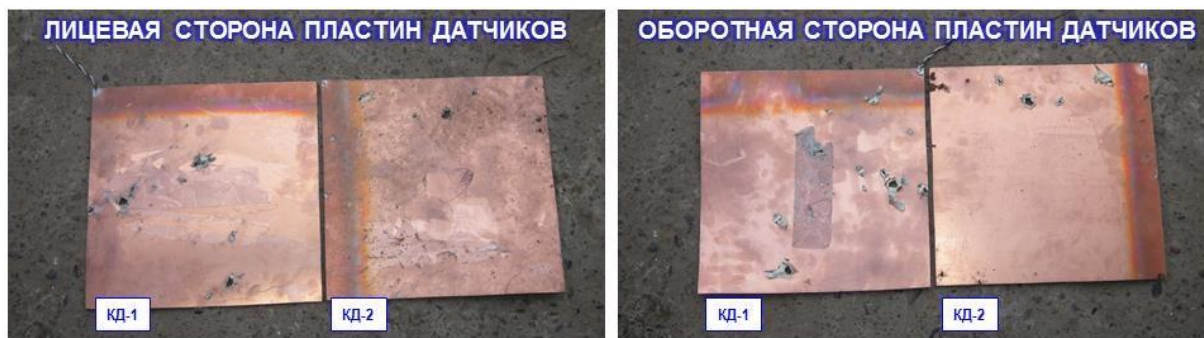
Fig. 7.1A shows a sensor located on the windscreen of the aircraft commander. Figure 7.1B shows two sensors ("input" 1B and "output" 2B) located in the seat of the aircraft commander.

Based on the data obtained from the sensor plates (1.5 mm thick double-sided foiled glass textolite), the maximum velocity of the leading preformed fragments was determined to be as follows:

MVS ¹⁷ windscreen, m/s	2 522
"input" MVS-1 of the crew commander, m/s	1 050
"output" MVS-2 of the crew commander's seat, m/s	813

The sensor plate from the windscreen did not survive the experiment (was completely destroyed), while the appearance of the sensor plates of MVS-1 and MVS-2 from the aircraft commander's seat is shown in figure 7.2.

¹⁷ MVS – monitoring velocity sensor.

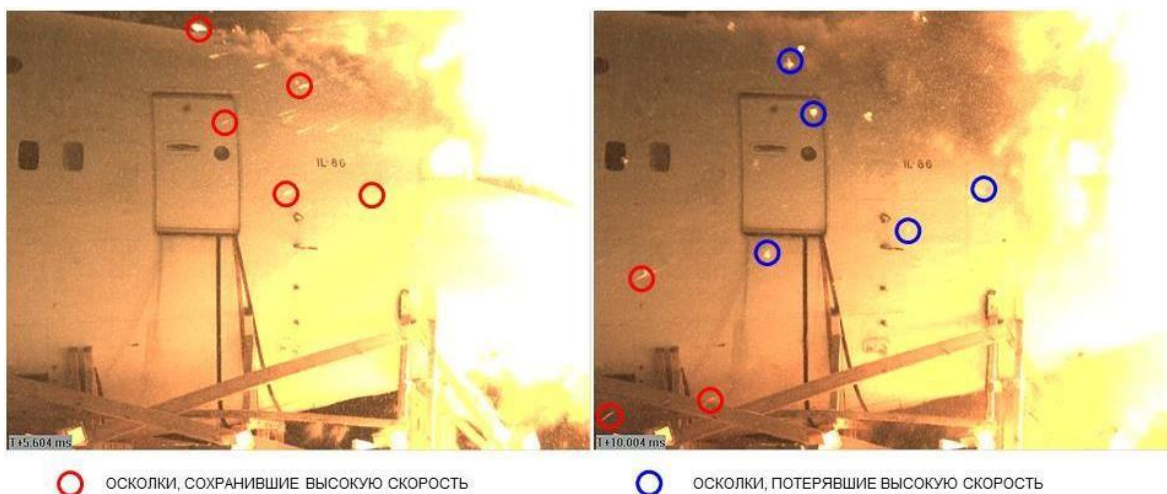


Face side of velocity sensor plates

Back side of velocity sensor plates

Figure 7.2 - Appearance of velocity sensor plates
(after the experiment)

Figure 7.3 contains still images from a high-speed camera (5,000 fps) showing traces (paths) of preformed fragments piercing through the aircraft's hull.



fragments that retained high velocity

fragments that lost high velocity

Figure 7.3 – Penetration by high-velocity fragments of the right side of IL-86
target aircraft's fuselage

In fig. 7.3, examples of paths of high-velocity fragment (white glowing dashes), which, after passing through the fuselage, retained high velocity and could have caused damage to the right wing or the right engine of the Boeing 777, are highlighted in red.

The examples of fragments (flares) that have lost high velocity and, therefore, kinetic energy after passing through the fuselage are highlighted in blue.

The examples of the appearance of exit holes on the right side of the target aircraft fuselage are shown in figures 7.4 through 7.7 and in section 5.1.4 of this Report¹⁸. The damage includes both through-and-through (piercing) and non-penetrating damage.



Figure 7.4 - Exit hole (left) and non-penetrating damage (right)



Figure 7.5 - Exit holes and non-penetrating damage to the starboard

¹⁸ Figures 5.83 through 5.105 in section 5.1.4 of Almaz-Antey's Report.



Figure 7.6 - Exit holes on the starboard side



Figure 7.7 - Exit holes on the starboard side

As shown by the analysis of the cockpit damage, the projectiles pierced not only the port side and cabinets with avionics and communication equipment, but also the floor, roof, bottom, starboard side, including through cabinets with equipment in the

flight engineer's workplace. Examples of such through-and-through penetrations are shown in figures 7.8-7.10.



Figure 7.8 - Through-and-through holes in the cockpit floor (bottom view)



Figure 7.9 - Instrumentation cabinet panel at the top of the starboard side behind the co-pilot's seat. In the upper right-hand corner is an exit hole in the right section of the cockpit roof



Figure 7.10 - Exit holes in the lower right-hand side of the first passenger compartment (rear view)

As noted earlier, when the 9H314M warhead of the 9M38M1 missile is detonated, the projectiles, according to the DSB Report, pierce through the cockpit structure. Figures 7.11-7.13 contain the still images with examples of starboard side penetration by the projectiles.



Figure 7.11 - Through-and-through hole in the starboard side made by a projectile



Figure 7.12 - Through-and-through hole in the starboard side made by projectiles

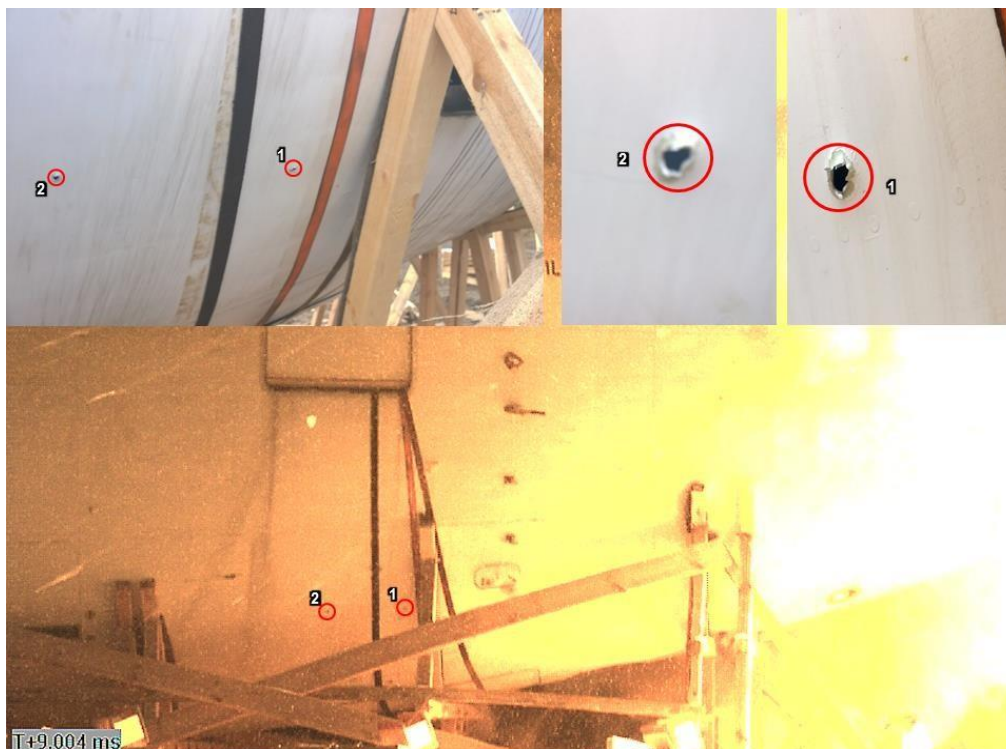


Figure 7.13 - Through-and-through hole in the starboard side made by projectiles

It should also be noted that the avionics of IL-86 target aircraft are of analogue design, using an electronic component base (ECB) from the 1970s-80s.

The presence of numerous material-intensive electronic and electromechanical components of the aircraft's avionics significantly weakened the penetration of the projectiles (figure 7.14).



Figure 7.14 - Elements of Ilyushin-86 target aircraft's avionics

Moreover, the projectiles that pierced the hull of the aircraft successively overcame at least three to five combined dispersed obstacles in varying combinations:

- elements of the outer skin of the aircraft on the port side and/or roof;
- thermal insulation and decorative panels on the port side and/or roof;
- panels or instrumentation cabinets on the port side or roof;
- cockpit floor, including longitudinal or transverse structural elements;
- panels or instrumentation cabinets on the starboard side or under the cockpit floor;
- thermal insulation and decorative panels on the starboard side or bottom;

elements of the outer skin of the aircraft on the starboard side or bottom of the aircraft.

The analysis of mechanical (penetration) capability of the preformed fragments showed that the characteristics set forth in the specifications¹⁹ are confirmed: the preformed fragments are able to pierce obstacles of up to 10-26 mm, Dural equivalent, depending on entry angles.

With regard to the version of the missile detonation under the conditions in the DSB Report, the preformed fragments of 9H314M warhead **pierce through the aircraft structure**, as evidenced by dozens of through-and-through holes on the starboard side, the right side of the roof and the bottom of the target aircraft.

In order to evaluate the penetration characteristics of the preformed fragments (9H314M 1-10, 9H314M 1-9, 9H314M 1-11) of the 9H314M warhead, a supplemental experiment was conducted in a shield target layout simulating other warhead detonation conditions (approach angles and distances from the blast point).²⁰

During the tests, projectiles of all three fractions pierce through up to 5-6 obstacles made of aluminium alloy AMg6M with thickness of 2.0 to 4.0 mm²¹. Figure 7.15 contains still images from the high-speed cameras that registered the order in which obstacles in the shield target layout were penetrated.

¹⁹ The mechanical (penetration) capability of 9H314M 1-10 projectiles, obtained experimentally, is as follows (Dural equivalent): at the angle between the velocity vector and the obstacle plane of 90 deg. – 23.0-26.3 mm; at angle of 30 deg. - 10.0-12.2mm. The source data on the penetration capability of the 9H314M projectiles was confirmed to DSB experts by Almaz-Antey's official letter No. 01-09/548k dated 29.07.2015.

²⁰ The conditions of the supplemental experiment in a shield target layout are set out in section 6.2.1. of the Almaz-Antey's Report.

²¹ The first obstacle consisted of two layers, the obstacles from the second to the fifth consisted of one layer of aluminium alloy AMg6M with thickness of 2.0 mm each.



high-speed camera No.1 10,000 frames per second

high-speed camera No.2 10,000 frames per second

Figure 7.15 - Consistent penetration of obstacles in the target layout by preformed fragments

In figure 7.15, numbers from "1" to "5" refer to the obstacles (targets Nos. 1-5) simulating the outline of a Boeing 777 aircraft and number "6" refers to a particularly robust obstacle (trap) designed to trap projectiles.

The maximum velocities of the leading projectiles (which were evaluated based on data from video cameras) were, after they passed through the obstacles²² in the shield target, as follows:

after obstacle No. 2, m/s	2 130 - 2 190
after obstacle No. 3, m/s	1 970 - 1 990
after obstacle No. 4, m/s	1 840 - 1 880
after obstacle No. 5, m/s	1 670 - 1 700

²² Taking into account the loss of speed when overcoming obstacles.

The average velocities of the main fragmentation flow were, after it passed through the obstacles in the shield target, as follows:

- after obstacle No. 3, m/s 1,100 - 1,630
- after obstacle No. 4, m/s790 - 1 270
- after obstacle No. 5, m/s 710 - 1 040

Figures 7.16 and 7.17 contain still images from the high-speed cameras that recorded the penetration of obstacles by leading preformed fragments.

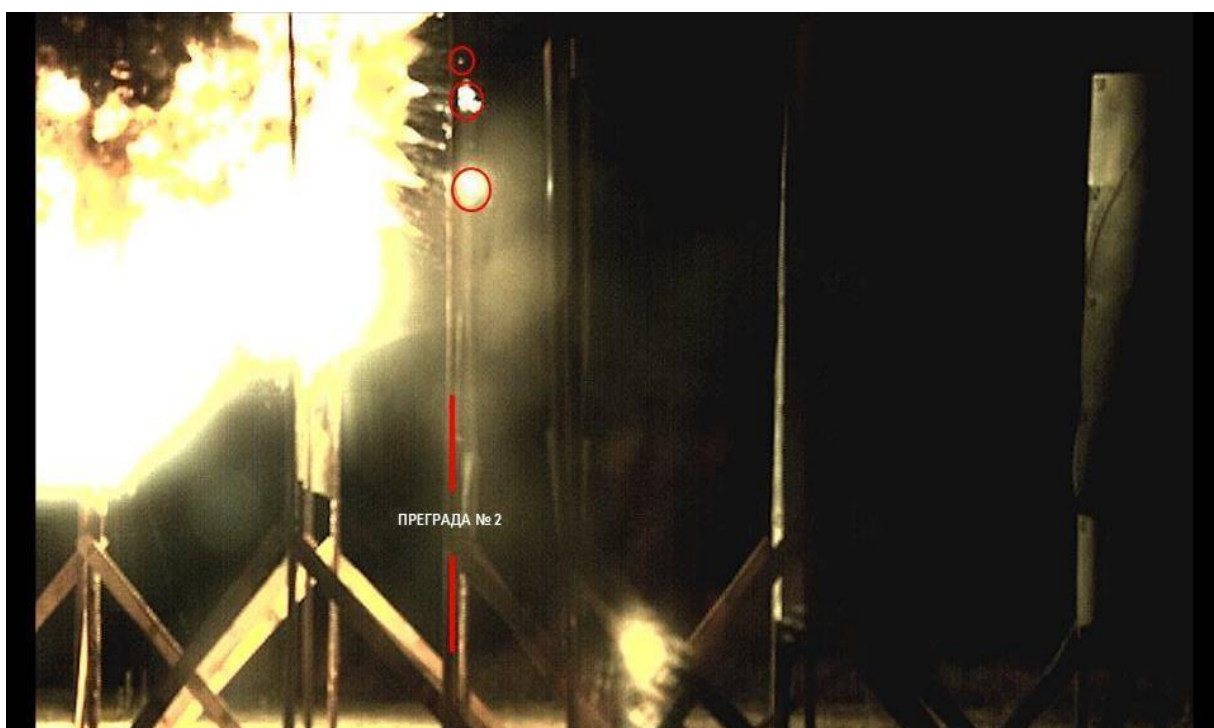


Figure 7.16 - Penetration of obstacle No. 2 (target No. 2) by leading fragments.



Figure 7.17 - Penetration of obstacle No. 3 (target No. 3) by leading fragments
 Some of the projectiles (mostly lightweight ones) did not pierce through obstacles No. 4 and No. 5. Examples of piercing and non-penetrating damage are shown in figure 7.18 and in Appendix A.

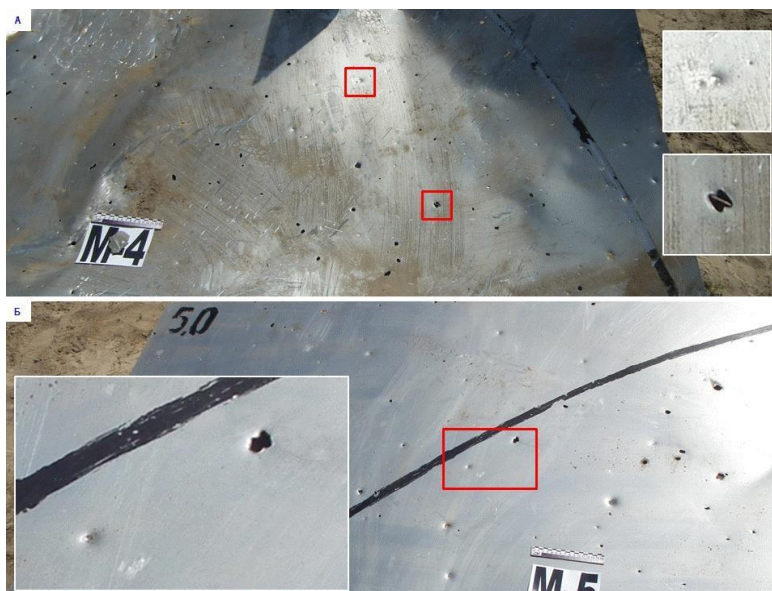


Figure 7.18 - Piercing and non-penetrating damage to obstacle No. 4 (A) and barrier No. 5 (B)

Other projectiles, after penetrating obstacles, pierced a reference steel screen (3.0 mm, St3) located on the ground or fell into a special trap.

Figure 7.19 shows the preformed fragments (highlighted in blue) at the moment of piercing the steel screen designed to gather elements from the terrain.



steel screen

Figure 7.19 – Fragments piercing through the steel screen

Figure 7.20 shows the moment when leading fragments penetrate the trap designed to trap preformed fragments.



Figure 7.20 – Leading fragments piercing obstacle No. 6, the trap (flashes in lower right corner)

Figure 7.21 contains photographs showing the condition of trap No. 1 (L1) barriers after the testing.²³

Photograph 7.21A - external trap obstacle (2.0 mm aluminium alloy sheet AMg6M), photographs 7.21B through 7.21G - PS-150 foam sheets (total thickness of 260.0 mm), photographs 7.21D and 7.21E - extraction of 9H314M 1-10 fragment (highlighted in red in photograph 7.21D) from boards at the depth of more than 400.0 mm.²⁴

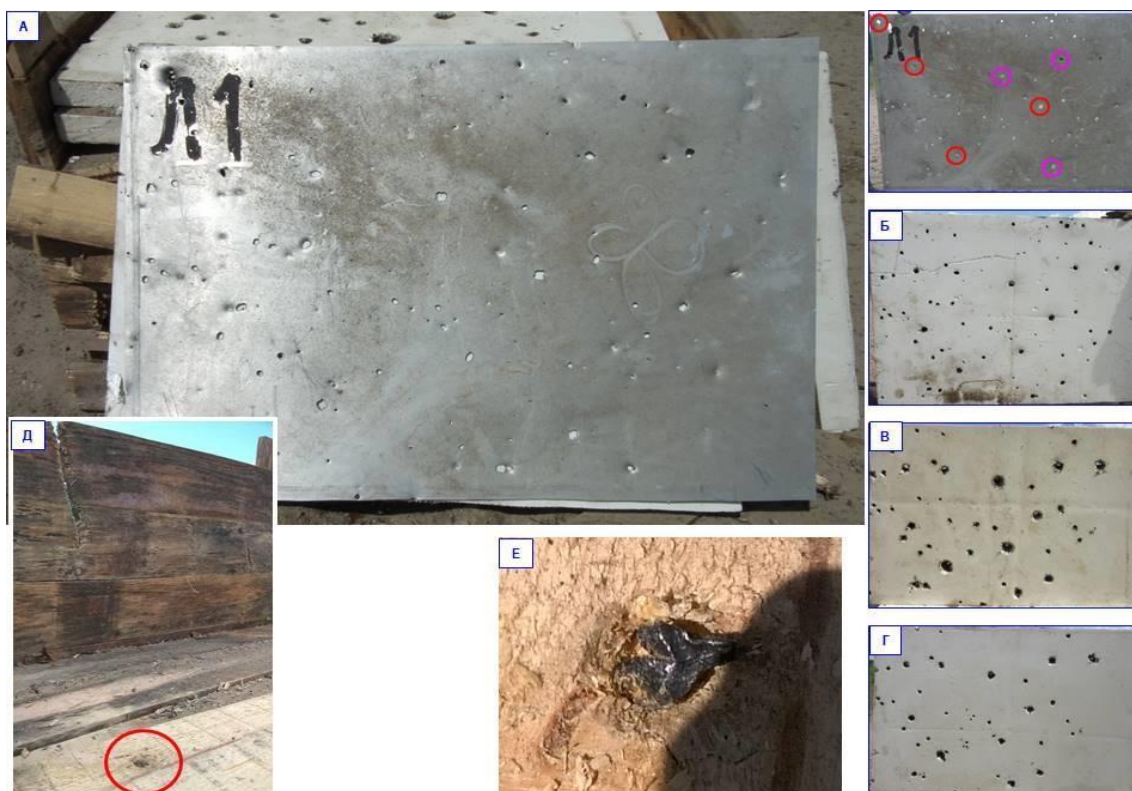


Figure 7.21 - Condition of trap L1 obstacles after the testing

²³ The trap obstacle was a wooden box with consecutive barriers - 2.0mm aluminium alloy sheet, PS-1-150 foam sheets with total thickness of 260.0mm and boards of up to 750.0mm.

²⁴ Taking into account the outer skin of the trap (2.0 mm aluminium alloy AMg6M) and the stopping foam PS-1-150 (three layers with combined thickness of 260.0 mm), the preformed fragments penetrated the complex combined obstacle to a depth of up to 400.0-450.0 mm.

The testing results show that the preformed fragments of 9H314M warhead are capable of penetrating dispersed obstacles of the target layout to a depth of greater than 14.0 mm, Dural equivalent.

Further, 9H314M 1-10 heavyweight ("bowtie") fragments leave distinctive butterfly-shaped holes not only on the first obstacle but also on all subsequent obstacles. Figure 7.22 shows examples of "butterfly" holes left in the dispersed shield target layout: obstacle No. 5 (shield target) and obstacle No. 6, the outer layer of a particularly tough obstacle (trap) designed to trap projectiles.



obstacle No. 5

obstacle No. 6

Figure 7.22 - Characteristic butterfly-shaped holes on dispersed obstacles in the shield target layout

Also, in the course of the experiment in the shield target layout, the penetration of preformed fragments of the 9H314M warhead was evaluated at various angles of interaction with obstacles.

The analysis of the photos of the targets shows that preformed fragments active in the main (primary) fragmentation field penetrate all single and double barriers of 2.0-4.0 mm thick aluminium alloy AMg6M at angles of attack of 20 degrees or more (figure 7.24).



Figure 7.23 - Fragment of shield target 1.5

Figure 7.23 shows a fragment of shield target 1.5 positioned at angles of 20-30 degrees to the direction of impact from the flow of preformed fragments.

There is no non-penetrating, non-piercing damage (ricochets) caused by preformed fragments to sheets in the first layer of the first obstacle in the target layout²⁵.

The analysis of the mechanical (penetration) capabilities of the ready-made projectiles showed that the characteristics set forth in the specifications are confirmed: the projectiles are able to pierce obstacles up to 10-26 mm, Dural equivalent, depending on the entry angles.

Thus, the results of the experiment carried out under the conditions specified in the DSB Report showed that the penetration of the preformed fragment flux generated by detonation of the 9H314M warhead was significantly higher than the penetration of preformed fragments that hit the Boeing 777.

²⁵ Additional research into penetration capability of projectiles of the 9H314M warhead confirmed the results of the experiment. The research showed that in all cases where an obstacle mounted at 15° angle was shot through and a projectile struck the obstacle flatwise, the obstacle was pierced through with the projectile penetrating behind the obstacle. The projectiles penetrating behind the obstacle maintained their orientation and subsequently pierced through cardboard and a test screen made of 5.0 mm thick steel.

8. Analysis of weight and size characteristics of preformed fragments of 9H314M warhead before and after the experiment

8.1. Weight and size characteristics of preformed fragments before the experiment

The main characteristics of the 9H314M warhead²⁶ are shown in Table 8.1.

Table 8.1 - Characteristics of the 9H314M warhead

Characteristic	Value
Weight of the warhead, kg	about 70
Weight of explosives, kg	33.5+0.8 -0.4
Weight of projectiles, kg	28.7
9H314M 1-9	9.635
9H314M 1-10	15.147
9H314M 1-11	3.927
Dimensions of projectiles, mm	
9H314M 1-9	8 x 8 x 5
9H314M 1-10	13 x 13 x 8.2
9H314M 1-11	6 x 6 x 8.2
Projectiles material	steel
Weight of one projectile, g	
9H314M 1-9	2.35 ± 0.15
9H314M 1-10	8.1+0.6-0.1
9H314M 1-11	2.1+0.01-0.17
Number of projectiles, pcs.	
9H314M 1-9	4 100 ± 100
9H314M 1-10	1 870 ± 47
9H314M 1-11	1 870 ± 47

²⁶ The main characteristics of the 9H314M warheads were communicated to the DSB experts in Almaz-Antey's official letter No. 01-09/548k dated 29 July 2015.

8.1.1. Heavyweight 9H314M 1-10 (bowtie shaped) projectiles

Table 8.2 shows the initial weight and size characteristics of the heavyweight projectiles. The dimensions of the 9H314M 1-10 heavyweight (bowtie shaped) projectiles as per the drawing are shown in figure 8.1.

Table 8.2 - Initial weight and size characteristics of ready-made 9H314M projectiles 1-10

Projectile	Dimensions, mm			Weight, g
	1*	2*	3*	
9H314M 1-10	$13.0^{+0.6-0.4}$	$13.0-0.7$	8.2 ± 0.2	$8.1^{+0.6-0.1}$

* - linear dimensions according to the drawing

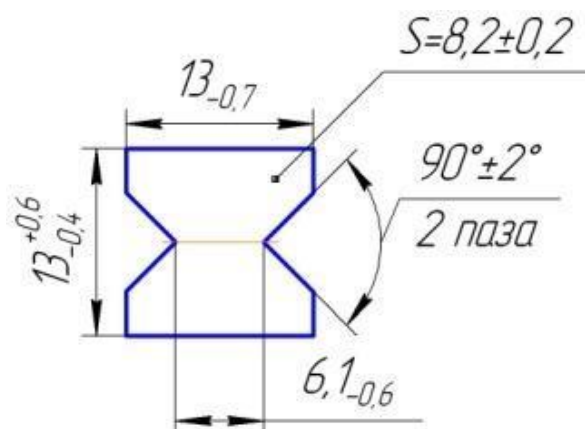


Figure 8.1 - Dimensions of 9H314M projectile 1-10

8.1.2. Lightweight 9N314M 1-9 and 9N314M 1-11 ("parallelepiped"-shaped) projectiles

Table 8.3 shows the initial weight and size characteristics of the lightweight (parallelepiped-shaped) 9H314M 1-11 and 9H314M 1-9 projectiles.

Table 8.3 - Initial weight and size characteristics of ready-made lightweight projectiles

Projectile	Dimensions, mm			Weight, g
	A	Б	В	
9H314M 1-11	6.0- 0.08	6.0- 0.08	8.2 ± 0.2	2.1+ 0.01- 0.17
9H314M 1-9	8.0- 0.09	8.0- 0.09	5.0+ 0.1- 0.2	2.35 ± 0.15

8.2. Weight and size characteristics of the ready-made projectiles after the experiment

In the course of the full-scale experiment, 18 projectiles of all three fractions of the 9H314M warhead were extracted from the IL-86 target aircraft.

The distribution of the extracted projectiles by type was as follows:

- 9N314M 1-10 ("bowtie" shaped) - 7 pieces (38.89 %);
- 9N314M 1-9 ("parallelepiped" shaped) - 5 pieces (27.78 %);
- 9N314M 1-11 ("parallelepiped" shaped) - 6 pieces (33.33 %).

An analysis of the experiment results shows that all three types of projectiles contained in 9H314M warhead are extracted from the elements of the target layout (structure of the target aircraft). Further, 9H314M1-10 heavyweight ("bowtie" shaped) projectiles account for **at least 38%** of the total number of projectiles extracted.

The appearance of the ready-made projectiles extracted from the target structure during the experiment is shown in figure 8.2.



PARALLELEPIPED (6x6x8.2 mm)

PARALLELEPIPED (8x8x5 mm)

Initial appearance of the projectile

Initial appearance of the projectile

BOWTIE 13x13x8.2 mm)

BOWTIE (13x13x8.2 mm)

top view

side view

Initial appearance of the projectile

Figure 8.2 - Extracted projectiles:

9H314M 1-11 (top left); 9H314M 1-9 (top right);

9H314M 1-10 (bottom)

Three out of the seven 9H314M 1-10 heavyweight ready-made projectiles extracted from the target retained their original shape, which accounts for more than

42% of all 9H314M 1-10 ready-made "bowtie" shaped projectiles extracted. The rest of the projectiles lost their "bowtie" shape as a result of destruction and were identified as 9H314M 1-10 only by their residual mass, which exceeds the original mass of the lightweight projectiles²⁷.

The appearance of the ready-made 9H314M 1-10 projectiles removed from the target is shown in figures 8.3 through 8.5.



Figure 8.3 - Extracted 9H314M 1-10 projectiles (top view)



Figure 8.4 - Extracted 9H314M 1-10 projectiles (top view)

²⁷ The mass of lightweight ready-made projectiles 9H314M 1-9 (8x8x5 mm "parallelepiped") and 9H314M 1-11 (6x6x8.2 mm "parallelepiped") is 2.35 ± 0.15 and $2.1^{+0.01}_{-0.17}$ g, respectively. The minimum mass of the destroyed bowtie shaped projectile 9N314M 1-10 exceeds the initial mass of lightweight ready-made projectiles 9N314M 1-9 and 9N314M 1-11.



Figure 8.5 - Extracted 9H314M 1-10 projectiles (Side view)

Part of the ready-made 9H314M 1-10 ("bowtie" shaped) projectiles was removed from the aircraft's avionics equipment.

An example of a 9H314M 1-10 projectile removed from the cockpit's avionics box is shown in figure 8.6.



Figure 8.6 - Removing a 9H314M 1-10 projectile from avionics equipment

The undestroyed heavyweight 9H314M 1-10 projectiles, the shape of which resembles an "bowtie" shape have a residual weight ranging from 7.3 to 7.9 g (1, 2 and 3 at the left in figures 8.3-8.5).

Their weight loss is between 3 and 10 %.

As a result of deformation due to interaction with obstacles, the linear dimensions of the 9H314M 1-10 "bowtie" shaped projectiles exceed their original linear dimensions (length and width).

Highly deformed and fractured projectiles that lost their "bowtie" shape have a residual weight in the range of 3.9 to 6.4 g (4-7 at the left in figures 8.3-8.5). Their weight loss ranges from 21 to 52%.

8.3. Results of a supplementary experiment in the shield target layout

In order to assess the residual weight and size of the ready-made 9H314M projectiles, a supplementary experiment was conducted in a shield target layout simulating other warhead detonation conditions (approach angles and distances from the detonation point)²⁸.

In the course of the experiment, 71 projectiles of all three 9H314M warhead fractions were extracted from the shield target and traps. Photographs showing examples of extracted projectiles of different fractions are shown in figure 8.7 and figures A.202-A.211 in Appendix A.

²⁸ The conditions for the supplementary experiment in a shield target layout are provided in section 6.2.1. of Almaz-Antey's Report.



PARALLELEPIPED (6x6x8.2 mm)

PARALLELEPIPED (8x8x5 mm)

Initial appearance of the projectile

Initial appearance of the projectile

BOWTIE (13x13x8.2 mm)

BOWTIE (13x13x8.2 mm)

top view

side view

Initial appearance of the projectile

Figure 8.7 – Ready-made 9H314M projectiles extracted from the target and traps

Distribution of extracted projectiles by type:

- 9N314M 1-10 ("bowtie")²⁹ - 39 pcs (54.93 %);

²⁹ Heavyweight 13 x 13 x 8.2 mm projectile.

- 9N314M 1-9 ("parallelepiped")³⁰ - 17 pcs (23.94 %);
- 9N314M 1-11 ("parallelepiped")³¹ - 15 pcs (21.13 %).

8.3.1. Heavyweight 9H314M 1-10 projectiles

Sixteen out of the 39 9H314M 1-10 heavyweight ("bowtie"-shaped) projectiles extracted from the target and traps retained their original "bowtie" shape, accounting for more than 41% of all 9H314M 1-10 projectiles extracted from the target and traps.

The appearance and weight of the 9H314M 1-10 projectiles which retained their "bowtie" shape after testing are shown in figures 8.8 and 8.9.



Figure 8.8 - 9H314M 1-10 projectile ("bowtie")

³⁰ Lightweight 8 x 8 x 5 mm projectile.

³¹ Lightweight 6 x 6 x 8.2 mm projectile.

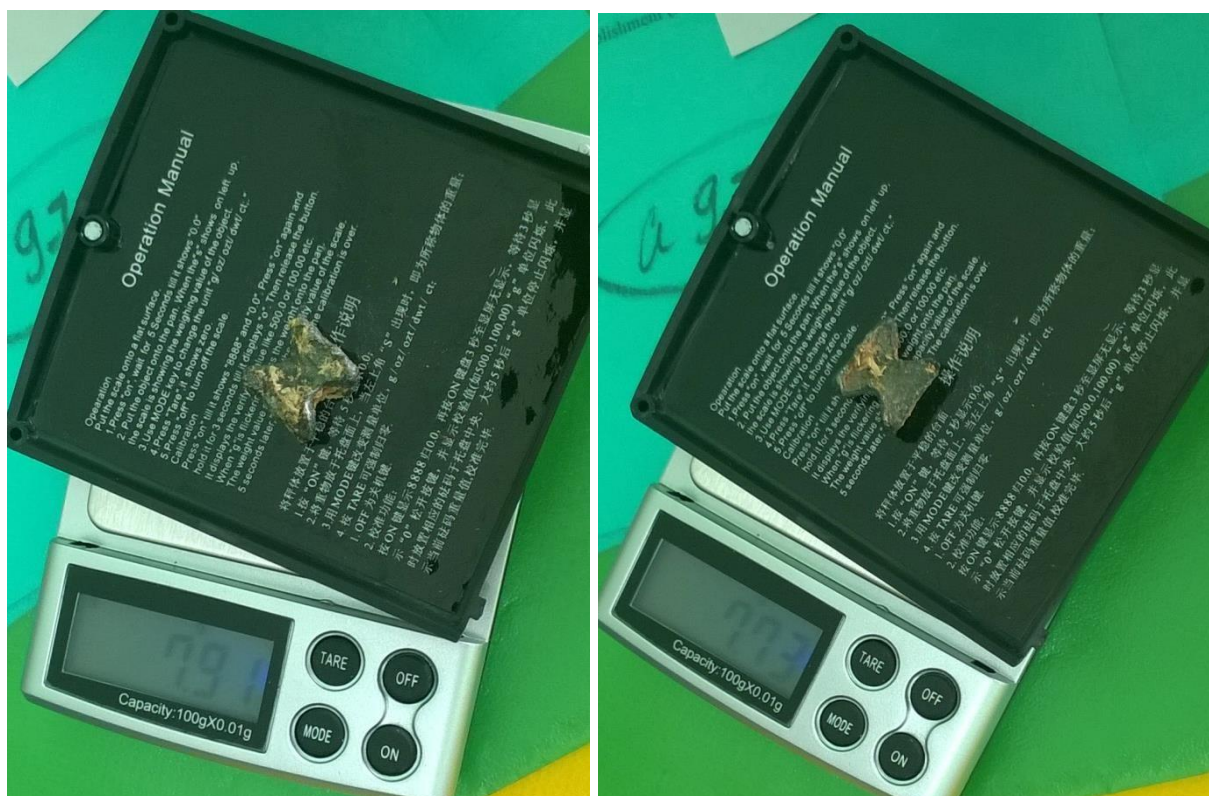


Figure 8.9 - Weight of 9H314M 1-10 projectiles after the testing

An analysis of the characteristics of the 9H314M 1-10 projectiles which retained their original "bowtie" shape shows that, as a result of the tests:

- the average weight of undestroyed projectiles that retained their "bowtie" shape is ~ **7.23 g**;

- the average weight loss³² by particular bowtie-shaped projectiles does not exceed ~**11%**;

- the linear dimension "A"³³ of undestroyed ready-made heavyweight projectiles is within the range of 14.40 to 21.50 mm;

- the linear dimension "B" of undestroyed ready-made heavyweight projectiles is within the range of 12.10 to 17.50 mm;

³² Based on a nominal weight of 8.1 g.

³³ The following dimensions were taken as the linear dimensions: "A" is the maximum linear dimension (length or width) obtained from the measurement of the projectiles after the tests; "B" is the second linear dimension (length or width); "C" is the height of the projectile.

- minimum dimension "B" (thickness) of ready-made heavyweight projectiles that retained their original shape resembling "bowtie" is **6.90** mm, the average value is **8.13** mm.

As a result of the deformation, the linear dimensions of the 9H314M 1-10 projectiles exceed their original linear dimensions (length and width).

As an example, figure 8.10 contains photographs of a 9H314M 1-10 projectile, which retained its "bowtie" shape.



Figure 8.10 - 9H314M 1-10 projectile: after removal from the trap (left), at weighing (centre) and after dimensional measurements (right)

The 9H314M 1-10 projectiles with a weight loss of more than 15 - 19% are deformed and destroyed, losing their shape resembling a bowtie. An analysis of the characteristics of the destroyed and deformed 9H314M 1-10 projectiles that lost their bowtie shape shows that, as a result of the tests, the weight loss and dimensional changes are within a substantial range.

Examples of 9H314M 1-10 heavyweight bowtie shaped (13x13x8.2 mm) projectiles extracted from the traps and the target structure are shown in figures 8.11 and 8.12.



Figure 8.11 - 9H314M 1-10 projectiles (top view)

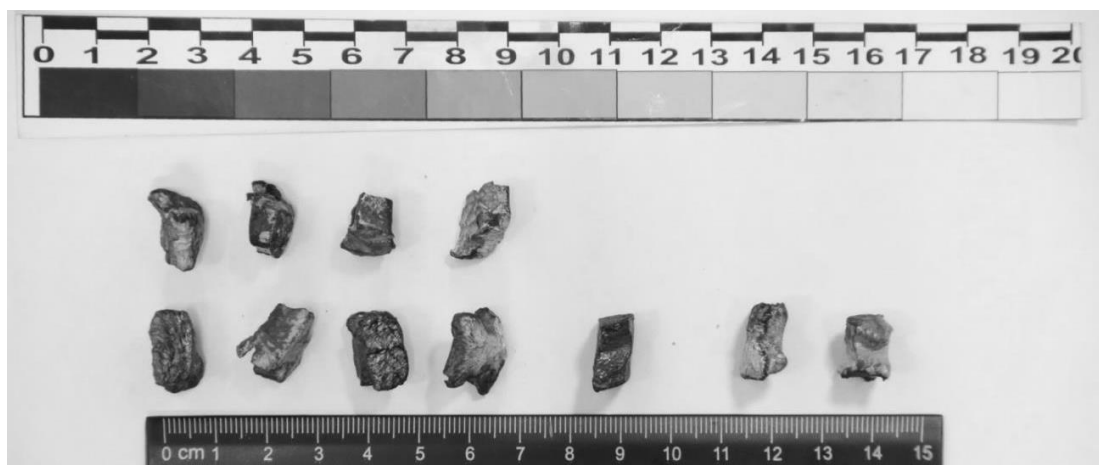


Figure 8.12 - 9H314M 1-10 projectiles (side view)

8.3.2. Lightweight 9H314M 1-9 and 9H314M 1-11 projectiles

Figures 8.13 and 8.14 show examples of 9H314M 1-11 and 9H314M 1-9 projectiles removed from the target structure.



Figure 8.13 - 9H314M 1-11 projectiles

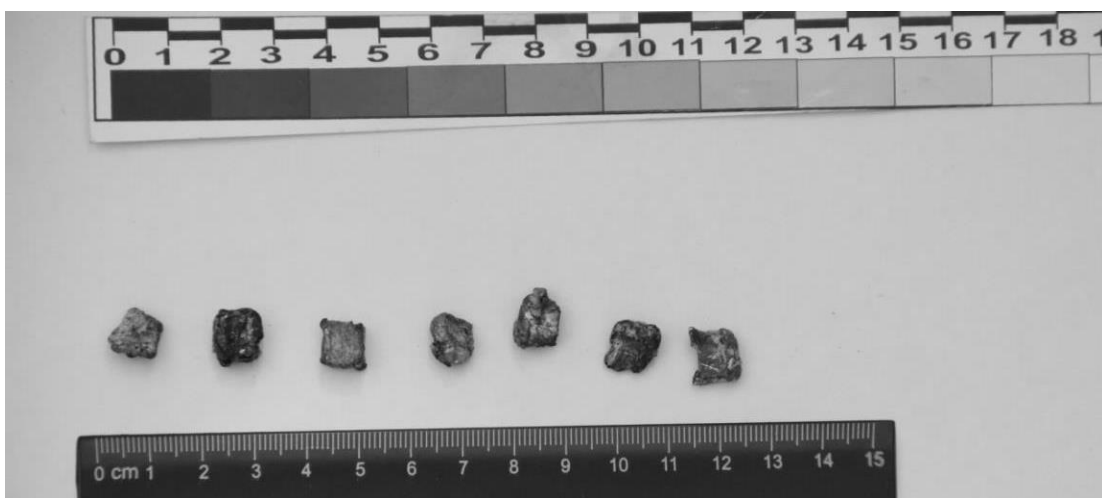


Figure 8.14 - 9H314M 1-9 projectiles

An analysis of the data on lightweight projectiles shows that, as a result of the tests:

- the average weight loss by a single 9H314M 1-11 (6x6x8.2 mm) projectile is ~24%;
- the average weight loss by a single 9H314M 1-9 (8x8x5 mm) projectile is ~ 21 %;
- the linear dimensions (length and width) of lightweight projectiles after impact with obstacles increase considerably and may reach 11.20 to 12.50 mm for 9H314M 1-9 projectiles and 10.40 to 11.40 mm for 9H314M 1-11 projectiles.

8.4. Comparative analysis of the projectiles

8.4.1. Comparative analysis of the projectiles with archival data

An analysis of the results of the experiments shows that all three types of projectiles contained in 9H314M warhead are extracted from the target layout (target aircraft structure). Further, 9H314M 1-10 heavyweight ("bowtie" shaped) projectiles account for **at least 38%** of the total number of projectiles extracted.

The results of the assessment of the weight and size characteristics of the ready-made projectiles extracted from the targets are consistent with the baseline data on projectiles derived from an analysis of archival test data from 9H314M warhead detonation tests.

The appearance of 9H314M 1-10 ("bowtie" shaped) projectiles removed during the experiments as compared to the archival data is shown in figure 8.15.



13x13x8 fraction

Photo No. 1

13x13x8 fraction

Photo No. 2

9H314M warhead testing report (archival data)

BOWTIE SHAPE (13x13x8.2 mm)

BOWTIE SHAPE (13x13x8.2 mm)

Experiment. Stage 1

BOWTIE SHAPE (13x13x8.2 mm)

Experiment. Stage 2

Initial appearance of bowtie shaped projectile

Figure 8.15 - Comparative analysis of 9H314M 1-10 ("bowtie" shaped) ready-made projectiles

Thus, according to the results of detonation tests at ground static conditions in the compartment hull of 9M38M1 missile and 9M38M1 missile assembled, which were conducted under different conditions of the encounter of projectiles with obstacles, the average weight loss by a single undestroyed projectile that retained "bowtie" shape does not exceed 10-11%, and the maximum weight loss is about 15%.

9H314M 1-10 projectiles with an initial weight loss of more than 15-19% deform significantly and deteriorate.

8.4.2. Comparative analysis of projectiles recovered following the experiment and those specified in the DSB Report

The DSB Report refers to more than 70 steel projectiles removed from the aircraft structure and human remains and not belonging to the aircraft structure. The Report provides only part of the characteristics for 20 fragments³⁴.

At the same time, although "numerous Bow-tie" fragments are constantly mentioned in the Report, there are photos of only two fragments which have remote

³⁴ Final Report. Table 11: Overview of the 20 selected fragments.

similarity with ready-made "bow-tie" shaped 9H314M 1-10 projectile. Another fragment (#2)³⁵ which has dimensions of 12x12x1 mm and weight of 1.2 g was also positioned as a "bowtie" in the Draft Final Report (figure 8.16).

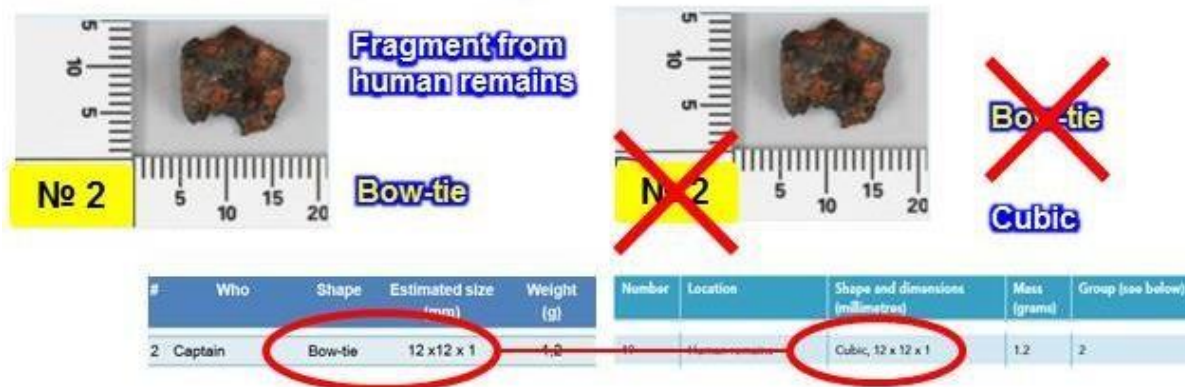


Figure 8.16 - Projectile No. 2 appearing in the Draft Final Report as a "bowtie"

This fragment cannot be a 9H314M 1-10 heavyweight bowtie-type projectile because weight mass is too low.

In the DSB Report this fragment is already referred to as "Cubic" (Fig. 8.16, right) and only two fragments (#1 and #3) are presented as "bowtie" shaped fragments.

The first of these two fragments, which are shaped like a 'bowtie', is shown in figure 8.17.

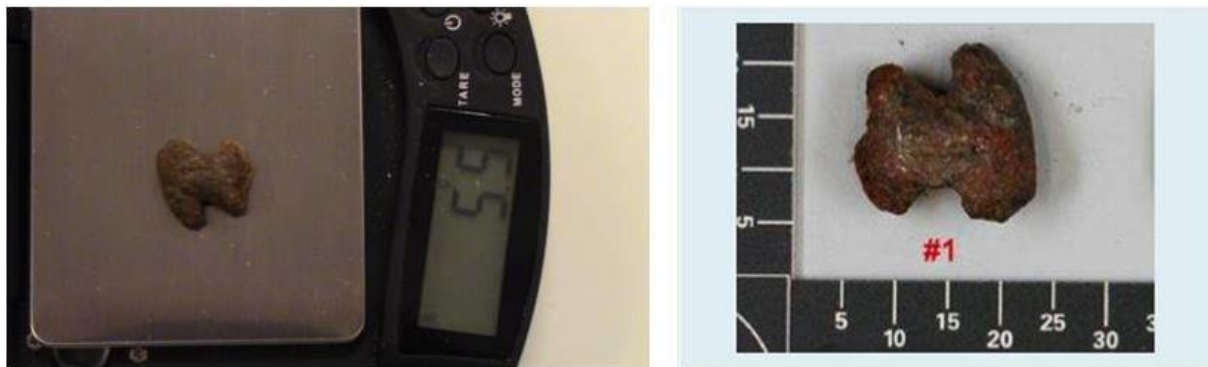


Figure 8.17 - Appearance of the # 1 target

³⁵ In Table No. 11 of the Final Report, this item is numbered "19".

This fragment (#1) was first shown to Russian experts in February 2015. When weighed in the presence of Russian experts, it weighed 5.5 g (left photo of figure 8.17). In the DSB Report, in Tables 11 (Overview of the 20 selected fragments) and 12 (Composition in (percentage) of elements found in steel of the two groups of fragment examined) the following data are given on this fragment³⁶:

weight, g	6.1
dimensions:	
dimension "A", mm	14.0
dimension "B", mm	14.0
dimension "B", mm	4.5
group (by composition)	1
discovery location.....	cockpit

However, the location where this projectile was recovered is unknown - unlike the other lightweight fragments, no logbook (passport) was provided for this fragment and, in the course of the commission's work, such locations as starboard noise insulation fragments, technical documentation and other locations were cited as locations of extraction.

The second fragment, which has a shape resembling a "bowtie" (fragment #3),³⁷ was removed from the pilot's body and, therefore, was not considered in the course of the work of the technical commission until the issuance of the Draft Final Report.

The appearance of this fragment (as per the DSB Report) is shown in figure 8.18.

³⁶ In Table 11 of the DSB Report, this item is numbered "10".

³⁷ In Table 11 of the DSB Report, this item is numbered "20".



Figure 8.18 - Appearance of projectile #3

The DSB Report contains the following data on this fragment:

weight, g	5.7
dimensions:	
dimension "A", mm	12.0
dimension "B", mm	12.0
dimension "C", mm	5.0
group (by composition)	1
discovery location	human remains

Given the characteristics of the 9H314M 1-10 projectile, which has an initial weight of $8.1^{+0.6}_{-0.1}$ g, the weight loss by fragment #3 is between 29 and 34%. With such degree of deformation, 9H314M 1-10 projectiles normally have linear dimensions greater than the initial ones.

However, the linear dimensions of this fragment are even slightly less than the minimum initial contours of the "bowtie", considering all three dimensions at the same time³⁸.

³⁸ See figure 8.1 and table 8.2 in section 8.1.1 of Almaz-Antey's Report.

Figures 8.19 and 8.20 show 3D printer produced 1:1 scale mock-ups of the projectiles: fragment (#3)³⁹ from the DSB Report and 9H314M 1-10 projectile from the experiment.



Figure 8.19 - Appearance of mock-ups of fragment #3 (top) and 9H314M 1-10 projectiles after the tests (bottom)



Figure 8.20 - Comparison of sizes of fragment #3 (from DSB Report) and 9H314M 1-10 projectile

At the same time, DSB materials contain images of fragments, information on which is not reflected in the Report or is not presented in its entirety. Thus, in table 11 of the DSB Report, linear dimensions are given only for four fragments, which are numbered "10", "15", "19" and "20".

Fragments numbered '10' and '20' are defined as resembling a 'Bow-tie', while fragments '15' and '19' are defined as 'Cubic 6x6x5' and 'Cubic 12x12x1', respectively. No linear dimension data is provided at all for the other fragments.

³⁹ In Table 11 of the final report, this item is numbered "20".

An analysis of the photographic material provided by the DSB experts⁴⁰ shows that some of the steel projectiles recovered from the aircraft structure and human remains and not belonging to the aircraft structure cannot be projectiles of 9H314M warhead.

Examples of such fragments are shown in figure 8.21.

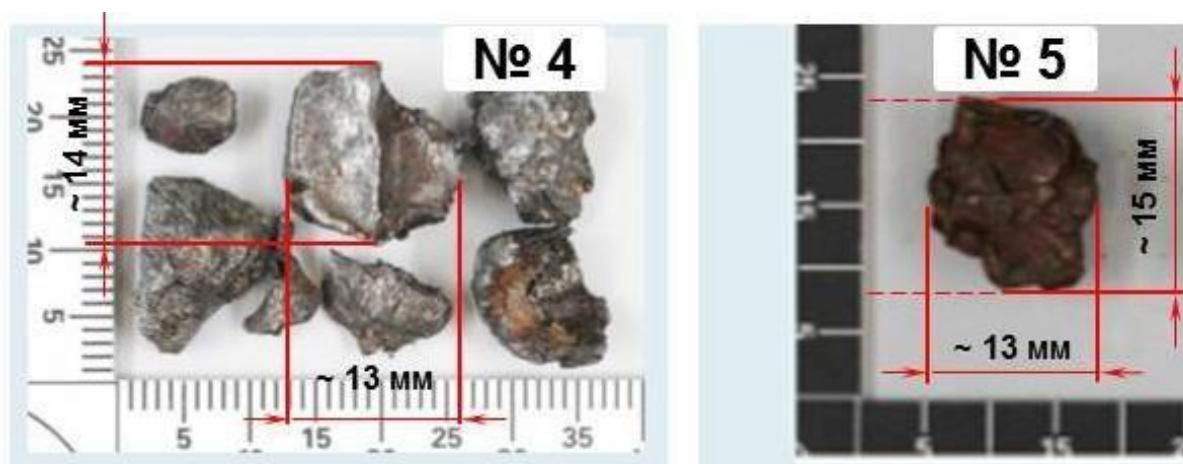


Figure 8.21 - Appearance of fragments #4 and #5

Fragment No. 4 was recovered from the body of a crew member and fragment No. 5 was recovered from the wreckage of the Boeing 777 structure⁴¹. These fragments have dimensions of approximately 13 x 14 mm and 13 x 15 mm, respectively. The lack of data on the third dimension (thickness) and the residual weight of the fragments in the DSB Report does not allow their unequivocal identification.

Their appearance resembles that of a parallelepiped, and their linear dimensions, which significantly exceed the dimensions of the maximally deformed lightweight

⁴⁰ Investigation MH17. Annex 13 meeting Gilze-Rijen. High Energy Objects. 11 August 2015.

⁴¹ According to the DSB materials.

projectiles (no more than 1,112.5 mm⁴²), rule them out as belonging to the 9H314M warhead.

Thus, the results of the experiment showed that the fragments available to the DSB do not match the 9H314M warhead in terms of their main weight and size characteristics.

9. Analysis of the pattern of destruction of missile's structural elements

For convenience, the fragments of destroyed structural elements of the 9M38M1 missile that was used during the experiment can be divided into two groups:

- hull fragments from the second compartment (warhead compartment), parts of the first and third compartments (located near the frames and mounting flanges) with dimensions comparable to those of ready-made projectiles, whose meridional angle of dispersion corresponds to the limits of the basic meridional angle of dispersion of the fragmentation field formed by ready-made projectiles;

- large fragments of other missile airframe compartments and structural components the dispersion of which is beyond the boundaries of the main meridional angle of fragmentation field.

See figures 9.1-9.4 for examples of hull fragments and the holes they leave behind.

The bulk of the fragments from the first group are concentrated in the main (primary) fragmentation field formed by the projectiles. The dimensions of large hull fragments reach 30-150 mm.

⁴² Based on the results of tests as part of full-scale experiments. For details, see section 8.2. of Almaz-Antey's Report.



Removed from the traps of the shield target layout Removed from Target No. 1 (aircraft nose section)

Experiment. Stage 1

Experiment. Stage 2

Figure 9.1 - Second compartment (warhead compartment) hull fragments



Comparison of dimensions of ready-made projectiles and warhead hull fragments

Comparison of dimensions of holes left by ready-made projectiles and warhead hull fragments

Target No. 1 (aircraft nose section)

Figure 9.2 - Comparison of dimensions of and holes left by hull fragments from the first group with the dimensions of and holes left by ready-made projectiles



Figure 9.3 – Holes left by second compartment hull fragments on the port side of the target in the area of door L1



Figure 9.4 - Second compartment hull fragments and holes left by them

The hull fragments shown in figure 9.4 were found in the cockpit of the target aircraft and are approximately 35mm and 50mm in size, respectively. The right side of the photograph in figure 9.4 shows the appearance of a hole in the roof of the cockpit left by one of such hull fragments.

The size of the hole exceeds 150 mm.

The compartments of the 9M38M1 missile, except for the second one (warhead compartment), are generally destroyed into large fragments, constituting the second group.

Examples of the 9M38M1 missile compartment fragments after the test are shown in figures 9.5 through 9.7.



Figure 9.5 - Fragments of the 9M38M1 missile compartments



Figure 9.6 - Fragments of the 9M38M1 missile compartments

The bulk of the first compartment fragments were found at the impact point (insert in the lower left corner of figure 9.7) at a distance of about 100 m from the test stand.

The linear dimensions of the main fragments of the first compartment reach 100-250 mm or more.



Figure 9.7 - First compartment fragments impact point
(the place where first compartment fragments fell is shown in the bottom left corner)

The third and fourth compartments of the missile are also destroyed into large irregularly shaped fragments. Photographs of the fragments of the 3rd and 4th compartments are shown in figure 9.8.



Figure 9.8 - Fragments of the third and fourth compartments of the missile

Figure 9.9 shows, for comparison, photographs of the third compartment (engine) from the experiment (top) and the item allegedly discovered at Boeing 777 crash site⁴³ (bottom).

In the photos of figure 9.9, the missile's lug is marked in red, indicating that the objects in question may be the third compartment of the missile mentioned in the DSB Report materials.

However, the undamaged condition of the shown part of the third compartment hull shown and the absence of traces of deformation caused by the explosion or deformation caused by its fall from an altitude of about 10,000 m and its hitting the ground, cast doubt that its belongs to the missile the impact of which caused the Boeing 777 to crash.

The effects of the explosion on the third compartment of the item 9M38M1 are shown in figures 9.10 and 9.11 (still images from the video recording of the experiment).

⁴³ Photo from the Dutch commission's materials (MH17 investigation meeting 11-12 August 2015 Gilze-Rijen).



• Missile part - Casing 2nd part (1.60 m)



Figure 9.9 - Comparison of fragments of the missile's third compartment: appearance of fragments following the tests (top) and of those from DSB materials (bottom)



Experiment: detonation of 9M38M1 missile

Figure 9.10 - Item 9M38M1 on the test stand before detonation

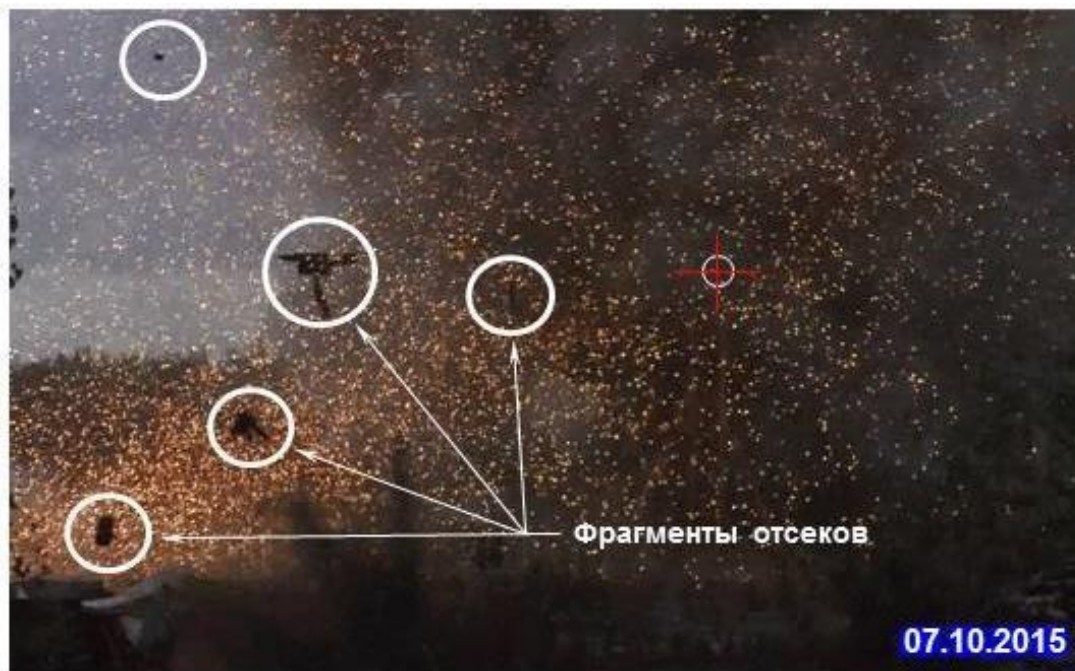


Figure 9.11 - Disintegration of fragments of compartments 3 and 4 of 9M38M1 missile as a result of the detonation of the 9H314M warhead

The structural elements of the 9M38M1 missile, except for the second missile compartment (warhead compartment), break up predominantly into large irregularly shaped fragments. The flight direction of the bulk of large fragments of the first compartment (the nose section of the missile) coincides with the longitudinal axis of the missile at the time of detonation. The linear dimensions of the main fragments of the first compartment reach 100-250 mm or more.

Thus, the appearance and damage assessment analysis and the analysis of the explosive deformation of a fragment of the third compartment of 9M38M1 missile body after its experimental detonation showed the existence of fundamental differences as compared to a similar fragment discussed in the DSB Report's working papers.

Such differences cast doubt as to whether the fragment of the body of the third compartment in the possession of the DSB belonged to the missile the impact of which caused the Boeing 777 to crash.

MAIN CONCLUSIONS FROM THE RESULTS OF THE EXPERIMENT

Based on the results of the analysis of the field experiment conducted under the conditions specified in the findings of the DSB Report, the results of special research into the penetration capability of projectiles, and the assessment of damage to the outer skin, the interior, and the structure of the Boeing 777-200 (MH17), it has been found that:

1. The credibility of the conclusion in the DSB Report "Crash of Malaysia Airlines Boeing 777-200, 9M-MRD, flight MH17" that the aircraft was hit by a 9M38-series anti-aircraft missile armed with a 9H314M warhead has not been confirmed.

2. The credibility of this conclusion is not confirmed in view of the following:

- the size and density of the fragmentation field produced by the detonation of the 9H314M warhead are not consistent with the characteristics of the fragmentation damage to the Boeing 777 fragments;

- the number and shape of the holes produced by the detonation of the 9H314M warhead are not consistent with the observed holes on the Boeing 777 fragments;

- the penetration of the flow of ready-made projectiles produced by the detonation of 9H314M is not consistent with the penetration of the weapon's projectiles that impacted the Boeing 777;

- the area and level of destruction and damage caused by the 9H314M warhead explosion are not consistent with similar characteristics of the Boeing 777 fragments;

- the weight and dimension characteristics of projectiles of the 9H314M warhead (degree of deformation, shape, dimensions and residual weight) are not consistent with the characteristics of fragments provided in the DSB Report;

- the level of destruction of the missile's structural elements following the experiment is not consistent with the level of destruction of the missile's fragments referred to in the DSB Report materials.

EXHIBIT A**Photo report in relation to the full-scale experiment in a shield target layout**

The exhibit contains photographs showing how the experiment was prepared and conducted.

The target layout consisted of five duralumin shields (alloy AMg6M) 2.0 mm thick¹, up to 7.4 m high² and 6.0 m long. In addition, a shield of steel (St3) plates (3.0 mm thick, 2.5 m long and 3.75 m high) was mounted at a distance of 22.3 m. Traps L1 and L2 were mounted on the opposite side of the target layout to capture striking elements.

1. Mounting the target layout

The mounting of the shields, warhead and traps in the target layout was done in accordance with the "Programme and Methodology for 9H314M Warhead Testing by Explosion in a Shield Target Layout". Figures A.1 through A.6 illustrate the stages of preparing the shield target layout.



Figure A.1 - Target barriers No. 4 and No. 5

¹ The first obstacle had two layers of duralumin shields with a total thickness of 4.0 mm.

² Taking into account the height of the supports which is 1.4m above ground level.



Figure A.2 - Target barriers Nos. 2, 3, 4 and 5



Figure A.3 - Target barrier No. 2

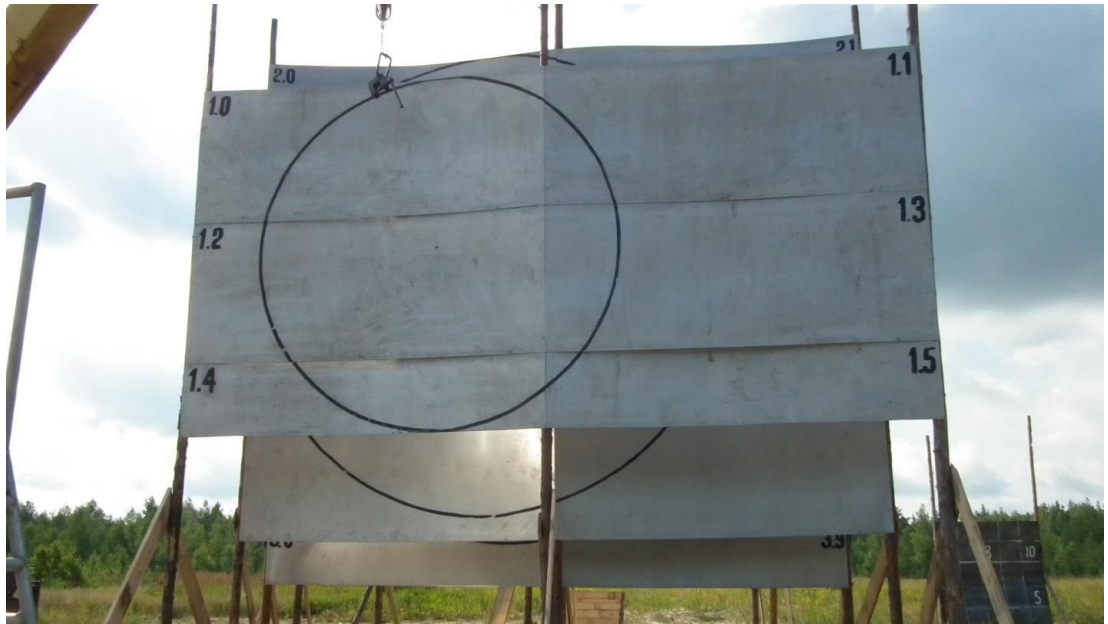


Figure A.4 - Target barrier No. 1



Figure A.5 - Target layout imitating the contours of the nose of a Boeing 777-200 aircraft



Figure A.6 - Additional shield target (target No. 6M.D) imitating the left engine of a Boeing 777-200 aircraft

Figure A.7 shows the mounting of one of extra strong barriers (traps) designed to collect (capture) striking elements.



Figure A.7 - Mounting of a trap (bottom right) to collect striking elements.
Rear view.

A 9H314M warhead with number 40-290 placed in the hull of 9M38.0201.040 missile compartment with number 05-05 (Figure A.8) was provided for the testing. The mounting of the warhead on a test bench is shown in figure A.9.



Figure A.8 - 9H314M warhead and second compartment hull



Figure A.9 - Mounting the 9H314M warhead in the second compartment hull
the test bench

The mounted target layout (shield target barriers, traps and the warhead in the compartment hull) is shown in Figure A.10.



Figure A.10 - Target layout at the first stage of the experiment

2. Conducting tests

The blasting of the warhead was initiated at the front end from the centre of a special assembly (MSNI.773979.011-01) containing an electric detonator ED-8M.

The overall straddle pattern and the times of arrival of ready-made projectiles at the targets were recorded using high-speed video cameras Phantom V7.3 and four certified panoramic video cameras mounted on the sides of the shield target layout.

The overall view of the experiment was recorded by four panoramic video cameras. The process of detonating the 9H314M warhead in the compartment hull is shown in Figures A.11 through A.29.

Figures A.11 through A.13 contain images from panoramic camera No. 1P (front view of the nose of a Boeing 777-200 imitation).



Figure A.11 - Camera No. 1P. Before detonation of the warhead



Figure A.12 - Camera No. 1P. Detonation of the warhead



Figure A.13 - Camera No. 1P. After detonation of the warhead

Figures A.14 to A.19 show still images from panoramic camera No. 2P (front view of the left side of the Boeing 777-200 aircraft imitation).



Figure A.14 - Camera No. 2P. Before detonation of the warhead



Figure A.15 - Camera No. 2P. Detonation of the warhead



Figure A.16 - Camera No. 2P. Beginning of the target layout destruction



Figure A.17 - Camera No. 2P. The target layout destruction by high-explosive effect



Figure A.18 - Camera No. 2P. The target layout destruction by high-explosive effect



Figure A.19 - Camera No. 2P. After detonation of the warhead

Figures A.20 to A.24 show still images from panoramic camera No. 3P (view of the left side of the Boeing 777-200 aircraft imitation).



Figure A.20 - Camera No. 3P. Before detonation of the warhead



Figure A.21 - Camera No. 3P. Detonation of the warhead



Figure A.22 - Camera No. 3P. Beginning of the target layout destruction



Figure A.23 - Camera No. 3P. The target layout destruction by high-explosive effect



Figure A.24 - Camera No. 3P. After detonation of the warhead

Figures A.25 through A.29 contain still images from panoramic camera No. 4P (rear view of the left side of the Boeing 777-200 aircraft imitation).



Figure A.25 - Camera No. 4P. Before detonation of the warhead



Figure A.26 - Camera No. 4P. Detonation of the warhead



Figure A.27 - Camera No. 4P. The target layout destruction by high-explosive effect



Figure A.28 - Camera No. 4P. The target layout destruction by high-explosive effect



Figure A.29 - Camera No. 4P. After detonation of the warhead

Figure A.30 shows a general view of the target layout after the testing.



Figure A.30 – View of the layout target after the testing

3. Initial testing results

3.1 Extra strong barriers - traps

Figures A.31-A.38 contain photographs of trap L1 after the testing.



Figure A.31 - General view of trap L1 after the testing

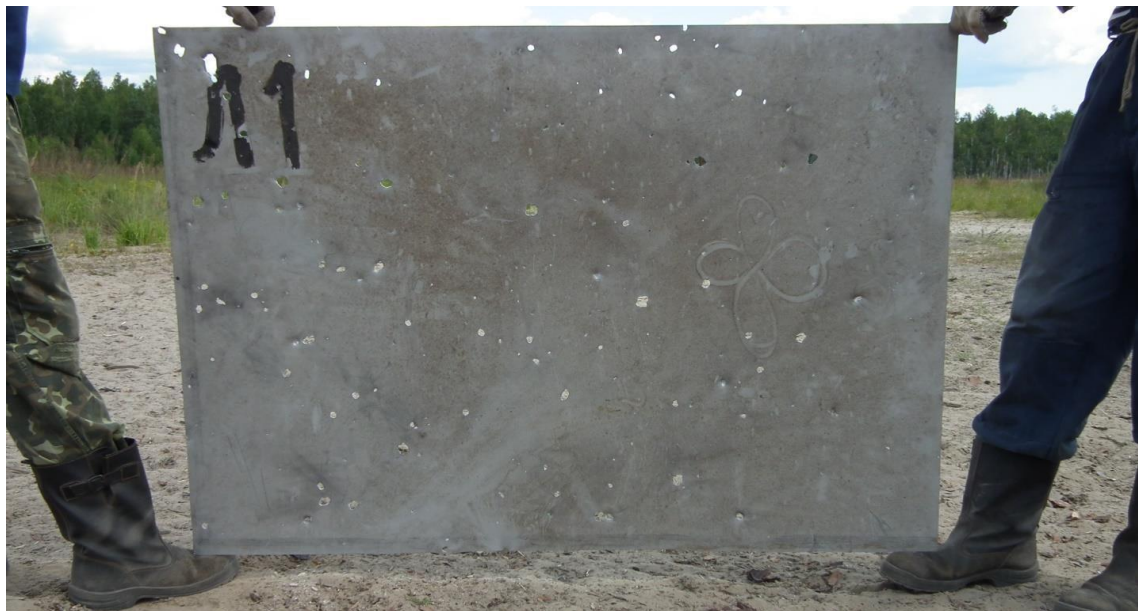


Figure A.32 - First barrier of trap L1 (2.0 mm thick sheet of aluminium alloy AMg6M) after the testing



Figure A.33 - Example of a "butterfly"-shaped hole in the first barrier of trap L1 after the testing



Figure A.34 - Second barrier of trap L1 (first layer of foam plastic PS-1-150) after the testing.



Figure A.35 - Second barrier of trap L1 (second layer of foam plastic PS-1-150) after the testing



Figure A.36 - Second barrier of trap L1 (third layer of foam plastic PS-1-150) after the testing



Figure A.37 - Hull fragment (that of the compartment hull) lodged in the third layer of stopping foam plastic PS-1-150



Figure A.38 - Third barrier of trap L1 (boards with a total thickness of 750 mm) after the testing

Figures A.39 through A.42 contain pictures of trap L2 after the testing.



Figure A.39 - General view of trap L2 and first barrier (2.0 mm thick sheet of aluminium alloy AMg6M) after the testing



Figure A.40 - Second barrier of trap L2 (first layer of PS-1-150 foam plastic) after the testing



Figure A.41 - Second barrier of trap L2 (second layer of foam plastic PS-1-150) after the testing



Figure A.42 - Second barrier of trap L2 (third layer of foam plastic PS-1-150) after the testing

The extraction of fragments from the traps L1 and L2 after the testing is shown in Figures A.43 through A.49.



Figure A.43 - Disassembling trap L1 to remove fragments



Figure A.44 - Depth of penetration of ready-made projectiles into trap L1



Figure A.45 - General view of a projectile lodged in trap L1



Figure A.46 - Projectile lodged in trap L1



Figure A.47 - Removal of 9H314M 1-10 projectile lodged in trap L1



Figure A.48 - Projectile lodged in trap L2



Figure A.49 – Removal of a projectile lodged in trap L2

The projectiles removed from the traps L1 and L2 are shown in Figures A.50 through A.52.



Figure A.50 – Ready-made projectiles of three fractions extracted from trap L1



Figure A.51 - Hull fragments (those of the compartment hull) recovered from traps



Figure A.52 - Ready-made projectiles and hull fragments (those of the compartment hull) removed from trap L2

3.2 The target layout

3.2.1 Shield target No. 1

Figures A.53 through A.71 show the appearance of target No. 1 and its fragments after they were collected. The sides of the target correspond to the simulated fuselage of the Boeing-777-200 aircraft. The left side of the aircraft is represented by shields, including the first layer: 1.1, 1.3 and 1.5; second layer: 1.1¹, 1.3¹ and 1.5¹; right side - first layer: 1.0, 1.2 and 1.4; second layer: 1.0¹, 1.2¹ and 1.4¹, respectively.



Figure A.53 - Target No. 1



Figure A.54 - Fragments 1.2 and 1.4 of target No. 1 (general view)



Figure A.55 - Left side of fragments 1.2 and 1.4 of target No. 1 (general view)



Figure A.56 - Left side of fragment 1.0 of target No. 1



Figure A.57 - Right side of fragment 1.0 of target No. 1



Figure A.58 - Left side of fragment 1.1 of target No. 1



Figure A.59 - Right side of fragment 1.1 of target No. 1



Figure A.60 - General view of fragment 1.1 of target No. 1

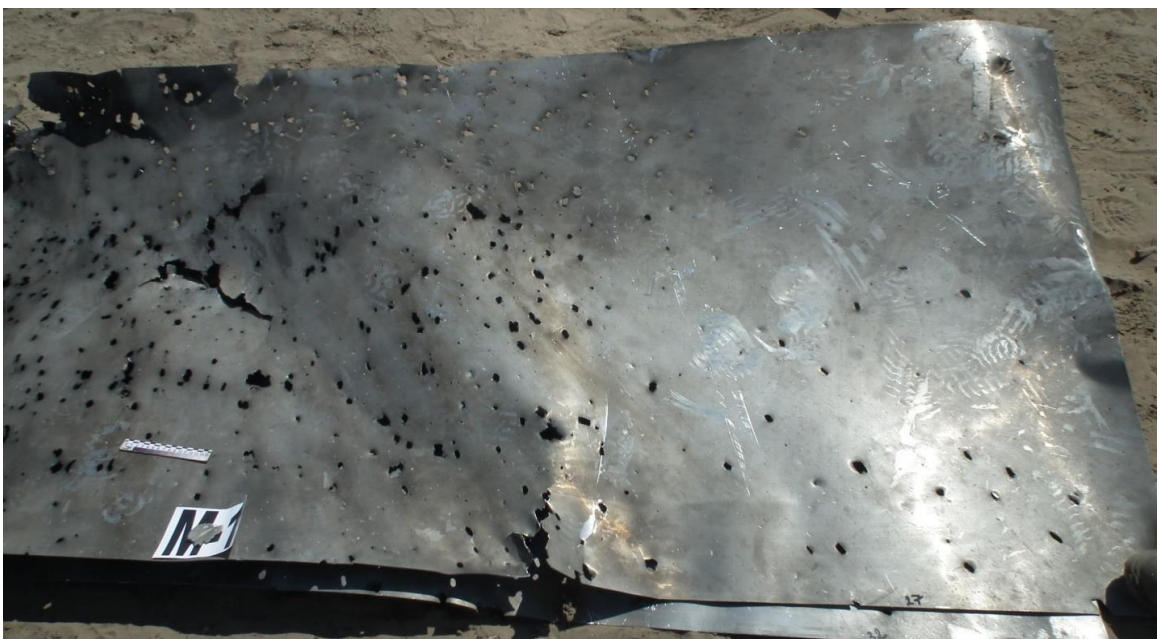


Figure A.61 - General view of fragment 1.1 of target No. 1

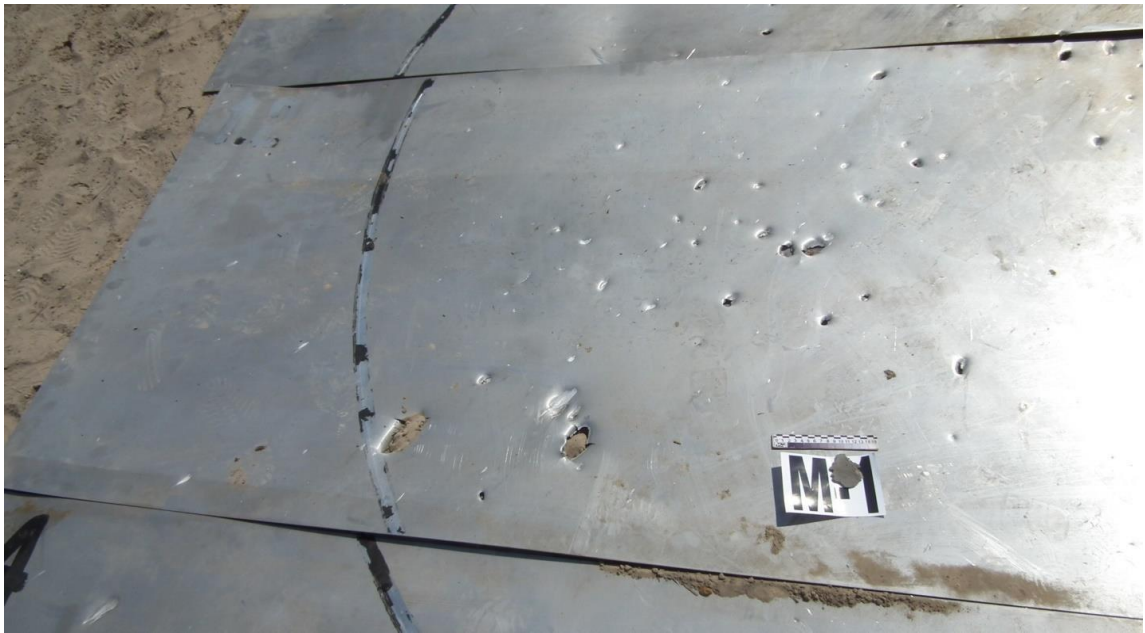


Figure A.62 - Left side of fragment 1.2 of target No. 1



Figure A.63 - Right side of fragment 1.2 of target No. 1



Figure A.64 - Left side of fragment 1.3 of target No. 1

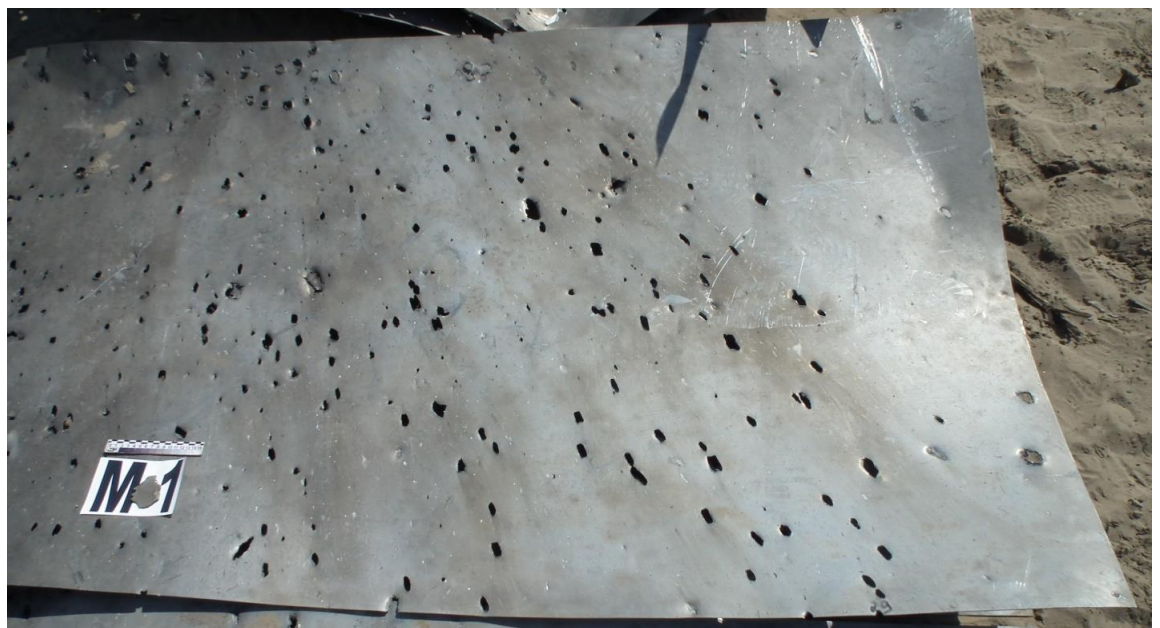


Figure A.65 – Right side of fragment 1.3 of target No. 1



Figure A.66 - Left side of fragment 1.4 of target No. 1



Figure A.67 - Right side of Fragment 1.4 of target No. 1

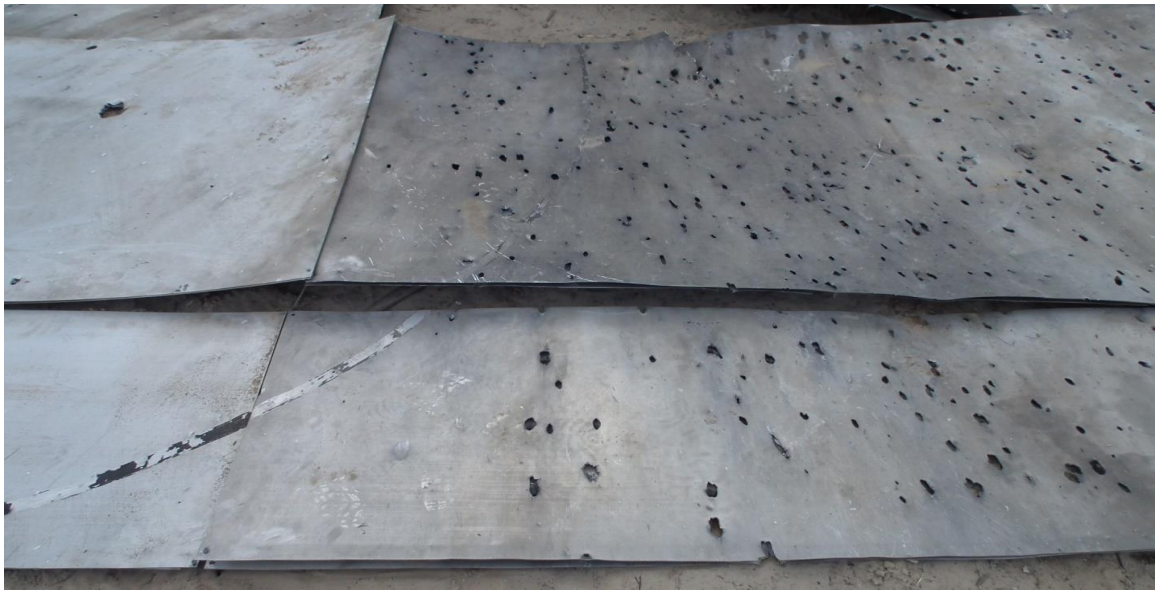


Figure A.68 - Left side of fragments 1.3 and 1.5 of target No. 1



Figure A.69 - Right side of fragments 1.3 and 1.5 of target No. 1



Figure A.70 - General view of fragment 1.1^I of target no. 1
(second layer of shields)



Figure A.71 - General view of fragment 1.1^I of target no. 1
(second layer of shields)

3.2.2 Shield target no. 2

Figures A.72 through A.97 show the appearance of target No. 2 and its fragments after they were collected. The sides of the target correspond to the simulated fuselage of the Boeing 777-200 aircraft. The left side of the aircraft is represented by shields 2.1, 2.3, 2.5 and 2.7; the right side by 2.0, 2.2, 2.4 and 2.6.

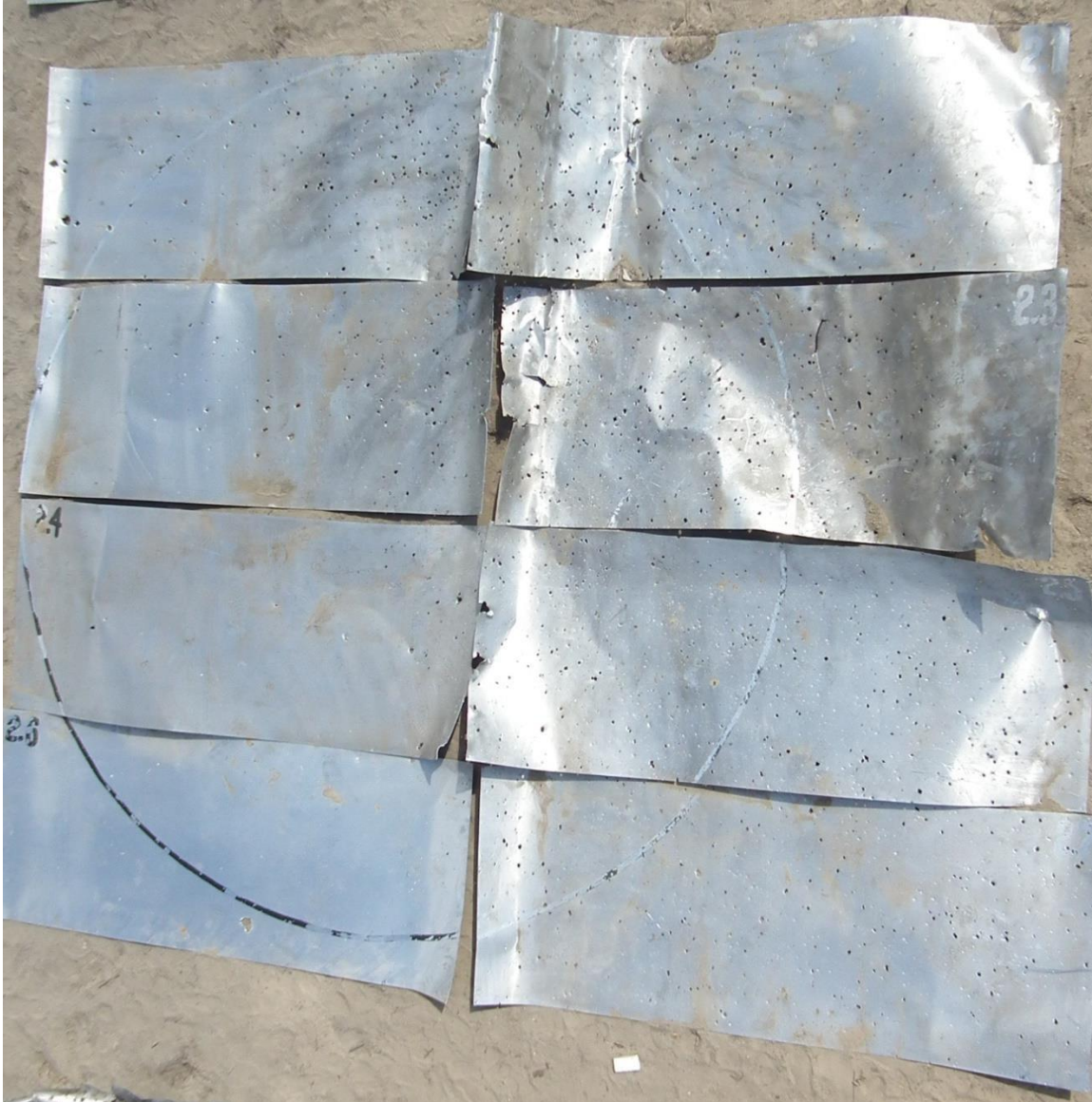


Figure A.72 - Target No. 2



Figure A.73 - Fragments 2.1 (top), 2.3, 2.5 and 2.7 (bottom) of target No. 2



Figure A.74 - Fragments 2.1 (top), 2.3 and 2.5 (bottom) of target No. 2



Figure A.75 - Fragments 2.5 and 2.7 of target No. 2



Figure A.76 - General view of fragments 2.0 (top), 2.2 and 2.4 (bottom) of target No. 2



Figure A.77 - Fragments 2.0 (top), 2.2, 2.4 and 2.6 (bottom) of target No. 2



Figure A.78 - General view of fragments 2.4 (top) and 2.6 (bottom) of target No. 2

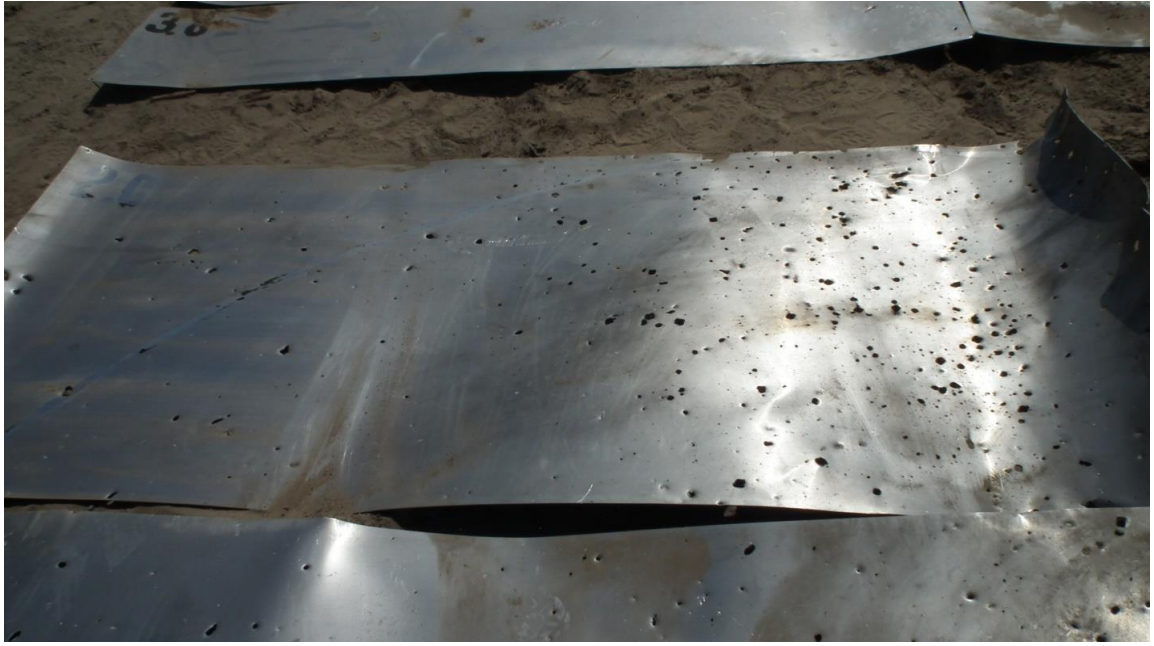


Figure A.79 - General view of fragment 2.0 of target No. 2



Figure A.80 - General view of fragment 2.1 (centre) of target No. 2



Figure A.81 - Left side of fragment 2.0 of target No. 2



Figure A.82 - Right side of fragment 2.0 of target No. 2



Figure A.83 - Left side of fragment 2.1 of target No. 2

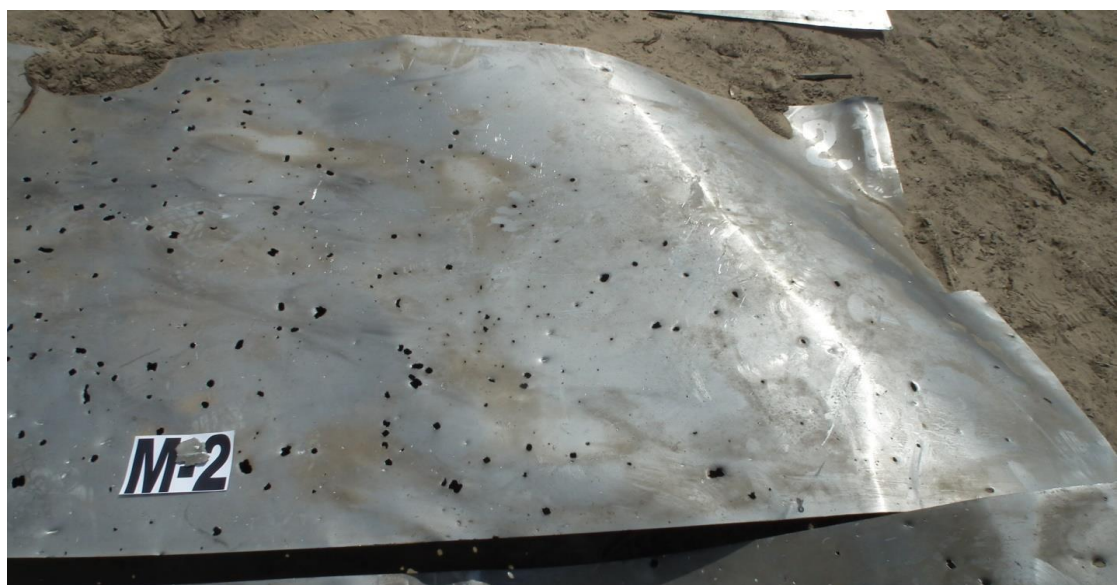


Figure A.84 - Right side of fragment 2.1 of target No. 2



Figure A.85 - Left side of fragment 2.2 of target No. 2



Figure A.86 - Right side of fragment 2.2 of target No. 2



Figure A.87 - Left side of fragment 2.3 of target No. 2



Figure A.88 - Right side of fragment 2.3 of target No. 2



Figure A.89 - Left side of fragment 2.4 of target No. 2



Figure A.90 - Right side of fragment 2.4 of target No. 2

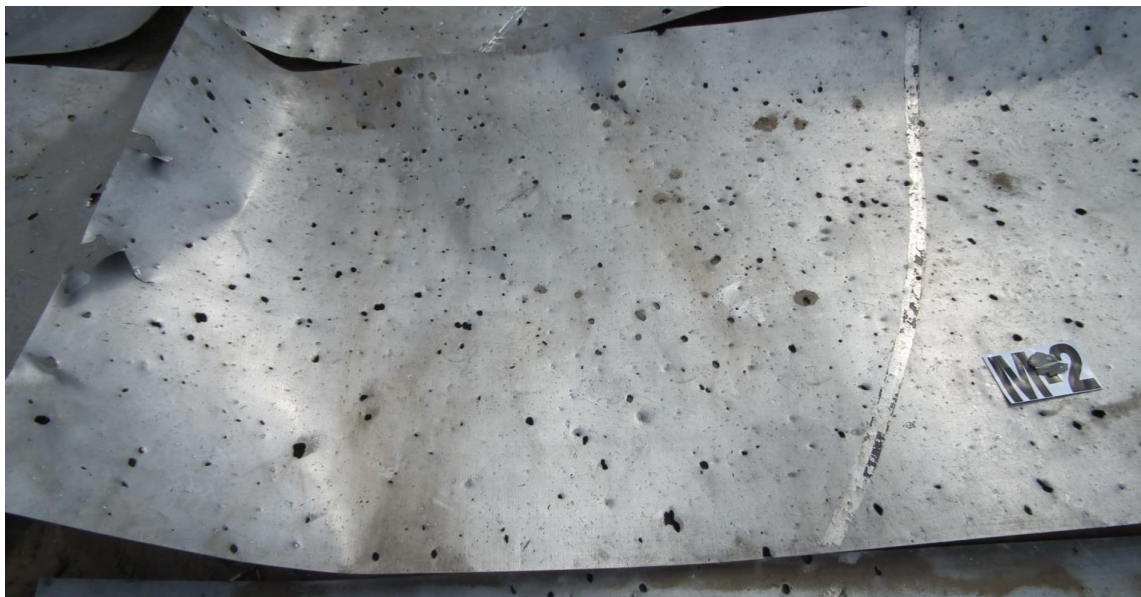


Figure A.91 - Left side of fragment 2.5 of target No. 2

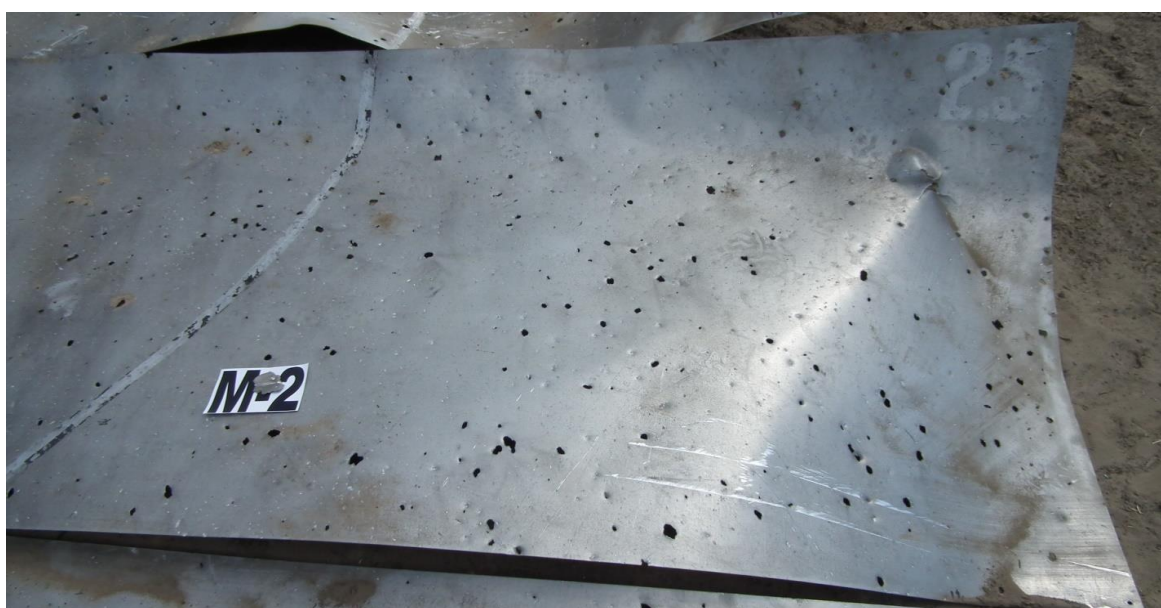


Figure A.92 - Right side of fragment 2.5 of target No. 2



Figure A.93 - Left side of fragment 2.6 of target No. 2



Figure A.94 - Right side of fragment 2.6 of target No. 2



Figure A.95 - Left side of fragment 2.7 of target No. 2



Figure A.96 - Right side of fragment 2.7 of target No. 2



Figure A.97 - General view of fragments 2.5 (top) and 2.7 (bottom) of target No. 2

3.2.3 Shield target No. 3

Figures A.98 through A.124 show the appearance of target No. 3 and its fragments after they were collected. The sides of the target correspond to the simulated fuselage of the Boeing 777-200 aircraft. The left side of the aircraft is represented by shields 3.1, 3.3, 3.5, 3.7 and 3.9; the right side by shields 3.0, 3.2, 3.4, 3.6 and 3.8.



Figure A.98 - Target No. 3

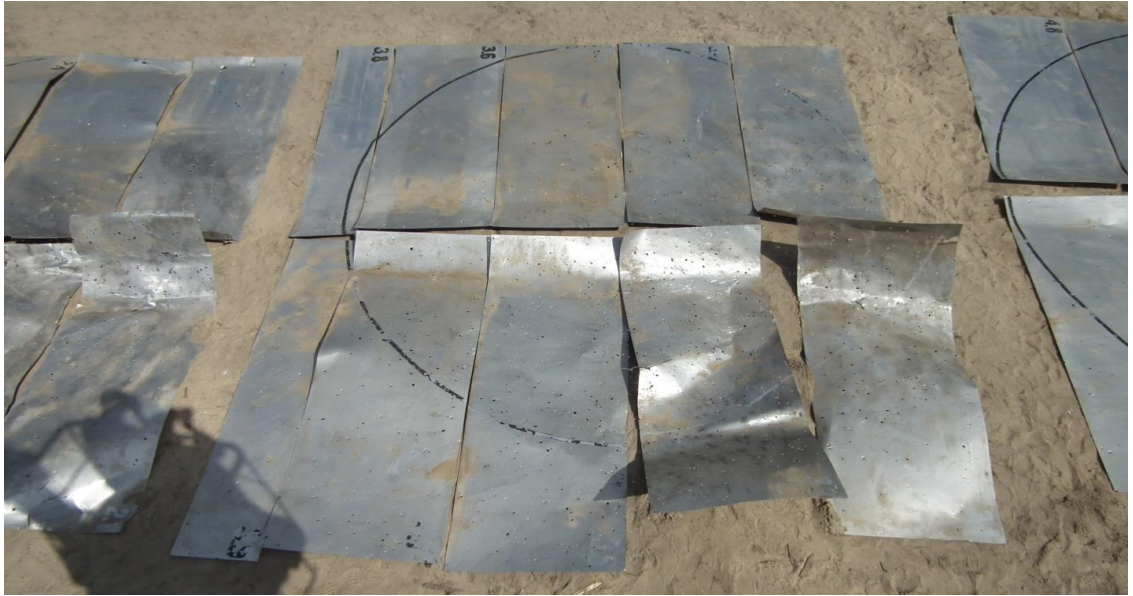


Figure A.99 - Target No. 3 (centre)



Figure A.100 - Fragments 3.0 (top), 3.2 and 3.4 (bottom) of target No. 3

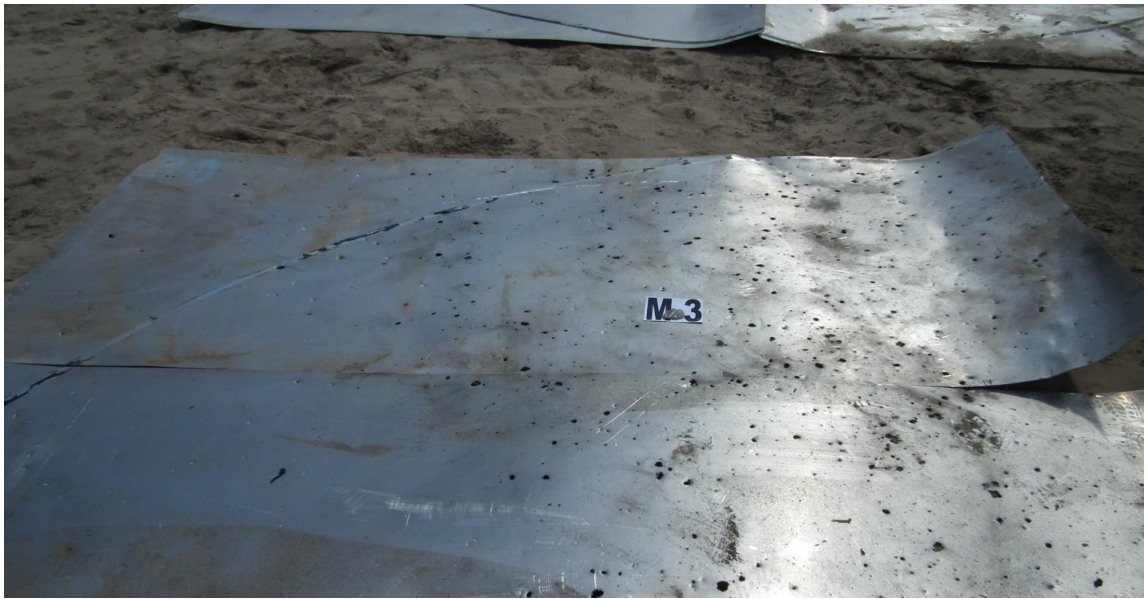


Figure A.101 - Fragments 3.0 (top) and 3.2 (bottom) of target No. 3



Figure A.102 - Fragments 3.3 (top), 3.5, 3.7 and 3.9 (bottom) of target No. 3



Figure A.103 - Fragments 3.4 (top), 3.6 and 3.8 (bottom) of target No. 3



Figure A.104 - Fragments 3.4 (top), 3.6 and 3.8 (bottom) of target No. 3



Figure A.105 - Fragments 3.2 (top), 3.4 and 3.6 (bottom) of target No. 3



Figure A.106 - Fragments 3.1 (top), 3.3 and 3.5 (bottom) of target No. 3



Figure A.107 - Left side of fragment 3.0 of target No. 3



Figure A.108 - Right side of fragment 3.0 of target No. 3



Figure A.109 - Left side of fragment 3.1 of target No. 3



Figure A.110 - Right side of fragment 3.1 of target No. 3



Figure A.111 - Left side of fragment 3.2 of target No. 3



Figure A.112 - Right side of fragment 3.2 of target No. 3



Figure A.113 - Left side of fragment 3.3 of target No. 3



Figure A.114 - Right side of fragment 3.3 of target No. 3



Figure A.115 - Left side of fragment 3.4 of target No. 3



Figure A.116 - Right side of fragment 3.4 of target No. 3



Figure A.117 - Left side of fragment 3.5 of target No. 3



Figure A.118 - Right side of fragment 3.5 of target No. 3



Figure A.119 - Left side of fragment 3.6 of target No. 3



Figure A.120 - Right side of fragment 3.6 of target No. 3



Figure A.121 - Left side of fragment 3.8 of target No. 3



Figure A.122 - Right side of fragment 3.8 of target No. 3



Figure A.123 - Left side of fragments 3.7 and 3.9 of target No. 3



Figure A.124 - Right side of fragments 3.7 and 3.9 of target No. 3

3.2.4 Shield target no. 4

Figures A.125 through A.145 show the appearance of target No. 4 and its fragments after they were collected. The sides of the target correspond to the simulated fuselage of the Boeing 777-200 aircraft. The left side of the aircraft is represented by shields 4.1, 4.3, 4.5, 4.7 and 4.9; the right side by 4.0, 4.2, 4.4, 4.6 and 4.8.



Figure A.125 - Target No. 4



Figure A.126 - Left side of fragment 4.0 of target No. 4



Figure A.127 - Right side of fragment 4.0 of target No. 4



Figure A.128 - Left side of fragment 4.1 of target No. 4



Figure A.129 - Right side of fragment 4.1 of target No. 4



Figure A.130 - Left side of fragment 4.2 of target No. 4



Figure A.131 - Right side of fragment 4.2 of target No. 4



Figure A.132 - Left side of fragment 4.3 of target No. 4

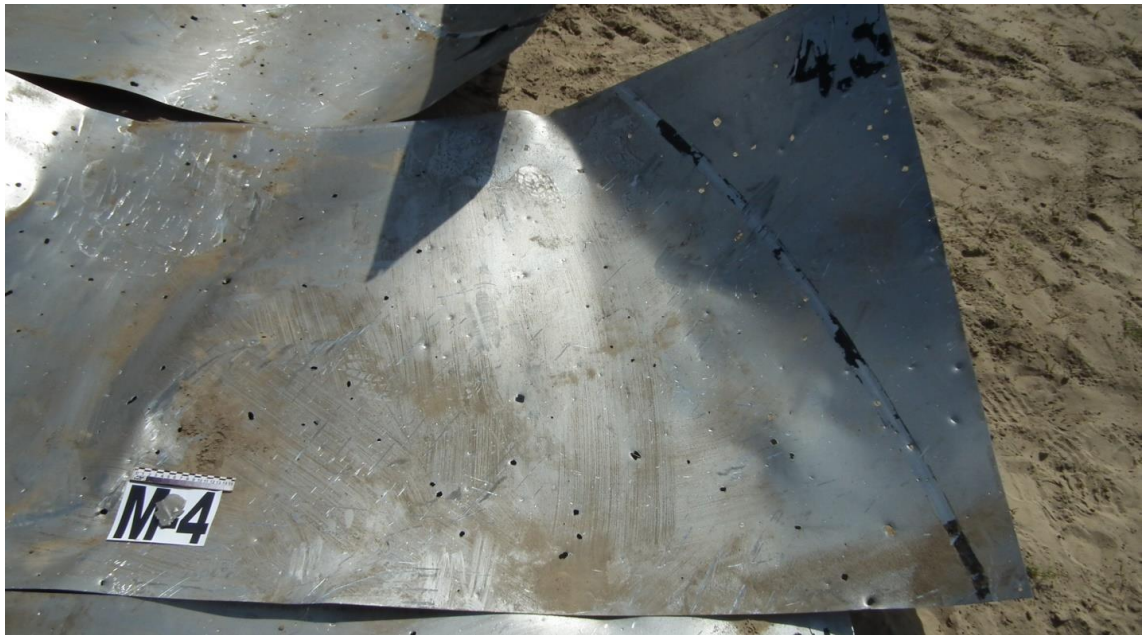


Figure A.133 - Right side of fragment 4.3 of target No. 4



Figure A.134 - Left side of fragment 4.4 of target No. 4



Figure A.135 - Right side of fragment 4.4 of target No. 4



Figure A.136 - Left side of fragment 4.5 of target No. 4

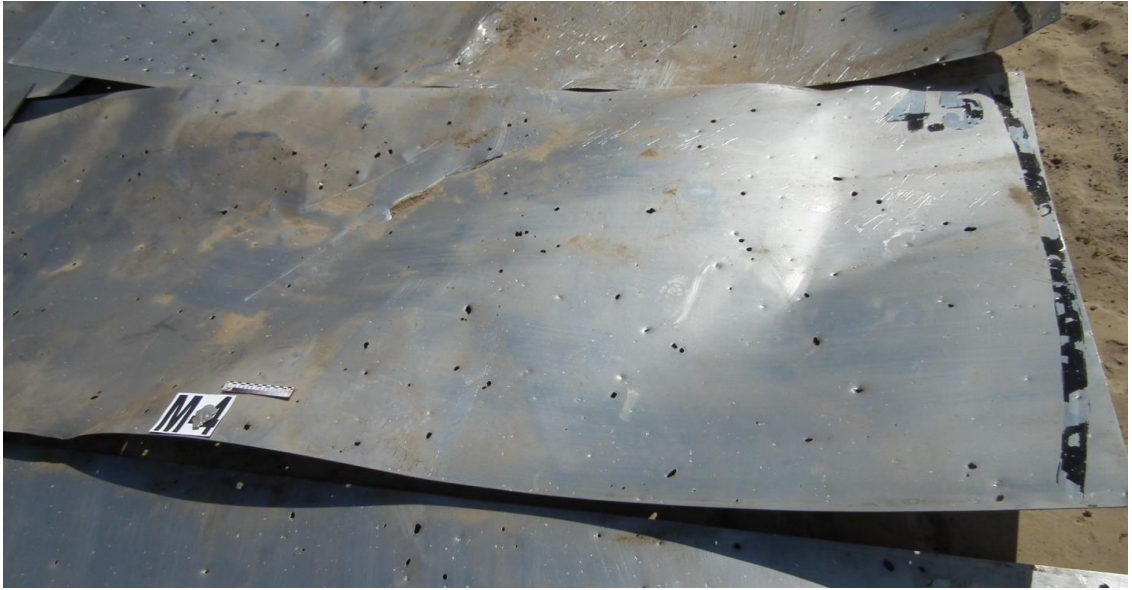


Figure A.137 - Right side of fragment 4.5 of target No. 4



Figure A.138 - Left side of fragment 4.6 of target No. 4



Figure A.139 - Right side of fragment 4.6 of target No. 4



Figure A.140 - Left side of fragment 4.7 of target No. 4



Figure A.141 - Right side of fragment 4.7 of target No. 4



Figure A.142 - Left side of fragment 4.8 of target No. 4



Figure A.143 - Right side of fragment 4.8 of target No. 4



Figure A.144 - Left side of fragment 4.9 of target No. 4



Figure A.145 - Right side of fragment 4.9 of target No. 4

3.2.5 Shield target No. 5

Figures A.146 through A.166 show the appearance of target No. 5 and its fragments after they were collected. The sides of the target correspond to the simulated fuselage of the Boeing 777-200 aircraft. The left side of the aircraft is represented by shields 5.1, 5.3, 5.5, 5.7 and 5.9; the right side by shields 5.0, 5.2, 5.4, 5.6 and 5.8.



Figure A.146 - Target No. 5



Figure A.147 - Left side of fragment 5.0 of target No. 5



Figure A.148 - Right side of fragment 5.0 of target No. 5



Figure A.149 - Left side of fragment 5.1 of target No. 5



Figure A.150 - Right side of fragment 5.1 of target No. 5



Figure A.151 - Left side of fragment 5.2 of target No. 5



Figure A.152 - Right side of fragment 5.2 of target No. 5



Figure A.153 - Left side of fragment 5.3 of target No. 5



Figure A.154 - Right side of fragment 5.3 of target No. 5



Figure A.155 - Left side of fragment 5.4 of target No. 5



Figure A.156 - Right side of fragment 5.4 of target No. 5



Figure A.157 - Left side of fragment 5.5 of target No. 5

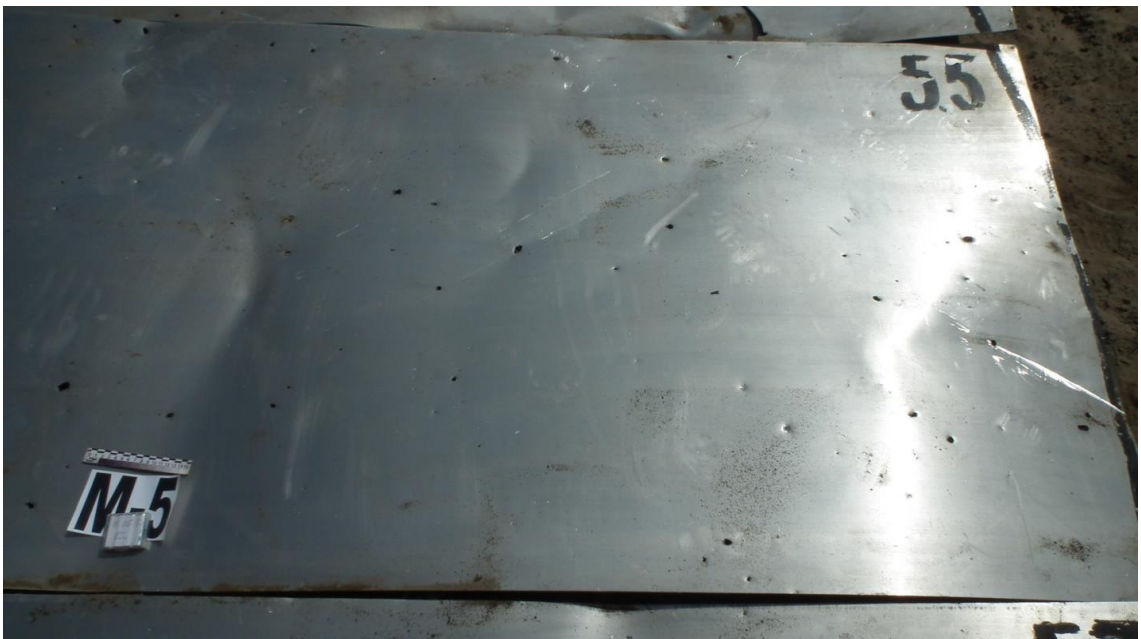


Figure A.158 - Right side of fragment 5.5 of target No. 5



Figure A.159 - Left side of fragment 5.6 of target No. 5

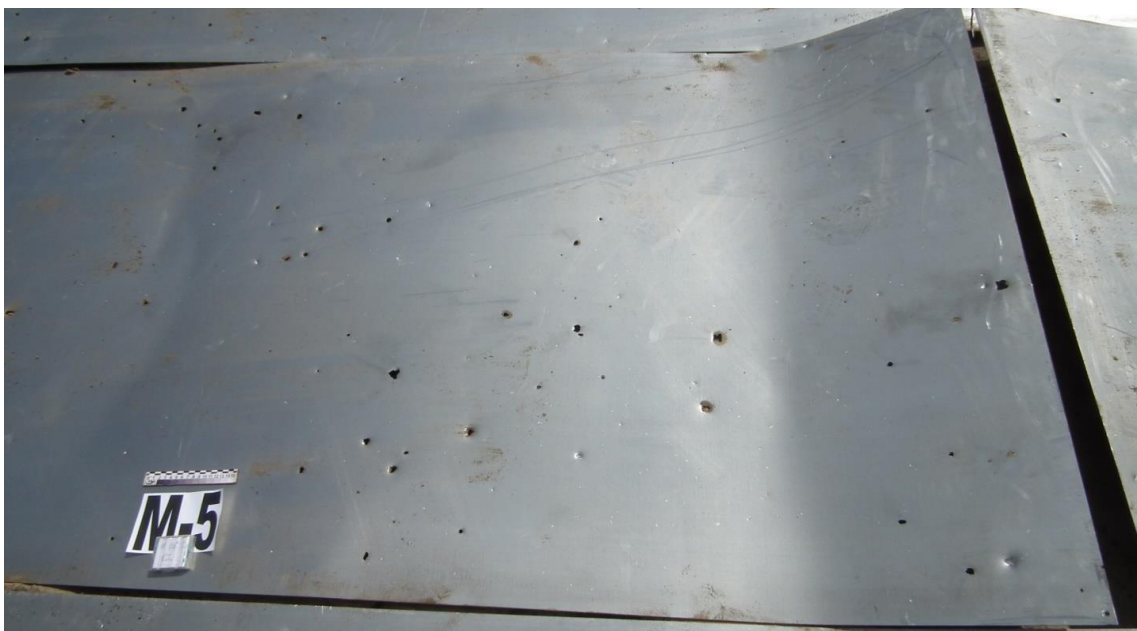


Figure A.160 - Right side of fragment 5.6 of target No. 5



Figure A.161 - Left side of fragment 5.7 of target No. 5

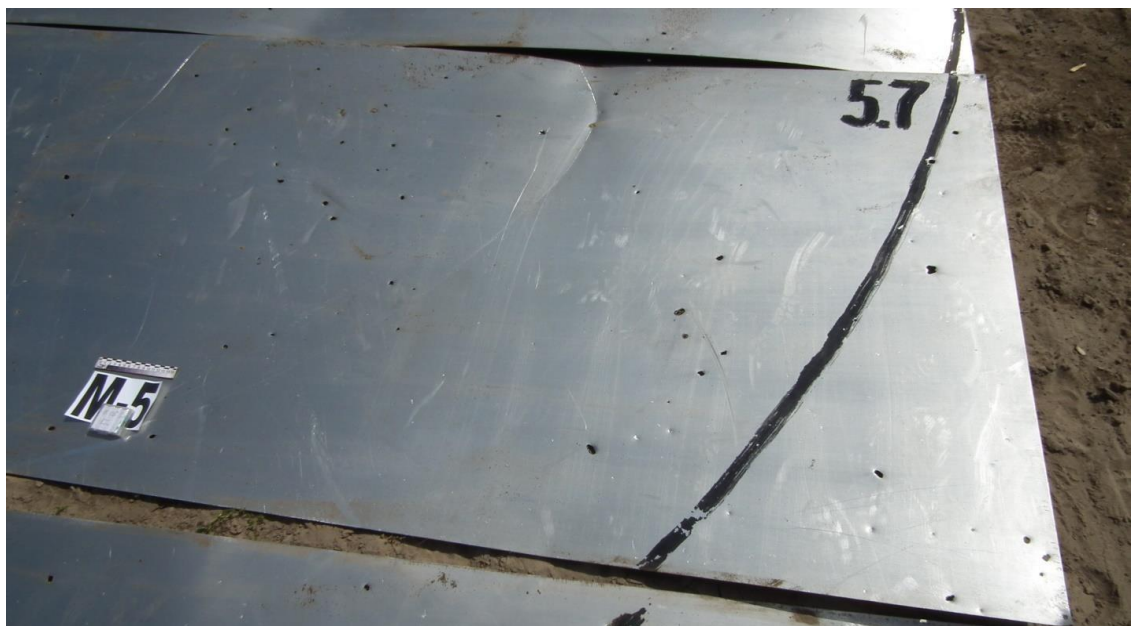


Figure A.162 - Right side of fragment 5.7 of target No. 5



Figure A.163 - Left side of fragment 5.8 of target No. 5



Figure A.164 - Right side of fragment 5.8 of target No. 5



Figure A.165 - Left side of fragment 5.9 of target No. 5



Figure A.166 - Right side of fragment 5.9 of target No. 5

3.2.6 Shield target No. 6M.D (left engine imitation)

Figure A.167 shows the appearance of target No. 6M.D (left engine imitation) and examples of piercing and non-penetrating damage. The through-holes are highlighted in red and non-penetrating damage is highlighted in yellow.

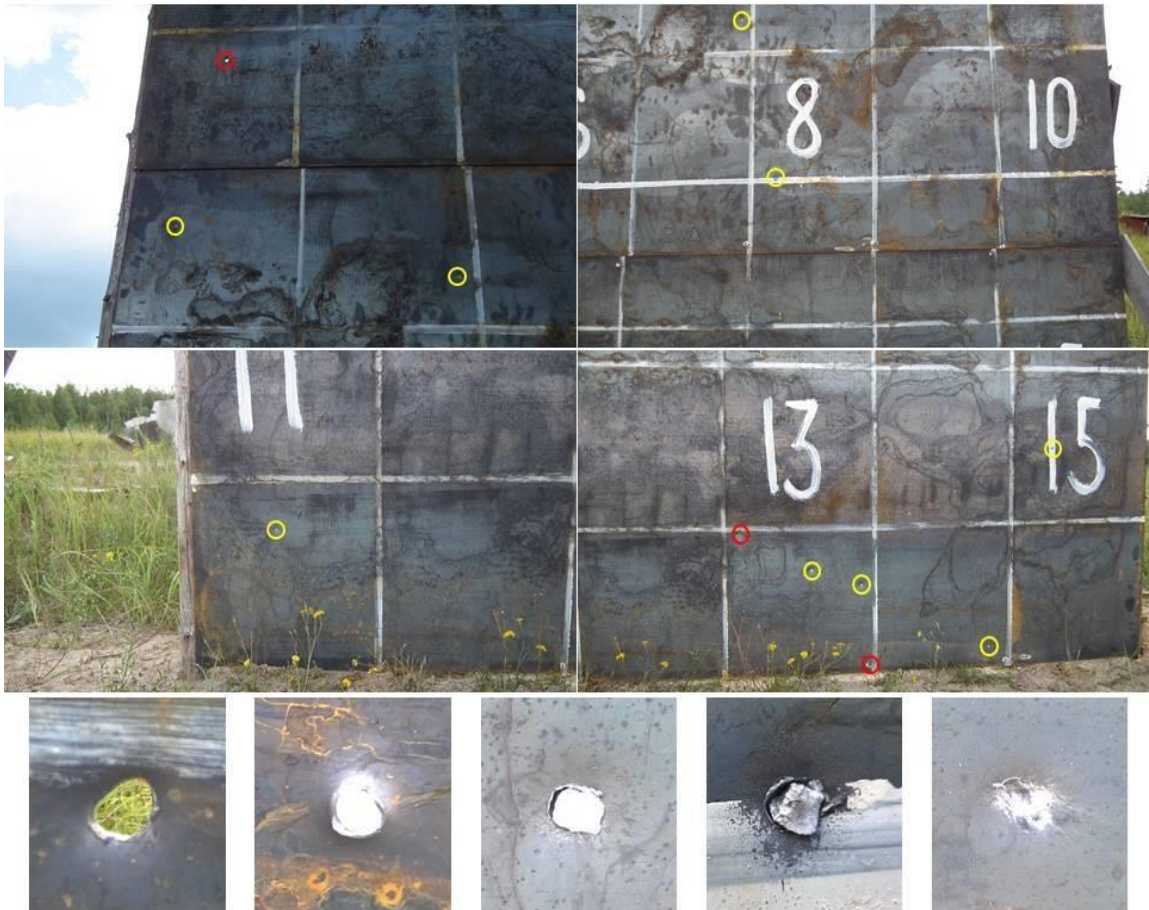


Figure A.167 - Fragments of target No. 6 (top) and examples of damage to the target (below)

3.3 Characteristic damage

3.3.1 "Butterfly"-shaped through-holes

An examination of damage to (through-holes in) fragments of the target layout revealed that all the targets made of duralumin alloy have a large number of "butterfly"-shaped holes, which are left the 9H314M 1-10 heavy fraction "bowtie"-shaped projectiles (Figures A.168 through A.174).



Figure A.168 - Characteristic "butterfly"-shaped holes

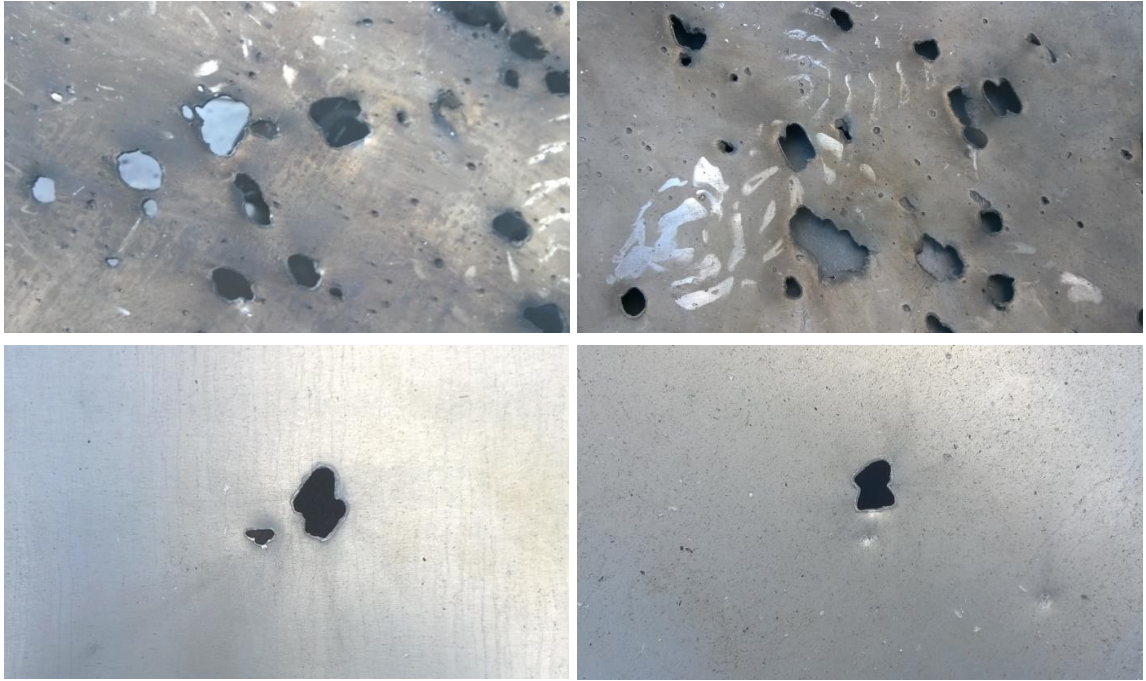


Figure A.169 - Characteristic "butterfly"-shaped holes



Figure A.170 - Characteristic "butterfly"-shaped holes



Figure A.171 - Characteristic "butterfly"-shaped holes

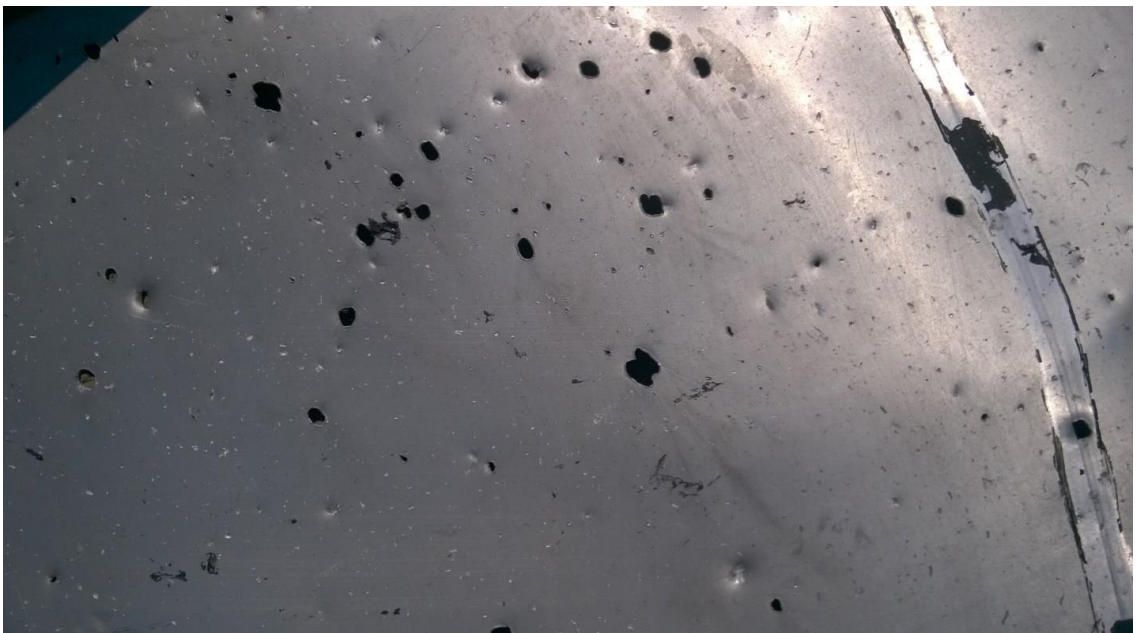


Figure A.172 - Characteristic "butterfly"-shaped holes

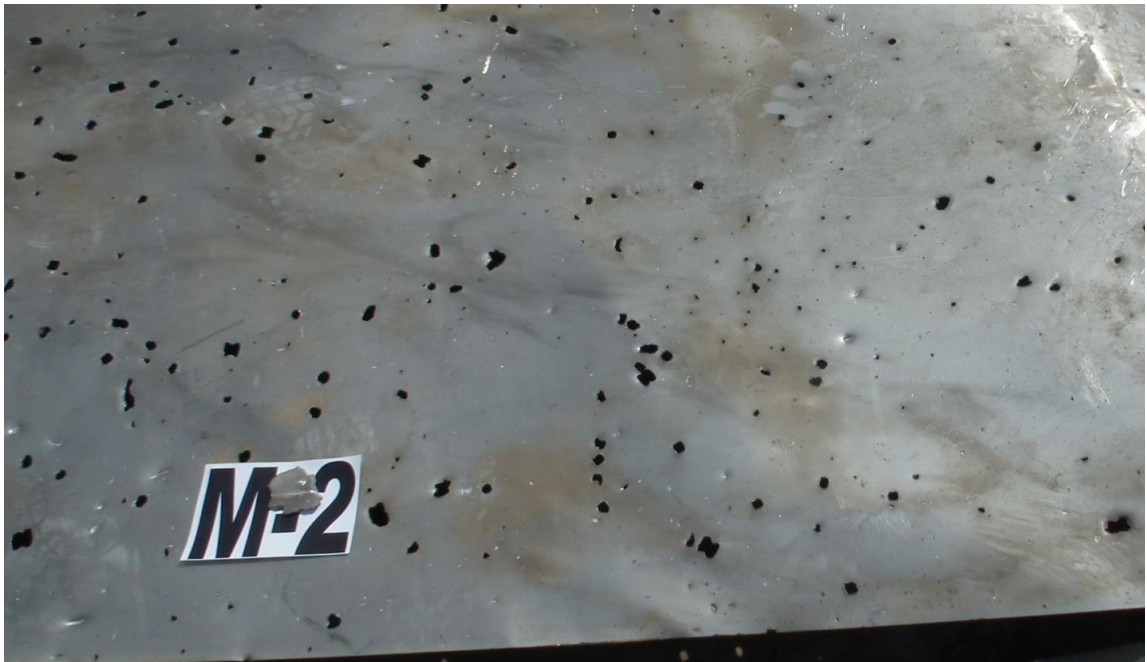


Figure A.173 - Characteristic "butterfly"-shaped holes



Figure A.174 - Characteristic "butterfly"-shaped holes

3.3.2 Damage caused by hull fragments

Hull fragments (those of the compartment hull) caused both piercing and non-penetrating damage to fragments of the shield target layout.

Some of the holes were significantly larger in size than the linear dimensions of the ready-made projectiles. Most of the "non-standard" through-holes left by hull fragments were located near the front and rear boundaries of the fragmentation flow, but within the meridional angle of dispersion of ready-made projectiles.

Examples of "non-standard" through-holes are shown in Figures A.175 through A.178.



Figure A.175 – Holes left by hull fragments



Figure A.176 - Piercing and non-penetrating damage caused by hull fragments



Figure A.177 - Hole left by a hull fragment



Figure A.178 - Hole left

None of the hull fragments that hit target No. 6M.D (left engine imitation) pierced the shields. An example of non-penetrating damage caused by a hull fragment is shown in Figure A.179.



Figure A.179 - Non-penetrating damage to target No. 6M.D
(left engine) caused by a hull fragment

3.3.3 Damage caused by effects of a close explosion

The traces left on the shield target fragments by the effects of a close explosion are manifested in the existence of micro-crater areas, thermal oxidation, compression, deformation and rupture of the target sheets. Examples of such damage are shown in Figures A.180 to A.187.



Figure A.180 - Target fragment with micro-crater marks and thermal oxidation



Figure A.181 - Target fragment with micro-crater marks and thermal oxidation

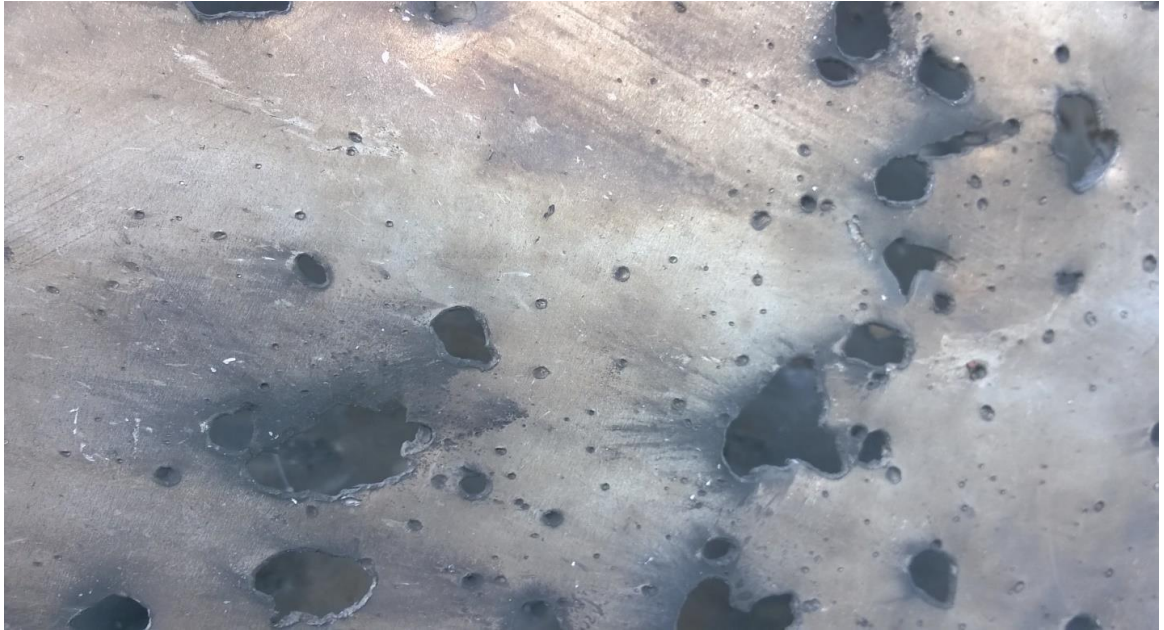


Figure A.182 - Target fragment with micro-crater marks and thermal oxidation



Figure A.183 - Target fragment with micro-crater marks and minor thermal oxidation

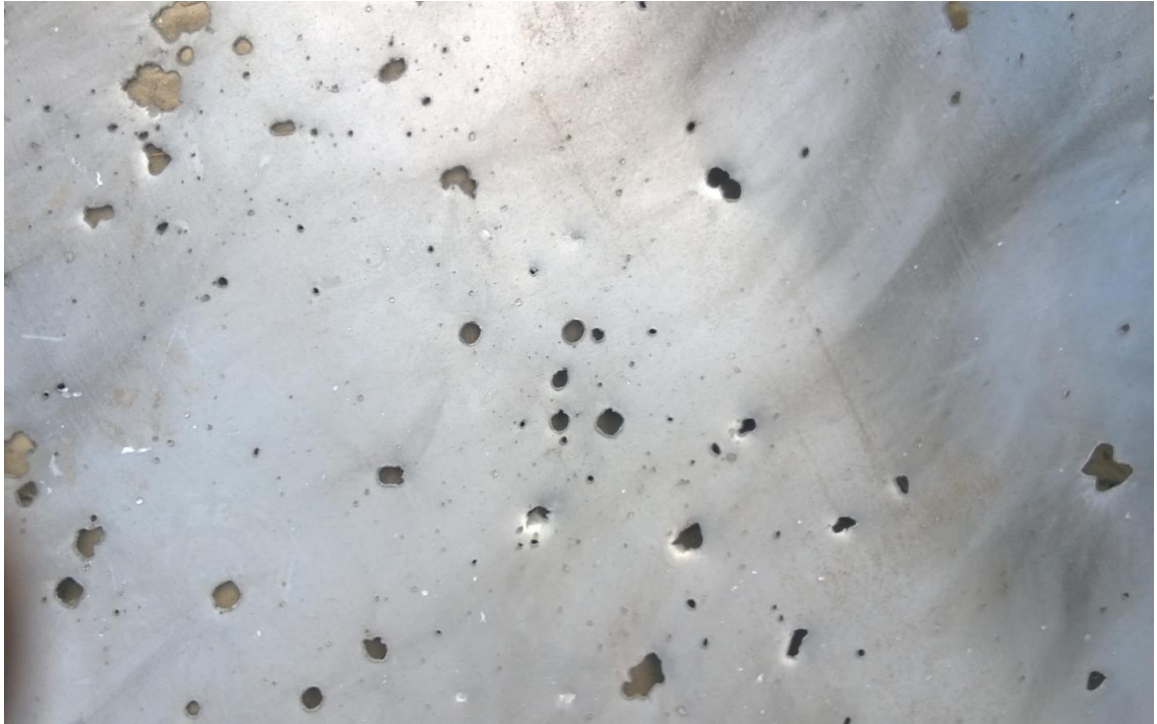


Figure A.184 - Target fragment with micro-crater marks and minor thermal oxidation



Figure A.185 - Target fragment with traces of compression, deformation and rupture of skin sheets



Figure A.186 - Target fragment with traces of deformation and rupture of skin sheets



Figure A.187 - Target fragment with traces of deformation and rupture of skin sheets

3.3.4 Secondary damage

Fragments of shield target #2 and #3 show a large amount of damage from secondary striking elements - fragments ("plugs") of the target sheets knocked out of the first /second barrier. Examples of such damage are shown in Figures A.188, A.189 and A.190.



Figure A.188 - Fragment of target with marks of secondary damage

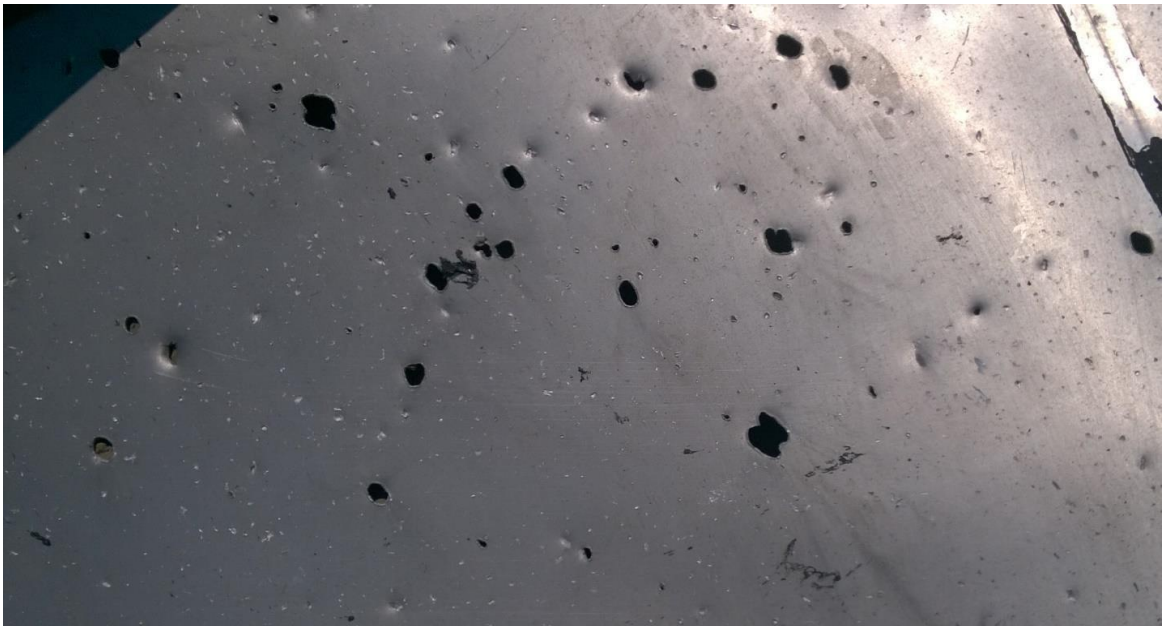


Figure A.189 - Fragment of target with marks of secondary damage



Figure A.190 - Fragment of target with marks of secondary damage

Figure A.191 shows a close-up view of secondary damage manifesting itself in "scratches" on target fragment No. 3.

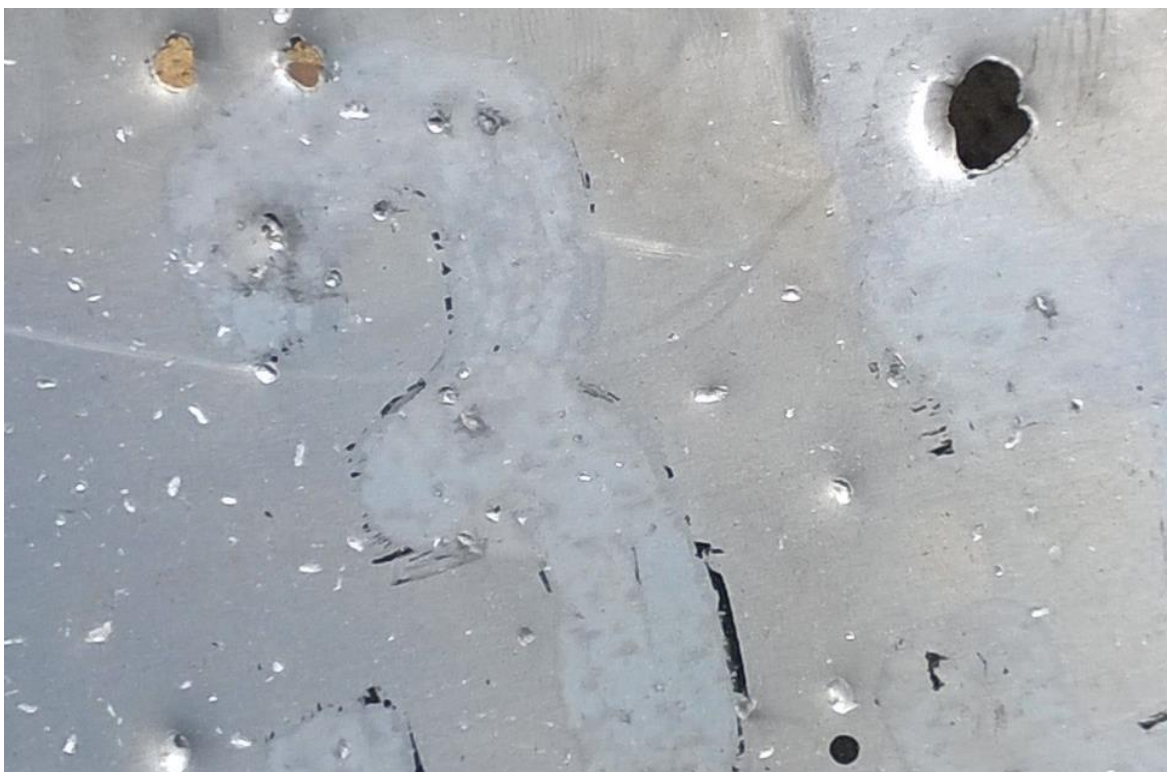


Figure A.191 - Fragment of target with "scratches" from secondary striking elements

Figures A.192 through A.194 show examples of secondary striking elements ("plugs" from target sheets).



Figure A.192 - Secondary striking elements ("plugs" from target sheets)



Figure A.193 - Secondary striking elements ("plugs" from target sheets)



Figure A.194 - Secondary striking element ("plug") shaped like a "bowtie"

3.3.5 Exit holes and non-penetrating damage

Figures A.196 through A.201 show examples of through-holes from ready-made projectiles and of non-penetrating damage from hull fragments and secondary striking elements in shield target sheets.



Figure A.196 - Exit holes and non-penetrating damage
(view from the back of the shield)



Figure A.197 - Exit holes and non-penetrating damage
(view from the back of the shield)



Figure A.198 - Exit holes and non-penetrating damage
(view from the back of the shield)



Figure A.199 - Exit holes with jagged edges and non-penetrating damage on
target No. 4 (view from the back of the shield)

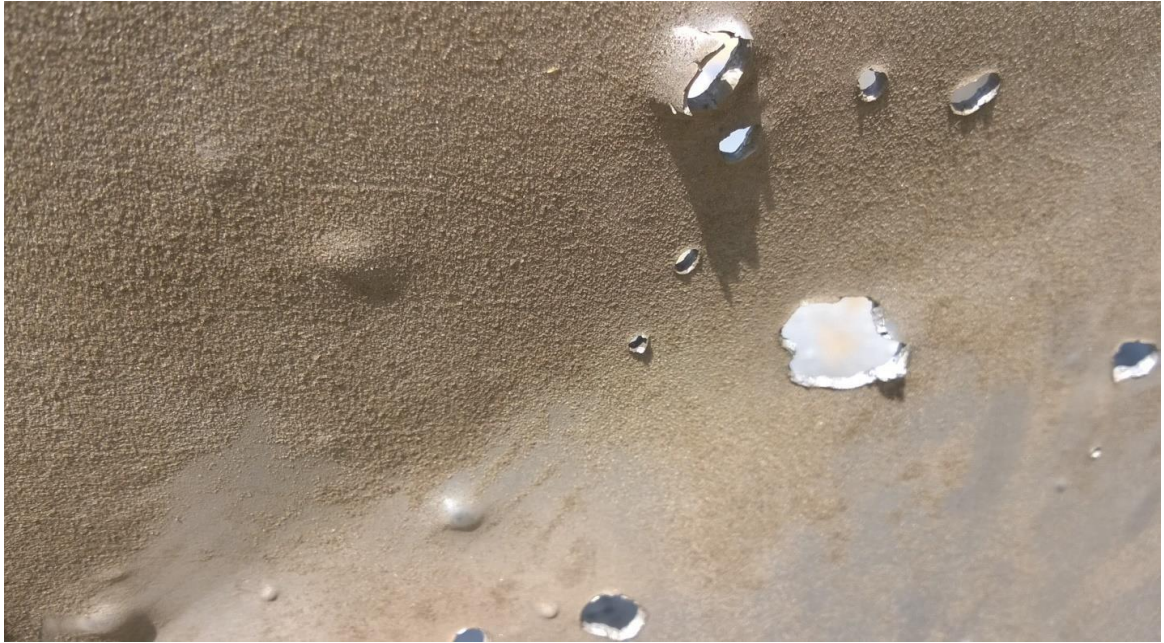


Figure A.200 - Exit holes with jagged edges and non-penetrating damage on target No. 4 (view from the back of the shield)



Figure A.201 - Exit holes and non-penetrating damage (view from the back of the shield)

3.4 Projectiles

During the testing, 71 projectiles of all three fractions of the 9H314M warhead were extracted from the target structure and traps:

- 9N314M 1-10 (heavy fraction "bowtie" 13 x 13 x 8.2 mm);
- 9N314M 1-9 (light fraction "parallelepiped" 8 x 8 x 5 mm);
- 9N314M 1-11 (light fraction "parallelepiped" 6 x 6 x 8.2 mm).

Photographs of examples of the extracted projectiles are shown in Figures A.202 through A.206.

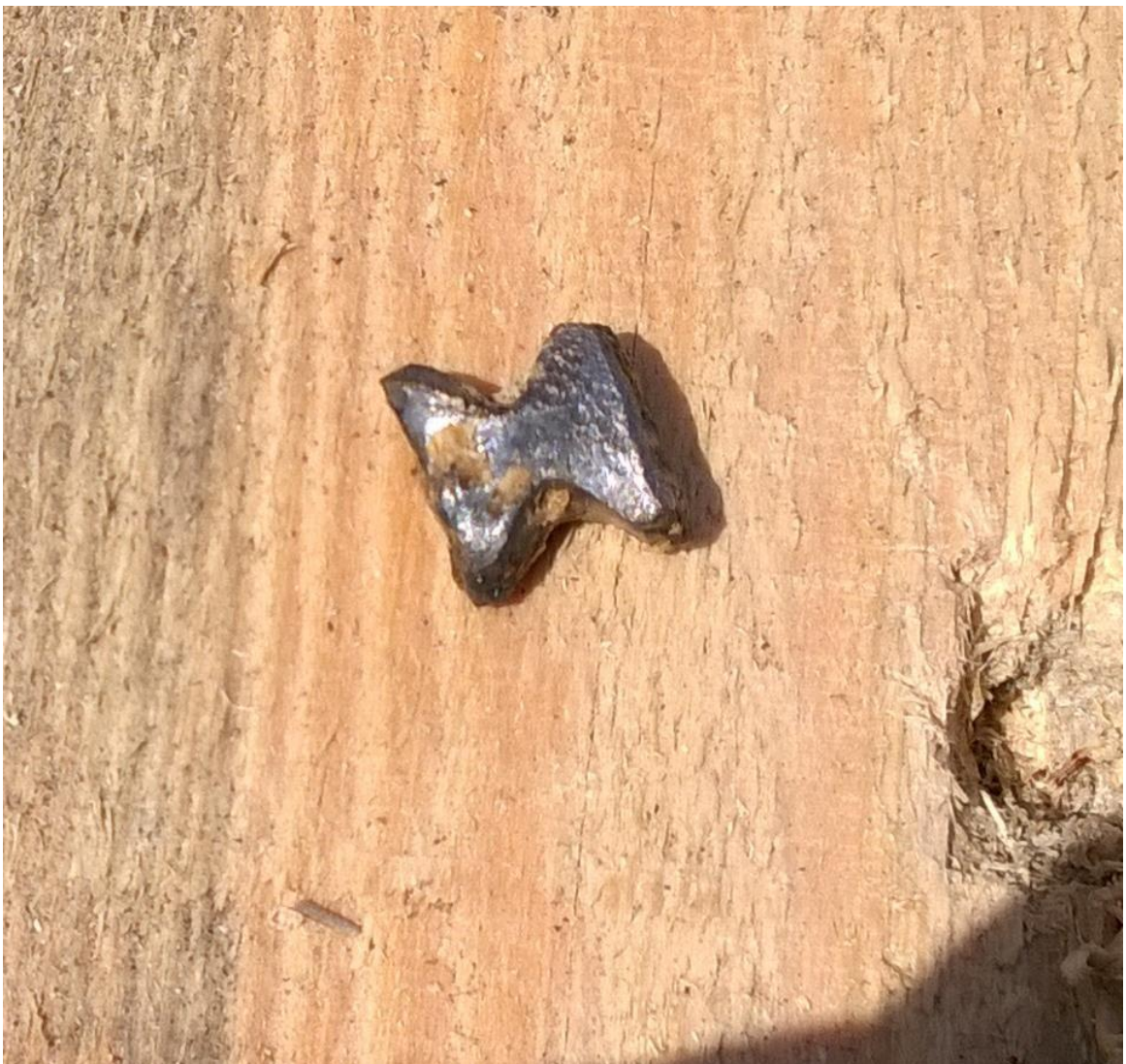


Figure A.202 - 9H314M 1-10 ("bowtie") projectile retaining its original shape



Figure A.203 - 9H314M 1-10 projectile ("bowtie ") which was deformed but retained its original shape



Figure A.204 - 9H314M 1-10 projectile ("bowtie") which lost its original shape



Figure A.205 - 9H314M 1-9 projectile ("parallelepiped")



Figure A.206 - 9H314M 1-11 projectile ("parallelepiped")

Distribution of extracted projectiles by type:

- 9N314M 1-11 "parallelepiped" 6x6x8.2 mm - 15 pcs. (21.13 %);
- 9N314M 1-9 "parallelepiped" 8x8x5 mm - 17 pcs. (23.94 %);
- 9N314M 1-10 "bowtie" 13x13x8.2 mm - 39 pcs. (54.93 %).

Examples of 9H314M 1-10 "bowtie"-shaped projectiles (13x13x8.2 mm fractions) recovered from traps and the target structure are shown in Figures A.207 through A.209.



Figure A.207 - 9H314M 1-10 projectiles (top view)



Figure A.208 - 9H314M 1-10 projectiles (side view 1)



Figure A.209 - 9H314M 1-10 projectiles (side view 2)

Examples of "parallelepiped"-shaped 9H314M 1-11 projectiles (6x6x8.2 mm fractions) extracted from traps and the target structure are shown in Figures A.210 and A.211.

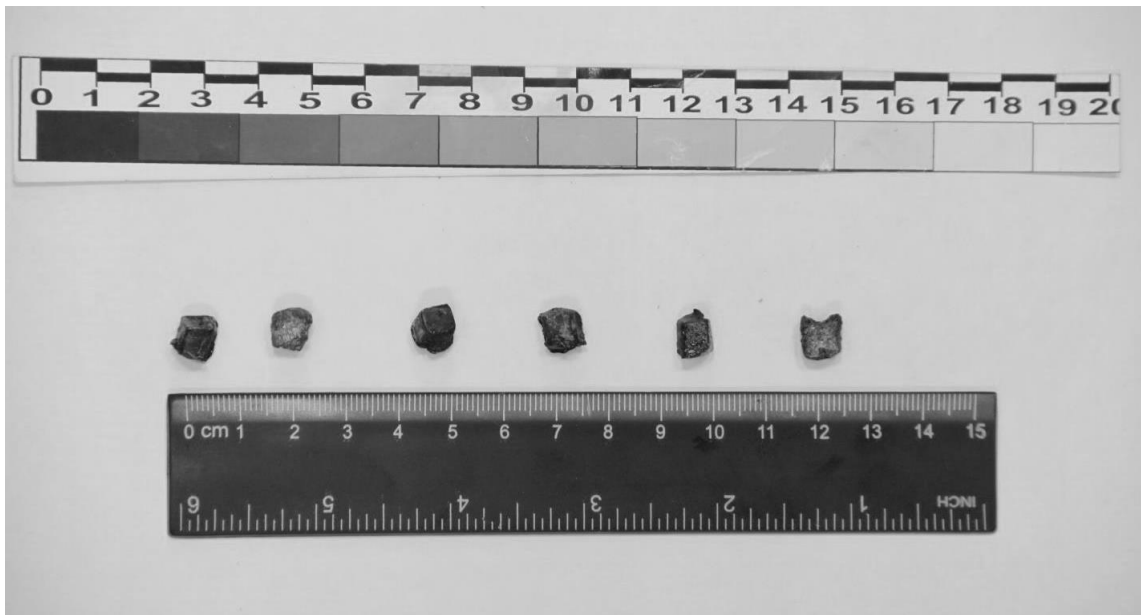


Figure A.210 - 9H314M 1-11 projectiles (top view)

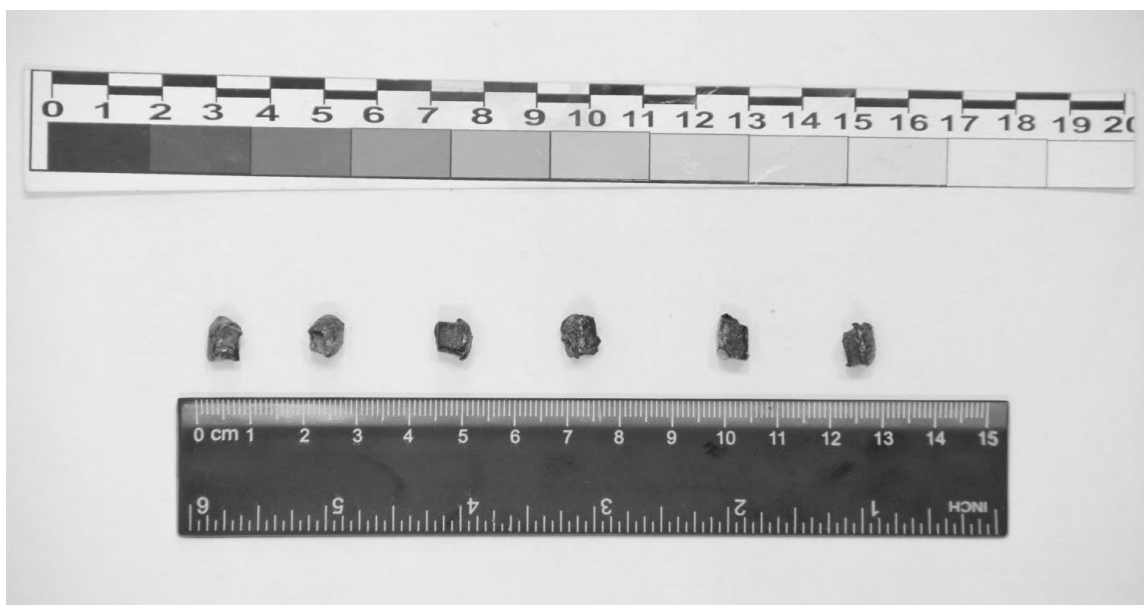


Figure A.211 - 9H314M 1-10 projectiles (side view)

Examples of "parallelepiped"-shaped 9H314M 1-9 projectiles (8x8x5 mm fractions) extracted from traps and the target structure are shown in Figure A.212.



Figure A.212 - 9H314M 1-9 projectiles (top view)

Examples of hull fragments (those of the compartment hull) recovered from traps and the target structure are shown in Figures A.213 and A.214.



Figure A.213 - Hull fragments



Figure A.214 - Hull fragments

Annex 3

Report of JSC Air and Space Defense Corporation "Almaz-Antey" on a flight test of the air-route radar complex "Utes-T" located at the air-route radar position "Ust-Donetsk" at the Rostov Regional Centre of the Russian Federation Unified Air Traffic Management System, 2019

(translation)

REPORT

on a flight test of the air-route radar complex "Utes-T"
located at the air-route radar position "Ust-Donetsk" at the Rostov Regional Centre
of the Russian Federation Unified Air Traffic Management System

Moscow, 2019

Designations and Abbreviations

AC	- aircraft
UATMS	- Unified Air Traffic Management System
PSR	- primary surveillance radar
PJ	- passive jamming
RI	- radar information
RC	- radar complex
RS	- radar station / radar
RF	- Russian Federation
MTS	- moving target selection
TRS	- technical requirement specification
ARRC	- air-route radar complex
MOR	- military operational requirement
RCS	- radar cross-section

Terms and Definitions

The following terms with their respective definitions were used in preparing this report:

False-alarm probability: The probability that noise or other interfering signals will erroneously cause a target detection decision. *See also:* detection probability (according to IEEE Std 686).

Detection probability: 1) (detection probability): the probability that a signal, when actually present at the input of the receiver, will be correctly declared a target signal based on observation of the receiver output. *See also:* false alarm probability;

2) (acquisition probability): the probability of establishing a stable track on a designated target (according to IEEE Std 686).

Secondary RI processing: The processing of primary RI that provides target trajectory detection, filtering and extrapolation of detected trajectory parameters and target tracking, as well as recognition of radar target classes based on signal and trajectory characteristics. The result of secondary processing is trajectory radar information on the target (trajectory parameters).

Range: Distance between a radar and a target (according to IEEE Std 686).

Minimum detectable velocity (MDV): In a Doppler processing radar for detection of moving targets, the minimum target velocity that can be detected (according to IEEE Std 686).

Minimum detectable signal (MDS): The minimum signal level that gives reliable detection in the presence of white Gaussian noise (according to IEEE Std 686).

Note: MDS must be described in terms of probability of detection and probability of false alarm, due to its statistical nature.

Slant range: The slant distance between a radar and a target (according to IEEE Std 686).

Slant distance: The distance between two points which are not at the same elevation. Used in contrast to ground distance (according to IEEE Std 686).

Radar coverage area: The area of space within which RI can be obtained and which is characterised by the coordinates of the area boundaries in terms of range, azimuth, elevation and scan period (rate).

Radar detection area: The part of the coverage area where detection of a specific type of target with predetermined characteristics of correct detection and

false alarm is provided. The detection area is characterised by RCS and flight speed of the target and the boundary values of range, altitude, elevation angles and azimuth.

Detection: Isolation of an object from the background and classifying it as an object of potential interest.

Detection of a radar target: establishing the presence of a target as a result of RI processing and determining the position of the target in space and identifying the nature of actions.

RI processing: the process of transforming RI, including by combining RI received from several radars, in order to improve its completeness, accuracy and reliability.

Radar signal processing: The process of converting radar signals to reduce interference and isolate useful RI.

Backscatter: Energy reflected or scattered in a direction opposite to that of the incident wave (IEEE Std 686).

Signal-to-noise ratio: In radar, the ratio of the power corresponding to a specified target measured at some point in the receiver to the noise power at the same point in the absence of the received signal (according to IEEE Std 686).

Primary RI processing: The processing (conversion) of radar signals received from the output of a receiving radar over a certain time interval or in a single space scanning session, which provides detection of a signal reflected from or emitted by a target, stabilization of false alarm level, obtaining primary measurement information about radar target coordinates. The result of the primary processing is RI on coordinates of the target (coordinate points).

Radar position: An area of the earth's surface on which a radar is located or which is prepared for the deployment of a radar or parts thereof.

Threshold: A value of voltage or other measure that a signal must exceed in order to be detected or retained for further processing (according to IEEE Std 686).

Potential (from Latin potentia: power): 1) energy characteristic of a system or a device; 2) an available resource that can ensure the implementation of a particular process.

Radar potential: A generalised characteristic of a radar which depends on the ratio of its transmitter power to the receiver sensitivity.

Radar information (RI): The totality of information about radar targets that is obtained by radar methods in the process of radar observations.

Radar station (RS, radar): (1) radar equipment that comprises structurally and functionally related components and is designed for radar observation; (2) an

electromagnetic system for the detection and location of objects that operates by transmitting electromagnetic signals, receiving echoes from objects (targets) within its volume of coverage, and extracting location and other information from the echo signal (according to IEEE Std 686).

Notes:

1. Radar is an acronym for radar detection and ranging.
2. Radar equipment can be operated with the transmitter turned off, as a passive direction finder on sources radiating within the band of the receiving system.

Radar target: A radar observation object in the form of an object or environment that is capable of emitting or altering the parameters of radio waves.

Radar observation: The process of obtaining information about objects and environment using radioelectric methods based on the phenomena of emission, propagation and scattering of radio waves. Radar observation of airborne objects includes: surveillance of a defined area of space, searching for and detecting various objects, determining their coordinates and radial velocity, and obtaining non-coordinate information about them.

Radar complex (RC): Radar equipment comprising one or more radars and communication and RI processing facilities which are functionally linked and shared for radar observation.

Radar scanning: The process of radar observation of targets in a defined coverage area, which is characterised by the distribution of emitted and received energy. The nature of the energy distribution is determined by the shape of the antenna directivity pattern, as well as the law of motion of antenna.

Radar signal: A signal in the form of radio waves used in the radar observation process to obtain information about radar targets.

Tracking: The process of following a moving object or a variable input quantity. In radar, target tracking in angle, range, or Doppler frequency is accomplished by keeping a beam or angle cursor on the target angle, a range mark or gate on the delayed echo, or a narrowband filter on the signal frequency, respectively (according to IEEE Std 686).

Note - This process may be carried out manually or automatically for one or more of the above input quantities. The beam, range gate, or filter can be either centered on the input quantity or can be coarsely placed, with interpolation measurements providing accurate data to a computer that does the fine tracking. *See also:* automatic tracking; tracking radar; track-while-scan.

Elevation angle: In radar, the angle between the line-of-sight in the direction of interest and a horizontal reference plane, measured upwards (according to IEEE Std 686).

Radar equation: a mathematical expression that relates the range of a radar at which specific performance is obtained to the parameters characterizing the radar, target, and environment. Synonym: radar range equation; range equation (according to IEEE Std 686).

Note: The parameters in the radar equation can include the transmitter power, antenna gain and effective area, frequency, radar cross section of the target, range to the target, receiver noise figure, signal-to-noise ratio required for detection, losses in the radar system, and the effects of the propagation path.

1. Purpose and Objectives of the Flight Test of Utes-T ARRC

The DSB's report "Crash of Malaysia Airlines Boeing 777-200, 9M MRD, flight MH17" claims that the crash of Boeing 777 was caused by the impact of "a 9H314M war head carried by a 9M38-series missile"¹ and concludes that the probable location of the missile launch is "eastern Ukraine"², indicating the possible launch area of about 320 km², as calculated by experts of the "Netherlands Aerospace Centre" (NLR)³.

The experts of Almaz-Antey Air-Defence Corporation ("Almaz-Antey") claim that if the 9M38 missile was launched from the area mentioned in DSB's report, there would be a high probability that the missile would have been detected by Utes-T ARRC deployed in the village of Ust-Donetsk in Rostov Region of the Russian Federation. However, a careful review of the documented primary radar information from Utes-T ARRC shows that the missile was not detected by the locator. This fact, along with an analysis of the performance features of: (i) the Buk surface-to-air missile system, (ii) 9M38 surface-to-air guided missiles, (iii) damage to the outer skin, internal equipment and load-bearing structure of the Boeing 777, and (iv) the results of experiments and special research conducted by Almaz-Antey led to the following conclusions:

- If the crash of the Boeing 777 was caused by a 9M38 missile, then this could only have happened in case the missile was on a "collision course" (the most likely angle of the missile's approach to the aircraft in the horizontal plane could be 72^{+2}_{-10} deg.;

- The launch area could be the area shown in yellow in Figure 1 and shown in the presentation⁴ at Almaz-Antey Air-Defence Corporation's press conference held in October 2015 to present the results of the full-scale experiment;

- When a 9M38 missile was launched from the area indicated by the Corporation's experts, Utes-T ARRC was not capable of detecting it;

- If a 9M38-type missile was launched from the area specified in the DSB's report, it would have had a high probability of being detected by Utes-T ARRC.

¹ The name of the weapon from the DSB's Report.

² Final Report. 11. Missile flight parts, p.256.

³ Final Report. Visualisation of NLR fly out simulation result. Figure 62, p.144.

⁴ "Results of a Field Experiment to Evaluate the Causes of the Crash of MH17", October 2015.

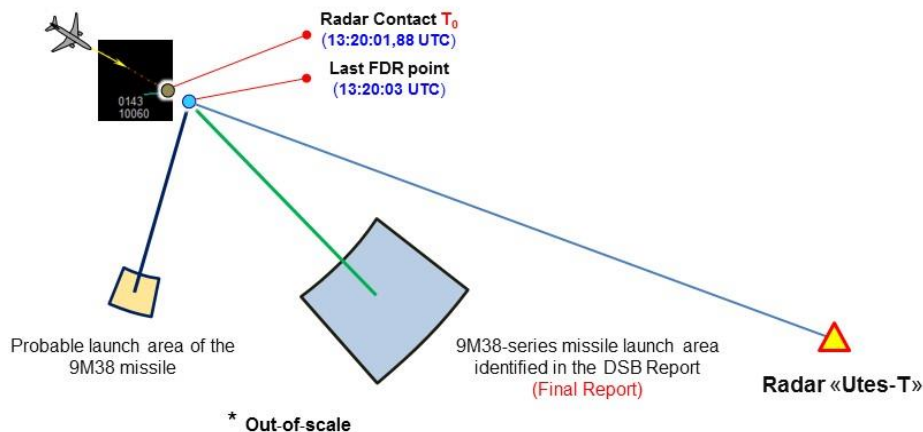


Figure 1 - Presumed missile launch areas

In order to confirm the conclusions drawn by experts of Almaz-Antey, a flight test of Utes-T ARRC was conducted.

The purpose of the flight test of Utes-T ARRC was to assess the spatial characteristics of Utes-T ARRC's primary surveillance radar (PSR) and its ability to detect airborne objects whose flight and reflection characteristics are similar to those of a 9M38-series missile.

The objectives of the flight test were:

1. Defining more precisely the acquisition radar range of Utes-T ARRC's PSR for airborne objects with radar visibility corresponding to a 9M38-type missile.
2. Determining the capability of Utes-T ARRC's PSR to detect and track airborne objects:
 - flying at supersonic speeds, including in the acceleration and deceleration areas;
 - suddenly appearing from below the radio horizon and moving along trajectories consistent with the hypotheses under consideration concerning the 9M38 missile intercept flight.

2. Conditions and procedures for conducting the flight test

The 9M38 missile detection capabilities of Utes-T ARRC's PSR was determined in two phases.

In the first phase, the potential capabilities were determined using known analytical relationships based on the PSR characteristics set forth in Utes-T ARRC operational documentation.

In the second phase, information on detection of real airborne objects manoeuvring under different conditions was gathered, and the PSR detection area diagram for 9M38-type objects was built.

The flight test was conducted in the airspace of the Russian Federation symmetrically in relation to the phase centre of Utes-T ARRC's PSR. The test diagram is shown in Figure 4.

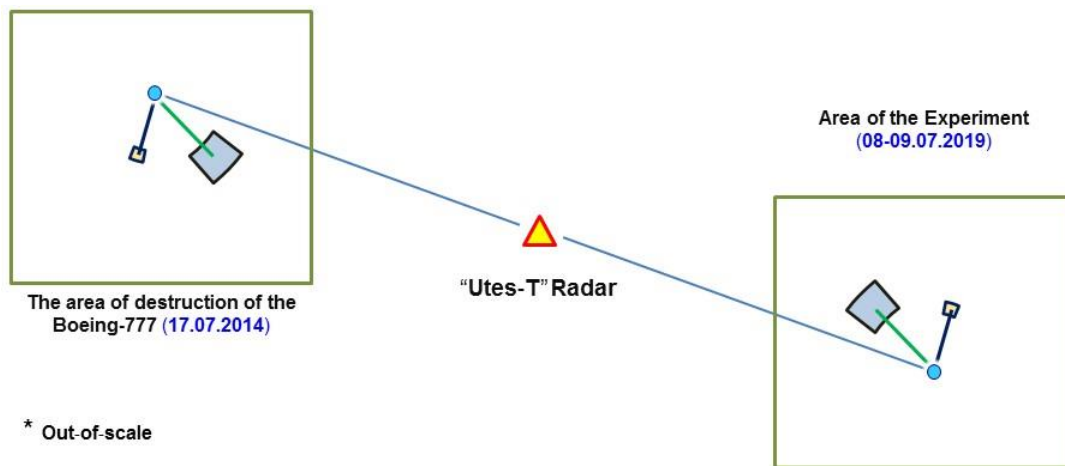


Figure 2 - Flight test diagram

During the test, all events were simulated under maximally similar initial conditions as to relative position of the radar and the reference airborne objects.

Utes-T ARRC operated in a routine automatic mode. The equipment operated in a routine mode and the operators did not interfere with the operation of the ARRC during the tests⁵.

In the test area (reference area), Utes-T ARRC's primary radar, which operated in an automatic mode, was detecting airborne objects in MTS mode. This is evidenced by the forms in respect of the aircraft which were travelling in international air corridors and the reference airborne objects.

⁵ Audio and video recording of the tests was carried out.

The weather conditions at the time of the test were equivalent to the actual weather conditions in the area of the Boeing 777 crash (Figure 4), which is also evidenced by weather radar data at Millerovo position (Figure 5).



Figure 3 - Actual weather conditions at the time of the test



Figure 4 - Weather radar data (Millerovo position)

MiG-29 and MiG-31 aircraft, as well as Orlan-10 UAV took part in the flight test of Utes-T ARRC.

The RCS of MiG-29 aircraft was about 5 m². Orlan-10 UAV RCS data obtained by means of statistical processing of the back reflection diagrams measured by the reference radar are shown in Table 1.

Table 1 - RCS of Orlan-10 UAV

Location angle sector*	$0^{\circ}\pm 45^{\circ}$	$90^{\circ}\pm 45^{\circ}$	$180^{\circ}\pm 45^{\circ}$
RCS value for level 0.5 ($\sigma_{0,5}$), m ²	0.23	0.26	0.13

* - 0° angle corresponds to location from the nose; 90° angle corresponds to location from the side; and 180° angle corresponds to location from the tail of the unit in the course plane (horizontal plane).

The test flight around the radar position was conducted over two days, 08 July 2019 and 09 July 2019, using the single programme and methodology.

At the boundaries of the area of ARRC detection by reference airborne objects (MiG-29), the test flight was performed at ranges of 280 to 380 km and altitudes of 7,000 to 12,600 m, which corresponds to the elevation position range of 0.3 to 1.0 degrees relative to the radar position.

The test flight was performed both by approaching and moving away from the ARRC position. When approaching the ARRC near the far edge of the detection area, the reference airborne objects flew with their transponders turned off.

The test plan included special reference trajectories of two types. The first type was a high-speed supersonic segment with preliminary acceleration, supersonic manoeuvring and subsequent deceleration. During the acceleration and manoeuvring and throughout the reference high-speed segment and deceleration segment, the reference targets (MiG-31) were flying with the transponder off.

The second type of reference trajectories is the simulation of a missile flight according to the versions of the hypothesis in question.

Before the flight along the special trajectories of the second type, the reference targets (MiG-29s) also switched off their transponders and descended below the radio horizon. When below the radio horizon, they manoeuvred and approached the point of origin of the special reference trajectory.

The reference targets then flew a trajectory consistent with the hypotheses under consideration: "in an opposite direction" and "on a collision course".

Test results were recorded using ARRC initial log files, recordings of parametric recorders, GPS sensors, and audio, photo and video equipment mounted on ARRC, reference airborne objects and other objects.

3. Brief Description of the Test Object

The object of the tests was Utes-T ARRC's PSR (serial number 208020) located at the Ust-Donetsk radar position at the Rostov Regional Centre of the UATMS of the Russian Federation (Figure 5).



Figure 5 - Utes-T ARRC in Ust-Donetsk village, Rostov Region, Russian Federation

Utes-T ARRC is used for air traffic control. Certificate of FAVT-RTOP-005 type issued for Utes-T ARRC by the Federal Air Transport Agency of the Russian Federation on 17 July 2018 confirms that Utes-T ARRC is a high-performance radar complex which meets the requirements of ICAO and Eurocontrol.

The operating area of the PSR at zero takeoff angle for aircraft with the RCS equal to 5 m² under probability of correct detection of at least 0.8 and probability of false alarms based on the receiver's own noise of no more than 10⁻⁶ is as follows:

- minimum elevation angle: not more than 0.5 deg.;
- maximum elevation angle: at least 45 deg.;

- maximum detection range: at least 360 km;
- maximum detection altitude: at least 20 km.

The threshold signal-to-noise ratio in terms of power for defined probabilities of correct detection (P_d) and false alarm (P_{fa}) is as follows:

$$q_0 = \frac{\ln P_{\text{ЛТ}}}{\ln P_0} - 1 \approx 60,9 \approx 17,85 \text{ дБ} \tag{1}$$

* $P_{\text{ЛТ}} = P_{fa}$
 $P_0 = P_d$
 дБ = dB (translator's note)

Using the above data, it is possible to determine from the radar equation the RCS potential (P_{RCS}), which must be at least

$$\Pi_{\text{ПОРЛ}} \geq \frac{q_0 \cdot D_{\text{макс}}^4}{\sigma_0} = \frac{60,9 \cdot (360000)^4}{5} = 2 \cdot 10^{23} \tag{2}$$

where $D_{\text{макс}}$ (D_{max}) is the maximum detection range of the PSR which is equal to 360,000 m;

σ_0 - target RCS equal to 5 m².

* $\Pi_{\text{ПОРЛ}} = P_{RCS}$ (translator's note)

The vertical section of the PSR detection area for a target with the RCS equal to 1 m² under detection probability of at least 0.8 and false-alarm probability of no more than 10⁻⁶ is shown in Figure 3.

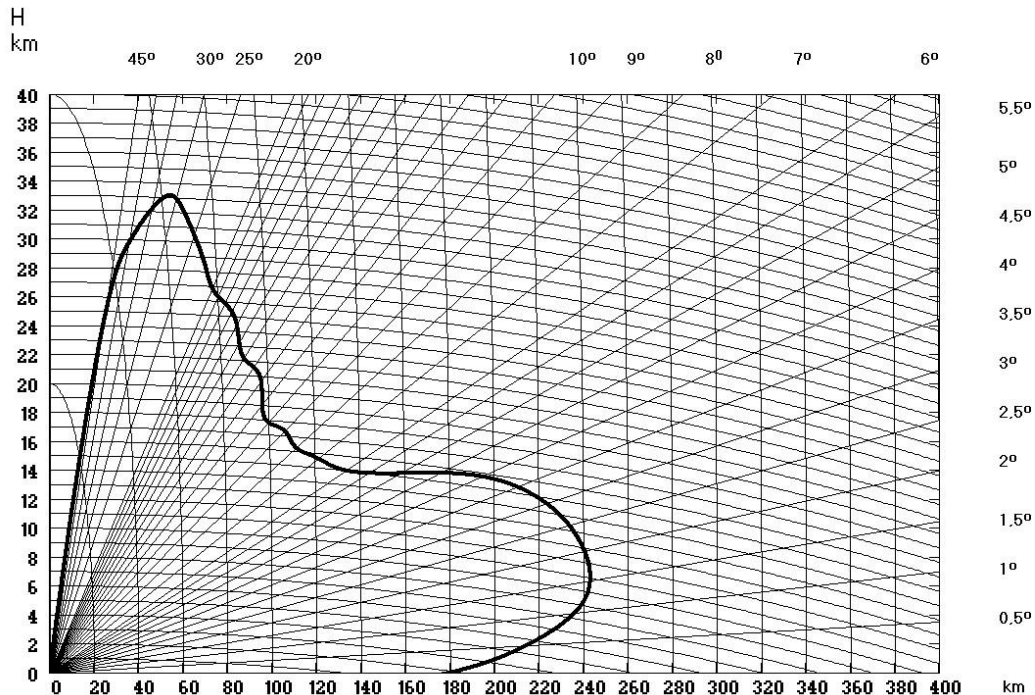


Figure 6 - Vertical section of Utes-T ARRC's PSR detection area for a target with RCS equal to 1 m^2 under detection probability of 0.8 and false-alarm probability of at least 10^{-6}

The PSR operates in the L-band (1215 - 1350 MHz).

The radar complex has high reliability and features automatic back-up, remote control, monitoring and diagnostics, and unattended operation, and is built on solid-state technology featuring state-of-the-art signal and information processing methods.

The signal and information processing system provides a dynamic range of digitally processed signals of at least 70 dB and primary and secondary processing of radar information. The complex ensures documentation and reproduction of all processed radar information.

The MTS algorithm is implemented in a special signal processor and is based on the principle of adaptive grid Doppler filtering. The MTS provides separation of reflected signals from aircraft moving with radial velocities of 40 to 500 m/s against the background of noise created by stationary objects and objects moving at a speed of less than 40 m/s (reflections from ground and water surfaces, moisture targets, etc.). In the area where the radial velocities are from 500 to 1,000 m/s, there are no long-term dips in the transmission ratio of more than 2-5 dB in depth (Figure 7).

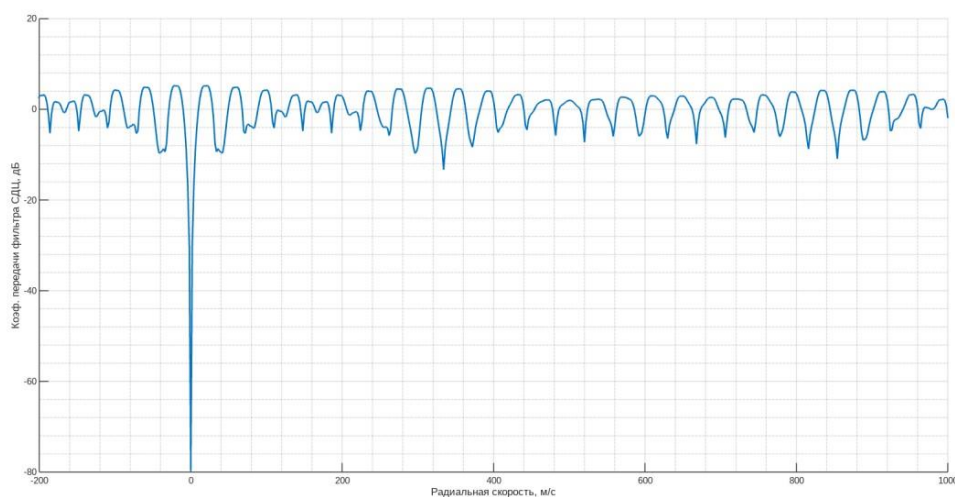


Figure 7 - Velocity performance of Utes-T ARRC's MTS system

* MTS filter transmission ratio, dB
Radial velocity, m/s

In order to eliminate "blind" velocities, wobbling of the repetition intervals of sounding signals is used. The use of signals with a non-equidistant pulse sequence makes it possible to create a passive noise rejection zone with no significant dips in the non-zero velocity zone. The passive interference suppression ratio is at least 50 dB.

4. Estimate of missile detection capability

The RCS values for a 9M38-type missile obtained from different observation angles when taking measurements at the reference radar complex in the L-band with horizontal polarization of the signal are shown in Table 2.

The radar performance was determined using a 9M38RM missile equipped with a standard radiotransparent radome and mounted target seeker device. The radar visibility characteristics of the 9M38RM unit were obtained by means of statistical processing of the measured back scattering diagrams.

Table 2 - RCS of 9M38 type-missile

Location angle sector*	$0^\circ \pm 10^\circ$	$90^\circ \pm 10^\circ$	$90^\circ \pm 30^\circ$	$165^\circ \pm 15^\circ$	$180^\circ \pm 10^\circ$
RCS value for level of 0.5 ($\sigma_{0,5}$), m^2	0,3	3,3	0,9	0,85	2,3

* - 0° angle corresponds to location from the nose; 90° angle corresponds to location from the side; 180° angle corresponds to location from the tail of the unit in the course plane (horizontal plane).

According to the transcripts of the Boeing 777's parametric recorders, the crash of flight MH17 occurred at 13.20:03 UTC.

The last measurement of Boeing 777's position was taken by Utes-T ARRC's PSR at $T_0 = 13.20:01.88$ UTC (Figure). Thus, about 1.12 seconds elapsed between the last measurement and the crash.

According to the DSB's report, the Boeing 777 airliner did not perform any manoeuvres three minutes before the Last FDR point, and its altitude, course and speed were constant. The experts of Almaz-Antey conducted a simulation of the 9M38-type missile's acquisition of a non-maneuvring aerodynamic target for two hypotheses:

- "in an opposite direction" launch
- "on a collision course" launch

The 9M38 missile flight trajectories for the two hypotheses are shown in Figure 9 (time T_0 corresponds to the time of the last measurement in relation to the Boeing 777, while time T_{-10} and T_{-20} correspond to 10 s and 20 s before the last measurement, respectively). One can see from the figure that given the time of the missile's flight to the Last FDR point, the missile should have entered the ARRC's coverage area at least twice in case of a flight "on a collision course" and should have entered that area three times in case of a flight in "an opposite direction".

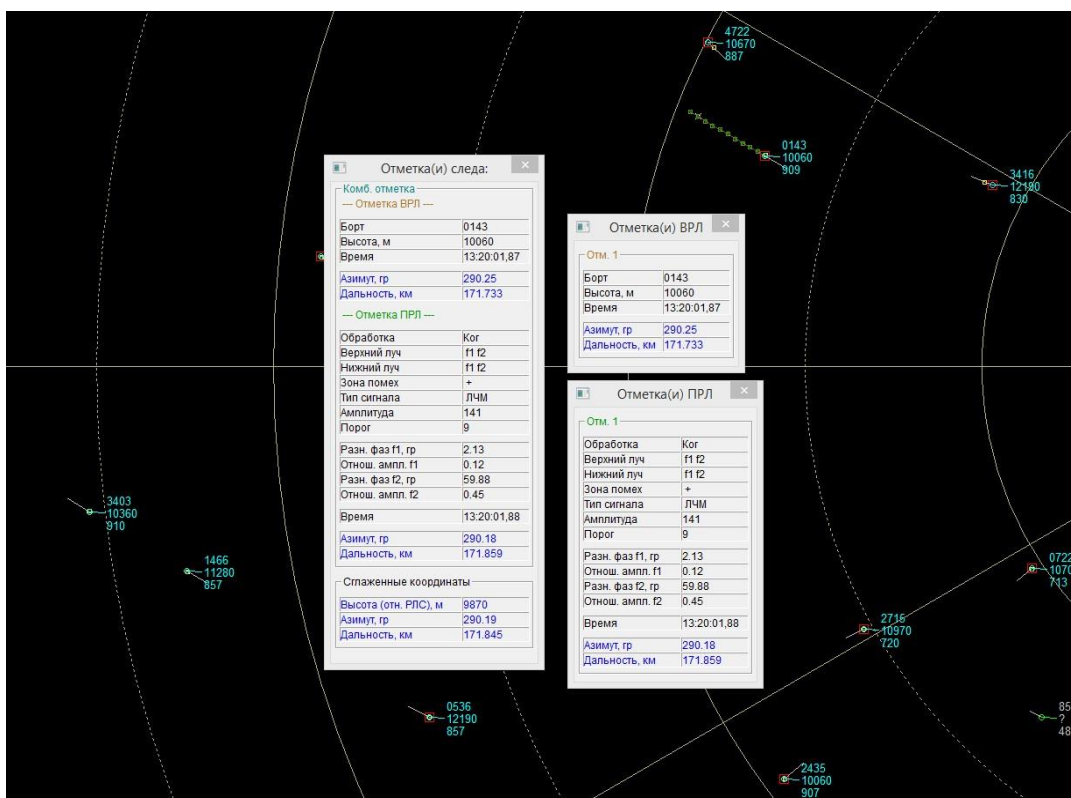


Figure 8 - Last measurement taken
by Utes-T ARRC in relation to Boeing 777 aircraft

*

Trail mark(s)

Combined mark - Secondary radar mark	
Board	0143
Altitude, m	10060
Time	13:20:01,87
Azimuth, deg..	290.25
Distance, km	171.733
- Primary radar mark	
Processing	Coherent
Upper beam	f1 f2

Lower beam	f1 f2
Interference area	+
Signal type	Linear frequency modulation
Amplitude	141
Threshold	9
Phase difference f1, deg..	2.13
Amplitude ratio f1	0.12
Phase difference f2, deg..	59.88
Amplitude ratio f2	0.45
Time	13:20:01,88
Azimuth, deg..	290.18
Distance, km	171.859
Smoothed coordinates	
Altitude (relative to radar), m	9870
Azimuth, deg..	290.19
Distance, km	171.845

Secondary radar mark(s)

Mark 1	
Board	0143
Altitude, m	10060
Time	13:20:01,87
Azimuth, deg..	290.25
Distance, km	171.733

Primary radar mark(s)

Mark 1	
Processing	Coherent
Upper beam	f1 f2
Lower beam	f1 f2
Interference area	+
Signal type	Linear frequency modulation
Amplitude	141
Threshold	9
Phase difference f1, deg..	2.13
Amplitude ratio f1	0.12
Phase difference f2, deg..	59.88
Amplitude ratio f2	0.45
Time	13:20:01,88

Azimuth, deg..	290.18
Distance, km	171.859

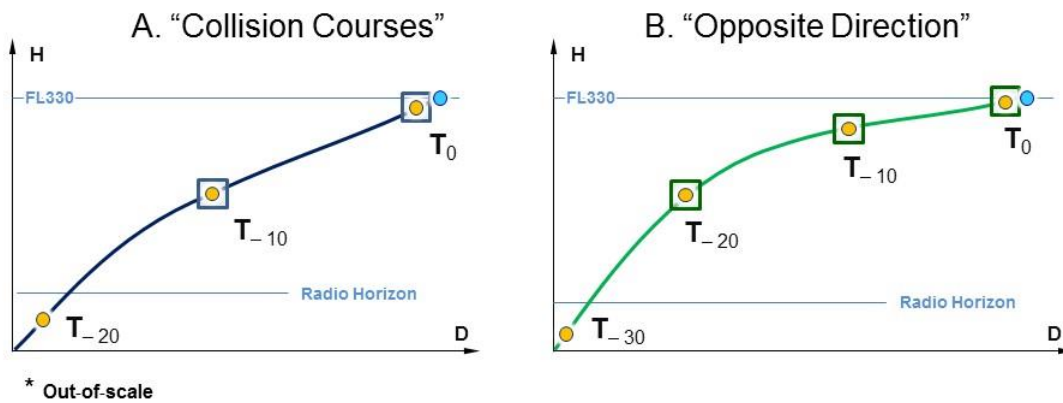


Figure 9 - Possible trajectories of 9M38 missile flight
A - "collision course"; B - "opposite direction"

The maximum distance of the missile from Utes-T ARRC at the time T_0 was about 170 km.

The maximum detection range for a radar target can be determined from the known characteristics of the radar and the RCS of the target (σ_{target}):

$$D_{\text{макс}} = \sqrt[4]{\Pi_{\text{ПОРЛ}} \cdot \frac{\sigma_{\text{ц}}}{q_0}} \quad (3)$$

$$\begin{aligned} * \quad D_{\text{макс}} &= D_{\text{max}} \\ \Pi_{\text{ПОРЛ}} &= P_{\text{RCS}} \\ \sigma_{\text{ц}} &= \sigma_{\text{target}} \end{aligned}$$

The maximum detection range for a 9M38 type missile (depending on the angle of its observation) for correct detection probability of 0.8 and false alarm probability of 10^{-6} is shown in Table 3.

Table 3 - Maximum detection range for 9M38 type missile

Location angle sector*	$0^\circ \pm 10^\circ$	$90^\circ \pm 10^\circ$	$90^\circ \pm 30^\circ$	$165^\circ \pm 15^\circ$	$180^\circ \pm 10^\circ$

Detection range, km	177	323	233	230	295
---------------------	-----	-----	-----	-----	-----

* - 0° angle corresponds to location from the nose; 90° angle corresponds to location from the side; and 180° angle corresponds to location from the tail of the unit in the course plane (horizontal plane).

It can be seen from the table that at any angle of observation, the maximum detection range for a 9M38 missile exceeds its maximum distance from the radar.

It is also possible to determine the signal-to-noise ratio and the probability of detecting the missile at times of its presumed location. The fact that the signal-to-noise ratio exceeds the threshold value also confirms the likelihood of its detection.

Given the known potential of Utes-T ARRC's PSR, the signal-to-noise ratio for the targets can be calculated using the following formula

$$q = \Pi_{\text{ПОРЛ}} \cdot \frac{\sigma_{\text{ц}}}{D_{\text{ц}}^4}, \quad (4)$$

where $\sigma_{\text{ц}}$ is the target's RCS;

$D_{\text{ц}}$ (D_{target}) - slant range equal to the distance from the radar to the target.

With fixed false alarm value, the probability of correct detection will be

$$P_0 = \exp\left(\frac{\ln P_{\text{ЛТ}}}{q + 1}\right) \quad (5)$$

$$* P_{\text{ЛТ}} = P_{\text{fa}}$$

In addition to the sufficient detection range, it is also important that the conditions for observing the missile correspond to the capabilities of the PSR in terms of elevation angles and radial velocity at the times of the missile location.

The estimated values of trajectory parameters and conditions for observation of a 9M38-type missile by Utes-T ARRC for the launch in an opposite direction and on a collision course at points in time T_{-20} , T_{-10} and T_0 are shown in Table 4.

Table 4 - Conditions for missile observation by Utes-T ARRC

Characteristic	Missile's course					
	Collision course			Opposite direction		
	T_{-20}	T_{-10}	0	T_{-20}	T_{-10}	0

Ground speed, m/s	680-740	975-990	750-770	930-970	770-850	635-670
Radial speed, m/s	- (9-11)	12-15	-(17-19)	790-820	730-810	606-630
Elevation angle, degrees	-(0.45-0.35)	1.2-1.4	2.4-2.6	1.6-2.1	2.4-2.75	2.6-2.75
Slant range (not more than), km	-	170	170	150	160	170
Observation angle, degrees	-	90°±30°	90°±30°	165°±15°	165°±15°	165°±15°
RCS, m ²	-	0.9	0.9	0.85	0.85	0.85
Signal-to-noise ratio	-	215	215	336	275	208
Probability of detection	-	-	-	0.96	0.95	0.94

It is seen from the table that a 9M38-type missile fails to enter Utes-T ARRC's coverage area in terms of elevation angles in one instance only: when it is below the radio horizon line (on a "collision course" at $T-20$).

Utes-T ARRC's PSR has sufficient capability to detect a 9M38-type missile in flight both in an opposite direction and on a collision course. The expected signal-to-noise ratio was significantly above the threshold in all scan periods. However, a 9M38-type missile could not be detected by Utes-T ARRC's PSR in case of a flight on a "collision course" because of excessively low radial velocity. The minimum radial velocity at which the radar can detect moving targets when the MTS equipment is on is 30(50) m/s. In contrast, the probability of detecting a 9M38-type missile flying to intercept a target in an "opposite direction" is high in each of the three scan periods. Further, the probability of detecting the missile in at least one of the three scan periods is close to 1 and is greater than 0.99.

The results of the flight test should confirm or refute the conclusions drawn from the analytical calculations.

5. Main results of the flight test

When flying around Utes-T ARRC's PSR in the far periphery of the detection area, the reference airborne objects both approached the position of the ARRC and moved away from it.

An example of detecting a reference airborne object, which was detected when it was approaching the radar position, is shown in Figure 10.

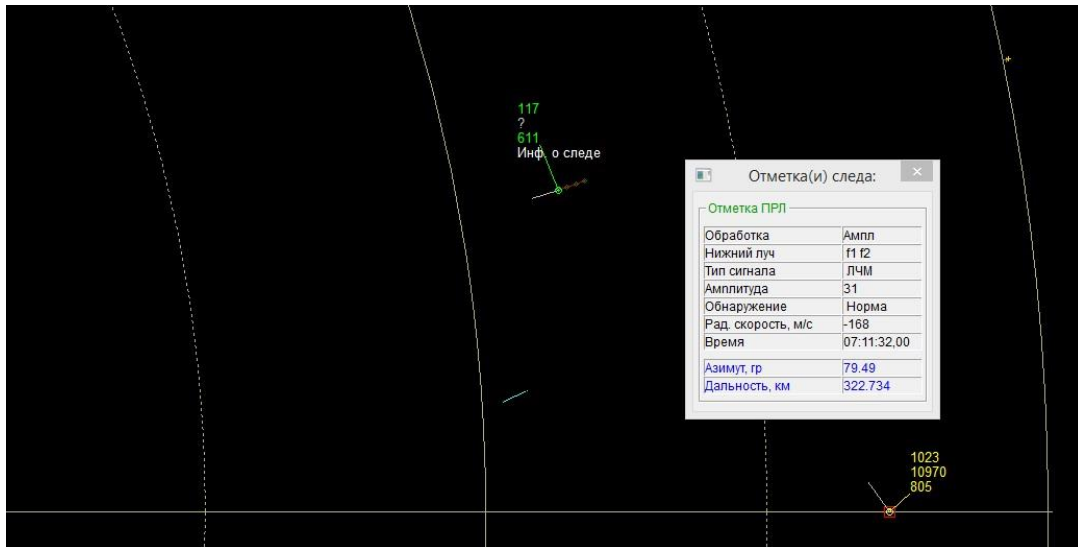


Figure 10 - Detection of reference airborne object No. 117 by the PSR at a distance of 322.7 km

* Trail mark(s)

- Primary radar mark	
Processing	Ampl.
Lower beam	f1 f2
Signal type	Linear frequency modulation
Amplitude	31
Detection	Standard
Radial velocity, m/s	-168
Time	07:11:32,00
Azimuth, deg..	79.49
Distance, km	322.734

The results of the test flight along the far edge of the detection area are shown in Table 5.

Table 5 - Range of reference targets detection

	Range, km	Radial speed, m/s
Approaching the ARRC	309,5...354,4	-245...-168
Moving away from the ARRC	304,3...360,9	172...256

According to the results of the flight around Utes-T ARRC, the detection range for an airborne object the RCS of which corresponds to that of a 9M38 missile (recalculated using the formula for free-space RCS, taking into account equal angular positions) should be at least 200-218 km. The results of confirmation of the far edge of the detection area for the RCS equal to 0.85 m^2 and 1.0 m^2 are shown in Figure 11.

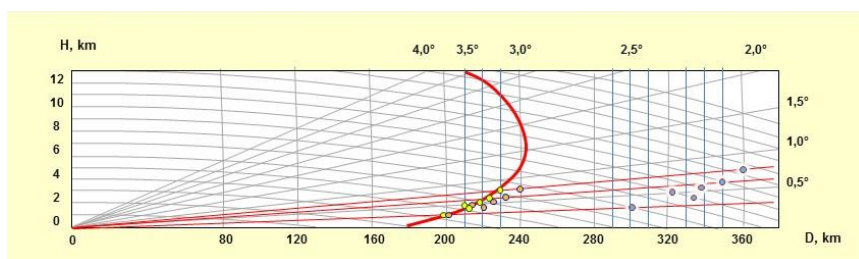


Figure 11 - Confirmation of estimated area of detection of a 9M38-type missile at altitudes above 3,500 m based on the results of reference targets' test flight

The primary radar's capability to detect small targets is additionally confirmed by the fact that at the time of the events that occurred on 17.07.2014 an Orlan-10-type UAV, the RCS of which is 3-5 times smaller than that of a BUK missile, was detected and tracked by the ARRC. The radar mark and the airborne object ("Orlan-10") form are shown in Figure 12.

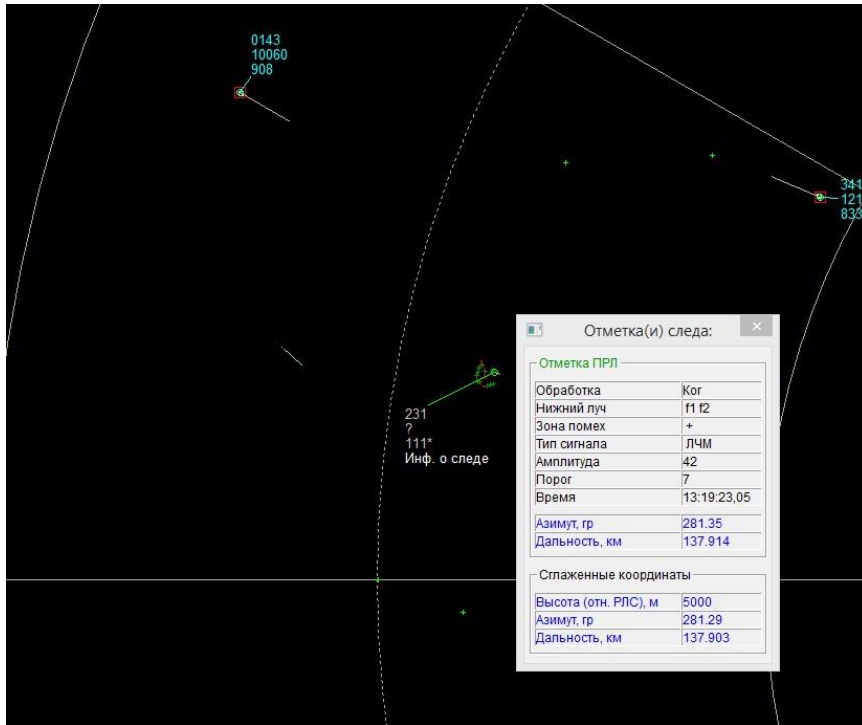


Figure 12 - Radar mark and form in respect of airborne object No. 231 (Orlan-10 UAV) at a distance of 137.9 km from Ute-T transponder. Time: 13:19:23.05 UTC (registration file "14-07-17_fragment.kt")

* Trail mark(s)

- Primary radar mark	
Processing	Coherent
Lower beam	f1 f2
Interference area	+
Signal type	Linear frequency modulation
Amplitude	42
Threshold	7
Time	13:19:23,05
Azimuth, deg...	281.35
Distance, km	137.914
Smoothed coordinates	
Altitude (relative to radar), m	5000
Azimuth, deg.	281.29
Distance, km	137.903

Thus, a missile flying at altitudes above the radio horizon can be detected by the primary radar at distances greater than 200 km.

Confirmation of the speed characteristics of the primary radar.

While circling Utes-T ARRC's primary radar, a reference supersonic airborne object in the area of the high-speed segment was manoeuvring and accelerating to supersonic speed:

true speed, max M= 2.04...2.1
 indicated speed, max M= 1.9...2.0

The airborne object was steadily observed in the entire reference segment of the trajectory. The radial velocity V_R measured by the ARRC ranged from 508 to 567 m/s (Figures 13 and 14).

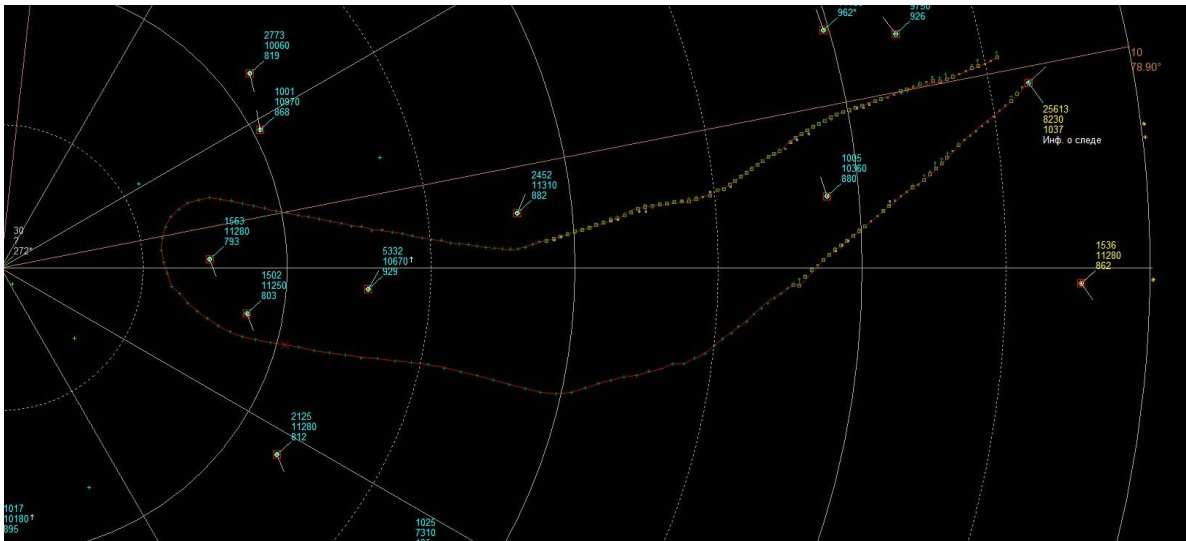


Figure 13 - Supersonic airborne object flight path including the reference segment of the trajectory

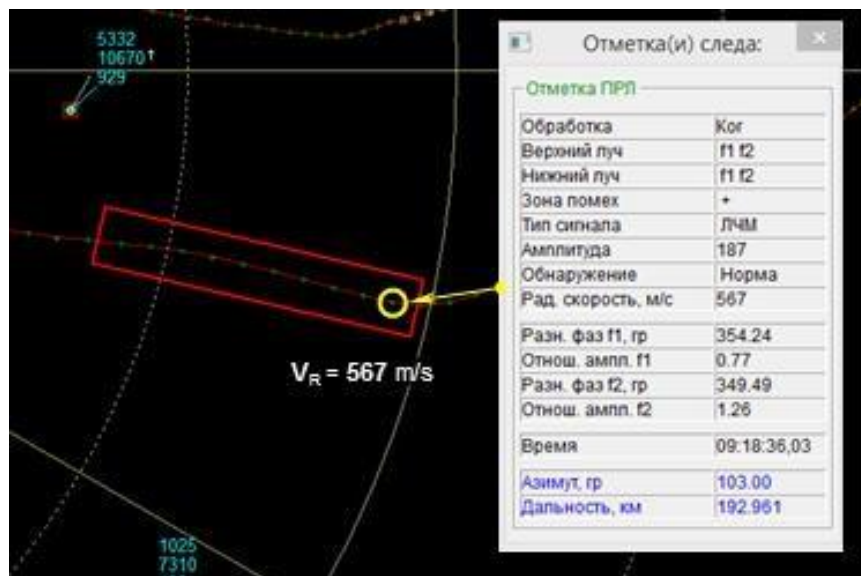


Figure 14 - Reference supersonic segment of the trajectory. True velocity of airborne object M= 2.04...2.1. Radial velocity measured by the ARRC is 567 m/s (time 09:18:36.03 UTC 09.07.2019)

* Trail mark(s)

- Primary radar mark	
Processing	Coherent
Upper beam	f1 f2
Lower beam	f1 f2
Interference area	+
Signal type	Linear frequency modulation
Amplitude	187
Detection	Standard
Radial velocity, m/s	567
Phase difference f1, deg..	354.24
Amplitude ratio f1	0.77
Phase difference f2, deg..	349.49
Amplitude ratio f2	1.26
Time	09:18:36,03
Azimuth, deg..	103.00
Distance, km	192.961

The capability of Utes-T ARRC to detect supersonic airborne objects is also confirmed by air situation data of 2001. This air situation data obtained by Utes radar at Gelendzhik position (earlier generation radar, which is a predecessor to Utes-T ARRC) in October 2001 was used in practice to determine the cause of Tu-154M RA85693 crash over the Black Sea.

At that time, the primary radar detected an unidentified airborne object moving in the direction of the Tu-154M aircraft's flight path at a speed of about 1,000 m/s. Subsequently, the recorded marks were identified as S-200 SAM missile that caused the crash⁶.

Figure 15 shows a fragment of "Findings of Damage Research on Fragments of Tupolev 154M RA85693 Crashed on October 4, 2001 over Black Sea" with the flight path of the Tu-154M in the last segment.

⁶ Final Report ACCID Tu-154 RA-85693 (EN), p.16-17.

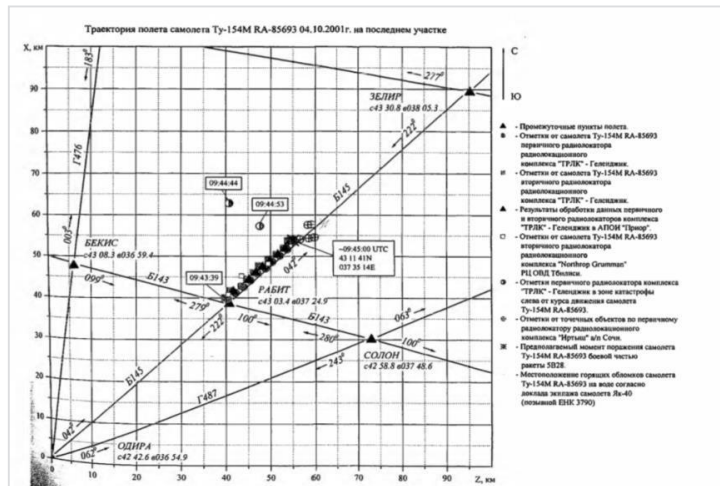


Figure 15 – The last segment of the flight path of Tu-154M RA-85693 on 04.10.2001. There are marks from an airborne object detected by the ARRC at Gelendzhik position to the left of the aircraft's path.

*

- Waypoints
- Marks from Tu-154M RA-85693 by the primary radar of the radar complex in Gelendzhik
- Marks from Tu-154M RA-85693 by the secondary radar of the radar complex in Gelendzhik
- Results of data processing by APOI Prior in relation to data from the primary and the secondary radars of the radar complex in Gelendzhik
- Marks from Tu-154M RA-85693 by the secondary radar of Northrop Grumman radar complex of RTs OVD Tbilisi
- Marks by the primary radar of the radar complex in Gelendzhik in the crash area, to the left of Tu-154M RA-85693 aircraft's course
- Marks from point-like objects according to the primary radar of Irtysh radar complex in Sochi
- Presumed moment when Tu-154M RA-85693 aircraft was hit by the war head of 5B28 missile.
- Location of burning debris of Tu-154M RA-85693 aircraft in water according to the report of Yak-40's crew (call sign EHK 3790)

Thus, a missile flying at a supersonic speed corresponding to the radial speed of up to 1,000 m/s can be detected by the primary radar within the detection area.

When testing the "opposite direction" hypothesis, the marks from the reference target were detected immediately after they crossed the radio horizon. The primary radar's marks with the derived data are shown in Figures 16 and 17.

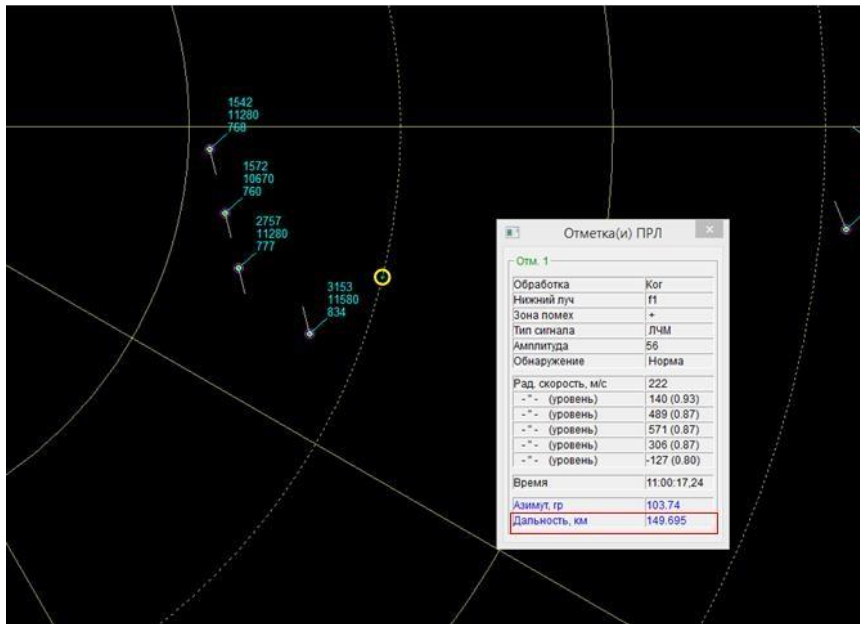


Figure 16 - First mark from the reference airborne object after it went beyond the radio horizon. The distance is 149.7 km

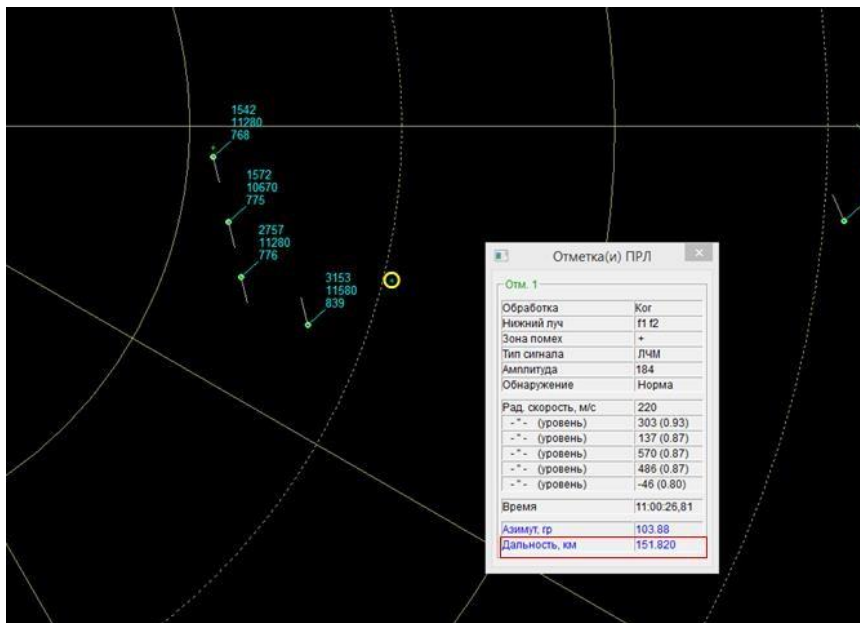


Figure 17 - Second mark from the reference airborne object after it went beyond the radio horizon. The distance is 151.8 km

- Primary radar mark(s)	
Mark 1	
Processing	Coherent
Lower beam	f1
Interference area	+

Signal type	Linear frequency modulation
Amplitude	56
Detection	Standard
Radial speed, m/s	222
- * - (level)	140 (0.93)
- * - (level)	489 (0.87)
- * - (level)	571 (0.87)
- * - (level)	306 (0.87)
- * - (level)	-127 (0.80)
Time	11:00:17,24
Azimuth, deg..	103.74
Distance, km	149.695

- Primary radar mark(s)	
Mark 1	
Processing	Coherent
Lower beam	f1
Interference area	+
Signal type	Linear frequency modulation
Amplitude	184
Detection	Standard
Radial speed, m/s	220
- * - (level)	303 (0.93)
- * - (level)	137 (0.87)
- * - (level)	570 (0.87)
- * - (level)	486 (0.87)
- * - (level)	-46 (0.80)
Time	11:00:26,81
Azimuth, deg..	103.88
Distance, km	151.820

The object simulating the missile flight "in an opposite direction" was detected immediately after it went beyond the radio horizon (during the first scan period). Following that, the reference airborne object was tracked steadily throughout its flight in the reference segment of the trajectory (Figure 18) and until it exited the detection area at a distance of over 320 km.



Figure 18 – Airborne object No. 116 in "an opposite direction" trajectory.
The airborne object in the reference segment of the trajectory was observed steadily

- Trail mark(s)	
- Primary radar mark(s)	
Processing	Coherent
Lower beam	f1
Interference area	+
Signal type	Linear frequency modulation
Amplitude	56
Detection	Standard
Radial velocity, m/s	222
Time	11:00:17,24
Azimuth, deg..	103.74
Distance, km	149.695

- Trail mark(s)	
- Primary radar mark(s)	
Processing	Coherent
Upper beam	f1
Lower beam	f1
Interference area	+
Signal type	Linear frequency modulation
Amplitude	107

Detection	Standard
Radial velocity, m/s	167
Time	11:01:43,37
Azimuth, deg..	106.25
Distance, km	169.906

Information about this object was continuously displayed on the radar operator's screen and saved as air situation data in the primary registration file "19-07-09.kt", which is similar to the one given to the Dutch experts.

Thus, a missile that is in the space observed by the ARRC and is within the area of detection on the basis of the main parameters, such as radar visibility, position above the radio horizon in the antenna directivity pattern, exceeding the MTS threshold for radial speed, etc., can be detected by the primary radar of Utes-T ARRC without any hindrance.

It follows from an analysis of the results obtained⁷ that if a moving object with characteristics corresponding to a BUK missile and travelling at a speed of 500 to 1,000 m/s was in Utes-T ARRC's observation area, it would have been detected with more than 0.9 probability at a distance of 200 to 240 km.

The distance to aircraft #0143 (MH17) recorded by the ARRC at the time of radar contact T_0 (less than 1.2 seconds before the tragedy) was ~ 171.8 km.

The distance to the weapon moving "in an opposite direction" at the time of radar contact T_0 would be about 170 km, and in time periods T_{-10} and T_{-20} the distance would be significantly less than 170 km.

Thus, at the time of radar contacts T_0 , T_{-10} and T_{-20} the main parameters of the missile flight (radial velocity, position above the radio horizon in the lower lobe of the antenna directivity pattern) made it possible, if the launch hypothesis under consideration is true, to record steady marks of echoes from an object moving towards the aircraft at a speed of 620-970 m/s.

At the time of these "hypothetical" radar contacts, the main parameters of the missile flight (radar visibility; radial velocity; position over the radio horizon in the antenna directivity pattern, etc.) made it possible, in the case of the "opposite direction launch" hypothesis by DSB/JIT, to record steady marks of echoes from an object moving towards the aircraft with a probability of ~ 0.9 in each scan period.

⁷ The tests were conducted over two days on 08.07.2019 and 09.07.2019. The results obtained during the two phases are the same.

The probability of recording at least one mark during three consecutive scan periods exceeds 0.99.

Such marks would have been recorded in the primary registration file containing all primary air situation data. They would have been detected when playing back and reviewing the file "14-07-17.kt" which was previously handed over to the Dutch side.

When playing back the registration file "14-07-17.kt" of Utes-T ARRC for the period from 13:02 to 13:32 UTC 17.07.2014, one can see that no marks were recorded, which suggests the absence of an object moving in the observed area in the direction of the Boeing 777 from the side of Pervomaisky (Snezhnoye) settlement in Donetsk region of Ukraine.

5.8. The airborne object simulating the missile flight from the southern direction ("on a collision course") was not observed by the primary radar in any part of the reference segment of the flight path.

The first mark appeared only after the airborne object completed its flight along the reference trajectory (at an altitude of "10,360 m" and with the MTS radial velocity threshold being exceeded ("-36 m/s")).

The first mark by the primary radar with the derived data is shown in Figure 19.

The reference airborne object was then tracked steadily (Figures 20 and 21).

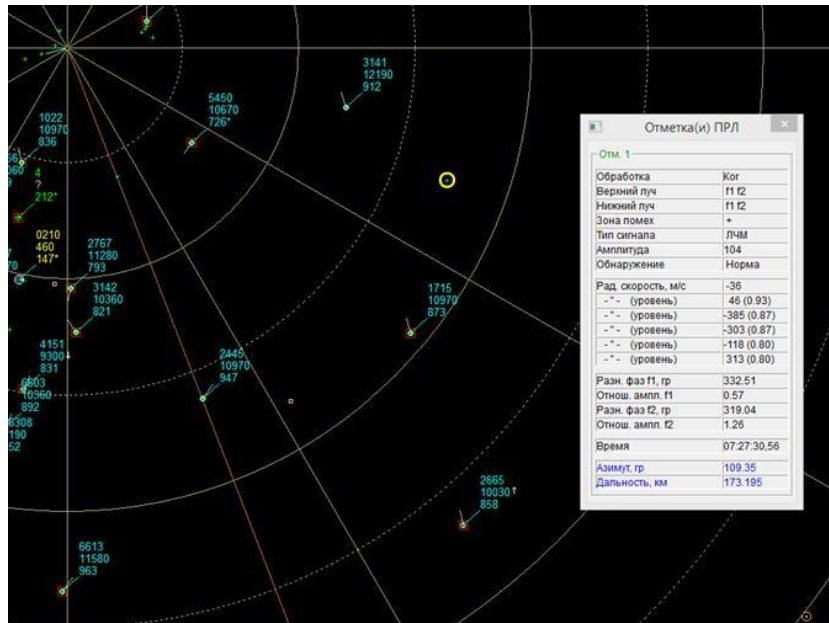


Figure 19 - First mark of the reference airborne object after completion of its flight along the special trajectory simulating the missile flight from the southern direction. The distance is 173.2 km

*

- Primary radar mark(s)	
Mark 1	
Processing	Coherent
Upper beam	f1f2
Lower beam	f1f2
Interference area	+
Signal type	Linear frequency modulation
Amplitude	104
Detection	Standard
Radial speed, m/s	-36
- * - (level)	46 (0.93)
- * - (level)	-385 (0.87)
- * - (level)	-303 (0.87)
- * - (level)	118 (0.80)
- * - (level)	-313 (0.80)
Phase difference f1, deg..	332.51
Amplitude ratio f1	0.57
Phase difference f2, deg..	319.04
Amplitude ratio f2	1.26
Time	07:27:30,56
Time	11:00:17,24
Azimuth, deg..	109.35
Distance, km	173.195

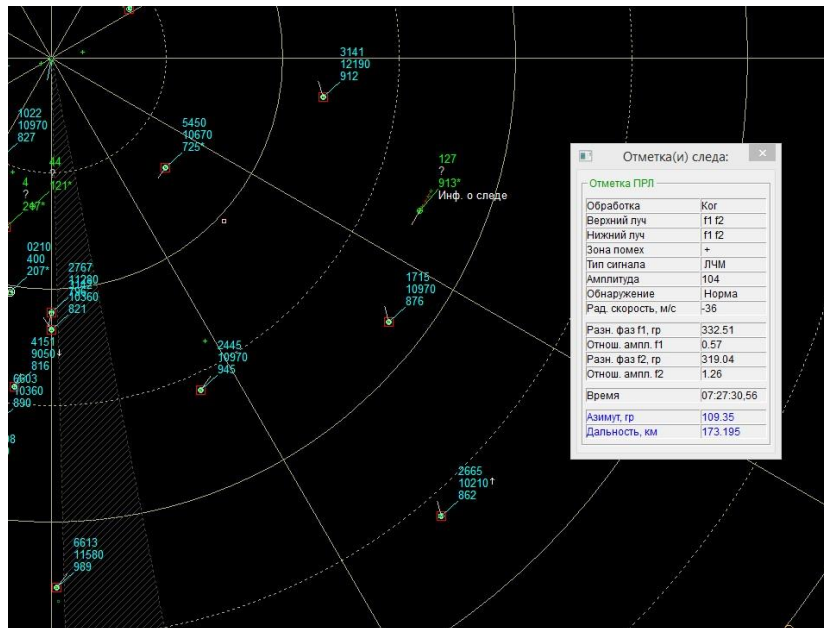


Figure 20 – Tracing of the reference airborne object

*

- Primary radar mark(s)	
Mark 1	
Processing	Coherent
Upper beam	f1 f2
Lower beam	f1 f2
Interference area	+
Signal type	Linear frequency modulation
Amplitude	104
Detection	Standard
Radial speed, m/s	-36
Phase difference f1, deg..	332.51
Amplitude ratio f1	0.57
Phase difference f2, deg..	319.04
Amplitude ratio f2	1.26
Time	07:27:30,56
Time	11:00:17,24
Azimuth, deg..	109.35
Distance, km	173.195

No information about this reference object flying along a special trajectory simulating the missile flight from the southern direction ("on a collision course") was displayed on the radar operator's screen or saved in the primary registration file "19-07-09.kt". The reference object was detected by the primary radar at 07:27:30,56 UTC at an altitude of 10,360 m only after completion of the trajectory flight, when the MTS radial velocity threshold of "-36 m/s" was exceeded.



Figure 21 – Tracking of the reference airborne object after completion of the flight along a special trajectory simulating the missile flight from the southern direction

Thus, a missile in the ARRC's observation area may fly undetected by the primary radar, if its radial velocity is below the MTS threshold (in this case below 30 m/s).

The analysis of primary radar data for 17.07.2014 showed that no objects moving towards the Boeing 777 "from the southern direction" ("on a collision course") were detected, when the registration file "14-0717.kt" was played back. According to the simulation results, the trajectory of the missile approaching the Boeing 777 "from the southern direction" ("on a collision course") has a characteristic feature: a low sign-variable radial velocity. The range of these velocities is -21 to 24 m/s.

In this case, taking into account the missile's trajectory and flight time and the coherent operation mode of Utes-T ARRC in the crash area due to weather conditions, the probability of detecting marks with low radial velocity is low. This was confirmed experimentally: the reference airborne object was only detected after the MTS threshold of -36 m/s for radial velocity was exceeded.

As the test results have shown, the absence of marks in the primary data registration file "14-07-17.kt" of Utes-T ARRC does not mean that there was no object moving towards the Boeing 777 at a high speed "from the southern direction" in the observed space.

6. Conclusions

1. The results of the simulation show that, in the case of the hypothesis suggesting that the Boeing 777 was hit by a BUK missile moving "in an opposite direction", the object would have been within Utes-T ARRC's detection area over three scan periods, while in the case of the hypothesis implying impact from the southern direction ("on a collision course") it would have been there over two scan periods.

2. The flight around of Ust-Donetsk radar position confirmed the main capabilities of Utes-T ARRC to detect small and high-speed airborne objects.

3. The probability of detecting an airborne object with parameters corresponding to a missile flying "in an opposite direction" relative to the Boeing 777 aircraft is about 0.9. At the same time, the probability of recording at least one mark over three consecutive scan periods exceeds 0.99.

4. The fact that the registration file "14-07-17.kt" of Utes-T ARRC for the period from 13:02 to 13:32 UTC 17.07.2014 contains no marks approaching the aircraft at a high speed "from the east of Ukraine" suggests there was no object travelling towards the Boeing 777 from the direction of the village of Pervomaisky in Donetsk Region of Ukraine in the area of observation.

5. According to the results of the completed full-scale experiment the conditions of which were as close as possible to those at the time of the crash, a BUK missile could approach the Boeing 777 without being detected by the radar from the southern direction only, if it was flying on a "collision course".

Thus, if BUK missiles are considered as the probable cause of the destruction of the Boeing 777 aircraft, such missile could approach the aircraft without being detected by Utes-T radar from the southern direction only, if it was flying on "a collision course".

The missile launch from the side of Snezhnoye and Pervomaisky settlements (Donetsk Region of Ukraine), i.e. "in an opposite direction", is not confirmed by air situation data recorded by Utes-T air-route radar complex. The primary data registration file "14-07-17.kt" of Utes-T ARRC for the period from 13:02 to 13:32 UTC 17.07.2014 contains no marks from the weapon, which suggests the absence

of an object moving in the direction of the Boeing 777 "on an opposite course" in the area of observation.
